Laboratoire de Constructions Hydrauliques
Ecole Polytechnique Fédérale de Lausanne

Communication 25

The influence of pool geometry and induced flow patterns in rock scour by high-velocity plunging jets

Pedro Manso

Editeur : Prof. Dr A. Schleiss

Lausanne, 2006

Communications du Laboratoire de constructions hydrauliques ISSN 1661-1179
Ecole Polytechnique Fédérale de Lausanne
Editeur: Prof. Dr A. Schleiss

Preface

The safety of hydraulic structures in general and dams in particular is very often endangered by the formation of scour near the foundation as a result of high-velocity jets leaving from appurtenant structures as spillways and plunging into the tailwater. Scouring is a very complex physical process and full physical understanding of the water-air-rock interaction in the scouring process is still lacking.

With his research, Dr. Pedro Manso filled up a considerable gap towards a better scientific understanding of the scouring process. For the first time the influence of pool geometry and induced flow patterns in rock scour by high-velocity plunging jets was studied in a systematic way by physical modelling and numerical analysis.

By the help of an experimental set-up producing near prototype jets, jet issuance conditions for cylindrical nozzles and typical prototype structures were described in detail. Impact pressures were measured for variable pool depths and jet velocities in pools with flat bottom. Systematic probabilistic analyses were carried out, which allowed a detailed description of jet diffusion in limited-depth pools. A new methodology for jet diffusion and time-averaged energy dissipation in limited-depth pools was worked out by Dr. Pedro Manso, compiled from previous research and compared with experimental data. Investigations of aerated pool flows under high velocity jets allowed describing air bubble behaviour in the vicinity of the pool bottom and presenting experimental evidence of air bubble contraction at stagnation.

For a large number of laterally confined pool geometries, the dynamic pressures at the pool bottom were measured and analysed, which allowed for the first time performing a systematic comparison of jet diffusion and flow patterns in pools with flat bottom and in laterally confined pools. Their combination can be applied for typical scour evolution scenarios under prototype conditions.

In a next step the propagation of dynamic impact pressures, generated in laterally confined pools, inside closed-end rock fissures were measured. The conditions of occurrence of pressure amplification and of column separation, as well as the configuration of typical spectral distributions inside fissures could be defined.

Finally Dr. Pedro Manso performed a systematic description of 1D, 2D and 3D approaches for rock block displacement analysis, considering the persistence and the likelihood of occurrence of given pressure fields as well as block dimensions. This is important for the dynamic impulsion of the rock blocks and therefore for the assessment of scour evolution. The persistence and energy content of pressure pulses with given extreme probability was also analysed.

We would like to thank Prof. Virgilio Fiorotto from the University of Trieste, Italy for his significant contribution in the fields of analytical and numerical analyses of the dynamic pressure measurements, as well as Prof. Jorge Matos, Technical University of Lisbon, Portugal and Prof. Michel Pirotton, University of Liège, Belgium for their support and guidance as academic guests at LCH-EPFL. We also thank gratefully the Foundation for Science and Technology (FCT) of Portugal and the Swiss Federal Office for Water and Geology for their financial support.

Prof. Dr. Anton J. Schleiss

Abstract

The influence of pool geometry and induced flow patterns in rock scour by high-velocity plunging jets

The dissipation of energy of flood discharges from water releasing structures of dams is often done by plunging jets diffusing in water and impacting on the riverbed downstream. The construction of expensive concrete structures for energy dissipation can be avoided but the assessment of the scour evolution is mandatory for dam safety. The scour growth rate and shape depend on the riverbed geology. The geometry of scour may influence the turbulent flow pattern in the pool, the dynamic loadings acting on the rock interface, and the pressures propagating inside rock joints. Up to present, dynamic impact pressures at the pool bottom have been investigated mainly in pools with flat bottom and are therefore described as function of the pool depth and the characteristics of the jets only. To approach the conditions found in practice, non-flat plunge pools and turbulent two-phase jets are investigated in this research work. This fundamental investigation focuses on the interaction between the development of plunging jets in the water and the geometry of the plunge pool. The influence of laterally confining jet diffusion is investigated by means of experimental work in near prototype conditions, in terms of jet velocities and air entrainment in the pool. Different pool geometries typical of prototype conditions are tested and compared with a reference pool with flat bottom. Pressure measurements at the jet outlet, at the pool bottom and inside a closed-end fissure are presented. The main emphasis of the text is on the analysis and the description of physical processes. The integration of the findings in existing scour estimation models is discussed.

The thickening of the water cushion downstream, artificially or by scour, is investigated for fully controlled jet issuance conditions. The dissipation of jet energy is estimated based on measurements of mean impact pressures and is compared with results from an analytical model. The developed model features jet diffusion in limited-depth pools and is tentatively applied to turbulent two-phase jets. Agreement is good in the early stages of scour and in deep flat pools. For pool depths about the jet core development length (i.e. transitional pools), analytical estimates are quite sensitive to the initial assumptions on the centreline velocity decay, dimensions of the impinging zone and pool aeration. The findings highlight the limitations of existing empirical laws in representing the diffusion of turbulent two-phase jets in pools with flat bottom. Turbulent impact pressures are also investigated for increasing pool depths. Based on an evaluation of high-order statistical moments and autocorrelation functions of pressure fluctuations at stagnation, jet development conditions at impact are distinguished in core and developed impact conditions. Core impact conditions are typical of shallow pools and generate negatively asymmetric distributions at stagnation. The end of core development is associated with highly intermittent flow conditions, with important pressure fluctuations (high kurtosis). For developed impact conditions, pressure fluctuations at stagnation are positively asymmetric. A Gaussian distribution fits satisfactorily the data, save for extreme high and low (cumulated) probabilities. Air-water measurements are carried out at selected points in pools with flat bottom. They allow describing the behaviour of air bubbles before, at, and aside stagnation. Void fraction estimates close to the entry of rock fissures show that air bubbles reduce in size under the influence of the high-pressure gradient at stagnation. The characteristic dimensions of the air bubbles close to the bottom are small compared to typical entry dimensions of rock fissures.

The investigations conducted in pools with flat bottom are used as a reference scenario in the investigation of plunge pools with more realistic geometries. The experimental results show that mean impact pressures at the pool bottom are lower in laterally confined pools than in equivalent pools with flat bottom. The length of core development can be reduced, depending on the degree of

confinement and pool depth. Enhanced pool turbulence is described by power spectra density and probabilistic distribution functions of impact pressures. It is concluded that the flow currents created by deflection of the jet on the lateral boundaries of the pool may interfere with the development of the jet, generate additional dissipation in the water column and hinder the propagation in depth of air bubbles in the pool. For shallow and transitional laterally confined pools, pressure fluctuations may have more energy than in corresponding pools with flat bottom. Power spectra of pressure fluctuations have higher energy content in the intermediate frequency range (e.g. 10 a 100 Hz). Extreme positive pressures increase. In terms of scour, there is a trade-off relatively to flat pools: there is hardly core impact and persistent hydro-fracturing (because mean impact pressures are lower), but fracturing may occur if high low-persistence pressure peaks are generated inside rock fissures (by transients due to enhanced impact pressure fluctuations). For deep laterally confined pools, the energy of pressure fluctuations is lower than in pools with flat bottom. Extreme positive pressures are similar, but increase in relative terms to the total energy of pressure fluctuations. Negative extreme pressures are lower. The most relevant flow features in laterally confined pools are identified using direct observations of flow patterns and in-depth analysis of the characteristics of turbulent pressures at impact. Large-scale pool flow features like surface oscillations, shear eddies and air-water ejections are described. The evolution of geometry-induced flow patterns and dynamic loading with scour development, for variable width of confinement and pool depth, are presented for four typical scour scenarios. The role of the deflected upward currents and shear eddies in the dissipation process depends on the degree of confinement, jet velocity and pool depth. The closer they are to the plunging jet, the higher is the dissipation of energy before impact. Recirculation currents may enhance jet development by either pushing upward currents into the jet.

The dynamic pressure measurements performed inside closed-end fissures allow concluding that the dynamic response of rock fissures varies with the turbulent character of impact pressures at the rock interface. It is shown that the dimensions of the entry of the fissure play an important role in filtering turbulent pressure fluctuations in the transition from the pool into the fissure: the larger the dimensions, the lower are the frequencies filtered out. It is observed that the energy of pressure fluctuations inside the fissure is always higher than at the entry, for all pool configurations tested. The energy of pressure fluctuations inside rock fissures is lower in narrow confined pools for transition and deep pools, but higher in shallow pools, compared with equivalent pools with flat bottom. This is also valid for positive extreme pressures. Negative extreme pressures are generally lower. Amplification of pressure peaks is observed inside a closed-end fissure for both shallow and deep pools; it depends of the degree of jet development, i.e. of relative pool depth, pool geometry and jet turbulent characteristics (and, indirectly, of the amount of entrained air reaching the bottom of the pool). Therefore, transient pressure peaks generated inside fissures are a potential agent of scour in laterally confined pools, from shallow to deep. Amplification occurs due to the development of transient flows inside the fissure, that may include column separation. The occurrence of resonance inside fissures is investigated numerically. Multiple resonant harmonics are replicated solving numerically the waterhammer equations inside the fissure with the hydraulic impedance method.

A probabilistic-based event analysis is developed to correlate the probability, persistence, duration and energy content of extreme pressure pulses. It is shown that pulses with high extreme (cumulated) probabilities have low persistence and high energy content. The concept of relevant probability is outlined, allowing for the selection of pressure events that should effectively be considered for the propagation of rock fissures or for the dynamic uplift of rock blocks. The role of extreme pressure events in the scouring processes of crack propagation and block displacement is discussed.

In conclusion, the experimental investigation of jet diffusion in pools with flat bottom and laterally confined pools shows the importance of pool flow patterns in the definition of impact pressures and transient pressures inside rock fissures. It provides detailed information on hydrodynamic processes involved in rock scour, as well as several contributions to engineering practice, in terms of jet issuance conditions, empirical relationships for impact pressures and recommendations for the design of pre-excavated pools.

Key-words: high-velocity jets, physical modeling, dynamic pressures, void fraction, turbulent pool flows, rock scour, induced-currents, interaction between jets and pool geometry.

Résumé

Impacts de jets plongeants à haute vitesse : l'influence de la géométrie de la fosse d'érosion et de ses courants induits sur l'affouillement du massif rocheux récepteur

Dans le cadre du dimensionnement d'évacuateurs de crue par jets plongeants, il est courant d'assurer la dissipation de l'énergie liée à la chute par un impact non protégé sur le massif rocheux de la rivière en aval. Cette solution économique permet en effet d'éviter la construction d'ouvrages de dissipation d'énergie en béton armé. Il est nécéssaire d'estimer le plus précisément possible l'étendue de la fosse d'érosion pendant la durée de vie de l'ouvrage, afin d'assurer la sécurité du barrage, des ouvrages annexes et des versants de la vallée. Le taux d'affouillement ainsi que la forme de la fosse dépendent de la géologie du lit de la rivière. En l'état actuel, la description des pressions dynamiques n'a été effectuée que pour des fosses à fond plat, en fonction de la profondeur de la fosse et des caractéristiques turbulentes du jet. Afin d'approcher les conditions trouvés en pratique, des fosses d'érosion non-plates ainsi que des jets biphasiques turbulents sont étudiés dans cette recherche. Ce travail porte d'abord sur l'analyse expérimentale du comportement de jets plongeants ayant un champ de vitesses et un processus d'entraînement d'air de conditions quasi-prototype. L'effet d'un confinement latéral de la diffusion du jet dans la fosse d'érosion sur les sollicitations transmises au rocher est mis en évidence. Différentes configurations types de fosses d'érosion sont testées et comparées avec la fosse à fond plat. Les pressions dynamiques sont mesurées à l'intérieur du jet lui-même, au fond de la fosse ainsi qu'à l'intérieur de fissures unifilaires à bout fermé. Ces mesures sont utilisés pour analyser le comportement turbulent de l'écoulement dans la fosse et des régimes transitoires dans les fissures du rocher. Le texte se focalise sur l'analyse et description de processus physiques. L'intégration des résultats dans des modèles existantes pour l'estimation de la profondeur d'affouillement est discutée.

L'épaississement du matelas d'eau en aval, artificiellement ou par affouillement, est étudié avec des jets produits en conditions contrôlés. La dissipation de l'énergie de jets dans des fosses d'affouillement est estimée à partir de mesures de pressions moyennes au fond de la fosse, à la zone d'impact. Les résultats expérimentaux sont comparés avec des valeurs obtenues avec un modèle analytique pour la diffusion de jets turbulents biphasiques en bassins à fond plat. Ce dernier fournit des résultats satisfaisants dans le cas de bassins profonds à fond plat ainsi qu'en phase initiale du processus érosif. Pour des profondeurs correspondant à la longueur de développement du jet (situation de transition), le modèle analytique est très sensible aux conditions initiales. Ces dernières portent sur les hypothèses liées à la décroissance de la vitesse à l'axe du jet, aux dimensions de la zone de stagnation et enfin à l'entraînement d'air dans la fosse. Les résultats montrent les limitations des lois empiriques existantes dans la description de la diffusion de jets turbulents biphasiques dans les bassins à fond plat. Les pressions turbulentes à l'impact du jet au fond de fosses à fond plat sont aussi analysés pour plusieurs profondeurs d'eau, à la zone de stagnation. Les conditions d'impact sont caractérisées en fonction de l'évaluation des moments statistique de troisième et quatrième ordre ainsi que des autocorrelations des fluctuations de pression. L'impact en "noyau du jet" est typique de bassins peu profonds et produit des fluctuations de pression d'asymétrie négative. La fin du développement du jet correspond à un caractère intermittent du jet signalé par une augmentation du kurtosis. L'impact d'un "jet développé" produit des fluctuations de pression d'asymétrie positive. Une distribution gaussienne permet un ajustement satisfaisant des pressions dynamiques, à l'exception des valeurs extrêmes de probabilité (cumulé) très haute ou très basse. Des mesures des concentrations en air de l'écoulement sont effectuées en trois points singuliers de fosses à fond plat et de profondeur variable. Les mesures permettent de décrire le comportement des bulles d'air à l'entrée, au milieu et à côté de la zone de stagnation. Les mesures du contenu en air au voisinage de l'entrée des fissures montrent une réduction des dimensions des bulles d'air sous l'effet du fort gradient de pression de stagnation. Les bulles d'air proche du fond sont petites par rapport aux dimensions caractéristiques des fissures du massif rocheux.

Les investigations menées sur des fosses à fond plat servent de référence pour l'étude de fosses confinées latéralement (i.e. non plates). Les résultats expérimentaux montrent que pour les dernières, les pressions

moyennes à l'impact sont plus faibles que celles mesurées dans les fosses à fond plat. D'autre part, la longueur de développement du noyau du jet peut être réduite, selon le degré de confinement latéral et la profondeur de diffusion. En effet, les courants créés par la déviation du jet plongeant par les parois latérales du confinement peuvent interférer dans le développement du jet; de la dissipation additionnelle sera générée et la pénétration de bulles d'air en profondeur sera rendue plus difficile. Dans les bassins confinés latéralement à faible profondeur ou de transition, les fluctuations de pression peuvent contenir plus d'énergie que dans le cas de bassins plats de profondeur similaire. Les fonctions de densité spectrale révèlent un surplus d'énergie dans la plage de fréquences intermédiaires (e.g. 10 a 100 Hz). L'amplitude des pressions extrêmes positives augmente. Du point de vue de l'affouillement il y des avantages et des inconvénients par rapport aux fosses à fond plat: la gamme de conditions qui produisent l'impact "du noyau" et la rupture de la roche par hydro-fracturing persistent est très limité (car les pressions moyennes à l'impact sont plus faibles), mais la rupture peut être effectuée par des pics de pressions de courte durée générés par des régimes transitoires à l'intérieur de fissures de la roche (dus à l'augmentation du comportement turbulent en surface). Par contre, à plus grande profondeur, l'énergie des fluctuations de pression est plus basse dans les bassins confinés latéralement que dans les bassins à fond plat. Les valeurs extrêmes de pressions positives n'augmentent pas en termes absolus, mais en termes relatifs par rapport à l'énergie totale des fluctuations de pression. Les valeurs extrêmes négatives sont plus basses qu'en bassin à fond plat, indépendamment de la profondeur. Les principales particularités de l'écoulement dans des fosses confinées latéralement, tels que oscillations du plan d'eau, éjections et structures tourbillonnaires sont identifiés sur la base d'observations directes de l'écoulement et des caractéristiques des pressions dynamiques à l'interface eau-rocher. L'évolution de la structure de l'écoulement et des sollicitations dynamiques à l'interface eau-rocher est analysée en fonction de l'évolution de l'affouillement, du degré de confinement latéral et de la profondeur de diffusion, pour quatre scénarios types d'affouillement. Le rôle des courants ascendants et des structures tourbillonnaires sont commentés en regard de leur participation au processus dissipative, selon le degré de confinement, la vitesse du jet et la profondeur de la fosse. Le plus proches elles sont du jet, le plus de dissipation sera produite dans la colonne d'eau avant l'impact. Les courants de re-circulation peuvent aussi contribuer au développement du jet en forçant les courants ascendants vers le jet lui-même.

Les mesures de pression effectuées à l'intérieur de fissures montrent que les régimes transitoires de l'écoulement dans les fissures du rocher varient selon les caractéristiques turbulentes des pressions dynamiques à l'impact. L'importance des dimensions de l'entrée de la fissure pour le transfert de pressions est mis en évidence : les plus larges sont les dimensions de la fissure, les plus basses sont les fréquences filtrées. L'énergie des fluctuations de pression mesurées à l'intérieur de la fissure est supérieure à celle mesurée à l'entrée dans chaque cas étudié. Pour les grandes profondeurs ou les profondeurs de transition, les fluctuations de pression dans les fissures sont plus basses dans les bassins latéralement confinés. Pour les faibles profondeurs de diffusion, ces fluctuations sont plus basses dans les bassins à fond plat. L'amplification des pics de pression à l'intérieur des fissures à bout fermé est observée dans le cas de faible profondeurs, ainsi que de grandes profondeurs, dans des bassins confinés latéralement. L'amplification dépend du degré de développement du jet, i.e. de la profondeur de diffusion, de la géométrie de la fosse et des caractéristiques turbulentes du jet (et, indirectement, de la quantité d'air proche du fond). De ce fait, des pics de pression générés par régimes transitoires à l'intérieur de fissures sont un agent potentiel de l'affouillement de fosses latéralement confinées. La rupture de la veine liquide à l'intérieur des fissures est documentée. La mise en résonnance de la fissure est simulée numériquement et comparée avec les mesures de pression. Les oscillations harmoniques sont reproduites par la résolution des équation du coup de bélier à l'intérieur de la fissure par la méthode d'impédance hydraulique.

Une méthode d'analyse temporelle des pressions dynamiques est developé. Elle permet de corréler la probabilité d'apparition d'événements de pressions avec leur persistance, durée et contenu énergétique. Son application à plusieurs séries de données expérimentaux montrent que la persistance des événements décroît considérablement pour des événements rares, ayant un contenu énergétique important. Ceci permet la définition d'une probabilité seuil pour la séléction des événements importants pour chaque processus physique. La participation des événements de pression extrêmes aux processus de propagation des fissures et de soulèvement de blocs est analysée.

En conclusion, ce travail expérimental démontre l'importance fondamentale de la description de la structure de l'écoulement dans la fosse d'érosion pour l'estimation des sollicitations dynamiques à l'impact et à l'intérieur des fissures du massif rocheux. Elle propose une documentation détaillée de processus hydrodynamiques existants lors de l'affouillement de lits de rivière rocheux par des impacts de jets, ainsi que plusieurs contributions pour la pratique en termes des conditions de sortie du jet, équations empiriques pour les pressions dynamiques à l'impact et recommendations pour le dimensionnement de pré-excavations.

Mots-clés: jets à haute-vitesse, modélisation physique, pressions hydrodynamiques, concentration en air, turbulence, affouillement, courants induits, interaction jet plongeant-géométrie de la fosse d'érosion.

Sumário

Influência da geometria da fossa de erosão e das correntes de recirculação induzidas, na erosão localizada de leitos rochosos provocada por jactos de grande velocidade

O impacto directo de jactos provenientes de órgãos de descarga de cheia de barragens num leito rochoso constitui uma alternativa à construção de estruturas dispendiosas em betão armado, para dissipação de energia hidráulica durante cheias. No entanto, a avaliação da evolução da erosão no período de vida útil da barragem é necessária para garantir a segurança da barragem, das estruturas anexas e das encostas das margens na zona da restituição do escoamento. As fossas de erosão criadas a jusante de grandes barragens desenvolvem-se em função do funcionamento dos órgãos de descarga e segundo a geologia do leito. A sua geometria pode influenciar o campo de escoamento turbulento no rio, bem como as acções hidrodinâmicas no seu leito e no interior de fissuras rochosas. As acções hidrodinâmicas no impacto com o leito rochoso são o agente motor do processo erosivo. Até ao presente, as pressões dinâmicas no impacto foram descritas para bacias com fundo plano. Nestas condições, as pressões dinâmicas dependem essencialmente da profundidade de difusão e das características turbulentas do jacto. Na maioria dos casos, os jactos investigados são menos turbulentos e energéticos do que os jactos em protótipo. Importantes efeitos de escala ligados ao défice de arejamento destes jactos dificultam a transposição de resultados de investigação a jactos turbulentos em protótipo. O trabalho de investigação agora apresentado evidencia a interacção entre o desenvolvimento de jactos em fossas de erosão e a geometria da excavação. A influência do confinamento lateral da difusão de jactos nas solicitações dinâmicas sobre o leito é documentada em trabalho experimental, realizado com jactos e condições de emulsionamento de ar de características quasi-protótipo. Diferentes geometrias de fossas de erosão, típicas de condições de protótipo, são testadas e comparadas com o cenário de referência de uma bacia com fundo plano. São apresentadas medições de pressão à saída do jacto, no fundo da bacia e no interior de uma fissura unifilar fechada.

O efeito do aumento da espessura do colchão de água a jusante, artificialmente ou por erosão do leito, é estudado utilizando jactos de características conhecidas. A dissipação de energia de jactos de velocidade elevada é estimada com base em medições de pressões médias na secção de impacto. Os resultados são comparados com estimativas obtidas a partir de um modelo analítico da difusão de jactos turbulentos arejados em bacias de fundo plano. O modelo analítico apresenta estimativas da eficiência de dissipação de energia concordantes com as medições, para a fase inicial do processo erosivo, bem como em bacias com profundidades de difusão elevadas. Em bacias com profundidades equivalentes à distância de desenvolvimento do núcleo potential do jacto (i.e. bacias de transição), as estimativas analíticas são muito sensíveis às hipóteses iniciais relativas ao decaímento da velocidade axial do jacto, à dimensão da zona de impacto e ao emulsionamento de ar na bacia. As pressões turbulentas na zona de impacto de bacias com fundo plano são investigadas em termos da sua distribuição probabilística no ponto de estagnação, para bacias com profundidade crescente. As condições de desenvolvimento do jacto na zona de impacto são divididas em condições de impacto do núcleo potencial e de jactos desenvolvidos, de acordo com uma avaliação de momentos estatísticos de terceira e quarta ordem e das autocorrelações de flutuações de pressão. As condições de impacto do núcleo são características de bacias pouco profundas e geram fluctuações de pressões com assimetria negativa, na zona de estagnação. A extinção do núcleo é associada a um caractér intermitente das fluctuações de pressão, reflectido em valores elevados do momento de quarta ordem. Para jactos desenvolvidos, as flutuações de pressão na zona de estagnação têm assimetria positiva. As fluctuações de pressão podem ser ajustadas por distribuições de probabilidade Gaussianas, excepto para probabilidades extremas. Medições do ar emulsionado são apresentadas para pontos seleccionados em bacias com fundo plano. As medições permitem descrever o comportamento de bolhas de ar antes, depois e na passagem pela zona de estagnação. As estimativas da concentração de ar emulsionado obtidas junto à entrada da fissura rochosa mostram que as bolhas de ar se reduzem em dimensão, sob a influência do forte gradiente de pressão na zona de estagnação. As dimensões características de bolhas de ar são inferiores às dimensões típicas de fissuras rochosas.

O trabalho experimental com fossas de fundo plano serve de referência para o estudo de fossas de geometria mais próxima da realidade prática. As medições de pressões médias na zona de impacto na soleira da bacia obtidas no presente estudo são menores em bacias confinadas lateralmente do que em bacias de fundo plano. Em consequência, o comprimento do núcleo do jacto pode ser reduzido, dependendo do grau de confinamento e de profundidade do colchão de água. A modificação do cáracter turbulento do escoamento dentro da fossa é descrito em função das funções de densidade espectral e de distribuição probabilística das flutuações de pressão transmitidas ao leito rochoso do rio. As correntes criadas pela deflexão do jacto nas fronteiras da fossa podem interferir com o desenvolvimento do jacto, gerar dissipação adicional e impedir a propagação em profundidade de bolhas de ar na bacia. Em bacias confinadas lateralmente e de profundidade baixa (shallow pools) ou de transição (transitional pool), as flutuações de pressão podem ter mais energia do que em fossas de profundidade equivalente e de fundo plano. Os espectros das flutuações de pressão têm mais energia em frequências intermédias (e.g. 10 a 100 Hz), e as pressões positivas extremas são mais elevadas, que em bacias de fundo plano. Para bacias profundas confinadas lateralmente, a energia das flutuações de pressão é menor do que em bacias com fundo plano. Os valores positivos extremos aumentam relativamente à energia total das flutuações de pressão comparativamente às bacias com fundos planos, mas mantêm-se semelhantes em termos absolutos. As pressões negativas extremas são menores em bacias confinadas lateralmente relativamente ao caso de referência do fundo plano. Fénomenos macro-turbulentos como oscilações do plano de água, células de recirculação dissipativas e ejecções, são identificados e caracterizados com base em observações directas do padrão de escoamento e em características turbulentas das acções dinâmicas no fundo da bacia. O seu papel no desenvolvimento dos jactos livres e no arrastamento de ar ma bacia é discutido. Os padrões de escoamento induzidos em diversos cenários de erosão característicos são apresentados e discutidos. É posto em evidência a evolução do campo de escoamento e das acções dinâmicas transmitidas ao leito rochoso em função das dimensões laterais da fossa e da profundidade do colchão de água.

As medições de pressão efectuadas no interior de fissuras unifilares fechadas permitem concluir que a resposta dinâmica de fissuras na rocha varia com o carácter turbulento das pressões dinâmicas à superfície, no impacto com o interface rochoso. Verifica-se que as dimensões da secção de entrada da fissura têm uma influência directa na filtragem das fluctuações de pressão na trânsição bacia-fissura: quanto maior for a fissura, menores serão as frequências filtradas. Observa-se que a energia das flutuações de pressão dentro da fissura é sempre mais elevada do que à entrada, para todas as configurações analizadas e colchões de água testados. A energia das flutuações de pressão dentro da fissura é menor em bacias estreitas e confinadas, para colchões de água transitórios e profundos, mas maior para colchões pouco profundos, relativamente a fundos planos. Estes resultados são igualmente válidos para pressões positivas extremas. As pressões negativas extremas são geralmente menores. A amplificação de picos de pressão ocorre em todos os colchões de água estudados; e é descrita como sendo função do desenvolvimento do jacto, i.e. da espessura do colchão de àgua, da geometria da bacia e das características turbulentas do jacto. Esta amplificação da energia turbulenta é devida ao estabelecimento de regimes transitórios, por vezes com rotura da veia líquida dentro da fissura. A ocorrência de resonância é investigada, replicando as frequências múltiplas superiores através da resolução numérica das equações do golpe de aríete dentro da fissura com base no método da impedância hidráulica.

Um método de análise probabilística de eventos de pressão é desenvolvido, correlaccionando a probabilidade, a persistência, a duração e conteúdo energético de pulsos de pressão extremos. Verifica-se que a persistência reduz-se abruptamente para pulsos de pressão de probabilidade (cumulada) elevada, que têm um importante conteúdo energético. O papel de eventos de pressão extremos nos processos de erosão de propagação de fissuras e na sobrelevação de blocos rochosos é discutido.

O trabalho experimental apresentado de análise da difusão de jactos em fossas com fundo plano e lateralmente confinadas demonstra a importância do conhecimento detalhado do padrão de escoamento na fossa para a definição das pressões dinâmicas na zona de impacto e dentro de fissuras rochosas. A dissertação apresentada informação detalhada sobre processos hidrodinâmicos envolvidos no processo erosivo de leitos rochosos. São incluídas diversas contribuições para a prática de engenharia, em termos das condições de emissão de jactos, equações empíricas para as pressões dinâmicas no impacto e recomendações para o dimensionamento de pré-excavações.

Palavras-chave: dissipação de energia por jactos, velocidades do jacto à escala de protótipo, modelação física, pressões dinâmicas, concentração de ar emulsionado, turbulência, geometrias de fossas de erosão, correntes induzidas, difusão de jactos, interacção ar-água-rocha.

This work is dedicated to

my grandparents,

my parents,

à Margarida e ao Miguel, and

to my dearest beloved Janina.

Contents

List of Tables

List of Figures

1. Introduction

Água mole em pedra dura, tanto bate até que fura[1].
Portuguese saying

1.1. Problematic of rock scour

High dams are built to store water and make it available for irrigation, drinking water supply, energy production and flood retention. These structures include by-pass channels or orifices to control the water level in the reservoir. In case the storage limit is attained during an important flood, water has to be released; further water level rise may be dangerous for dam safety. The discharges release water that is stored a few dozen meters higher than the river downstream. The potential energy of the water is converted in kinetic energy of flows passing in channel spillways or through orifices. The velocities reached by such flows are largely in excess of the corresponding flow velocities in natural floods in the downstream reach and may produce uncontrolled erosion of the riverbed and banks. Therefore, part of this kinetic energy has to be dissipated locally, so that restitution velocities become lower.

The direct impact of falling jets on the riverbed downstream of high dams is often used as a solution for the dissipation of water energy from floods. The construction of expensive concrete structures for energy dissipation can thus be avoided. In these cases, the assessment of the evolution of scour is mandatory for dam safety. It is a complex water-air-rock interaction problem.

For large dams, scaled physical model tests are often performed. The results are combined with prototype observations in order to develop empirical formulae for ultimate scour prediction. The applicability of empirical methods is limited to the range of tested parameters and it does not represent the complex interaction between a highly aerated water jet and the rock. Correction factors have been added in previous research to account for jet aeration, two-phase pool flow, as well as local rock characteristics but are limited to the conditions for which they were obtained. Therefore, the use of empirical methods is often limited to the preliminary stages of a project.

The applicability of existing formulae for scour progression in loose sand or gravel beds to rock riverbeds is very limited. These formulae do not consider the time needed for rock break-up by crack formation and propagation, nor for block downsizing (ball-milling). A comprehensive review and discussion about scouring downstream of dams can be found in Schleiss (2002).

[1] Soft water in hard rock, wears it at last (free translation).

The hydrodynamic pressures generated by the impact of the jet at the pool bottom can cause the failure of reinforced concrete structures built to confine energy dissipation (e.g. stilling basin or lined plunge pools) and are the driving agent for scour progression in unlined plunge pools. Locher and Hsu (1984) reported that:

"Damage caused by fluctuating pressures and forces is often spectacular. Turbulence in the stilling basin at Nezahualcoytl (Malpaso) dam in Mexico for example, resulted in displacement and transport of floors slabs 12 m x 12 m x 2 m that weighted 720 tons[2]*. The basin floor was damaged extensively and about 46 % of the floor had to be reconstructed*[3]*. Laboratory studies (Bribiesca and Viscaino) showed that the slabs could be lifted vertically as a consequence of differential pressure fluctuations between the upper and lower surfaces of the slab. An extensive series of measurements of cross-correlation and spectra of the pressure fluctuations on slabs in stilling basins was reported in Sanchez-Bribiesca and Fuentes-Mariles (1979).".*

Displacement of large concrete slabs by differential pressure fluctuations has been investigated experimentally for stilling basin under the influence of hydraulic jumps, as well as under the impact of falling jets. In unlined plunge pools, the rock mass is first disintegrated before the loose blocks can be removed. Unlined pools are highly heterogeneous by nature, whereas lined pools are the results of engineering design. There is increasing interest in the definition of dynamic impact pressures at the pool bottom, for typical prototype conditions of jet velocity, turbulence and pool depths. Traditionally, the most current solutions considered in engineering practice to increase safety of lined pools or prevent uncontrolled scour in unlined pools are:

- the increase of the pool depth over the riverbed, by construction of a tailpond dam or weir;
- the decrease of the unit discharge q at impact, either increasing the number of water-releasing structures, or increasing the spreading of the jet before entering the pool downstream by manipulation of jet issuance conditions (e.g. splitters, type of hydro-mechanical device); and,
- the pre-excavation of a pool in the riverbed, increasing the initial pool depth over the impact zone, and inducing scour in a given direction.

The first solution corresponds to additional costs and, depending on the imposed pool depth, can hinder or enhance the turbulent pattern of impacting pressures at the bottom of the pool. The second solution may reduce the throw of the jet or generate undesired spreading and spray. If possible, the most cost-effective solution is not to line the pool and avoid the construction of additional structures. Finally, pre-excavation may represent an additional cost but the excavated material may sometimes be used in construction.

A recent example of the combination of solutions is presented in Figure 1.1 for the Karun III HEPP dam project in Iran. Lining of the 400 m long, 50 m wide plunge pool was considered necessary, as well as the construction of a 60 m high tailpond dam (45 m from foundation to Ogee crest). The analysis of the dynamic pressures generated by the multiple spillways and outlet jets is of utmost importance for the design of the lining structure and drainage system, as well as for the definition of the tailpond dam height and of the operation guidelines for flood routing.

[2] i.e. 7200 kN

[3] The gross head from reservoir to stilling basin was H_0 = 118 m and the unit discharge q = 40 m^3/s/m.

Figure 1.1.: Karun III arch dam in Iran, H = 205 m, maximum discharge capacity of 18'000 m^3/s through chute and overfall spillways and orifices. Photo courtesy of Soleyman Emami of Mahab Ghodss Cons. Eng. Co., Tehran, Iran.

A sound understanding of the dynamic loadings generated by plunging jets is crucial for the definition of innovative design solutions for new and existing schemes. In the case of existing dams, such understanding may be instrumental in improving the design of repair works and the assessment of the degree of safety of dam foundations against local scour by uncontrolled overtopping.

For the majority of dam schemes, the design solutions are optimized performing physical model studies at reduced-scale. Evaluation of rock scour is qualitative due to significant scale effects. Only a few number of design solutions are normally investigated. Enhanced knowledge of the governing physical processes could allow for a mathematical-numerical assessment of scour for a larger range of solutions, i.e. of design parameters.

The physical processes involved in rock scour have for long been overlooked or bundled together. More attention is given to the overall implications, in disfavour of identifying the influence of each relevant process on rock scour.

In practice, rock scour is a three-dimensional complex process. Unlined prototype pools evolve during the operation of water-releasing structures from dams. The geometry of the pool may influence the turbulent flow pattern and therefore the dynamic loadings transmitted to the rock. Pressures propagating inside rock fissures are directly dependent on those acting at the water-rock interface. A sound knowledge of impact pressures in

prototype conditions, taking into account the geometry of the pool, is necessary and has not been addressed before.

Rock scour by plunging jets is an interface problem concerning air, water and rock. The interaction of air and water has been object of research in the past but important questions remain unanswered regarding: (1) the definition of the conditions at plunging point, (2) the interaction of air bubbles with the turbulent pool flow, (3) the presence of air close to the rock interface, (4) the eventual entry of air in rock fissures and (5) its role in transient flow regimes inside rock fissures.

There is also a large ground for research in terms of the interaction between hydrodynamic pressures and the rock mass. Crack opening by high dynamic pressures has yet to be studied in the framework of plunging jets. Propagation of fissures is the object of research in various fields of engineering and a first attempt to adapt theoretical developments based on the stress intensity factor at the crack tip to the process of rock scour is included in Bollaert (2002b); Bollaert and Schleiss (2005). The analysis of the influence of the heterogeneity of rock masses, in terms of intrinsic mechanical characteristics, as well as fissuring pattern, fissure interlocking and fissure filling material, in rock scour remains an open field for research.

Furthermore, once blocks are created, they can only be ejected from the rock matrix by a net uplift pressure field persisting during a certain time interval, as observed for concrete slabs by Fiorotto and Rinaldo (1992a). The pressure field that induces block displacement results from the spatial and temporal correlation of instantaneous local pressures over the blocks. The process of block displacement depends on a coupling of hydraulic and geologic site-dependent factors: it is based on a correlation between the turbulent flow structures imposed by the jet and the pool boundaries, and the dimensions of typical rock blocks created by rock fracturing.

In summary, there is a severe lack of knowledge on the interaction between hydrodynamic and rock mechanics aspects. Impact pressures govern the physical processes involved in scour progression and their description for conditions closer to those found in practice is of utmost importance to improve existing scour assessment tools.

1.2. Purpose of the study

The present work concerns the interaction between plunging jets and the geometry of rock scour. It focuses on the physical processes (Figure 1.2) involved in the definition of hydrodynamic pressures at the rock interface and inside underlying rock fissures.

In prototype, plunge pools are quite varied in shape in correlation with the local geology (Figure 1.3). Depending on the geometry of the pool, the flow pattern may vary considerably inside the pool. The currents that are induced by the diffusion of plunging jets in a given geometry may interfere with the jet itself as well as with the entrainment of air. Hence, impact pressures transmitted to the rocky riverbed are expected to depend on the pool geometry and on the induced pool flow pattern.

Up to present, pool bottom pressures generated by aerated turbulent water jets have only been described for pools with flat bottoms. Furthermore, hardly any research has been conducted with jet velocities and aeration conditions close to those found in practice, which considerably hinder the application of research findings in practice.

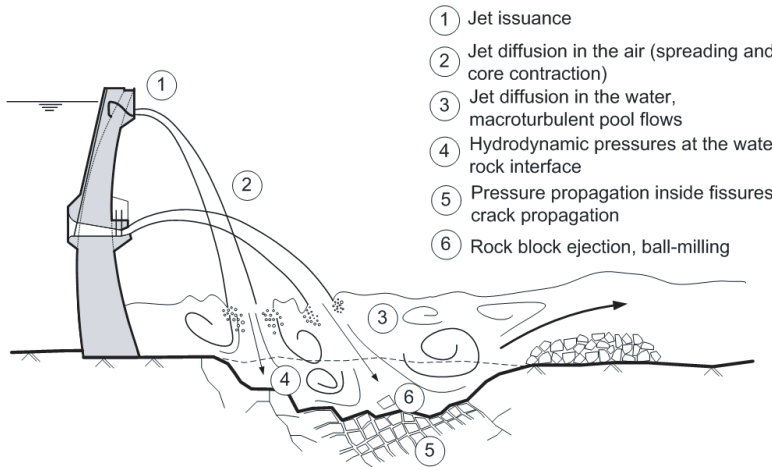

Figure 1.2.: Main physical processes involved in rock scour.

The present research project aims at:

- Documenting the characteristics at issuance of high-velocity plunging water jets found in engineering practice.
- Investigating the diffusion of plunging jets in simplified prototype-like pool geometries.
- Documenting the influence of pool geometry on the turbulent impact pressures under the jet.
- Investigating the behaviour of entrained air bubbles inside plunge pools, in particular close to the riverbed.
- Studying the transfer of impact pressures into a fissured rock mass.
- Documenting the influence of pool geometry on pressure propagation inside fissures.
- Evaluating the persistence of dynamic pressures at impact and inside fissures.
- Contributing to the development of mathematical-numerical tools for simulation of governing physical processes in rock scour.

These topics are addressed by means of experimental work with high-velocity jets and analysis of the corresponding results.

A detailed study of the issuance characteristics of the near-prototype jets produced in the experimental set-up was conducted. This study had not been initially considered in the terms of reference for this work but was considered necessary to set a sound basis for the investigations that followed. For practical reasons, this obliged dismissing the study of different configurations of fissures as initially planned.

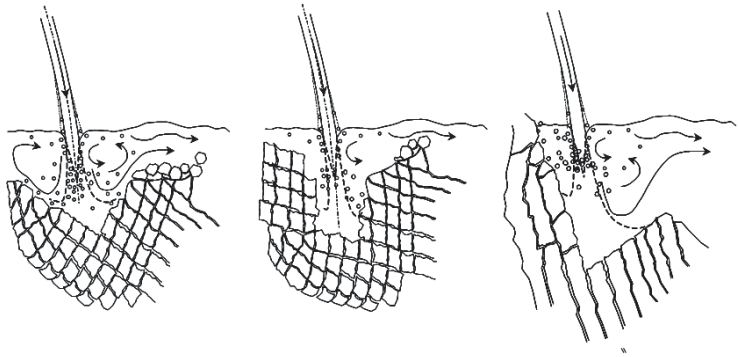

Figure 1.3.: Three different shapes of the plunge pool bottom, as a function of the joint set patterns and the degree of fracturing of the rock mass (Bollaert et al., 2004).

1.3. Outline of the work and of the document

The dissertation consists of 12 chapters, introduction being the first.

Chapter 2 presents a review of previous studies in rock scour, with particular focus on scour geometry and on the most recent research developments. Among other topics, it includes a review of the behaviour of prototype plunge pools as compared to laboratory model studies; as well as a discussion on the influence of air entrainment in the pool on rock scour (Section 2.11).

The experimental arrangement as well as the instrumentation used for the test campaign are presented in Chapter 3. Three test series were performed concerning the study of (1) the characteristics of the jet at issuance, (2) impact pressures at the pool bottom and their propagation inside closed-end fissures, and (3) the behaviour of air bubbles entrained by high-pressure jets in pools with limited depth.

The analysis can be divided in five parts, presented sequentially in Figure:

Part 1 - Evaluation of the hydraulic characteristics of the jets produced in the LCH test facility in comparison to practice (in Chapter 4).

Part 2 - Investigation of impact pressures and air bubble behaviour at stagnation in pools with flat bottom (Chapters 5, 6 and 7). It sets the reference conditions for Part 3.

Part 3 - Investigation of impact pressures and pool flows in laterally confined pools (in Chapters 8 and 9).

Part 4 - Investigation of transient pressures inside fissures in pools with flat and non-flat bottoms (in Chapter 10).

Part 5 - Applicability of findings: (1) for the development of probabilistic based model for selection of relevant persistent events (in Chapter 11); and 2) in terms of suggestiosn for existing scour models (in Chapter 12).

Chapter 4 presents the hydraulic characteristics of the jets produced in the LCH facility based on detailed measurements performed at the jet outlet, defining the upstream boundary conditions of system. Modifications in the supply system of the experimental set-up are

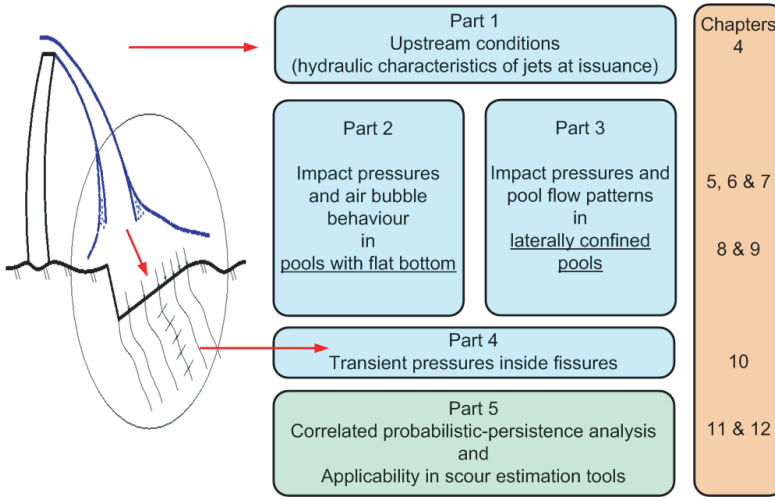

Figure 1.4.: Organization of the analysis: from upstream to downstream.

presented and discussed. Based on the experimental results and on a review of water-releasing structures, the characteristics of typical prototype jets are defined.

In Chapter 5 an analytical model to assess energy dissipation in plunge pools with flat bottom is compiled. Analytical estimates of the energy dissipation efficiency are computed and compared with estimates based on experimental measurements. Recommendations for the use of the analytical model in engineering practice are outlined.

Chapter 6 presents experimental measurements of impact pressures generated by rough turbulent plunging jets on pools with flat bottom in fully controlled issuance conditions and variable pool depths. The probabilistic distribution of impact pressures at stagnation is assessed and used to describe local flow features and the intermittency of plunging jets.

Measurements of air entrainment by plunging jets in pools with flat bottom are presented in Chapter 7. Void fraction estimates at several locations in the pool provide further insight on the behaviour of entrained air bubbles under the influence of strong pressure gradients.

Impact pressures in pools with non-flat geometry are presented in Chapter 8. The influence of laterally confining jet diffusion in the pool is discussed.

Four typical scenarios of scour evolution are composed and investigated in Chapter 9, combining experimental data from test with various pool geometries. The influence of the geometry-induced flow patterns on impact pressures and air entrainment in the pool is studied. Coherent flow features are identified and documented.

In Chapter 10 the propagation of impact pressures inside a closed-end fissure is investigated for both flat and non-flat pools. The turbulent pattern of dynamic pressures at the pool bottom (i.e. fissure's entry) and inside the fissure is compared. The transition from free surface pool flow to pressurized flow inside fissures is studied. Transient regimes inside fissures are simulated and directly compared with experimental data.

The persistence of pressure fluctuations is assessed in Chapter 11. An analytical model relating the probabilistic distribution of turbulent pressures with its persistence and energy content is developed. Based on the obtained results, the interest of extreme pressure events for rock scour is discussed.

Finally, conclusions for both research and engineering are drawn in Chapter 12, including suggestions for application of the findings in existing scour assessment tools. Additional experimental details and complementary information on the procedures are presented in the appendixes at the end of the document.

2. Literature review on rock scour geometry and air entrainment in the pool

Scour downstream of large dams is due to jet impact from water releasing structures. Dissipating water energy by jet diffusion in a water pool and impact with the river bottom allows saving the cost of building large concrete structures for the same purpose. Scour growth with time should be carefully estimated in the design phase to prevent undermining of the dam's foundation or side slopes during the operation lifetime. An equilibrium scour state is reached once the water cushion created by the deepening of scour becomes thick enough, so that impact pressures are no longer capable of further scour.

This chapter presents a brief review of available literature on the rock scour process, focusing on the assessment of pool geometry and corresponding induced-flow patterns, as well as on pool aeration.

2.1. Overview of previous studies relevant for rock scour

Systematic research on rock scour may be assumed to have started in the 60's when the number of existing schemes and feedback from prototype behaviour became available, allowing for comparison of estimation methods. Before, dams were studied individually in laboratory and only a few empirical tools were derived and used.

Reviews were performed by Martins (1973a,b, 1975); Taraimovich (1979, 1981); Whittaker and Schleiss (1984) presenting and discussing the empirical methods that had been developed from hydraulic models and prototype observations for the estimation of rock scour.

Yuditskii (1963) presented the first method to assess rock scour based on hydrodynamic pressures and rock characteristics.

Regarding the evolution of rock scour, systematic research has been pursued in controlled conditions with mobile bed of given grain size distribution and block interlocking conditions. This corresponds to simulating non-cohesive riverbeds or rocky riverbeds after break-up of the rock. The process of rock break-up has been simulated for a limited number of prototype cases by binding the aggregates with different materials (Martins, 1973a,b) but the results do not allow extracting general rules. Formulae for scour development both in time and space have been proposed based on experimental tests with mobile bed (Rajaratnam and Mazurek, 2002, 2003) and compared with numerical simulation (Salehi-Neyshabouri et al., 2003).

Estimation methods based on the energy of the jet have been developed by Spurr (1985) and Annandale (1995). These methods take into account the characteristics of local geology and are, in this sense, closer to the real situation of plunge pools than empirical models

obtained from reduced-scale experiments in laboratory. Annandale et al. (1998) performed large-scale tests to validate the semi-empirical "Erodibility Index" approach.

In parallel, systematic research on the jets has been going on since the 1920's. Based on experimental data with air jets, Albertson et al. (1948) set the foundations of the theory of free jet diffusion. Abramovich (1963) developed analytical solutions for typical jet applications (e.g. with counter-flow, with co-flow) based on *potential flow* theory. Kraatz (1965) discussed the behaviour of water jets diffusing in a medium of different density (e.g. air).

By that time, Cola (1965, 1966) presented the first study with bounded diffusion, i.e. diffusion of a submerged water jet in a pool with finite depth, describing how jet streamlines are deflected close to the pool bottom.

Soon afterwards the first studies with plunging jets appeared (Henderson et al., 1970; Hartung and Häusler, 1973). Henderson et al. (1970) opened a research line on the entrainment of air by plunging jets and was soon followed by, amongst others McKeogh and Elsawy (1980); McKeogh and Ervine (1981); Ervine and Falvey (1987); Sene (1988); Bín (1993). Experimental work has been pursued with increasing Reynolds numbers and turbulence intensities, approaching prototype conditions found in spillways of dams.

The trajectory of jets in the air was studied by Martins (1977). A review on this topic was presented in Melo (2001). The development of the jet in the air has been discussed by, amongst others, Kraatz (1965); Henderson et al. (1970); Ervine and Falvey (1987); Ervine et al. (1997). The influence of the issuance conditions were studied by Ervine and Falvey (1987); Zaman (1999); Burattini et al. (2004). However, the development of aerated core jets such as those issued from ski-jump spillways is barely documented.

The jet characteristics at entry in the pool (i.e. plunging point) are still matter of discussion. The works of Bonetto and Lahey Jr (1993); Bohrer et al. (1998); Cummings and Chanson (1997); Chanson et al. (2004) provide experimental data on air entrainment conditions for developed and undeveloped plunging jets. However, these works have mainly been conducted with smooth turbulent jets.

Submerged jet diffusion (i.e. the density of the jet is equal to that of the surrounding medium) and impact pressures in flat surfaces have been studied by Cola (1966); Kamoi and Tanaka (1972); Beltaos and Rajaratnam (1973, 1974); Gutmark et al. (1978).

Plunging jet diffusion and corresponding impact conditions have been investigated by, amongst others, May and Willoughby (1991); Puertas-Agudo (1994); Ervine et al. (1997); Melo (2001); Bollaert (2002b). Despite the existence of a wide database of pressure measurements for different conditions of jet shape, jet turbulence intensity, jet velocity, travel distance in the air, relative degree of break-up, pool aeration, a.s.o., there is no systematic analytical model to describe the diffusion of a two-phase turbulent shear layer in pools with limited-depth.

Turbulent pressures generated by high-velocity jets typical of prototype dams are still far from being well documented; they have been studied for low velocities and at impact on flat surfaces, e.g. by May and Willoughby (1991); Ervine et al. (1997); Melo (2001); Bollaert (2002b).

Extreme pressure events that may cause crack propagation or block ejection have even been less documented and discussed. Bollaert (2002b) studied systematically pressure propagation inside different types of fissures, showing that pressure wave superposition may lead to

pressure amplification. He highlighted the existence of two fracture modes: by brittle failure and by fatigue. The first may be generated by important steady loads or by short-duration peaks of pressure inside fissures; whereas the second mode depends on short-duration cyclic loadings. The short duration event are typically derived from transient flows inside fissures and are generated for intermediate or deep water cushions for which the turbulent jet is well developed at impact. These findings allowed confirming the scour potential associated with transitional and deep water cushions.

Turbulent pressures are still poorly described in terms their probabilistic definition. It is possible that pressure values with given probability of occurrence and magnitude are relevant for brittle or fatigue crack opening, whilst some others are relevant for block displacement. In fact, it is not known which extreme pressure values are relevant and for which processes. The major difficulties in studying fluctuating pressures are the sampling duration and the representativeness of pressure measurements performed in reduced-scale models. Regarding plunging jets, only short duration runs have been performed at near-prototype conditions (Ervine et al., 1997; Bollaert, 2002b). In general, fairly good estimates of mean and RMS pressure values can be obtained within reasonable laboratory times. This is not the case for extreme pressures.

Long duration runs were performed by several authors (Toso and Bowers, 1988; Fiorotto and Rinaldo, 1992a,b) in order to assess extreme pressures under hydraulic jumps at reduced-scale.

Fiorotto and Rinaldo (1992a) presented a stability criterion for concrete slabs under hydraulic jumps based on maxima and minima pressure fluctuations, correlating slab dimensions with the integral scales of the turbulent pressure field. They used pressure estimates obtained from 24 hour-runs at reduced-scale. The notion of time and space correlation is implicit in the definition of the integral scales. According to these authors, a given degree of time-space correlation is fundamental for slab displacement.

Hartung and Häusler (1973) were the first authors to show experimentally that dynamic pressures can break open a fissured concrete mass. Their work paved the way for future research on the interaction between plunging jets and pressure propagation inside rock joints by, e.g. Montgomery (1984); Amelung (1996); Bollaert (2002b) or under concrete slabs by Sanchez-Bribiesca and Fuentes-Mariles (1979); Fiorotto and Rinaldo (1992a,b); Liu et al. (1997); Melo (2001).

At the present stage of knowledge, at least two physically based engineering model for prediction of scour in rock as a function of time are available for practice: the one by Yuditskii (1963) and the one by Bollaert (2004); Bollaert and Schleiss (2005). Such models relate hydrodynamic pressures in rock joints with the resistance of these joints against cracking.

Once blocks are created, they are ejected from the rock matrix by a net uplift pressure field. As observed for concrete slabs by Fiorotto and Rinaldo (1992a), a given time persistence of the pressure field is necessary for the blocks to be displaced. The pressure field results from the spatial and temporal correlation of instantaneous local pressures over the blocks.

The process of block displacement has recently been addressed by Melo (2001) for concrete slabs under the impact of plunging jets. Stability models for various conditions of open and closed joints were presented and validated.

However, pool bottom pressures generated by aerated turbulent water jets have only been described for flat impact surfaces, e.g. Hartung and Häusler (1973); May and Willoughby

(1991); Puertas-Agudo (1994); Ervine et al. (1997); Melo (2001); Bollaert (2002b). A few researchers working in the field of aeronautics with air and water jets have documented impact pressures with curved surfaces (Ho et al., 1977; Gilard and Brizzi, 2005) but the range of test parameters is far from those found in hydraulic engineering practice (i.e. single-phase, lower velocities, lower Reynolds number).

2.2. Previous research at LCH-EPFL

Systematic investigation of the physical processes involved in rock scour is carried out at the Laboratory of Hydraulic Constructions (LCH-EPFL) since the late 1990's. The long-term purpose is to develop and enhance tools to simulate scour evolution based on a profound understanding of all physical processes from jet impact to crack propagation.

A first Ph.D. Dissertation in this line of research was presented in 2002 (Bollaert, 2002b). It focused on the transient regimes developing inside rock fissures, under the impact of plunging jets. An innovative experimental installation was built that includes a module simulating a fissured rock mass. It allowed measuring for the first time the transient pressures in rock joints due to high-velocity jet impact. New phenomena could be observed, such as the reflection and superposition of pressure waves, resonance pressures. Quasi-instantaneous air release and re-solution due to pressure drops in the joints was identified as a possible explanation for the reduction of pressure wave celerity. If the corresponding stresses due to the hydrodynamic pressures at the tip of the joint exceed the fracture toughness of the rock, depending on its tensile strength and initial compressive stresses, the rock will crack and the joint can grow further. In the case of open-end rock joints in fully jointed rock, the pressure waves inside the joints create a significant dynamic uplift force on the rock blocks. This dynamic uplift force will break up the remaining rock bridges in the joints by fatigue and, if high enough, eject the so formed rock blocks from the rock mass into the macro-turbulent plunge pool flow. Based on the experimental results and numerical simulations as well as on an extensive physical analysis, a new scour model was derived, which includes the main relevant processes starting from the free falling jet to the fissured rock mass. This new model is a significant step in research towards a better assessment of the scour process. It is discussed in Section 2.3.5.

2.3. Estimation of scour

Scour is normally studied using reduced scale physical models of the dam and downstream river reach. One may say that scour is a function of:

- The jet type and travel distance in the air;
- The discharge time series;
- The downstream pool depth, obtained from the local rating curve or imposed by a built structure (e.g. tailpond dam);
- The riverbed's resistance to jet impact, i.e. the rock characteristics and its mechanical state (surface weathering, fissures, etc.).

Each one of these items presents incertitude. Therefore, in most practical cases, the priority is estimating the scour depth and spatial extent that are likely to be reached during the

lifetime of the dam. From these results, additional protection measures may be considered or the design and operation rules of the scheme redefined.

Several methods exist to estimate the ultimate scour, i.e. the scour depth that corresponds to an equilibrium situation. The scour estimation methods can be divided into hydrodynamic methods (Hartung and Häusler, 1973), empirical methods derived from model or prototype observations (Martins, 1973a; Mason and Arumugam, 1985), semi-empirical methods (Spurr, 1985; Annandale, 1995) and physically based methods (Yuditskii, 1963; Bollaert, 2002b; Bollaert and Schleiss, 2005).

2.3.1. Hydrodynamic methods

Hydrodynamic methods consider the diffusion of a given jet in an unbounded water pool. Energy dissipation is done by mixing (i.e. turbulent diffusion) and ultimately by viscous diffusion. Hartung and Häusler (1973) estimate the influence depth t_{hyd} of a plunging jet as 20 times its diameter D (circular jet) or 40 times its thickness B(rectangular nappe) at impact. According to these authors, the mean remaining energy at that depth is of about 85 % and 70 % of the plunging jet energy for circular and rectangular jets respectively. The lateral influence of the jet is defined according to the theory of linear diffusion of a free jet in an infinite pool. This depth can be fairly well approximated by the "depth of bubble penetration" D_p, i.e. the maximum distance that air bubbles entrained at plunging point travel in water. It provides a purely hydrodynamic estimate of the distance influenced by the jet. In fact, air bubbles that are entrained into the pool are transported axial and radial wise by the jet. These bubbles reach a maximum depth where the buoyancy forces surpass the viscous drag exerted by the jet (Clanet and Lasheras, 1997). Several authors have suggested expressions for this depth and reviews can be found in McKeogh and Elsawy (1980); Bín (1993). In this case, the extent of scour correspond roughly to $t_{hyd}/3$ to either side of the jet axis. This method provides a conservative envelope estimation of the ultimate scour depth t_{hyd}. It does not take the resistance of the rock into account.

As an example, one of the deepest scour holes documented in literature is that of the Kariba Dam (River Zambeze). Scour has reached a depth of 87.5 m below the initial river bed, despite the relatively important tailwater level of about 40 m that is imposed by the natural rating curve of a control section in the d/s river reach. Hartung and Häusler (1973) assumed a characteristic jet diameter of 6.9 m: for these conditions, the actual scour in 1979 was of ≈18D in total. It is not clear if equilibrium conditions have been attained or not. In this particular case, jet diffusion is far from being "free".

2.3.2. Reduced scale physical model tests for dams

Reduced scale model tests of dams are normally undertaken during the final design stage to refine engineering design options and assess the good hydraulic behaviour of the structures.

Laboratory studies allow the investigation of various design solutions and observation of the main flow features. This last topic is often disregarded but is of utmost importance to prevent erosion of the side slopes by return currents.

Tests are normally conducted under Froude similarity due to the governing effect of gravitational forces. In the case of large dams, small scales ranging from 1/35 to 1/100

are normally used, due to space and cost constraints. The small scale of the models limits the representation of prototype conditions. Phenomena depending on Weber and Reynolds similarity are not reliably accounted for scales smaller than 1/20. Therefore, jet behaviour in the air and jet diffusion in the pool is simulated with insufficient air mixing. This is rather conservative but may lead to an overestimation of scour and of the impact point downstream.

On the other hand, representing the rocky riverbed is a major difficulty. While selecting a material with similar intrinsic mechanical properties does not pose a major problem, modeling its ensemble response to dynamic pressure taking into account rock weathering and rock fracturing is quite complex.

Martins (1973a,b) performed a review of laboratory studies that remains quite updated and listed alternative methods for the simulation of rock riverbeds. The most important parameters to look for are the nature of the gravel being used (density, etc.), its shape (rolled, irregular, etc.), the use of a binder to simulate a given degree of cohesion, as well as the nature of binder.

After 1973, several research groups explored the topic of erosion in mobile river beds with the goal of obtaining generalized relationships for scour growth. Some of the most important contributions have been made by the group of Prof. Rajaratnam in Alberta University (several papers on erosion in mobile beds from the 70's up to 2003). This group has focused on the evolution of scour with time evolution for different type of jet velocities, bed material and impinging angle, in "submerged" jet conditions. Their approach is valid whenever rock fracturing is not a key issue. They have not addressed the two-phase character of the problem. Their work provides straightforward solutions for practical cases in irrigation channels and pools with non-cohesive loose sediments.

2.3.3. Empirical methods

Empirical formulae to estimate the ultimate scour depth (i.e. equilibrium scour depth) have been derived from laboratory model studies and observations in prototype. Comprehensive reviews have been made by Whittaker and Schleiss (1984), updated by Mason and Arumugam (1985) and discussed by Bollaert (2002b). The most well known and used are those of Martins (1975) and Mason and Arumugam (1985).

Empirical evidence has been gathered from prototypes, e.g. Taraimovich (1979), which allow having a preliminary idea of the pool slopes. However, it is not known to what stage of scour evolution these observations correspond to.

2.3.4. Semi-empirical methods

Semi-empirical methods combine observations with theoretical developments. Spurr (1985) presented a method based on the evaluation of the power of the plunging jet and on the definition of a energy scour index. Annandale (1995) presented a method based on a comparison between the ability of the flow to generate erosion and the resistance of the riverbed material. It is called the Erodibility index method and was validated experimentally in a large scale facility by Annandale et al. (1998). These methods do not take into account the evolution of scour in time. A detailed discussion of these methods can be found in Bollaert (2002b).

Recently, Liu (2005) proposed a new method for calculating the ultimate depth of scour. It comprises a scour coefficient that depends on the local bedrock. Based on a calibration of his method on observed data from 14 plunge pools in China, Liu (2005) provides indications for this coefficient for four types of bed rock. The pioneering character of this approach is remarkable, taking also in consideration the immense difficulty in collecting data. Extending the calibration to a larger set of examples would be desirable. The prototype examples provide valuable information: the ratios scour depth/water head t/H and pool depth /water head Y/H are only >0.5 in less than 30% of the cases, all of these having specific discharges between 47 and 60 m^2/s.

2.3.5. Pressure-gradient dependent methods

Pressure-gradient methods are based on an evaluation of the dynamic loading around existing rock blocks, i.e. on the upper face (at the water-solid boundary interface) and inside the joint separating the block from the rock matrix.

Yuditskii (1963) presented what is probably the first conceptual model of the rock scouring process based on pressure fluctuations on rock blocks. His procedure is based on an evaluation of the maximum instantaneous pressure that can separate a rock block from the matrix. For increasing pool depths, the maximum pressure gradient amplitude originated by jet impact is compared with a limit pressure value corresponding to the equilibrium situation.

He conducted experimental work (more than 2000 tests) focusing on the mechanisms of block ejection for varying scour depths, relative size of blocks, block density and joint thickness. One interesting observation that remains quite up-to-date is: "[..]*the block is ejected, not by one pressure fluctuation of high amplitude nor by a succession of pressure fluctuations of high amplitude, but by one large average pressure that is established in the joint underneath the block following a small vertical displacement. The opening of the joint that allows this small vertical displacement is done by one pressure fluctuation of high amplitude.*"

Yuditskii clearly separated the pressure events that break-open the rock from those displacing rock blocks. Displacement would require a given pressure field persistence, to allow for a high mean pressure value to establish underneath the rock block and trigger its displacement. This topic is one key issue still being discussed nowadays.

Several researchers have worked on pressure-gradient methods for block displacement on rock plunge pools (Liu et al., 1998), in lined pools for plunging jet impact (Melo, 2001; Melo et al., 2006) and in hydraulic jump stilling basins (Sanchez-Bribiesca and Fuentes-Mariles, 1979; Fiorotto and Rinaldo, 1992a,b). The displacement of concrete slabs in lined pools and stilling basins shows some analogy with the rock scour process. The most

The first works of dynamic pressures were presented by Sanchez-Bribiesca and Fuentes-Mariles (1979); Fiorotto and Rinaldo (1988); Toso and Bowers (1988). Fiorotto and Rinaldo (1992a,b) presented experimental and analytical work leading to a design criteria for concrete slabs. It is based on pressure fluctuations, turbulent scales, pressure propagation in construction joints, development of waterhammer transients flows in the joints and block ejection by a net positive pressure gradient resulting from the correlation of surface pressures and joint pressures. They presented a criteria for slab stability under hydraulic jumps. Liu et al. (1997) presented a variant of the latter, using the theory of random vibration to define the design criteria; their criteria includes explicitly a Strouhal number for the vibrating

slab. Liu et al. (1998) presented a 2D version of the previous model. They also discussed the interaction between pressure fluctuations at the pool bottom and inside fissures, based on measurements of fluctuation *forces* and space-time correlations. Melo (2001) presented a stability concept for slabs under the impact of plunging jets, considering open joints and closed joints with one failed waterstop. He presented a four-stage procedure for the design of stable slabs, include evaluation of the impingement zone with the downstream water level, of the hydraulic characteristics of the jet at the same location, of the mean dynamic loadings at the pool floor, and of slab stability and dimensions, for variable pool depth, jet velocities and discharge durations. The stability criteria is presented in detail in Melo et al. (2006) and considers that failure is primarily a consequence of a mean pressure gradient. These authors argue that the turbulent pressure field is not in phase in the upper and lower faces of the slabs, due to poor spatial correlation at the surface and frequency filtering inside the joints. Despite studying conditions that are different from those in rock scour, namely in terms of the relative dimensions between the main structures of the flow field and the solid elements to displace, as well as joint characteristics, these developments provide valuable insight on the physical processes governing rock scour.

The method presented by Yuditskii (1963) assumes a fissured rock mass; it does not account for crack propagation. Recently, Bollaert (2002b) combined experimental measurements both at the pool bottom and inside typified fissures to define a *crack propagation method*, as well as a *dynamic impulse method for block ejection*. He used jets with near-prototype velocities. The methodology relies on the dynamic pressures transmitted to the foundation under given jet characteristics at issuance and given tailwater levels downstream. Based on pressure measurements inside fissures, the hydrodynamic loads at the tip of a fissure are estimated.

The *crack propagation method* is based on a direct comparison of stress intensity coefficients, on the one side resulting from pressure propagation inside the fissure - the hydrodynamic loading at the fissure tip - and, on the other side, the admissible stress of a given rock mass - i.e. the resistance. The modulation of pressure fluctuations inside fissures was described and three mechanisms of fissure propagation were identified:

- by hydrofracturing due to a high mean pressure ("hydrojacking") leading to brittle failure at the fissure tip;
- idem, but caused by very high amplitude instantaneous pressure fluctuation resulting from pressure modulation in transients flow inside the fissure; and,
- by fatigue, due to the cyclic loading of the fissure's tip and that depends explicitly on time.

The *dynamic impulse method for block ejection* is based on the conversion of an important instantaneous uplift pressure in kinetic energy, lifting the block of a given height eventually out of the matrix. This method accounts for the oscillatory character of the transient pressures inside the fissure, but does not consider the time required for the joint to be filled by water (i.e. the persistence of the pressure field) as well as the necessary spatial correlation of the pressure field. Scour evolution is simulated by erosion of successive flat rock layers.

In summary, the most straightforward method for estimation of the ultimate scour based on experimental evidence of pressure gradients capable of ejecting block for the riverbed is the one presented by Yuditskii (1963). However, experiments were performed at reduced-scale and do not consider aeration or crack propagation. The idealisation of the scouring process

presented in that model is remarkably up-to-date. The recent developments presented by Bollaert (2002b) in terms of experimental evidence of transient regimes inside fissures and identification of crack propagation methods is an important step forward in the understanding of rock scour. The procedure presented by the latter can explicitly account for the duration of the input discharge, since the fatigue mechanism depends on a number of loading cycles per unit of time. However, it is yet not clear if transient peaks will develop inside real-nature fissures up to the amplitudes found experimentally using smooth simple-shaped fissures.

The main physical processes governing rock scour have been identified. However, it is necessary to further approach prototype conditions. Existing scour assessment tools include important simplifications and yet do not properly represent the interactive evolution of scour as a three-dimensional, three-phase process. This can only be done by further fundamental research and continuous uprating of existing tools.

2.4. Behaviour of prototype plunge pools compared to laboratory models

Plunge pools are used in modern dam construction to dissipate energy by jet impact for at least 80 years. Assessment of scour downstream of dams is normally performed in models at scales less than 1:30, often close to 1:100, so that most of the dam and appurtenant structures are included. Model predictions and prototype observations fairly correlate most of the times. Reduced-scale model results are often quite conservative, meaning that the ultimate scour state is deeper and attained faster than observed in reality. This is mainly due to the difficulty to simulate the damping effect of jet aeration in reducing mean pressures and to the use of loose gravel to simulate the riverbed, neglecting the time needed for rock fracturing.

A selected number of examples are presented in Table 2.1 and Appendix A. These examples show that scour development has to be addressed on a case-to-case basis and that local geological features are quite important for the definition of the plunge pool geometry.

Taraimovich (1979) analysed 16 cases of scour below high-head ski-jump spillways and showed that most pools are asymmetrical longitudinal-wise, with a milder upstream slope, between 14° and 22° for impacting angles from 24 to 46° in case of rock foundation. The downstream slope is approximately equal to the impacting jet angle. For non-rock foundations, the upstream slope is between 12° and 14°. Both Taraimovich and Martins (1973b) cited Yuditskii's recommendation to take an upstream slope of 24° and downstream slope of 33° for an exiting ski jump angle of 35°; however, no indication of the elevation difference between issuance and impact is given.

A review of selected publications and dam cases summarised in tables 2.1 to 2.3 allows concluding that:

1. Hydraulic model tests provide reasonable estimates of scour depth and its evolution in time. If the bar created by the deposition of loose material is removed during testing, scour depth is overestimated and the equilibrium scour is attained faster in laboratory than in prototype. Reduced-scale models fail to reproduce air-water interaction and, thus, the impinging energy in model is often higher than in prototype. The processes of crack

Table 2.1.: Selected examples of dams with plunge pools described in literature. The energy to dissipate is given relative to the initial riverbed elevation. References: [1] Quintela and Cruz (1982), [2] Ramos (1982), [3] Whittaker and Schleiss (1984), [4] Quintela et al. (1987), [5] Hartung and Häusler (1973), [6] Martins (1973b), [7] Taraimovich (1979), [8] Melo (2001), [9] Locher and Hsu (1984), [10] Fahlbusch (1994), [11] Schleiss (1993), [12] Attari et al. (2002), [13] Sarkaria et al. (2003), [14] Melo (2002a), [15] Furstenburg et al. (1991).

Dam	Jet outlet	Unit discharge at issuance, q [m^2/s]	Energy to dissipate [MW/m]	References
Cahora-Bassa, 1975 (Mozambique)	8 sluices (32°), 6.00 x 7.80 m^2	270 (total 13'100 m^3/s)	147.3	1, 2, 3, 4
Kariba, 1960 (Zambia/Zimbabwe)	6 orifices 6.90 x 9.00 m^2	156 (total 8'400 m^3/s)	125.4	2, 3, 5
Picote, 1958 (Portugal)	Gated, ski jump (8°)	170 (total 11'000 m^3/s)	50.3	6, 7, 8
Krasnoyark (Russia)	Gated, ski jump (35°)	69 (total 12'000 m^3/s)	-	7
Inguri, 1980 (Georgia)	Orifices (49°)	95 (total 2'500 m^3/s)		7, 9, 10
Karun I, 1976 (I.R. of Iran)	Gated, flip bucket (new, 20°)	40 (new) / 290 (old) (total 16'200 m^3/s)	9.6	11, 12
Estreito, 1969 (Brasil)	Gated, flip bucket (35°/42°), 11.5 x 16.6 m^2	155 (45 passed) (total 13'000 m^3/s)	79.4	13
Foz do Areia, 1980 (Brasil)	Gated, flip bucket (20°), 14.5 x 19.45 m^2	145 (125 passed) (total 10'250 m^3/s)	150.8	13
Furnas, 1963 (Brasil)	Gated, flip bucket, 11.5 x 17.36 m^2	145 (52 passed) (total 12'297 m^3/s)	114.8	13
Itaipú, 1982 (Brasil)	Gated, flip bucket, 20 x 21.34 m^2	186 (120 passed) (total 62'200 m^3/s)	126.5	13
São Simão, 1978 (Brasil)	Gated, flip bucket, 15 x 18.78 m^2	154 (80 passed) (total 24'100 m^3/s)	72.7	13
Tucuruí, 1984 (Brasil)	Gated, flip bucket, 20 x 20.75 m^2	207 (90 passed) (total 100'000 m^3/s)	81.1	13
Xingó, 1982 (Brasil)	Gated, flip bucket (17°), 14.83 x 20.76 m^2	151 (15 passed) (total 33'000 m^3/s)	130.5	13
Santa Luzia, 1942 (Portugal)	Gated, overfall 2 bays/6.4 m wide	15 (total 240 m^3/s)	12	14
Katse, 1997 (Lesotho)	Free overfall, 10 bays/15.9 m wide	38 (-) (total 6252 m^3/s)	41.04	15

Table 2.2.: Pool geometry and relative pool depth (Y/D), assuming D_0 equal to flow depth at issuance for overfall and ski-jumps, or orifice height. The parameter h is the initial water level in the river, and t, L_s, W and Y_t are respectively the depth, the length, the breadth and the measured pool depth of the scour hole.

Dam	t [m]	L_s [m]	W [m]	h/D_0	Y_t/D_0
Cahora-Bassa (CB)	30	200	80-100	≈10	≈14
Kariba (K)	87.5	150	-	5.5	≈18
Picote (P)	22	163	80	≈7-8	≈11-12.5
Krasnoyark (Kr)	17	102	-	-	-
Inguri (I)	80	124	60	-	-
Karun I (Ka)	≈ 18	188	-	-	-
Estreito (E)	-	-	-	-	-
Foz do Areia (FdA)	25	237	80	-	-
Furnas (F)	-	-	-	-	-
Itaipu (I)	30	-	-	-	-
São Simão	5	300	165.4	-	-
Tucuruí (T)	-	-	-	-	-
Xingó (X)	-	70-100	200	-	-
Santa Luzia (SL)	7	-	-	-	-
Katse (model)(Kt)	13	70	50	≈6	≈10

Table 2.3.: Pool type according to riverbed geology.

Geology	Dam	t/W	side slope	t/L_s	u/s slope	d/s slope	angle of jet impingement
Granite/Gneiss	CB	≈0.30-0.38	33° - 50°	0.15	≈ 14°	≈ 14°	$\approx 32 - 35°$
	K	-	-	≈ 0.78	33°	steep	≈ 60°
	P	0.25	steep	≈ 0.13	18.4°	18.4°	$\approx 8 - 15°$
	Kr	-	-	0.17	21°	-	-
Limestone	I	1.33	-	-	32°	-	≈ 50°
Quartzite	E	-	-	-	-	-	-
	F	-	-	-	-	-	-
	SL	-	-	-	-	-	≈ 90°
Basalt	Kat(M)	0.26	$25 - 30°$	0.19	20°	25°	≈ 90°
	SS	-	-	0.02	-	-	-
	It	-	-	-	-	-	-
	FdA	-	-	-	-	-	-
Not defined	Kar	-	30° - 40°	0.07	35°	11°	-
	Tu	-	-	-	-	-	-
	X	-	-	-	-	-	-

opening, crack propagation and block formation are not replicated. Scour development is often faster in model than in prototype.

2. Scour geometry depends not only on the characteristics of the jet but also on **local rock characteristics**, on **gate operation guidelines** and on the **induced return currents**. Despite advanced model studies at the design stage, it has often been important to conduct new tests after the first years of operation and/or operation with large floods. These new series of tests allow adjusting gate operation procedures and test corrective works. They can also be used to investigate the best laboratory granulate-binder mixture to simulate the rock mass, based on the observed scour in prototype.

3. Pre-excavated pools can considerably reduce unexpected evolutions of the scour hole, inducing and confining scour evolution. Pre-excavation is often limited to the removal of alluvial deposits or superficial weathered rock.

4. Prototype observations have shown that the heights of bars created by deposition of scoured material predicted in model studies, are generally larger than actual prototype bar heights (Amanian and Urroz, 1993). In prototype, rock blocks are reduced in size by collision and therefore transported further downstream.

5. The size of typical rock blocks is related to the fracturing spacing and intrinsic rock characteristics in the pool area. For concrete dams in narrow valleys, sound rock foundations are often a basic requirement for dam construction. Thus, typical significant diameters (d_m) range from 0.25 to a few meters. Large blocks are normally ground by collision/abrasion in the pool before being swept downstream. Mason (1993) suggested a value of 0.30 m for use in empirical formulae, which are often used at the feasibility stage of a project[1]. In general, alluvial deposits and superficial weathered rock are removed at an initial stage. For large spillways with buckets, like the examples selected from Russia and Brazil, local rock foundation conditions are more varied.

6. There is little information about the relative pool depths Y/D (or Y/B) considered in model and/or observed in prototype. From the fifteen examples, only three were sufficiently documented to allow obtaining this parameter. For the Cahora-Bassa and the Kariba dams, the natural rating curves of the d/s reach assure water cushions of $8 - 10B_0$ and $5.5B_0$, respectively. For the Cahora-bassa dam, the diffusion length in 1987 (12 years of operation) was already larger than $\approx 10B_0$ (inclined diffusion), whereas for Kariba it was $\approx 18B_0$ after 19 years. For Katse dam, the tailpond dam assures a minimum cushion of $7D_0$ (vertical diffusion) but scour is not expected to grow deeper than $9-10D_0$. Martins (1973b) mentioned nine model tests by Solov'eva with sky-jump spillways and rocky riverbeds, unit discharges from 28-62 m^2/s and fall heights from 39 to 104 m, for which ultimate scour depths were estimated between 4.5D to 37D for initial water cushions of 2.6D to 14.5D respectively.

7. Most of the available information concerns ski-jump spillways. The selected examples reflect the scarcity of data for orifices and free or gated crest overfalls. Orifices and crest overfalls are highly convenient for high dams in narrow valleys, since they allow sparing the investment in excavation and reinforced concrete structures necessary for ski-jump chutes or spillway galleries.

8. For large spillways that have been in operation for a considerable percentage of the total operational life (e.g. during construction of other dam sections), scour has reached a stable configuration. This has been observed even in cases for which the total discharge has not

[1] Mason and Arumugam (1985) recommended the use of d_m instead of d_{90} and 0.25 m as input for empirical formulae.

approached the design flood (expect in Foz do Areia dam). In such cases, the most frequently used bays may have passed specific discharges very close to the design unit discharge, as indicated for instance by Quintela et al. (1987); Schleiss (1993).

9. For non-concentric jets, scour is mainly a function of q and not of Q. For a given site, equilibrium scour is defined by combinations of q and discharge duration T.

10. Scour can reach equilibrium in a few years depending on the number of hours of operation of the spillway. Operation duration is a function of the size of the catchment area and of the ability to store water in the reservoir. For large schemes in wide rivers (e.g. Itaipu, Tucuruí, Krasnoyark) or in large watersheds (e.g. Cahora-Bassa), diversion of the river is done through the spillways while the remainder of the scheme is under construction. This may lead to continuous operation for years and to considerable scour during construction. Operation of gated spillways is mostly done with each gate at full opening (to avoid vibration in partial openings), eventually varying the number of bays/orifices being used. Therefore, high specific discharges are used during long periods. In this case, the scour hole corresponding to the most used chutes/orifices may attain equilibrium in a couple of decades, and even in a few years.

The first reference to the importance of pool morphology was made by Studenichnikov around 1962 (Martins, 1973b). He mentioned the importance of the ratio of the riverbed width (W) to the spillway width (nappe width W_0). The ratio W/W_0 should be larger than about 2.5 to avoid interference of the side slopes in the scouring process. In these conditions, the return currents generated in the pool would be assumed not to disturb jet diffusion in the water cushion.

Confining the lateral diffusion of the jet may modify the macro-turbulent flow pattern. Depending on the degree of confinement, the pressure loads transmitted to the rock foundation will be modified in comparison with pools with infinite width.

In summary, the evolution of scour geometry depends considerably on local geology, namely on the rock mechanical characteristics (e.g.admissible tensile strength, elastic modulus) and on the rock fissuring pattern (spacing, depth, slope). Besides pressure-driven mechanism, abrasion by loose blocks also contributes to the scour process by smoothing out the rock surface.

2.5. Scour in mobile or quasi-fixed riverbeds

Most research on plunge pool scour has been conducted with uniform grain sized material, simulating a fully disintegrated rock foundation. The predominant sediment transport mechanism is the shear stress generated by the laterally expanding wall jets. In this case a distinction should be made between the ultimate dynamic scour depth and the static scour depth. The latter is smaller than the former, since it results from suspended material deposition and sliding to the scour hole after the jet facility has been shut down.

2.5.1. Scour profiles

Rajaratnam and Mazurek (2002, 2003) presented experimental results of tests with non-cohesive bed material and provided empirical laws for the scour profile and its evolution in time, for different jet velocities and angles of impact. Pool profiles are presented as a function

of a densimetric Froude number, that accounts for the grain size. Scour growth follows a logarithmic law. The expressions proposed by these authors have wide applicability for scour assessment downstream of structures in alluvial riverbeds, for which the average grain size is one or two orders of magnitude smaller than the jet's dimensions.

Jia et al. (2001) presented a computational model that takes into account the unsteady behaviour of turbulent jet fluctuations and the corresponding influence in the sediment pick-up rate. The unsteadiness of pressure loading on bed material was defined based on empirical values. Agreement of computational results with experimental data was reasonably good.

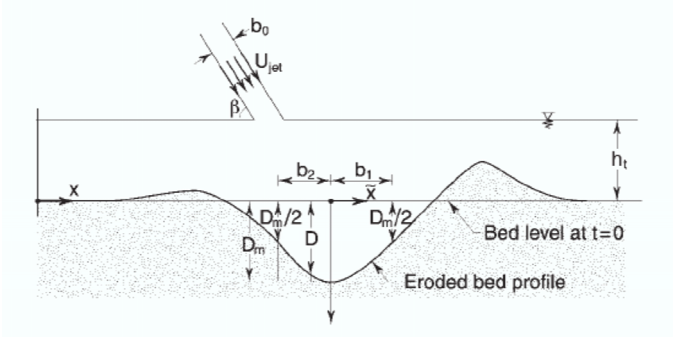

Figure 2.1.: Definition sketch (Salehi-Neyshabouri et al., 2003)

Salehi-Neyshabouri et al. (2003) developed another mathematical model that showed good agreement with empirical methods for scour estimation. Their model also fits very well the experimental relationship describing the scour profiles, as defined by Rajaratnam (1981)(see Figure 2.1 for definitions):

$$\frac{D}{D_m} = exp[-0.693(\frac{\tilde{x}}{b_i})^2] \tag{2.1}$$

The scour profile is defined as an asymmetrical sinusoidal curve for non-vertical impact angles, being steeper downstream rather than upstream.

Rocky plunge pools tend to have a rather polygonal "rough" surface created by fracturing of the rock and by block ejection. Loose blocks that remain in the pool may abrade the boundaries (Amelung, 1996). After being reduced in size by collision, these blocks are swept away from the pool. The final scour configuration differs from site to site, according to the local geology and the relative role of individual scouring mechanisms.

The mechanisms of crack opening and propagation are difficult to reproduce in laboratory. Research on this field has been done in parallel with model tests for large dam projects, but results can hardly be extrapolated for other local conditions. Martins (1973a,b) studied 90 combinations of angles of impact, gate openings, size of concrete blocks (r = 2200 kg/m^3) and tailwater levels. He observed the formation of roughly symmetrical longitudinal pool profiles, the slopes of which were between 30° and 55° in 80 % of the cases. He mentioned a close dependence between the shape of the scour profiles and the type of loose blocks (cubes) used for the experiments. The cube's dimensions were of the same order of magnitude of the dimensions of the jet.

The use of a somewhat cohesive material mixture to bind the loose material provided better correlation with prototype observations. It allows a more realistic reproduction in the model of the local rock constitution and cracking pattern. However, this can only be done (1) once the structure is in operation (to allow calibration) and (2) on a case-to-case basis, not being reasonable to repeat systematic model tests for numerous geological conditions.

Amelung (1996) performed tests at reduced-scale simulating a completely fissured rock mass composed of loose concrete cubes tightly packed. He used a vertical jets impinging on a riverbed made of 5.0 cm side uniform cubes of 2160 kg/m^3, varying jet thickness, velocity (maximum 6.4 m/s at model scale), impinging angle and tailwater depth. The ratios between jet thickness (b) and cube side length (l) varied from 0.5 to 3 by steps of 0.5. He documented the formation of symmetrical pools for vertical jets, presenting photos for the submerged jet case (otherwise aeration would unable visual observation). Tests were performed for a wide range of block Froude numbers from 2.5 to 40 defined as:

$$F_B = \frac{U_0}{\sqrt{g.L_B}} \tag{2.2}$$

where the length scale L_B is the side length of the cube. Different modes of block displacement and block collision within the pool were described. For high velocities, deep symmetrical steep pools were observed and large number of blocks remained rotating in suspension within the pool limits (15 - 28 m/s assumed for prototype, taking blocks with 1 m side length).

2.5.2. The influence of jet impingement angle on scour geometry

Martins (1973a) mentioned that little differences exist in scour and flow patterns for impingement angles between 60° and 90°. Rajaratnam and Mazurek (2002) performed tests with mobile beds and impingement angles from 7.5° to 60°. They concluded that oblique jets produce scour holes that are wider than perpendicular jets. Amanian (1993) performed experimental work with gravel and observed that for lower angles the scour pit is necessarily longer and shallower than for steeper impingement angles. Oblique jets tend to produce asymmetric u/s and d/s rollers[2] in the plunge pool. When the jet width is close to the river or pool width, the absence of contact between the u/s and d/s rollers may lead to a reduction of the tailwater level on the u/s side. This may reduce the protective effect of the water cushion over the riverbed (Puertas-Agudo, 1994). Furthermore, for low impingement angles, less energy is dissipated by impact on the rocky riverbed. Violent circulation currents are created. However, the horizontal component of flow allows a greater capacity for transport of loose blocks out from the scour hole. Therefore, the impingement angle is an important design parameter, in particular for impact angles lower than 60°.

2.6. Temporal development of scour

From prototype observations and model tests, the temporal evolution of scour follows an exponential law (Spurr, 1985):

$$t = A(1 - e^{BT}) \tag{2.3}$$

[2] u/s and d/s are abbreviations for the words "upstream" and "downstream".

where t is the scour depth, T the time and A and B are two constants that can be determined from scour measurements during a given period of operation $\Delta\ t$. According to prototype observations Akhmedov (1988), scour evolves initially rapidly, only to slow down progressively. The rate of evolution depends on the evolution of the hydrodynamic driving agents regarding the geometry of the pool. Model tests, with either non-cohesive or somewhat cohesive material, aim at reaching a reasonable estimate of the equilibrium scour in acceptable laboratory hours, using criteria such "number of observed block movement per interval of time" to stop the tests. This is considered sufficient to have an order of magnitude of scour extension, such estimate suffering from the limitations mentioned in previous paragraphs. However, for detailed design of rock plunge pools, an improved knowledge on rock scour evolution is necessary.

2.7. Notes on the design of pre-excavated pools

Definition of pre-excavation geometry is normally based on model studies. The literature is scarce on this topic. The geometry of the pre-excavated pools is defined to approximately confine the macro-turbulent flow generated by jet impact and induce a given scour progression direction away from the main structures. A well defined geometry may generate enough dissipation, by macro-turbulent confined flows, to reduce scour. The design challenge is to select the adequate geometry for each site.

Amanian and Urroz (1993) performed model studies at reduced scale using flip buckets spillways with exiting angles of 22, 30 and 45° and jet impact in a gravel river bed with variable tailwater level. Based on a total of 63 experiments and a maximum test duration of 6 hours, they suggested a series of equations for the design of pre-excavation scour holes. The expressions suggest upstream, downstream and lateral slopes between 22 and 26° in gravel bed rivers. For rocky riverbeds, it is more difficult to predict how will the scour hole evolve, in terms of breadth, depth, and side slopes. Depending on the intrinsic mechanical characteristics of local rock and on its fracturing and weathering character, scour can evolve quite differently compared to gravel bed rivers.

2.8. Air entrainment by undeveloped plunging jets in unbounded pools

Air is entrained in the pool around the jet when it plunges in the pool or inside the jet. The presence of air in the pool may interfere with jet diffusion. For vertical plunging jets, buoyancy of air bubbles opposes jet momentum. This topic has been object of research in the past for various types of jets and diffusion conditions. In the present framework, only turbulent jets are discussed.

2.8.1. Air entrainment by smooth turbulent jets

According to McKeogh and Ervine (1981), the depth of bubble penetration D_p is given by:

$$D_p = 2.6(V_i D_i)^{0.7} \tag{2.4}$$

The maximum concentration $C_{air,max}$ at a given depth has to be derived from the centreline air-water ratio using

$$C = \frac{\beta}{1+\beta} \tag{2.5}$$

where β is given by:

$$\beta = \frac{Q_{air}}{Q_w} = 1.4\left[\left(\frac{\varepsilon}{r}\right)^2 + 2\left(\frac{\varepsilon}{r}\right) - 0.1\right]^{0.6} \tag{2.6}$$

and ε is the surface roughness as defined in plots of the original paper. As an example, for V =10 m/s and jet turbulence intensities (Tu) larger than 5 % the surface roughness can be obtained from:

$$\frac{\varepsilon}{r} \approx 0.828\frac{L}{L_b} + 0.09 \tag{2.7}$$

where L is the distance travelled in the air and L the break-up length that should be carefully estimated according the turbulence level of the jet at issuance. It should be stressed that the computation of *beta* takes explicitly into consideration the turbulent conditions of the issuing jet. The radial distribution of the air concentration can be computed at any given depth based on the centreline value $C_{air,max}$ by:

$$\frac{C_{air,x}}{C_{air,max}} = \frac{1}{1+3(\frac{x}{D_p})^3} \tag{2.8}$$

which have been obtained for V = 1 - 7 m/s and fully disintegrated rough jets.

2.8.2. Air entrainment by rough turbulent jets

Ervine and Falvey (1987) present an alternative methodology for rough turbulent jets valid in the **zone of established flow** (ZEF). The average air discharge at a given cross-section is given by:

$$Q_{air,i} = \beta_i Q_{w,i} \tag{2.9}$$

where β_i is the air-water ratio at impact (plunging) defined as:

$$\beta_i = K\left(\frac{L}{D_0}\right)^{\frac{1}{2}} \tag{2.10}$$

assuming K = 0.4 (from Table 1 in Ervine and Falvey (1987)) for rough turbulent circular falling jets with $L/D_0 < 50$. Inside the pool, the air discharge in the ZEF is assumed to decay *linearly* according:

$$\frac{Q_{air,y}}{Q_{air,i}} = 1 - \frac{D}{D_p} \tag{2.11}$$

where D_p can either by obtained from Figure 12 in Ervine and Falvey (1987) or given by:

$$D_p = K_1\frac{V_i}{V_r}D_i \tag{2.12}$$

where V_r is the bubble rise velocity that depends on bubble size and on the difference in density with the ambient fluid. The constant K_1 ranges from 1.33 to 1.5 depending on the

turbulence intensity of the jet. Finally, the average air-water ratio at a given depth can be obtained from:

$$\beta = 3.12\beta_i\left(1 - \frac{D}{D_p}\right) \tag{2.13}$$

2.8.3. Discussion

The two methods presented have both been derived from experiment data. They differ slightly on physical background, since Ervine and Falvey (1987) included the bubble rise velocity to account explicitly for the size of air bubbles. The formulae for rough turbulent jets can be applied to high-velocity prototype conditions if proper estimates of air bubble sizes are available.

2.8.4. Jet core development in the air

Ervine et al. (1997) completed the previous procedure by clarifying the dependency of the development of the jet core in the air from the turbulence intensity at issuance. The perturbations on the jet surface where air is entrapped and pushed into the pool are defined as:

$$\varepsilon = \frac{1.14.T_u.U^2}{g}\left[\sqrt{\frac{2.L}{D_0.F_0^2} + 1} - 1\right] \tag{2.14}$$

where F_0 is a jet Froude number defined in terms of D_0. These perturbations grow from the boundaries inwards and outwards. The jet core disappears when:

$$\frac{D_c}{2} = \frac{\varepsilon}{2} \tag{2.15}$$

where D_c is the mean diameter of the jet core. The distance of travel in the air necessary for the core to vanish, i.e. for break-up of the jet, can be computed from the following system of equations:

$$C^2 = \frac{1}{\left(\frac{2L_b}{D_0F_0^2} + 1\right)\left(\sqrt{\frac{2L_b}{D_0F_0^2} + 1} - 1\right)^2} \tag{2.16}$$

and

$$C = 1.14T_uF_0^2 \tag{2.17}$$

where C is a turbulence parameter. When L $< L_b$ the jet core persists at entry in the plunge pool and the jet is said to be undeveloped. The terms "unbroken" or "with potential core" are synonymous for undeveloped found in literature.

2.9. Diffusion of turbulent jets

The diffusion of turbulent high-velocity aerated water jets presents many difficulties for experimental research due to the complex two-phase environment. The hydrodynamic flow field is often inferred from non-aerated conditions, neglecting the contribution of air in the diffusion process. Enhanced knowledge on jet diffusion in extreme conditions of turbulence, aeration and compressibility is of interest in industrial two-phase flows, as encountered in

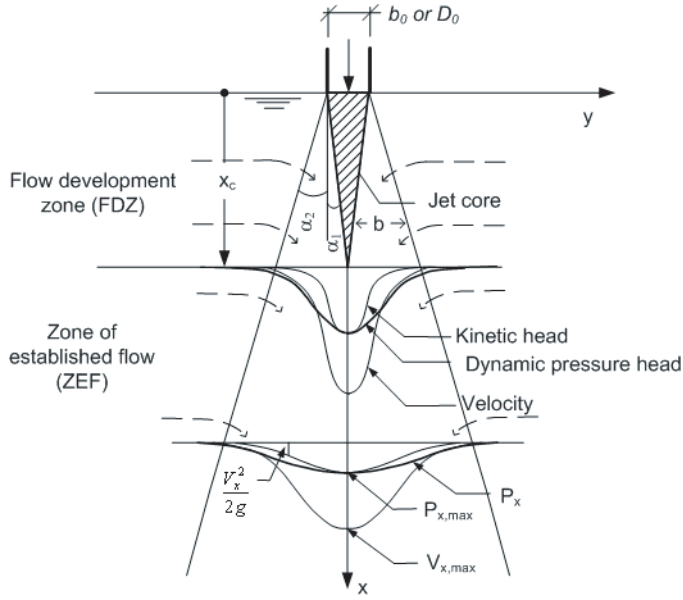

Figure 2.2.: Free jet diffusion (adapted from Hartung and Häusler 1973), where α_1 is the core contraction angle, α_2 the shear layer boundary spreading angle and x_c the core development length.

the dam and the water treatment industries. Jet diffusion in a water pool depends on jet entry velocity, density, turbulence intensity and jet and pool dimensions. Diffusion defines the rate of mixing with the surrounding fluid and the distance influenced by the jet. Mixing is important when dealing with pollutants but, first and foremost, to define the energy remaining at a given depth and thus the dynamic loading acting on the solid structural boundaries or on a natural riverbed. However, existing theoretical tools as the theory of free jet diffusion and centreline velocity decay are hardly valid if flow streamlines deform due to the presence of obstacles or in two-phase conditions.

Systematic research on jet diffusion started during the $1920's$ with the analysis of jet propagation in unbounded media of identical density. A comprehensive review of the research performed over the first half of the XX^{th} century was presented by Albertson et al. (1948). Jet diffusion is divided in two flow regions (see Fig. 2.2): the flow development region ($x \leq x_c$), where the jet potential core persists; and the established flow region further downstream ($x > x_c$).

Kraatz (1965) studied plunging water jets and discussed the influence of mixing fluids with different densities (typically air and water). Cola (1966) studied submerged vertical water jets and documented for the first time jet streamline deflection close to the bottom of the pool. Beltaos and Rajaratnam (1974) presented a review of studies with impinging jets and defined theoretically the deflection zone for circular air jets. For air jets and velocities from 45 to 90 m/s, they observed a deviation of the centreline velocity decay law from the free jet diffusion law after 86 % of the total distance from issuance to impact. McKeogh and Ervine (1981) related jet diffusion with the degree of jet turbulence, jet development in the air and

air entrainment in the pool, which influence mixing and jet core development. Ervine and Falvey (1987) studied rough turbulent water jets as issued from dams, and described jet spreading and core contraction in the air and inside a water pool. Compared with the first test from the 1920's, the velocities tested, as well as the jet's turbulence intensity and pool aeration, have been approaching typical prototype applications.

McKeogh and Elsawy (1980) described how pool aeration is modified when restraining free jet diffusion. They documented the influence of the distance from plunge point to pool bottom upon the bubble penetration depth and void fraction at given depths for jet velocities up to 5 m/s. Gutmark et al. (1978) studied submerged plane water jets with V = 35 m/s and showed that mean pressures at impact with the bounding surface decrease with increasing diffusion distance. They too suggested that the jet starts being deflected at about 75% of the diffusion length.

Impact pressures have mainly been studied in reduced scale models (May and Willoughby, 1991; Puertas-Agudo, 1994). In both studies, plane jets were used. The thickening of the water cushion was shown to reduce mean pressures at the bottom of the pool. These studies, however, do not reliably account for pool aeration, thus neglecting enhanced mixing and energy dissipation due to air bubble buoyancy. Melo (2002b) studied the impact conditions of submerged water jets with artificial air entrainment in lined pools with velocities of up to 10 m/s. He showed experimentally the influence of air entrainment in reducing mean pressures at impact with the pool floor, by directly and fully controlling the amount of air being entrained. In resume, several studies have approached different relevant topics for two-phase jet diffusion in plunge pools but a comprehensive analysis combining high velocities, aeration, bounded pools, dynamic pressures, prototype turbulence levels and therefore reduced scale effects, is still missing.

Recently, Ervine et al. (1997) presented mean, RMS, maxima and minima statistics of impact pressures for velocities up to 29 m/s, varying travel distances, initial jet turbulence, jet velocity and pool depths. Bollaert (2002b) studied the radial pressure distribution at the pool bottom, as well as the propagation of surface pressure fluctuations inside rock fissures (or structural joints).

Research on jet diffusion in conditions where jet diffusion is modified by lateral solid boundaries or counter-flows has only been object of analytical developments. Experimental evidence is missing.

2.10. Conclusions and need for further research

Methods for scour estimation concern mainly the definition of the maximum depth of scour. Laboratory model studies at reduced scale have been the best means to assess the performance of the hydraulic structures as well as the flow patterns in the plunge pool. The development of scour estimation methods was initially empirically-based. Recently, research has been directed in the sense of improving the physical background of estimation methods. Several alternative methods exist for the simulation of scour evolution based on the most important physical processes. Further research should allow improving the representativeness of such tools. Several aspects merit further investigation:

1. The *interaction between jet diffusion in the water and the geometry of the plunge pool.* In fact, scour evolution depends on the impact pressures at the water-rock interface. However, they have only been documented for flat surfaces. This interaction

is considered of utmost importance to the definition of the dynamic loading acting on the rocky riverbed. Furthermore, pool flow patterns can reduce the effectiveness of a given water depth in diffusing the falling jet, as well as induce erosion of side slopes and failure of appurtenant structures. Several incidents in prototype plunge pools are related with pool flow patterns and not directly with jet impact. They justify a more in-depth approach to the genesis, development and behaviour of return currents[3]. These currents are related with the morphology of pool, as well as with the tailwater level and the characteristics of the jets.

2. The *scale effects* in terms of aeration and turbulence characteristics. Most of past research was conducted with either low velocities, single phase, low Reynolds number, poorly representing typical jets found in dams. There is little prototype information on dynamic pressures in plunge pools. The few data acquired with near-prototype velocities correspond to short-duration runs, simulating jet impact with flat metallic surfaces equipped with measuring devices. Larger sets of data are available from reduced-scale models, but entrain significant scale effects in terms of turbulence characteristics and air entrainment in the pool. Enhanced knowledge on pressure fluctuations requires the continuation of research on dynamic pressures in prototype facilities.

3. The definition of *relevant loading events* for crack propagation and for block ejection. One the one hand, there is only one model for crack propagation. It requires validation and upgrading for conditions closer to real-nature, in terms of fissure characteristics and impact pressures. On the other hand, several pressure gradient methods have been proposed that are not unanimous in the definition of the ejection conditions. Furthermore, the methodologies proposed up to present are rather deterministic, neglecting the probabilistic character of the loadings and of the hydrological events that are at the basis of the scouring process.

2.11. Discussion of "Effect of jet air content on plunge pool scour" by Canepa and Hager (2003)

Kraatz (1965) and Melo (2001, 2002b) have showed that mean impact pressure are reduced with increasing air content in the pool. Canepa and Hager (2003) investigated the effect of jet aeration in scour of mobile bed pools. This section corresponds to a published scientific discussion (Manso, Fiorotto, Bollaert and Schleiss, 2004) to the paper "Effect of jet air content on plunge pool scour" published in the Journal of Hydraulic Engineering by Canepa and Hager (2003). The authors of the original paper presented experimental results with plunging jets in loose gravel plunge pools. They discussed and analysed in detail the influence of the initial air content of the jet on the evolution and final extent of scour. The results confirm a reduction of scour with increasing air content in the pool. However, their experimental work concerns gravel riverbeds or rocky riverbeds for which the material is already loose.

[3]In the famous Tarbela dam, important return currents led to plunge pool damage. Undermining of the foundation of the main spillway and sliding of large amount of material from a side slope into the pool lead to partial collapse of the structure. This forced the increased use of the auxiliary spillway, the foundation and side abutment of which were eroded also by recirculation currents (Melo, 2001). Very important repairing works had to be undertaken, mounting to a total of US$210 millions. Other operational problems related with return currents have been reported for Itaipu HPP scheme by Sarkaria et al. (2003).

2.11.1. Introduction

The influence of jet and plunge pool aeration on scour formation is not yet fully known and the authors' work constitutes an important contribution to this issue. In the following, the discussers would like to comment the experimental set-up and the physical principles pertaining to the comparison of water and air-water jets. Furthermore, a different view on the authors' experimental data is given.

2.11.2. Experimental set-up

Concerning the estimation of the ultimate depth and extent of scour, Froude scale models poorly represent the interactions between air, water and the riverbed material, unless very large scales are used. Air-water interaction depends on the Weber number and Froude models cannot scale down surface tension. Also, since pool aeration depends mainly on jet velocity and jet turbulence intensity (McKeogh and Elsawy, 1980), Reynolds similarity is of relevance. Hence, for given hydrodynamic conditions, model air entrainment is lower than at equivalent prototype conditions.

Scaled physical modelling often overestimates the ultimate scour depth. Water jets remain compact over larger distances and excavate further, due to an overestimation of the impact energy. Further problems in similarity are created by the use of loose or artificially-bind gravel to simulate the rocky riverbed. For more reliable design, aeration must be taken into account, as well as the geological and geotechnical characteristics of the rock mass.

In the authors' experimental procedure, air is added under pressure to the water in the supply conduit, resulting in a homogeneous air-water mixture at issuance. This type of aeration differs from that of free overfall chutes or orifices, where a jet core remains non-aerated. The main air entrainment occurs during the travel of the jet through the air and depends on jet velocity and jet turbulence intensity at issuance (Ervine and Falvey, 1987; Ervine et al., 1997; May and Willoughby, 1991). The aeration effects start at the outside layer of the falling jet, increasing progressively inwards as the jet further develops. But aeration does not normally concern the whole jet section, except for small jet dimensions and very long trajectories, for which the jet may fully break-up. The use of jet splitters at ogee crests and ski jumps may largely decrease the break-up length of the jet, but generally jet trajectories are not long enough for a complete break-up before impact with the downstream water cushion. Therefore, at impact, often a non-aerated core remains and thus an average air concentration cannot be defined.

As implied by the authors, adding air to the water flow in the supply system increases the velocity (and energy) of the mixture

$$V_{aw} = V_w(1 + \beta) \tag{2.18}$$

by continuity as the total mixture discharge increases and the density of the outgoing flow is reduced to the same degree. Furthermore, the flow distribution at issuance may significantly change at low velocities or at high air-water ratios (Manso, Bollaert and Schleiss, 2004b).

Therefore, in the authors' experimental set-up and for any given discharge, the kinetic jet energy increases with increasing β, since the reduction of mixture density is linear while the increase in velocity is quadratic. Hence, scour increases with increasing β since the mixture's

velocity V_{aw} at impact is higher than the equivalent clear-water velocity V_w. However, in reality, the jet velocity is equal to V_w as long as the core exists.

Pool aeration depends mainly on the velocity of the jet at impact. Plunging of the jet in the pool produces a highly aerated shear layer around a non-aerated jet core (McKeogh and Elsawy, 1980; Ervine and Falvey, 1987). The latter only disappears for pools deeper than 4 to 6 times the impact jet diameter Bollaert (2002a).

The high air content modifies the density and viscosity of the flow mixture and thus the spreading and dissipation of the jet's energy in the pool.

In the authors' experimental set-up, pool aeration is a combination of air entrainment at issuance, which hardly exists in reality, and air entrainment by the impact of the jet. Air entrainment along the travel in the air is not reproduced in the authors' installation.

Experimental investigations by Melo (2002b) with submerged jets show that increasing pool aeration reduces the mean hydrodynamic loading on plunge pool bottoms. The water jet spreads over a larger area while diffusing in an aerated pool. Energy is dispersed over a larger area and the corresponding pressures at the pool bottom are reduced. Melo placed aeration slots at depressed zones close to the jet issuance, which allowed full control of the amount of air entrained in the pool without altering the total energy of the jet.

From these considerations, it may be concluded that the experimental set-up used by the authors' makes it difficult to transfer the results to prototype situations.

2.11.3. Comparison of air-water jets under prototype and laboratory conditions

Assuming that prototype jets at impact in a plunge pool consist of a non aerated core surrounded by a highly aerated area, jets with equal water discharge but different air-water ratios should be compared to assess the effect of aeration in equal water releasing conditions and, consequently, to mitigate the scale effects of physical modelling. This could be envisaged either by modelling jets with equal initial turbulence intensity but for different travel lengths, corresponding to different degrees of jet spreading and breaking-up, or by modelling jets with different initial turbulence intensities, which requires appropriate issuance devices.

Therefore, an approach complimentary to the authors' one would be to compare jets of equal impact velocity or total discharge

$$Q_T = Q_w(1 + \beta) \tag{2.19}$$

and equal turbulence intensity. This ensures equal pool aeration and allows straightforward comparison. The only difference is the air mixed in the jet core. The discussers' invite the authors to present a direct comparison of their data for jets with the same impact velocity and different density.

Also, in the discussers' viewpoint, when performing scaled model tests, prototype aeration is largely underestimated. Hence, an aerated jet with lower water discharge with respect to the scaled prototype water discharge should be used to correctly estimate corresponding prototype scour. Thus, for increasing β at prototype scale, both the modelled water discharge and mixture's density should be adapted in accordance.

For the same velocity at impact, a highly aerated jet will have *less energy* and will produce less scour than a clear water jet.

2.11.4. Alternative analysis of the authors' results

The mixture flow is considered as a pseudo-fluid where water and air velocities are equal for each β value. The analysis assumes fully developed jets and uniformly distributed air across the falling jet. For comparison purposes, the sediment grain size is kept constant.

The authors' Figure 5 shows that ultimate scour depth $Z_m = z_m/D$ increases with the flow velocity. For aerated jets, the experimental data are plotted all together in Figure 6 and maximum scour results are presented as a function of β but rendered dimensionless with the densimetric Froude number F_{aw}. However, the latter also depends on β and increases its value accordingly. Therefore, Figure 6 does not allow a direct comparison between equivalent jets with same impact velocity and different density due to aeration.

In the discussers' analysis, the dimensionless scour depth Z_m is plotted as a function of the kinetic energy (dimensionless as well). The density of the pseudo-fluid is defined by:

$$\rho = \frac{1}{1+\beta}\rho_w + \frac{\beta}{1+\beta}\rho_{air} \tag{2.20}$$

where ρ_w, ρ_{air} = density of water and air, respectively. For practical β values, the second term can be neglected since $\rho_w \gg \rho_{air}$. Therefore, the kinetic energy of the mixture flow is given by:

$$E_c = \frac{1}{2}\rho_w V_{aw}^2 \frac{1}{1+\beta} \tag{2.21}$$

On the other hand, according to the authors' equation (5) the dimensionless maximum scour depth Z_m is:

$$Z_m = (1+\beta)^{-0.75} 0.37 \frac{V_{aw}}{\sqrt{g' d_{90}}} \tag{2.22}$$

Figure 2.3 is obtained by plotting Z_m against E_c, varying the air content β from 0 to 3 and V_{aw} between 0.5 and 20 m/s. It shows that scour, on the one hand increases with the impact kinetic energy, which is in agreement with prototype observations and, on the other hand decreases (for a given E_c) with increasing air content.

However, this correction to the jet's density and velocity at impact with the pool does not consider what happens inside the plunge pool. The analysis can be improved by including in a simplified way the effect of jet diffusion through the water cushion. When increasing the air content, both inside the jet and in the pool, the angle of diffusion of the jet increases and the corresponding mean dynamic pressures at the pool bottom decrease (McKeogh and Elsawy, 1980).

Melo (2002b) suggested the following relationship between mean dynamic pressures at a given depth for aerated and non-aerated conditions, based on the works of Kraatz (1965); Amelung (1996)[4]:

$$\frac{P_{air}}{P} = (1-C)^{1.345} \tag{2.23}$$

where C is the initial air concentration at a given depth. Considering the short travel distance in the authors' set-up, the air concentration at impact C_0 can be assumed equal to

[4] the additional exponent 0.345 was presented by Kraatz (1965) to relate the jet core length in plunging and submerged conditions, i.e. with and without a difference in the densities of the jet and the surrounding environment

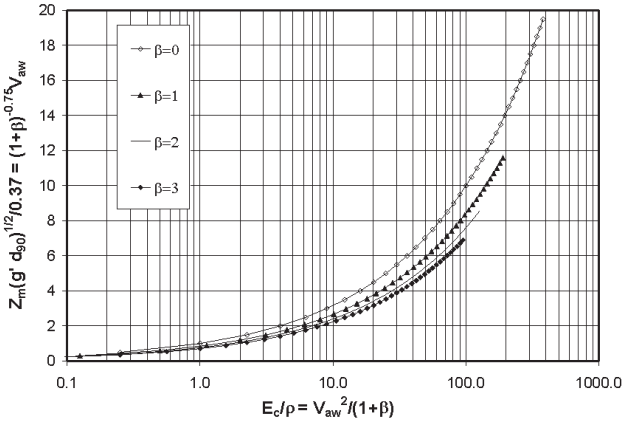

Figure 2.3.: Maximum scour depth Z_m as a function of kinetic energy E_c for different air-water ratios.

$\beta/(1+\beta)$. According to Equation 2.21 and Equation 2.23, the kinetic energy corresponding to the diffusion of an initially aerated jet in a two-phase plunge pool can then be estimated by:

$$E_c = \frac{1}{2}\rho_w V_{aw}^2 (1 - C_0)^{1.345} \tag{2.24}$$

which is better presented as:

$$\frac{2}{\rho_w} E_c = \frac{V_{aw}^2}{(1+\beta)^{1.345}} \tag{2.25}$$

By plotting Z_m against Equation 2.25, the curves for different β values almost match (Figure 2.4). Therefore, when accounting for (1) the reduction in density, (2) the increase in mean water velocity and (3) the effect of diffusion of the jet through the pool due to the air content β, the analysis of the authors' data shows that jets with equal energy create similar scour.

Full matching of the curves can be achieved when correcting C_0 by a factor of 1.04, which might be due to a slight increase in air content that merits further investigation.

In the discussers' opinion, Figures 2.3 and 2.4 allow a straightforward understanding of the authors' data. For future experimental works, the discussers believe that the direct comparison of jets of equal impact velocity and different densities due to air entrainment is particularly adequate for the assessment of the influence of aeration on the scour process.

2.11.5. Particular case of scour in fractured rock

The authors' experiments were performed for loose, non-cohesive bed material and can therefore not be transferred to prototype scour of fractured rock. Recent research (Bollaert, 2002b; Bollaert and Schleiss, 2003b) revealed that, when considering the particular geometric

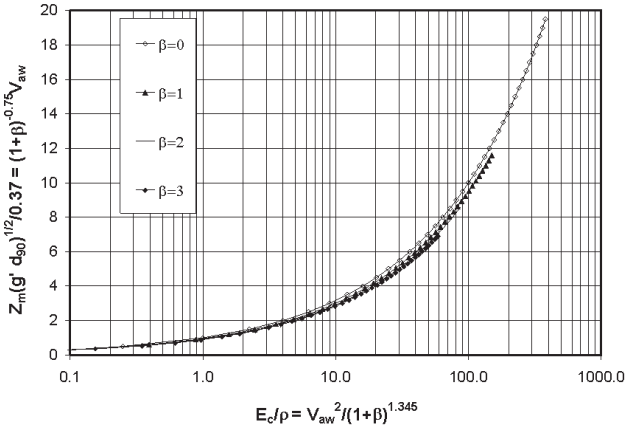

Figure 2.4.: Maximum scour depth Z_m as a function of kinetic energy E_c for different air-water ratios, after correction to account for jet diffusion through the pool.

and geomechanic characteristics of fractured rock instead of loose particles, scour is not only related to the incoming kinetic energy of the jet, but also to the ability of the jet to develop pressure fluctuations in rock joints at the water-rock interface.

This ability depends on several aspects, such as plunge pool aeration, the stability of the jet and its geometry upon impact compared to the depth of the pool. The generated pressure fluctuations inside the rock joints are enhanced by air presence and are able to break up the rock mass into distinct particles and to generate net uplift forces on the particles that eject them from their mass. Hence, air presence in plunge pools is directly relevant to scour of fractured rock.

3. Experimental arrangement and description of the test campaign

The investigation of two-phase pool flows created by the diffusion of turbulent plunging jets is quite challenging. At present, experimental research is the best means to improve the understanding of highly aerated turbulent flows, but only a limited number of existing instrumentation tools can be used in such conditions.

This chapter presents the experimental facility and the test campaign undertaken. Experimental tests are divided into three series, two concerning the measurement of dynamic pressures and one focusing on air-water mixed flow characteristics.

The main objective of the test campaign is investigating the interaction between the diffusing jet and the geometry of the pool, as well as the implications of such interaction on dynamic pressures at the pool bottom and inside underlying fissures.

3.1. The LCH facility for high-velocity plunging jets

3.1.1. Overview of the facility

The existing facility was built at the Laboratory of Hydraulic Constructions (LCH) of the *Ecole polytechnique fédérale de Lausanne* (EPFL) in 1998. The experimental facility is presented in Figure 3.1. It aims at reproducing the most important hydrodynamic processes involved in rock scour. Real-life rock scour being a quite complex process, considerable simplifications are necessary to perform experimental research.

Its structure consists of four main parts, as described by Bollaert (2002b):

- A 300 mm diameter water supply conduit, with a cylindrical or convergent-shaped jet outlet system at its end, models the jet. Due to constructive limitations, the supply conduit has a 90° bend just upstream of the jet outlet system. A rigid steel frame, consisting of three I-shaped steel profiles that are welded together, guarantees the support of the supply conduit.
- A 3 m diameter cylindrical basin in steel reinforced Lucite simulates the plunge pool. The height of the basin is 1 m, and the steel reinforcement is provided by 10 T-shaped profiles. The bottom of the basin is made of a rigid steel frame, covered by a 10 mm opaque Lucite plate. Inside the basin, two rectangular boxes made of Lucite adjust the water level by a flat plate that is inserted. The water that flows over these plates is conducted downstream into four restitution conduits.
- A three-parts pre-stressed steel structure models the jointed rock mass. The rock joint is simulated by a 1 mm thin steel sheeting with a particular form. This sheeting is pre-stressed by means of 10 steel bars of 36 mm of diameter between two 100 mm thick steel plates of 1 ton each. These plates are 1 m high and wide and are connected, at

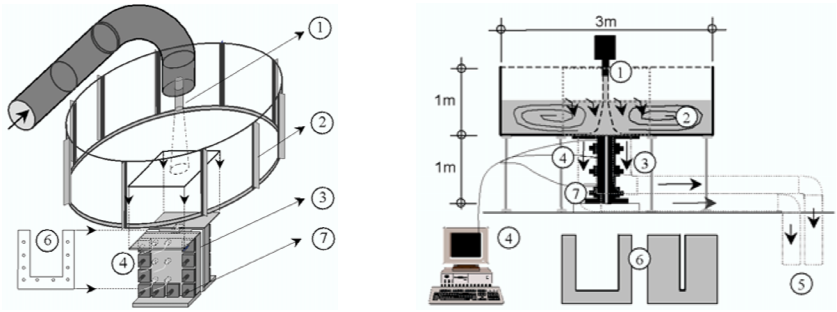

Figure 3.1.: Perspective and side view of the facility with the following elements (Bollaert, 2002b): 1) cylindrical jet outlet, 2) reinforced plastic cylindrical basin, 3) pre-stressed two-plate steel structure, 4) PC-DAQ and pressure sensors, 5) restitution system, 6) thin steel sheeting pre-stressed between steel structure (defining the form of artificial 1D and 2D joints), 7) pre-stressed steel bars.

their top and bottom, with two horizontal steel plates. The top plates form the pool bottom, while the bottom plates stabilize the structure. In the top plates, pressure sensors can be inserted.

- A restitution system consisting of 4 conduits of 220 mm of diameter simulates the river downstream. These conduits are connected to the overflow boxes and conduct the water into the main reservoir of the laboratory.

3.1.2. Types of jets investigated in the present study

The jet outlet is cylindrical with a nozzle diameter of 0.072 m. The facility produces jets with velocities up to 30 m/s and a maximum Reynolds number of 1.87 x 10^5. The 300 mm diameter upstream conduit supplies a maximum discharge of 120 l/s by means of a 63 m high head pump.

The present facility is similar to that of Ervine et al. (1997). It generates **high jet velocities** within the range found in engineering practice. The range of velocities produced by this facility allows replication of **near-prototype pool aeration**. From literature review, few examples with similar velocities were found (Gutmark et al., 1978; Ervine et al., 1997). The former studied submerged water jets, while the latter studied plunging water jets.

Ervine et al. (1997) and Bollaert et al. (2002) state that facilities producing near-prototype jet velocities and pool aeration are able to produce dynamic pressure statistics at impact with the pool floor (i.e. root-mean-square and positive and negative extreme fluctuations) that are significantly higher than previous values obtained in reduced-scale models. A comprehensive comparison of RMS values can be found in Bollaert (2002b).

Bollaert et al. (2002) state that the present facility generates **near-prototype power spectra of dynamic pressure fluctuations**. The obtained power spectra with high velocities and representative Y/D ratio values were considered to replicate prototype jet spectra. This, at least, in the range of frequencies relevant for slab instability and rock block

displacement (i.e. roughly between 10 and 100 Hz). Low frequencies (<10 Hz) depend on site specific currents and are therefore characteristic of the experimental basin. Frequencies higher than 200 Hz are not expected to contribute for block displacement. This topic is discussed further in Chapter 11.

At the beginning of the present study, the facility that had been used for Bollaert (2002b) produced jets with axial and transversal turbulence intensities of about 4.1 - 5.2 % and 1 - 1.3 % respectively. The behaviour of the jet showed the presence of low-frequency turbulence and an unstable character. In order to investigate in detail the characteristics of the jets produced in this facility, a first experimental test series was included in the work program. It is presented in section 3.2. The assessment of origin of such instability was of utmost importance to define proper input conditions in the test facility.

The experimental work was carried out with (axisymmetric) **circular jets**. In practice, circular and rectangular jets are found. Jets deform as a function of the turbulence intensity at issuance and of the jet travel length. [1]

In the present experimental facility, the jet trajectory in air is maximum 0.70 m. For a typical Tu of 4 % the degree of jet break-up will not exceed 0.44, according to Equation 2.16. This means that in all cases the core persists at the plunging point. Comparing to prototype jets, this facility can only reproduce **undeveloped jets**. To the author's knowledge, only the works of McKeogh and Ervine (1981) and Bohrer et al. (1998) dealt with developed jets. These situations are less common in dam hydraulics; they require long trajectory lengths.

The investigated jets have **non-aerated cores**. Only a limited number of attempts of reproducing aerated core jets, as observed in the case of ski-jumps after long chute spillways, have been done in the past. In these structures, the water column is progressively aerated along the chute. However, in reduced-scale models velocities are generally not sufficient to overcome the surface tension. Large scale models would be required. Aerated cores have been obtained by artificially injecting air into the core in the supply system (Ervine et al., 1997; Canepa and Hager, 2003). Ervine et al. (1997) compared different air to water ratios for several degrees of jet break-up ($0 < L/L_b < 0.5$). They showed that an aerated core can reduce mean pressures at impact. Apparently it can also reduce pressure fluctuations (RMS values) at impact, even if only a reduced number of results was available. Canepa and Hager (2003) used a reduced scale facility to assess the influence of the air concentration in the evolution of scour and ultimate scour extent in loose gravel riverbeds. A detailed comment on their work is presented in section 2.11.

All in all, little is known about the behaviour of an aerated jet along its trajectory in the air. This lack of knowledge poses many questions relatively to jet characteristics at plunging point and about the significance of the research results obtained with artificially aerated-core jets. This remain a challenging topic for future research, though a rather cumbersome one to explore. The facilities necessary to study jet behaviour in the air with reduced scale effects and high velocities would be lengthy and massive.

[1] Zaman (1999) showed that rectangular jets deform similarly to circular jets for length/width section ratios up to 10, except when issuance conditions are significantly changed by inclusion of protrusions at the outlet section. For jets issued from high dams (e.g. fall heights 50 - 100 m), the jet's shape at impact with the tailwater surface d/s is rather circular. Gravity and surface tension tend to keep the core of the jet compact while turbulence intensity enhances spreading and core contraction. This topic is consensual amongst experts on large dams and has been explicitly mentioned in the past, for e.g. Martins (1973b); Spurr (1985).

3.1.3. Plunge pool

The plunge pool is simulated by means of a round flat basin with variable pool depth. By increasing the pool depth, the travel length in the air is reduced. At entry in the pool, the jet entrains air in near-prototype conditions. The travel length in the air varies from 0.63 to 0.03 cm for the shallowest and deepest pools tested respectively. The corresponding degrees of break-up at entry of the pool are L/L_b = 0.02 for Y/D = 9.3 and L/L_b = 0.44 for Y/D = 1.04. All tested jets are undeveloped at entry in the plunge pool.

The initial pool depth Y varies from 7.5 to 67 cm for plunging jet conditions (about $1D$ to $9.3D$) and 82 or 87 cm for submerged jet conditions (Y/D ratios of 11.4 and 12.1). Jet diffusion is axisymmetrical. Dynamic pressures at impact with the pool are representative of prototype conditions.

The pool flow is not fully symmetrical; the two side-weirs at the East-West extremes reduce the full breadth of the basin locally. Enhanced by this unevenness, circulatory flows develop, which are clearly visible at high jet velocities. For the particular case of an intermediate pool depth Y = 0.60 m (Y/D = 8.3) the horizontal circulation reduces the pool depth at point of jet entry of up to 15 cm (twice the jet's diameter). This effect is not relevant in all the other test conditions.

3.1.4. Fissured rock mass

A four-element pre-stressed steel structure (Figure 3.2) simulates a jointed rock mass (Bollaert, 2002b):

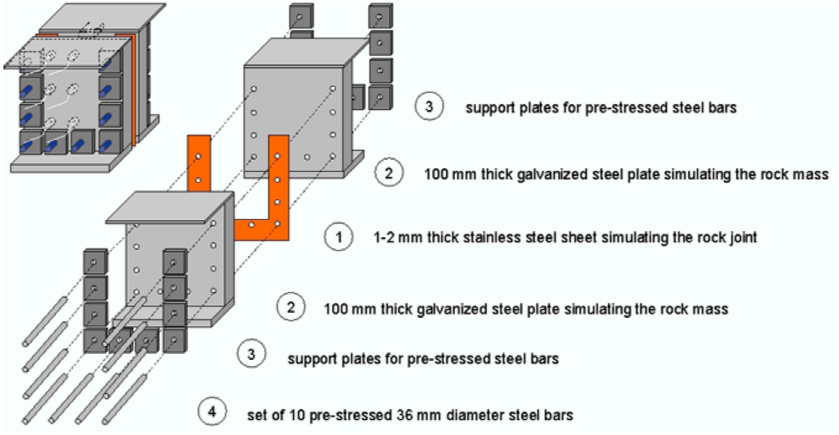

Figure 3.2.: Pre-stressed steel system showing the four main elements and their disposition (Bollaert, 2002b): 1) thin stainless steel sheeting (2D-joint), 2) two thick steel plates simulating the rock mass, 3) a set of support plates, 4) a series of 10 pre-stressed steel bars.

"The first element corresponds to a 1 mm thin stainless steel sheeting with a particular form. This sheeting can have any form, but for a constant thickness, and allows modelling one-and two-dimensional rock joints at prototype scale. The second element represents two

100 mm thick steel plates, with a weight of 1 ton each, that simulate the surrounding rock mass. These plates have a height and a width of 1 m and, at their top and bottom, two small horizontal steel plates have been welded. The top plates form a 1 m^2 pool bottom and exactly correspond to the size of the hole that has been made inside the plunge pool basin. The bottom plates stabilize the structure. The third element constitutes a set of 20 support plates of 0.20 m x 0.20 m that are necessary to transmit the stresses of the steel bars into the steel plates in a homogenous manner. Finally, the fourth element is formed by a series of 10 DIWYDAG steel bars of 36 mm of diameter and 430 mm of length. These bars allow pre-stressing the thin stainless steel sheeting between the two thick steel plates. Hence, an extremely rigid and watertight system has been created, with a 1-2 mm small opening in the middle. The advantage of this system is its facility to modify the form and the thickness of the sheeting, as well as the stresses in the DIWYDAG steel bars. Within this steel system, a series of holes have been made in order to introduce the pressure sensoring devices. The stresses are induced in the DIWYDAG steel bars by means of a hydraulic piston. With this system, forces of up to 1'000 kN can be generated. For steel bars of 36 mm of diameter, this corresponds to a stress of maximum 1018 N/mm^2. The forces induced in the steel bars during the test runs fluctuated between 150 and 300 kN, corresponding to stresses of between 152 and 305 N/mm^2. This is safely situated in the elastic range. The yield stress of the bars is 1'080 N/mm^2, and the tensile strength is 1'230 N/mm^2. The modulus of elasticity of the steel bars E_s is 205 kN/mm^2. The particular form of the rock joint under investigation has been obtained by cutting a piece out of the 1 m^2 stainless steel sheeting. This precision work is done by jet cutting. The sheetings are fabricated with a thickness tolerance of $+0/+0.1$ mm."

A closed-end fissure is used in the present study. The metallic sheet is 1 by 1 m^2 and the fissure is 800 mm long and 10 mm wide. It was placed in between the metallic plates mentioned above. The opening is thus a hole with 1 by 10 mm^2, which was aligned with the jet axis. The basin and the supply conduit are independent structures. Therefore, any eventual vibration of any of these may induce some misalignment of the jet axis with the fissure.

3.2. Experimental investigation of jet characteristics at issuance

The objective of this test series is to study the jet characteristics at issuance from a cylindrical nozzle. The assessment of jet characteristics is carried out by means of pressure measurements spatially distributed over the diameter of the nozzle[2].

Prototype jet mean velocities of up to 30 m/s, corresponding to Reynolds numbers of maximum $2E+6$ are used. The jet nozzle extends 30 cm out of the supply conduit and 15 cm inside, the ratio between its lengths and diameter l/D is 6.3. The 300 mm diameter conduit upstream supplies a maximum of 120 l/s by means of a 63 m high head pump. Discharge measurements are performed with an electromagnetic flowmeter placed on the supply system, with 1 % accuracy.

Pressure measurements are performed at the outlet of a 72 mm diameter jet nozzle using a piezo-resistive micro-transducers of type KULITE XTL-190-17BAR-A. The measuring pressure transducer is placed in a mobile metallic structure right below the jet supported

[2]This section is part of the scientific publication Manso et al. (2005b) presented in Chapter 4.

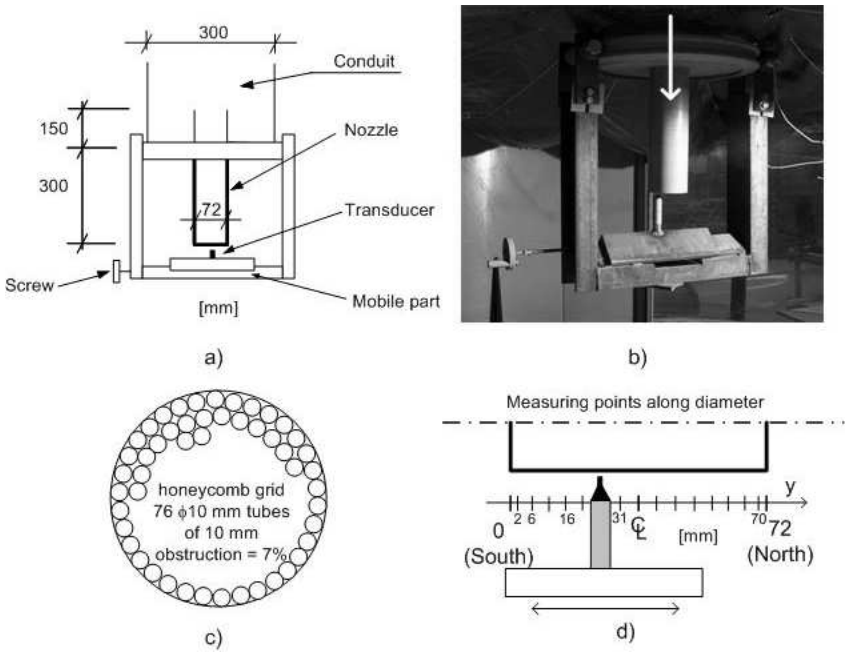

Figure 3.3.: Experimental set-up: a) schematic view and b) photo of the measuring frame installed under the jet nozzle, c) honeycomb grid which was placed 25 nozzle diameters upstream, d) measuring points spaced of 4 - 5 mm each.

Table 3.1.: Test conditions for the experimental investigation of the hydraulic characteristics of jets at issuance

Test series	Discharge $[m^3/s]$	Velocity [m/s]	Reynolds [-]	Comments
1^{st} series	0.030	7.37	4.61E+05	13 measurement
	0.040	9.82	6.15E+05	points spaced
	0.050	12.28	7.69E+05	by 5 mm
	0.060	14.74	9.23E+05	
	0.072	17.56	1.10E+06	
	0.081	19.77	1.24E+06	
	0.091	22.35	1.40E+06	
	0.102	24.93	1.56E+06	
	0.114	28.00	1.75E+06	
	0.120	29.47	1.85E+06	
2^{nd} series	0.047	11.62	7.27E+05	15 measurement
with an	0.059	14.37	9.00E+05	points, by
air vent	0.071	17.46	1.09E+06	addition of
and a	0.083	20.48	1.28E+06	2 points
honeycomb	0.095	23.36	1.46E+06	close to wall
bundle	0.107	26.16	1.64E+06	
	0.118	29.08	1.82E+06	
	0.125	30.73	1.92E+06	

by a rectangular steel frame (Figure 3.3). The transducer's membrane has a measuring diameter of 3.8 mm and is mounted on an elongated 90 mm long hollow stainless steel cylinder. The top of this cylinder is conically shaped to minimise the influence of the cylinder upon the turbulent flow characteristics. Measurements were performed at points evenly spaced of 5 mm, the points closest to the walls were 2 mm from the nozzle inner sidewalls (Table 3.1). The transducer has an accuracy of ± 0.1 % of the full-scale output (17 bar absolute) due to non-linearity and hysteresis. The transducer's natural resonance frequency is 750 kHz. The acquisition system allowed sampling at a maximum frequency of 20 kHz, the signal being conditioned by a lowpass hardware filter set at the Nyquist frequency. The pressure signal was sampled at 2 kHz during 32.5 sec. This frequency was selected to guarantee the acquisition of eventual low and high-frequency instabilities. The duration selected assures ergodic sampling of the first moment of the data series and provides reliable representation of the high frequency fluctuations contained in the corresponding spectra. Pressure measurements were collected via a multi-channel acquisition card. The signal was conditioned by hardware low-pass filtering at 1 kHz. The filtered signal was digitized by means of an ARCNET PCI 14 bits card.

Two different supply conditions were tested. The upstream circuit has several 90° bends, which induce secondary currents at the exit for the lowest velocities tested. These conditions [3], have been considered for the first series of tests. For the second series of tests, a honeycomb grid was placed immediately upstream of the last bend of the supply conduit. The grid consists of 10 cm long, 10 cm diameter metallic tubes. In addition, an air vent was added at the highest point of the supply system.

On prototype, a large range of jet conditions can be distinguished. For orifices with high Reynolds numbers at issuance, the turbulence characteristics of either rectangular or circular jets do not substantially differ, except for hollow jet valves due to their special configuration. In the case of free overfall weirs, which have relatively low turbulence conditions at issuance, this difference can be more significant. However, since the fall distance is rather long on high-head dams (relatively to the break-up length), the jet will often deform towards a circular shape. A quite different situation occurs for jets issuing from ski-jump spillways at the end of long chutes for which the jet core is aerated. It reduces surface tension and jet compactness, enhancing the disintegration of the jet. The jets produced in the LCH experimental facility show the same behaviour of orifices, free-falling high-velocity undeveloped nappes and submerged outlets encountered in practice, in all cases with non-aerated cores at impact with the pool.

3.3. Experimental investigation of dynamic pressures at impact and inside underlying fissures

3.3.1. Pressure measurements in pools with flat bottom

The influence of the pool geometry in jet diffusion and dynamic pressures at the pool bottom is firstly studied in pools with flat bottom, following previous researchers and, secondly, in other pool geometries. The aim is to approach real-life plunge pool conditions.

Based on the experimental results and extensive review of previous literature, the impact pressures in pools with flat bottom are defined as the reference scenario for comparison

[3] similar to conditions used by Bollaert (2002b).

with other pool geometries. To measure dynamic pressures generated by high-velocity jets, pressure transducers are flush-mounted on the pool bottom as described in Fig. 3.4.

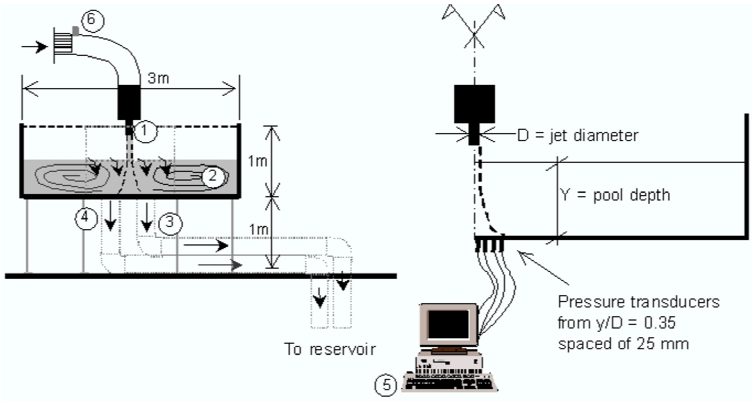

Figure 3.4.: Schematic representation of the experimental facility (except the "rock mass" module): 1) cylindrical jet outlet (D = 0.072 mm), 2) cylindrical basin, 3) and 4) restitution system, 5) DAQ system for pressure transducers, which are installed at x = 0.70 m and y = 25, 50, 75, 95, 150 and 200 mm from jet axis, 6) air vent and honeycomb grid; x and y are the vertical and horizontal co-ordinates, respectively.

Dynamic pressures were measured at the bottom of the pool at nine different locations. Due to the existence of a limited number of transducers (maximum 6) not all interesting positions could be tested simultaneously and thus several series were required (Table 3.2).

Table 3.2.: Test series in pools with flat bottom

Name	♯ transducers, position	Remarks
FB0	4 (25, 50, 75, 95)	non-simultaneous tests and previous to modifications in issuance conditions
FB1	6 (25, 50, 75, 95, 150, end of I-fissure)	transducer at 25 mm failed in ≈ 90 % of tests
FB2	5 (all at 200 mm, spaced of 10° each)	perimetrical evaluation
FB3	4 (25, 150, middle and end of I-fissure)	partial repetition of FB1 series and study of the transfer of pressures to the fissure

The water depth in the plunge pool can vary from 0 to 0.9 m. Water is evacuated in two rectangular boxes equipped with variable height weirs symmetrically placed regarding the plunging jet. The height of these weirs sets the initial tailwater level. This allows creating a high-velocity diffusing turbulent shear layer that impacts the pool bottom. The turbulence intensities at the jet outlet are between 0.04 and 0.08, the lowest value corresponding to velocities from 20-30 m/s (see Chapter 4 for details). At impact with the pool surface, the observed jets are rather compact due to their small fall heights (max. 0.50 m) and small degree of break-up (max. 0.44). Tests were performed for velocities ranging from 7.4 to 29.5 m/s and for relative pool depths Y/D from 1.0 to 11.4 (or 12.1). The latter corresponds to a submerged jet at the outlet. The distance from jet nozzle to pool bottom is 0.70 m, thus resulting in travel distances L in the air of maximum 0.625 m or $L/D = 8.6$. Test conditions are presented in Table 3.3 and Table 3.4.

For test series "FB0" only one transducer was available. It was moved over the four central

Table 3.3.: Tests conditions with flat bottom pools (FB), where Q is the discharge, V_0 the velocity at issuance, Re the Reynolds number and Fr the Froude number (using D_0).

Tests	Q [l/s]	V_0 [m/s]	$Re * 10^5$ [-]	Fr [-]
	30	7.4	4.6	8.8
	40	9.8	6.2	11.7
	50	12.3	7.7	14.6
	60	14.7	9.2	17.5
	70	17.2	10.8	20.5
Flat bottom	80	19.6	12.3	23.4
	90	22.1	13.8	26.3
	100	24.6	15.4	29.2
	110	27.0	16.9	32.1
	120	29.5	18.5	35.1

positions, while repeating the test procedure for all discharges and weir levels. These tests were performed prior to the modification to the supply system. Test series "FB1" employed a group of transducers placed radially outwards regarding the jet axis. Transducers were flush-mounted on the pool bottom at 25, 50, 75, 95 and 150 mm from the jet axis. One transducer was placed at the end section of the closed-end fissure ("I-fissure"). For test series "FB2", five transducers were mounted at 200 mm from the jet axis but displaced along a perimetrical line and spaced of 10° each. The last series "FB3" was performed in similar conditions to series "FB1", repeating measurements at 25 and 150 mm. Two transducers measured dynamic pressures at the middle and end sections of the I-fissure. Repetition was necessary due to failure of the transducer placed at 25 mm (y/D = 0.35) during a large part of the "FB1" series tests.

Table 3.4.: Pool water level conditions for the tested velocities. The other parameters are the length of travel in the air L, the length of travel in the pool Y (pool depth), the relative pool depth Y/D and the relative degree of jet break-up L/L_b (L_b being the break-up length).

Y [m]	Y/D [-]	L [m]	L/L_b [-]
0.075	1.0	0.625	0.40-0.44
0.20	2.8	0.50	0.32-0.35
0.30	4.2	0.40	0.26-0.28
0.40	5.6	0.30	0.19-0.21
0.50	6.9	0.20	0.13-0.14
0.60	8.3	0.10	0.06-0.07
0.67	9.3	0.03	0.02
0.82	11.4	submerged	-
0.87	12.1	submerged	-

3.3.2. Dimensional analysis of impact pressures in confined pools

The purpose of this dimensional analysis is twofold: (1) to identify the governing parameters concerned in jet diffusion in confined pools; and, (2) to combine these parameters in dimensionless numbers that can be used for the analysis of the confined diffusion process.

Jet issuance characteristics can be described by the mean velocity V_0 (or the energy H_0), the discharge Q, the turbulence intensity Tu_0, the jet diameter D_0 (or jet thickness B_0 for

plane jets), the kinematic viscosity μ and the mass density ρ of the fluid. Additional features of the issuing section can be accounted for in Tu_0 and ρ, as shown by Zaman (1999).

The deformation of the jet in the air depends on the issuance characteristics as well as on the water surface tension σ. Surface tension contributes to keep the core compact and defines shear conditions between air and water. It thus plays a key role in the air-water mixing process. An extensive review of jet deformation in the air can be found in Melo (2001). It includes also a comprehensive discussion on the interest of the Weber number for simulation of jet development in the air at reduced scale in laboratory (not the present case). If Weber similarity conditions are respected, jet surface disturbances ε depend on Tu_0, V_0 and F_0, where "0" stands for issuance conditions[4]. This is typically the case for We $\gg$ 100 (Boes, 2000).

Furthermore, the deformation of the jet in the air depends also on the reduced mass density of the jet ρ. Jet's density may be lower than that of water ρ_w already at issuance (i.e. ski-jump at the toe of long chute) or from increasing air mixing in the jet surface. This effect can be accounted for in the void fraction C_{air} over a characteristic cross-section of the jet. The gravitational acceleration g and the length of travel in the air L are necessary to properly estimate the actual spreading and core contraction, as well as the geometry of the jet at the entry of the plunge pool. The jet characteristics at the plunging section can be defined considering:

$$(D_i, V_i, C_i) = f(Tu_0, Q_0, D_0, \rho_w, C_{air}, \mu, \sigma, g, L) \tag{3.1}$$

Diffusion of a plunging jet inside the pool can hardly be considered a one-way process. Even in free diffusion conditions, the rise of entrained air bubbles opposes jet diffusion. Jet diffusion can be assumed to be depth-bounded if there is an obstacle at a distance inferior to, at least, the maximum depth of bubble penetration[5]. In this circumstances, jet streamlines are disturbed. The pool flow patterns may induce changes in jet diffusion itself. Therefore, physical processes related with jet travel in the air and its diffusion in the water must be considered for dimensional analysis.

To describe the behaviour of the jet in the pool, the diffusion length (or pool depth Y) and the pool geometry should be added. The dynamic pressures generated by the impact of a circular plunging jet can be considered as a function of:

$$p(x, y, z, t) = f(Tu_0, Q_0, D_0, \rho, C_{air}, \mu, \sigma, g, L, Y, pool - geometry) \tag{3.2}$$

The group of selected parameters can be reduced for the dimensional analysis. The void fraction can be accounted for in $\rho = \rho_w(1 - C_{air})$. The surface tension σ and kinematic viscosity μ are accounted for in the Weber and Reynolds' numbers respectively, and need not be further developed. Since the gravitational and inertial forces are the most relevant ones, Froude similarity governs the physical processes under investigation.

The survey of prototype plunge pool geometries presented in Chapter 2 leads to selecting stepped conical and cylindrical configuration for the experimental tests. They are described by the diameter D_c and the height t (c stands for confinement). The pool depth Y is $t + h$, where h is the initial tailwater level.

[4] The surface disturbances ε were defined by McKeogh and Ervine (1981) for Tu_0 = 0 - 5 % and $V_0 < 10$ m/s and by Ervine et al. (1997) for Tu = 0 - 8 % and $V_0 < 29$ m/s (see also section 2.8).

[5] Some authors argue that $1.2D_p$ should be considered.

Thus, the equation to be solved in the dimensional analysis is:

$$F(p, H, Q, D, \rho, g, h, D_c, t) = 0 \tag{3.3}$$

where the length of fall L is replaced by the total energy H and the total pool depth Y by h and t.

The Vaschy-Buckingham theorem (also known as the fundamental theorem of Dimensional Analysis) states that any homogeneous relation between n parameters can be replaced by another relation between $(n - p)$ dimensionless numbers, with p being the number of the independent units needed to explain the phenomenon. Since all parameters in Equation 3.3 can be described in the MLT (mass, length, time) system, three units are used. The dimensionless numbers $\prod_i$ are:

$$\prod_i = \frac{A_i}{A_k^{x_i} A_l^{y_i} A_m^{z_i}} \tag{3.4}$$

where A_k, A_l and A_m are three fundamental independent parameters. The parameters ρ, g and D_c are selected. They are described in the MLT system as:

$$[\rho] = [kg/m^3] = [M^1 L^{-3} T^0]$$
$$[g] = [m/s^2] = [M^0 L^1 T^{-2}]$$
$$[D_c] = [m] = [M^0 L^1 T^0]$$

The determinant of the 3 x 3 matrix created with the x, y, z exponents different from zero. Six dimensionless numbers are obtained:

$$\prod_1 = \frac{p}{D_c . \rho . g} \tag{3.5}$$

which is similar to the Euler (Eu) dynamic pressure coefficient if D_c is replaced by H (i.e. same units allow direct replacement). Also:

$$\prod_2 = \frac{Q}{D_c^{5/2} . \sqrt{g}} \tag{3.6}$$

which is a type of Froude number (more evident if D_c is replaced by D). The remaining four numbers are the ratios H/D_c, $\frac{D}{D_c}$, $\frac{h}{D_c}$ and $\frac{t}{D_c}$.

Typically, parameters such as the relative pool depth Y/D, the dynamic pressure coefficients C_p (or E_u), the jet's turbulence intensity Tu_0, and the air concentration C_{air} are used to describe dynamic impact pressures $p(t)$ for given Reynolds (Re), Froude (Fr) and Weber (We) jet propagation conditions.

The parameter $\frac{h}{D}$ (i.e $\frac{Y}{D}$ when h = Y) is used to define the diffusion length in pools with flat bottom. For confined pools, $\frac{H}{D_c}$ and $\frac{h}{D_c}$, however, mix hydrodynamic and geometry-induced processes. Two parameters are selected in this study to describe the interaction between the pool geometry and the diffusion of the jet: (1) $\frac{D}{D_c}$, defining the degree of lateral confinement (DLC); and (2) $\frac{t}{D_c}$ the scour hole (aspect) ratio (SHR).

In addition, the Strouhal number defined as $St = f\mathrm{d}/V$ is considered in the analysis of the turbulent pressure field. The selection of the characteristics length scale d depends on the phenomena being investigated. For instance, Kobus et al. (1979) used the jet diameter D_0 as reference length to study scour geometry, whereas Ervine et al. (1997); Bollaert and Schleiss (2003b) used the pool depth Y to study impact pressures. According to Levi (1995), the length scale d should be related to the scale of the predominant motion.

3.3.3. Idealised impact pressures in laterally confined jet diffusion

Current knowledge on impact pressures and dynamic pressure loads propagating inside rock joints is based on experiments in plunge pools with flat bottoms. In that case, the impinging jet spreads laterally without constraints and depends mainly on the characteristics of the jet and on the travel distance inside the water. The jet core disappears by shear at a depth of about 4 to 6 times the jet diameter D_i at impact with the water cushion (Ervine et al., 1997). Core (compact) jets generate high mean pressures at impact that can lead to crack formation and propagation by hydraulic fracturing (brittle failure). Once the core disappears, the mean pressures at impact decrease (Figure 3.5).

For pools deeper than the core development length, impact pressure present a low mean value and important pressure fluctuations. Bollaert (2002b) showed that pressure fluctuations have sufficient energy to further scour the rock. Pressure fluctuations at the rock interface can generated transient flows inside fissure. Due to the superposition of pressure waves, pressure peaks may exceed the maximum pressure at the entry and lead to crack propagation by (instantaneous) brittle failure. Regular pressure fluctuations can open up cracks by fatigue. Scour in pools with flat bottom is assumed to be driven by mean pressures for core jets and by a combination of mean and fluctuating pressures for developed jets (Bollaert, 2002b; Bollaert and Schleiss, 2005).

Confining diffusion may not only change flow patterns in the pool but also the dynamic character of impacting pressures. Since scour depends on both mean and fluctuating characteristics of impacting pressures, any apparent enhancement, damping or change in energy-carrying frequencies may have significant consequences on the existing "perception" of the rock scour process.

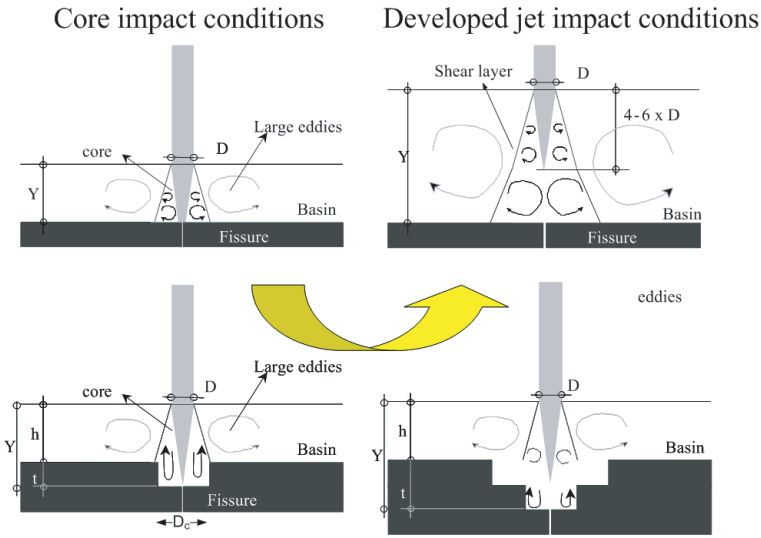

Figure 3.5.: Schematic representation of core (CJ) and developed jets (DJ) for flat bottom plunge pools (top) and expected contribution of a lateral confinement (bottom).

The scour process in real-life plunge pools is likely to follow a sequence of alternating vertical and lateral erosion steps. The hydrodynamic pattern of pool flows and impact pressures are modified accordingly. Once a first scour hole is created, the return currents induced by wall jet reflection on the boundaries may well disturb the falling jet. If scour is narrow, reflected currents may destroy the jet core not by shear diffusion but by direct collision. The empirical reasoning presented in Figure 3.5 shows that confining laterally the diffusion of plunging jets may enhance jet development, at least during the first scour stages.

3.3.4. Pressure measurements in laterally confined pools

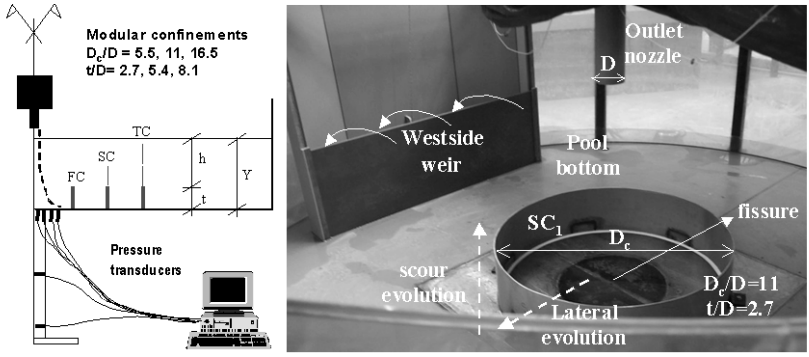

Figure 3.6.: Detailed cross-section and photo of the experimental set-up. Pressure transducers were alternatively set in the pool bottom at radial distances of $y/D = 0.35, 0.69, 1.04, 1.32, 2.08$ and 2.78, and along the closed-end fissure (y = 0) at axial distances from the fissure's entry of $\Delta x/D = 5.56$ (middle) and $\Delta x/D = 11.04$ (end). The confinements were composed by fixing modular cylinders of diameter D_c and height t.

The interaction between the falling jet and pool geometry is studied by means of pressure measurements at the pool bottom, lateral walls and inside a closed-end I-shaped fissure.

Existing plunge pools downstream of large dams do not have a flat bottom and develop into shapes that are directly related to local geological characteristics (Figure 1.3). The experimental study focuses on a limited number of pool geometries that should allow identifying the most important flow features.

A modular system of steel cylinders with different heights t and diameters D_c ("c" stands for confinement) was conceived that allows simulating lateral and depthwise growth of symmetrical scour holes - Figure 3.6. Three different lateral confinement conditions D_c are simulated, which correspond to 5.5, 11 and 16.5 times the diameter of the jet at issuance D. The confinement is created by 20, 40 and 60 cm high cylinders, used separately, fixed to the pool bottom. The cylinders have 40, 80 and 120 cm of diameter respectively. The height (i.e. depth) of scour and the distance of the confinement to the jet axis were selected to be of the same order of magnitude as the jet diameter and typical rock block dimensions.

First, the effect of a changing confinement diameter is studied, for a constant scour depth $t = Y - h = 2.8D$, h being the pool depth above the initial riverbed level. They simulate a first step of scour depth t.

Table 3.5.: Test conditions for flat bottom pools (FB) and lateral confinements D_c/D of 5.5 (FC), 11 (SC) and 16.5 (TC).

Tests	Y [m]	Y/D [-]	D_c/D [-]	t [m]	t/D [-]	t/D_c [-]
Flat bottom (FB 0,1,2,3)	0.075-0.82	1.0-11.4	infinity	-	-	
First cylinder (FC 1/2)	0.20 -0.87	2.8-12.1	5.6	0.20	2.8	0.50
Second cylinder (SC 1/2)	0.20 -0.82	2.8-11.4	11	0.20	2.8	0.25
Second cylinder (SC3)	0.40 -0.82	5.6-11.4	11	0.40	5.6	0.50
Third cylinder (TC1)	0.20 -0.82	2.8-11.4	16.7	0.20	2.8	0.17
Third cylinder (TC2)	0.40 -0.82	5.6-11.4	16.7	0.40	5.6	0.33
Third cylinder (TC3)	0.60 -0.82	8.3-11.4	16.7	0.60	8.3	0.50
Combined I (FS)	0.40 -0.82	5.6-11.4	5.6-11	0.40	5.6	0.50-1.0, conical
Combined II (FST)	0.60 -0.82	8.3-11.4	5.6-16.7	0.60	8.3	0.17-1.5, conical

Second, the influence of an increasing scour depth is investigated using cylinders of different heights corresponding to $t/D = 2.8$, 5.6 (for $D_c/D = 11$) and also 8.3 (only for $D_c/D = 16.7$). Finally, the existing cylindrical modules are combined to create conical stepped pools, the smallest having $t/D = 5.6$ and $D_c/D = 11$ ("combined FS"), and the largest $t/D = 8.3$ and $D_c/D = 16.7$ ("combined FST").

These combinations allow testing nine different pool geometries, including the flat bottom surface used as a reference. The bottom of the pool on the leeside of the cylinders was not raised up to the top level of the cylinders since the volume of water in this region hardly contributes to pool dynamics. The FC geometry is of particular interest for analysis; it is often named "narrow pool".

Approximately 1100 tests were performed with the nine geometries, for varying jet velocity V, initial pool depth h, and number and position of pressure transducers. The characteristics of these tests are summarised in Table 3.5. The geometries tested are presented in Table 3.6. A schematic representation of the geometries with the total number of transducers and their position is presented in Appendix B. For some tests, one pressure transducer was flush-mounted on the lateral wall of such confinement to measure dynamic pressure resulting from bottom wall jet impact. The names of the data files follow are standardized according: name of pool test series, weir height, flow discharge and run number, for example: 1FB with Y = 0.40 cm and Q = 100 l/s, the file for the run No.1 is 1FB040Q100-1-ASCII.txt.

Table 3.6.: Tested pool geometries in terms of relative scour depth t/D and relative confinement ratio D_c/D

	t/D			
D_c/D	> 2.8	> 5.6	> 8.3	> 1.0
5.6 (Narrow)	FC1/FC2			
11.1 (Intermediate)	SC1/SC2	SC3		
16.7 (Wide)	TC1	TC2	TC3	
20.8 (∞)				FB1,FB2,FB3
combined		FS	FST	

3.3.5. Pressure measurements inside a closed-end fissure

The rock fissure is simulated placing a thin (1 mm thickness) metallic sheet in between two main steel plates. A closed-end fissure is used (Figure 3.7). Its simple geometry and surface

smoothness produce friction losses that are of minor importance when compared to the energy losses generated by the superposition of pressure fluctuations in a compressible air-water mixture. The fissure was regularly drained and vacuumed in running water conditions in order to assure that it was completely full with water. The transducer at the lowest position was screwed off for this operation and then screwed back in against running water. This operation was repeated at the beginning of each test session and whenever the opening of the fissure was not submerged.

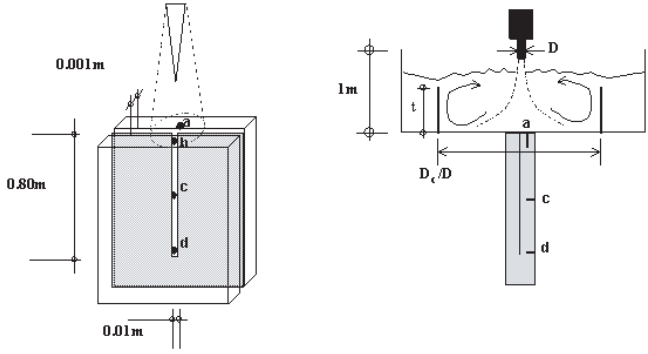

Figure 3.7.: Schematic representations of the closed-end fissure and corresponding measuring points: a) pool bottom, 25 mm from the jet axis, c) inside fissure, 0.40 m below pool bottom (middle point), d) inside fissure, 0.795 cm from the surface (end point).

3.3.6. Transducers for dynamic pressure measurements

For pressure measurements at the pool bottom, a maximum of six transducers type ©KULITE $XTM-190-17BAR-A$ (3 mm diameter diaphragm, details in Table 3.7) were flush-mounted on the pool bottom and along the closed-end fissure.

Table 3.7.: Characteristics of micro pressure transducers from KULITE type XTM-190M-17BAR-A

Pressure range (FSO)	0-17	bar absolute
Over presure	35	bar absolute
Non-linearity and hysteresis	± 1%	FSO
Output	75	mV at full scale
Resonance frequency	425	kHz
Working frequency range	0-15	kHz
Temperature drift	± 1%	of full scale per 55° C

The XTM-190 miniature pressure transducer utilizes a metal diaphragm as a force collector with a piezoresistive sensor as its sensing element. Whereas the previously used XTL transducer incorporated a fully active four arm Wheatsone Bridge dielectrically isolated on a silicon-on-silicon diaphragm, the XTM have a metallic diaphragm mounted on an equivalent basis. XTL transducer presented a high failure rate. XTM are apparently more robust. According to the supplier, they are specifically packaged to perform pressure measurement in severe environments. Only one out of six transducers failed over 2 years of tests ($>$ 400 hours of exposure).

This second group of pressure transducers allows obtaining readings with a potential combined non-linearity, hysteresis and repeatability (CNL&H) of ± 1 % of the full-scale output (FSO = 17 bar A), i.e. max. 0.17 bar ≈ 1.7 m. The reference zero may shift by ± 2 % FSO, i.e. max 3.4 m. It did not did not exceed 1.5 m during an extended 24-hour check run. The conversion from volt to bar is made using a linear calibration equation of type $y = m.x + b$. The supplier's sensitivity (m) was double-checked to take into account the differences in tension used by the acquisition cards. The supplier's electrical excitation was rated 10 VDC to a maximum of 15 VDC, and the used acquisition cards had 11.77 and 11.89 VDC respectively.

Calibration was performed at the Laboratory of Hydraulic Machinery (LMH-EPFL) by comparing the relative pressure readings provided by the data acquisition system (DAQ) with those of a reference (HUBER) transducer for increasing-decreasing static pressure levels. The sensitivities of the transducers were corrected by maximum 0.009. The maximum difference between predictions using the supplier's sensitivity or the corrected ones was ± 0.02 bar. The offset of the calibration curve (b) was continuously updated, performing measurements of the local atmospheric pressure and relating these with hourly measurements provided by the Swiss Meteorological Service.

These transducers have a diameter larger than the Kolmogorov length scale in the pool, estimated in less than 5 mm (reference size of the smallest air bubbles found in the pool, see Chapter 7 and indicative thickness of the bottom boundary layer). They were spaced on the pool bottom every 20 - 25 mm, which is larger than the spacing recommended by Löfdahl and Gad-el Hak (1999) of 3 to 5 times the Kolmogorov scale for a good resolution of the smaller scales. Averaging of scales smaller than the transducer is done and the corresponding energy is counted in the mean field.

3.3.7. Data acquisition system for dynamic pressure measurements

The hardware system and the acquisition system were developed at the Laboratory of Hydraulic Machinery (LMH-EPFL). The hardware system comprises a DAQ module (Figure 3.8) that contains an 8-channel platform of two A/D cards of 4 channels each. The DAQ system allows pre-amplification of the signal, as well as lowpass filtering. The analog filter is a 5^{th} order low-pass filter of the Bessel kind (excluding all frequencies higher than a given cutoff frequency f_c), by means of a jumper selectable at 60, 120, 234, 469, 938, 1875, 3750 and 7500 Hz. The output signal is filtered at ± 10 V maximum. The alimentation is simultaneous for the 4 channels of each card (± 12 VDC or 160 mA, tolerance ± 5 V).

During 2003, both the hardware and the software systems were upgraded and gained in efficiency and conviviality. The hardware system comprises two multiple entry acquisition cards for A/D conversion, a hardware lowpass filter and a PCI ARCNET card for data storage on a Pentium III PC. The conversion of the signal from analog to digital is made at 14 bits (± 10 V) with a 1.22 mV/bit sensitivity. One card is master and the other slave, but acquisition is simultaneous. In terms of memory, a maximum of about 4Mb, or 65536 data per channel times 8 channels can be stored in a single file. Output files can be either ASCII or binary. Transfer and storage take about twice the time of the measurement duration (i.e. total 3 min runtime for 1 min of sampled data).

The acquisition software was prepared in the ©LabView environment and allows operation of multiple cards, automatic acquisition of multiple runs, visualization of the signal and of primary statistics. It is readily available as an autonomous application (.exe file) and runs

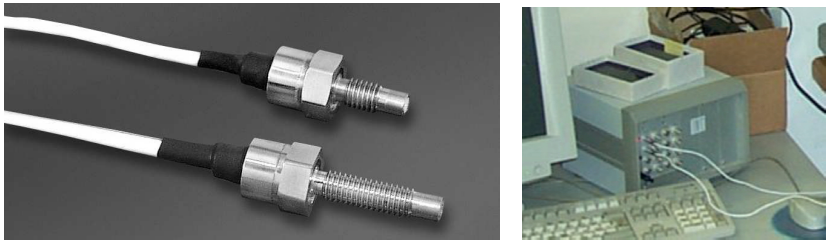

Figure 3.8.: Left: XT-190 micro-pressure transducers (the longest one was used, L =19.3 mm); Right: DAQ module containing the two cards, the lowpass filter and the amplification selectors.

in Windows 2000. The software allows defining a value offset from +5 V to -5 V, as well as a gain (amplification by simple product) of 1, 2, 4 and 8 per channel to improve the visualization of the signal. The acquisition rate can be set between 100 Hz and 20 000 Hz per channel. The parameters of the calibration curves (i.e volts-bar) can be included and basic statistics of the ongoing runs (mean, RMS, maxima and minima values) observed. This allows for fast screening of the data. The latest version of the acquisition software allows performing multiple acquisition automatically and saves them in individual 4Mb ASCII files or lighter Binary files.

The pressure signal at the pool bottom and inside the fissure was sampled at 1 kHz for a maximum of 65536 points during each run (approx. 65 s). Control runs at 10 and 20 kHz were performed regularly to verify appropriate recording of extreme values. The acquisition system allows sampling at a maximum frequency of 20 kHz, the signal being conditioned by a lowpass hardware filter set at the corresponding Nyquist frequency but maximum 7.5 kHz.

3.3.8. Error margins of dynamic pressure measurements

The combination of error sources is relevant for the assessment of absolute pressure statistics like the mean, maxima and minima. Inaccuracy margins were estimated as: ±0.04 mwc for the tailwater level during tests, ±0.3 mwc for the variation of the atmospheric pressure during the tests (12 h period), ±1.5 mwc due to the transducer's zero drift, ±1.7 mwc due to the CNL&H, and ±0.2 mwc due to eventual differences in the transducer's sensitivity. The combination of these values leads to an average error margin of 4 mwc (0.4 bar) for pressure measurements. This corresponds to 80 % of the incoming energy for V = 9.8 m/s and about 9 % for V = 30 m/s.

Due to a 1 % flowmeter error margin, an additional error of ±2% in terms of the estimated issuance kinetic energy should also be considered. The error margins mentioned above are a highly unfavourable and unlikely cumulation of all error sources. Nevertheless, they show that dynamic pressure measurements can vary significantly. This should be kept in mind when comparing data from different experimental campaigns and authors. The estimates of mean pressure may therefore present considerable error margins, which decrease with increasing jet velocity.

Estimates of turbulent pressure fluctuations p' like the RMS value and the maximum and minimum extreme fluctuations p'^{+} and p'^{-} are less affected by these sources of error. These

statistics are differences between individual pressure values and the mean value, obtained during ergodic runs. For individual runs, the error in absolute pressure measurements can be assumed consistent and therefore not reflected in the statistics of p'.

Only one reference of the error margins of dynamic pressure measurements was found. Gilard and Brizzi (2005) performed dynamic pressure measurements at the impact of laminar and smooth turbulent air jets with a curved surface. A digital micro-manometer was used and wall pressures were sampled at 0.5 kHz. The precision of the manometer was 1 % FSO and the error margin of the measurements was estimated in about 15 % of C_p values.

3.3.9. Additional experimental features

The flowmeter installed in the pumping circuit was calibrated several times. For that purpose a calibration tank with a known volume-level curve was used and measurements were performed for different time intervals and flow discharges. This allowed obtaining calibration curves to correlate observations with the automatic readings provided. Correlation factors were always higher than $R^2 = 0.999$.

Since the previously used pressure transducers XTL-190 had presented a high rate of failure, a comparison between these and one test transducer XTM-190 was performed before command of new ones. The comparison comprised analysis of pressure statistics and power spectra at the pool bottom.

Several tests were object of photo and video recordings. With the flat bottom, there is little visibility in the pool due to the large amount of air entrained by the jet. For some of the confined pool configurations tested, less air is entrained. This allows for the observation of typical flow features. Several attempts were made to improve visualization of such flow patterns using injected dye and pressurized air, as well as stroboscope video recordings. These topics are described in detail in section 9.2.

3.4. Experimental investigation of air bubble behaviour inside limited-depth plunge pools

3.4.1. Air-water measurements

The first studies of air entrainment by plunging jets concerned the estimation of the amount of air entrained and of the depth of bubble penetration D_p (Henderson et al., 1970; McKeogh and Ervine, 1981; Sene, 1988; Bín, 1984, 1993). More recently, the local air concentration and flow velocity at the vicinity of the plunging point has been addressed by several authors (Bonetto and Lahey Jr, 1993; Bohrer et al., 1998; Chanson et al., 2004). However, there has been limited research in limited-depth pools. Figure 3.9 illustrates the differences in pool aeration in the case of free jet diffusion compared to bounded jet diffusion in the laboratory.

McKeogh and Elsawy (1980) focused on the amount of air entrained in bounded jet diffusion conditions comparatively to free jet diffusion using the air hood volumetric method. Observations in a laboratory installation in fully controlled aeration conditions have shown that increasing air content in the pool reduces mean pressures at the pool bottom Melo (2001, 2002b). However, it also increases RMS values as well as positive and negative extreme

Figure 3.9.: Left: free jet diffusion (Chanson et al., 2004), D = 12.5 mm, V = 3.3 m/s, freshwater (courtesy of Dr Hubert CHANSON); Right: Plunging jet diffusion in a flat shallow pool, D = 72 mm, Y/D =5.6, V = 20 m/s.

pressure fluctuations (Melo, 2001). The likelihood that air bubbles may enter rock fissures, thus reducing pressure wave celerity inside fissures is still an open topic of discussion.

The present experimental investigation has two purposes: contribute to the understanding of the behaviour of air bubble in depth-limited plunge pools and, while doing so, test the adequacy of optic-probes for air-water measurements in pool flows. The exploratory character of such tests should be stressed. Measurements in highly turbulent regions of the pool are performed using advanced instrumentation in unprecedented conditions of turbulence and velocity[6]. The measurements aim at comparing air-water flow characteristics between pool regions with important pressure gradients, namely close to the pool bottom. The influence that jet streamline deflection at the pool bottom has on aeration is discussed.

3.4.2. Double-fibre optic probe for air-water measurements

A double fibre-optical probe has been used to measure air concentration and velocity. The probe was developed by RBI Instrumentation, Meylan, in France. The measuring system comprises three components: the probe, the optoelectronic module and the computer interface board. The measuring principle is based on the different *refraction* indices of the air and the water. Emitted light hitting the sensitive tip surface is refracted when liquid surrounds the tip and is reflected when gas is present (Figure 3.10). A detailed description of the probe tip can be found in Cartellier and Achard (1991). The interfaces between air bubbles and water can be identified. The optic fibre tips have minimum diameters of 20 μm. The probe includes a light guide and a sensitive cone-shaped tip. It can withstand pressures up to 5 bar and temperatures up to 80° C. According to Cartellier and Achard (1991) successful tests have been performed in water with velocities up to 20 m/s.

A specific optoelectronic module emits light through two optical fibres connected to the two probe tips located in the flow and converts the optical signal (i.e the quantity of light

[6]To the author knowledge, air-water measurements with velocities higher than 10 m/s have only been investigated by Henderson et al. (1970) to estimate the air entrainment rate in free diffusion conditions.

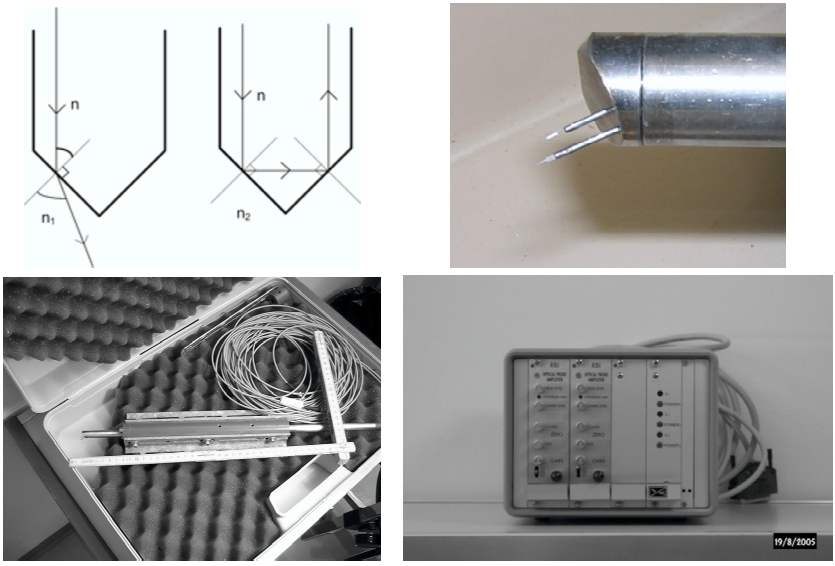

Figure 3.10.: Top, left: definition of refraction (n_1) and reflection (n_2) angles. Top, right: detail of probe tips, distance between tips is $\Delta x = 2.5$ mm. Bottom, left: double-fibre optical probe with specific set-up to fix at the pool bottom. Bottom, right: optoelectronic module for optic signal emission, conversion to digital signal with thresholds and transfer to output files.

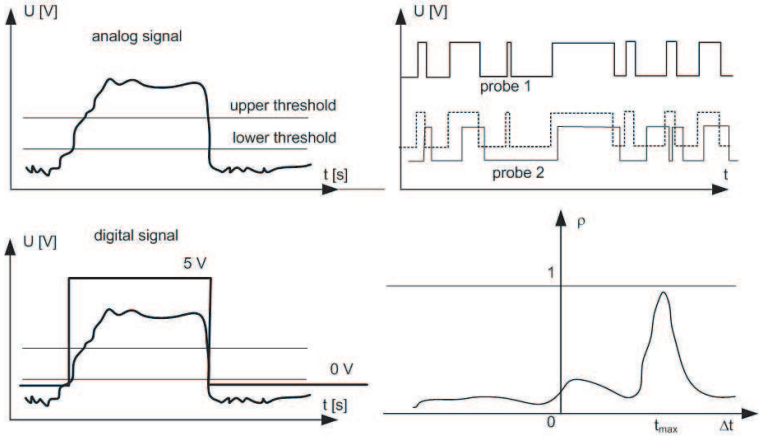

Figure 3.11.: Left: transfer of analog into digital signal for a single probe. Right, top: schematic of the signals at the two tips, probe 2 shifted; bottom; bottom: results of time-spatial cross-correlation between both signals (adapted from RBI 1999, Boes and Hager (1998)).

reflected) into an electrical signal by means of a photosensitive diode. Detailed information on the electronic components, signal handling and data processing can be found in the supplier's manual (RBI, 1999).

3.4.3. Signal processing principle

Signal amplification by the optoelectronic module and threshold selection of the raw analogue signal results in a digital Transistor-Transistor-Logic (TTL) signal, corresponding to the air or water phases in the vicinity of the probe tip (Figure 3.11). Two thresholds must be set on the optoelectronic module, in order to define which part of the signal is considered as water and air respectively. When the raw signal rises above the upper threshold, it is transferred into a digital signal of 5 V (gas phase) until it falls under the lower threshold, where the digital signal returns to 0 V (liquid phase). An oscilloscope can be connected to the analogue BNC port of the opto-electronic module for visual signal control. The digital signals are transferred to the interface board. The response time of the double fibre-optical probe is 0.033 μs and the data was collected at sampling frequency ranging between 0.5 and 1 MHz. The threshold values are set at 1.5 and 2.5 V.

3.4.4. Data processing

The void fraction C is the proportion of time that the probe tip is in the air. It is defined as the time fraction or percent of air in flowing water by volume (Figure 3.12):

$$C_{air} = \frac{1}{T} \sum_{i=1}^{N} \Delta\tau_i \tag{3.7}$$

The void fraction is a local average. A preliminary analysis to set the adequate acquisition duration to obtain ergodic results of the void fraction was performed and is presented in Chapter 7. Air concentrations can be obtained in both probe tips. Only the value of the leading probe tip is herein considered since the intrusion of the leading probe may reduce the accuracy of the trailing probe tip data.

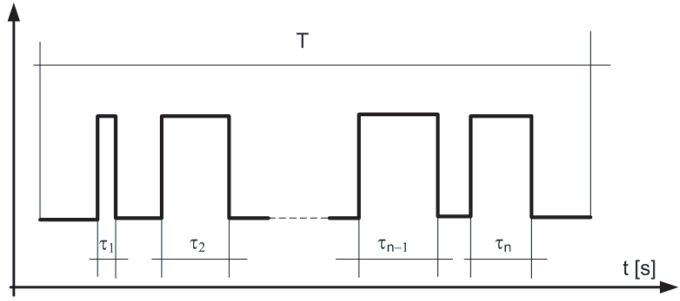

Figure 3.12.: Typical TTL output signal and definition of gaseous time intervals

The estimation of the interfacial velocity is made possible by the use of two tips, placed at a known distance. The local air-water velocity is given by:

$$V_{aw} = \frac{\Delta x}{\tau_{\rho_{max}}} \tag{3.8}$$

where τ results from a cross-correlation analysis of the measurements at both tips. The principle of determination consists in recognising the similarity of probe signal spaced of a given time lag τ. It assumes that a given bubble passes at both tips. This is likely to happen when the flow is unidirectional and well aligned with the tips, during the acquisition interval. The time interval τ is the most likely time of travel between the two tips. According to Matos et al. (2002), this technique assumes that bubbles and droplets are not significantly affected by the leading tip. In ideal conditions, the two signals would be identical but separated by a time delay. In practice they differ because the leading probe disturbs slightly the flow.

The distance between tips should not be very large to assure that the same bubble passes through both tips. This however is difficult to verify in two-phase turbulent flows. As an order of magnitude, Cain and Wood (1981) suggested that Δx should not be larger than 10 bubble diameters. In this case, it means that bubbles with less than 0.25 mm of diameter may not be accurately accounted for. The correlation process constitutes thus a mathematical tool that replaces physical evidence.

The correlation consists on shifting the signal of the second probe of a given Δt::

$$R(x, \Delta x, \tau) = \lim_{T \to \infty} \int_0^T V_1(x,t).V_2(x + \Delta x, t + \tau)dt \tag{3.9}$$

The normalised correlation between the two signals is computed according to:

$$\rho(x, \Delta x, \tau) = \frac{\widehat{R}(x, \Delta x, \tau)}{\sqrt{\sigma_1^2.\sigma_2^2}} \tag{3.10}$$

A correlation function is thus obtained for different time lags. The time lag $\tau_{\rho_{max}}$ corresponding to the maximum correlation is retained for the computation of the interfacial velocity.

The bubble count rate F is the number of bubbles impacting the probe tip. The bubble chord time τ_{ch} is defined as the residence time of the bubble on the probe tip. It is often assumed that the bubbles are spherical (Cartellier and Achard, 1991).

When multiplying the bubble (or droplet) cord time by the estimated interfacial velocity, characteristic bubble cord lengths are obtained. Histograms of cord lengths can thus be plotted, allowing to estimate the dominant bubble length range.

$$L_i = T_i.V_{aw} \tag{3.11}$$

Another estimate of the bubble size is obtained by computing the characteristic Sauter diameter by:

$$d_{Sauter} = \frac{6.C}{\gamma} \tag{3.12}$$

where γ is the specific air-water interface area given by:

$$\gamma = \frac{4.F}{V_{aw}} \tag{3.13}$$

The cumulated statistics presented above can be obtained for each individual run with the acquisition and data treatment software VIN 2.0 by RBI. This software is presented as a closed source application and it does not allow direct access to the raw signals. Post-processing of the standartised output files was undertaken for extraction of only the necessary statistics, by means of routines programmed in ©MatLab and ©VisualBasic for the analysis of multiple runs.

This type of instrumentation was been intensively used over the last decade mainly for research over stepped spillway chutes (Boes, 2000; Matos et al., 2002; André, 2004; Renna et al., 2005) and in conditions where flow streamlines are rather straight and perpendicular to the probe tips. An eventual misalignment of the tips with flow streamlines tends to reduce the cross-correlation values used for the estimation of interfacial velocities. RBI suggests that for correlation values below 0.7 the signals are "rather badly correlated" and that the information passing on the first tip does not necessarily pass through the second one. Matos et al. (2002); André (2004) compared air-water flow measurements in stepped chutes using double-fibre optic probes, back-flushing pitot tubes and acoustic doppler velocity meter (ADV). They observed that the velocity estimates obtained with the optic probe where flow curvature was more pronounced were somewhat off-trend. The difference was assumed to depend from misalignment of the probe tips compared with flow direction. Based on experimental measurements and observations of flow pattern, André (2004) suggests that the threshold value for acceptance of relevant interfacial velocity results should be rather 0.5 than 0.7 whenever some misalignment between the streamline and the tips is expected. Assuming values lower than 0.7, may be a valid means of obtaining proper information of flow characteristics as indicated by Matos et al. (2002) and André (2004).

3.4.5. List of experimental tests for air-water measurements

Three measuring points were selected inside the pool, in the impinging zone (measuring point 1, MP1), in the wall jet region (MP2) and in the plunging jet region (MP3). The measuring points are presented in Figure 3.13.

First, measurements were performed very close to the pool bottom under the jet axis. The probe was fixed directly to the pool bottom, with the tips aligned vertically and at less than 2 cm of vertical distance from the entry of the fissure.

The second measuring point was set in the wall jet region, 10 cm aside the jet axis. The probe was rotated 90° to align the tips horizontally.

The third measuring point is in the plunging jet region. The probe was elevated at 10 cm from the bottom and placed over a rigidified structure to reduce eventual vibration. The probe tips were aligned vertically and along the plunging jet axis.

A list of the test performed is presented in Table 3.8. Different acquisition times were set in order to compare estimations of the parameters under investigation. The results are presented and discussed in Chapter 7.

Check runs were performed to evaluate the variability of void fraction estimates. The thresholds were never set less than 0.6 V apart. For lower thresholds between 1.0 and 2.0 V, and upper thresholds between 2.0 and 2.6 V, bubble count rates varied less than 5 % and less than 2 % for the lowest and highest velocities tested, respectively.

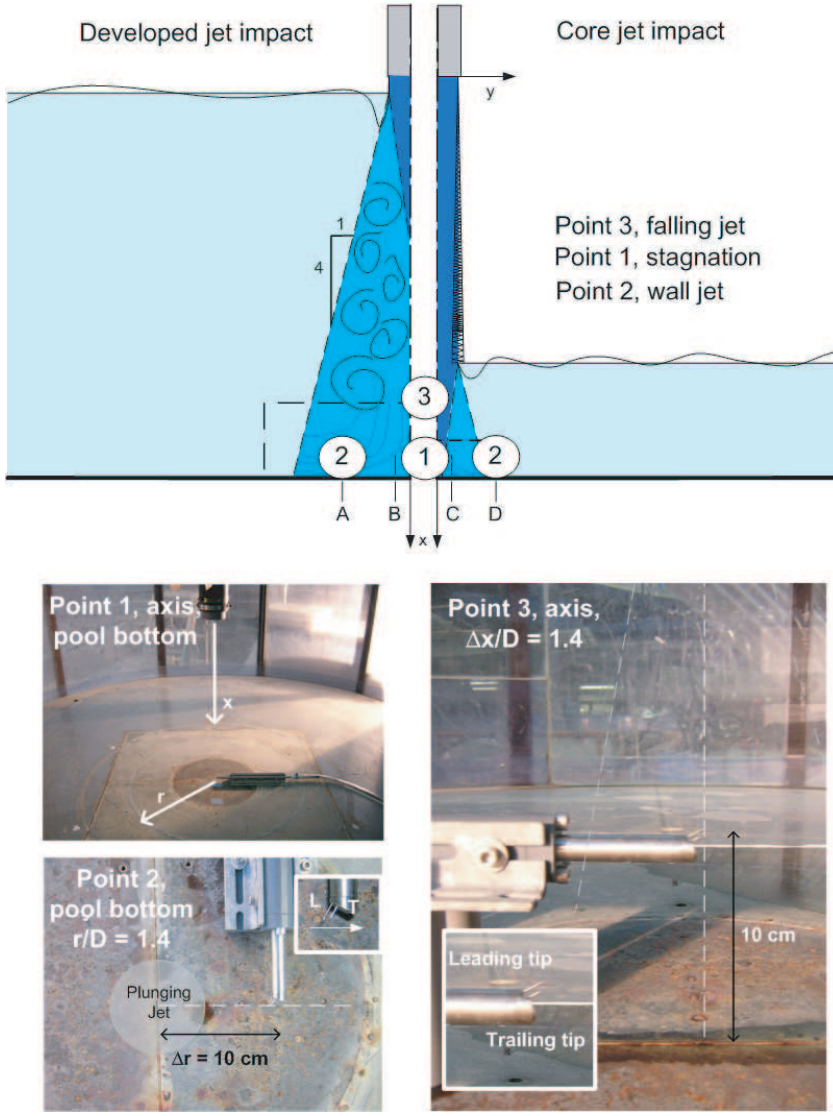

Figure 3.13.: Top: Measuring points for variable pool depths. Bottom: probe set-up used to fix the probe at the three measuring points.

Table 3.8.: List of experimental runs. Y is the pool depth.

Measuring point	Y [m]	Velocities [m/s]	Runs per V	Duration [s]	Number of bubbles
1, stagnation	trial tests	6.1 - 17.2	-	6, 60, 300	3000 - 100'000
	0.67	6.1 - 19.7	60, 1, 5	5, 60, <1	220 - 7450
	0.40	6.1 - 20.9	60, 30	5	900 - 5200
	0.30	6.1 - 19.7	60, 30, 10	5	1000 - 5450
	0.20	6.1 - 22.1	10	5	560 - 5700
		9.8	1	24.7	9110
2, wall jet	0.20	6.1 - 22.1	10	5	210-10'000
		6.1 - 22.1	1, 2 ,3	60 - 8.9	10'000
	0.40	6.1 - 24.6	10	5	800 - 6450
		6.1 - 24.6	1	60	13'000 - 64'000
	0.67	6.1 - 24.6	10	5	300 - 10'000
		7.4 - 24.6	3	60	8'000 - 10'000
3, falling jet	0.20	6.1 - 22.1	10	5	700 - 10'700
		6.1 - 22.1	3	60 - 37.5	14'000 - 70'000
	0.40	6.1 - 29.5	10	5	1000 - 16'000
		6.1 - 24.6	3	60- 33.5	3'500 - 72'000
	0.67	6.1 - 24.6	10	5	750 - 10'000
		6.1 - 24.6	3	60 - 37	8'000 - 64'000

3.5. Scale effects

Free surface flows are studied under Froude dynamic similarity. The facility produces very high velocity jets that can be considered prototype velocities and, pressure, inertia and gravity forces are correctly accounted for. Assuming the viscosities of both the liquid phase (water) and gas phase (air) as representative of prototype conditions, Reynolds similarity is also complied with.

The deformation of the jet in the air, however, is also depending on the Weber number. Weber similarity law is complied with, up to the point where the liquid phase characteristics (tap sweet water) are not fully representative of real-life problems, i.e. water with different densities, particles in suspension, viscosity, temperature and surface tension. However, at the present stage of research, this is considered of secondary importance. Recent studies on scale effects in air-water flows in stepped chutes concluded that surface tension and viscosity effect are well accounted for if the Weber number is higher than 100, and the Reynolds number is higher than 10^5 (Boes, 2000). These statements are considered valid for the present experimental work and pool aeration may be assumed to be exempted from scale effects.

The geometry of the basin can be seen as a distortion of the equivalent reality, since the jet diameter is relatively small compared with prototype structures. Therefore, all spatial turbulence features (large vortices, integral scales, etc.) are characteristic of this facility and cannot be used as prototype references. Dimensionless ratios may be explored. The most common length scales for dynamic similarity of the jet diffusion process are the jet diameter D or the jet thickness B, for circular and plane jets respectively. For instance, considering D as representative of the jet's smallest dimension allows studying jet diffusion as function of relative pool depths in the present facility. Pool flow interpretation is possible in radial planes of the pool.

Studying the behaviour of air bubbles under high-pressure gradients is unprecedented. This

raises several questions relatively to compressibility of air bubbles and slip between the liquid and gas phases.

Under a plunging jet, there is hardly slip between the two phases. Away from the jet, where bubbles ascend in an almost quiescent liquid (e.g. very large pools and low velocities) slip between air and water is important. In free jet diffusion, slip can be said to gain importance as soon as the velocity of air bubbles becomes lower than that of water droplets. This occurs close to the maximum depth of bubble penetration D_p. In pools with $Y < D_p$, it is not yet clear whether slip/no slip conditions are relevant for jet diffusion. This topic is considered of secondary importance for the present study and is not discussed further.

Buoyancy is also related with the size of the air bubbles. The larger the bubbles the larger the contribution of buoyancy forces to flow motion. The size of the bubbles is directly related with the entrainment velocity and with local pressure. However, since most previous studies of air-water flows have been performed for channel flows in laboratory, pressure gradients have hardly been a few dozen cm (i.e. maximum 0.2-0.3 m). In such circumstances, the compressibility of the fluid does not play a significant role in enhancing or hindering turbulence. Since the present study deals with pressure gradients up to 3 bar close to stagnation, the possibility that air bubbles may vary in volume cannot be ruled out *a priori*. Eventual compressibility of air bubbles in near-prototype high-velocity jet experiments is discussed in Chapter 7.

4. Evaluation of jet issuance characteristics as a basis for rock scour analysis

This chapter provides insight on turbulence intensity and velocity distribution at jet issuance (Figure 4.1) by presenting results of extensive systematic experiments with jets at near prototype velocities. Sound insight is obtained on the influence of upstream approach flow conditions, including aeration and outlet geometry. At the end, a summary of issuance characteristics for the most encountered hydraulic structures is presented, compiling information from both experimental tests and literature.

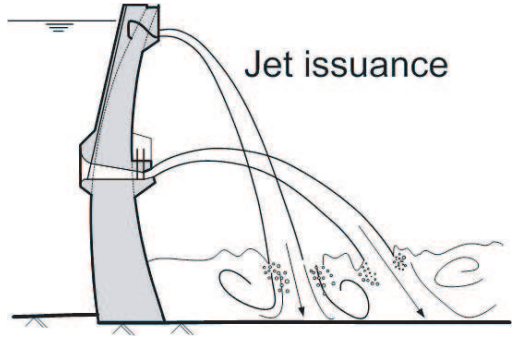

Figure 4.1.: Issuance conditions of high-velocity jets in dams: a key element for the definition of jet behaviour in the air and in the plunge pool.

4.1. The importance of jet issuance characteristics for jet development and for the definition of impact pressures

Appurtenant[1] structures of dams used for flood control and/or reservoir management make often use of plunging jets. The energy of these high-velocity jets is generally dissipated in natural or concrete lined plunge pools. The hydrodynamic loading produced by jet impact on the plunge pool bottom directly influences its design. This loading is governed by jet issuance characteristics, jet deformation in the air and jet diffusion through the downstream water cushion (Hartung and Häusler, 1973). For both natural and man-made plunge pools, it is necessary to ensure that scour or concrete slab damage due to jet impact does not endanger

[1] This chapter is based on the scientific manuscript Manso et al. (2005b) submitted to the Journal of Hydraulic Research in April 2005.

the foundation of the dam and its abutments. Design of plunge pools is traditionally based on physical model testing and assessment of ultimate scour from empirical formulae (Schleiss, 2002). Step-by-step modelling of scour evolution, however, is of increasing importance in practice. To evaluate the spatial and time evolution of scour, as well as the efficiency of counter-measures, key information such as the **issuance conditions** and the corresponding **hydrodynamic loading at the water-rock interface** for different types of jets, tailwater levels and pool geometries are required. Bollaert (2004) and Bollaert and Schleiss (2005) developed a physically based engineering model for evaluation of plunge pool scour as a function of time. This model points out the importance of the characteristics of plunging jets on scour formation. Recently, Manso, Bollaert and Schleiss (2004b,a) presented experimental evidence of the reduction of mean and fluctuating pressures transmitted to the rock due to the lateral confinement of jet diffusion in the pool, compared to flat pools (in Chapter 8 of this dissertation).

The hydrodynamic characteristics of the jet at impact with the downstream water cushion are closely related to jet issuance conditions. They define jet deformation in the air in terms of spreading and break-up (Ervine and Falvey, 1987; Zaman, 1999; Burattini et al., 2004). Jet behaviour in the air depends mainly on mean jet velocity, air drag and initial jet geometry. These parameters allow estimating the mean trajectory and impact energy, but do not account for the jet deformation needed to assess the impact area. Ervine and Falvey (1987) studied the mechanisms of jet spreading and break-up in the air and jet diffusion in the plunge pool. They found that the key parameter governing jet deformation in the air is the initial turbulence intensity Tu of the jet. Turbulence intensity is defined as:

$$Tu = u'/U \tag{4.1}$$

where u' is the root-mean-square (RMS) value of the axial velocity fluctuations and U is the mean axial velocity. It defines the rate of increase of the jet outer limits and the rate of core contraction by respectively outward and inward development of surface disturbances. The degree of break-up is directly related to the size of the core of the jet at impact. The extent of the outer limits of the jet delimitates the zone at impact that is subjected directly to fluctuating pressures. For practice, a compromise is needed between increasing the throw distance (which means keeping the jet as compact as possible) and increasing the wetted impact area (which means enhancing spreading). Rouse et al. (1951) dealt with a similar dilemma for fire monitors and nozzles. By performing systematic experiments, they highlighted the importance of controlling the initial turbulence of the flow. More recently, Zaman (1999) assessed jet spreading from nozzles of various geometries for jet Mach numbers ranging from 0.3 to 2.0. Zaman (1999) concluded that rectangular jets deform similarly to circular ones for length/width ratios up to 10, except when issuance conditions are significantly changed by inclusion of protrusions at the outlet section.

Issuance conditions also influence jet diffusion inside the water cushion downstream, especially in the case of undeveloped jets at impact with the pool. Jet core diffusion depends on both jet velocity and turbulence at impact (McKeogh and Elsawy, 1980; McKeogh and Ervine, 1981), which are closely related to the issuance conditions and the travel distance. The higher the turbulence intensity at impact, the shorter will be the development length of the core. If no core remains at impact with the pool bottom, a fully turbulent two-phase shear layer impacts the bottom, generating significant pressure fluctuations. In the opposite case, when a core persists at impact, it generates high quasi-steady pressure on the bottom. A turbulent shear layer impacts more radially outwards with large pressure fluctuations. For pools with flat bottom, the shear layer can freely develop laterally. In confined pools,

the geometry is expected to interfere with the development of the jet core and shear layer. Therefore, one can say that the turbulent shear flow in the plunge pool depends on jet turbulence intensity at impact, pool water depth and pool geometry.

Real-life jets and plunge pools may generate hydrodynamic loadings that significantly differ from those obtained from theoretical models based on ballistic jet trajectory and 2D jet diffusion in an unbounded medium at rest. Single-point measurements of Tu have been obtained by McKeogh and Elsawy (1980); Ervine and Falvey (1987); May and Willoughby (1991) for velocities lower than 10 m/s and by Ervine et al. (1997); Bollaert (2002b) for velocities up to 30 m/s. They used different instrumentation and velocity ranges. However, these authors do not explicitly account for the shape of the velocity profile at issuance nor for eventual influences of upstream supply conditions. Recently, Burattini et al. (2004) studied horizontal air jets with velocities up to 12 m/s and radial Tu values of about 2 % and up to 20 % without and with a large meshed grid, respectively. Small mesh grids were reported to reduce jet instability, decrease radial growth and extend the potential core length. Some of their conclusions may be valid for vertical water jets but need experimental validation.

No prototype information on jet initial Tu is available[2]. The velocity profile at jet issuance is often assumed uniform. Nevertheless, by assuming a fully developed turbulent profile rather than a uniform one, an increase of 10 to 20 % of the maximum impact energy that can be transferred to the rock mass is obtained. The latter assumption seems realistic under prototype conditions and substantially increases the jet's erosion potential during the early stages of scour, comparing to the former assumption.

4.2. Jet issuance experiments in near-prototype conditions

4.2.1. Experimental set-up and test conditions

The experimental installation and instrumentation used are described in Section 3.2 of this dissertation. The experimental data is processed by means ©Matlab routines for volt-bar conversion, computation of local mean velocity, RMS value of presssure fluctuations p', conversion to velocity fluctuations, turbulence intensity computation, a.s.o., for each discharge tested and for each measuring position investigated.

4.2.2. Mean and fluctuating velocity distributions

The jets being rather compact at issuance, the pressure transducers measure a highly efficient conversion of kinetic energy head into piezometric head. The velocity fluctuations $u^{'}$ are obtained from the pressure fluctuations $p^{'}$ using equation 6.3 proposed by Arndt and Ippen (1970). It neglects higher order terms when converting pressures into velocities, with a maximum estimated error of 5 % for a turbulence intensity level of 10 %. This is considered acceptable compared to the expected prototype turbulence intensities.

$$RMS(u') = \sqrt{\overline{u'^2}} = \frac{\sqrt{\overline{p'^2}}}{\rho.U} \tag{4.2}$$

[2]This was one key topic of discussion in the final roundtable of the International Workshop on Rock scour by falling jets held at EPFL in September 2002.

In Equation 6.3, ρ is the water density $[kg/m^3]$ and p' is the RMS value of pressure fluctuations $[kN/m^2]$. The mean and RMS pressure values are computed at each measurement position. The time-averaged local velocity V_y at all points along the diameter is derived from:

$$V_y = \sqrt{\frac{2(\overline{p} - p_{atm})}{\rho}} \tag{4.3}$$

In Equation 4.3, $\overline{p}$ is the mean local pressure $[kN/m^2]$ and p_{atm} is the atmospheric pressure $[kN/m^2]$. Time-averaged local velocities are estimated within $\pm$ 0.5 % for Tu values of about 10 % (Arndt and Ippen, 1970). The distribution of non-dimensional local outlet velocities is plotted in Figure 4.2 as a function of y/D, in which D stands for the nozzle diameter and y is the coordinate along the diameter.

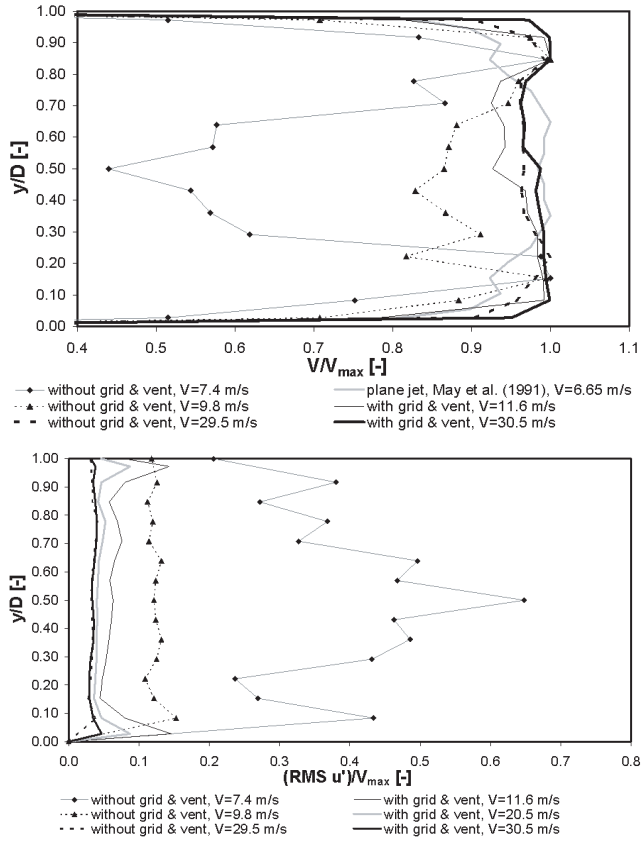

Figure 4.2.: Top: Mean local velocity from pressure measurements along the diameter (circular jet, 72 mm diameter) compared with data from May and Willoughby (1991)(plane jet, 38 mm thickness). Bottom: RMS velocity profiles. V_{max} is the maximum local velocity in the section.

The experimental profiles do not follow theoretical turbulent flow profiles. For velocities lower than 12 m/s, the profiles show very low velocities in the jet core.

During the *first* series of tests, the secondary currents in the supply conduit tend to keep most of the flow close to the outer walls of the nozzle. In *second* series of tests, with the honeycomb grid and the air vent, a better flow distribution inside the conduit is achieved for low and intermediate velocities (up to 20 m/s). The grid improves flow homogenization in the section, rendering the operation of the outlet more regular. The additional head loss does not reduce the range of tested velocities.

For high velocities (V > 25 m/s), the velocity profiles tend to be uniform, mainly due to the extreme contraction produced by the nozzle. This is more evident in the second series, for which upstream swirling is reduced. Flow is better distributed across the section and a good ventilation of the upstream circuit is assured. No secondary current effects are observed during the second set of tests, most likely due to the combined effect of the grid, the air vent and the contraction.

The RMS velocity profiles show a clear reduction of the jet fluctuating pattern in tests with the grid and air vent. Furthermore, a quite homogeneous repartition of turbulence fluctuations across the section is observed, with some amplification close to the boundaries. Burattini et al. (2004) observed similar amplifications at about 1.5 times the boundary layer thickness from hot-wire and anemometer measurements, with a circular jet of 55 mm diameter at 12.9 m/s.

The boundary layer thickness corresponds to $V_y/V_{max} = 0.99$ (Streeter and Wylie, 1983) and is 4 to 5 mm in the present experimental set-up. In fact, due to the length of the nozzle, the *vena contracta* created downstream of the nozzle entrance may still influence the readings at the points closest to the wall of the nozzle. Measurements in these points may exhibit pressure and velocity fluctuations characteristic of flow separation boundaries.

4.2.3. Probability distribution of pressure fluctuations

The probability density functions (PDF) of the measured data are compared with the corresponding Gaussian distribution fit in Figure 4.3 and Figure 4.4, using linear and logarithmic scales. Placing the grid and adding the air vent seems to slightly increase the skewness C_s and further increase the peakedness of the data PDF at $y/D = 0.5$ (jet axis) and at y/D = 0.083.

These data series show negative skewness, meaning that in comparison with a standard Gaussian distribution ($\mu = 0$, RMS $p^{'} = 1$, $C_s = 0$) asymmetry is more pronounced for extreme low pressure values.

The origin of negative skewness values under a highly compact jets is object of detailed discussion in Chapter 6. In brief, instead of the expected positive skewness resulting from relevant fluctuations *in the direction of the flow*, stagnation conditions at the pressure transducer's tip provide negative skewness.

A detailed analysis of the histograms presented in Figure 4.3 and Figure 4.4 shows that the number of positive fluctuations p'^{+} is indeed larger than that of negative fluctuations p'^{-}, which is in accordance with the general behaviour of the plunging jet. However, the maximum amplitude of p'^{-} is larger, reaching values of 6 to 8 times σ in a single 30 s run. This is the results of strong deflection in stagnation conditions.

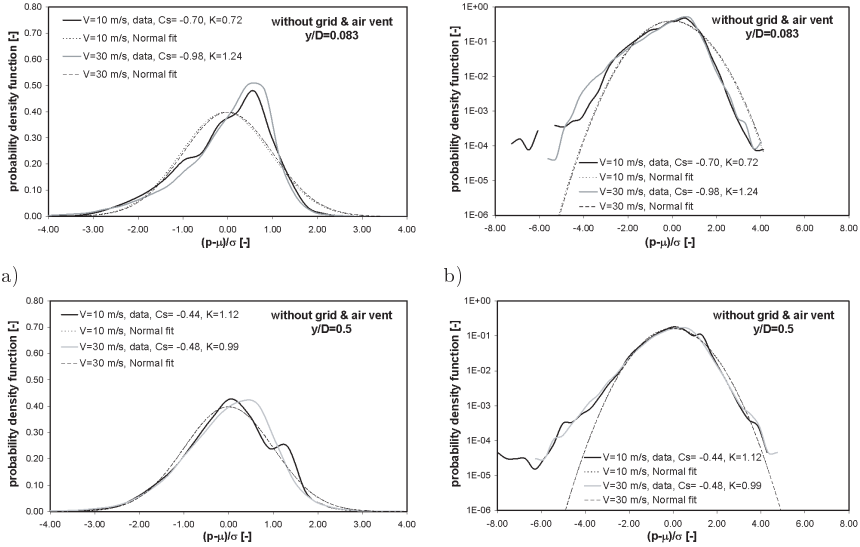

Figure 4.3.: Probability density functions of pressure measurements (using 30 data bins) across the jet compared with the corresponding Normal distribution fits for data series **WITHOUT** grid and air vent.

a) y/D=0.083 (6 mm from boundary); b) y/D=0.083 (6 mm from boundary);
c) y/D=0.500 (jet axis); d) y/D=0.500 (jet axis);

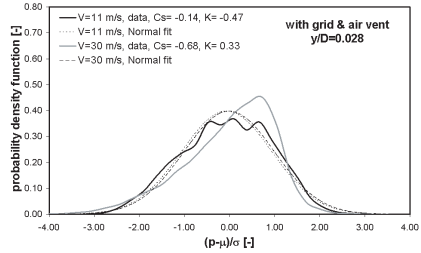

e)

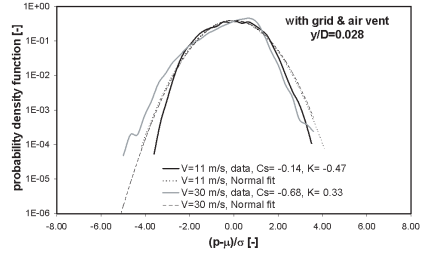

f)

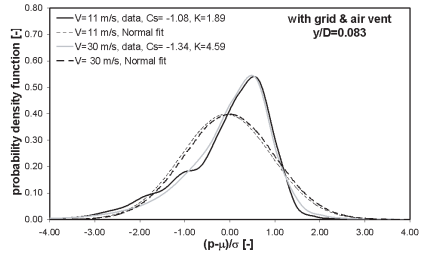

g)

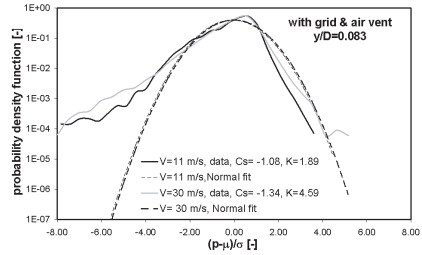

h)

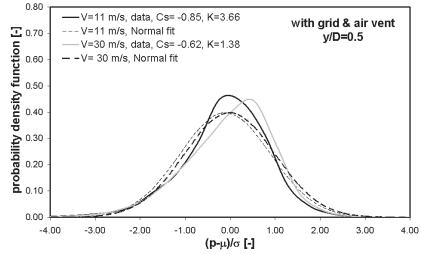

i)

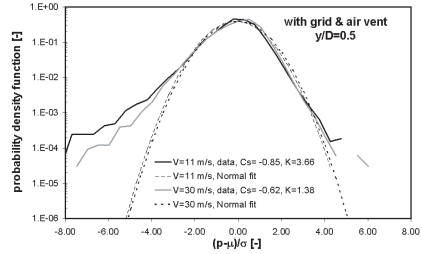

j)

Figure 4.4.: (cont.) **WITH** grid and air vent.

e) y/D=0.028 (2 mm from boundary); f) y/D=0.028 (2 mm from boundary);
g) y/D=0.083 (6 mm from boundary); h) y/D=0.083 (6 mm from boundary);
i) y/D=0.500 (jet axis); j) y/D=0.500 (jet axis);

All but one series present positive relative kurtosis values, reflecting the peakedness of the functions. Closer to the nozzle boundaries, the PDF functions for low velocities (i.e. V = 10 m/s) show (excess) kurtosis closer to a Normal fit (K = 0) than at the jet centreline. At the jet axis, the trend is inverted. The PDF functions for high velocities (i.e. V = 30 m/s) show kurtosis closer to the Normal fit at the axis than at the boundaries.

Data PDF at y/D = 0.028 obtained without grid and air vent show the flattest functions (lowest relative kurtosis), namely for low velocities. This is most likely representative of wall turbulence due to interference with the boundary layer or with the *vena contracta* separation zone created by the sudden section contraction.

For Reynolds numbers up to 10^6, intrusive methods will always generate stagnation conditions, reflected in particular in the skewness and kurtosis parameters. In the absence of non-intrusive measuring methods for such conditions, this effect has to be accepted for the estimation of mean and RMS pressures.

Figure 4.5 shows that for the highest velocities tested (quasi-prototype high-velocity jets), dynamic pressures at the jet axis seem to fairly agree with the Gaussian distribution, except for very high extreme probabilities. In fact, for probabilities beyond 0.999, pressure values drift from the Gaussian fit. Assuming a Gaussian distribution can lead to an underestimation of necessary extreme pressure values (non-conservative) for design purposes. For low-pressure extremes, however, such assumption provides conservative pressures estimates.

Each acquisition run lasted 32.5 sec satisfying ergodicity for the mean value within a 1% accuracy margin. Nevertheless, it may not be excluded that higher and lower extreme pressure values occur in reality or when larger sampling durations are used.

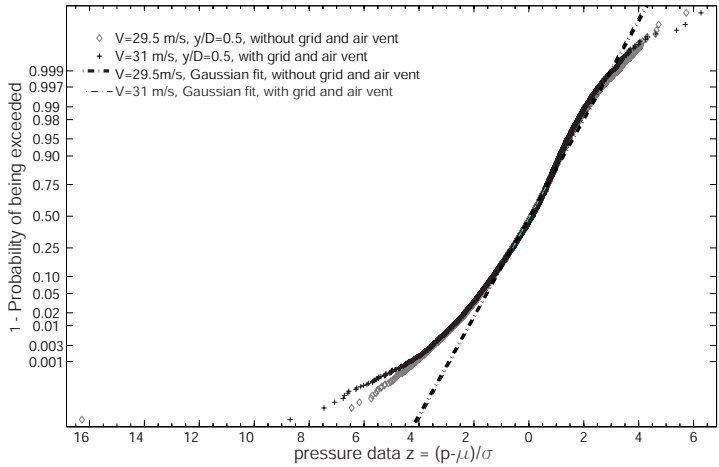

Figure 4.5.: Comparison of pressure data probability at y/D = 0.5 with Gaussian fits, for data series without grid and air vent (V = 29.5 m/s) and with grid and air vent (V = 30.7 m/s).

4.2.4. Turbulence intensity and kinetic energy correction factor

Section-averaged and local turbulence intensities are computed using the mean section-averaged velocity U and the mean local velocity V_y respectively. For section-averaged Tu values, eventual errors depend on both transducer and flowmeter calibration accuracy, whereas for local Tu estimates, only the calibration accuracy of the transducers is concerned. In Figure 4.6, section-averaged and local turbulence intensities (at the jet axis) are presented. Results of Bollaert (2002b) with convergent and pipe nozzles are also included.

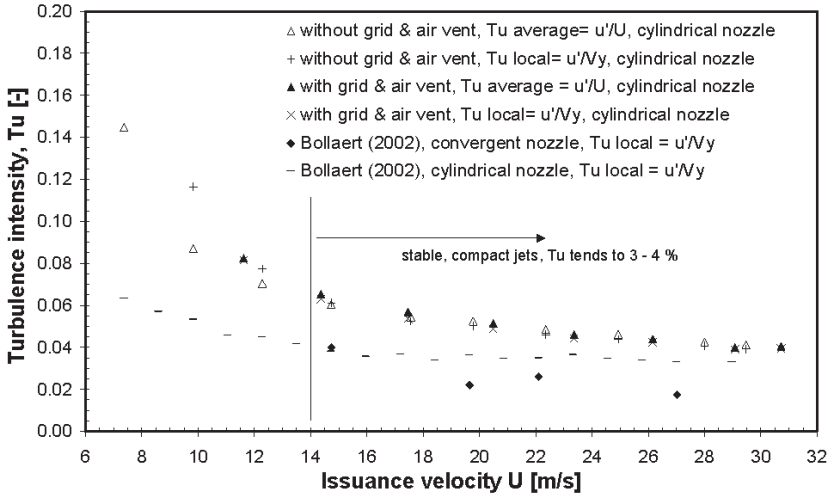

Figure 4.6.: Initial turbulence intensity Tu at the jet centreline (y/D = 0.5) from pressure measurements as a function of section-averaged mean jet velocity (Tu average) and local mean velocity (Tu local).

Jet turbulence intensities are below 8 %, except for velocities lower than 12 m/s. For higher velocities, the results tend to 3 - 4 % for both supply conditions (with/without honeycomb grid). The convergent nozzle reduces turbulence intensities to values of 2 to 3 %. They are complementary to observations by previous authors for lower velocities:

- McKeogh and Elsawy (1980) obtained Tu values of less than 1 % for laminar jets and 2 % for turbulent jets with velocities lower than 5 m/s, using pressure transducers;
- May and Willoughby (1991) used a total-head Pitot tube to measure the RMS value of pressure fluctuations and estimated Tu in the range of 5.5 to 5.8 % for velocities between 4.9 m/s and 6.6 m/s;
- Ervine and Falvey (1987) presented initial turbulence intensities of 0.3 % for almost laminar plunging jets, 1.2 % for smooth turbulent plunging jets and 5 % for rough turbulent plunging jets, based on experiments using a laser Doppler velocimeter, velocities from 3.3 m/s up to 29 m/s and a smooth tapered nozzle.

The present results agree with those of Ervine and Falvey (1987) with similar conditions. As an example, their 25 m/s jet had a turbulence intensity estimated at 7 %, which is slightly

higher than the present findings with pressure measurements.

As prototype velocities and aeration are used, it is assumed that the results are exempt of significant scale effects. It should be kept in mind, though, that local Tu estimates depend on the estimate of local velocity V_y obtained from an average pressure measurement. The accuracy of these measurements reduces the farther the measured pressures are to the full-scale output value of the transducer (17 bar A), i.e. for low velocities. Cumulated variability of the measurements is estimated in $\approx$ 0.4 bar, which represents approximately 80 % of the incoming energy for U = 9.8 m/s and 9 % for U = 30 m/s (Manso et al., 2005c). RMS statistics have lower error margins, since they represent differences between absolute pressure values taken in relatively short time intervals that may, each one of them, present equal deviations.

The differences between Tu local values between the present data without grid and air vent and Bollaert (2002b)'s observations (i.e. similar conditions) are within the error margin of the pressure measurements. All results present the same trend and converge to $Tu \simeq 3$ - 4 % for the range of velocities most relevant for engineering practice.

The velocity profiles allow computing the kinetic energy correction factor, which is defined as:

$$\alpha = \frac{1}{A}\int_A \frac{V_y^3}{U^3} dA = \frac{1}{\pi . r_0^2} \sum_{i=1}^{6} \left(\frac{\frac{V_{i+1}+V_i}{2}}{U} \right)^3 2\pi \left(\frac{r_{i+1}^2}{2} - \frac{r_i^2}{2} \right) \tag{4.4}$$

where r_0 is the radius [m] of the nozzle. The velocity profile is assumed valid over the entire cross-section. This coefficient is used to define the kinetic energy and dynamic pressure coefficients of a falling jet impacting in a plunge pool. For the first series of tests, α is less than 1 for velocities lower than 15 m/s since the flow section is not completely full and core velocities are very low. For velocities higher than 15 m/s, α varies from 1.0 to 1.1 as the influence of the observed secondary currents is reduced. Values close to 1.1 correspond to well-developed turbulent profiles, while values close to 1 are typical for uniform profiles (Streeter and Wylie, 1983). For comparison, Bollaert (2002b) found α values of 1.0 at low jet velocities and 1.05 at high jet velocities (up to 30 m/s) with similar supply conditions, performing measurements only under the jet axis and assuming a turbulent velocity profile as given by:

$$\frac{V(y)}{V_{max}} = \left(\frac{y}{D/2} \right)^{1/n} \tag{4.5}$$

where $n \approx 7$ (typical value for turbulent rough flows). Streeter and Wylie (1983) presented a value of 1.06 for a 7-power law turbulent velocity profile, whereas May and Willoughby (1991) suggested 1.158 for $n = 6.33$ for plane jets. Using the honeycomb grid and the air vent, α values are always higher than 1.0 for V > 10 m/s and rapidly decrease to 1.0 for velocities up to 30 m/s.

The turbulence intensity is plotted against the kinetic energy correction factor in Figure 4.7. For 10 < V < 30 m/s, the following equation was obtained ($R^2 = 0.947$):

$$Tu = 0.85\alpha - 0.824 \tag{4.6}$$

Whereas for 20 < V < 30 m/s ($R^2 = 0.974$):

$$Tu = 1.092\alpha - 1.071 \tag{4.7}$$

from the results with grid and air vent, both with a confidence interval of 99 %.

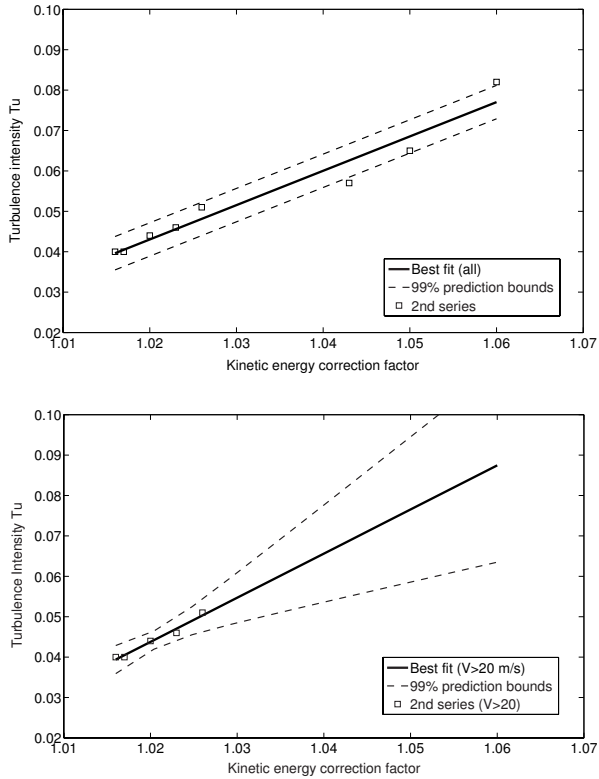

Figure 4.7.: Relationships between section-averaged turbulence intensity Tu and kinetic energy correction factor a for circular jets taking Tu values for $10 < V < 30$ m/s (top image) and $20 < V < 30$ m/s (bottom image). The velocity profile at issuance is rather uniform (2^{nd} series of measurements). The dashed lines show the prediction bounds for 99 % confidence estimates.

4.2.5. Influence of a sudden contraction and of the upstream supply system in issuance conditions

The 17.4 to 1 surface contraction ratio forces the flow from the conduit through a narrow nozzle, increasing the velocity accordingly. Comte-Bellot and Corrsin (1966) were the first to observed that a contraction accelerates axial flow, which approaches an isotropic turbulent flow pattern. According to Chassaing (2000), the contraction reduces the difference between axial fluctuations (either velocity or pressure in compact jets) and lateral (radial) fluctuations, while increasing the mean velocity. Turbulence intensity should thus decrease with increasing contraction influence (with velocity), which is in good agreement with the experimental observations.

Since the used contraction is rather sudden than smooth, the velocity profile presents slightly higher velocities close to the sidewalls. The relatively long nozzle length (l/D =

6.25) assures the re-attachement of the streamlines to the nozzle walls upstream from the measuring section. Contractions of many different types are often present in large-size hydraulic structures, namely in orifices and other gated structures, and their eventual influence in jet behaviour should be accounted for whenever possible.

The differences between local and average Tu values observed at low velocities in the first tests are eliminated in the second series of test by the addition of the honeycomb bundle and the air vent.

Spectral analysis of the pressure fluctuations measured is conducted, in order to identify the eventual existence of secondary currents, disturbances due to pump regime or any additional fluctuations due to inefficient air release at start of testing. Power spectral density functions of pressure fluctuations at the nozzle outlet are presented in Figure 4.8, for low and high velocities, without and with the honeycomb grid. The cut-off frequency is 1 kHz.

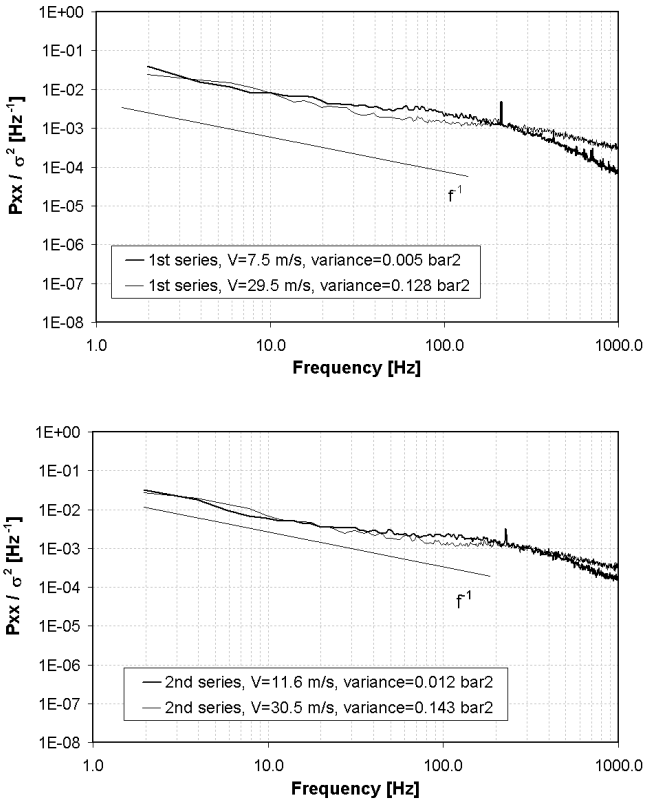

Figure 4.8.: One-sided Power Spectra Density estimates (Pxx) normalised using the data variance σ^2 from pressure measurements with acquisition frequency of 2 kHz performed under the jet axis: a) data from the 1^{st} series of measurements, b) data after addition of flow conditioner and air vent in the supply system. Spectra obtained with the Welch periodogram method.

The spectra are computed using both the Fast Fourier Transform (FFT) and the Welch algorithm for comparison. The latter uses windowing (Hamming) and overlapping in order to improve the accuracy of the spectral estimates (Lyons, 1997; Stearns, 2003). The former provides a raw, straightforward but often quite irregular spectral estimation. The differences in the computation of the data variance (integral of the spectra) from the results of the two methods are found negligible for the present application.

Spectra for high velocities show rather mild slope decrease with frequency of maximum f^{-1}, corresponding to highly compact jets (Bollaert, 2002b; Bollaert and Schleiss, 2003b). For low velocities spectra enter dissipation at about 100 Hz. No relevant accumulation of energy at a given frequency (that could reflect the presence of a characteristic supply system perturbation) is observed.

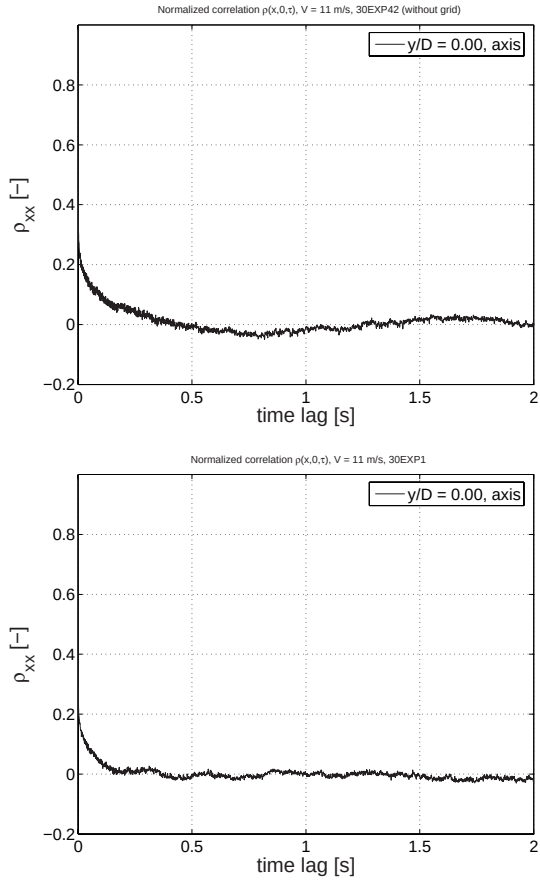

Figure 4.9.: Time autocorrelations ρ_{xx} at the jet axis (y/D =0.00). Acquisition frequency of 2 kHz: top, without grid and air vent (1^{st} series); bottom, with grid and air vent of measurements (2^{nd} series).

Comparing high and low velocity spectra without the grid, they are in general quite alike. However, the low velocity spectrum is almost flat at intermediate frequencies up to 80 Hz (log-log scales), then entering the dissipation range. The flatness reveals a transfer of energy from larger to intermediate scales. This corresponds to a less compact jet somewhat influenced by geometry-related turbulence. After placing the honeycomb grid, the low and high velocity spectra tend to collapse when divided by the corresponding variances. In these conditions, no isolated energy peaks are observed and eventual interferences of secondary currents, pump regime or oscillations due to deficient air expelling are excluded.

Time autocorrelations ρ_{xx} are computed at the jet axis for velocities 10-11 m/s before and after the addition of the honeycomb grid and air vent (Figure 4.9). Without grid the autocorrelation at the jet axis shows the presence of an oscillating phenomena that should correspond to a low frequency, eventually swirling flow. The left hand side figure shows an identical picture for a time series obtained with grid and air vent, for comparison. The oscillating behaviour is less evident in the measurements performed after addition of grid and the air vent.

4.3. Issuance conditions of prototype jets

4.3.1. Typical prototype jets

The hydraulic characteristics of seven typical jet-issuing structures are summarised in Table 4.1. The experimental results are used to compile suggestions for turbulence intensity and kinetic energy correction factor, which may be considered as first-hand indications for design. They can be used as input for jet trajectory and jet spread computations.

Table 4.1 is non exhaustive and highlights the absence of sound knowledge on the flow patterns of the most widely used hydraulic structures in large dams. The information on pressure and velocity profiles is rather qualitative since detailed research is often missing. Particular geometric features (splitters, deflectors, etc.) of each type of outlet are not taken into account and may significantly alter the presented values.

4.3.2. Overfall weirs

Overfall weirs are characterised by relatively low approach velocities. The flow accelerating over the weir can be considered potential. Along the downstream face, surface roughness initiates boundary layer development. For some cases such as the ogee crest, velocity and pressure at crest level have been systematically studied and assessed. Jets issuing from such structures are often quite compact and non-aerated.

For chutes shorter than the distance needed by the turbulent boundary layer to reach the surface (point of inception), the velocity profile in the upper part of the water column corresponds to a non-developed potential flow and is rather uniform (Vischer and Hager, 1998). The turbulence intensity is considered very low. The distance from the highest crest point to the inception point measured along the crest and chute may be computed directly, as shown by Ferrando and Rico (2002)'s method based on boundary layer thickness development as given by Wood et al. (1983). An example is presented in Appendix C.

For a typical case where q = 10 m^2/s, k = 2 mm and q = 45° a distance of about 54 m would be required to reach inception. In most practical cases of overfall weirs, the chute

length does not exceed 20 m and the issuing jet may be assumed to have a non-aerated core with a uniform velocity profile and a turbulence intensity of less than 3 % (case 4 in Table 4.1).

For chutes sufficiently long for the turbulent boundary layer to reach the flow surface, the jet section is entirely aerated at issuance and the velocity profile correspond to that of a partially developed turbulent flow (case 5 in Table 4.1). The turbulence intensity is then about 4-5 % (Ervine and Falvey, 1987).

Non-controlled overtopping of concrete dams can be modelled as flow over a broad-crested weir (case 6).

Whenever weirs are equipped with jet splitters or deflector blocks issuing conditions are difficult to assess (case 7). These devices reduce the unit discharge and enlarge the streamwise span of the issuing jets, as well as the impact area. They enhance jet disintegration and reduce impacting pressures downstream. Their study by Froude scaled model tests is hardly representative since processes like jet aeration, jet spread and jet break-up largely depend on Weber and Reynolds numbers. The effects of viscosity and surface tension become less relevant only at scales larger than 1/15.

4.3.3. Orifices

Orifices comprise bottom and intermediate level outlets. Issuing jets are initially non-aerated, save in case of reduced intake submersion. They tend to be operated with full opening of the gates to prevent vibration. Flow streamlines smoothly contract at the intake and the flow accelerates towards the issuance section. The exiting velocity depends on the upstream head in the reservoir. For small gate openings, there is an additional contraction of the streamlines close to the gate. In such case, the velocity profile at issuance is rather uniform and low turbulence intensity values are expected.

For large gate openings in orifices of thin arch dams, the length of the orifice is around 3 - 6 times its largest dimension (height). In this case, the contraction from the reservoir to the orifice conduit prevails and conditions similar to small gate openings should be found.

Jets issuing from high head orifices are considered rough (high Reynolds number) with high mean velocity. They have rather uniform flow distribution and low turbulence intensity.

For low head orifices (typically less than four times the height of the opening or exiting velocities less than 9 m/s, for which the difference between the velocity at the upper and lower streamlines is larger than 10 %), the contraction will not have such an important role and the flow pattern may exhibit secondary currents. Jets issuing from low head orifices are less affected by streamline contraction and flow acceleration, and are thus more likely to have higher turbulence intensity, eventually with uneven flow distribution due to swirling.

Based on the experimental results, a Tu value higher than 8 % should be considered if secondary currents are expected. For low head orifices (case 2), Tu should be lower than 8% if the flow section is fully occupied, values as low as 3 to 4 % being possible for smoothly converging sections producing rough jets. Thus, for high head orifices and bottom outlets (case 3), Tu values lower than 4 %, which can reach 2 to 3 % for prototype velocities larger than 30 m/s, can be considered.

Table 4.1.: Hydrodynamic characteristics of seven typical spillways and orifices configurations. P(n) and V(n) stand for pressure and velocity profile at issuance, respectively. Initial jet turbulence intensity and kinetic energy correction factor α for each type of outlet are based on experimental results with high-velocity jet flows.

Case	Schematic	Type of jet	Type of Intake	Boundary layer development	Outlet structure	Hydrodynamics	Aeration	Angle of lower nappe	Angle of upper nappe	Turbulence intensity Tu [%]	Kinetic energy correction factor [-]
1		Trajectory	WES weir (gated or non-gated)	Fully or partially developed	Ski jump (plane bucket)	P(n) concave, V(n) deformed logaritmic tending to uniform	Partially or fully aerated core	tang(lip)	approx. tang(lip), eventual correction	4 -8 %, take 4% for high velocities	tending towards 1.0 for high velocities
2			Orifice, low head	Non-developed	Curved lip	P(n) hydrostatic, V(n) turbulent ev. swirling tending to uniform for high V	Depending on submergence	tang(lip)	approx. tang(lip), eventual correction	3 - 8 %	tending towards 1.0 for high velocities
3			Orifice, high head	Non-developed	Curved lip	P(n) hydrostatic, V(n) quasi uniform	None	tang(lip)	approx. tang(lip), eventual correction	2 – 4 %	approx. 1.0
4		Overfall	WES weir, short chute	Partially developed	Straight lip	P(n) approx. parabolic, V(n) almost uniform	None	tang(lip)	approx. tang(lip)	Low, < 3 %	approx. 1.0
5			WES weir, long chute	Partially or fully developed	Straight or curved lip	P(n) hydrostatic, V(n) turbulent uniform	Partially aerated	tang(lip)	approx. tang(lip)	4 - 5 %	approx. 1.1
6			Broad-crested weir	Non-developed	Straight lip	P(n) approx. parabolic, V(n) freefall quadratic	None	horizontal	approx. 4 to 5°	Low, < 3% but may depend on crest details	approx. 1.0
7		Complex overfall	WES weir	Partially or fully developed	blocks or deflectors	Mixed	Partially or fully aerated	tang(lip)	approx. tang(lip)	8 % overall or more	-

4.3.4. Ski-jumps

The length of the chute being often larger than the distance to the inception point, aeration is either partially or fully developed and quasi-uniform flow conditions may be found at the toe of the chute. For gated structures, Toso and Bowers (1988) estimate the distance needed for the boundary layer to reach the surface to about 50 times the gate opening. At the entrance of the flip bucket, the pressure gradient is hydrostatic and the velocity profile approaches that of a uniform free surface turbulent flow. The mean air concentration is a function of the slope and the characteristics of the water (Falvey, 1980). The concave shape of the bucket deforms the streamlines that tend to remain parallel to the bottom. Streamline contraction modifies the pressure profile, which becomes different from the hydrostatic triangular shape. Some air detrainment may occur. Maximum bottom pressures increase with decreasing invert radii. For an equal takeoff angle, most designers rather reduce the radii in the downstream part of the bucket to prevent pressures from dropping to inconvenient values (Mason, 1993). An extensive study on takeoff angles is presented in Juon and Hager (2000). At issuance, though, one can readily agree that neither the pressure profile is hydrostatic nor the velocity profile is steadily turbulent.

Due to the lack of sound knowledge, one can assume that these jets have an aerated core with approximately the same mean air content as computed for the chute. The velocity profile may approach the uniform flow shape. Due to the pressure increase, U is expected to decrease in the flip-bucket, thus increasing Tu when compared to values at the toe of the chute. The influence of the reduced core density in the trajectory of the issuing jet is still a topic of discussion. On one hand, state-of-the-art developments by Ervine et al. (1997) do not apply directly to aerated jet cores. On the other hand, prototype observations like those done by Kawakami (just two observations, cited in Martins 1977) and by Taraimovich (1981), focused on the length of the trajectory but do not follow the same procedures. They are not only few but often lead to over-conservative corrections of the ballistic jet trajectory estimate.

For ski jump outlets where no contraction is imposed but the effect of longitudinal curvature somewhat uniforms the velocity profile, Tu values similar to rough jets, i.e. 4 - 8 %, are suggested for feasibility purposes.

4.4. Conclusions

The complex physics of high-velocity air-water jets demands for prototype scaled studies. Experiments with a circular jet nozzle at prototype velocities of up to 30 m/s are performed to assess the hydraulic characteristics of the jet core. This is done by measuring dynamic pressures across the jet outlet and analysing the shape of the velocity profile and the turbulence intensity of the jet. The experimental investigations show that:

1. Jet outlet turbulence intensities are generally below 8 %, reaching larger values if the outlet section is either not fully occupied or swirling occurs (secondary flows). For near-prototype velocities, jet turbulence intensities are close to 4 % if the outlet has a pronounced contraction, and close to 2 - 3 % if the outlet is smoothly convergent.

2. An abrupt contraction renders the mean velocity and pressure profiles almost uniform. The kinetic energy correction factor varies between 1.0 and 1.1, which influences the

impact kinetic energy downstream. Using a value of 1.1 for design purposes leads to conservative calculations.

3. At very high mean velocities, a more uniform profile corresponds to a lower turbulence intensity.

4. Core pressures follow fairly well a Gaussian distribution for non-exceedence probabilities between 0.1 and 0.999. Extreme pressures drift from a Gaussian distribution. Extreme pressures normally used in design procedures can be fairly well estimated with such distribution, in the case of compact jets with low turbulence intensity for which the core remains at impact downstream. For most real-life jets, however, this is hardly the case at impact, and extreme pressure distributions should be considered for design.

5. Based on experimental results and on extensive literature survey, a synthesis of hydraulic characteristics in typical structures is presented. Turbulent jet parameters at issuance, such as initial turbulence intensity, velocity profiles and pressure profiles are described. These allow estimating the jet deformation in the air, the extent of the impact area downstream, the dimensions of the remaining jet core, and the resulting jet impact energy downstream.

5. Diffusion and energy dissipation of plunging jets in pools with flat bottom

The present chapter (1) presents a review of diffusion of turbulent plunging jets (Figure 5.1) in free, limited-depth and laterally confined pools; (2) a compilation of an analytical model for the assessment of average energy dissipation of rough turbulent jets in pools with flat bottom ; (3) a comparison between analytical estimates and experimental measurements of impact pressures and energy dissipation in pools with flat bottom; and, (4) a discussions of the significance of the available empirical relationships for the diffusion of turbulent jets in pools with flat bottom. The experimental work with prototype jets allows comparing state-of-the-art empirical principles with measurements with near-prototype plunging jets in a pool with flat bottom.

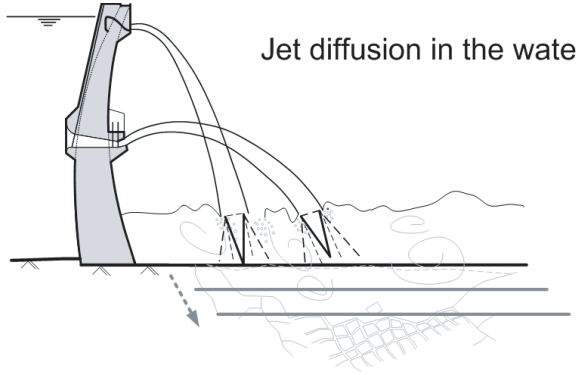

Figure 5.1.: Diffusion of turbulent plunging jets in water pools with flat bottoms.

5.1. Energy dissipation by diffusion of jets

The dynamics of plunging water jets is an important feature of many hydraulic works, such as water releasing structures in dams and in industrial plants (e.g aerator tanks). In the case of high dams, prototype jets have velocities significantly higher than 10 m/s and entrain air at impact with the downstream pool. The energy of the jet can be dissipated by diffusion (i.e. development) in an aerated pool. The understanding of the energy dissipation process is of utmost importance for the design of protection measures like concrete slabs used as linings, or for estimating the evolution of scour in unlined rock pools. The representation of such complex flow and structural conditions in reduced-scale laboratory Froude models does not adequately replicate the complex interactions between water, air and rock.

Up to the 1960's research focused on free jet diffusion, e.g. Albertson et al. (1948); Holdhusen (1948). Initially, mainly laminar and smooth turbulent air jets were studied. Soon afterwards, the first experiments with water jets diffusing in the air were presented by Kraatz (1965).

From the 1960's, major research can be divided into three fields:

- the influence of confining jet propagation, both in the stream-wise and lateral directions;
- the influence of jet turbulence; and,
- the incidence of the previous two points on impact pressures and, thus, on energy dissipation.

Research on jet diffusion in pools with flat bottom was initiated by Cola (1965, 1966) and Beltaos and Rajaratnam (1973, 1974, 1977). Abramovich (1963) and Rajaratnam (1976) presented analytical solutions for jet diffusion assuming potential flow for various situation of lateral confinement, co-flow and counter-flow. Their work set the foundations of the theory of jet diffusion. However, many applications of jet deviate from such theoretical conditions.

Of particular interest for this thesis is the progress made in the investigation of jets with high-Reynolds numbers ($10^4 - 10^6$). The role of jet's turbulence intensity in diffusion of turbulent jets was documented by McKeogh and Ervine (1981) and Ervine and Falvey (1987). Just recently, Manso, Bollaert and Schleiss (2004b) estimated initial turbulence for typical outlet structures encountered in practice, based on experiments with plunging jets with V $\leq$ 30 m/s (Chapter 4).

The entrainment of air by plunging jets in water pools has been addressed by several authors, e.g. McKeogh and Elsawy (1980) in limited-depth pools and, e.g. McKeogh and Ervine (1981); Ervine and Falvey (1987); Bonetto and Lahey Jr (1993); Bohrer et al. (1998); Chanson et al. (2004) in free jet diffusion conditions.

A typical engineering concern is the definition of the dynamic pressures generated at impact in the pool bottom. Dynamic pressures have been studied for submerged outlet conditions by, e.g Cola (1965); Gutmark et al. (1978), and for plunging jets by, e.g. Hartung and Häusler (1973); Kobus et al. (1979); May and Willoughby (1991); Puertas-Agudo (1994); Ervine et al. (1997); Melo (2001); Bollaert (2002b); Manso et al. (2005c). These studies have shown that impact pressures are a function of:

$$p(x, y, z, t) = f(V, Tu, C_{air}, L, Y) \tag{5.1}$$

where V is the jet velocity, Tu is the jet's turbulence intensity, C_{air} is the air content and L and Y are the travel distances in air and water respectively.

When considering rough turbulent plunging jets alone, as in the case of large dams, research results from laboratory work are scattered by falling angles, degrees of development, velocities and densities at plunging point. It is not clear if the existing relationships obtained from various types of jets and diffusion conditions in laboratory conditions suit the reality of prototype jets. Often the velocities used are too low, and the turbulence intensity of the jet and the amount of air entrainment are not assessed.

5.2. Free jet diffusion

5.2.1. Jet development length in unbounded media

Albertson et al. (1948) performed extensive tests with *air jets*. They documented the existence of two diffusion zones, namely the flow development zone (FDZ) and the zone of established flow (ZEF), depending on the distance to emission and on the mixing process. They reviewed the results of preceding research and described the evolution of the jet contours, velocity profile, kinetic energy and pressure head with distance, taking into account turbulent mixing. Free jet diffusion zones are presented in Figure 2.2.

According to Albertson et al. (1948) the angle of jet diffusion ($\alpha_1 + \alpha_2$) should be constant. The normal distance between the core and the outer spreading boundary b (i.e. the thickness of the mixing layer) can be related to the travel distance x by means of b/x=C. C is the turbulent constant:

$$C = \tan\alpha_1 + \tan\alpha_2 \tag{5.2}$$

Based on theoretical work, Abramovich (1963) provided C values ranging from 0.10 for jet diffusion in equal density media at rest, ≈0.20 in a co-flowing stream or ≈0.06 in counter-flow[1].

The diffusion coefficient C_d is defined as:

$$C_d = \frac{1}{\sqrt{\pi}C} \quad \text{or} \quad C_d = \frac{x_c}{D_0} \tag{5.3}$$

The length of the flow development region is given by $x_c = C_d.D_0$, where D_0 (or B_0 for plane jets) is the initial jet diameter.

In case of free diffusion of submerged jets (i.e. propagation in a surrounding media of identical density), C_d ranges from 5 to 6.2. A summary of values obtained by previous researchers is presented in Table 5.1.

The core contraction angle can be defined as:

$$\alpha_1 = \arctan\frac{1}{2C_d} \tag{5.4}$$

and the spreading angle as:

$$\alpha_2 = \arctan C - \alpha_1 \tag{5.5}$$

For circular submerged jets, Albertson et al. (1948) suggested a spreading angle α_2 of 14° in the established flow region (i.e., $x/y = 4$, where x and y are, respectively, the longitudinal and normal coordinates as given in Figure 2.2).

Kraatz (1965) studied free jet diffusion in air using a *circular water turbulent* jet, stressing the importance of the difference in density between the fluid in motion and the ambient fluid. In these conditions, the value of C is much lower than for submerged jets; this case is representative of the behaviour of a turbulent water jet in the air.

[1] This evidence is one of the few references found in literature which is somewhat representative of diffusion conditions in laterally confined pools (also described in literature as "dead-ends").

Table 5.1.: Diffusion coefficient C_d from selected references: P - plane jets, C - circular jets, P.A. = practical applications.

Type of jet	Tu_0 [%]	C	C_d	Re	Reference
Free jet diffusion					
C, submerged, air	-	0.081	6.2	> 1500	Albertson et al. (1948)
P, submerged, air	-	0.109	5.2	> 1500	Albertson et al. (1948)
C, free, water in air	-	0.01	50	10^3–10^6	Kraatz (1965)
C, plunging	0.3 - 8	0.37-0.41	2.96	10^3–10^4	McKeogh and Ervine (1981)
C, plunging, water	1 - 9	-	3.55	10^5–10^6	Ervine and Falvey (1987)
C, air	-	-	2.7-3	10^4–10^5	Malmström et al. (1997)
C, submerged	-	0.07-0.09	6.2-8.05	-	Rinaldi and Valentin (2005)
Diffusion in pools with flat bottom					
P, submerged, air	1-5	-	6-8	$2x10^4$	Kamoi and Tanaka (1972)
P, C, plunging	-	-	5	P.A.	Hartung and Häusler (1973)
P, submerged, air	-	-	8	10^3–10^4	Beltaos and Rajaratnam (1973)
P, submerged, water	-	-	≈ 5	10^5–10^6	Cola (1965)
C, submerged, air	-	0.10	5.6	P.A.	Rajaratnam (1976)
C, submerged, air	-	-	5.5-8.3	$3\text{-}5x10^4$	Beltaos and Rajaratnam (1977)
C, plunging	0.3 - 8	-	4-5	10^5–10^6	Ervine et al. (1997)
Diffusion in other conditions					
P, C, submerged, co-flow		0.22-0.27	-	-	Abramovich (1963)
P, C, submerged, counter-flow		0.06-0.10	-	-	Abramovich (1963)

McKeogh and Ervine (1981) studied experimentally the behaviour of *circular water jets* with a turbulence intensity (Tu) of 0.3 to 8%, travelling in the air and *plunging* into a water pool. They also described the mechanisms of pool aeration and the consequences for free jet diffusion. For turbulent plunging jets, they showed that spreading and core contraction depend not only on jet velocity but also on the turbulence intensity Tu. They suggested a spreading angle of $13 - 14°$ in the FDZ and $14 - 15°$ in the ZEF *in the pool*, the angle depending on the value of Tu.

Also for turbulent plunging jets, Ervine and Falvey (1987) suggested a ratio between α_1 and α_2 *in the water* based on an approximate momentum balance, mentioning that this angle had not yet been measured successfully. For most practical cases of turbulent jets, α_1 is thus between $7 - 9°$. They also studied spreading and break-up of jets *in the air* from photographs taken in laboratory and indicated an outer spread rate of 3 - 4 % and inner core decay of 0.5 - 1 % for typical turbulent rough jets. To the author's knowledge no other attempt of measuring α_1 has been made since.

5.2.2. Centreline velocity decay in unbounded media

As long as the core persists the velocity at the centreline is either equal (e.g. submerged jets) or directly proportional to that at issuance. For instance, for *falling* jets in the air, the mean velocity of the jet at a given fall height L is:

$$V_L = \sqrt{V_0^2 + 2gL} \tag{5.6}$$

For ski-jump jets, suitable formula can be found in Martins (1977); Whittaker and Schleiss (1984).

In practical terms, this means that for undeveloped plunging jets, the velocity in the core inside the water can be assumed identical to that at the entry of the pool V_i.

Table 5.2.: Centreline velocity decay *in free jet conditions*

Type of jet	Tu_0	C_v	Re	Reference
C, submerged, air	-	6.2	> 1500	Albertson et al. (1948)
P, submerged, air	-	5.2	> 1500	Albertson et al. (1948)
P, submerged, water	-	≈ 5	$10^5 - 10^6$	Cola (1965)
P, submerged, air	1 %	5	$2x10^4$	Kamoi and Tanaka (1972)
	2-3 %	4		
	5 %	2.5		
C, submerged, air	-	6.3 - 6.8	$10^4 - 10^5$	Beltaos and Rajaratnam (1974), D_0=6.4 - 23 mm
C, plunging, water	1-9 %	4	$10^5 - 10^6$	Ervine and Falvey (1987)
C, air	-	5.7 - 6.1	$10^4 - 10^5$	Malmström et al. (1997)
C, air	-	4-5.7	$10^4 - 10^5$	Malmström et al. (1997), D_0=15 mm and 2<V< 12 m/s

Beyond the flow development zone (FDZ), the centreline velocity of the plunging jet decays according to the following law:

$$\frac{V_{max,x}}{V_0} = C_v . \frac{D_0}{x} \tag{5.7}$$

where $V_{max,x}$ is the centreline velocity at distance x, V_0 is the initial velocity and C_v a coefficient that depends on *the diffusion conditions*. It can be interpreted as the inverse rate (or slope) of velocity decay in the FDZ; the lower C_v, the faster velocity decays.

For plunging jets, x is measured from the pool surface, and V_0 and D_0 are normally replaced by the corresponding values at entry in the pool V_i and D_i. The physical definition of V_i and D_i is still a topic of discussion. A summary of values of C_v obtained in previous investigations is presented in Table 5.2.

According to theoretical developments by Abramovich (1963); Rajaratnam (1976), C_v is an universal constant due to the self-similarity of the velocity profiles in the ZEF. This can be considered as a reference scenario for the analysis of turbulent jets, keeping in mind that the assumptions made in such theoretical developments may not suit every application.

C_v should be of the same order of magnitude of C_d. Values from 5.8 to 7.4 have been reported. In fact, it is C_d that depends directly from issuance conditions and not C_v as shown, for instance by Burattini et al. (2004). These authors discussed the influence of the initial turbulence intensity in jet deformation *in the near-field* after issuance for different outlet configurations.

For smooth and rough turbulent plunging jets, McKeogh and Ervine (1981) proposed:

$$\frac{V_{max,x}}{V_i} = 3.3 \left(\frac{D_0}{x} \right)^{1.1} \tag{5.8}$$

Yu cited in Liu et al. (1997) presented an alternative expression obtained from experimental work with two-phase impinging jets:

$$\frac{V_{max,x}}{V_i} = \left(\frac{D_0}{x} \right)^{0.53} \tag{5.9}$$

This is the only expression found in literature that does not consider explicitly a constant, and for which D_0/x varies with an exponent < 1.

Bohrer et al. (1998) performed experimental tests with developed and undeveloped jets at entry in the pool. They performed 20 tests with undeveloped jets, with velocities from 0.48 to 3.01 m/s, and air contents at entry from 0.38 to 0.52. They obtained another equation for the centreline velocity decay (R^2=0.864):

$$\frac{V_{max,x}}{V_i} = 0.0675.\frac{\rho_i}{\rho_w}\frac{V_i^2}{gx} + 0.1903 \tag{5.10}$$

where "i" stands for *entry* in the pool. This expression is valid within $0.51 < \frac{\rho_i}{\rho_w}\frac{V_i^2}{gx} < 5.76$.

C_v is 6.2 for submerged jets (Albertson et al., 1948) and 4 for rough turbulent jets (Ervine and Falvey, 1987). The velocity profiles in the established flow region are self-similar and follow a Gaussian error function (Albertson et al., 1948; Kraatz, 1965). These profiles die out at a distance $y/x \approx 0.25$ for circular jets (Holdhusen, 1948).

5.3. Jet diffusion in pools with flat bottom

Cola (1966) studied experimentally the diffusion of a *submerged water jet* in a pool with flat bottom, and described the deflection of flow streamlines at the bottom of the pool, as well as the creation of bottom wall jets[2]. The stagnation effect changes free jet velocity close to a solid surface. Jet behaviour diverges from that of a free jet when jet streamlines are deflected due to the presence of the obstacle. Cola (1966) was the first to describe this process. Following his pioneering work, several other researchers have documented the influence of the obstacle for various types of jets. He developed an expression for centreline velocity decay in limited-depth diffusion conditions:

$$V_{max,x} = \sqrt{V_0^2 \frac{1}{\sqrt{\pi}C}\frac{B}{H}\frac{1}{1-\eta_A}\left(1 - e^{-\frac{ln a}{\eta_A^2}(\frac{x}{H})^2}\right)} \tag{5.11}$$

where $\eta_A Y$ defines the distance from the bottom at which the jet streamlines start being deflected (named point A), and a is a constant that relates the maximum pressure head created by impact of the jet core (i.e. $V_0^2/2g$) with the pressure head at point A. He mentioned that the value of η_A varies between 0.25-0.35 for values of a from 10 to 500, if C is assumed 0.109 as defined by Albertson et al. (1948) for plane "submerged" air jets. This expression has not been validated or tested in other jet diffusion conditions. It depends on several parameters that are poorly documented for plunging aerated jets like η_A, C and a.

Three flow regions have been defined in wide pools with flat bottom (Kamoi and Tanaka, 1972; Beltaos and Rajaratnam, 1974; Liu et al., 2003): the free jet region (or plunging region), the impinging region (or stagnation region) and the wall jet region (Figure 5.2). In the impingement region, the jet is deflected by the presence of the flat pool bottom. Moreover, the velocity decay no longer follows free jet diffusion laws. Velocity is progressively converted into pressure head and reconverted back into kinetic head downstream of the stagnation point.

[2]Part of this work was published in English (Cola, 1965) but the version in Italian is much more comprehensive and detailed.

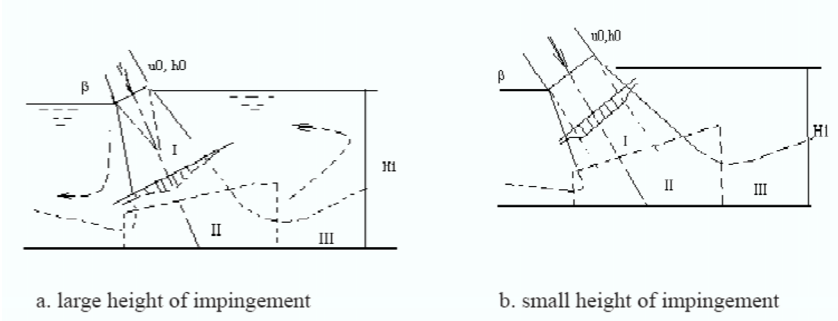

Figure 5.2.: Schematic representation of flow regions in limited-depth pools with flat bottom (Liu et al., 2003) divided in (I) plunging jet region, (II) stagnation or impinging region and (III) wall jet region: a) in deep pools; b) in shallow pools.

Beltaos and Rajaratnam (1977) described the stagnation zone as a small radial flow region of radius $\approx 0.14D_0$ around the stagnation point. This estimate was derived from experimental data using a circular air jet (in "submerged" conditions) impinging on a flat surface. They proposed three different impingement conditions based on the evolution of stagnation pressures:

- $Y/D_0 < 5.5$ for small impingement heights (i.e. shallow pools);
- $5.5 < Y/D_0 < 8.3$ for transitional conditions;
- and, $Y/D_0 > 8.3$ for large heights (i.e. deep pools).

The threshold between impingement conditions is somewhat related to the C_d defined for free jet conditions. A summary of C_d in limited-depth pools is also presented in Table 5.1.

Several attempts to define the dimensions of the impinging zone have been done, for various levels of jet turbulence, density and shape. It can be defined by η_A and by the radial distance from the jet axis ξ. The free diffusion length is defined as β_A = 1- η_A. A summary of values of β_A and ξ is presented in Table 5.3.

Table 5.3.: Free diffusion length, β_AY, and stagnation width, ξY, in pools with flat bottom

type of jet	β_AY	ξY	Reference
C, submerged, air	-	0.24	Holdhusen (1948)
P, submerged, air	-	0.33	Holdhusen (1948)
C, submerged, air	0.86	0.22	Beltaos and Rajaratnam (1974)
P, submerged, water	0.65-0.75 0.724	0.33	Cola (1966), V = 1.30 - 4.80 m/s by regression
P, submerged, air	0.70	0.35	Beltaos and Rajaratnam (1973)
C, submerged, air	η_A=1.2D_0	ξ=1.4D_0	Beltaos and Rajaratnam (1977)
P, submerged, air	0.75	-	Gutmark et al. (1978), V = 35 m/s

The experimental study with the highest Reynolds is the one by Gutmark et al. (1978), who measured dynamic pressures generated by a *submerged plane water jet* at 35 m/s at impact with a flat surface. They suggested β_A= 0.75 and showed that mean impact pressures decrease with increasing diffusion distance. This is one of the numerous studies

from the Mechanical or Aerospatial engineering domains on jet diffusion and impact in solid boundaries (Barata et al., 1993).

None of the works mentioned in Table 5.3 dealt with two-phase flow mixing or discussed the influence of the jet's turbulence level. Turbulence increases the spreading angle (McKeogh and Ervine, 1981), and air reduces mean pressures at impact with the surface (Melo, 2001, 2002b). These two aspects are bound to modify β_A and ξ and merit further research.

The previous examples show that the estimation of impact pressures is closely depending on the validity range of free diffusion centreline velocity decay laws, as well as on the dimensions of the impinging zone. The major difficulty to investigate these two topics is the two-phase character of the flow.

5.4. Jet diffusion in laterally bounded pools

Little is known about diffusion of plunging turbulent jets in laterally confined environments. However, studies in different conditions and with other types of jets may provide useful information[3].

Abramovich (1963) also studied jet diffusion and flow patterns in confined media analytically, as well as in co-flowing and counter-flowing streams. Rajaratnam (1976) presented extensive information on laterally confined jets as encountered in jets expanding inside ducts without a longitudinal confinement. The ratio between the confinement's diameter D_c and the jet's diameter D was identified as the main parameter enhancing reverse flow.

In the case of plunging water jets diffusing in aerated pools, reverse flows will travel upwards opposing gravity. The dimensionless ratio D_c/D_i, where D_c is the diameter of the confinement, may be used for analysis. A schematic representation of this reasoning is presented in section 3.3.3. For increasing values of D_c/D_i, the plunging jet will be less influenced by direct impact with the upward currents. Theoretically, this situation is similar to jet diffusion with counter-flow. Rajaratnam (1976) discussed centreline velocity decay in counter-flows for submerged jets, suggesting $C_v = 5.83$, which is somewhat *lower* than his suggestions for free jets. Hence, jet spreading is disturbed in the presence of a counter-flow. The lateral decay of velocity is probably faster and the influenced zone narrower, comparatively to the free jet situation. In these circumstances, both C_d and C_v are expected to be lower than the values presented for diffusion in pools with flat bottom and no lateral confinement.

5.5. Experimental work for dynamic pressure measurements in pools with flat bottom

The experimental facility and test procedures have been presented in Chapter 3. Pressure measurements close to the jet axis are used in this chapter. The mean dynamic pressure coefficients C_p from tests in pools with flat bottom and jet velocities between 17 and 30

[3] These notes on jet diffusion in laterally confined pools are included in this chapter to complete the previous analysis. This topic is not discussed further in this chapter.

m/s, are presented in Figure 5.3. C_p is defined as:

$$C_p = \frac{[\overline{p} - p_{atm}] - Y}{\frac{\alpha V_0^2}{2g}} \tag{5.12}$$

where Y is the initial static level of the pool and $[\overline{p} - p_{atm}]$ is the mean relative pressure head measured. The kinetic energy correction factor is assumed $\alpha = 1$ for all velocities tested. The experimental mean pressure $\overline{p}$ corresponds to the ensemble average of ergodic samples of pressure values sampled at 1 kHz.

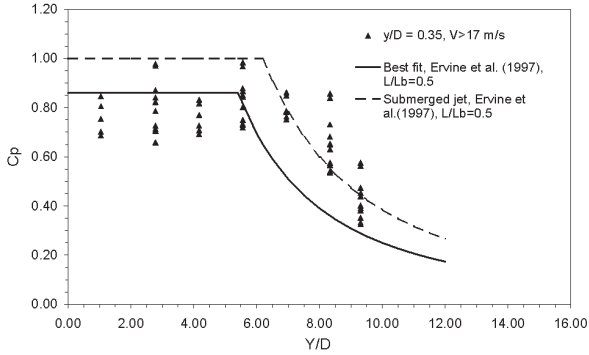

Figure 5.3.: Mean dynamic pressure coefficient C_p at y/D =0.35 as a function of the relative pool depth Y/D. Comparison with best fit and submerged jet data by Ervine et al. (1997). Data from experiments with flat pools (all FB test series in the present study) and V > 17 m/s

Only undeveloped jets at the entry of the plunge pool are considered. Broken-up jets produce comparatively lower impact pressures, even if only a shallow water depth is provided for diffusion. In fact, such jets impact as a succession of separate packs of water. The velocity of these packs of water depends mainly on the jet fall height (i.e. $V = \sqrt{2gL}$) and less on the issuance conditions. For higher fall distances, the packs become smaller and smaller.

5.6. Limited-depth diffusion model for the estimation of average energy dissipation in pools with flat bottom

In the case of turbulent plunging jets in flat pools, two situations can occur (see Figure 5.4): the core development length x_c is shorter than the distance from the surface to the impinging region x_A; or $x_c > x_A$. In the first case, impact pressure at stagnation (point B) should be approximately the incoming kinetic energy. In the second case, there is some energy dissipation by mixing and buoyancy from x_c to x_A.

The energy dissipation efficiency is defined as:

$$\eta = \frac{E_1 - E_2}{E_1} \tag{5.13}$$

where E_1 is the mean kinetic energy at pool entry and $E_2 = (\overline{p}\text{-}Y\text{-}p_{atm})$ is the measured or estimated excess pressure head at the pool floor (point B in Figure 5.3). The experi-

mental estimates of the energy dissipation efficiency are based on mean dynamic pressure measurements closest to the jet axis, i.e. at y/D=0.35.

A limited-depth diffusion model (LDDM) for the estimation of the energy dissipation efficiency in flat pools of variable depth is defined based on:

- the two diffusion scenarios presented in Figure 5.4, according to the relation between x_c and x_A;
- the velocity at impact with the pool surface, which is estimated as $U_i = \sqrt{U_0^2 + 2gL}$ (where L is the fall height in the air);
- the diameter at impact D_i, assumed as the mean diameter of the jet core according Ervine et al. (1997): $D_i = D_0\sqrt{U_0/U_i}$;
- the impinging zone, as defined by Gutmark et al. (1978), i.e. with $\beta_A = 0.75$Y;
- the core development length x_c, which is defined considering $C_d = 5$ as representative of the rough turbulent jets produced in the present experimental installation;
- a constant outer diffusion angle of the shear layer, as defined by Ervine and Falvey (1987) for jets with $Tu \approx 5\%$;
- the pressure head at B, estimated based on a 100 % efficient conversion of the kinetic energy available at A (i.e. 0 % energy losses in the impingement region);
- the velocity inside the jet core, assumed $V_{max,x} = V_i$;
- the hypothesis that in case $x_A > x_c$, the velocity at point A is estimated assuming C_v = 5 in Equation 5.4 for free jet diffusion in unbounded media, and using V_i;
- the hypothesis that in case $x_A > x_c$, the pressure head in B computed from the kinetic energy at A is corrected to account for the influence of air. The correction factor is $(1 - C_{air})^\theta$ where C_{air} is the mean air concentration in the diffusion layer at x_A;
- the C_{air}, which is computed according the procedure by Ervine and Falvey (1987) for rough turbulent jets, which are undeveloped at impact with the pool surface (section 2.8). This procedure is based on a linear decay of the air flow rate from impact. Mean air concentrations at impact from 21 to 45 % resulted in air concentration at point A between 9 and 37%. For $x_A < x_c$ and for submerged conditions, there is no pressure reduction at the bottom due to pool aeration.
- the exponent $\theta = 1.345$ according to Melo (2002b), for mean pressures at the plunge pool floor.

The excess energy at impact E_2 is computed for each case from:

$$E_2 = \frac{P_B}{\gamma} = \frac{V_i^2}{2g} \quad \text{for Y} < \frac{C_d.D_i}{\beta_A} \tag{5.14}$$

$$E_2 = \frac{P_B}{\gamma} = \left[\frac{C_v D_i V_i}{\beta_A Y}\right]^2 \frac{1}{2g}(1 - C_{air})^{1.345} \quad \text{for Y} > \frac{C_d.D_i}{\beta_A} \tag{5.15}$$

The measured pressure values are transposed to the jet centreline using (Ervine et al., 1997):

$$P_{axis} = \frac{P_{y/D=0.35}}{e^{-30\left[\frac{y}{DY}\right]^2}} \quad \text{for Y/D} \leq 5.6 \tag{5.16}$$

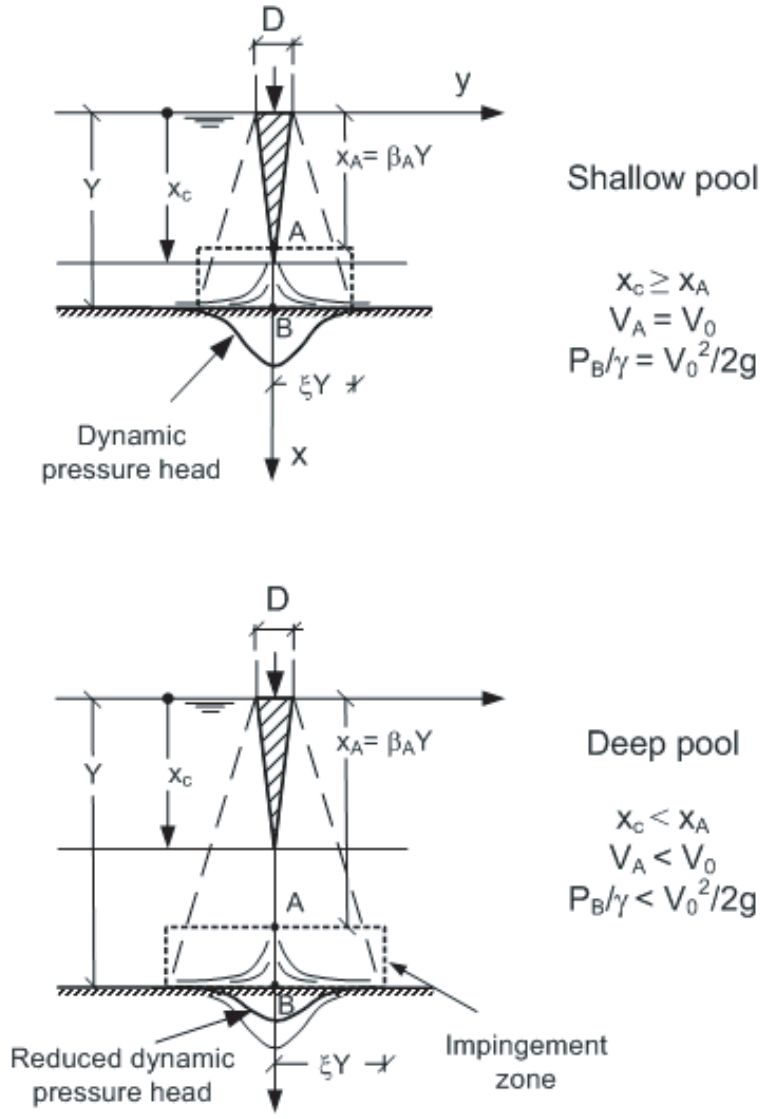

Figure 5.4.: Diffusion pattern of turbulent plunging jets in aerated pools according to the Limited-Depth Diffusion Model (LDDM). P_B/γ is the mean excess pressure head at B.

and

$$P_{axis} = \frac{P_{y/D=0.35}}{e^{-50\left[\frac{y}{DY}\right]^2}} \quad \text{for Y/D} > 5.6 \tag{5.17}$$

This corresponds to assuming that the maximum pressure is reached at the centreline, which may not always be the case due to displacement of the stagnation point (Kamoi and Tanaka, 1972; Melo, 2001).

The transfer of pressures to the centreline leads to an increase in mean dynamic pressure values of about 7% for $Y/D = 9.3$ and 13 % for Y/D = 6.9. For Y/D $\leq$ 5.6 values higher than 1.00 are obtained and cannot be accepted. Therefore, no correction is made for Y/D=2.8, 4.2 and 5.6. For these pool depths, the measurements at y/D=0.35 correspond to core impact conditions.

5.7. Comparison between analytical and measured estimates of energy dissipation

A comparison between the excess energy heads at impact E_2 obtained analytically with LDDM and experimentally is presented in Figure 5.5.

For deep pools with Y/D = 9.3, the estimates obtained with the LDDM are in good agreement with the experimental data. For shallow pools with Y/D $\leq$ 4.2, a reasonable accordance with measured data is obtained for the highest values of E_2 (i.e. V = 27 and 29.5 m/s). The analytical estimates for lower velocities are consistently higher than measured estimates.

For the remaining (intermediate) pool depths, the measured pressures are larger than the LDDM estimates. This means that the LDDM is "generating" too much dissipation.

Figure 5.6 shows that LDDM estimates of the energy dissipation efficiency η are generally higher than the values obtained from experiments. The LDDM estimates are rather constant in the tested range of velocities from 17 to 30 m/s, whereas measurements show a clear reduction trend in Figure 5.7.

Table 5.4.: Energy dissipation efficiency: comparison between limited-depth diffusion model (LDDM) and experimental measurements.

Y/D	V	Diffusion Model	Measured	η_M/η_{LDDM}	Comments
2.8	17.2	0.00	0.24	1.24	LDDM underestimates η
	29.5	0.00	0.04	1.04	good agreement
4.2	17.2	0.00	0.26	1.26	LDDM underestimates η
	29.5	0.00	0.03	1.03	good agreement
5.6	17.2	0.46	0.28	0.82	LDDM overestimates η
	29.5	0.47	0.02	0.56	LDDM overestimates η
6.9	17.2	0.40	0.16	0.75	LDDM overestimates η
	29.5	0.41	0.03	0.62	LDDM overestimates η
8.3	17.2	0.51	0.42	0.91	LDDM overestimates η
	29.5	0.51	0.07	0.55	LDDM overestimates η
9.3	17.2	0.55	0.57	0.98	good agreement
	29.5	0.55	0.53	1.03	good agreement

For velocities higher than 17 m/s, differences between LDDM and measured estimates of η are:

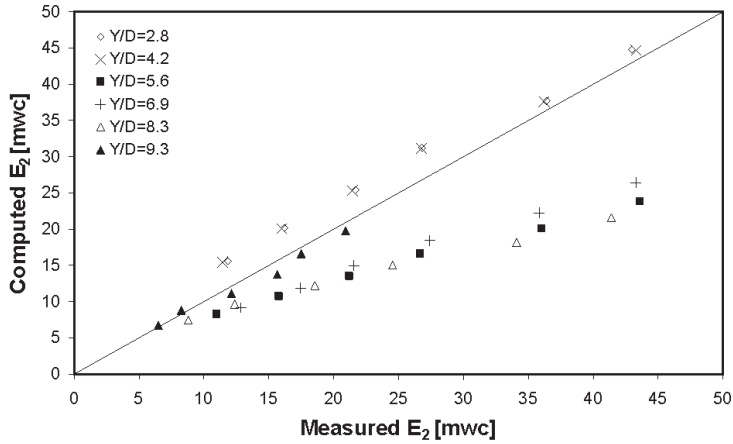

Figure 5.5.: Measured and computed values (according Eq. 5.14 and Eq. 5.15) of the excess energy head E_2 in pools with flat bottom and variable pool depth Y/D.

- +3 to -45 % for developed jet impact conditions (Y/D > 6);
- -18 to -44 % for intermediate impact conditions (Y/D = 5.6); and,
- +3 to +26 % for core impact conditions.

For Y/D = 2.8 and 4.2, average dynamic pressure coefficients C_p are less than 1.0 (Figure 5.4), i.e. lower than what is assumed in the LDDM model ($V_A = V_i$). Thus, the LDDM underestimates the pool's energy dissipation efficiency. It is conservative in estimating impact pressures in shallow pools with flat bottom.

Table 5.4 shows that the LDDM underestimates the energy dissipation efficiency of shallow pools, especially for lower jet velocities (within the tested range 17-30 m/s). It assumes that no dissipation at all occurs in core impact conditions, which is almost the case for 30 m/s but not for 17 m/s. For deep pools (e.g. Y/D = 9.3), the LDDM provides fairly good estimates for the range of velocities analysed.

5.8. Discussion of the limited-depth diffusion model

The previously presented model for estimation of the energy dissipation efficiency in a flat pool is based on a series of assumptions that merit further discussion.

5.8.1. Impinging zone

The previous two cases assume that there is no additional mean head loss inside the impinging zone. This assumption is difficult to verify. The definition of the dimension η of the impinging zone depends considerably on the type of jet.

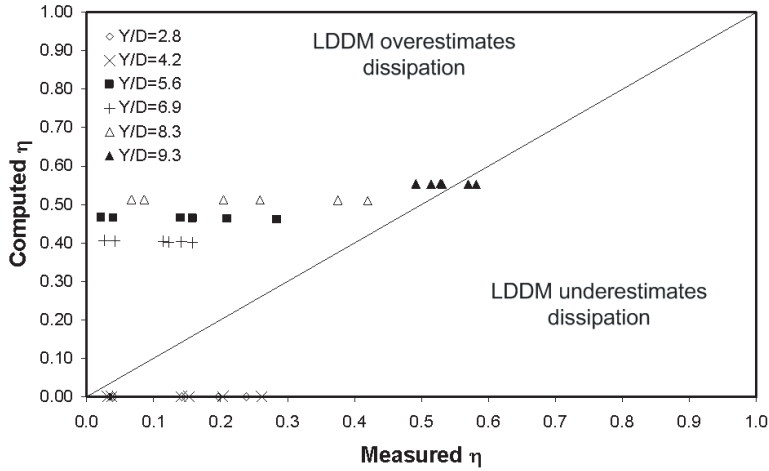

Figure 5.6.: Average energy dissipation in flat pools (V = 17.2 - 29.5 m/s).

In the present case, the selection of the free diffusion length β_A is arguable since no specific measurements of the pool velocity field are available. In the absence of values for two-phase jets, $\beta_A = 0.75$Y was selected from experiments with water jets and similar velocities (Gutmark et al., 1978). It is considered a conservative value since it reduces the decay (i.e. dissipation) distance in comparison with higher values (e.g. 0.86).

However, since Tu and C_{air} are a function of V_0, then C_d is likely to be a function of V_0 also. And not constant, as assumed. Therefore, C_v should also be a function of V_0 and Tu, as well as β_A.

5.8.2. Core development length

Assuming $C_d = 5$ is a compromise between the low values proposed by Ervine and Falvey (1987) (i.e. 3.55) or by McKeogh and Ervine (1981) (i.e. 2.76), and the experimental evidence gathered in this thesis.

The present facility produces undeveloped rough turbulent jets at entry of the pool with long core persistence, of at least[4], C_d= 5.6.

Therefore, the selection of a value of C_d for the model should be tailored for the *jet* being considered in each application.

Moreover, C_d (and C_v) is considered constant with V, in the case of turbulent plunging jets in pools with flat bottom. These coefficients should depend on Tu, as outlined by McKeogh and Ervine (1981) and Ervine and Falvey (1987). In fact, they should depend on Tu_i, i.e. Tu at impact, which is also a function of the relative fall height L/D_0.

[4]This topic is presented in detail in Chapter 6.

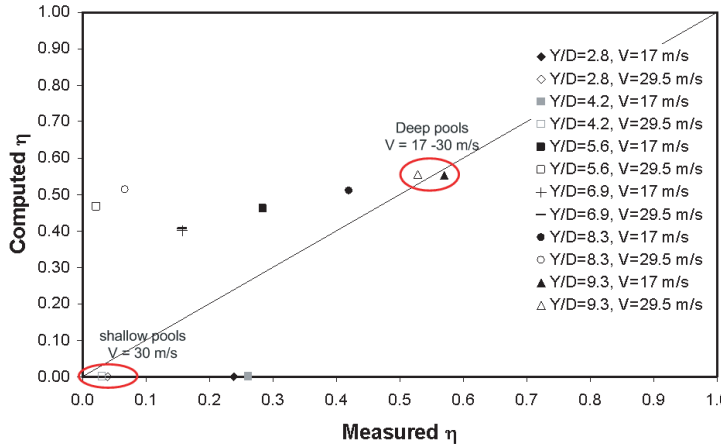

Figure 5.7.: Average energy dissipation efficiency η in flat pools, as a function of the issuance velocity V_0.

5.8.3. Jet characteristics at entry in pool

The velocity at impact was computed based on the fall height. The diameter at impact D_{imp} that is used to compute x_c using C_d is assumed to be the mean diameter of the jet core according Ervine et al. (1997): $D_i = D_0\sqrt{U_0/U_i}$. However, this is a simplified representation of the jet, since it neglects the momentum equivalent to the spreading and boundary layers. A clear definition of a "representative" impact diameter is yet to be found. Therefore, estimating $x_c = C_d.D_i$ is rather hardy. On the one hand, D_i depends on Tu, L and on the definition of a "representative" diameter. On the other, C_d depends on Tu_i, which itself depends on D_i, Tu and L.

For undeveloped plunging jets, the margin of accuracy in estimating D_i and x_c is likely to be within $\approx 20\%$ of their real physical value.

For jets with longer trajectories (e.g. trajectory jets from ski-jumps or orifices), the representativeness of D_i estimates is often connected to the degree of break-up. A sensitivity analysis should be performed to this parameter since the pool length depth "potentially available for energy dissipation" (Figure 5.8) depends directly on D_i.

5.8.4. Air content decay rate

The decay rate of the air content entrained by rough turbulent jets in the pool is assumed linear after Ervine and Falvey (1987). This is based on the work of McKeogh and Ervine (1981) and may not be valid if the flow pattern in the pool is modified, for instance, by the presence of a lateral confinement disturbing jet diffusion.

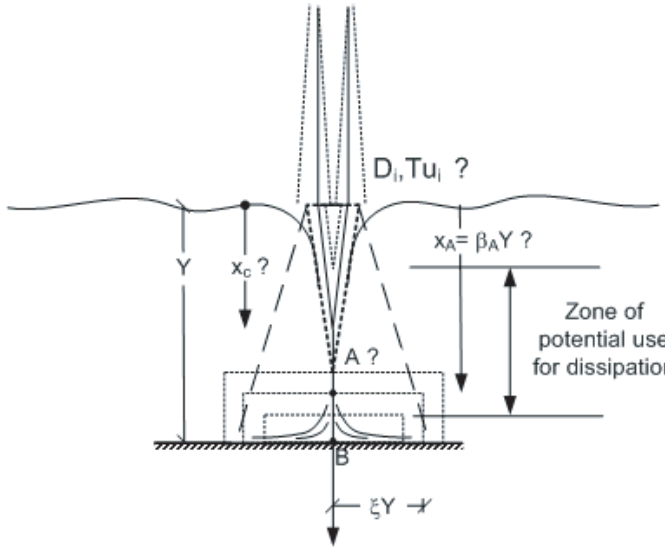

Figure 5.8.: Synthesis of parameter for which assumption are necessary for the assessment of the diffusion of turbulent plunging jets in flat pools: x_c, β_A, D_i, Tu_i

5.8.5. Mean pressure reduction due to air content in pool

A correction factor for mean pressures equal to $(1-C)$ was suggested by Ervine and Falvey (1987). This factor corresponds to a correction of the mass density ρ at given depth in free diffusion conditions.

Melo (2002b) suggested a correction factor of $(1-C)^{1.345}$ in case of limited-depth plunge pools, as opposed to non-aerated conditions. The additional 0.345 in the exponent θ is thought to be due to the contribution of the air bubbles to the diffusion process. An exponent of 1 reflects a reduction in density only, but does not reflect the *mechanical* effects due to the presence of the air bubbles. Air bubbles tend to migrate to lower pressure zones and if this is predominantly done in counter-current (with buoyancy) then it may enhance dissipation.

5.9. Synthesis and conclusions

The energy dissipation of a circular plunging jet in a flat pool with variable depth is studied both experimentally and analytically.

Impact dynamic pressures generated by a near-prototype plunging jet with velocities between 17 and 30 m/s diffusing in pool with flat bottom are measured at the pool bottom using piezoresistive transducers. These pressure measurements are used to estimate mean dynamic excess pressure head at impact for bounded diffusion conditions in a water cushion of variable depth. Undeveloped turbulent jets are considered.

A model for the assessment of the energy dissipation efficiency of given water cushions was compiled (Eq. 5.14, Eq. 5.15 and Fig. 5.4), based on previous research findings for free jet diffusion and jet diffusion in pools with flat bottom (numerous references mentioned in previous sections). The model was named limited-depth diffusion model (LDDM) and is valid for pools with flat bottom.

Experimental and analytical estimates of impact pressure head and corresponding energy dissipation efficiencies are compared. Results show that the LDDM is suitable for practical purposes with high-velocity jets, i.e. 20-30 m/s, both at the initial stages of scour and for deep flat pools. For intermediate pool depths, the model is quite sensitive to the initial assumptions, namely those on the centreline velocity decay, dimension of impinging zone and pool aeration.

In summary, the LDDM depends considerably on the assumptions made for β_A, C_d, impact diameter D_i, and air flow rate decay. For each application of LDDM, a sensitivity analysis should be performed to the assumptions made on these parameters. As observed, diffusion theory is in continuous development. The compiled limited-depth diffusion model for pools with flat bottom highlights the fairly good representativeness of existing laws but also its weaknesses.

Pools with flat bottom are considered as the reference scenario in the framework of rock scour. In reality, unlined rock plunge pools developed into quite complex geometries as defined by the interaction between the plunging jet loading and local geology. The modification of pool flow patterns in prototype scour compared to pools with flat bottom is expected to induce changes in the mathematical description of centreline velocity decay, pool aeration and jet core development. In those circumstances, the LDDM may provide first hand estimates of the mean loading at the water rock interface.

In depth knowledge of flow behaviour in prototype-like pools is the first step to the definition of more suitable governing laws, namely for centreline velocity decay, core development length and pool aeration.

The present analysis focused solely on mean pressures, but can be extended by considering the RMS pressure values, and the corresponding contribution to energy dissipation in the pool. This discrete analysis can also give way to a probabilistic analysis by replacing discrete definitions by probability-based definitions of parameters like air content at given depth and jet core length.

6. Intermittency and impact pressures of high-velocity jets in pools with flat bottom

The analysis of jet diffusion in pools with flat bottom is a first step in the analysis of the dynamic interaction between jet diffusion and pool morphology. Considerable experimental results and experience of impact pressures in flat surfaces (Figure 6.1) allow establishing a reliable reference scenario for comparison with other pool geometries. This chapter presents experimental work with turbulent jets at velocities ranging from 7.5 to 30 m/s plunging in a water pool with variable depth and flat bottom.

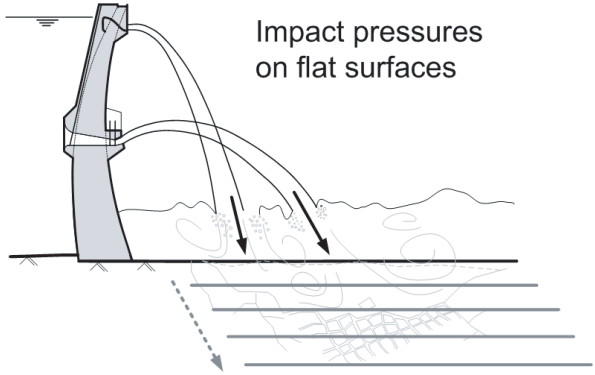

Figure 6.1.: Schematic representation of scour evolution by flat rock layers (pools with flat bottom) due to the impact of plunging jets.

6.1. Definition of impact pressures in limited-depth pools

The[1] diffusion of turbulent high-velocity aerated water jets presents many difficulties for experimental research due to the complex two-phase environment. The hydrodynamic flow field is often extrapolated from non-aerated conditions. Enhanced knowledge on jet diffusion in extreme conditions of turbulence, aeration and compressibility is of interest in industrial two-phase flows encountered in dam construction and in the water treatment industry. Jet diffusion in a water pool depends on jet entry velocity, density, turbulence intensity and jet and pool dimensions. Diffusion defines the rate of mixing with the surrounding fluid and the distance influenced by the jet. Mixing is important when dealing with pollutants but,

[1] This chapter is based on the manuscript of the scientific publication Manso et al. (2005a) submitted to the journal Experiments in Fluids in August 2005.

in the context of the hydraulics of dams, to define the energy remaining at a given depth and thus the dynamic loading acting on the solid structural boundaries or on a natural riverbed. However, existing theoretical tools as, for example, the theory of free jet diffusion and centreline velocity decay, are hardly valid if flow streamlines deform due to the presence of obstacles or in two-phase conditions.

Systematic research on jet diffusion started during the $1920's$ with the analysis of jet propagation in unbounded media of identical density. A comprehensive review of the research performed over the first half of the XX^{th} century was presented by Albertson et al. (1948). Jet diffusion is divided in two flow regions (see Fig. 2.2): the flow development region ($x \leq x_c$), where the jet potential core persists; and the established flow region further downstream ($x > x_c$).

Kraatz (1965) studied plunging water jets and discussed the influence of mixing fluids with different densities (typically air and water). Cola (1966) investigated submerged vertical water jets and documented for the first time jet streamline deflection close to the bottom of the pool. Beltaos and Rajaratnam (1974) presented a review of studies with impinging jets and defined theoretically the deflection zone for circular air jets. For air jets and velocities from 45 to 90 m/s, they observed a deviation of the centreline velocity decay law from the free jet diffusion law after 86 % of the total distance from issuance to impact.

McKeogh and Ervine (1981) related jet diffusion with the degree of jet turbulence, jet development in the air and air entrainment in the pool, which influence mixing and jet core development. Ervine and Falvey (1987) studied rough turbulent water jets as issued from dams, and extensively described jet spreading and core contraction in the air and inside a water pool. Compared with the first test from the 1920's, the velocities tested, as well as the jet's turbulence intensity and pool aeration, are approaching typical prototype applications.

McKeogh and Elsawy (1980) described how pool aeration is modified when restraining free jet diffusion. They documented the influence of the distance from the plunging point to the pool bottom upon the bubble penetration depth and the void fraction at given depth. They used jet velocities up to 5 m/s but did not consider impact pressures. Gutmark et al. (1978) studied submerged plane water jets with V = 35 m/s and showed that mean pressures at impact with the bounding surface decrease with increasing diffusion distance. They suggested that the jet starts being deflected at about 75% of the diffusion length, which is in agreement with the findings of Cola (1966). However, they did not discuss the influence of air entrainment or jet turbulence intensity.

Impact pressures have mainly been studied in reduced scale models (May and Willoughby, 1991; Puertas-Agudo, 1994). In both studies, plane jets were used. The thickening of the water cushion was shown to reduce mean pressures at the bottom of the pool. These studies, however, do not reliably account for pool aeration, thus neglecting enhanced mixing and energy dissipation due to air bubble buoyancy. Melo (2002b) documented the impact conditions of submerged water jets with artificial air entrainment in lined pools with velocities of up to 10 m/s. He showed experimentally the influence of air entrainment in reducing mean pressures at impact with the pool floor, by directly and fully controlling the amount of air being entrained. As a summary, several studies have approached different relevant topics for two-phase jet diffusion in plunge pools but a comprehensive analysis combining high velocities, aeration, bounded pools, dynamic pressures, prototype turbulence levels and therefore reduced scale effects, is still missing.

Ervine et al. (1997) were the first to present mean, RMS, maxima and minima statistics of impact pressures for velocities up to 29 m/s, varying travel distances, initial jet turbulence, jet velocity and pool depths. Bollaert (2002b) and Bollaert and Schleiss (2003b) studied the radial pressure distribution at the pool bottom, as well as the propagation of surface pressure fluctuations inside rock fissures or structural joints. Bollaert et al. (2002) and Manso, Bollaert and Schleiss (2004a) pointed out the importance of the scale of the model in terms of jet velocities and aeration in order to have comply with Froude, Reynolds and Weber similarity. A summary of existing studies on bottom pressures in flat plunge pools can be found in Bollaert (2002b) and Bollaert and Schleiss (2003b).

6.2. Experimental work in pools with flat bottom

The experimental facility and test procedures are presented in Chapter 3.

The impact pressures generated by the rough turbulent jets produced are described statistically for variable jet velocities and pool depths.

First, the procedure for ergodic sampling is presented. Second, pressure measurements performed at jet issuance are compared with measurements at the pool bottom in the impinging zone (y/D = 0.35 and 2.08) in shallow pool conditions (depth less than 4-6 jet diameters). The influence of the modifications performed in the supply system of the experimental facility upon impact pressures at the pool bottom is discussed. Finally, probability density functions of pressure measurements at the same two points at the pool bottom are analysed for variable jet velocities and pool depths. The analysis of the kurtosis and skewness parameters allow gaining further insight on the intermittent character of pool turbulence.

6.3. High-order ergodicity analysis of pressure signals

An ergodicity analysis is performed to define the cumulated acquisition duration that provides estimates of at least the first moments of a data series, i.e. the mean μ and the standard deviation σ, within 5 % of the corresponding ensemble moments $< \mu >$ and $< \sigma >$. An evaluation of the range of variation of skewness and kurtosis estimation is also presented. Obtaining estimates of the latter within such stringent boundaries requires very long duration runs and was not the main objective of the study.

Table 6.1.: Selection of long duration test for ergodicity analysis (n = number of runs). The number of samples varies between 32768 and 65536. Comparison between moments after 3 min of cumulated acquisition time and ensemble moments obtained from cumulated 30 min.

Test	y/D	Y/D	V	n	samples	$\Delta\mu$	$\Delta\sigma$	ΔC_s	ΔK
Shallow pool	0.69	5.6	27	30	65536	$< 1\%$	$< 2\%$	$< 10\%$	$< 2\%$
	end					$< 1\%$	$< 1\%$	$< 40\%$	$< 2\%$
Deep pool	0.69	9.3	27	30	65536	$< 6\%$	$< 10\%$	$< 32\%$	$< 26\%$
	end					$< 5\%$	$< 6\%$	$< 22\%$	$< 30\%$
Submerged jet	0.69	11.4	24.6	60	32768	$< 1\%$	$\pm 1\%$	$\pm 5\%$	$\pm 3\%$
	end					$< 1\%$	$\pm 1\%$	$\pm 5\%$	$\pm 3\%$

The sampling frequency selected was 1 kHz following the work of Bollaert (2002b), which outlined the existence of considerable spectral energy at frequencies as high as 300 Hz. This is an intrinsic characteristic of near-prototype pressure measurements generated at LCH jet facility (Bollaert et al., 2002).

Long duration runs were performed up to a net maximum duration of $\approx 0.5 hour$ (1.5 hours of total acquisition time). Instantaneous pressures at the pool bottom (y/D=0.35 and 0.69) for different tailwater levels and jet velocities were used for this analysis [2]. The mean value, the standard deviation, the skewness and the kurtosis parameter of each single run were computed for each transducer, as well as the cumulated statistics for the sum of n runs. The skewness and kurtosis parameters reflect the importance of extreme pressure values in the probabilistic pressure distribution and are herein considered as follows:

$$C_s = \frac{\sum_{n=1}^{N}(p_i - \overline{p})^3}{(N-1)RMS(p')^3} \tag{6.1}$$

$$K = \frac{\sum_{n=1}^{N}(p_i - \overline{p})^4}{(N-1)RMS(p')^4} - 3 \tag{6.2}$$

A selection of test cases is presented in Table 6.1. The successive comparison of the n^{th} run average with the ensemble average of all the runs (Figure 6.2) allowed selecting a cumulated acquisition time of 3 min at 1 kHz, which guarantees an ensemble average estimate $< \mu_{3min} >$ within ± 3 % of the long-term ensemble average $< \mu_{60} >$. An equivalent method is to divide the entire set of data in sub-sets of given duration, e.g equal to the sum of 2, 3 , 5, and 20 consecutive runs, and compare the statistics of such subsets with the ensemble statistics obtained with the total set of data (Bellin and Fiorotto, 1995). The larger the duration of the sub-sets the lower will be the range of variation. In the present case, both approaches gave the same results.

Estimates of mean pressure values vary considerably for individual runs with deep tailwater levels, in particular for the submerged jet case. This is likely due to the absence of the cushioning effect introduced by pool aeration (by buoyancy and compressibility). For the second moment, $< \sigma_{3min} >$ is within ± 2 % of $< \sigma_{60} >$. For the skewness and kurtosis, only the most case with the most enhanced fluctuations was studied in detail. The estimates of the third and fourth moments obtained with cumulated 3 min of acquisition are within $\pm 5 - 10$ % and ± 2 % of the ensemble value, respectively.

This analysis considers data from tests performed before the addition of the honeycomb grid and air vent in the supply system. Since these changes to the supply system have rather contributed to an increase in jet stability, these conclusions are considered to remain valid.

The analysis was also repeated for pressure measurements more radially outwards at $y/D =$ 0.35, 0.69, 1.04, 1.32, 2.08 and the end of the closed-end I-shaped fissure (Figure 6.3) with similar results.

For the submerged jet case, individual run average values vary considerably from one run to the following but are overall in the same range of accuracy has presented before. The

[2] The results corresponding to the "end" position are not included in the submitted paper. The paper deals exclusively with impact pressures. The position of the end of I-fissure transducer is presented in Figure 3.6 and Figure 3.7

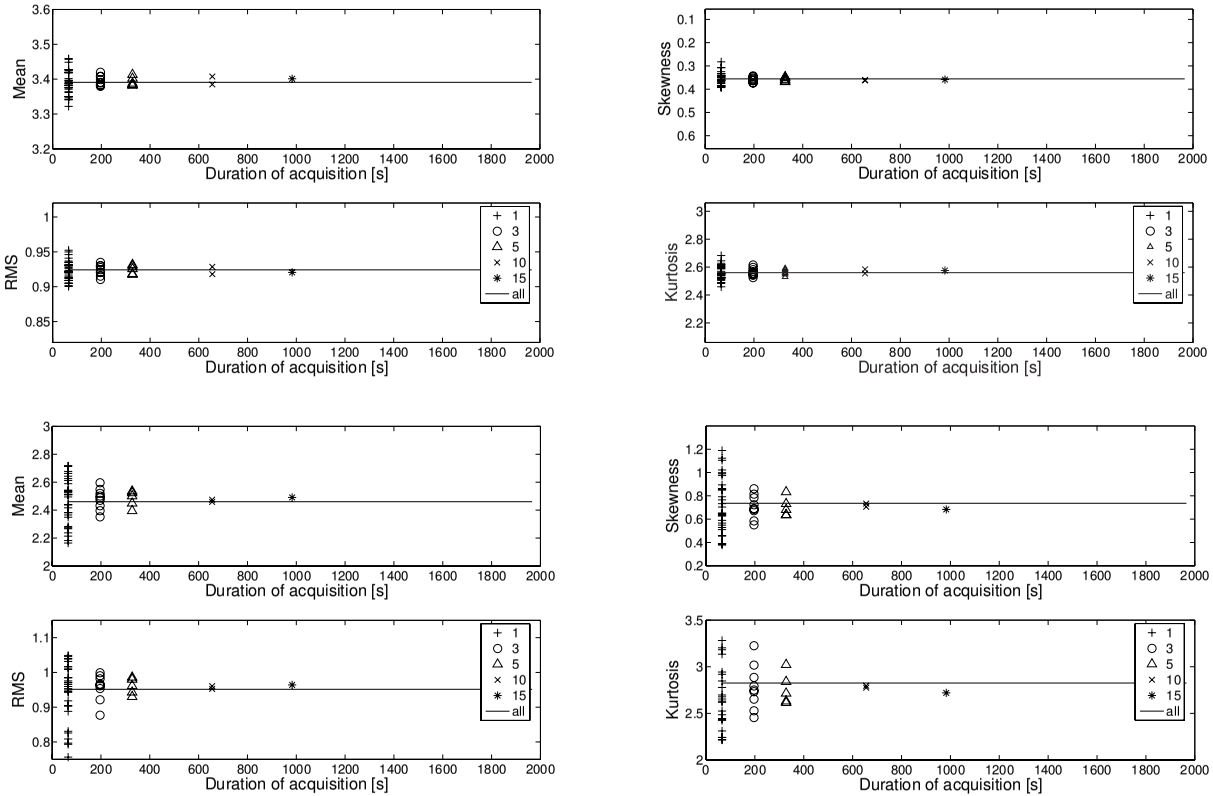

Figure 6.2.: Estimates of the mean, standard deviation, skewness and kurtosis of pressure data series **at $\mathbf{y/D = 0.35}$** compared with ensemble statistics in terms of acquisition duration. Pressure measurements performed close to the jet axis. Rows are: top, shallow pool; bottom, deep pool.

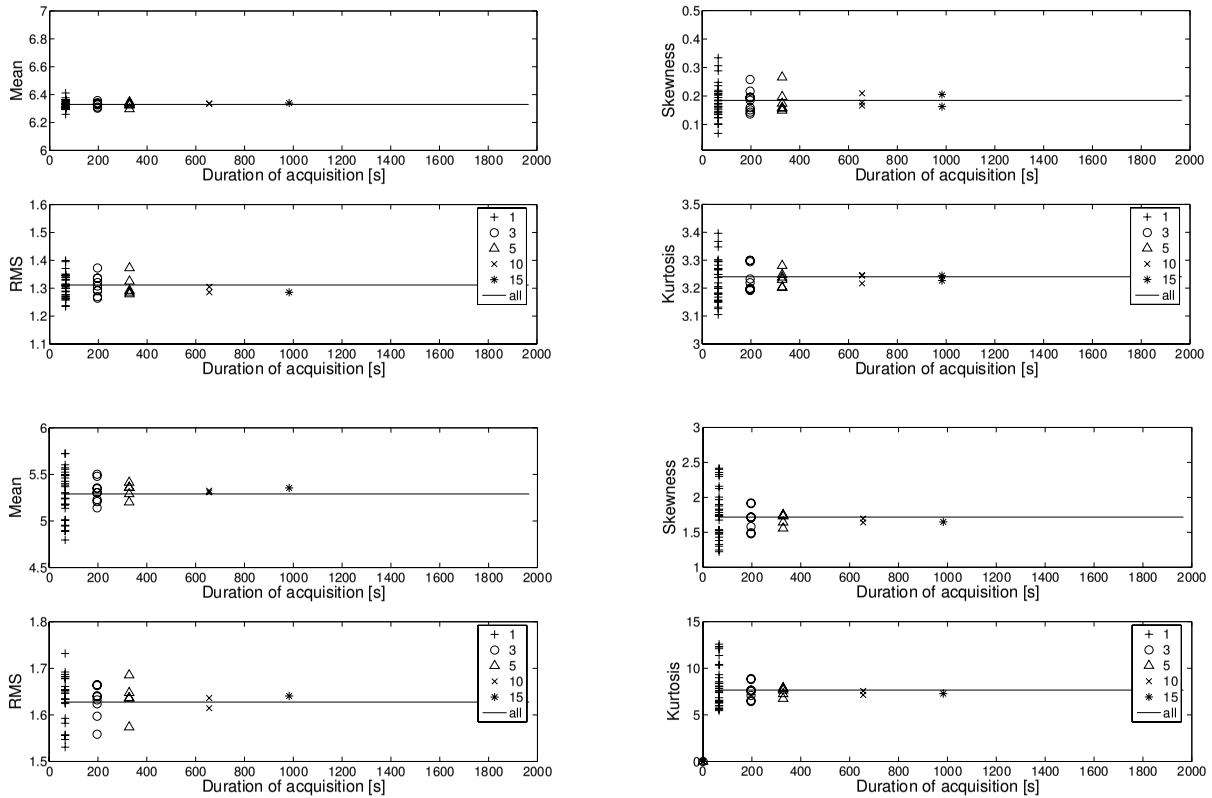

Figure 6.3.: Estimates of the mean, standard deviation, skewness and kurtosis of pressure data series **at the end of the fissure**, compared with ensemble statistics in terms of acquisition duration. Pressure measurements performed close to the jet axis. Rows are: top, shallow pool; bottom, deep pool.

Table 6.2.: Statistics of selected tests (at issuance, each file has 32768 points sampled at 0.5 kHz and at impact with the bottom 65536 points sampled at 1 kHz). C_s is the skewness coefficient, K the flatness excess kurtosis, and z_{min} and z_{max} are the minimum and maximum values of the Gaussian distribution variable.

Test series	Configuration	Y/D	y/D [-]	U [m/s]	P_{mean} [bar]	RMS_p [bar]	p'^+ [bar]	p'^- [bar]	C_s [-]	K [-]	z_{max} [-]	z_{min} [-]
Issuance	without grid		0.00	9.82	1.234	0.083	0.373	0.681	-0.44	1.12	4.49	-8.20
				29.47	5.856	0.359	2.062	2.321	-0.47	0.99	5.74	-6.46
	with grid		0.0	11.62	1.660	0.110	0.563	1.080	-0.85	3.67	5.11	-9.80
				30.73	6.016	0.381	2.389	3.311	-0.62	1.38	6.27	-8.69
Pool bottom	without grid	2.78 (0.20 m)	0.35	9.82	0.207	0.202	0.797	0.570	0.60	-0.24	3.94	-2.82
				29.47	3.747	1.056	3.271	4.030	-0.49	-0.22	3.10	-3.82
		9.31 (0.67 m)	0.35	9.82	0.204	0.088	0.633	0.271	1.06	2.54	7.18	-3.07
				29.47	1.627	0.741	4.517	1.735	1.33	2.34	6.09	-2.34
	with grid	2.78 (0.20 m)	0.35	9.82	1.254	0.077	0.237	0.420	-0.96	1.22	3.09	-5.46
				29.47	5.274	0.737	2.208	4.171	-1.13	1.57	3.00	-5.66
		9.31 (0.67 m)	0.35	9.82	0.988	0.073	0.415	0.195	0.91	1.09	5.68	-2.67
				29.47	3.102	1.042	4.532	2.303	0.77	-0.03	4.35	-2.21

absence of air seems to enhance the fluctuating pattern but not the amplitude of such fluctuations.

For the deep pool case, the average values of individual runs fall within a slightly larger 3 % margin after a cumulated runtime of 3 min. In this case, large pressure fluctuations inside the fissure have been documented by Bollaert (2002b). They result from the amplification inside the fissure of impact pressure fluctuations.

Based on this analysis, a cumulated runtime of 3 minutes was selected for most of the tested cases. This corresponds to performing at least 3 runs of 65 s using the selected frequency of 1 kHz.

6.4. Impact pressures in pools with flat bottom

6.4.1. Effect of adding honeycomb grid and air vent

The characteristics at issuance of the high-velocity jets produced in this facility are presented in Manso, Bollaert and Schleiss (2004b)[3]. These characteristics play a major role in the definition of jet behaviour in the air and in the water cushion. The influence of adding a honeycomb grid in the supply system and improving air exhaustion on jet behaviour at issuance was discussed. For velocities between 10 and 20 m/s jet stability at issuance was considerably improved. These modifications being more recent than previous research results presented in Bollaert and Schleiss (2003b), a comparison between the pressures at impact with the pool bottom generated previously (without grid and air vent) and those produced with the current apparatus (with grid and air vent) was considered necessary.

A selection of tests was used for the comparison of pressure statistics (mean value, standard deviation, maxima, minima, skewness and kurtosis) for low and high velocities (approx. 10 and 30 m/s), taking measurements at issuance and after diffusion through shallow (Y/D = 2.8) or deep (Y/D = 9.3) pool. These statistics are presented in Table 6.2.

The grid and air vent allow to eliminate swirling flow and render the velocity profile almost uniform for velocities from 10 to 30 m/s (Manso, Bollaert and Schleiss, 2004b). Pressure

[3]see also Chapter 4 of this dissertation

distributions are not Gaussian. Skewness values are negative under the jet axis. For highly compact jets, positive skewness would be expected, showing direct impact in the pressure transducer tip. However, due to the intrusion created by the transducer, jet reflection close to the stagnation point generate negative skewness values.

In Figure 6.4 and Figure 6.5, the empirical probability density functions (epdf) of the pressure measurements obtained for two velocities, 10 m/s and 30 m/s, along the jet axis at issuance and at the closest measuring station to the axis at the pool bottom (y/D = 0.35) are compared. Pressure distributions at issuance are compared with the impact pressures after plunging through a water cushion (shallow pool, Y/D = 2.8 and deep pool, Y/D = 9.3) and with the corresponding Gaussian fits (Npdf).

For a low pool tailwater level (Y/D = 2.8) and without grid, pressures at impact present negative kurtosis (i.e pdf flatter than Gaussian pdf) and negative and positive skewness for $V = 10$ m/s and $V = 30$ m/s respectively. The difference in skewness sign is thought to correspond to a higher degree of turbulence development at impact for V = 10 m/s due to the non-homogeneity of the jet core and of a swirling-like velocity profile. After addition of the grid and air vent, pressure statistics at the bottom are fairly close to those measured at issuance. The jet being more compact and uniform, it passes through the water cushion. These pressure statistics likely reflect the impact of a potential core.

The interpretation of the figures with linear y-scale is however counter-intuitive: negative skewness is herein obtained when the epdf central lob is to the right side of the Gaussian pdf; the opposite for positive skewness. In these circumstances, the use of log-scales helps perceiving the weight of the pdf tails (see sub-Figures 6.5 e) and f)). These plots show that for the studied jet velocities, dynamic pressures at issuance and at impact in shallow pools do not follow a Gaussian distribution. In fact, epdf's at impact in a shallow pool show important negative tails. Such negative extremes are somewhat surprising since associated with counter-current fluctuations and may correspond to the effect of jet reflection of the pressure transducer's tip at stagnation. The deviation from a gaussian behaviour is also reflected in the high values of the kurtosis parameter. After the changes to the experimental set-up, both measurements at issuance and at the bottom (Y/D = 2.8) have positive (excess) kurtosis.

When comparing shallow and deep pools (Y/D = 2.8 and 9.3 respectively, Figure 6.5 g) and h), it becomes apparent that the addition of the grid and air vent reduces the weight of the positive tail of the pdfs by increasing that of the negative tail, for V = 10 m/s and 30 m/s and for both pools.

Measurements close to the jet axis in deep pools are positively skewed, in opposition to the observation at the same location with a lower tailwater level. On the other hand, the kurtosis parameter reduces: it is higher at issuance, and progressively lower for the shallow and deep pools considered, for both velocities studied. It reflect an approach to gaussianity with increasing jet development. These conclusions reflect changes in the pool flow pattern that will be discussed in the following sections.

6.4.2. Turbulence intensity

Jet behaviour in the air is quite dependent on jet turbulence intensity (Tu) at issuance (Ervine and Falvey (1987)). Turbulence intensity is defined as $Tu = u'/U$ where u' is the root-mean-square (RMS) value of the axial velocity fluctuations and U is the mean axial

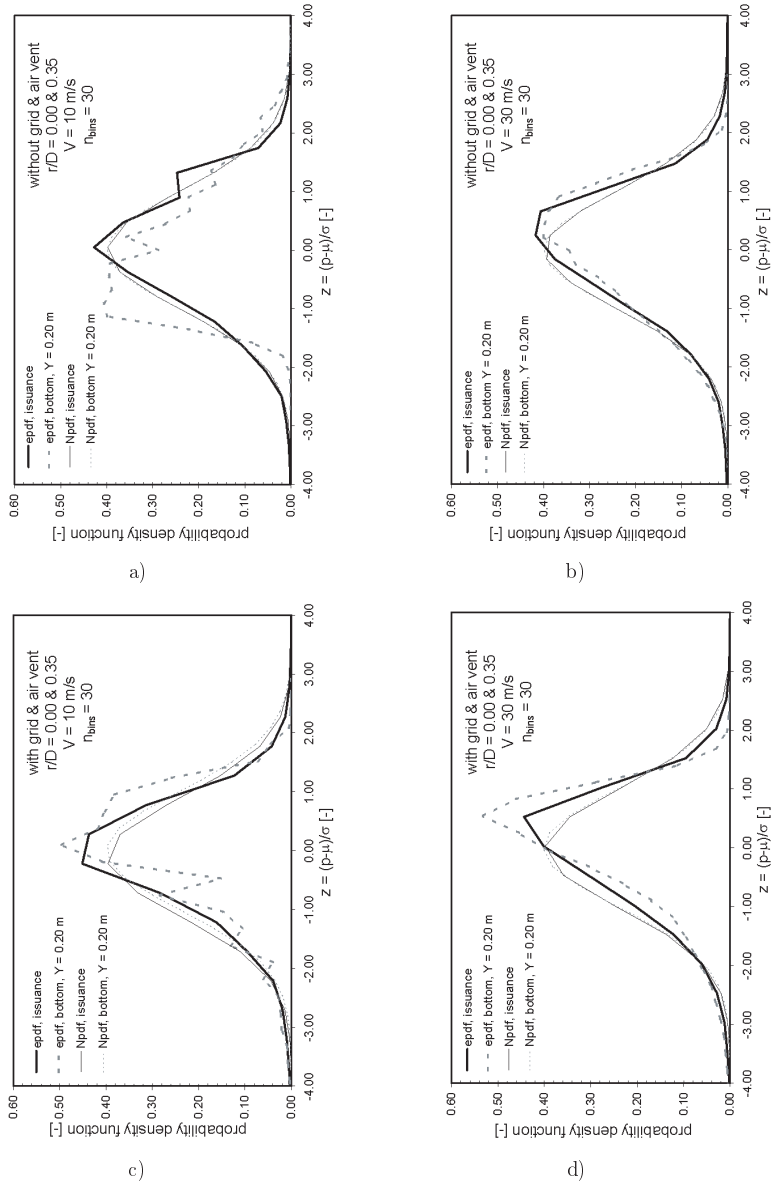

Figure 6.4.: Normalised empirical probability density functions (epdf) and corresponding Gaussian fits (Npdf) of pressure measurements at issuance and for shallow and deep pools (Y/D = 2.8 and 9.3), using 30 class bins for 32768 points at issuance and 65536 points at the pool bottom. Data series:

a) without grid, V = 10 m/s; b)without grid, V = 30 m/s;
c) with grid, V = 10 m/s; d)with grid, V = 30 m/s;

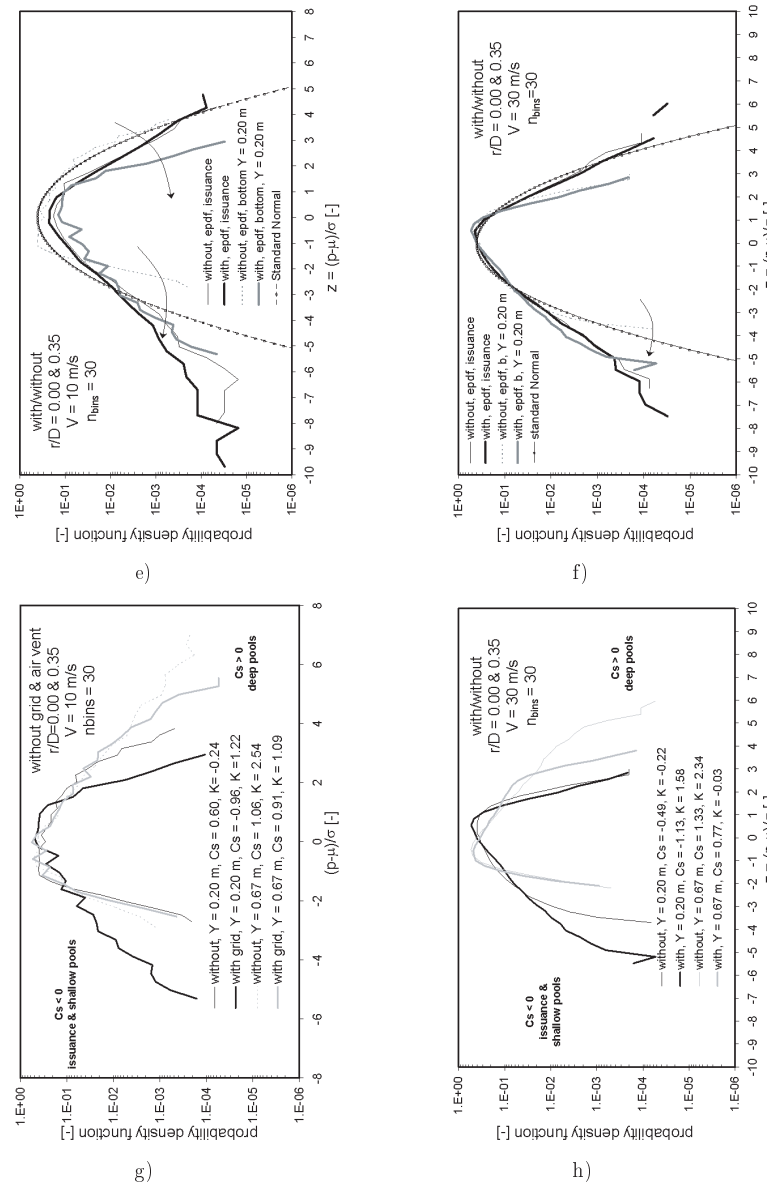

Figure 6.5.: cont.

e) with/without grid, 10 m/s, issuance/shallow pool; f) with/without grid, 30 m/s, issuance/deep pool;
g) with/without grid, 10 m/s, shallow/deep pools; h) with/without grid, 30 m/s, shallow/deep pools.

velocity. Arndt and Ippen (1970) proposed Equation 6.3 and Equation 6.4 for computation of Tu from pressure fluctuations. Higher order terms are neglected when converting pressures into velocities with an estimated error of maximum 5 % for a turbulence intensity level of 10 %, which is considered acceptable, when compared to the expected prototype turbulence intensities.

$$RMS(u') = \sqrt{\overline{u'^2}} = \frac{\sqrt{\overline{p'^2}}}{\rho.U} \tag{6.3}$$

$$Tu = \frac{RMS(u')}{U} = \frac{\sqrt{\overline{p'^2}}}{\rho.U^2} = \frac{RMS(p')}{\rho.U^2} \tag{6.4}$$

Tu estimates at impact can be obtained from the relation between turbulent pressures at the pool bottom relatively to the incoming jet kinetic energy, as defined by Equation 6.5:

$$C'_p = \frac{\frac{RMS(p')}{\gamma}}{\frac{U^2}{2.g}} = \frac{RMS(p')}{\frac{\rho.U^2}{2}} = 2.Tu \tag{6.5}$$

where $RMS(p')$ is the root-mean-square (or standard deviation) of the dynamic pressures (in Pascal), assuming the validity of Equation 6.3. This hypothesis seems adequate for shallow pools. Table 6.3 presents a comparison between Tu estimates at issuance and at the bottom of a shallow pool (Y/D = 2.8).

Table 6.3.: Turbulence intensity estimates from tests with and without grid (and air vent) measured at issuance (y/D = 0.00) and impact with the pool bottom (y/D = 0.35, shallow pool with Y/D = 2.8)

V	Issuance		Y/D=2.8	
[m/s]	no grid	with grid	no grid	with grid
9.8/11.6	0.087	0.081	0.206	0.080
29.5/30.7	0.041	0.041	0.119	0.085

At issuance, Tu values between 4 and 8 % were measured for velocities ranging from 10 to 30 m/s. The lowest Tu corresponds to the highest velocity. At impact with the pool bottom, Tu values of 20 % and 12 % for respectively 10 and 30 m/s were obtained. This is considerably more than measured at issuance, which is rather surprising due to a short travel distance in the air ($\pm 6.9D$). It reflects enhanced jet deformation in the air due to the jet instability created by swirling flow and air accumulation in the supply system. After the changes in the supply system, the velocity profile becomes uniform at issuance. Tu at impact are reduced to about 8 %, which is much closer to the values at issuance. The jet is less developed at plunging point, the degree of break-up is 0.32-0.35 and, therefore, the jet core cuts through the water cushion. Nevertheless, for $V = 30$ m/s, Tu at impact is still doubled compared to that at issuance (it was three times more without the grid). Detailed analysis of the corresponding time series confirmed the existence of intense pool surface instabilities. In fact, bottom wall jet reflection in the basin boundaries generates a feedback phenomena that disturbs the jet's entry in the pool and somewhat increases Tu. This is a typical facility artifact.

It seems plausible to state that jet deformation in the air is small and that core impact conditions are found at the bottom for Y/D = 2.8 and travel lengths of maximum 6.9 times the jet diameter. Therefore, the issuance velocity profile is highly important for the

Table 6.4.: Selected statistical parameters of pressure measurements at $y/D = 0.35$ and differences at negative and positive extreme values between the empirical probability distribution function (E) and the corresponding Normal (N) and Gumbel (Gu) fits. Statistics obtained from a data set of 3 times 65536 points sampled at 1 kHz, (i.e. $\approx$ 3.25 min)

Y/D	V [m/s]	C_s	K	Z'_{min} [-]	Z'_{max} [-]	$\Delta Z'_{0.1\%}$ [E−N]	$\Delta Z'_{0.1\%}$ [E−Gu]	$\Delta Z'_{99.9\%}$ [E−N]	$\Delta Z'_{99.9\%}$ [E−Gu]	Close to Gaussian pdf
2.8	24.6	-0.48	0.45	-6.36	3.72	-1.34	-2.79	-0.50	-1.30	$\approx$ P(0.05-0.90)
	29.5	-1.10	1.44	-5.65	3.70	-	-	-	-	-
5.6	29.5	-1.06	2.05	-7.88	4.78	1.55	-2.72	-0.55	-2.60	$\approx$ P(0.10-0.90)
6.9	29.5	-0.88	0.39	-3.70	3.01	-0.06	-1.27	-1.11	-1.11	$\approx$ P(0.25- 0.75)
8.3	29.5	-1.02	0.44	-4.34	3.11	-	-	-	-	-
9.3	29.5	0.86	0.27	-2.46	4.71	2.32	0.09	-1.76	-1.50	$\approx$ P(0.25 - 0.75)

definition of the turbulent pressure fluctuations in shallow pools. It will certainly be less important for deep pools due to enhanced jet development. Ervine et al. (1997), Bollaert and Schleiss (2003b) and Manso et al. (2005c) presented values of Cp' at impact (flat pools) that do not exceed 0.28 for relative pool depths Y/D of up to 11. Assuming the validity of Equation 6.5 as long as the core persists, and in the absence of any further disturbance, one can generally say that Tu at impact in flat pools is not more than 14 % for shallow pools ($Y/D < 4 - 6$).

The remainder of the chapter deals solely with pressure measurements obtained with grid and air vent.

6.4.3. Bottom pressure distribution for variable pool depths

After modification of the supply system (grid, air vent) the produced jets were considered exempt of laboratorial effects. Two categories of jet impact conditions were defined: core impact and developed jet impact. Core jet impact conditions are encountered at issuance and in shallow pools (Y/D = 2.8) and have negative skewness and positive (excess) kurtosis. Developed jet impact conditions are found in deep pools, for which the skewness values presented in Table 6.2 are positive. The kurtosis is expected to approach zero with increasing jet development.

In Figure 6.6, empirical probability density functions (epdf) are compared with the corresponding Normal (Npdf) and Gumbel (Gpdf) fits. The Normal (or Gaussian) distribution is often assumed as valid for engineering practice. There is growing interest to know how accurate this assumption is. The Gumbel pdf is also quite widely used to estimate extreme values and has the practical advantage of depending (as the Normal pdf does) on only two parameters (mean value and standard deviation). It has been used formerly for the analysis of independent (i.e. non correlated) extreme pressure values obtained at reduced laboratory scale in 24-hour duration runs (Toso and Bowers, 1988). However, due to the small duration of the herein presented near-prototype measurements, their comparison with the Gumbel extreme probability distribution is merely exploratory. Figure 6.6 shows that the experimental data does not follow Normal distributions. The epdf's in the left hand side column show the decrease in importance of the negative extreme values tail for growing pool depths (Y/D values of 2.8, 5.6, 6.9 and 9.3). From the right hand side comparison it can be seen that a Gaussian assumption is valid for probabilities of approximately 0.05-0.25 to 0.75-0.90, all cases considered (Table 6.4). The evolution from negative to positive skewness

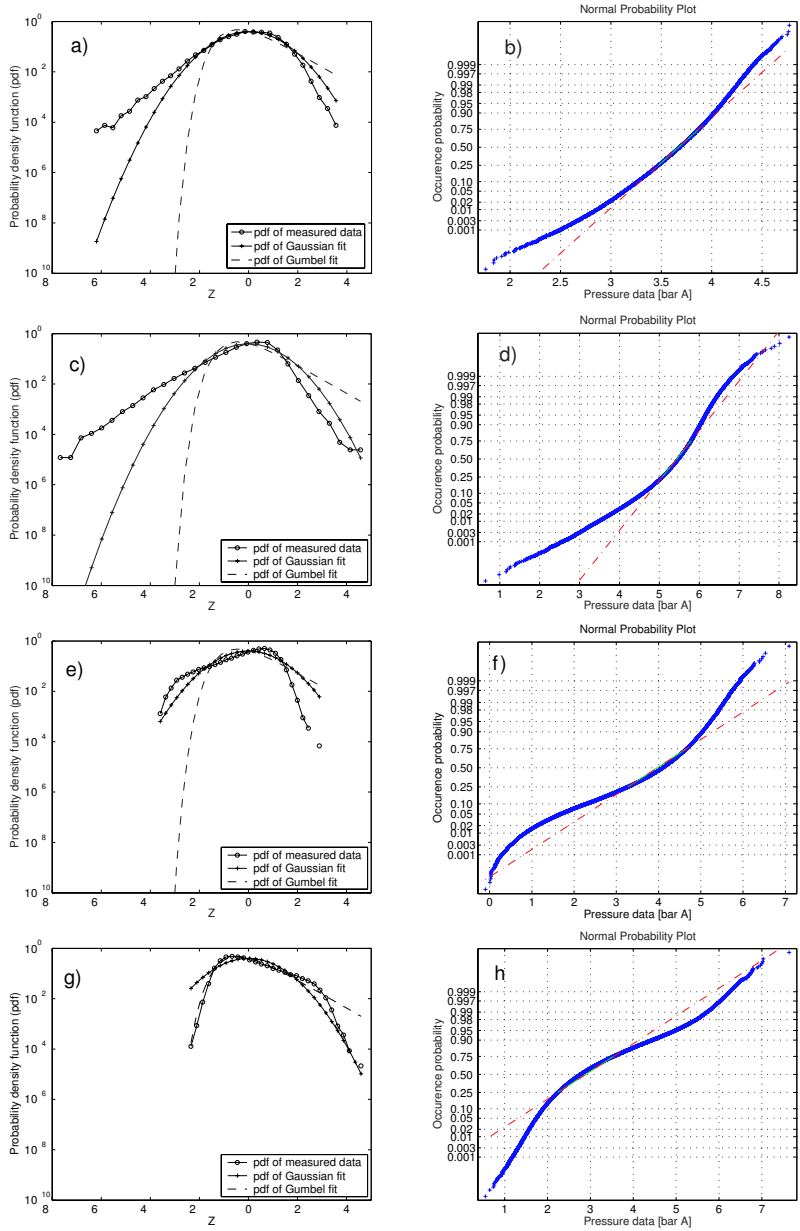

Figure 6.6.: Left: empirical density functions (epdf) of pressure measurements at y/D = 0.35 compared with the respective Normal (Npdf) and Gumbel fits (Gpdf). Right: direct comparison between epdf and the respective Normal fit. Data series:

a) and b): Y/D = 2.8, V = 24.6 m/s; c) and d): Y/D = 5.6, V = 29.5 m/s;
e) and f): Y/D = 6.9, V = 29.5 m/s; g) and h): Y/D = 9.3, V = 29.5 m/s.

at $y/D = 0.35$ with growing pool depth can be observed by the behaviour of the negative and positive tails of the pdfs.

Table 6.4 presents also the differences in terms of number of multiples of σ between the pressure estimates using a Normal or Gumbel distribution for probabilities of 0.1 % and 99.9 %. For both the negative and positive tails, the largest difference between estimates from a Gaussian fit and the measured data pdf's were obtained for $Y/D = 9.3$. The analysis of the semilog-scale plots is helpful in showing whether assuming a Normal distribution assumption is conservative or not.

According to previous observations by Lopardo and Henning (1985) and Fiorotto and Rinaldo (1992b) the skewness parameter changes sign below the hydraulic jump roller where the wall jet starts moving away from the bottom. It can be interpreted as being positive for predominantly incident pressure fluctuations and negative in the oppositive situation. Table 6.4 clearly shows that close to the jet axis (y/D = 0.35), core jet impact conditions (observed at issuance and at least for Y/D = 2.8) correspond to a negative C_s, while developed jet impact conditions ($Y/D = 9.3$) correspond to a positive C_s. The explanation for such counter-intuitive results should be sought on the local flow pattern. For that purpose, the autocorrelation functions of pressure measurements at $y/D = 0.35$ were computed. The space-time unidirectional correlation function is defined as:

$$R(x, \Delta x, \tau) = \lim_{T \to \infty} \int_0^T p'(x,t).p'(x + \Delta x, t + \tau)dt \tag{6.6}$$

where p'(x,y,t) = $p(x, y, t) - \overline{p}$. The autocorrelation at $y/D = 0.35$ can be estimated by:

$$\rho(x, 0, \tau) = \frac{\widehat{R}(x, 0, \tau)}{\sigma^2} \tag{6.7}$$

The initially rapid decay observed in Figure 6.7 provides information on local fluctuations, whereas the slow decaying tail represents a second (larger) structure. This in good agreement with the analogous observations of Carreras et al. (1998). In the case of a shallow pool (Y = 0.20 m, i.e. Y/D = 2.8), one may associate the local fluctuations (with negative skewness) with flow deflection close to the stagnation point. According to free jet diffusion theory by Ervine and Falvey (1987), the jet core boundary should impact the bottom at 28 *mm* from the axis (assuming 8° for the core contraction angle and the impact diameter as the issuance diameter). The measurements at 25 *mm* (y/D = 0.35) were expected to correspond to a predominant downward motion and positive skewness, which is clearly not the case. These *empirical* assumptions do not account for jet deflection close to the bottom. In the present case, it is believed that the transducer's readings are influenced by a fluctuating behaviour of the stagnation point (also observed by Melo 2001 and Kamoi and Tanaka 1972), due to jet core instability and streamline deflection. The negative skewness reflects some type of local correlated structure (e.g. formation of a turbulent boundary layer at the bottom), also shown by the autocorrelation function.

At y/D= 2.08 skewness is positive (Figure 6.8), kurtosis is positive and the autocorrelation drops rapidly to negative values. This is believed to correspond to the presence of a roller. In this case, the transducer is slightly upstream the hydraulic jump created between the wall jet (resulting from jet deflection at the bottom) and the oscillating tailwater level. This hydraulic jump was clearly visible during the tests.

For a deep pool (Y = 0.67 m, i.e Y/D =9.3), pressures at the bottom reflect the impact of a developed turbulent shear layer. Close to the axis (y/D = 0.35), skewness is positive

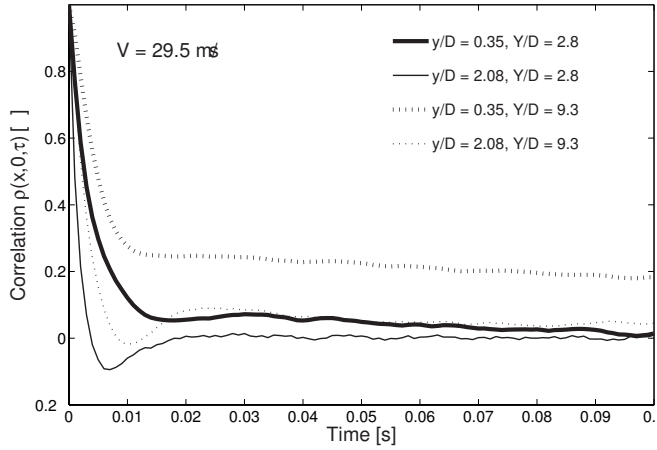

Figure 6.7.: Normalized time correlation function of dynamic pressures at impact with a shallow pool (Y/D = 2.8) and a deep pool (Y/D = 9.3), at y/D = 0.35 and 2.08, created by a plunging jet with V =29.5 m/s (from the expected value FFT of 3 files of 65536 points each, f =1 kHz).

and the autocorrelation drops also sharply. Small local fluctuations should correspond to the developed jet turbulence level, whereas the mild decay of the autocorrelation may correspond to the impcat of the turbulent shear layer of the (developed) jet. At y/D = 2.08, farther from the jet axis, skewness is also zero and the autocorrelation becomes negative at about 0.01 s. The transducer should be under a rotating vortex. Compared to the equivalent situation for shallow pools, the autocorrelation crosses zero at about the double of the time distance. Therefore, the rotating vortex is larger for deep pools than shallow pools, which is in good agreement with observation. Nevertheless, such vortex is smaller than the tailwater level, as observed by Puertas-Agudo (1994).

To accurately determine the tail of the autocorrelation function, improved estimates of high order moments are required (Carreras et al., 1998). In free jet diffusion, turbulence tends to self-similarity and dynamic pressures should be gaussian. In these circumstances, the Hurst parameter is 0.5 and it can be related with the decay of the autocorrelation function. In the present case, the Hurst parameter is expected to be $\neq 0.5$, as observed by Carbone et al. (2000)[4].

6.4.4. Core persistence

The persistence (core length) of turbulent plunging jet is not precisely defined. Ervine and Falvey (1987) suggested a core contraction angle of $7-9^{\circ}$ based on an α_2/α_1 ratio obtained from momentum considerations and variable air concentrations. No direct measurements

[4]This topic may open another line of research on pool turbulent flows, based on the analysis of the fractal dimensions of given turbulent structures induced by the pool geometry in relation with the resulting impact pressures. Mandelbrot (2002) may be a good starting point.

existing, it is often assumed that the core persist until a depth of about 5 times the diameter, instead of the 3-4 diameters mentioned by these authors for rough turbulent jets.

In turbulent flows, a departure from gaussianity in the PDF tails is a sign of intermittency (Carbone et al., 2000), which is directly related to the kurtosis. Sporadic extreme pressures (both negative and positive) generated by intermittent motion tend to increase considerably the 4^{th} statistical moment. They do not necessarily have high energy due to low persistence but their amplitude to the 4^{th} power contributes to a high kurtosis value. This is thought to correspond to the situation where the core is interrupted by turbulent structures. The highest fluctuations should correspond to an intermediate situation for which core impact conditions are the most intermittent. From Table 6.4 and Figure 6.8, the highest kurtosis closest to the jet axis ($y/D = 0.35$) is obtained for Y/D = 5.6. The corresponding time series shows very low pressure extreme values compared to the mean (up to -8σ) and also very high positive extreme values (up to 4.8σ).

Based on these observations, the core development length is hereafter assumed as $Y/D = 5.6$. This is rather long comparing with the indications by Ervine and Falvey (1987), but it could be a direct consequence of the high stability and compaction of the jet. Burattini et al. (2004) observed an increase in core persistence of air jets of approximately 50 % after adding a grid (mesh size about 6 % of jet diameter, 3 % with the present facility), which may partly explain the long persistence of the simulated jets. The relatively low degree of break-up (max L/L_b of 0.35), also contributes to the compaction of the jet at entry in the pool.

On the other hand, and since existing indications of core persistence for rough turbulent plunging jets correspond only to free jet diffusion, it is also possible that the low energy dissipation occurring in the deflection zone results in core impact conditions for slightly larger distances than expected. This, however, can only be verified with direct measurements of the flow field, which merits further research.

6.4.5. Radial pressure distribution

Below the jet, C_s is only positive ($y/D = 0.35$) for deep pools. At $y/D = 2.08$, skewness is almost always positive (Figure 6.9). The highest values of C_s at $y/D = 2.08$ correspond to Y/D = 2.8 (shallow), for which the shear layer does not impact the transducer. Such positive skewness rather reflects the presence of a wall jet disturbed by fluctuations of the pool surface (very low tailwater level). For increasing pool depths (Figure 6.8), C_s at $y/D = 2.08$ tends to zero (i.e. as a Gaussian pdf), reflecting the establishment of a well-developed wall jet. Similarly, the kurtosis at y/D = 2.08 is also higher for shallow pools (more intermittent), approaching gaussianity for Y/D higher than $\approx$ 7. This is in good agreement with the findings of Knowles and Myszko (1998) using air jets. They observed peak levels of wall jet turbulent fluctuations at about y/D = 2, which decrease with increasing distance from nozzle to impact surface (with Y/D ranging from 2.0 to 10 and Reynolds of $\approx 9E04$).

Figure 6.10 shows the evolution of C_s and K with velocity at two locations in the pool bottom, and for several pool depths Y/D. For Y/D = 8.3, C_s at y/D = 0.35 changes sign with velocity. Due to the establishment of a strong recirculation inside the basin, the tailwater level was lowered of 10 to 20 cm at the point of jet entry. This considerably reduces the diffusion length, approaching conditions typical of shallow pools. This effect was only relevant at this relative tailwater level and is considered an artifact of the facility.

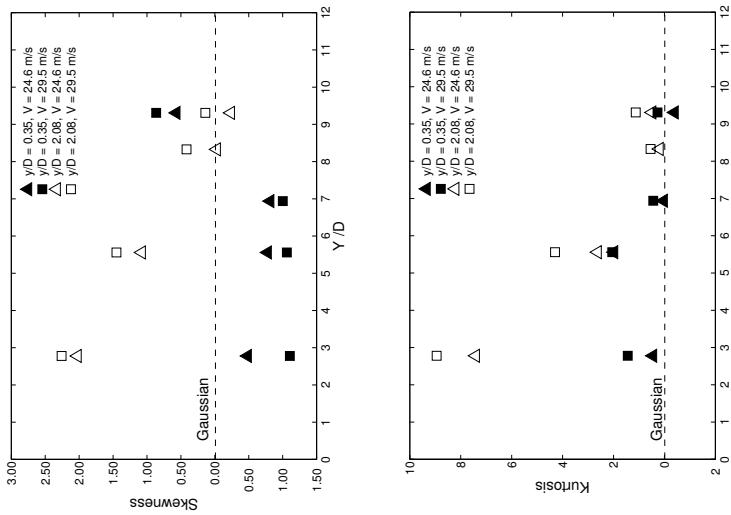

Figure 6.8.: Evolution of C_s, K with relative tailwater depth Y/D.

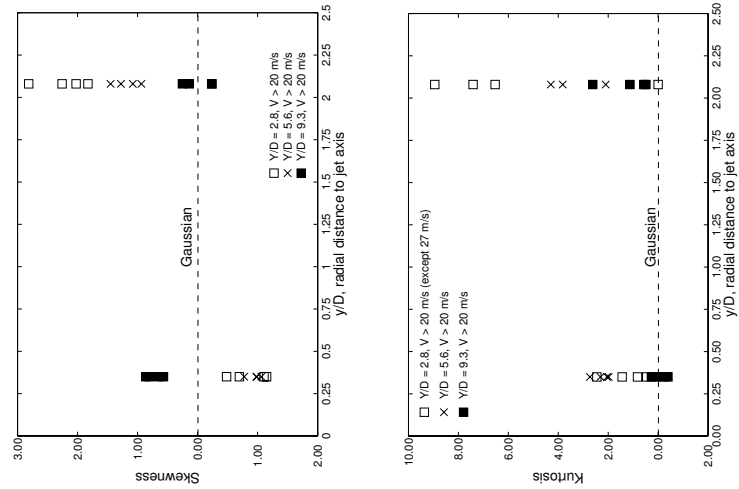

Figure 6.9.: Evolution of C_s, K with distance to jet axis

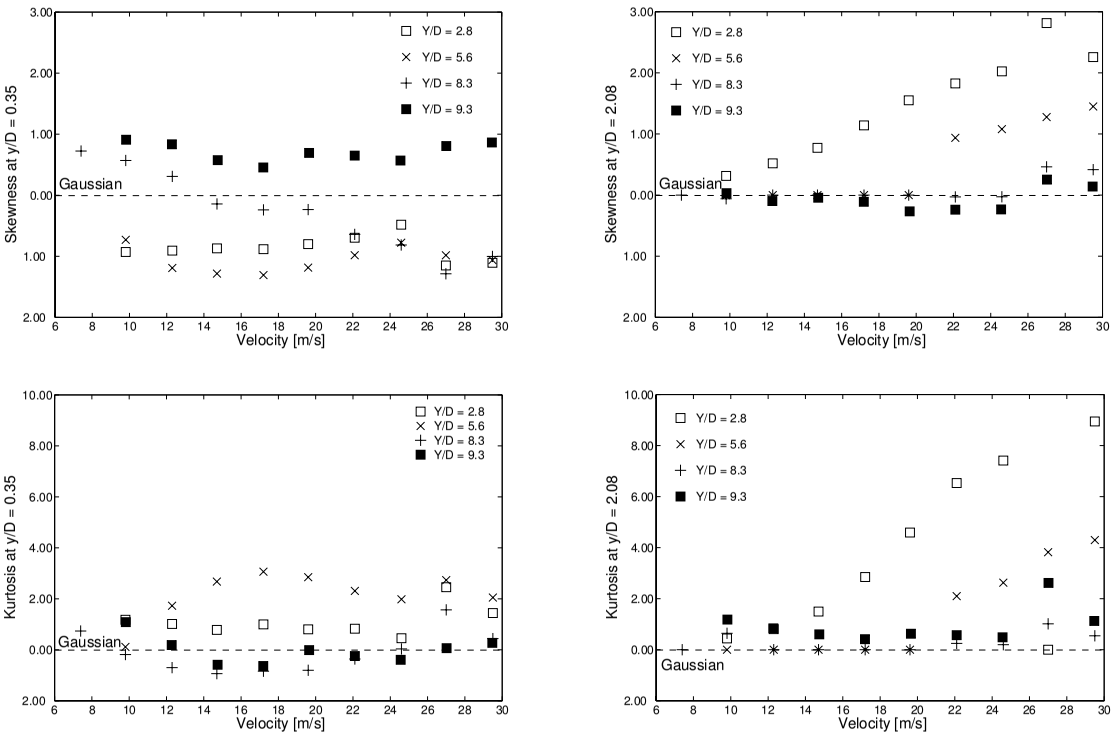

Figure 6.10.: Evolution of C_s and K with velocity. Right column: y/D = 0.35. Left column: y/D = 2.08

In terms of kurtosis, intermittency is higher at $y/D = 0.35$ for the intermediate pool of $Y/D = 5.6$ and for almost all velocities tested. For the remaining Y/D values, the kurtosis are close to zero, corresponding to compact jet impact and developed turbulence for respectively shallow and deep pools. At $y/D = 2.08$, K increases considerably with velocity for shallow pools. If a steady wall jet would exist, K would be close to zero at this position. In this case, jets are deflected with little energy dissipation and hit the experimental facility side walls at high-velocity; since the water cushion is relatively small, its low inertia cannot prevent the readings at y/D = 2.08 from being influenced by pool surface oscillations. In most practical applications, this is also likely to occur for such low submergence ratios, due to the creation of a confined scour hole. For deep pools, the kurtosis values reduce significantly.

For V = 27 m/s, very high kurtosis were registered at $y/D = 2.08$. Three spurious peaks of approximately 5 times the mean incoming kinetic energy were registered during a 3.5 min cumulated run time, each lasting about 1 ms. They were considered outliers and are not presented. For the same reason, the corresponding skewness is somewhat off trend.

A schematic summary of the observations for the two extreme cases of a shallow pool (Y/D = 2.8) and a deep pool (Y/D = 9.3) is given in Figure 6.11.

6.5. Conclusions

Experimental work has been done with high velocity jets at prototype scale. Dynamic pressure measurements both at issuance and after diffusion in a water pool allow concluding that:

1. Compact jets at issuance remain quite compact after travel distances of $L/L_b = 0.35$ and diffusion in pools with relative depths $Y/D \leq 2.8$.

2. Dynamic pressures both at issuance and at impact with shallow and deep pools do not follow a Gaussian (Normal) distribution.

3. The deviation from Normal fits can be analyzed by means of the third and fourth moments of the pressure empirical distribution function, i.e the skewness and the kurtosis. Impact pressures under the jet have negative skewness in shallow pools, due to a deviation of the negative extreme tail from the normal pdf. Skewness at that location becomes positive for deep pools due to an increasing weight of the positive extreme value tail.

4. A combined analysis of high order pressure statistics and autocorrelation functions at the pool bottom allows inferring some characteristic of the pool flow patterns, as radial wall jets at the bottom and depth-dependent rollers.

5. Negative skewness under the jet for shallow pools coincides with a double-structure time autocorrelation function of pressure measurements. Local fluctuations close to the stagnation point may reflect an acute deflection of jet streamlines.

6. An increasing tailwater level (or pool depth) enhances the development of the jet core and increases turbulence in the pool. The highest kurtosis under the jet axis was registered for $Y/D = 5.6$, which approximates the core development length. For such plunging rough turbulent high-velocity aerated jet, the core contraction angle is likely 5°.

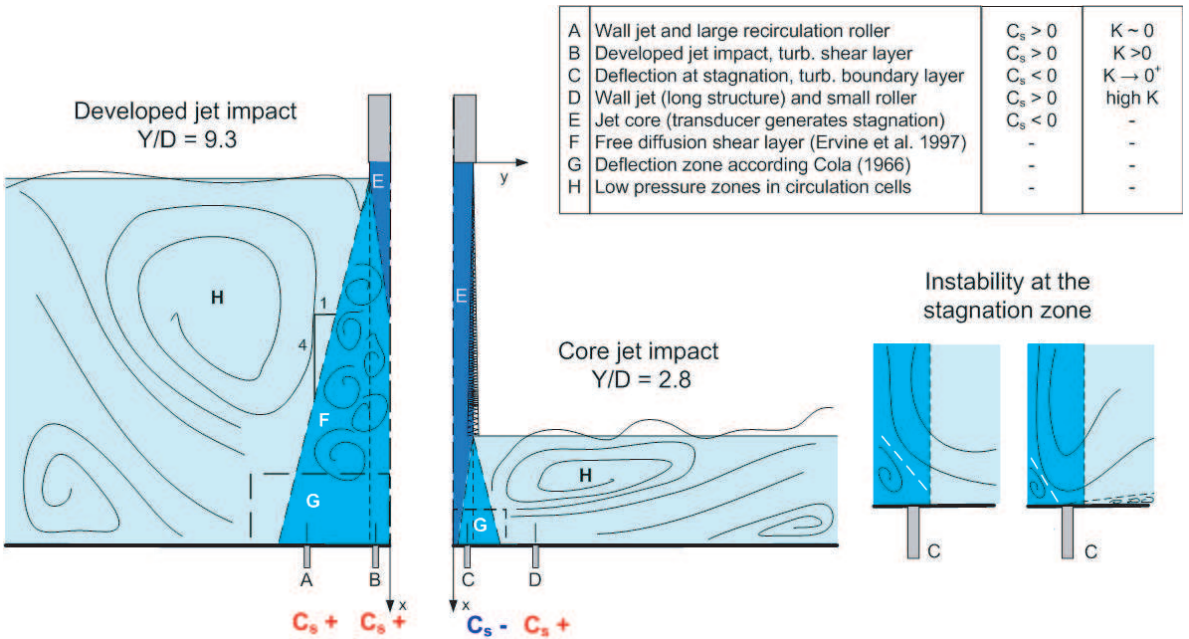

Figure 6.11.: Schematic representation of flow patterns and statistical parameters as C_s and K, according relative pool depth Y/D and distance to axis y/D. Detail of presumed local flow pattern at the stagnation point, including fluctuating pattern due to jet instability.

7. An increasing tailwater level also leads to a change in sign of the skewness parameter under the jet and a more pronounced deviation from Normal fits. Extreme values with occurrence probabilities beyond, on the average, 0.10 and 0.90, merit further investigations based on longer acquisition runs.

8. Bottom pressures further outwards, at $y/D = 2.08$, reveal the presence of a well developed wall jet for deep pools (with slightly negative skewness and almost nil kurtosis) and the intermittent character of pool surface oscillations for shallow pools (increasing positive skewness and kurtosis with velocity) combined with depth-dependent rollers.

The above results contribute to the description of impact pressures generated by plunging rough turbulent high-velocity aerated jets in flat pools. The flat pool geometry is the reference scenario for this research on the interaction between jet diffusion and real-life pool geometries (laterally confined, skewed, etc.) by analysis of impact pressures. This type of complex multi-phase flows hardly allows any other type of measurement technique.

6.6. Complements on the asymmetry of pressure fluctuations

The physical meaning of a change in sign of the skewness parameter of pressure fluctuations in plunge pools is investigated in detail hereafter.

For shallow pools, pdf's under the jet have negative skewness and positive excess kurtosis. For deep pools, skewness becomes positive.

Skewness is defined as a cubic power (see Eq. 6.1). It is negative when the sum of the negative differences p'^- at the power 3 is larger than the sum of the positive differences p'^+.

This may correspond to :(1) the number of p'^- in a sample set is larger than the number of p'^+ or, (2) the amplitudes of the p'^- are larger than those of the p'^+ or, (3) a combination of both.

In supercritical flows, the occurrence of many values lower than the mean reflects turbulent events that should be induced from downstream. In the present case, the impact with the pool surface at very high velocities (or with the transducer's tip close to the outlet) results in strong reflection and thus important local counter currents.

On the other hand, if the skewness is positive, then p'^+ are more important (in number, amplitude or both). In this case, fluctuations are predominantly in the same direction of the mean flow. In fact, their energy can be added up to that of the mean flow.

In order to assess in more detail the origin of negative and positive values of the skewness parameter, a break-down analysis of pressure fluctuations was performed and is presented in Table 6.5. The number of positive/negative fluctuations and their weight on the computation of the C_s for V = 29.5 m/s and various relative pool depths Y/D is presented.

The results in Table 6.5 show that the sign of C_s is more influenced by the amplitude p'^+ or p'^- than by their numbers.

For compact jet impact conditions, the mean value is very high. Even if the majority of fluctuations are positive, their amplitude is rather small comparatively to the mean.

Table 6.5.: Breakdown of p' values using one single run (65'536 samples at 1 kHz)

Test	y/D	C_s	Y/D	V	$\sharp p'^-$	$\sharp p'^+$	$\sum p'^{-3}$	$\sum p'^{+3}$
	-	-	-	[m/s]	-	-	$[bar^3]$	$[bar^3]$
shallow	0.35	-1.13	2.8	29.5	26688	38848	-39261	9683
deep	0.35	0.77	9.3	29.5	37979	27557	-30266	87185
shallow	2.08	2.20	2.8	29.5	41867	23669	-28	236
	2.78	0.79	2.8	29.5	34258	31278	-140	281
deep	2.08	0.23	9.3	29.5	39664	25872	-45223	457781
	2.78	-1.04	9.3	29.5	37693	27843	-753	230

Reflection at the pool bottom creates negative fluctuations, that are quite important in amplitude and are responsible for the negative skewness.

For developed jet impact conditions, turbulent pressure fluctuations carry more energy comparatively to compact jet impact conditions. As the predominant motion is still downwards, despite the interference of pool currents, positive pressure fluctuations are larger in amplitude regarding negative fluctuations.

In fact, this analysis of the relative weight between number and amplitude of fluctuations of given sign, confirms the relation between the C_s and the Gaussian Z' variable. In Table 6.4, it was visible that Z'_{min} was always larger than Z'_{max} for negative C_s, and vice-versa.

On the other hand, the interpretation of velocity and pressure fluctuations also depends on the predominant flow motion. In the region directly influenced by the falling jet, predominant motion in perpendicular to the surface, whereas in the wall jet region it is approximately parallel to the surface.

Results for measuring points more radially outwards, approaching the wall jet region, show that the energy in the fluctuations normal to the surface is much smaller comparatively to that in the impact zone. C_s is positive at y/D =2.08, due to the large contribution of the positive fluctuations (about 10 times higher than that of the negative fluctuations).

While moving radially away from the centre of the jet, the pressure fluctuations should reflect the degree of a given "predominant motion" impinging at an angle with the pool bottom: when predominantly downwards, skewness is positive; when predominantly upwards, skewness is negative; and, when parallel, gaussian. The last situation corresponds in the present case to a parallel wall jet under a large roller, as shown by the breakdown performed for $y/D = 2.78$ in a deep pools. C_s becomes negative and the point of gaussianity is likely to be between 2.08D and 2.78D. In fact, for y/D = 2.78 C_s is negative, with a majority of negative fluctuations. This means that the number of fluctuations of given sign is also important if the amplitudes are small. It may be concluded that the skewness of wall pressure fluctuations may be used to identify flow motion.

7. Deformation at stagnation of air bubbles entrained by high-velocity jets in pools with flat bottom

This chapter present experimental work to assess the air concentration at selected position inside plunge pools with flat bottom (Figure 7.1), using advanced instrumentation in unprecedented conditions of turbulence and high pressure gradient (maximum 3 bar) close to the pool bottom.

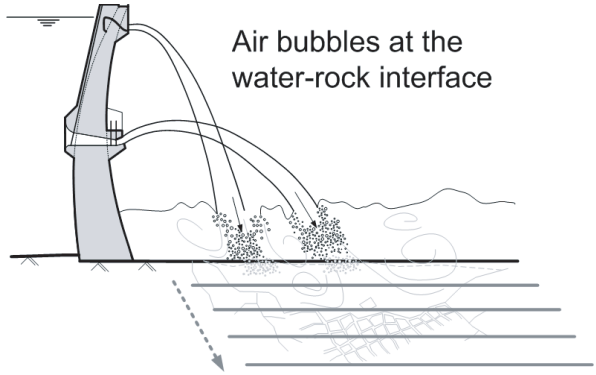

Figure 7.1.: Schematic representation of air entrainment by plunging jets in pools with variable depth (and flat bottom).

7.1. The role of entrained air in rock scour

High-velocity plunging jets are found in many hydraulic schemes, namely in large dams. The process of energy dissipation has to be confined in a plunge pool, either lined or unlined. It is of course highly advantageous economically not to line the riverbed at impact, saving the investment that would correspond to the construction of large lined pools. In either case, impact pressures have to be estimated and compared with the resistance capacity of the plunge pool bottom. Unlined plunge pools may scour until an equilibrium condition is reached, but should not endanger dam stability or that of the valley side slopes. Lined pools should be designed to withstand a given dynamic load throughout the entire lifetime of the dam. Air entrainment in the pool reduces mean pressures at impact (Melo, 2002b). The buoyancy of air bubbles is in counter-flow and hinders jet diffusion. It is also expected to reduce the extent of scour in mobile-bed rivers (Canepa and Hager, 2003).

The process of air entrainment during the jet trajectory in the air has been extensively studied and depends mainly on jet characteristics at issuance such as velocity, geometry and turbulence intensity (Ervine and Falvey, 1987; Zaman, 1999). Additional air is dragged into the pool when the jet pierces the pool surface. McKeogh and Ervine (1981) described the mechanisms of air entrainment in the pool for jets with different turbulence intensities from laminar to rough turbulent. The diffusion of rough turbulent plunging water jets inside a water pool has been object of systematic research by, amongst others, Henderson et al. (1970); Hartung and Häusler (1973); McKeogh and Ervine (1981); Ervine and Falvey (1987); Bonetto and Lahey Jr (1993); Bohrer et al. (1998). In unbounded (free) diffusion conditions, the air bubbles entrained by rough turbulent jets have diameters in the order of a mm (Bonetto and Lahey Jr, 1993).

Extensive literature is also available for smooth turbulent jets, e.g. Cummings and Chanson (1997); Brattberg and Chanson (1998); Chanson et al. (2004) . A comprehensive review of air entrainment by plunging liquid jets, independently of their turbulence level, performed by Bín (1993) remains a good reference.

However, only few studies are performed for bounded diffusion conditions, i.e. when jet streamlines are deflected at impact with a solid surface (McKeogh and Elsawy, 1980). In these circumstances, the stagnation pressure gradient can be sufficiently high to modify air bubble behaviour in the pool regarding free diffusion conditions. Phenomena like bubble compressibility (Zhao and Li, 2000) may significantly alter the dynamic loading transmitted to the pool bottom by interfering with jet diffusion. Besides reducing mean pressures at impact, the presence of air may interfere with the turbulent character of the pressure loading.

The presence of air inside rock fissures is relevant for the process of rock scouring (Bollaert, 2002b). Air bubbles in the fluid mixture inside fissures reduce the celerity of pressure waves. The dimensions of the air bubbles vary with local pressure according to the Law of Ideal Gases. The amount of air dissolved in the liquid may also vary with local pressure according Henry's Law if adequate thermodynamic conditions are verified. Apart from what may occur, it has been verified that pressure wave propagation and superposition may generate transient regimes with important spurious pressure peaks and/or important regular pressure oscillations. This superposition depends on the celerity of pressure waves. Hence, air may interfere in the dynamic response of joint systems, both in fractured rock and under concrete slabs of lined pools. There is great interest to know if air bubbles reach the pool bottom and if they can enter rock fissures.

7.2. Air entrainment by plunging jets in limited-depth conditions

Most air is entrained at the plunging section, around the jet. This air is entrapped in the surface disturbances of the jet and in the air boundary layer just outside the spreading limits of the jet. For developed jets or for jets with aerated cores (as those issued from long chute spillways with ski-jumps), air enters the pool directly under the jet. Air is dragged to larger depths by flow momentum. The mechanisms of air entrainment by plunging jets are described by McKeogh and Ervine (1981). Methodologies to compute the air-water ratio β and the corresponding air concentration C_{air} in free jet diffusion conditions have been presented in section 2.8.

The pressure gradient between different zones of the pool pushes air bubbles to travel to lower pressure zones. In hydrostatic conditions, this corresponds to bubbles moving upwards. In high-velocity pool flows, air bubbles are trapped and transported by the jet and by the shear layer vortices. Bubbles may be forced move to higher pressure regions (e.g jet diffusion when approaching the pool bottom) and will reduce in size.

In developed flow conditions, bubbles rise as soon as the downward turbulent velocity fluctuations become less important than the bubble rise velocity. For decreasing jet velocities, bubble migration to low pressure zones becomes predominant.

Bubbles follow pressure gradients faster than water does, due to their lower inertia. Close to the pool's bottom and in particular close to the stagnation point, the pressure gradient is so important that it is highly unlikely to find any air there. However, if there is an opening in the pool bottom (e.g. a fissure), stagnation conditions are modified (Kobus et al., 1979). The velocity at the bottom is not nil and mass exchange between the pool and the foundation may occur. Thus, air may eventually travel up to the solid boundary.

McKeogh and Elsawy (1980) indicate that the volume of air retained in the pool is in a state of dynamic equilibrium. Despite the continuous movement of air into and out of the aerated zone, the overall volume of air in the pool remains rather constant. Their analysis is based on an evaluation of volume rather than local or mean air concentration. They performed test with jet velocities up to 5 m/s, $Tu < 5$ %, jet diameters of 6 and 9 mm and variable jet fall height, to assure undeveloped and developed plunging conditions. Two conclusions are relevant for the present study: (1) the volume of air retained in the pool in bounded diffusion conditions can be as much as 20 % higher than that in free diffusion conditions (i.e. Y $<$ D_p, where D_p is the depth of bubble penetration); and, (2) the maximum relative increase in the volume of air retained compared to free jet diffusion is reached for Y/D_p=0.6. Such increase is likely related with the ability of pool flow pattern to entrap the air in the pool, preventing it from ascending.

7.3. Experimental work

The experimental facility, the instrumentation, the test procedure and the methodology for post-processing of the experimental data have been presented in section 3.4.

7.4. Void fraction measurements

The void fraction C is the proportion of time that the probe tip is in the air, as described in detail in Section 3.4.4. Void fraction statistics can be obtained for both probe tips, but only those of the leading tip are herein considered for analysis.

For each measurement point a first analysis was performed to define the duration of acquisition necessary to have representative estimates of the local void fraction. Several runs with different duration, from 5 to 60 s, are performed. Since the void fraction varies linearly with the duration of acquisition, it was possible to sum up several runs to obtain the void fraction of the cumulated duration. Longer duration runs, typically from 60 to 300 s, are used to obtain estimates of the ensemble average. This analysis is hereafter presented in detail for measurement point 1 (MP1) and is summarized for points 2 and 3 (MP2 and MP3).

7.4.1. In the impinging region, close to stagnation (MP1)

Void fraction estimates for individual runs of 5 s and 60 s, as well as for cumulated runs of 50 s and more, for four pool depths are presented in Figure 7.2.

All the results for MP1 are presented in these plots. Despite the apparent scatter, the plots show that steady estimates of the local void fraction can be obtained within reasonable laboratory durations. A summary of void fraction estimates is presented in Table 7.1.

Table 7.1.: Void fraction at jet centreline, in the impinging zone, z = 25 mm, measurement point 1 (MP1)

Y (Y/D)	V	cumulative duration	average	maxima [5 s runs]	minima [5 s runs]
0.20 (2.8)	6.14	50	0.043	0.069	0.029
	9.82	50	0.047	0.074	0.028
	14.74	50	0.041	0.068	0.030
	19.65	50	0.043	0.058	0.026
	22.10	50	0.038	0.057	0.026
0.30 (4.2)	6.14	50	0.052	0.064	0.039
		300	0.053	0.074	0.039
	9.82	50	0.036	0.046	0.031
		150	0.036	0.050	0.028
	14.74	50	0.029	0.036	0.021
		150	0.030	0.036	0.021
	19.65	50	0.032	0.050	0.024
0.40 (5.6)	6.14	50	0.058	0.067	0.052
		300	0.055	0.072	0.051
	9.82	50	0.047	0.056	0.036
		300	0.050	0.064	0.034
	14.74	50	0.033	0.036	0.028
		300	0.035	0.046	0.027
	19.65	50	0.031	0.037	0.026
		300	0.035	0.057	0.026
	20.88	50	0.035	0.048	0.027
0.67 (9.3)	6.14	50	0.017	0.021	0.014
		300	0.017	0.030	0.014
	9.82	50	0.062	0.110	0.037
		300	0.061	0.110	0.022
	14.74	50	0.071	0.096	0.048
		300	0.072	0.115	0.043
	19.65	50	0.067	0.085	0.052
		300	0.064	0.097	0.047

The differences between the shorter (50 s) and the longer runs (150 s or 300 s) are mostly below 6 %, with one single exception as indicated in Table 7.2. For the remaining measurements, regular acquisition durations of "cumulated 50 s" (sum of 10 runs of 5 s) or single runs of 60 s were done. Summing up several runs of equal duration allows obtaining the void fraction of a given cumulated duration. Longer duration runs, typically from 60 to 300 s, were used as estimates of the ensemble average. The differences of the 50 s or 60 s statistics regarding the ensemble statistics were also less than 6 %.

At MP1, void fraction is generally between 0.02 and 0.08 for all the pool depths investigated and for velocities from 6.1 to 22 m/s (Figure 7.3).

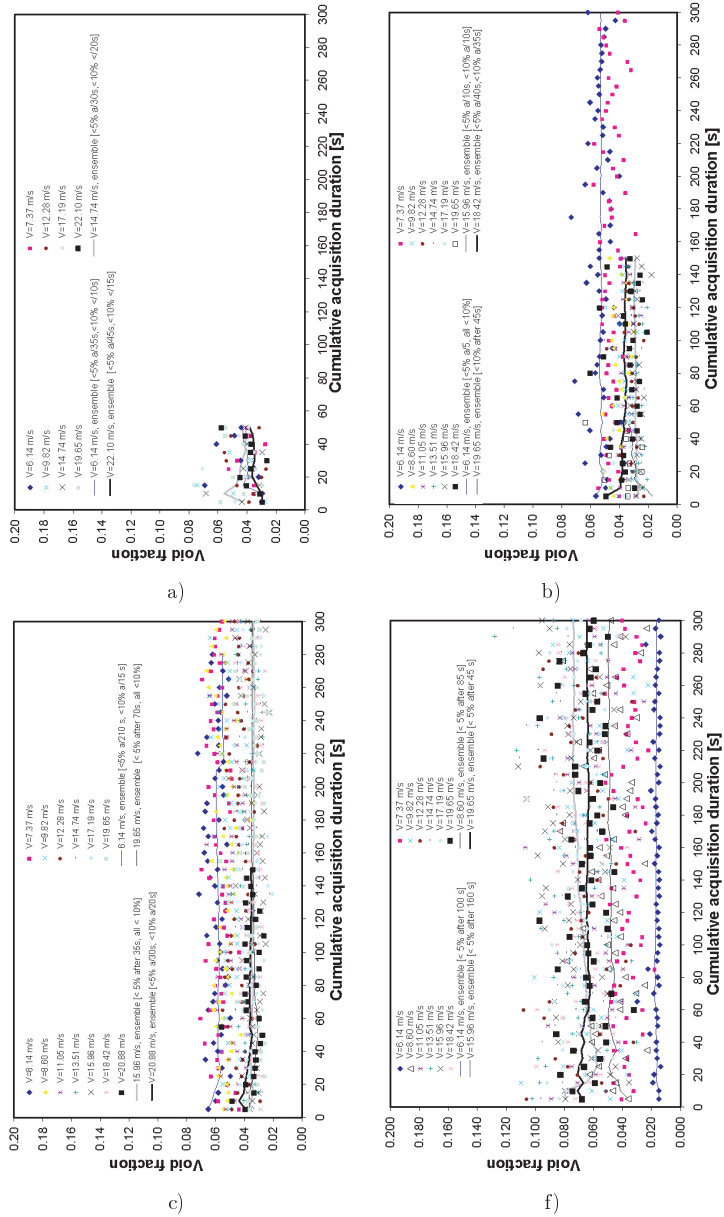

Figure 7.2.: Void fraction at jet centreline, in the impinging zone, z = 25 mm, measurement point 1 (MP1, note: these figures are intended for a global and not a detailed interpretation):

a) Y = 0.20 m (Y/D = 2.8) b) Y = 0.30 m (Y/D = 4.2)
c) Y = 0.40 m (Y/D = 5.6) d) Y = 0.67 m (Y/D = 9.3)

Table 7.2.: Differences between void fraction estimates obtained at measurement point 1 (MP1) from cumulated 50 s of acquisition and the ensemble void fraction estimates (durations of 150 to 300 s)

Y	V	cumulative duration	ensemble duration	Difference to ensemble C_{air}
0.30	6.14	50	300	2.4 %
	9.82	50	150	1.0 %
	14.74	50	150	3.6 %
	19.65	50	50	-
0.40	6.14	50	300	5.5 %
	9.82	50	300	6.4 %
	14.74	50	300	5.9 %
	19.65	50	300	10.1 %
	20.88	50	150	2.0 %
0.67	6.14	50	300	0.6 %
	9.82	50	300	2.2 %
	14.74	50	300	1.4 %
	19.65	50	300	3.6 %

For Y = 0.20, 0.30 and 0.40 m the highest values correspond to the lowest velocities (6 - 10 m/s), but for Y = 0.67 m they correspond to the highest velocities (18 - 22 m/s).

This is good agreement with jet development and turbulent pattern. Low velocity jets with higher Tu will entrain more air, whereas higher velocity jets (with lower Tu) remain compact farther. For shallow pools (Y/D<6), it is less likely that the core persists up to the pool floor for the lower velocities. For the highest velocities, the core is expected to persist longer and therefore these measurements reflect the nearly non-aerated character of the jet core.

For deep pools, and despite the differences in Tu for the different velocities, it is the pool flow pattern that governs the air content close to the bottom. For lower velocities, the depth of bubble penetration is less deep and therefore less air is found close to the pool bottom.

7.4.2. In the transition from the impinging to the wall jet region (MP2)

The second measurement point (MP2) is 10 cm radially away from the jet centreline, which corresponds theoretically to the impinging zone for shallow pool levels and the wall jet zone for deeper pools.

Void fraction values are much higher at MP2, after deflection of the plunging jet, than at MP1 (Figure 7.3, middle). The amount of entrained air increases with the velocity of the plunging jet at issuance V_0, and varies from 5 to 70 % for velocities of 6 to 24.5 m/s and relative pool depths Y/D between 2.8 and 9.3.

Most of the estimates lay between 5 and 40 %, save for the Y/D = 2.8 and V > 17 m/s; in these conditions, the falling jet pierces through the pool surface violently and the deflected wall jet creates a free hydraulic jump (circular) away from the centre of the pool. For increasing Y/D values the hydraulic jump approaches the falling jet and eventually becomes submerged for large pool depths. In these particular conditions, the deflected wall jet at the pool bottom is of the same order of magnitude of the distance between the optic probe tips and the pool bottom (i.e. 25 mm). Hence, the probe is either (1) in the top layer of a free surface horizontal flow (bottom wall jet), more precisely at the flow depth equivalent to 70 % of air and 30 % of water or, (2) close or even inside the hydraulic jump. In the latter case,

the flow is not unidirectional so it is hardly possible to assess if a given air bubble passes through the tip more than once during the measurement time window.

7.4.3. In the transition from the free jet region to the impinging region (MP3)

The third measurement point (MP3) is aligned with the jet centreline. The leading tip of the probe is 10 cm higher than the pool bottom (i.e. z = + 10 cm, z being a vertical co-ordinate opposite to x). According to the relative pool depth, this location can be classified as presented in Table 7.3.

Table 7.3.: Classification of MP3 according relative pool depth and jet diffusion

Y	z/Y	Pool region	x/D_0	Jet development
20	0.50	Free jet	1.4	Flow development zone (shallow pool)
40	0.25	Impinging - Free jet	4.2	Flow development zone (ev. transition)
67	0.15	Impinging - Free jet	7.9	Zone of established flow (deep pool)

In this case, void fraction values are globally lower than those at MP2 but higher than those at MP1 (Figure 7.3). For Y = 0.20 m (shallow pool), C_{air} ranges from 0.20 to 0.30 and grows with velocities from 6 to 22 m/s. For Y = 0.67 m (deep pool), C_{air} varies between 4 and 12 % for velocities from 6 to 24.5 m/s. It also grows with velocity. For an intermediate water level of Y = 0.40 m, C_{air} is as low as values for a deep pool for low velocities (i.e. $C_{air} < 15$ % for V < 15 m/s) but increases up to values close to those of a shallow pool for high velocities (i.e. $C_{air} \approx 0.25$ for 22 < V < 29.5 m/s). In summary, C_{air} at MP3 decreases with the increase of the pool depth and jet development.

7.5. Comparison between void fraction measurements and estimates with existing laws for air entrainment in free diffusion conditions

Air entrainment in plunge pools has been studied extensively, mainly in unbounded jet diffusion conditions. Test conditions are quite varied and not all relevant for the present study. Laminar to smooth and rough turbulent jets have been studied, in monophasic conditions (submerged) or in biphasic conditions (air-water). Circular and plane jets, of either air or water have been investigated.

The void fraction measurements performed are hereafter compared with other experimental results obtained in unbounded jet diffusion conditions:

1. Plunging circular jet data by McKeogh and Ervine (1981), for rough turbulent jets with $Tu = 5$ %, $D_0 = 9$ mm and V = 3.13 m/s. However, these jets are fully broken-up at impact.

2. Plunging circular jet data by McKeogh and Ervine (1981), for smooth turbulent jets. According to the authors, these jets are undeveloped at impact ($L/D_0 < 33$). However, smooth jets are known to entrain smaller air bubbles than rough jets (Bonetto and Lahey Jr, 1993) and therefore C_{air} is necessarily lower.

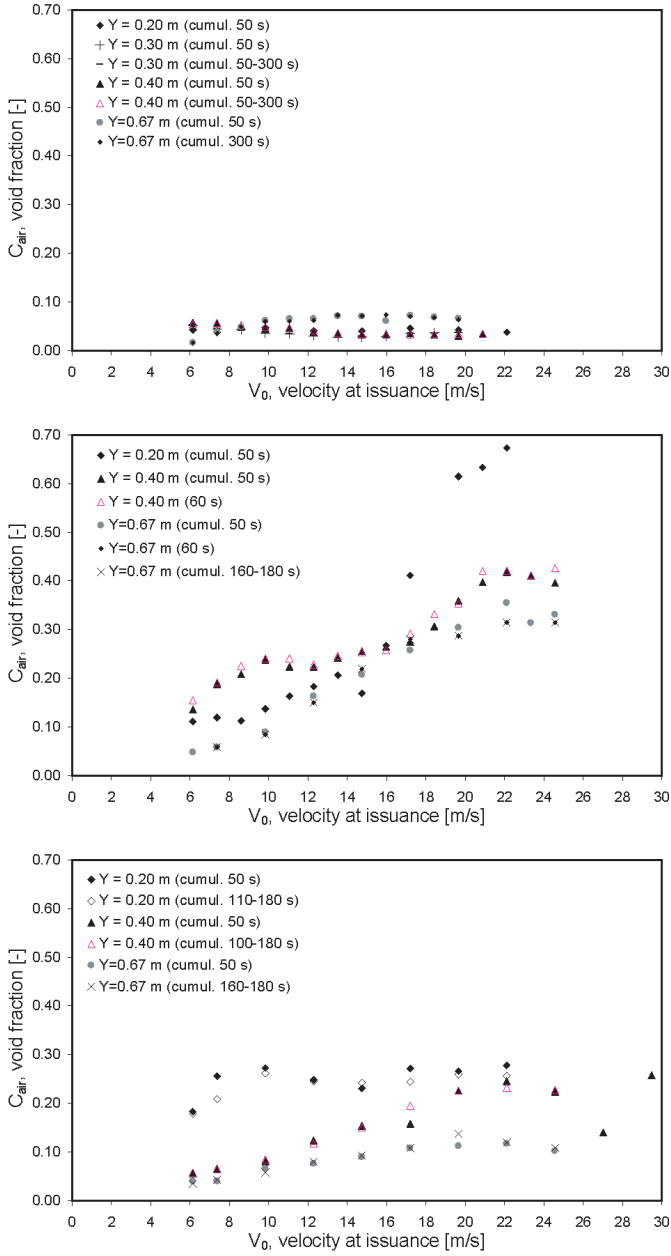

Figure 7.3.: Void fraction at: top, MP1; middle, MP2; bottom, MP3.

Table 7.4.: Comparison of void fraction estimates from optical probe measurements in *bounded diffusion* conditions with values obtained from existing laws for *free diffusion*: (a) McKeogh and Ervine (1981); (b) Ervine and Falvey (1987); (c) Bonetto and Lahey Jr (1993). Experimental data with optical probe for V = 19.65 m/s (Fr = 23.4). CL stands for centreline, R for rough jets and S for smooth jets.

Y [m]	L/D_0 [−]	V_i [m/s]	D_i [mm]	x/D_i [−]	C_{mea} [−]	C_{CL}(R) [−](a)	C_{CL}(S) [−](a)	C_i(R) [−](b)	C_{CL} [−](b)	C_{CL} [−](c)
MP3						Broken	Undevel.			
0.20	6.94	19.90	72.45	1.38	0.27	0.39	0.02	-	-	0.02
0.67	0.42	19.66	72.02	7.91	0.11	0.33	0.02	0.21	0.09	0.14
MP1										
0.20	6.94	19.90	72.45	2.48	0.04	0.38	0.02	-	-	0.05
0.67	0.42	19.66	72.02	9.02	0.07	0.32	0.02	0.21	0.08	0.12

3. Plunging circular jet formulae presented by Ervine and Falvey (1987), for smooth to rough turbulent jets, obtained from tests with jet velocities up to 29 m/s, D_0 = 50-100 mm and Tu values from 0.3 to 8 %. Only undeveloped jets at impact are considered for comparison.

4. Plunging circular jet data by Bonetto and Lahey Jr (1993) for a rough turbulent jet with V =4.96 m/s, D_0 = 5.1 mm and $Tu \approx$3 %.

5. Plunging circular jet data by Chanson et al. (2004) for a smooth turbulent jet with V = 4.4 m/s, D_0 = 25 mm and Tu = 0.96 %, undeveloped at impact (L/D_0=4).

Centreline void fraction values obtained with the fibre-optic probe C_{mea} are compared with rough and smooth turbulent estimates in Table 7.4.

The depth of bubble penetration D_p was computed using:

$$D_p = 2.6(V_i D_i)^{0.7} \tag{7.1}$$

as defined McKeogh and Ervine (1981) and as defined by Ervine and Falvey (1987) and Melo (2002b):

$$D_p = K_1 \frac{V_i}{V_r} D_i \tag{7.2}$$

where V_r is the bubble rise velocity that depends on bubble size and on the difference in density with the ambient fluid. The constant K_1 ranges from 1.33 to 1.5 depending on the turbulence intensity of the jet. In this case, V_r was assumed 0.25 m/s and K_1=1.33. The first equation provides D_p = 3.32 - 3.36 whereas the second D_p = 7.54 - 7.67 for respectively L/D_0 = 0.42 and 6.94.

Void fraction estimates obtained from an interpolation of experimental data presented by McKeogh and Ervine (1981) for broken-up jets at impact are clearly larger than the herein obtained results. On the other hand, the void fraction indications given by the same authors (i.e. an average value of 2 % per section until x < $0.5D_p$) for undeveloped smooth jets at impact are clearly lower than the present measurements. Since the present jet is non-broken at impact and rough turbulent, no direct comparison is possible.

According to Ervine and Falvey (1987) the air-water ratio at impact β_i can be estimated as:

$$\beta_i = K(\frac{L}{D_0})^{\frac{1}{2}} \tag{7.3}$$

assuming K = 0.4 (from Table 1, Ervine and Falvey (1987)) for rough turbulent circular falling jets with $L/D_0 < 50$. The void fraction at impact C_i can then be obtained by:

$$C_i = \frac{\beta_i}{1 + \beta_i} \tag{7.4}$$

The values of C_i are plausible regarding the measurements for deep pools. From impact values it is possible to compute the air -water ratio β and the void fraction C at MP3 assuming a linear decay given by:

$$\beta = 3.12\beta_i(1 - \frac{x_3}{D_p}) \tag{7.5}$$

This expression is only valid in the zone of established flow (ZEF) and provides values which are in close agreement with the measurements at MP3. It should be stressed that C_i is a section-averaged value and not a local value. In the flow development zone (FDZ), C_{air} is assumed nil in the jet axis (non-aerated core).

Comparison with the experimental data presented by Bonetto and Lahey Jr (1993) was performed by interpolating C_{air} values for the present x/D_0 diffusion distances. For a similar jet but with lower mean velocity at issuance V_0 they obtained a slightly higher C_{air} for the x_3/D_i=7.91 (i.e. MP3 in a deep pool). For x_3/D_i=1.38 (i.e. MP3 in a shallow pool), their estimate is much lower than the present measured value and the core can be considered almost non-aerated. The present measurements correspond to a degree of break-up of 0.35 and the core is expected to be non-aerated at impact. However, the current measurements are much higher (i.e. C_{air} = 0.27) which is likely to be due to the reflection of the jet at the pool bottom and enhanced air entrainment.

A similar exercise was performed for MP1, comparing void fraction measurements in a flat pool with free diffusion data by other authors. For the shallow pool case, the C_{air} estimate obtained by Bonetto and Lahey Jr (1993) with a fibre-optic phase anemometer is quite close to the present measurements. For the deep pool case, the present measurements are just slightly lower than the estimate obtained using the empirical procedure presented by Ervine and Falvey (1987) and almost half that than observed by Bonetto and Lahey Jr (1993).

At this stage of research, it is possible to conclude that:

- The void fraction C_{air} at the centreline of the jet for shallow pools are quite different from those predicted by free diffusion formula.
- The void fraction C_{air} in the core of the jet in free diffusion conditions is often assumed nil, as measured by Chanson et al. (2004) using a smooth turbulent jet. This is not the case for rough turbulent jets. Bonetto and Lahey Jr (1993) have shown that the air concentration at the jet centreline increases with distance from tests with undeveloped jets at impact. C_{air} ranged from very low values (i.e. less than 1%) at impact to a maximum value of 14 % at x/D_i= 8, for V =4.96 m/s, $Tu \approx 3\%$ and free jet diffusion conditions. The present measurements show C_{air} = 0.27 for x/D_i = 1.4 for which the free jet diffusion hypothesis is still valid. So why is C_{air} this high? In first hand, one would tend to associate it with a high degree of break-up, as studied by McKeogh and Ervine (1981). However, the present measurements correspond to a maximum L/L_b of 0.35, there must be some other reason for additional entrainment between the surface and MP3. One possibility is the additional entrainment of air due to some type of feedback phenomena due to jet impact in the pool bottom.

- The air concentration C_{air} at the jet centreline could be fairly well estimated in deep pools, using the procedure presented in Ervine et al. (1997) for undeveloped jets at impact. However, the estimates obtained with this procedure are section-averaged values and despite the probable flatness of air concentration distribution (radially) in the studied "control volume", it would be convenient to perform more measurements in the future. Moreover, Ervine et al. (1997) assume a linear decay of the air volume with depth, which is likely modified when approaching stagnation and does not account for the increase in air content in limited-depth pools as observed by McKeogh and Elsawy (1980).

The current analysis shows the interest of performing air-water measurements in pools with flat bottom because existing air entrainment models obtained for free jet diffusion fail to provide good estimates of the void fraction in bounded diffusion conditions. This research should be continued and extended with a larger set of data, in terms of jet velocity, pool depth and radial distribution.

7.6. Spatial distribution of the void fraction in pools with flat bottom and variable depths under large pressure gradients

With the results of the previous analysis, direct comparisons between void fraction at the three locations are presented in Figure 7.4.

For all pool depths, the void fraction at stagnation is the lowest.

For a shallow pool (Y/D = 2.8), jet centreline air concentration (at MP3) of about 20-30 % are either decreased for V < 15 m/s or considerably increased for V > 15 m/s at MP2. Considering that the predominant motion forces the air bubbles sampled at MP3 to flow in the direction of MP2, why does the C_{air} change? For shallow pools, there might be detrainment for low velocities, and additional entrainment for high velocities (i.e. visible hydraulic jump front and free surface wall jet). Detrainment is related with the balance between jet momentum (and corresponding dynamic forces acting on a particle) and air bubble buoyancy.

For a transition pool (Y/D = 5.6)[1], C_{air} increases smoothly with velocity at every MP. However, C_{air} decreases regularly from MP3 to MP1, and increases from here to MP2 reaching values even higher than those at MP3. In this situation no additional entrainment from the surface is possible in the trajectory from MP3 to MP1 and to MP2. From MP3 to MP1, air bubbles are either:

- deviated from stagnation due to the *high pressure gradient* and may not reach MP1;
- change in volume due to pressure gradient;
- dissolved in water due also to the large pressure gradient;
- or, a combination of the previous

Comparing directly MP3 and MP2, C_{air} increases regularly with velocity. In this case, there is either additional entrainment at MP2 coming from the outer pool flow; or, the air bubbles

[1] The previous chapters suggest a core persistence of at least Y/D = 5 and fully developed jet conditions only for Y/D = 9.3 in the present experimental set-up.

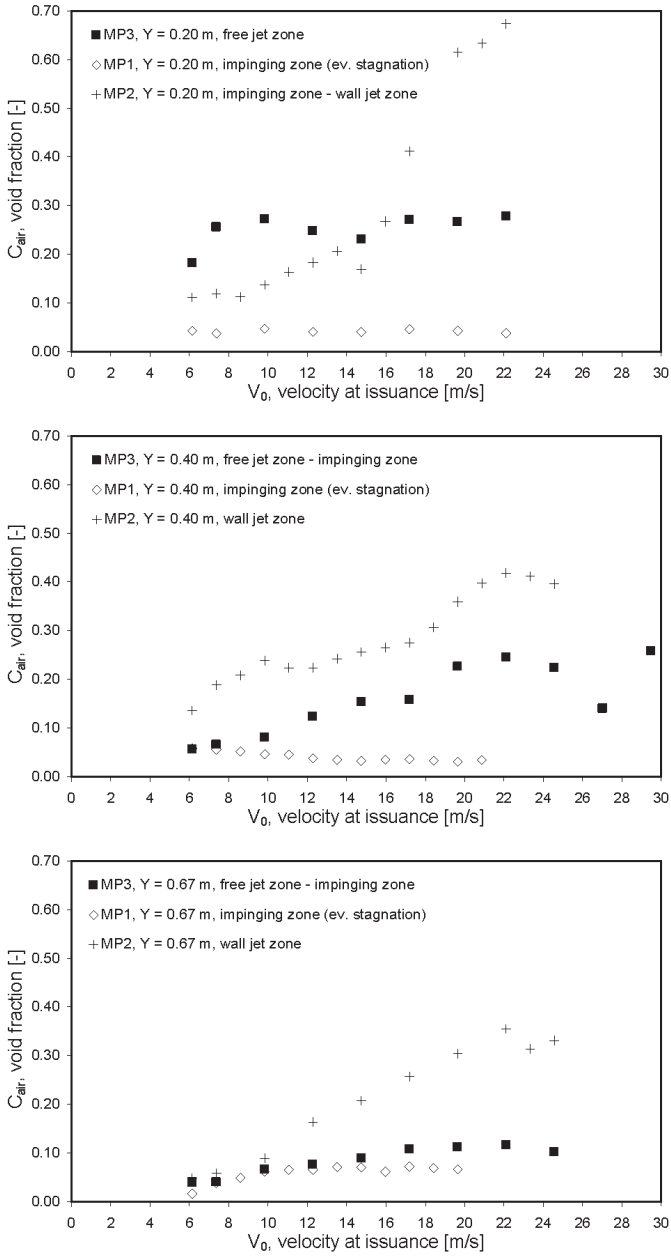

Figure 7.4.: Void fraction at: top, shallow pool (Y=0.20 m, Y/D =2.8); middle, shallow/transition pool (Y=0.40 m, Y/D=5.6); bottom, deep pool (Y=0.67 m, Y/D=9.3)

that have passed through MP3 have larger volume at MP2 due to a comparatively lower local pressure; or, there is gasification of air that was in solution in water; or, a combination of the previous.

For a deep pool (Y/D = 9.3), the differences between C_{air} estimates at MP3 and MP1 are small. Since the jet is already developed at MP3 the pressure gradient between MP3 and MP1 is less pronounced than in the previously discussed case of a transition pool. C_{air} is practically the same for V < 15 m/s. For V > 15 m/s, the same hypothesis as presented for shallow pools seem plausible: air bubbles are either deviated from MP1 due to the pressure gradient, or they shrink, or they are dissolved, or a combination of the previous.

Comparing directly estimates of C_{air} at MP3 and MP2, large differences are perceptible for V > 10 m/s. Even if for this pool depth the wall jet momentum is lower than for shallower pools, air bubbles that passed through MP3 should move to the vicinity of MP2. Since the probe is close to the pool bottom and still in the quite close to the impinging zone, these measurements are not expected to be influenced by air dragged by recirculation currents from the remaining areas of the pool. Therefore and again, there is either a decrease in bubble volume, a solution of air in water, migration by buoyancy or a combination of these processes.

It should be stressed that C_{air} is a time-averaged statistical parameter and thus any eventual change in volume of air bubbles will lead to a variation of this parameter *even if the quantity of air in the flow does not change*. The word "quantity" can be interpreted in this context as synonymous of mass or amount. A change in volume is said to occur by *compressibility* when a bubble is exposed to a pressure gradient, as defined by the Ideal Gas Law:

$$PV^n = mRT \tag{7.6}$$

where P is pressure, T is temperature, R a thermodynamic constant that depends on the properties of the fluid, m the mass of the existing moles of the gas in volume V and n a constant that depends on the type of thermodynamic process (n=1 for adiabatic processes)[2]. In this case, the time interval of bubble contact with the probe is reduced. The amount of entrained air does not change, only the size of the bubbles changes. Compressibility is discussed in detail in the next section.

In most of the bottom-influenced region directly influenced by the conversion of the falling jet into a wall jet (i.e. close to the boundaries including the measurement points) the amount of air should be identical.

If there is no apparent additional air entrainment or detrainment in between measurement points, a change in the void fraction could eventually occur by solubility of air bubbles into the liquid phase due to a pressure gradient. However, the processes of solution or gasification require the establishment of a thermodynamical equilibrium: a given time is necessary for a given amount of air to dissolve in water at a constant pressure or, inversely, to gasify. In a first approach, solubility of air bubbles in water seems farfetched.

As an example, the time scale of CO_2 gasification when opening a champagne bottle is in the order of a second. Coincidence or not, a champagne bottle cork withstands 5-6 bar, which is similar to the upper bound impact pressure in the present experimental set-up. In the present case, however, a given air bubble is not expected to remain longer than 0.01 s

[2] An adiabatic process is a reversible thermodynamic process that occurs without gain or loss of heat at constant level of entropy

in the impinging zone, considering entry/exit velocities in the order of 10 m/s. At this point of research, it would be speculative to describe the influence of this phenomena, as it would be to discard it. One suggestion for future research is perform high-speed video recording to clarify this issue.

7.7. Compressibility of air bubbles at stagnation under high-pressure gradients

Compressibility of air bubbles is investigated by analysis of the Sarrau-Mach number (Ma) and of the size of the captured air bubbles.

7.7.1. Air bubble cord length u/s and d/s of stagnation

Data sets with a similar amount of intercepted interfaces were selected for comparison of air bubble characteristic dimensions. The bubble cord length can be estimated from the time of flight between tips using the estimated interfacial velocity (Eq. 3.11). The estimates of interfacial velocity showed quite varied correlations, depending considerably on the local flow pattern (e.g. streamline curvature, degree of jet development) and on the acquisition duration. For the current study, only interfacial velocities corresponding to correlations higher than 0.50 were considered.

The cumulated density function (i.e the probability distribution function) of the bubble cord length at MP2 and MP3 for two typical pool depths (shallow/pool) and V = 19.65 m/s is presented in Figure 7.5. At MP1, strong curvature of the streamlines reduces significantly the correlations obtained. The representativeness of most of the V_{aw} measurements is under investigation and is not presented herein. These bubble cord length distributions were obtained with a large number of intercepted air-water interfaces, significant correlation and meaningful interfacial velocity estimates. They show that air bubbles at MP2 are in general larger than at MP3, for both the shallow pool and the deep pool cases investigated.

Two parameters were selected for comparison (Table 7.5): the Sauter diameter (d_S) and the diameter corresponding to a probability of 0.50 (d_{p50}). They both depend on the representativeness of the interfacial velocity estimate. The Sauter diameter seems to correspond to a cumulative probability of 0.80.

At MP1, the d_S and d_{p50} were estimated based on the corresponding values at MP3 and MP2, using the following expression derived from the Ideal Gas Law:

$$d_a = d_b \left(\frac{p_b}{p_a} \right)^{1/3} \tag{7.7}$$

where p_a and p_b are the local mean excess pressure at two random points (a) and (b). Local mean pressure at MP3 was estimated based on the Bernoulli equation and on the model of jet diffusion in limited-depth pools (Chapter 5).

For the shallow pool case, both d_S and d_{p50} are larger at MP2 than MP3. The estimate of d_S at MP1 is physically arguable; air bubbles size should not decrease from MP1 to MP2 but rather increase. In this sense, the estimate of d_{p50} is more plausible. For deep pools, both d_S and d_{p50} estimates at MP1 are lower than values at MP3 and MP2. This suggests that air bubbles may shrink from MP3 to MP1 and swell from MP1 to MP2.

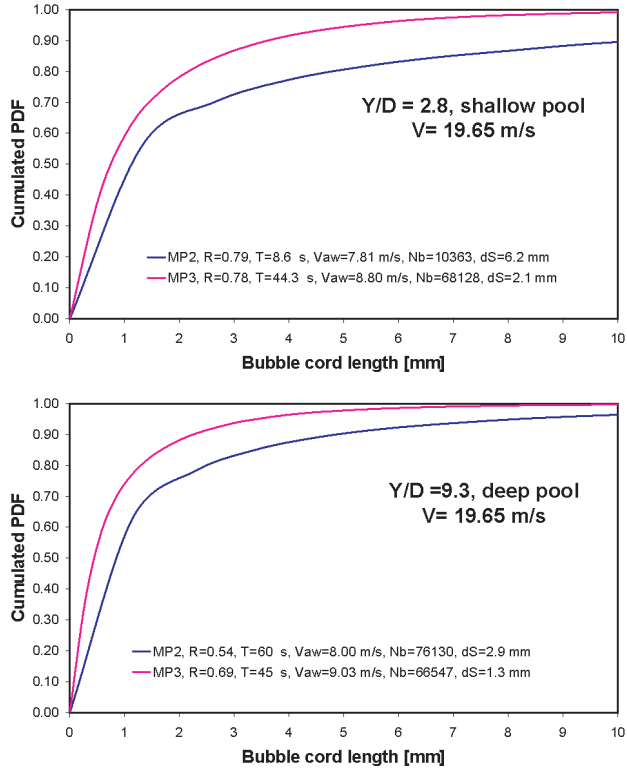

Figure 7.5.: Linearized probability distribution functions of the local void fraction C_{air} at MP3 and MP2, jet velocity 19.65 m/s: top, shallow pool (Y=0.20 m, Y/D =2.8); bottom, deep pool (Y=0.67 m, Y/D=9.3). Specific parameters: R is the correlation, T is the duration of acquisition and Nb is the number of intercepted interfaces air-water.

The present measurements at MP2 and MP3 show unprecedented evidence of the variation in air bubble distribution in pool flows generated by high-velocity jets and under large pressure gradients. At this stage, the bubble cord length at MP1 should be considered indicative.

7.7.2. Pressure wave (sound) velocity and Sarrau-Mach number

The Sarrau-Mach number is described as follows:

$$Ma = \frac{u}{a} \tag{7.8}$$

where u is the local flow velocity and a the sound celerity (Chanson, 1997; Zhao and Li, 2000). The Sarrau-Mach number is a dimensionless parameter somewhat similar to a Froude number. A threshold has been defined between subsonic and supersonic flows for

Table 7.5.: Sauter diameter and diameter with 50 % of probability, jet velocity 19.65 m/s. The values within brackets were computed from measured values (i.e. MP3/MP2 and p stands for mean local pressure minus the hydrostatic and atmospheric pressures).

Y [m]	MP	C_{air}	p [mwc]	d_S [mm]	d_{p50} [mm]
0.20	3	0.27	-	2.1	0.8
	1	0.04	17.35	(-/3.0)	(-/0.6)
	2	0.61	2.01	6.2	1.2
0.67	3	0.11	4.92	1.3	0.5
	1	0.07	7.88	(1.1/1.0)	(0.4/0.3)
	2	0.30	0.30	2.9	0.9

respectively $Ma < 1$ and $Ma > 1$. The analysis of this parameter may help understanding the contribution of phenomena like feedback from impact in a downstream surface and shock waves. Regarding two-phase flows, Zhao and Li (2000) defined a value of Ma = 0.3 as the threshold value above which compressibility effects should be taken into account; flow is still subsonic but is classified as "transonic flow".

Sound celerity is 300 m/s in the air and about 1500 m/s in the water. The Sarrau-Mach number can be computed using the Wood adiabatic formula (Zhao and Li, 2000) assuming that there is no velocity slip between the two phases:

$$a = \sqrt{\frac{\gamma_w p}{C_{air}(1 - C_{air})\rho_w}} \tag{7.9}$$

where p is the local mean (absolute) pressure (in bar), γ_w is the specific weight of water (in N/m^3) and ρ_w is the mass density of water (in kg/m^3).

For the computation of the sound velocity a series of assumptions are necessary.

For the shallow pool case (Y/D=2.8), the core of the jet impacts the pool bottom and p_1 is assumed as $0.86\frac{V_i^2}{2g}$. The velocity at impact is $\sqrt{V_0^2 + 2gL}$, where L is the travel length.

Velocity at MP1 was computed assuming a linear velocity decay in the impinging region (i.e. region 0.25Y high close to the pool bottom). This last assumption is rather conservative, since decay is rather exponential than linear (Cola, 1966).

For the developed pool case, is is assumed that there are no additional energy losses between MP3 and MP1. In fact, MP3 is at 0.57 m from the surface, which is already inside the impinging zone if a characteristic height of about 0.75Y (i.e. 0.50 m, point A) is considered.

Regarding velocity, the local velocity at MP3 was estimated using a centreline velocity decay law of free jet diffusion up to A (i.e. $x_A = 0.75$Y):

$$V_A = V_i C_v \frac{D_i}{x} \tag{7.10}$$

assuming $C_v = 5$ (see previous Chapter) and D_i and V_i equal to the diameter and velocity at issuance respectively. This velocity was transposed to MP3 assuming also a linear velocity

Table 7.6.: Computation of the Sarrau-Mach number. The values within brackets are interfacial velocity estimates obtained experimentally

Y $[m]$	MP	C_{air}	$\overline{p}/\gamma$ $[mwcA]$	u (V_{aw}) $[m/s]$	a $[m/s]$	Ma	Remarks
0.20	3	0.27	9.75	19.65 (8.80)	-	-	potential jet flow
	1	0.04	27.30	7.96 ($\longrightarrow$0)	26.66	0.30	>0.3 transonic, compressible
	2	0.61	11.96	16.28 (7.81)	7.09	2.30	>0.3 transonic, compressible
0.67	3	0.11	15.34	8.32 (9.03)	12.52	0.66 (0.72)	>0.3 transonic, compressible
	1	0.07	18.30	1.67($\longrightarrow$0)	16.77	0.10 (-)	at 2 cm from stagnation
	2	0.30	10.72	6.73 (8.00)	7.14	0.97 (1.12)	>0.3 transonic, compressible

decay from A to stagnation (slope = 83.22):

$$V_3 = V_A - [x_3 - x_A]\frac{V_A}{0.25Y} \tag{7.11}$$

where V_0 = 19.65 m/s, V_A = 14.15 m/s and V_3 =8.32 m/s.

From here, p_3 was estimated with the Bernoulli equation assuming that the mean excess pressure head at impact p_B is 39 % of the incoming kinetic energy (based on experimental results presented in Chapter 5). The mean pressure head at MP2 is obtained from pressure measurements performed at a radial distance of 95 mm from the jet axis, which is the closest (pressure) measurement station to MP2.

Mean local velocities at MP2 are computed from a simplified momentum balance between MP3 and MP2, assuming a wall jet uniform velocity in a region $h_{wj} = 0.50D_i$ close to the bottom, using:

$$U_2 = U_3 D_3 \sqrt{\frac{C_3}{C_2}\frac{1}{8yh_{wj}}} \tag{7.12}$$

where D_3 is the diameter of the shear layer at MP3, i.e. $D_0 + 0.25x_3$.

7.7.3. Discussion

On bubble cord length

Bubble sizes in chute flows are expected to be between 1 and 20 mm, as observed in the Aviomore dam spilway (Cain and Wood, 1981). McKeogh and Ervine (1981) observed the entrainment of bubbles with diameters in the range 1- 3 mm for a jet with a turbulence intensity of 3 %. In the present case, about 80 % of bubble cord lengths obtained experimentally are less than 2.1 mm in the free diffusion region (MP3) and less than 6.2 mm in the wall jet region (MP2). The probability that values lower than 0.8 mm are found in the free jet region or lower than 1.2 mm are found in the wall jet region is of 50 %. It is believed that these characteristic dimensions are linked to the high pressure gradients close to the pool bottom (max. 3 bar for the documented case with V = 19.65 m/s).

The large pressure gradient observed near to stagnation may lead to a reduction of amount of air bubbles in the vicinity of the probe tips. Bubbles tend to migrate to lower pressure regions. This stagnation effect was also observed near the stagnation of a back-flushing Pitot tube (Matos et al., 2002): the local air concentration is lower than that which would occur without the presence of the tube. Nevertheless, the fibre optic probes are much smaller than most Pitot tubes and the stagnation effect should be less important.

The strong curvature of flow streamlines close to MP1 did not allow obtaining representative estimates of the interfacial velocity at this location. Therefore, no direct measurements of bubble cord length at MP1 are presented. However, estimates based on momentum balance from neighbouring points revealed that air bubbles at MP1 are likely to be in the order of 1 mm, with a considerably percentage of their distribution below this threshold.

On pressure wave (sound) velocity estimation

Several expressions to compute the sound celerity were found in literature. No specific indication on the pressure to consider was found. The present computations were performed using the absolute local pressure. Very limited experimental data is available for comparison. Only three other references were found: Cain and Wood (1981), Shuai (1995) mentioned in Zhao and Li (2000) and Volkart and Rutschmann (1984) mentioned in Chanson (2004b). All three correspond to chute flows.

The hypothesis of no-slip was considered adequate in the free diffusion and impinging regions under the direct influence of the tested (rough turbulent plunging) jets and for pool depths not exceeding $\approx 9D_i$ (or 10% D_p). However, it is likely not valid for pools deeper than a given (large) percentage of D_p. As mentioned by Bonetto and Lahey Jr (1993) it is also not valid outside the shear layer created by the plunging jet or, in general terms, in any location in the pool where the bubble rise velocity exceeds the downward motion due to the jet. Therefore, due care should be taken in extrapolating the conclusions of this section for deeper pools.

The minimum value of the pressure wave velocity a found in literature is 18-20 m/s, for C_{air} = 0.5 at absolute pressures close to 1 bar. (Chanson, 2004b). The present result range from 7 to 27 m/s for similar atmospheric pressure but local mean absolute pressures under the of maximum 3 bar. For these conditions the flow was found to be compressible. This is highly important when trying to reproduce prototype plunge pool flows in laboratory at reduced scale (i.e. with important scale effects regarding aeration) or mathematically.

7.8. Conclusions

Acquisition duration of 50 to 60 s were considered satisfactory to provide ergodic estimates of the local void fraction, for measurement points in either unidirectional or potential flow in a plunge pool. This is typically the case inside the potential core of the jet and at the transition from the jet impingement to the wall jet region (in this case, save for very shallow pools). For developed flow conditions (e.g. in the mixing layer of the jet, recirculation zones, etc.) longer acquisition durations might be necessary due to the turbulent character of the flow.

Void fractions at three characteristic points in the free diffusion zone, the jet impingement zone and in the wall jet region, show that the air content in the pool varies significantly with the pool flow pattern and with local pressure. Void fraction decreases close to the pool bottom regarding values in the free diffusion region, and increases at the pool bottom sideways from the jet axis. At this stage of research, several hypotheses for air bubble behaviour were outlined: air bubbles may vary in volume; dissolve in water or release from water; or migrate to lower pressure regions; or, be entrained from outer pool flows; or be submitted to a combination of these processes.

For shallow pools, the core of the jet impacts the pool bottom and very little air is found close to the stagnation. In the wall jet region, additional entrainment may occur from the pool surface. For a deep pool, entrained air remain under the influence of the jet as long as flow velocities are higher than the bubble rise velocity (i.e. 0.25-0.50 m/s).

The most relevant processes considered herein were air bubble migration and air bubble compressibility. Bubble migration is particularly important in the vicinity of the pool bottom. Air bubbles tend to move away from the high-pressure region at stagnation, pushing air bubbles radially outwards and upwards enhancing buoyancy. High-velocity jets generated dynamic forces that are much larger than buoyancy in the free diffusion and the jet impingement regions. Air bubbles are entrapped in the flow. Air bubbles follow flow velocity and a no-slip conditions is usually considered valid. Therefore, air bubbles either change in volume or dissolve. Bonetto and Lahey Jr (1993) showed that rough turbulent jets entrain larger air bubbles than smooth turbulent jets. In this case, a no-slip assumption may not be the most adequate for the larger bubbles, whereas smaller bubbles (i.e. less than 1 mm) do flow with the liquid phase. For larger bubbles, buoyancy becomes more relevant. However, Bonetto and Lahey Jr (1993) tests were performed with a maximum velocity of 4.96 m/s and therefore the jet momentum acting on the air bubbles is significantly lower than in the present experimental investigation.

Computations of the pressure wave (sound) velocity and of the Sarrau-Mach number show that the flow in the measurement points may be considered transonic. In this case, the air-water flow is compressible.

The pressure gradients and jet velocities investigated are close to values found in prototype, which allows extrapolating these conclusions to typical engineering works in dams.

7.9. Suggestions for future research work in air-water flows

The existing measurement data base allows pursuing investigation on the topics of interfacial velocity and bubble count rate and size. The in-depth analysis of these parameters was not possible during the time frame of this thesis and remains one alternative for future work.

This topic merits further investigation to understand the relative importance of different processes like compressibility, solubility, entrainment and detrainment (e.g. bubble migration). Performing extensive measurements with high-velocity video recording and simultaneous air-water measurements at two stations (e.g. MP1 and MP3) could provide a closer insight on bubble migration regarding compressibility and even solubility effects.

Suggestions for further analysis include the definition of bubble cord length probabilistic distribution (ev. Rayleigh), the comparison of velocity estimates with existing empirical relationship for centreline velocity decay (e.g. McKeogh and Ervine 1981, Bohrer et al. 1998) and the systematic assessment of compressibility of air bubbles for variable jet velocity, turbulence intensity, degree of break-up and diffusion length.

The analysis of Cp' values of impact pressures in aerated and non-aerated conditions based on available data from literature and existing databases is also of interest for engineering practice.

8. Stagnation pressures generated by plunging jets in laterally confined pools with constant scour depth

This section present experimental results of pressure measurements performed in plunge pools for which the lateral diffusion of the jet is bounded (Figure 8.1). Experimental work was carried out with a wide range of typified plunge pool geometries, pool water levels and jet velocities.

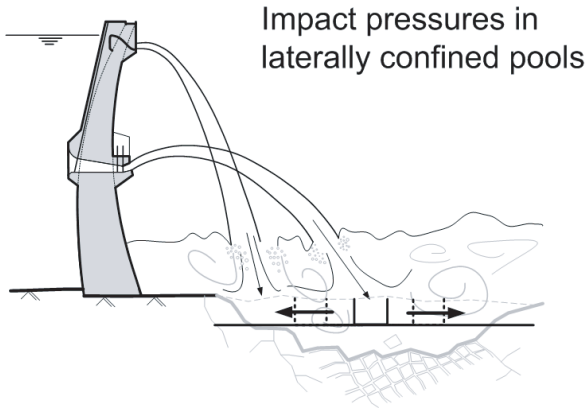

Figure 8.1.: Scour evolution due to the impact of plunging jets schematically represented by a sequence of stepped laterally confined pool geometries.

8.1. Experimental work in laterally confined pools with constant scour depth

The influence of laterally confining jet diffusion is investigated by testing cylindrical confinements with diameters D_c of 5.6, 11 and 16.7 times the jet diameter D, and comparing the results with a pool with flat bottom ($D_c = \infty$). They are named "narrow", "intermediate" and "wide" geometries in this chapter, respectively. The experimental installation and the test procedure are described in detail in Chapter 3.

First, mean pressure at the centremost point at the pool bottom (i.e y/D = 0.35) are presented. Three geometries that correspond to a similar scour depth and variable degree of confinement are compared with a very wide pool (i.e. a pool with flat bottom). The narrowest pool geometry of the three (i.e. D_c/D = 5.6) is studied in further detail.

Second, turbulent pressures at the same point are analysed for the three laterally confined pools, and compared to the reference case of pool with flat bottom.

Finally, extreme pressures and spectral energy distribution of pressure fluctuations are presented for the narrowest pool and compared with the reference pool.

Dynamic pressure values (mean, RMS, maxima and minima pressures), and the corresponding dynamic coefficients have been computed for each test and each measuring point. Extensive post-processing of data was performed using author-made ©Matlab routines for conversion of measured values using the corrected calibration curves (one for each transducer, updated at least once during each day of experimental work), summation of the necessary data files for ergodic sampling (3 acquisition files were systematically used for most cases), computations of statistical values for each transducer and storage of output files. The information not included in this analysis is available with the author.

To the author's knowledge only few scientific publications have included pressure measurements in non-flat pools. Very recently Amri and Verrette (2005) presented dynamic pressure measurements for four different plunge pool geometries, downstream of a ski-jump spillway. They simulated four different stages of scour evolution by fixing the riverbed with concrete after tests with loose gravel. Pressure taps were installed aligned with the jet axis and distributed in the downstream direction. They observed a reduction of mean pressures at impact with growing scour. However, the representativeness of the results is hindered by the scale effects associated with the use of a reduced scale model (total height ≈ 1 m, maximum head difference of 0.69 m) and maximum velocities of 4 m/s at entry in the pool.

8.2. Mean pressures in laterally confined pools

8.2.1. Mean pressure coefficient

The mean loads transmitted to the rock can be defined as the ratio between the measured mean pressures at the rock interface and the incoming jet kinetic energy (Equation 8.1):

$$C_p = \frac{[\overline{p} - p_{atm}] - Y_0}{\frac{\alpha V_0^2}{2g}} \tag{8.1}$$

where Y_0 is the initial static level in the pool, and $[\overline{p} - p_{atm}]$ is the mean relative pressure head. The kinetic energy correction factor was assumed to be $\alpha = 1$ for all velocities tested as presented in Chapter 4.

Detailed discussions of the effect of the tailwater level on mean pressures for plunging jets in pools with flat bottom can be found in Cola (1965, 1966); May and Willoughby (1991); Puertas-Agudo (1994); Ervine et al. (1997); Melo (2001); Bollaert (2002b) (naming only a few amongst the most recent). Several authors, however, have rather used a dimensionless parameter composed of $C_p \cdot \frac{h}{D}$, in quest of a collapse of the results for different h values. This approach can not be envisaged for non-flat pools.

A selection of Cp vales at $y/D = 0.35$ for flat and non-flat pools is presented in Figure 8.2. Due to the extension and diversity of the accumulated experimental data, it was necessary to select a limited number of cases for analysis in this chapter. In the following sections, a scour hole with a constant depth of $t/D = 2.8$ (t=20 cm) and variable degree of confinement

D_c/D is studied, for variable pool depths Y and jet velocities V_0. This analysis combines data from the FC1/2, SC1/2 and TC1 test series. Similar plots of $Cp_{y/D=0.35}$ for the remaining geometries (SC3, TC2, TC3, FS and FST) are included in the Appendix D.

For the three lateral confinements presented in Figure 8.2, the mean pressures at impact are lower than obtained in the reference scenario of a pool with flat bottom (FB series).

As pointed out in the dimensional analysis, several parameters play an important role in the definition of impact dynamic pressures. The herein presented analysis focuses on the diffusion length Y/D, jet velocity V and pool confinement ratio t/D_c, combined with D_c/D. However, it does not address pool aeration. Air entrainment has been observed to play an important role in the definition of impact pressures in pools with flat bottom, and it may play an important role in the diffusion process in confined pools also.

8.2.2. Reference scenarios of pools with flat bottom

For flat pools, Ervine et al. (1997) defined Cp_{axis} as a function of Y/D and of the air concentration $C_{air,i}$, at the impact point with the pool bottom :

$$C_{paxis} = 0.85 \quad \text{for } Y/D < \text{4-6} \tag{8.2}$$

$$C_{paxis} = 38.4(1 - C_{air})\left[\frac{D}{Y}\right]^2 \quad \text{for } Y/D > \text{4-6} \tag{8.3}$$

The range of application of the two equations depends on the core development length. The diffusion length is discussed in Chapter 5. The decay rate of C_p presented in Equation 8.3 is directly related to the centreline velocity decay. Such decay has been considered linear (Albertson et al., 1948; Ervine and Falvey, 1987) or depending on $(\frac{D}{Y})$ at a power of 1.1 for free diffusion up to 20D.

Cola (1966) described experimentally for the first time jet deflection close to the bottom. He suggested the use of an exponential decay law in the vicinity of the pool bottom, based on experiments with submerged plane jets and relative pool depths Y/D up to 72.

The air concentration at impact $C_{air,i}$ is defined as a linear function of the volumetric air-to-water ratio β, which was object of extensive research in the past, e.g. McKeogh and Elsawy (1980); McKeogh and Ervine (1981); Sene (1988); Bín (1993); Melo (2001). Discussed summaries of expressions for β can be found in Bín (1993); Melo (2001); Bollaert (2002b). A summary is presented in Chapter 2.

The previous expression should be used with caution since the C_{air} strongly depends on jet velocity (McKeogh and Elsawy, 1980; Bín, 1993; Melo, 2001), jet turbulence intensity (McKeogh and Ervine, 1981; Ervine and Falvey, 1987; Manso et al., 2005b), jet degree of break-up (McKeogh and Ervine, 1981; Ervine and Falvey, 1987; Ervine et al., 1997; Bohrer et al., 1998) and relative pool depth (submergence) in comparison with the maximum distance of air bubble penetration (McKeogh and Elsawy, 1980).

The values of $Cp_{y/D=0.35}$ obtained in the present study (see Figure 8.2) are somewhat different from those of Bollaert (2002b), whose data showed good agreement with the previous Equation 8.2 and Equation 8.3 presented by (Ervine et al., 1997). In fact, higher $Cp_{y/D=0.35}$ values are herein reported for pool depths between 4D and 6D (a few also for ≈8D). This is thought to correspond to an increased stability of the jet core, obtained after the modification in the supply system and turbulence intensity Tu presented in Chapter 3

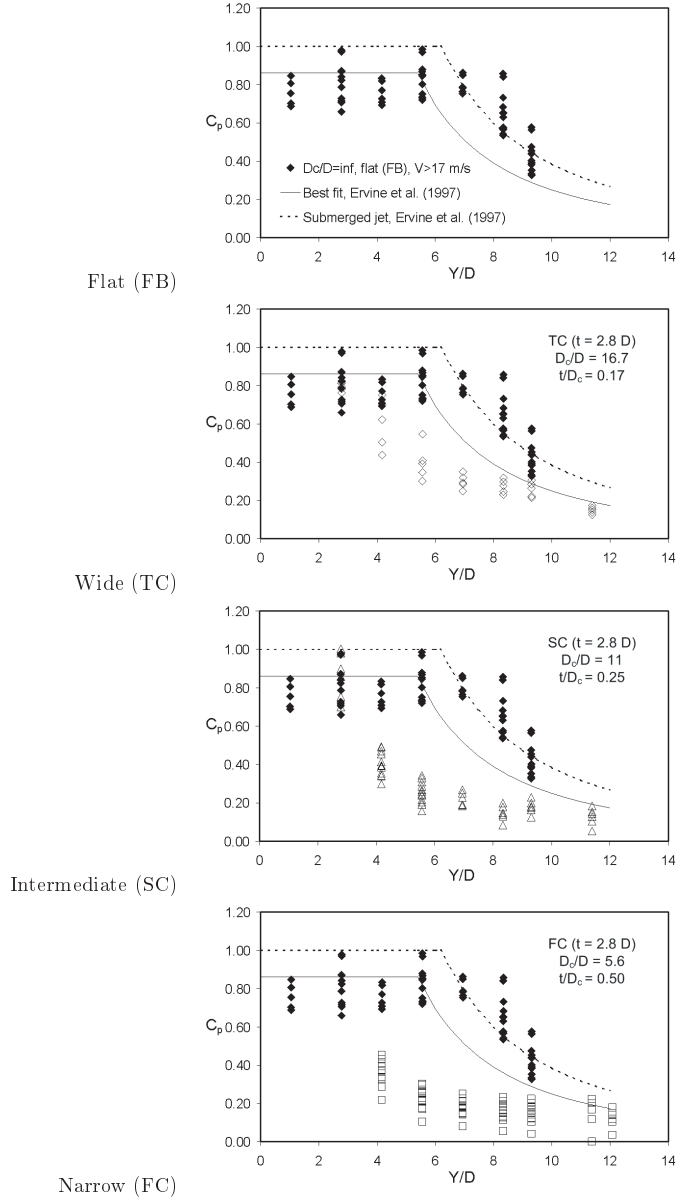

Figure 8.2.: Dimensionless mean pressure coefficient C_p close to the jet axis ($y/D = 0.35$) as a function of the relative depth ratio Y/D, for pools with flat bottom (FB) and laterally confined pools (wide, intermediate, narrow). Comparison with Ervine et al. (1997)'s best fit of data (continuous line) and submerged jet data (dotted line). All FC, SC and TC data are for the same scour depth t/D=2.8 and tests with $V > 17$ m/s.

and discussed in detail in Chapters 4 and 6. This has led to a redefinition of the concept of shallow, transition and deep pools that is used hereafter:

- **shallow pools**, characterized by $Cp_{y/D=0.35} > 0.70$ for V > 17 m/s and kurtosis at y/D = 0.35 lower than the maximum obtained value, i.e. pools with Y/D < 5;
- **transition pools**, characterized by $Cp_{y/D=0.35}$ from 0.50 to 0.70 for V > 17 m/s, large differences between the pool dissipation efficiency results obtained experimentally and based on the turbulent diffusion model, high intermittency (maximum for Y/D = 5.6), i.e. pools with 5 < Y/D < 8-9
- **deep pools**, for which a decay in $Cp_{y/D=0.35}$ for V > 17 m/s is observed and the previous analysis of Chapter 5 and Chapter 6 show a characteristic behaviour of developed jet impact conditions, i.e. Y/D > 9.

The range of transition from the core to the developed impact conditions depends on several parameters that are discussed in Chapter 5. This is thought to be a direct consequence of the impact on the pool bottom, which is not accounted for directly in the equations defined by Ervine et al. (1997).

8.2.3. Analysis of laterally confined pools with constant scour depth

From the previous remarks, one may expect that a lateral confinement will change the pool flow patterns with eventual incidence on jet diffusion. This may be reflected on two main processes: the decay of jet velocity with depth and the entrainment of air in the pool. Performing direct measurements of these processes is not part of this study. However, these processes are reflected in the measured impact pressures.

Visual observation of the flow in the pool during the experiments provides very limited information; generally the whole pool is occupied by a highly aerated flow mixture. Nevertheless, it is possible to say that the entrainment of air in the pool is done in three ways:

- By transport of air inside the core of the plunging jet; in the present case, the water is pumped from a basin. The pump intake is deeply submerged. Air exhaustion measures are applied in the supply system. The presence of air in the jet itself is highly unlikely, but is not directly assessed;
- By air entrainment at the plunging point, within the surface disturbances of the jet surface, as described by McKeogh and Ervine (1981), and in the surrounding air boundary layer;
- By air entrainment at re-plunging of the ascending deflected jets. For increased submergence, the re-plunging region behaves as a surface boil where little to no air is entrained. For shallow pools, the upward moving deflected jets pierced through the pool surface, re-plunging further outwards. This process was clearly visible for shallow pools and the whole range of tested jet velocities.

The qualitative description of these mechanisms, however, is insufficient to say whether more air or less air is entrained and found at a given depth, regarding free jet diffusion, or even diffusion in pools with flat bottom.

For the narrowest confinement tested (t/D_c=5.6), one may expect the diffusion shear layer to be severely affected by the change of pool flow patterns. Deflected jets collide with the

diffusing plunging jet. This is reflected in the reduction of C_p decay with relative pool depth Y/D presented in Figure 8.2, in comparison with the flat bottom.

Figure 8.2 shows C_p measurements close to the jet axis are lower for higher degrees of confinement.

At this stage of research it is not known if the centreline velocity decay is linear, quadratic or whether it follows any other type of law in function of pool depth.

As for air entrainment, the closer the confinement is to the jet axis, the more enhanced flow mixing *seems* to be. For a very shallow pool (Y/D = 2.8), the flow is reflected upwards, more brutally for the narrower confinement. For D_c/D=11 and 16.7, the non-aerated jet core impacts the bottom. For D_c/D=5.6, it is not possible to visually ascertain if there is direct contact between the upward going jets and the plunging jet. For increasing pool depths, several situations are observed:

- For transition pool depths and velocities up to 17.2 m/s, phenomena like pool surface oscillations are observed. These oscillations do not change the characteristics of the pool surface at plunging point and, therefore, air entrainment should be rather similar to free diffusion conditions.

- For transition pool depths and velocities up to 17.2 m/s but for other combinations of Y/D and V_0, rhythmic oscillations *inside* the confined region[1] generate inward currents that disturb plunging conditions. In this case, air entrainment conditions at plunging point may be reduced.

- For deep pools and large confinements (TC, D_c/D=16.7), the upward currents move radially inwards in the direction of the plunging jet. These currents may collide with the plunging jet close to the plunging point at the surface or inside the pool (i.e. interfering with the shear layer). In the first situation they may hinder air entrainment conditions at plunging point (i.e. interfering with the formation of an induction trumpet as defined by Chanson (1997)). In the second situation, they may hinder air bubble penetration.

Therefore, air entrainment conditions and air bubble penetration conditions may vary in a certain extent in comparison to free diffusion conditions of undisturbed plunging jets.

In the absence of experimental data or theoretical background on C_{air} and centreline velocity decay in laterally confined diffusion conditions, the following analysis provides empirical relationships between C_p and other dimensionless parameters as a function of the jet initial velocity.

The previously used relative pool depth ratio Y/D may no longer be sufficient for a proper representation of independent data series of a given two-phase jet. Whenever diffusion and pool aeration are disturbed by the geometry-induced flows, Y/D mixes geometry effects and hydrodynamic effects.

C_p is plotted in Figure 8.3 as a function of Y/D for direct comparison of the three pool geometries with t/D=2.8 and the flat reference case. It can be observed that:

- For $4 < Y/D < 9$, C_p values are generally lower than those in flat pools;

[1] Large-scale pool flow patterns are discussed in the chapter 9.

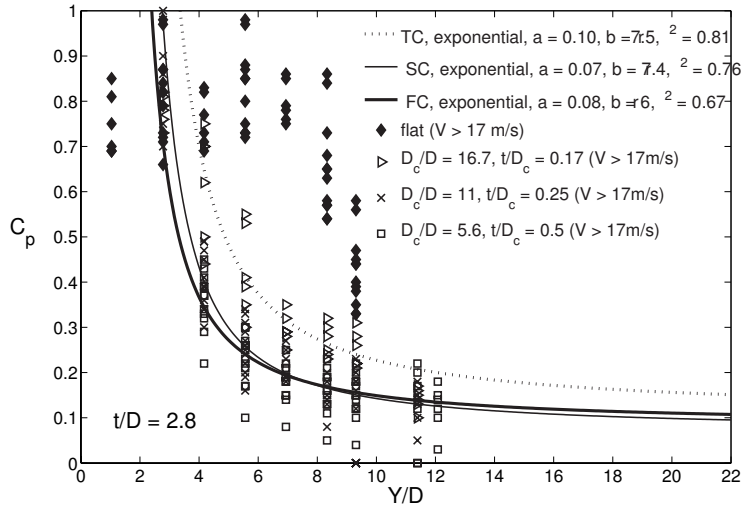

Figure 8.3.: Exploratory attempts for the analysis of the mean pressure coefficient close to the jet axis (y/D =0.35) for three lateral confinements with D_c/D ranging from 5.6 to 16.7, for a scour depth of t/D=2.8 (data from cases FC1/2, SC1/2,TC1).

- For Y/D = 4 - 6, C_p values are lower than 0.7 for all velocities presented (i.e. 17.2 - 29.5 m/s) for D_c/D = 5.6 to 16.7, with the exception of V = 29.5 m/s for D_c/D = 16.7;
- For Y/D > 4 and for the three confined geometries, C_p decay is no longer quadratic but eventually exponential. An exploratory fitting suggests that an expression of the type $C_p = ae^{bD/Y}$ could be adequate. The parameter a influences the location along the x-axis (somewhat related with the core development length), whereas the parameter b provides the energy decay rate in the established flow region (somewhat related with the centreline velocity decay and pool aeration);
- For a given geometry, data scattering can be associated with the different air entrainment conditions in the pool.
- Comparing the four geometries, differences in C_p values are thought to spring from differences in the induced pool flow patterns.

Three preliminary empirical expressions were obtained for:

1. The narrowest confinement, D_c/D=5.5 and t/D_c = 0.5 (r^2= 0.67):

$$C_{p,axis} = 0.08e^{6D/Y} \quad \text{for V} > 17 \text{ m/s} \tag{8.4}$$

2. The intermediate confinement, D_c/D=11 and t/D_c = 0.25 (r^2 = 0.76):

$$C_{p,axis} = 0.07e^{7.4D/Y} \quad \text{for V} > 17 \text{ m/s} \tag{8.5}$$

3. The widest confinement, D_c/D=16.7 and t/D_c = 0.17 (r^2= 0.81):

$$C_{p,axis} = 0.10e^{7.5D/Y} \quad \text{for V} > 17 \text{ m/s} \tag{8.6}$$

These tentative empirical expression are considered the baseline scenario for the detailed analysis that follows.

8.2.4. Analysis of the narrowest pool (FC)

For pools with flat bottom, previous authors showed that C_p data scattering was related to V_0 and the corresponding Tu as well as C_{air}, for both compact and developed jet impact conditions (Ervine et al., 1997; Bollaert, 2002b).

The modification of the flow pattern in the pool is reflected by the transition from one type of impact conditions to the other. In the present experimental set-up this transition occurs for flat pool depths Y at about 5.6D, as previously defined. The FC case is the narrowest confinement tested. Disturbances to the development of the jet core are reflected on the results obtained with the FC pool, rather than in others.

C_p values are reduced for shallow pools between 4< Y/D <6. As an example, for Y/D = 4.2 (Y = 0.30 m) $Cp_{y/D=0.35}$ reduces from around 0.8 (flat pool) to 0.56 (FC). The difference in energy at impact was either converted into fluctuations or dissipated by jet collision within the confinement. For Y/D = 9.3, the differences to the flat case are less pronounced. One can thus say that all the values presented correspond to a *developed jet impact condition in "confined" diffusion.*

For $Y/D > 4$, C_p values correspond to an exponential decay law[2]. Data fitting was performed for sets of data with equal velocity (Figure 8.4). The obtained r^2 for individual velocity series presented in Table 8.1 are higher than for the entire bundle of velocities (Equation 8.4, Equation 8.5 and Equation 8.6).

Table 8.1.: Regression parameters for exponential expression type $C_p = ae^{bD/Y}$ corresponding to Figure 8.4. The intervals correspond to the 95% confidence estimating bounds.

V $[m/s]$	a	b	r^2
29	0.080 [0.06-0.09]	6.613 [5.71-7.51]	0.98
27	0.058 [0.04-0.07]	7.594 [6.24-8.94]	0.94
24.6	0.116 [0.09-0.14]	5.061 [3.89-6.23]	0.89
22.1	0.096 [0.07-0.12]	5.510 [3.90-7.11]	0.84
19.6	0.063 [0.05-0.08]	6.992 [5.85-8.12]	0.94
17.2	0.030 [0.02-0.04]	9.148 [7.19-11.11]	0.92

To explore the evolution of C_p for a given pool depth Y, an analysis in terms of the confinement Froude number Fr_c is performed. Figure 8.5 shows that:

- C_p values decrease with growing pool depth Y/D, as occurs in pools with flat bottom;
- C_p values tend to increase with velocity up to Fr_c= 11 and remain fairly constant for Fr_c> 11. There is a slight decrease for Fr_c = 13.6.

[2] As a suggestion for future research, the centreline velocity decay in the developed flow region is likely to follow a similar exponential law where the exponent is $\approx b/2$.

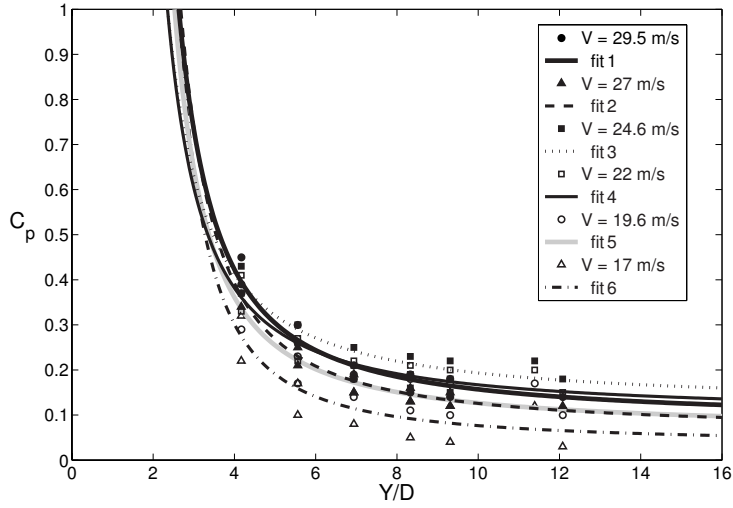

Figure 8.4.: Mean pressure as function of Y/D at jet axis (y/D =0.35) for the $D_c/D = 5.6$, $t/D_c = 0.5$ lateral confinement and a scour depth of t/D=2.8 (data from cases FC1/2)

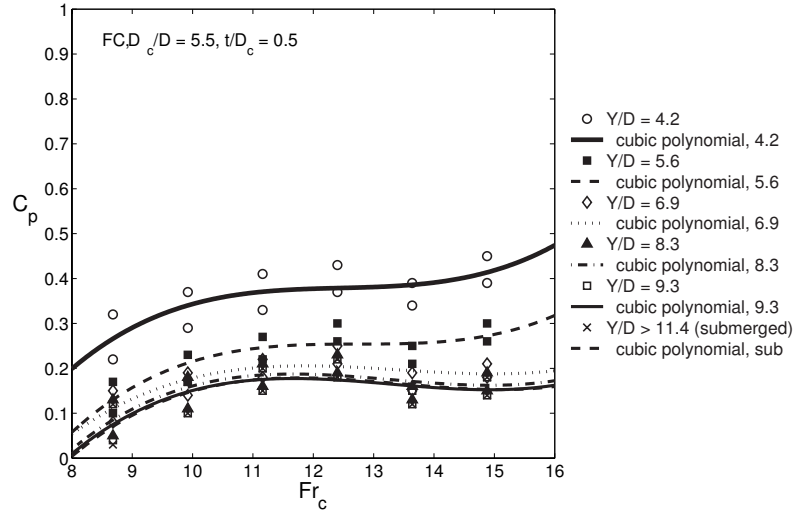

Figure 8.5.: Mean pressure as function of Fr_c, at the jet axis (y/D =0.35) for the $D_c/D = 5.6$, $t/D_c = 0.5$ lateral confinement and a scour depth of t/D=2.8 (data from cases FC1/2)

Fitting C_p values with a cubic polynomial of the kind:

$$C_p = a_1 Fr_c^3 + a_2 Fr_c^2 + a_3 Fr_c + a_4 \tag{8.7}$$

where a_1, a_2, a_3, a_4 are the polynomial coefficients, provided r^2 values between 0.5 and 0.7 when considering all the available data (from mixed test cases FC1 and FC2). Correlation coefficients r^2slightly increase when data sets for each of the FC series are considered separately.

Figure 8.5 suggests the existence of a velocity dependent process for the FC confinement ($D_c/D = 5.6$, $t/D_c = 0.5$). In flat pools, processes like air entrainment, core development and centerline velocity decay in the established flow zone depend on velocity. There is no reason to think the contrary in this case. However, in the presence of upward and inward flow currents induced by the confinement, these processes are likely to be modified.

The quantity of entrained air could be pointed out as one reason for the variation of C_p. A detailed analysis would require direct air concentration measurements.

McKeogh and Elsawy (1980) showed that the volume of air retained in a flat pool could be increased in comparison with an infinite pool, if the pool depth ranges between 30 - 100 % of the maximum depth of bubble penetration D_p. Their experiments were performed with smooth and rough turbulent jets with velocities up to 5 m/s. They showed that the volume of air retained in the pool is not constant for flat pools. In fact, it can even be less than for unbounded pools if Y $< 0.3 D_p$. This is exactly the case for the Y values used herein. Indeed, for V $>$ 17 m/s, D_p ranges from 3.00 to 4.40 m (Equation 7.1).

Ervine and Falvey (1987) described air entrainment of undeveloped rough turbulent jets *in unbounded conditions*, and provided an expression for the computation of the linear decay of the section-averaged air concentration, valid in the zone of established flow (ZEF, i.e. deep pools). However, for the present laterally confined pools, it is yet not clear what is the degree of jet development at impact. One could assume that, at least for the narrow pool, some type of jet development is achieved for Y/D $>$ 4. Nonetheless, C_p decay is not quadratic and, therefore, the velocity decay is not linear along the jet axis. Therefore, the air entrainment decay is likely not linear also.

Despite these contributions, and in view of the previous description of the observed mechanisms of air entrainment in laterally confined pools, any attempt to infer the evolution in depth of the air concentration for such pools, by extrapolating from known relationships valid for the (free) diffusion of rough turbulent plunging jets in unbounded pools is considered premature. In fact, pool aeration should still be a topic of further research in pools with flat bottom, as concluded in Chapter 7.

Furthermore, the jet core development may also be pointed out as a process interfering with the evolution of C_p in terms of Fr_c. If pool aeration is neglected, one can assume that for increasing jet velocities the upward moving currents also have increasing jet velocities. Therefore, for narrow confinements where upward and downward currents collide, additional resistance (i.e. friction) may enhance jet diffusion. This seems to be the case for the narrow (FC) pool. Under these conditions, one would expect a reduction of C_p with Fr_c. However, this is not the general trend within the tested range of velocities and pool depths: the increase in C_p derived from an increase in V is still larger than the corresponding increase in dissipation by the return currents.

The close similarity, almost collapse, of the $Y/D = 9.3$ and submerged jet series seems to indicate that the amount of entrained air may not be the governing parameter inducing the above mentioned C_p evolution with Fr_c.

In summary, C_p values for the narrow (FC) pool ($D_c/D = 5.6$, $t/D_c = 0.5$) are lower compared to the reference pool (FB). For transition pool depths between $4 < Y/D < 9$, the relative reduction of mean pressures at impact is quite important. For instance, for Y/D = 5.6 C_p values for V > 17 m/s range from 0.10 to 0.30, whereas for flat bottoms they vary between 0.70 and 1.00. A reduction of at least 50 % in C_p is achieved in this case.

The centreline mean pressure decay for in narrow pools (FC) is exponential and not quadratic as for pool with flat bottom (FB). The decay of C_p with growing pool depth is similar within the range of velocities 17 < V < 30 m/s, as showed in Figure 8.4. The differences in the amount of entrained air seem to play a secondary role in the diffusion process in this range of velocities. The induced flow patterns interfere with jet diffusion and generate additional friction with the plunging jet. They are likely to contribute to a non-linear evolution of C_p with velocity (i.e. with Fr_c).

A systematic computation of the differences between C_p values for the narrow and flat pools can be envisaged, based on the previously described equations, but the conclusions would be limited to the range of tested parameters. The governing processes of velocity and aeration decay in the pool merit further research.

The diversity of jet diffusion conditions is such, that each of the nine pool geometries tested should be studied separately.

8.2.5. Lateral evolution of scour with constant depth

As observed in Figure 8.2, the results obtained for the intermediate (SC) and wide (TC) pools are somewhat in between the "enveloping" cases of the narrow pools (FC) and pools with flat bottom (FB). The consecutive analysis of the narrow, intermediate, wide and flat pools can simulate a *lateral evolution of scour*, or inversely, highlight the contribution of the lateral confinement. The analysis of these two intermediate geometries is carried out hereafter. These pools have the same depth (t/D=2.8) as the narrow (FC) pool but have a different scour (aspect) ratio t/D_c.

For the intermediate pools (SC, Figure 8.6), an exponential decay provides a fairly good fit to the data for Y/D $\geq$ 4.2 (all r^2 values between 0.85 and 0.96).

Data for Y/D = 2.8 are fairly similar to those in flat pools. Values higher than 0.85 were obtained for V > 22 m/s, which is often considered to document the impact of the jet core (Ervine et al., 1997). According to this criteria, the flow establishment region is at least 2.8D deep for V > 22 m/s in the intermediate (SC) pool. Compared with C_p values in flat (FB) pools (Figure 8.2), this interpretation may be extended to C_p values as low as 0.7.

Data for Y/D = 5.6 to 9.3 (Figure 8.6a) show a wavy up-and-down pattern, despite being somewhat hidden by the fitting curves. C_p values for V = 27 m/s are quite similar to those for V = 17.2 m/s. The combined influence of the governing physical processes reflected in C_p does not vary in a one-way direction.

Figure 8.6b shows that C_p values do not follow a constant trend with Fr_c.

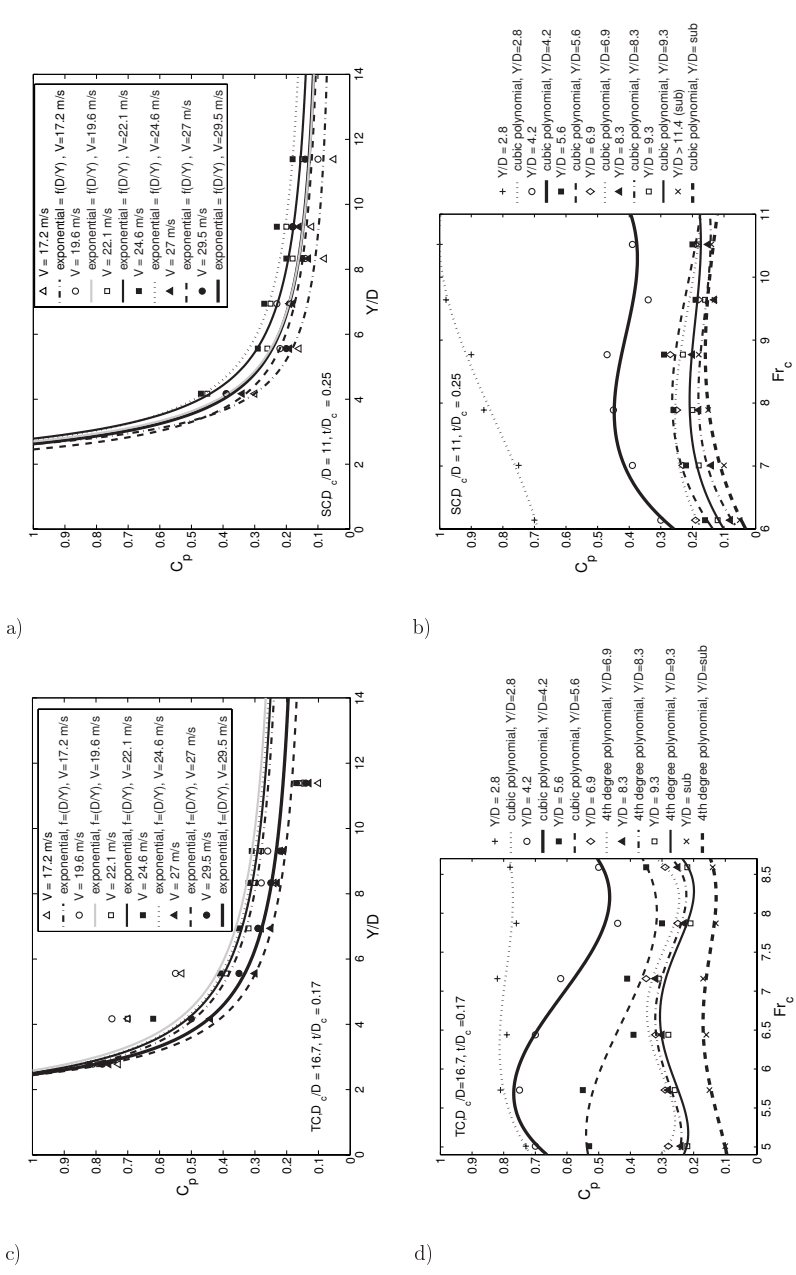

Figure 8.6.: Mean pressure coefficient C_p at jet axis (y/D=0.35) for the intermediate (SC) and wide (TC) pools with a scour depth of t/D=2.8: left, as function of Y/D; right, as function of Fr_c. Data from test series SC1/2 and TC1.

For a very shallow pool with Y/D=2.8, C_p increases up to 1; in this case the core should impact the pool bottom. High-velocity jets cut through very shallow pools. Such water level is non-effective for high-velocities, according to the definition of Puertas and Dolz (2002). Apparently, the intermediate (SC) confinement is not narrow enough for the deflected wall jets to bounce back and disturb the plunging jet directly for pool with $Y/D \leq 2.8$.

For $Y/D = 4.2$, C_p values start to decrease from a given $Fr_c \approx 8.8$.

For $Y/D \geq 4.2$, there is a decrease in C_p for Fr_c>9 and in particular for $Fr_c \approx 9.6$.

Figures 8.6c. and d. present the evolution of C_p with Y/D and Fr_c for the TC confinement ($D_c/D = 16.7$). In this case :

- Mean pressure decay seems to follow fairly well an exponential law for $V \geq 22.1$ m/s (Figure 8.6c.). However, for V = 17.2 and 19.6 m/s the energy decay rate is closer to a quadratic decay law as observed for flat pools. Therefore, *centreline mean pressure decay in confined pools depends on jet velocity.*

- Correlation coefficients r^2 are between 0.72-0.84 for V = 17.2 , 19.6 and 22.1 m/s, and 0.92, 0.98 and 0.96 for V = 24.6, 27 and 29.5 m/s respectively. If for V = 17 m/s the values for Y/D = 2.8 are excluded from the data series, the exponential fit r^2 increases for 0.92. Therefore, for the lowest velocities tested, C_p decay for Y/D > 4 approaches the type of decay observed in pools with flat bottom. On the contrary, for the highest velocities tested, and exponential decay reflects the behaviour of a laterally confined pool.

- Figure 8.6d. shows that the core development may *depend on jet velocity.* In fact, for $Y/D = 2.8$, all data corresponds to core impact conditions. However, for $Y/D = 4.2$, only the values corresponding to velocities from 17.2 - 22.1 m/s are higher than 0.7. This may reflect the importance of the deflection of the bottom wall jets. For low velocities, these wall jets do not bounce back towards the plunging jet after hitting the confinement, whereas for growing velocities they tend to disturb the development of the core of the jet.

- When comparing the series for Y/D = 2.8 in Figures 8.6b. and d.[3], C_p values for the highest velocities tested are higher with the SC pool than with the TC pool. The difference is about 20 % of the incoming kinetic energy. This is rather contradictory with the increasing influence of the reflected currents for narrower confinements. Values close to 1 are only found for SC pools; this indicates that a possible reason for a reduction in C_p in pools with flat bottom may be the air entrainment in the pool. This, however, can only be confirmed with direct measurements of air concentration along the jet centreline.

- When performing an identical comparison for Y/D = 4.2, C_p values for a given velocity are regularly higher than those for SC, and these higher than those for FC. The differences are larger for lower velocities. For this pool depth, the influence of the confinement is consistent: the narrower D_c is, the lower C_p is in the range of velocities tested;

- For deeper pools, the reduction of C_p with pool depth is consistent.

[3]Reading the x-axis in terms of V in lieu of Fr_c is possible since the other components are constant for each data series

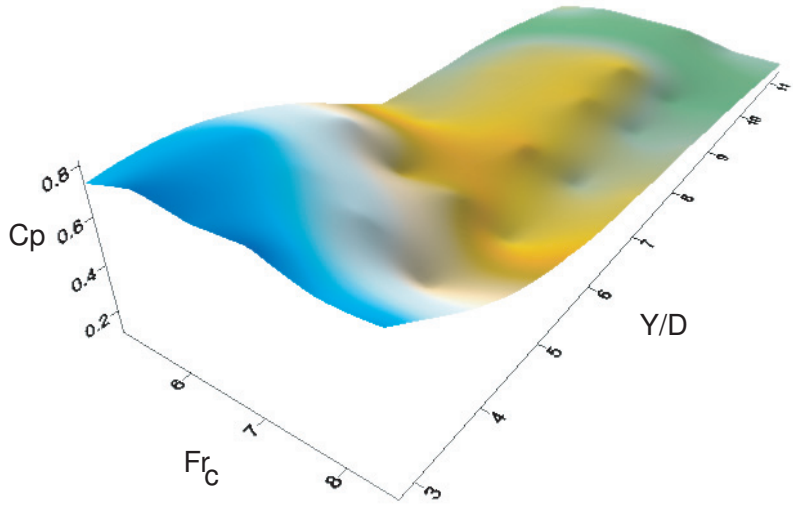

Figure 8.7.: Mean pressure coefficient C_p at jet axis (y/D =0.35) as function of Fr_c and Y/D for wide (TC) confined pools with a scour depth of t/D=2.8 (data from case TC1)

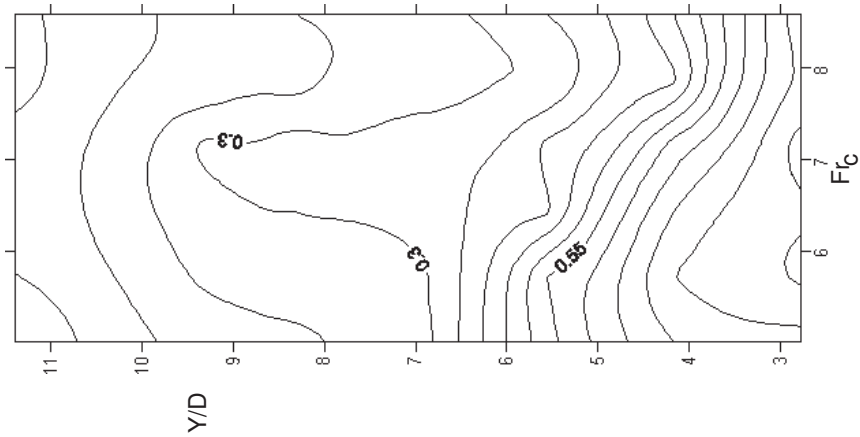

Figure 8.8.: Isolines of the mean pressure coefficient C_p at jet axis (y/D =0.35) as function of Fr_c and Y/D for wide (TC) confined pools with a scour depth of t/D=2.8 (data from case TC1). Line spacing = $0.05\frac{V^2}{2g}$.

- For deeper pools, the evolution of C_p with Fr_c presents a quite irregular pattern. Third and fourth-order polynomial are fitted to the measurements and present r^2 values between 0.73 and 0.92. Considering the size of each data set, these fits are merely indicative to help interpretation of the data.

The previous plots define a 3D surface (Figure 8.7) with a correlation of $r^2 = 0.95$ within the range of the parameters tested. The C_p isolines of such surface can be used to assess interesting combinations of pool depth and jet velocity (Figure 8.8). Similar isoline plots can be produced for the remaining geometries.

In summary, C_p decay laws in laterally confined pools are rather exponential than quadratic as previously observed in pools with flat bottom. Although no direct measurements were performed, the changes in flow patterns (discussed in Chapter 9) likely reduce air bubble penetration. The developments of the core of the jet and of the diffusion shear layer are accelerated due to counter currents inside the confined region. The participation of these processes in energy dissipation in the pool depend on the distance between the jet axis and the confinement; dissipation over the pool depth is higher for the narrow pools and decreases as the confinement becomes larger, i.e. for intermediate, wide and flat pools respectively in this order.

8.3. Fluctuating pressures in laterally confined pools

8.3.1. Turbulent pressures coefficient

Local dynamic pressures can be described as:

$$p(t) = \overline{p} + p'(t) \tag{8.8}$$

where $\overline{p}$ is the time average and $p'(t)$ the turbulent (i.e. fluctuating) component, in what is called the Reynolds decomposition (Chassaing, 2000). The turbulent pressure coefficient C'_p is defined as:

$$C'_p = \frac{\frac{\sigma_{p'}}{\gamma}}{\frac{\alpha V_0^2}{2g}} \tag{8.9}$$

where $\sigma_{p'}$ is the RMS value of the pressure fluctuations p'. The energy of such fluctuations is given by the variance of p', i.e. σ^2. Several authors have previously studied C'_p generated by jets in flat pools, e.g. Kamoi and Tanaka (1972); Gutmark et al. (1978) using air jets and May and Willoughby (1991); Puertas-Agudo (1994); Ervine et al. (1997); Melo (2001); Bollaert (2002b); Bollaert and Schleiss (2003b) using plunging water jets.

Figure 8.9 presents the evolution of C'_p with Y/D for four pool geometries, from the widest ($D_c/D = \infty$) to the narrowest ($D_c/D = 5.6$).

8.3.2. Reference scenarios of pools with flat bottom

Data in pools with flat bottom (FB) are compared with envelope curves presented by Ervine et al. (1997). These were obtained in a similar experimental facility and jet characteristics[4].

[4]However, the range of break-up degree was wider than in the present study.

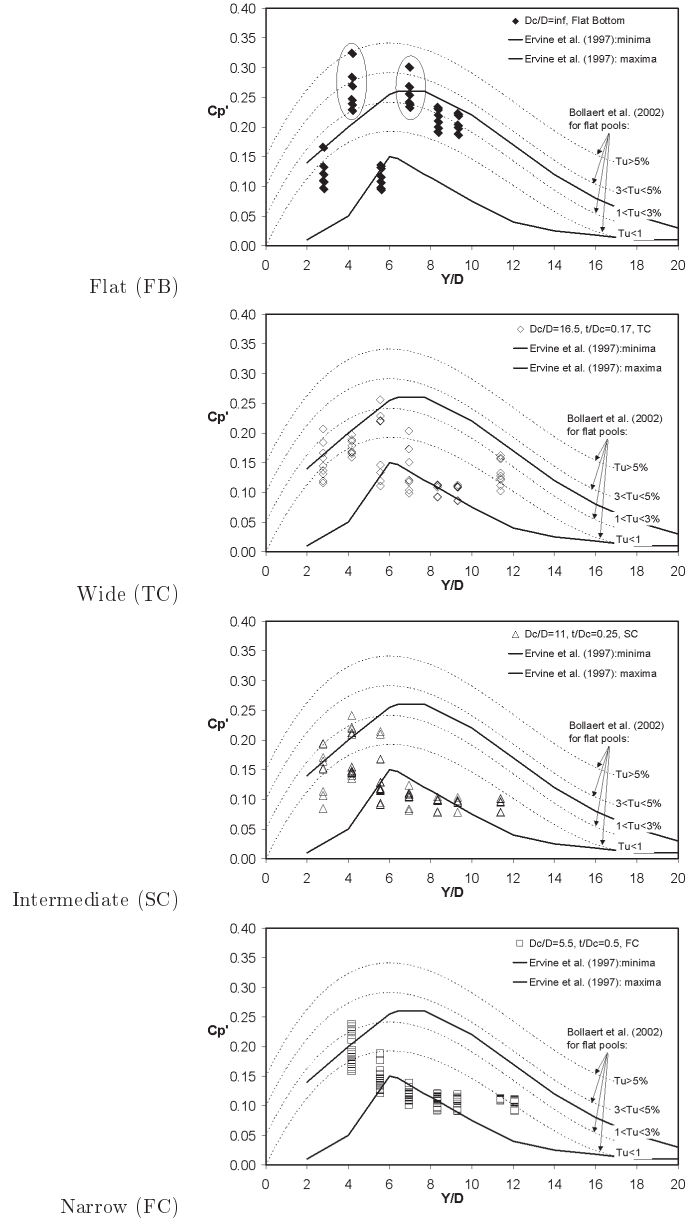

Figure 8.9.: Dimensionless RMS pressure coefficient C'_p close to the jet axis ($y/D = 0.35$) as a function of the relative depth ratio Y/D, for pools with flat bottom (FB) and laterally confined pools (wide, intermediate and narrow) with constant scour depth t/D=2.8. Comparison with empirical curves by Ervine et al. (1997) and Bollaert et al. (2002). Data from test series FB0/3, FC1/2, SC1/2 and TC1 with $10 < V < 30$ m/s. The circled data correspond to the FB0 series.

The agreement is fairly good, save for Y/D = 4.2 and 6.9 for which all C'_p are larger than the maxima of Ervine et al. (1997).

The Y/D = 4.2 and 6.9 series are part of the FB0 test series. They are outside Ervine et al. (1997) enveloping curve due to the unstable character of the jet produced during the FB0 test series. In fact, both the FB0 series and some of the tests of Bollaert (2002b) were performed with more unstable jets than those used by Ervine et al. (1997), even if in the same range of Tu_0. This was due to swirling flow in the supply system of the experimental facility, as discussed in Chapter 4.

Bollaert et al. (2002) proposed a group of curves for C'_p as a function of Tu_0 that fit their data with $r^2 = 0.99$. These curves are somewhat similar in shape to the enveloping curves of Ervine et al. (1997) but with peak values shifted towards shallower pools. This is likely due to the different degree of core instability in the two experimental set-ups. The differences between these authors (and also the present FB0 series) are nevertheless limited to core impact conditions in shallow pools with Y/D < 5-7 and jet velocities lower than 20 m/s.

The jets obtained in the FB3 test series, after modification of the supply system of the experimental facility, generate lower turbulent impact pressures for core impact conditions than those obtained during the FB0 test series and also those reported by Bollaert (2002b). The values of the FB3 test series are in good agreement with those of Ervine et al. (1997).

In laterally unbounded pools, C'_p maximum values are about 0.25. Values between 0.20 and 0.25 were measured for Y/D = 5.6 (low velocities) and Y/D > 6 and V > 10 m/s (Figure 8.10, left). These data indicate that the jet core persists at Y/D = 5.6 for high velocities.

Assuming a threshold value of $C'_p = 0.15$ developed jet impact conditions can be characterized by Y/D > 5.6, and Y/D = 5.6 with V < 15 m/s, in the present experimental set-up. This is an additional contribution to the definition of jet impact conditions in the present experimental set-up.

Farther from the jet axis, at y/D = 2.08, C'_p values are lower than 0.06 save for V < 10 m/s (Figure 8.10, right).

8.3.3. Lateral evolution of scour with constant depth

Figure 8.9 shows that C'_p is generally reduced for Y/D > 6 in laterally confined pools, when compared directly with the reference curves by Ervine et al. (1997) for pools with flat bottom. This reduction is more important for the narrowest pool (FC). The decrease in mean pressures observed previously is thus caused by increased dissipation along jet diffusion inside the confined zone.

8.3.4. The ϕ confinement ratio for turbulent impact pressures

In order to assess the conditions for which there is an increase in turbulent pressures, the confinement ratio for turbulent impact pressures is defined as:

$$\phi = \frac{C'_{p,confined}}{C'_{p,flat}} \tag{8.10}$$

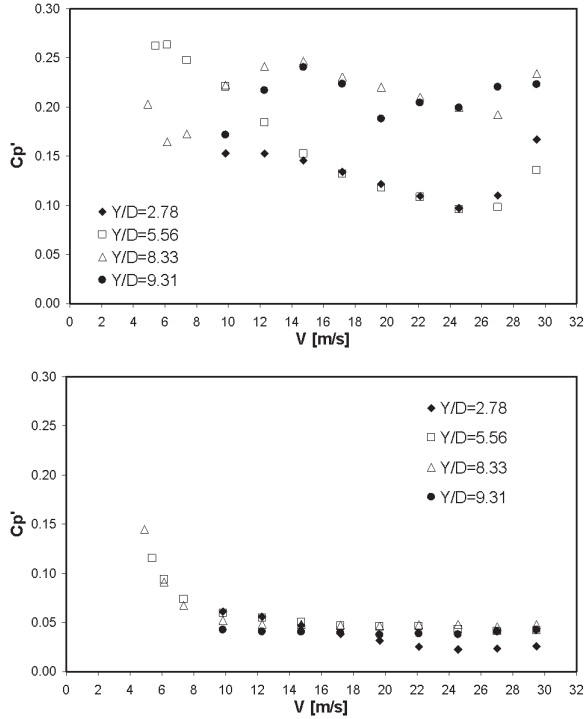

Figure 8.10.: Dimensionless RMS pressure values for the FC pool as function of V : left, at y/D = 0.35; right, at y/D = 2.08. Data from test series FB3.

Figure 8.11 presents the values of ϕ for the three pool configurations with t/D=2.8 (TC, SC, FC) when compared with laterally unbounded pools with flat bottom (FB3 test series).

For pools with Y/D > 8, C'_p values decrease in presence of any of the three confinements when compared with laterally unbounded pools.

For Y/D < 8, results are unanticipated: (1) C'_p values increase for almost all velocities tested with the TC pool; (2) C'_p values increase in the SC pool but only for velocities lower than 23-25 m/s; and, (3) C'_p increase for all V > 17 m/s with the FC (narrowest) pool. Interpretation of such results is rather complex due to the the scarcity of information on the variation of air entrainment, core development and pool flows.

According to the experimental observations by Melo (2001), *increasing* air content in the pool *increases* pressure fluctuations in the impinging zone at the pool bottom. Turbulence is enhanced by the different behaviour of the air and the water particles (Bonetto and Lahey Jr, 1993). Therefore, such observations may be due to:

- increase in air entrainment by re-plunging of the deflected upward currents, in the TC and SC cases;

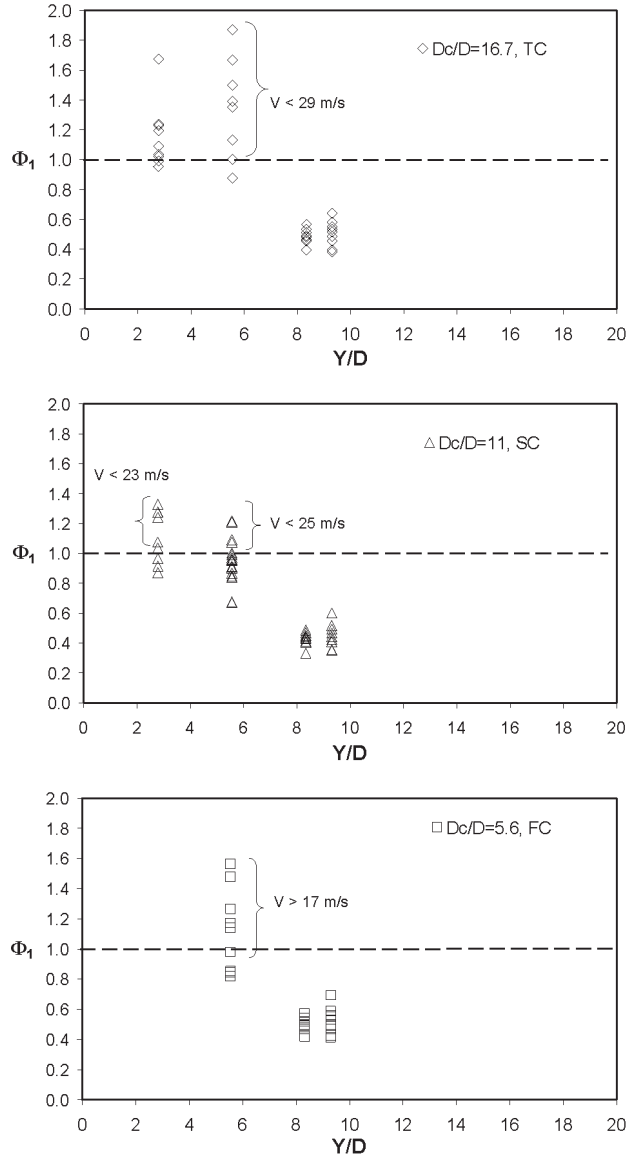

Figure 8.11.: The ϕ confinement ratio for turbulent impact pressures close to the jet axis (y/D =0.35) for the wide (TC), intermediate (SC) and narrow (FC) pools (t/D=2.8) as function of Y/D. Data from test series FC1/2, SC1/2 and TC1.

- direct collision between the plunging jet and the ascending currents, enhancing flow mixing and consequently turbulence, in the narrowest pool (FC).

Since the analysis of ϕ does not indicate the frequencies for which turbulent energy is modified, a spectral analysis for the most illustrating case (FC) is performed in Section 8.5.

8.3.5. Tentative fitting of C'_p in terms of Y/D

The data series per velocity for V > 17 m/s for the FC, SC and TC pools are plotted as function of the relative pool depth Y/D, in Figure 8.12. These series are fitted with third-degree polynomial functions, or with rational functions with polynomial numerators and denominators. In view of the limited size of the data sets (6 pool depths per V), this analysis is considered exploratory.

For the narrow pool (FC), correlation coefficients r^2 range between 0.97 and 0.99, whereas for the intermediate pool (SC) $r^2 > 0.99$, and for the wide pool (TC) r^2 range between 0.85 and 0.99. The lowest r^2 value corresponds to the V = 24.6 m/s series in the wide (TC) geometry.

Regarding the wide pool (TC), bell-shaped curves are obtained for velocities from 17 to 25.6 m/s. They are somewhat similar to the curves proposed by Ervine et al. (1997), at the exception of the submerged jet values for Y/D = 11.4. In the absence of air, C'_p values are increased, which may be explained by a decrease in air-induced turbulence and an increase in flow-pattern-induced turbulence. In fact, since there is no air moving upwards the influence of the large-scale recirculation currents generated in the pool upon the jet may increase[5]: the barrier of ascending air bubbles separating the plunging jet from the recirculation currents is no longer there. For the highest velocities, C'_p decreases with Y/D, save for the submerged jet conditions.

For the intermediate pool (SC), C'_p decreases with Y/D for all velocities tested and pool depths Y/D > 5.6. The data series are grouped in two sets, one for $C'_p \approx 0.10 - 0.12$ for V = 17.2 - 22.1 and for $C'_p \approx 0.08 - 0.10$ for V = 24.6 - 29.5 m/s. In this pool, there is no sudden increase in C'_p for submerged jet conditions. This may indicate a minor influence of the recirculation currents. For shallower pools, there are more turbulent fluctuations for Y/D =4.2 than for deeper pools for all the velocities presented. However, for Y/D = 2.8 the data scatter is higher and it is not possible to identify a clear trend for all velocities.

For the narrow pool (FC), C'_p decrease with increasing Y/D and for all the velocities between 17.2 and 29.5 m/s. C'_p values are higher for V = 24.6 - 29.5 m/s than for V = 17.2 - 22.1 m/s in the range Y/D = 4.2 and 5.6. This trend is inverted for deeper pools. This means that for small pool depths, the higher the velocity the more turbulent is the flow pattern induced by the confinement; or, the higher is the resistance to jet diffusion by the upward currents. The FC pool is so narrow that part of this resistance to jet diffusion is by friction in the air between the falling jets and ejections that come out of the water. In these circumstances, air entrainment conditions at plunging point are considerably modified. For deeper narrow pools (FC), interpretation is less straightforward. C'_p for submerged jet conditions are rather similar to those with Y/D = 9.3. Therefore, the presence/absence of air seems less relevant in this pool geometry. Friction between the upward currents *outside of the pool* and the falling jet travel in the air is reduced due to increased submergence of the former. On the

[5] This phenomena has been matter of video recording by the author. A schematic representation of such flow conditions is presented in the chapter 9.

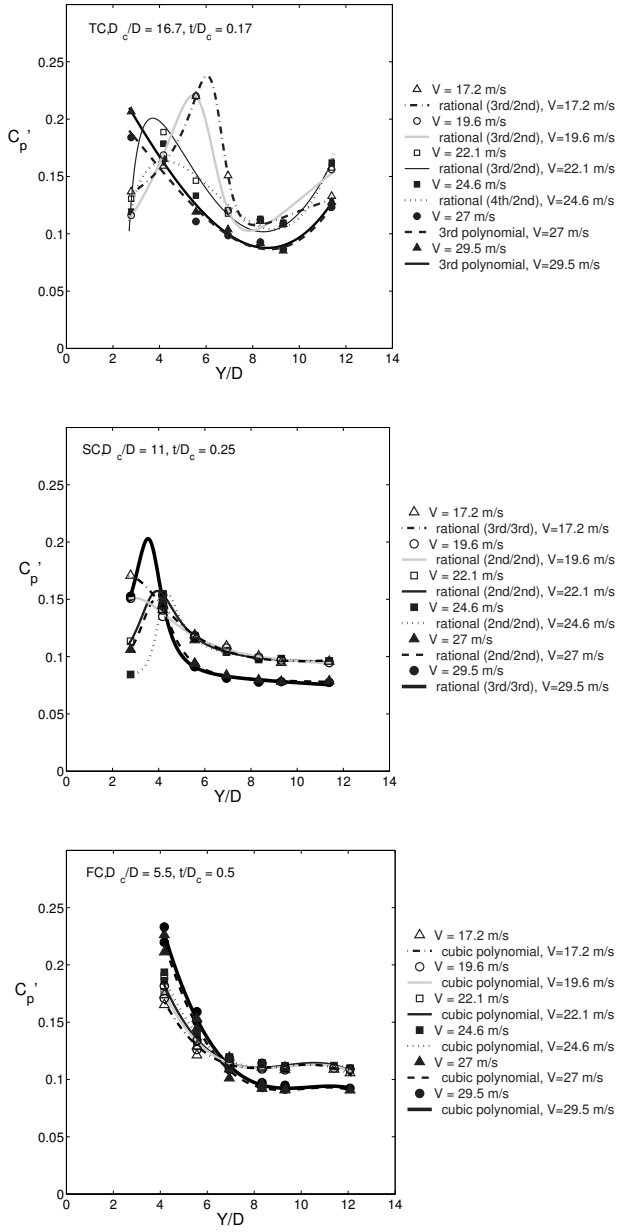

Figure 8.12.: RMS pressure values at jet axis (y/D =0.35) for the wide, intermediate and narrow pools (t/D=2.8) as function of Y/D. Data from test series FC1/2, SC1/2 and TC1 and V $>$ 17 m/s. From top to bottom: TC, SC and FC test series

other hand, there is increasing interference of the recirculation currents. These currents are the more efficient in redirecting the upward deflected jet to the center of the pool (against the plunging jet itself), the lower the velocity of the jet is.

8.3.6. Tentative fitting of C'_p in terms of Fr_c

The same data series are used to plot C'_p as a function of the Fr_c (i.e. V) per Y/D, in Figure 8.13. Correlation coefficients between 0.80 and 0.97 are obtained for the FC pool, 0.80 to 0.98 for the SC pool and 0.88 to 0.98 for the TC pool using 3^{rd} and 4^{th} order polynomial functions. Due to the limited data, this curve fitting analysis is carried out with the only purpose of supporting the physical interpretation of the results within the tested range. The three plots are analyzed separately.

For the wide pool (TC), C'_p values lie between 0.10 and 0.23. The largest variations with velocity are observed for Y/D = 5.6. For the lowest velocities, there is more turbulence in the pool due to an enhanced jet development. For the highest velocities, C'_p reduces to values similar to those for Y/D = 2.8 and low velocities, i.e. core jet impact conditions. In this case, the reflection of bottom wall jets generates violent upward currents that disturb the plunging jets. For deeper pools, C'_p decreases gradually with velocity. Dissipation must be done higher up in the water column and not close to the bottom. The upward currents may reduce air bubble penetration in the pool and thus reduce air-induced turbulence. The submerged jet data show clearly that the air content in the pool has direct influence in the turbulent character of impact pressures. A direct comparison of the Y/D = 9.3 and 11.4 (submerged) series shows a similar behaviour of both series in terms of Fr_c. However, the submerged jet series has 3 to 5% more energy. One would expect the opposite for such Y/D: for increasing pool depth $C_{p'}$ would reduce from Y = 9.3D to Y = 11.4D. For the SC and FC pools, the increase of $C_{p'}$ in submerged jet conditions is not observed: in those pools, flow-generated turbulence is likely to be more important than aeration-induced turbulence.

For the intermediate pool (SC), a smooth decrease of C'_p with Fr_c (i.e. V) was observed for Y/D$\geq$5.6. For Y/D = 4.2, C'_p values are almost constant with Fr_c, in what might be a compromise between the variations of air-induced turbulence and flow-induced turbulence. For Y/D = 2.8, C'_p reduces with Fr_c (with velocity) as the jet momentum progressively overbalances other processes until reflected currents start disturbing the jet.

For the narrow pool (FC), C'_p increases with Fr_c for Y/D$\leq$ 5.6. This is the result of flow-induced turbulence, generated by direct friction between the quite compact plunging jet and strong upward currents, in the air and in the water. Since the space between the falling jet and the ascending currents is very narrow, diffusion is done with hardly any spreading. The jet core must vanish before 4.2D at a higher dissipation rate due to increased friction. This is shown by the low C_p values discussed in Section 8.2. For pools deeper than 5.6D, C'_p decays slowly with velocity to values around 0.10.

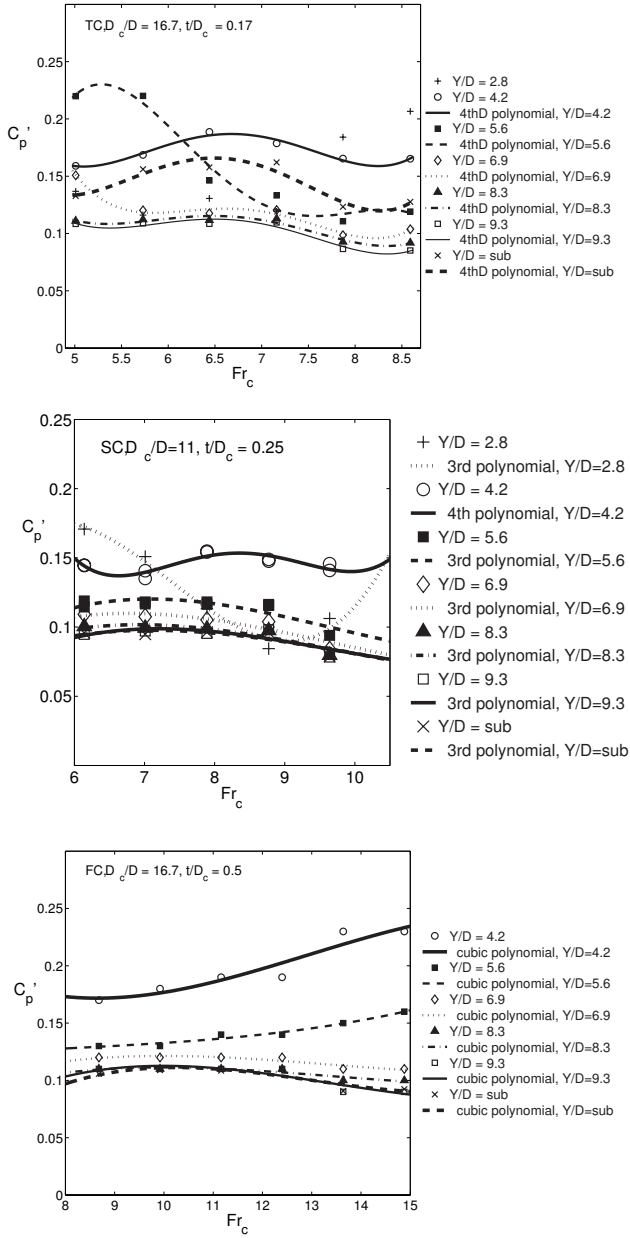

Figure 8.13.: RMS pressure values at jet axis (y/D = 0.35) for the wide, intermediate and narrow pools (t/D=2.8) as function of Fr_c. Data from test series FC1/2, SC1/2 and TC1 and V > 17 m/s. From top to bottom: TC, SC and FC test series

8.4. Extreme pressure peaks generated by plunging jets in narrow pools

8.4.1. Positive and negative extreme pressure fluctuations

Extreme instantaneous pressures coefficient for positive and negative fluctuations are defined as:

$$C_{p'}^{+} = \frac{p'^{+}}{\frac{\alpha V_0^2}{2g}} \tag{8.11}$$

and

$$C_{p'}^{-} = \frac{p'^{-}}{\frac{\alpha V_0^2}{2g}} \tag{8.12}$$

for positive p'^{+} and negative p'^{-} fluctuations respectively. Several authors have previously studied extreme pressures generated by plunging jets in laterally unbounded pools, e.g. May and Willoughby (1991); Ervine et al. (1997); Melo (2001); Bollaert (2002b). May and Willoughby (1991) sampled p' for 5.5 min at 0.1 kHz from jets with V = 3.3, 5.0 and 6.6 m/s. Ervine et al. (1997) presented p'^{+} and p'^{-} from 2-min runs at 0.1-0.23 kHz and velocities up to 25 m/s. Melo (2001) used 2-min runs at 0.075 kHz at maximum 4.7 m/s. Bollaert (2002b) sampled p' systematically during 1-min runs at 1 kHz from jet with V up to 30 m/s.

The following data correspond to pressure measurements during 3-min at 1 kHz, for V $\leq$ 30 m/s. Control runs at 7.5 kHz and 15 kHz show that p' values higher than those obtained in ergodic 3-min runs may occur, even though their duration is inferior to 1 ms. Toso and Bowers (1988); Fiorotto and Rinaldo (1992a); Bellin and Fiorotto (1995) showed that p'^{+} and p'^{-} can further increase if the duration of acquisition is increased up to 24 hours, under hydraulic jumps, using frequencies up to 150 Hz. Such large durations of acquisition have not yet been tried with plunging jets.

Figure 8.14 presents the evolution of $C_{p'}^{+}$ at y/D = 0.35, in terms of Y/D and V, in narrow pools and pools with flat bottom. For the latter case, $C_{p'}^{+}$ values larger than 1.0 are obtained only for velocities less than 20 m/s with the FB0 series (unstable jet before supply system modification, Y/D = 4.2 and 6.9). For the remaining series, $C_{p'}^{+}$ tends to 1.0 for high velocities and deep pools. If the FB3 test series alone is considered, $C_{p'}^{+}$ values for V=10-30 m/s *increase with pool depth*, from about 0.40 - 0.60 for shallow pools (Y/D = 2.8) to 0.8 - 1.0 for deep pools (Y/D=9.3).

The narrow confinement D_c/D = 5.6 and t/D = 2.8 generates $C_{p'}^{+}$ that are almost all lower than 1.0 for Y/D > 5.6. *They decrease with increasing pool depth*. The lowest values of $C_{p'}^{+}$ are obtained for Y/D = 8.3 and for the submerged jet conditions (Y/D > 11) for velocities from 9 to 30 m/s. Values higher than 1.0 where only observed for Y/D = 4.2.

The *negative* extreme values $C_{p'}^{-}$ (Figure 8.15) for laterally unbounded pools are almost all lower than 1.0, except for V < 15 m/s in the FB0 series with Y/D = 4.2. They tend to increase with submergence up to Y/D =8.3 but decrease beyond Y/D = 9. They are higher for shallow pools than deep pools (0.40 - 0.60 for Y/D = 9.3) and vary slightly with velocity.

With the confinement, $C_{p'}^{-}$ becomes lower than 0.6, save few exception with V = 9.8 m/s. For pools deeper than Y/D = 6, $C_{p'}^{-}$ tends to 0.40.

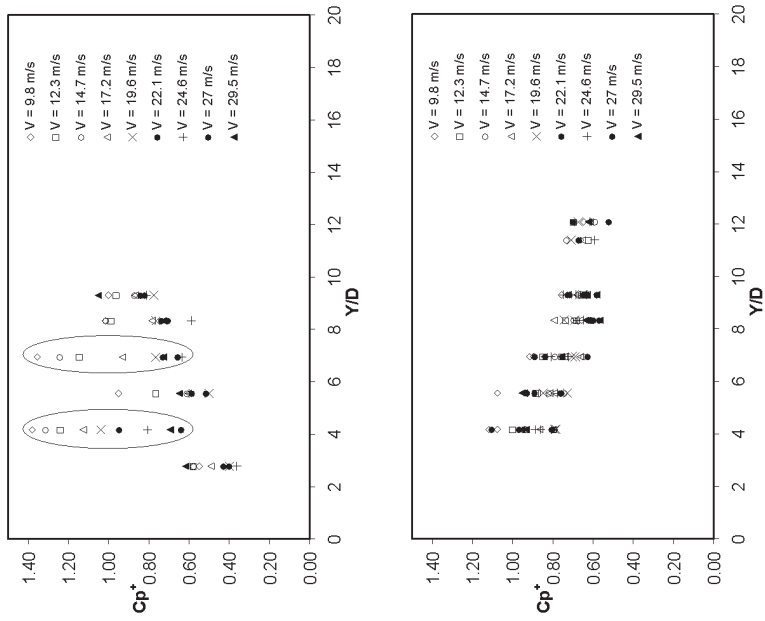

In terms of Y/D: left, pools with flat bottom (FB); right, narrow pools (FC).

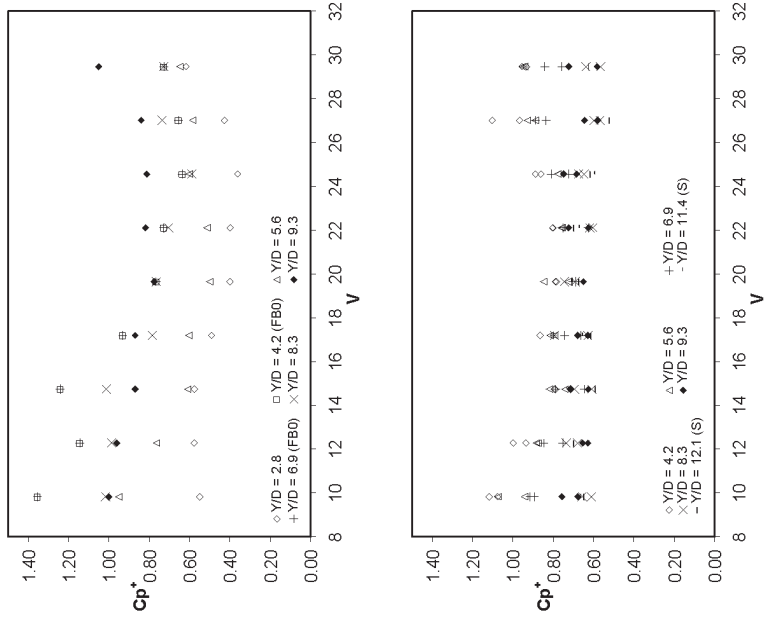

In terms of V: left, pools with flat bottom (FB); right, narrow pools (FC).

Figure 8.14.: $C_{p'}^{+}$ at y/D = 0.35: left, pool with flat bottom (FB); right, narrow pool (FC). Test series FB0 (encercled), FB3 and FC1/2.

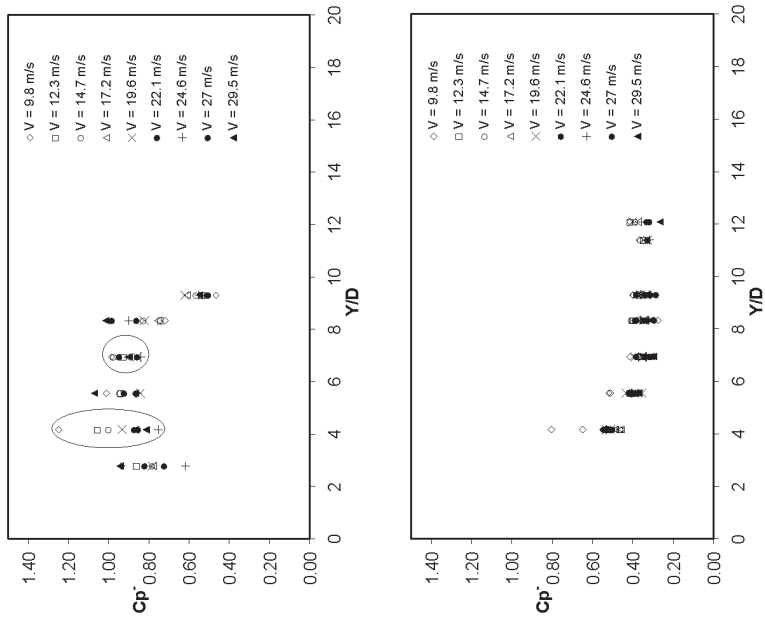

In terms of Y/D: left, pools with flat bottom (FB); right, narrow pools (FC).

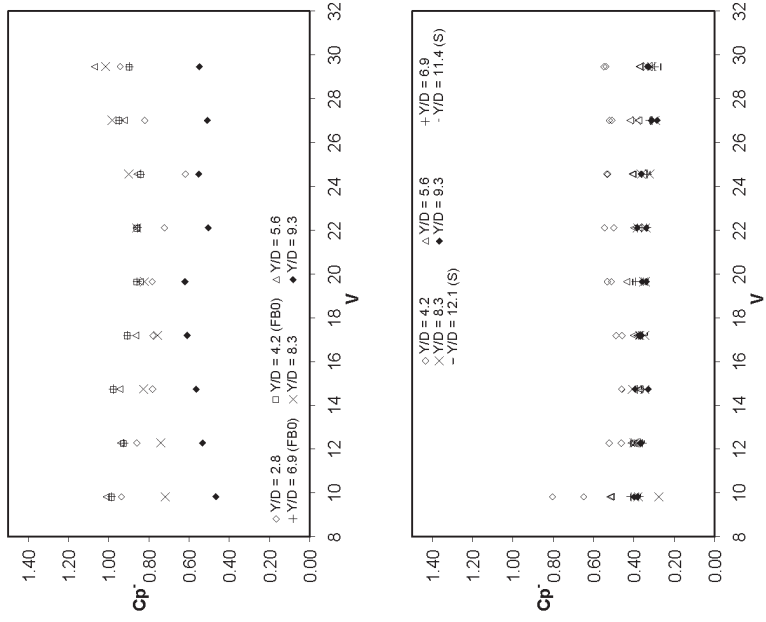

In terms of V: left, pools with flat bottom (FB); right, narrow pools (FC).

Figure 8.15.: $C_{p'}^{-}$ at y/D = 0.35. Test series FB0 (encercled), FB3 and FC1/2.

8.4.2. Pressure distribution at stagnation

As discussed in Chapter 6, the probabilistic distribution of pressure fluctuations is directly dependent on the pool turbulent flow conditions and is related to the degree of jet development.

Table 8.2 presents a selection of statistics of impact pressures in narrow pools (FC) for the highest velocity tested, V = 29.5 m/s, and various pool depths. These data can be compared with Table 6.4 in Chapter 6 for pools with flat bottom (FB).

Table 8.2.: Selected statistical parameters of pressure measurements at y/D = 0.35 with the FC pool and V = 29.5 m/s. Statistics obtained from data sets with 65'536 points sampled at 1 kHz (i.e. ≈ 1.1 min)

Y/D	$\overline{p}$ [bar]	σ [bar]	p'^{+} [bar]	p'^{-} [bar]	C_s	K	Z'_{min}	Z'_{max}	C_p	$C_{p'}$	$C^{+}_{p'}$	$C^{-}_{p'}$
4.2	3.000	1.032	7.228	0.572	0.56	-0.08	-2.4	4.1	0.45	0.23	0.95	0.55
5.6	2.311	0.704	6.530	0.672	1.01	1.40	-2.3	6.0	0.30	0.16	0.95	0.37
6.9	1.952	0.489	5.307	0.635	0.89	1.28	-2.7	6.9	0.21	0.11	0.76	0.30
8.3	1.855	0.431	4.358	0.477	0.81	1.00	-3.2	5.8	0.19	0.10	0.57	0.31
9.3	1.811	0.420	5.014	0.366	0.86	1.19	-3.4	7.6	0.18	0.09	0.72	0.33
12.1	1.659	0.409	4.421	0.487	0.81	1.05	-2.9	6.8	0.14	0.09	0.62	0.26

Dynamic pressure coefficients are lower than in pools with flat bottom, as described in the previous sections. The skewness values are always positive, indicating the impact of the turbulent shear layer of the plunging jet. The (excess) kurtosis values are almost all positive, save for Y/D = 4.2 where it is almost zero (i.e. Gausssian). The values of K are lower than the maximum value obtained in laterally confined pools.

In good agreement with the positive skewness, p'^{-} are 2 - 3 σ (i.e. Z'_{min} = 2-3), whereas p'^{+} can be almost 8σ. The increase in Z'_{max} is a consequence of the decrease in σ and $\overline{p}$, rather than an increase in p'^{+}, as discussed for $C^{+}_{p'}$.

An extensive analysis for other velocities and pool geometries may be performed with the available data.

8.5. Spectral energy distribution of impact pressure fluctuations generated by plunging jets in narrow pools

Pressure fluctuations are analysed by means of spectral analysis. Spectra of turbulent fluctuations present three main features from low to high frequencies Chassaing (2000): (1) the production zone, related to the mean characteristics of the energy source (i.e. the jet), (2) the energy redistribution zone from large eddies at low frequencies to progressively smaller vortices (cascade of energy), and (3) the dissipation or viscous zone, where the energy of the small turbulent structures (high frequencies) is dissipated by viscosity.

Density power spectra are computed using the Welch periodogram method for Fast Fourier Transforms, with 50% overlapping, a Hamming window, a maximum of 3 x 65'536 points sampled at 1 kHz, and 64 blocks.

8.5.1. The influence of jet velocity on spectral energy distribution

Spectral energy distribution of pressure fluctuations at stagnation in pools with flat bottom and narrow pools (FC) are presented in Figure 8.16.

For shallow pools (Y/D =4.2), the narrow pool spectra at y/D = 0.35 have higher energy at f < 10 Hz than those of pools with flat bottom at y/D = 0.69. Even if the comparison is not exactly at the same point, the differences are of two orders of magnitude for the highest velocities. This difference is in any case larger than the radial decrease of p' in such a short distance.

In pools with flat bottom, p' reflects the impact of the turbulent shear layer of a relatively compact plunging jet. The pool depth (Y/D = 4.2) is still lower than the estimated core development length (Y/D = 5.6 for Y > 15 m/s).

The p' data corresponding to the narrow pool represent the impact of a developed jet. The FC spectra enter the viscous dissipation range at about 20 Hz for low velocities (i.e. 9.8-12.3 m/s), and 50 Hz for high velocities (V = 27 - 29.5 m/s), whereas spectra in pools with flat bottom decay mildly from low to high frequencies.

The log-scales are deceiving: the integral of the spectra of narrow pools are lower than those of pools with flat bottom, as shown by the lower $C_{p'}$ values. The slow decaying spectra in pools with flat bottom have more energy at high frequencies. In all cases, spectral energy increases with jet velocity and similarly for all frequencies.

For deep pools (Y/D =9.3), spectra at the same point are compared. The shape is similar, corresponding to developed jet impact conditions. Overall, the FC spectra have less energy than the corresponding spectra in flat bottoms, which is in good agreement with the decrease in $C_{p'}$ values. Furthermore, FC spectra enter the dissipation range at lower frequencies, in the range 10-40 Hz. The transition of spectra in pools with flat bottom is done at about 30 Hz for V = 9.8 m/s, and 100 Hz for V = 29.5 m/s.

8.5.2. The influence of relative pool depth (Y/D) on spectral energy distribution

A detailed analysis for two flow velocities and increasing submergence is presented in Figure 8.17.

In pools with flat bottom and V = 17.2 m/s, spectra at y/D = 0.35 change from mild sloped spectra for Y/D $\leq$ 5.6 (i.e. core impact conditions, undevelop jet) to a double-sloped spectra for deeper pools. In the latter case, spectral energy is redistributed between turbulent scales up to 20-30 Hz, where the spectra enter the dissipation range. The equivalent spectra in FC pools are all "doubled-sloped". For shallow pools (e.g. Y/D = 2.8), FC spectra have higher energy content for intermediate frequencies between 20-100 Hz than spectra in pools with flat bottom. For deep pools, the energy content in FC spectra is generally lower than in the corresponding spectra in pools with flat bottom.

For V = 29.5 m/s, spectra in both pools with flat bottom and narrow pools (FC) correspond to developed jets. For Y/D = 2.8, the FC spectrum has almost the same energy as the spectrum in the corresponding pool with flat bottom. The entry in the dissipation range occurs for lower frequencies. For a deep pool with Y/D = 9.3, there is clearly less energy at all frequencies in the FC pool, when compared to the case of pools with flat bottom.

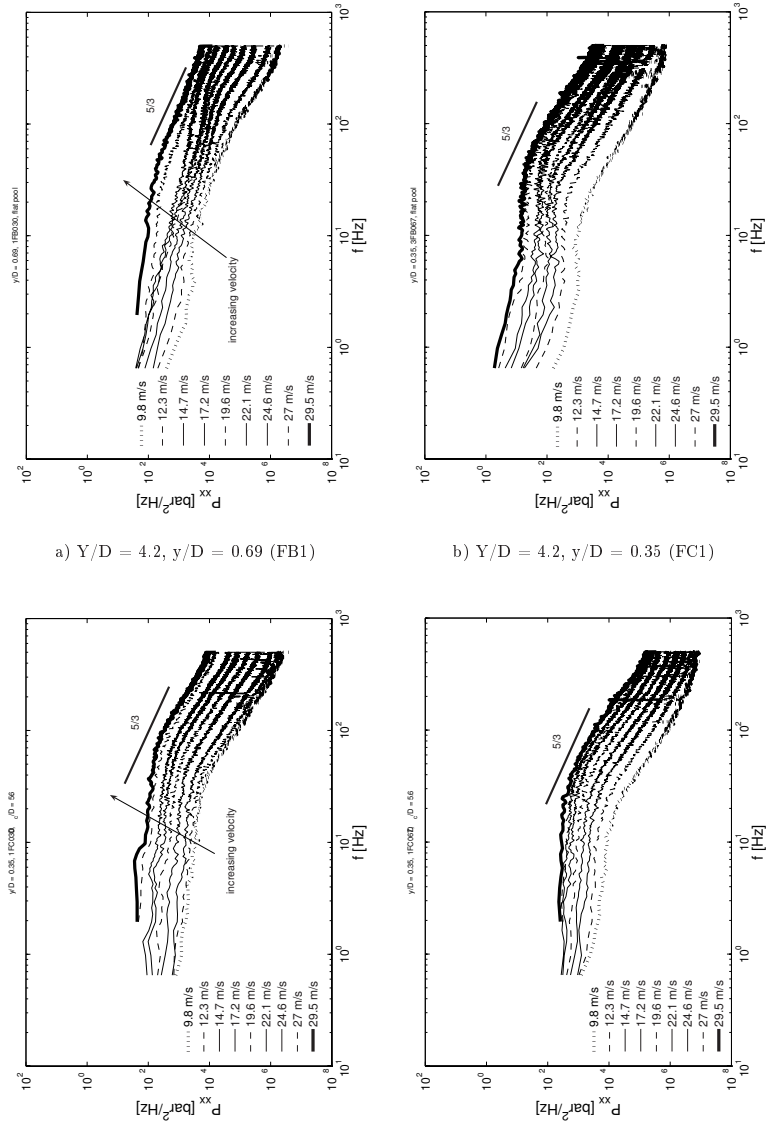

a) Y/D = 4.2, y/D = 0.69 (FB1)

b) Y/D = 4.2, y/D = 0.35 (FC1)

c) Y/D = 9.3, y/D = 0.35 (FB3)

d) Y/D = 9.3, y/D =0.35 (FC1)

Figure 8.16.: Power spectral density P_{xx} of pressure fluctuations in terms of velocity: left, pool in flat bottom (FB); right, narrow pool (FC). Test series indicated in brackets. All spectra computed with Welch's periodogram method and 3 x 65'536 samples from runs at 1 kHz, save few exceptions for 29.5 m/s with one single run.

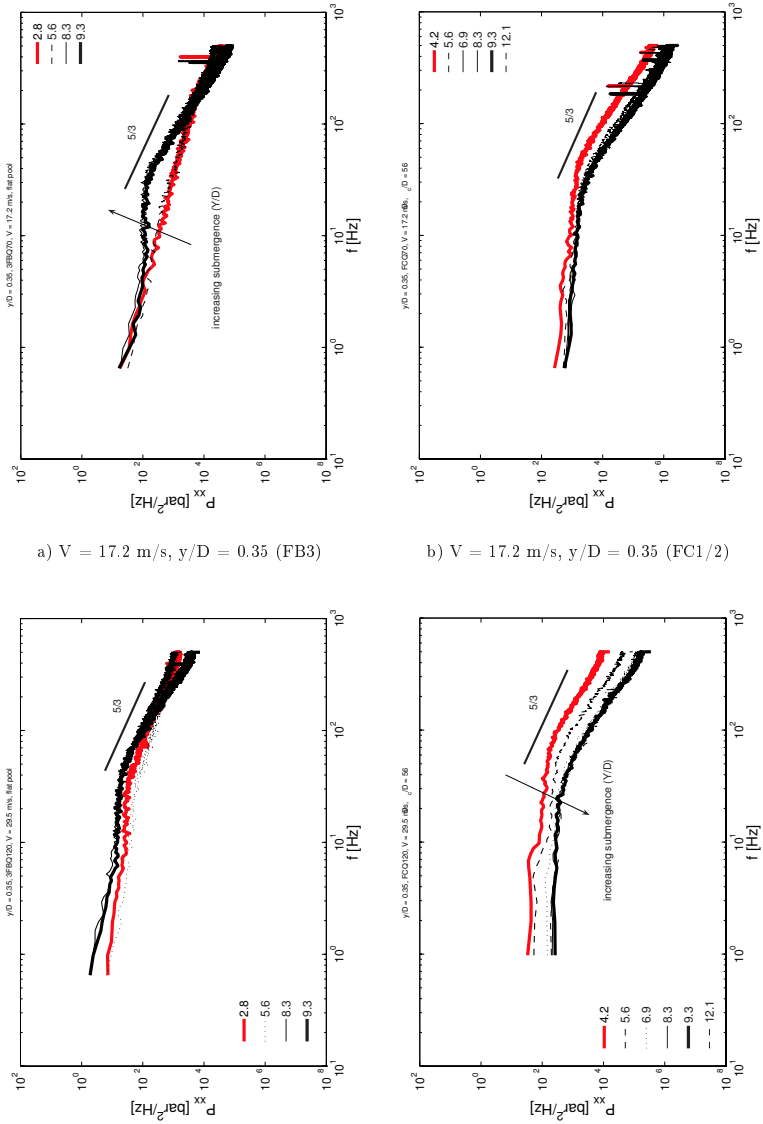

a) V = 17.2 m/s, y/D = 0.35 (FB3)

b) V = 17.2 m/s, y/D = 0.35 (FC1/2)

c) V = 29.5 m/s, y/D = 0.35 (FB3)

d) V = 29.5 m/s, y/D = 0.35 (FC1/2)

Figure 8.17.: Power spectral density P_{xx} in terms of velocity: left, pool with flat bottom (FB); right, narrow pool (FC). Test series indicated in brackets. All spectra computed with Welch's periodogram method and 3 x 65'536 samples from runs at 1 kHz, save few exceptions for FC at 29.5 m/s with one single run.

As a conclusion, the lateral confinement of the jet not only reduces energy in p' for frequencies < 500 Hz in deep pools, but it also precipitates the entry in the dissipation region. In shallow pools, there is more energy at frequencies capable of exciting rock fissures, i.e. about 10-100 Hz.

Confining jet diffusion in shallow pools presents thus the advantage of reducing mean pressures and eventually fluctuating pressures. However, spectral energy may increase at frequencies capable of generating important transient pressures oscillations inside simple-shaped fissures.

8.6. Conclusions and outlook

This chapter presents experimental evidence of the influence of the pool geometry on plunging jet diffusion, based on direct measurements of the dynamic pressures transmitted to the pool bottom. Systematic model tests were performed with circular jets at prototype velocities impacting in plunge pools with flat and non-flat bottoms.

Laterally confined pools with ratios of confinement to jet diameter of 5.6, 11 and 16.7, and a constant scour depth of 2.8 times the diameter of the falling jet are investigated.

Dynamic pressures are sampled at the pool bottom at 1 kHz. Mean, fluctuating and extreme positive and negative pressure coefficients, as well as density power spectra functions of pressure fluctuations are presented.

Results show that the mean dynamic pressures transmitted to the foundation are reduced in the presence of any of the three lateral confinements investigated, with $D_c/\mathrm{D} = 5.6$, 11 and 16.7 and scour depth of $\mathrm{t}/\mathrm{D} = 2.8$, when compared to a reference pool with flat bottom. For a given confinement, the reduction grows with velocity. For a given velocity and pool depth, the reduction becomes more significant for lower D_c/D. Jet development is enhanced, notably for shallow and transition pools.

Pressure fluctuations are lower for $\mathrm{Y}/\mathrm{D} > 6$ in laterally confined pools than in corresponding pools with flat bottom. However, they increase for shallower pools in the three confinements tested. Pressure distribution at stagnation are positively skewed and slightly peaked. Extreme positive and negative pressure values do not increase in absolute terms. However, the extreme positive pressures p'^{+} may reach 8 times the RMS values of pressure fluctuations. Extreme negative pressures p'^{-} do not exceed 2 - 3 times the corresponding RMS values.

Moreover, spectral density functions of centreline pressure fluctuations in narrow pools show an enhancement in jet development for shallow and transition depths. For shallow pools, the energy at frequencies capable of exciting rock fissures may increase. For deep pools, spectral energy is generally reduced for all frequencies and spectra enter the dissipation range at lower frequencies than in pools with flat bottom.

These results outline the importance of pool geometry in modifying both the mean and the turbulent pool flow patterns. They also highlight the need for in-depth research on the processes of velocity and aeration decay in pools with prototype-like geometry (i.e. laterally confined pools).

9. Mapping of coherent flow motion generated by the diffusion of plunging jets in laterally confined pools

This chapter presents experimental work with plunging jets in laterally confined plunge pools. The analysis of the fluctuating characteristics of bottom pressures is used to define the characteristic scales of coherent flow motion (Figure 9.1). This analysis is correlated with direct observations of the flow motion. The procedure is applied to several pool geometries, representing the lateral and depth evolution of cylindrical or stepped shaped scour holes.

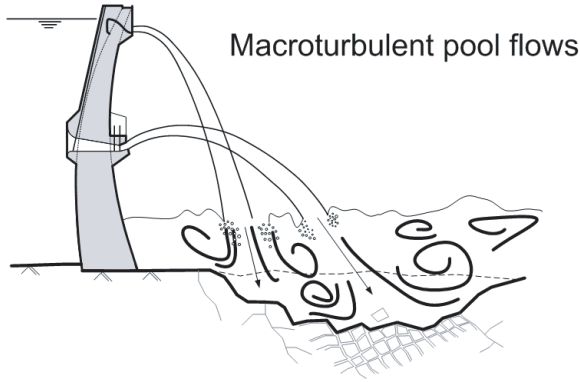

Figure 9.1.: Schematic representation of macro-turbulent pool flows in prototype rock scour (laterally confined pools) generated by plunging jets.

The impact of a turbulent shear layer generated by the diffusion of high-velocity jets in the pool may scour the riverbed, downstream of water releasing structures. Recirculation currents in plunge pools may create undesirable erosion of riverbanks. These two phenomena are directly related: the deflection of the plunging jet in the pool boundaries is the driving agent of larger-scale recirculation currents. Besides observations in prototype facilities, such processes have been studied in reduced-scale laboratory facilities.

The physical process of jet diffusion has been studied by several authors in pools with flat bottom (see Chapter 2 and Chapter 5). Few studies have been performed with non-flat pools, using mobile beds, e.g. Rajaratnam and Mazurek (2002). A combination of these two approaches is necessary to assess the interaction between the impact pressures at the pool bottom with the geometry of the pool. The understanding of the physical processes governing the interaction between the pool flow patterns and jet diffusion is expected to

help engineers infer the behaviour of a given plunge pool and provide adequate solutions for the mitigation of scour and of erosion induced by recirculation currents.

9.1. Experimental work in typified scour geometries

9.1.1. Definition of scour scenarios for analysis

A selection of data series from the entire database presented in Chapter 3 allows composing four typified scenarios of scour evolution for analysis of the induced flow patterns. The four scenarios selected correspond to (Figure 9.2):

1. Four shallow pool configurations, including three variable degrees of lateral confinement D_c/D and a pool with flat bottom, i.e. "lateral evolution of scour in shallow pools" (LAT-SHA);
2. Four deep pool configurations, including three variable degrees of lateral confinement and a flat pool, i.e. "lateral evolution of scour in deep pools" (LAT-DEEP);
3. Four pool configurations with variable depth, starting with a flat shallow pool and including three pools with *identical* degree of lateral confinement, i.e. "depth evolution of scour in vertical pools" (DEP-VERT);
4. Four pool configurations with variable depth, starting with a flat shallow pool and including three pools with *variable* degree of lateral confinement, i.e. "depth evolution of scour in symmetrically-stepped pools" (DEP-STEP).

The terms "deep" and "shallow" should be considered hereafter as defined by jet development conditions in pools with flat bottom. The analysis presented hereafter can be repeated for the remainder of the data. Multiple scour evolution scenarios can be composed with the available data library.

A schematic representation of the tested pool geometries can be found in Appendix B. Before the systematic analysis of the four scour scenarios, a detailed analysis of large-scale flow patterns that could be observed during the tests is presented.

9.1.2. Tools used in the analysis

Dynamic pressures are analysed in terms of mean and fluctuating pressure coefficient, defined according Equation 5.12 and Equation 6.5 respectively.

The third and fourth moments of the probabilistic distribution function (PDF) of pressure fluctuations are defined according Equation 6.1 and Equation 6.2, respectively for the skewness (C_s) and for the (excess) kurtosis (K). The C_s parameter provides an indication of the relative importance of the positive and negative extreme fluctuations regarding the pressure values closer to the mean. It is positive if the combined weight of the positive fluctuations is higher than that of the negative fluctuations and vice-versa. As discussed in Chapter 6 the change of sign of C_s is an indication of a change in the behaviour of the impinging turbulent flow. The analysis of the radial variation of the C_s parameter for wall pressure fluctuations allows documenting the flow behaviour in the impinging zone and in the transition to the wall jet zone. Lopardo and Henning (1985) and Fiorotto and Rinaldo (1992b) showed that the C_s changes sign under hydraulic jumps when the bottom wall jet

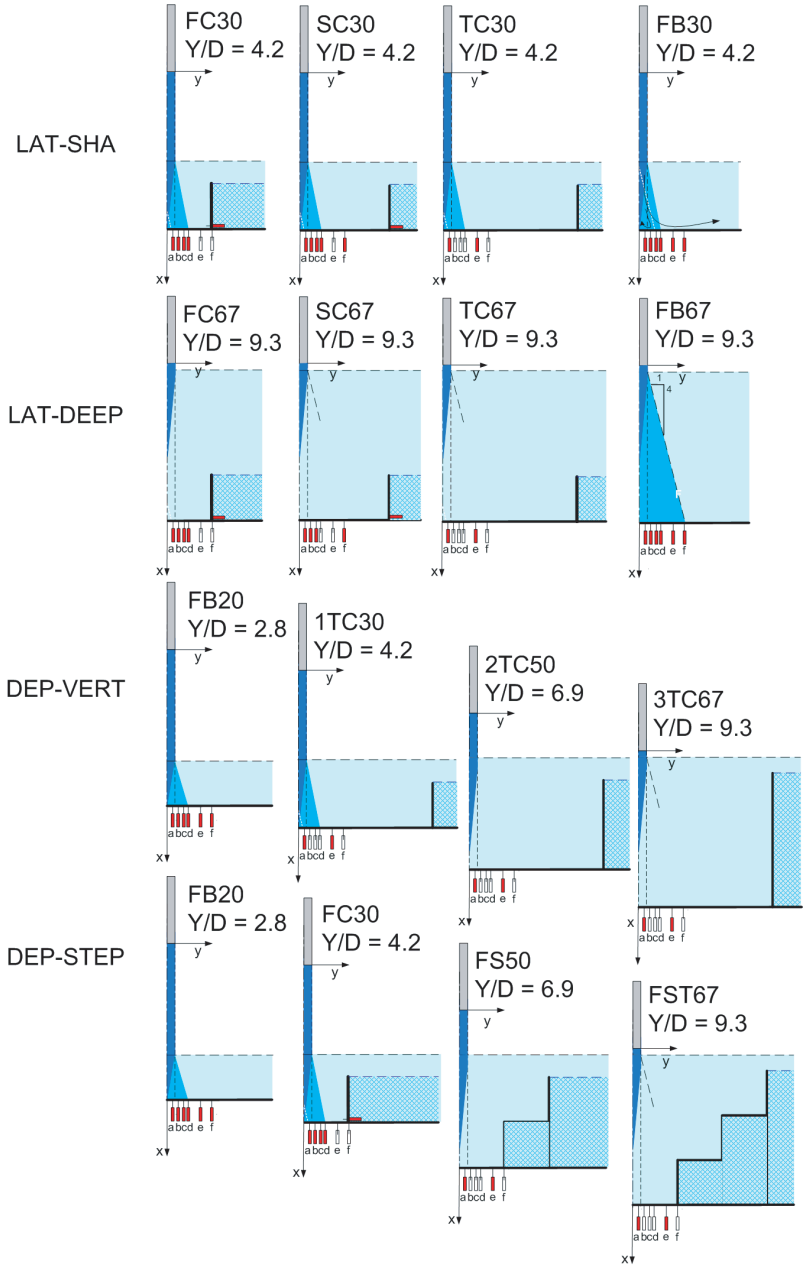

Figure 9.2.: Schematic representation of the four scour scenarios studied and corresponding measuring stations used.

is no longer predominantly impinging but rather detaching from the bottom, giving rise to a turbulent boundary layer. This has also been observed at impact of plunging jets in the analysis presented in Chapter 6.

The kurtosis parameter indicates the relative importance of the extreme fluctuations, either positive or negative, regarding the smaller fluctuations. Higher kurtosis represents a highly intermittent impinging turbulent flow, generating pressure extremes that even if few, have a large weight in this parameter.

Space-time correlations have been presented in section 6.4. Other examples of their application for the analysis of turbulent pressures can be found, for instance, in Fiorotto and Rinaldo (1992a); Ursino and Da Leppo (2003).

The spectral analysis of pressure fluctuations allows identifying the energetic content of each frequency. In brief, a time series of turbulent pressures may be seen as a superposition of sinusoidal functions of different amplitude A and phase ϕ. The energy content of each frequency is A^2. The power spectra is the cumulated series of given frequencies and corresponding energy contents. The variance of p' is the total energy of the fluctuations and therefore the power spectra can be defined as a decomposition of the variance per frequency. Inversely, the variance is the integral of the power spectra. Detailed information relevant for spectral analysis of digital signals can be obtained in Bendat and Piersol (1971); Lyons (1997); Stearns (2003).

The power spectrum can also be seen as the Fourier transform of the correlation function. In order to identify the relevant sinusoidal functions (i.e. the energy-carrying frequencies) for the measured data series, Fourier analysis is performed. In the present case, two approaches are compared and used alternatively for different purposes:

1. the direct computation of the Fourier transform terms using the FFT algorithm;
2. the lumped computation of the Fourier terms using the algorithm called the "Periodogram of Welch".

Author-made routines in ©Matlab allowed for the post-processing of pressure series, namely addition and calibration of numerous acquisition files, and computation of either of the processes. The latter presents the practical advantage of allowing for the straightforward handling of sub-sets of data, as well as windowing and overlapping corrections. These manipulations considerably improve the quality of the final spectral estimates. Implementation of these manipulations together with the FFT algorithm requires further programming. Nevertheless, the FFT approach has the advantage of providing the raw complex spectral estimates; they can be used for further analysis of the turbulent characteristics of the flow (e.g. correlations). Specific details of function and data handling are presented in the Appendix E.

9.2. Large-scale motion induced by turbulent plunging jets in river pools

Large scale flow patterns such as surface oscillations inside the confined region, intermittent ejections, pool surface oscillations and ring vortexes, are observed and analyzed for D_c/D = 16.7.

9.2.1. Description of observed flow patterns in laterally confined pools

For relative pool depths Y/D < 5.6 (tests cases Y=0.20, 0.30, 0.40 m), the confinements generate geyser-like flow ejections. The lateral confinements deflect the bottom wall jet upward in the direction of the pool surface.

For increasing pool depths (tests cases Y=0.50, 0.60, 0.67, 0.82 m), the upward flow is hindered by increased submergence and the ejections are reduced to a surface boil. This is observed for all three lateral confinements tested.

Tests with the D_c/D = 16.7 confinement allow visual observation and documentation of particular pool flow features. For low velocities, there is little air in the outer pool region and the flow features inside the confinement are perceptible.

For Y/D = 4.2 (test case Y = 0.30 m), periodic surface oscillations are observed between the confinement and the falling jet with an estimated frequency of ≈ 1 Hz. The impact of these oscillations with the falling jets is clearly visible, leading to upward ejections (Figure 9.3, left). With regular frequency, these ejections reach heights of approximately four times the jet's diameter.

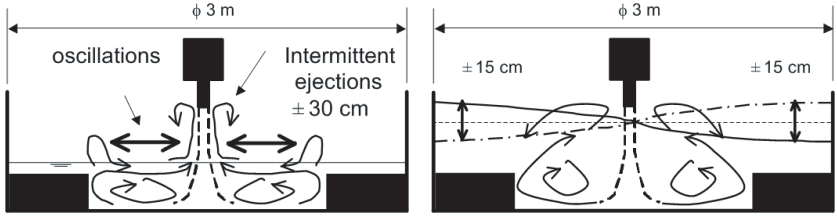

Figure 9.3.: Schematic representation of: left, oscillations inside the confinement with intermittent ejections; right, pool surface oscillations.

For deeper pools, i.e. Y/D > 4.1, the surface oscillations are observed over the whole pool (Figure 9.3, right). The peaks and nodes of the pool surface oscillations rotate slowly clockwise in plan view. The amplitude of the oscillations is visually estimated to be twice the jet's diameter. The pressure signal obtained at y/D = 2.08 confirmed the presence of pressure head oscillations of approximately 15 cm occurring with a frequency of 1 - 2 Hz.

For deep pools with Y/D = 9.3 and 11.4, the jet outlet is either intermittently submerged or permanently submerged, respectively. The formation of a ring vortex between the falling jet (in the centre) and the upward deflected jet (along the perimeter of the confinement) is clearly visible due to the presence of trapped air bubbles from initial pool filling (Figure 9.4).

When jet velocity is reduced, pool currents fade out and the air bubbles go up by buoyancy. When the outlet is initially submerged, no air is entrained in the pool by the jet. Only a small quantity of air is entrained at the surface through the boil. The ring vortex is saddle-like; its peaks and nodes rotate clockwise in plan view. It is a low pressure and low velocity flow region. For the range of jet velocities allowing visual observations (9.82 - 19.6 m/s), the vortex rotating frequency is estimated between 1 and 4 Hz. The vortex also expands and contracts in the radial direction. For V > 19.6 m/s, observation becomes difficult due to increased air entrainment through the surface boil. Depending on the ratio D_c/D, the

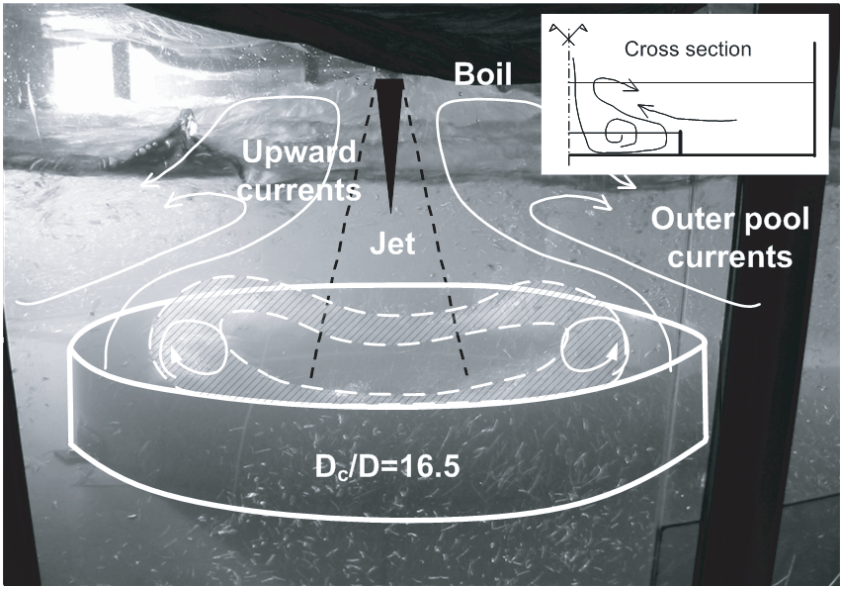

Figure 9.4.: Main flow features inside pool with D_c/D = 16.7, submerged nozzle (Y/D = 11.4) and V = 12.33 m/s. Entrapped air bubbles can be seen in the ring vortex.

upward currents may influence the development of the plunging jet and the dissipation of energy before impact with the bottom.

9.2.2. Turbulent characteristics of observed flow patterns in pools with Dc/D = 16.7 and t/D = 2.8

All the three lateral confinements change the pressure fluctuations at the pool bottom compared to the flat reference case. In most cases, this change corresponds to a reduction of their energy content, i.e. σ^2. Despite the reduction, more energy can be concentrated at frequencies corresponding to undesirable flow phenomena. As an example, macro-turbulent pool flows may produce ejections of spray or of mixed air-water packets that may affect ancillary structures located in the banks downstream of dams.

Pressure distribution

Selected statistical properties of 3-min data sets simultaneous to the previous mentioned observations are presented in Table 9.1.

For Y/D = 4.2, the (excess) Kurtosis is positive and thus the data probability density function (pdf) is more peaked than the Normal Gaussian pdf (mean = 0, RMS = 1, K = 0). For Y/D = 5.6, the opposite occurs, whereas for Y/D = 6.9 and 9.3 the differences to the Normal pdf are small.

For Y/D = 4.2, C_s is negative and should correspond to the creation of a turbulent boundary layer at the bottom in the vicinity of the core impact. For Y/D = 5.6, the skewness

changes from positive to negative with increasing velocity as a consequence of the increased persistence of the jet core for higher velocities.

Table 9.1.: Statistics of pressure fluctuations at y/D=0.35 for a selection of wide pools, D_c/D=16.7.

Y/D	V_0 [m/s]	σ [bar A]	p'^+ [bar A]	p'^- [bar A]	z_{max}	z_{min}	K	C_s	Comments
4.2	9.82	0.082	1.435	0.772	3.0	-5.0	1.58	-1.07	Oscillations in
	12.28	0.151	1.839	0.730	2.7	-4.6	0.52	-0.95	confinement with f ≈ 2.5 Hz
	14.74	0.206	2.367	0.836	3.4	-4.0	0.48	-0.93	Ejections with f ≈ 1 Hz
	17.19	0.240	2.791	0.808	3.1	-5.2	1.82	-1.24	
5.6	9.82	0.109	1.480	0.836	2.9	-3.0	-0.82	0.01	Pool surface oscillations,
	12.28	0.197	1.842	0.859	2.6	-2.4	-1.18	0.10	with f ≈ 1 Hz
	14.74	0.253	2.270	0.885	2.6	-2.9	-0.88	-0.20	
6.9	9.82	0.085	1.412	0.762	4.8	-2.9	0.28	0.68	Pool surface oscillations
	12.28	0.156	1.802	0.722	4.0	-3.0	-0.29	0.49	with f ≈ 1 Hz, not so
	14.74	0.192	2.187	0.748	4.5	-3.0	0.07	0.64	relevant for V=14.74 m/s
9.3	9.82	0.054	1.300	0.834	5.6	-3.0	0.39	0.58	Visible ring vortex
	12.28	0.086	1.565	0.836	5.4	-3.0	0.41	0.62	Energy peaks at
	14.74	0.121	1.836	0.799	5.3	-3.3	0.35	0.61	70 - 110 Hz
	17.19	0.163	2.431	0.836	6.6	-3.2	0.41	0.62	for increasing velocities
	19.65	0.214	2.711	0.834	5.4	-3.3	0.32	0.58	Strouhal = 3 - 4

Power spectral density

The measured series of pressure fluctuations are used to compute power spectra (PSD) estimates. The distribution of energy of the pressure fluctuations per frequency shows the presence of low-frequency surface oscillations and ejections. A detailed analysis at y/D = 0.35 for V = 12.3 m/s and various pool depths is presented in Figure 9.5. These spectra are typical of developed jet impact conditions, meaning that no core remains at impact with D_c/D = 16.7 and Y/D > 4. Disregarding the low-frequency disturbances, the spectra have a rather mild slope for f < 25 Hz.

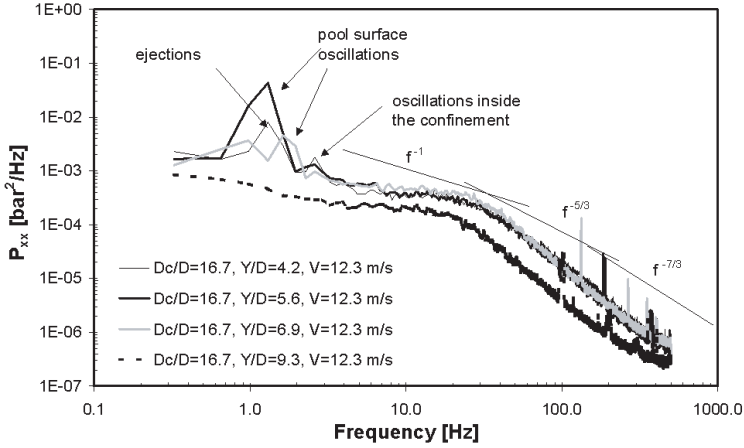

Figure 9.5.: Power spectral density P_{xx} for wide pools D_c/D = 16.7, t/D_c = 0.17, at y/D = 0.35 with V = 12.3 m/s.

In pools with flat bottom, the impact of the core has previously been observed in pools with Y/D < 4.2 for velocities from 7.5 - 30 m/s (Bollaert and Schleiss, 2003b). After the modifications to the supply system of the experimental installation, core impact conditions are observed up to Y/D = 5.6 and 17 < V < 30 m/s.

Detailed analysis of pool oscillations and ejections

Power spectra for Y/D =4.2 have been computed for all the velocities tested and are presented in Figure 9.6 for two positions on the pool bottom: at y/D =0.35 and 2.08. Each spectrum is obtained from 3 runs of 65536 points sampled at 1 kHz, divided in 64 blocks with 50 % overlapping using Welch's periodogram method.

Low frequency oscillations of about 1 - 4 Hz are identified at y/D = 0.35 for V = 12.3 to 17.2 m/s. All spectra at this position correspond to develop jet impact conditions. The peaks in spectral energy at low frequencies are related to the ejections and pool surface oscillations.

At y/D =2.08, there are three things worth mentioning:

- low frequency oscillations are also observed at about 1 Hz for V = 12.3 - 17.2 m/s;
- all spectra for V < 27 m/s show much less energy than those for V = 27 and 29.5 m/s up to 40 - 50 Hz. Beyond these frequencies, all spectra decay similarly;
- for f > 50 Hz, the spectra decay with a slope ≤ -5/3 and thus is not clear if the dissipation range is attained.

The reduction of spectral energy for f < 40 - 50 Hz is related to the formation of a bottom wall jet. The bottom wall jet does not have the same spectral energy of the impacting turbulent shear layer (TSL). For V = 27 and 29.5 m/s, the TSL impacts the bottom at y/D = 2.08. For V = 12.3 to 17.2 m/s, the ejections are superposed to the wall jet.

The mentioned low-frequency flow patterns can also be clearly identified in dimensionless spectra for Y/D = 4.2 (Figure 9.7) for Strouhal number of maximum 0.1. These oscillations disappear with increasing submergence, as shown for Y/D = 9.3. PSD estimates are divided by the variance σ^2 and frequency replaced by a Strouhal number (St = f.d/V) with $D_c/2$ as length scale d.

The selection of the most adequate length scale for each phenomena is a key task of a Strouhal analysis. The governing length scale responsible for the oscillations and ejections is the distance from the jet axis to the confinement R_c.

The spectra enter the energy dissipation range for $St \approx 1.0$. Pressure fluctuations observed between 70 and 110 Hz reduce with increasing Reynolds for $St > 4.0$. These fluctuations may correspond to a high-frequency perturbation of the diffusion shear layer.

The P_{xx} functions at y/D = 0.35 and 2.08 are quite different, Figure 9.8.

For an intermediate velocity (top row), P_{xx} varies considerably with pool depth and radial position at the pool bottom. At y/D = 0.35, the oscillations inside the confinement occur only for Y/D = 5.6. Core impact occurs for Y/D = 2.8. The remaining spectra reveal "developed jet impact" conditions, with transition to dissipation at about 40 - 50 Hz. At y/D = 2.08, there are oscillations for Y/D =4.2. The spectra for Y/D = 8.3 shows rather "incipient" developed jet impact conditions. The spectra for Y/D = 6.9 and 9.3 are identical.

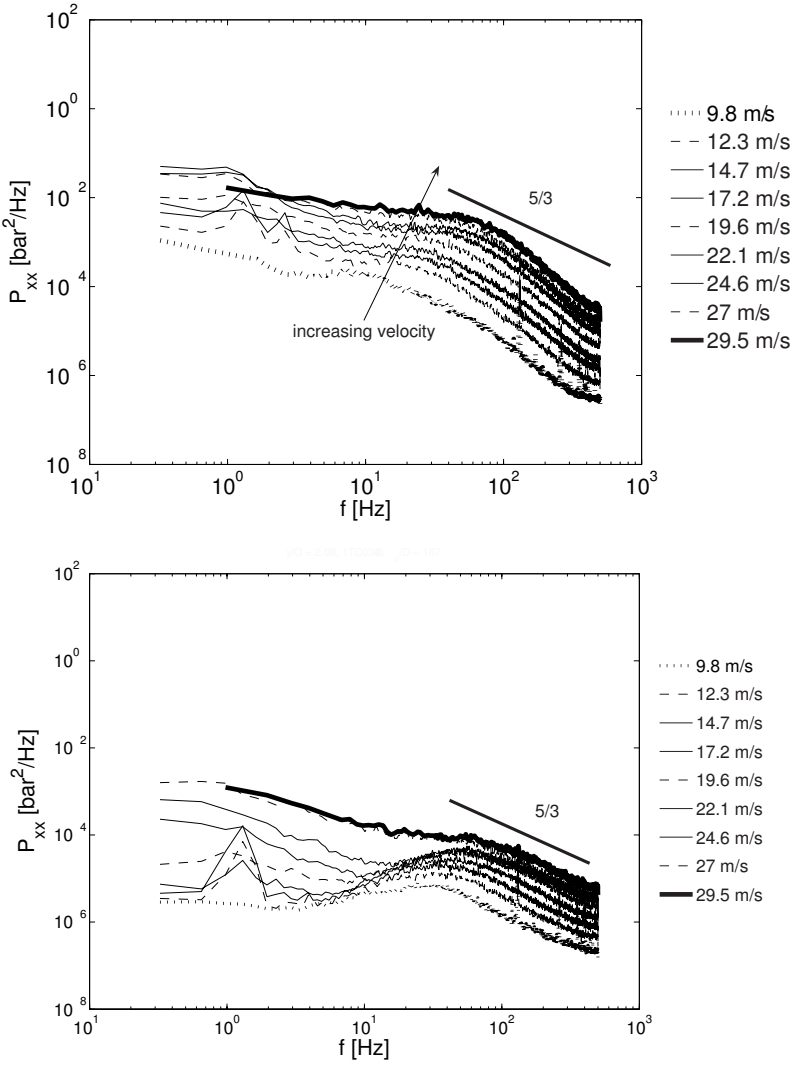

Figure 9.6.: Spectral density functions in **shallow laterally confined pools**, V_0 = 10 - 30 m/s, pool with D_c/D = 16.7, t/D_c = 0.17 with Y/D = 4.2: top, y/D = 0.35; bottom, y/D = 2.08. Test series 1TC030. Envelope cases are highlighted.

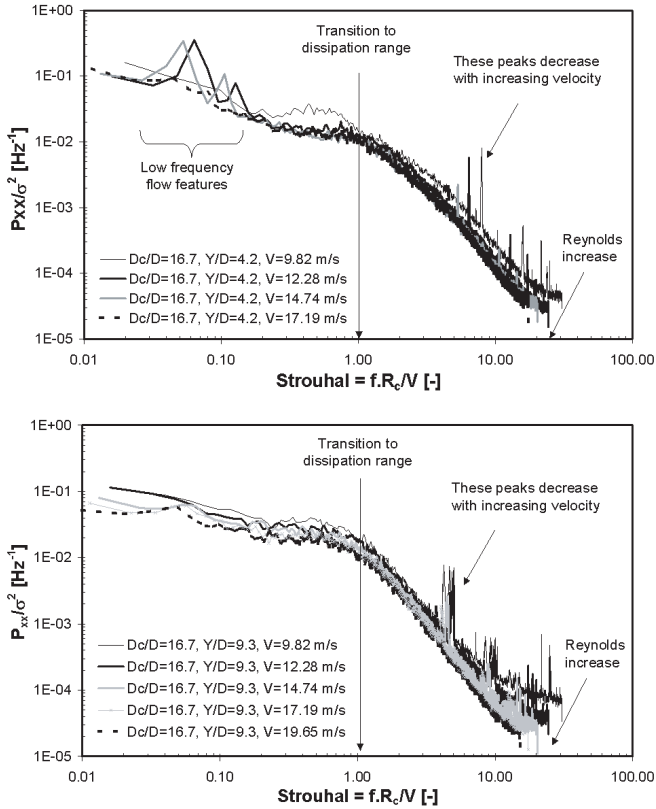

Figure 9.7.: Dimensionless power spectral density as a function of the Strouhal number, for wide pools D_c/D = 16.7, t/D_c =0.17, at y/D = 0.35: top, Y/D = 4.2; bottom, Y/D = 9.3.

For the maximum velocity tested (bottom row), there are less differences between the spectra. At y/D = 0.35, P_{xx} are typical of developed flow conditions, *even* for Y/D =2.8. At y/D = 2.08, there is 10 times less energy than at y/D = 0.35, for f < 30 Hz. For Y/D =2.8, the spectrum does not seem to enter the dissipation range within the acquisition range. For increasing submergence (Y/D), spectra correspond also to "incipient" developed jet conditions.

The term incipient is used to classify spectra that are neither that of "core impact conditions" nor of "developed jet impact conditions", even though closer to the latter. There seems to be a transition to the dissipation range since the slope at high frequencies is steeper or equal to -5/3. The redistribution range of these "incipient" developed spectra is, however, steeper ($\approx$ -1) than observed at y/D = 0.35 ($\approx$ 0).

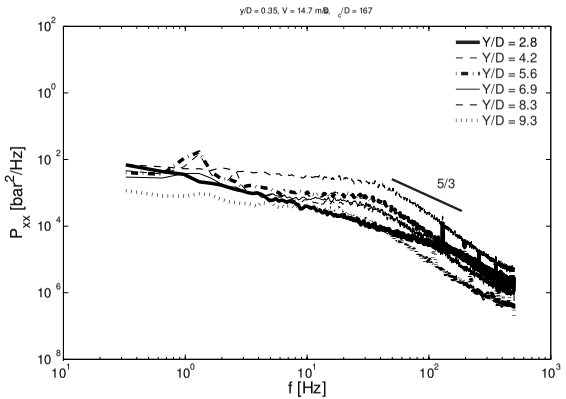

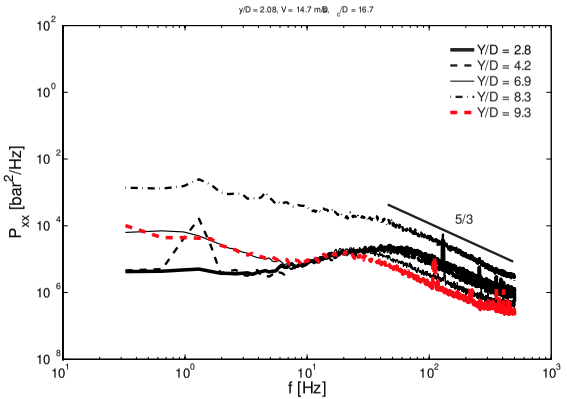

V_0 = 14.7 m/s: left, y/D = 0.35; right, y/D = 2.08.

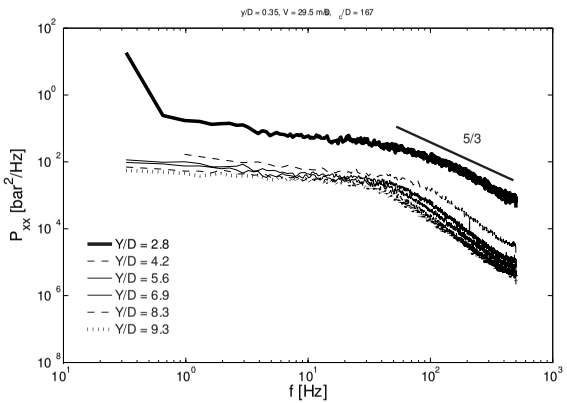

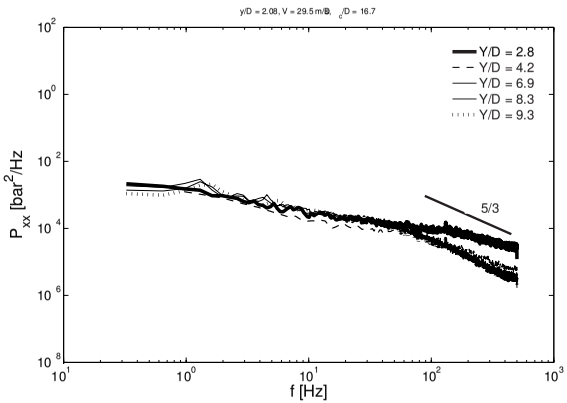

V_0 = 29.5 m/s: left, y/D = 0.35; right, y/D = 2.08.

Figure 9.8.: Spectral density functions for wide pools, D_c/D=16.7 and t/D_c=0.17.

9.2.3. Summary

Confining laterally the free diffusion of plunging jet modifies the flow pattern in the pool. This is reflected in the impact pressures at the pool bottom. Pressure fluctuations spectra show developed jet impact conditions for pool depths as shallow as Y/D = 4. Low-frequency oscillations observed in the pool during the tests are identified in the spectra of p' at the pool bottom. The oscillations can be associated to a Strouhal number. If defined as fR_c/V, oscillations are observed at about 0.1 and the dissipation range corresponds to Strouhal numbers larger than 1.

The previous analysis allows defining pool oscillations of frequency f_δ within the confinement as:

$$f_\delta = f(R_c, \frac{Y}{D}, V_i, ..) \tag{9.1}$$

In the present case, they are only observed for Y/D $<$ 5.6. Pool surface oscillations of amplitude δ can be defined as:

$$\delta = f(R_c, \frac{Y}{D}, V_i, \bigvee, d/s, ..) \tag{9.2}$$

where $\bigvee$ is the total volume of the pool and d/s stands for downstream conditions. In the present case, such oscillations are observed for 5.6 $<$ Y/D $<$ 9.3.

Quintela et al. (1987) reported the occurrence of large flow projections reaching important heights during large flood discharge operation in the Cabora-Bassa dam. This is the single description of **observations in prototype** of phenomena somewhat similar to the oscillations and ejections inside the confinement found in literature.

Full description of the shear eddy cells (i.e. the "ring vortex" observed with the help of air bubbles), requires measurements of the velocity flow field.

9.3. Coherent motion mapping in evolving scour

9.3.1. Radial evolution of mean pressure

Figure 9.9 shows the radial distribution of mean pressures for the highest velocity tested of V = 29.5 m/s. For shallow pools, mean pressures are reduced regarding the case of a pool with flat bottom and in a quite similar way for the intermediate (SC) and narrow (FC) pools. The wide (TC) pool presents the closest results to the flat (FB) pool.

If scour would start by a first narrow hole (FC) and evolve laterally, mean pressures at the centre would progressively increase. This increase is visible up to a radial distance of about $1.3D_i$ (assuming $D_i \approx D_0$ in the present set-up) and can be of $0.40E_0$ within that reach (E_0 is the jet kinetic energy at issuance).

In "deep" pool conditions (LAT-DEEP), an evolution from narrow to wide and flat shows a similar increase in C_p. The four geometries provide similar results beyond y = D. Within this distance, C_p values can vary of about $0.20E_0$ or 50 % relatively to the flat reference scenario (see Table 9.2).

The narrow (FC) series shows that C_p values at 1.3D tend rapidly to zero; this is precisely half of the distance to the confinement $R_c/2$.

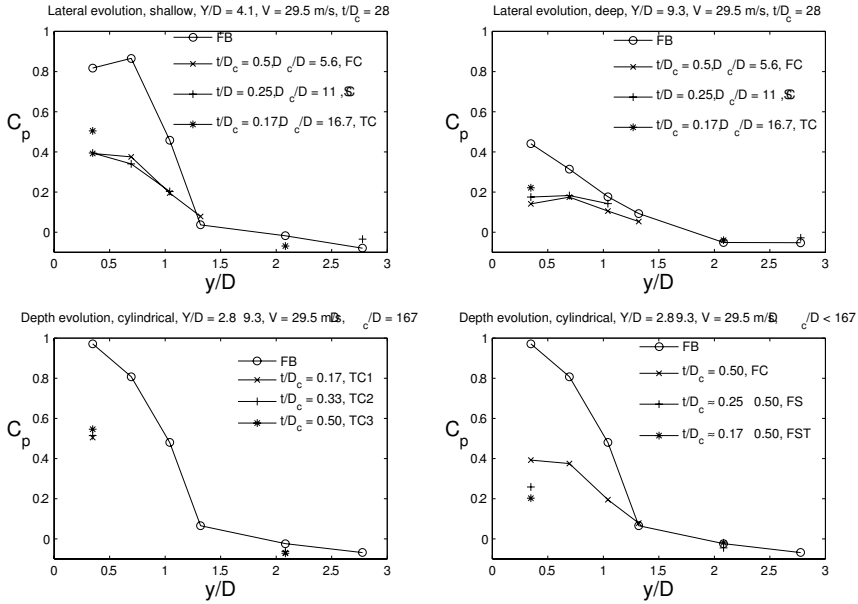

Figure 9.9.: Radial distribution of mean pressure coefficients for the selected scour evolution scenarios. Note: linear interpolation between available points is meant to help interpretation only.

Top, left: lateral evolution, shallow (LAT-SHA);
Top right: lateral evolution deep pool (LAT-DEEP);
Bottom, left: depth evolution, vertical slopes (DEP-VERT);
Bottom, right: depth evolution, stepped slopes (DEP-STEP).

Table 9.2.: Ratio of mean pressure coefficients C_p at each evolution stage regarding the corresponding initial flat pool scenario, for the selected scour scenarios and measuring positions.

		y/D					
	Compared series	0.35	0.69	1.04	1.32	2.08	2.78
Lateral, shallow	FC30/FB30	0.48	0.43	0.43	2.14	-	-
	SC30/FB30	0.48	0.39	0.44	-	-	0.44
	TC30/FB30	0.62	-	-	-	3.89	-
Lateral, deep	FC67/FB67	0.32	0.56	0.60	0.57	-	-
	SC67/FB67	0.40	0.58	0.80	-	-	0.54
	TC67/FB67	0.50	-	-	-	0.78	-
Depth, vertical	TC1-30/FB20	0.52	-	-	-	2.90	-
	TC2-50/FB20	0.53	-	-	-	2.63	-
	TC3-67/FB20	0.56	-	-	-	3.01	-
Depth, stepped	FC30/FB20	0.40	0.46	0.41	1.19	-	-
	FS50/FB20	0.27	-	-	-	1.89	-
	FST67/FB20	0.21	-	-	-	0.83	-

The DEP-VERT evolution in depth of a scour hole with D_c/D = 16.7 leads to a reduction of mean pressures from values as high as $0.98E_0$ to $0.55E_0$ at the centreline and for the three confinements despite the increasing pool depth. Mean dynamic pressures drop to almost zero in a distance of approximately 1.3D for the flat pool and at least not more than 2D for the confined configurations. The wide (TC) confinement is at y = 8.3D.

One interesting comparison is that of the wide 3TC case with the flat (FB) series for Y/D = 9.3 (LAT-DEEP plot): the C_p value closest to the axis for the flat (FB) pool is about $0.10E_0$ lower than the value obtained with the wide TC3 configuration. The wide TC3 pool is less dissipative, most likely due to a reduction in the air entrainment or to a decrease in flow-induced dissipation.

The DEP-STEP evolution in depth of a scour hole with stepped slopes shows that initial mean pressures (FB) are quite relevant up to 1.3D, reduce of almost $0.60E_0$ with a first narrow scour evolution, and of additional $0.20E_0$ with two consecutive steps of scour evolution in depth. When compared to the DEP-VERT final stage, C_p values at the centre of the scour hole are lower by almost $0.30 - 0.35E_0$. When compared to the FC data for LAT-DEEP, C_p values for the DEP-STEP are higher. A stepped "deep" pool with low tailwater (Y/D=9.3 and h/D = 0.4) dissipates less energy in average, than a narrow pool with high tailwater level (Y/D = 9.3 and h/D = 6.9).

9.3.2. Radial evolution of RMS-pressure fluctuations

The LAT-SHA evolution from narrow to wide pool with constant "shallow" pool depth presents very similar C'_p values within 1.3D for the narrowest and widest pools (see Figure 9.10). The intermediate and wide pools (SC and TC) have C'_p values that are some $0.10E_0$ lower. The SC pool has $C'_p \approx 0$ at $\approx 2.8D$, which is exactly $R_{sc}/2$. The pool with flat bottom and the wide (TC) confinement have similar C'_p values at y = 2.1D. The narrow FC pool presents C'_p values very close to those of FB but at 1.3D (i.e. $R_{fc}/2$) there is still an important level of turbulence fluctuations (≈ 0.13).

The LAT-DEEP case shows that all the three confinement contribute to a significant reduction of the turbulent fluctuation at the pool bottom, by as much as $0.15E_0$ within 1.3D. The C'_p values for the flat (FB) and wide (TC) pools are similar beyond 2D. For both the narrow (FC) and intermediate (SC) pool, the $R_c/2$ distances are still within the investigated region: for SC, C'_p at 2.8D is very low; and, for FC, C'_p at 1.3D is still significant regarding C'_p closer to the jet axis. In fact, the FC pool is so narrow that the turbulence level hardly reduces in the radial direction.

In the case of the DEP-VERT scenario, there is apparently less information. However, for the three confined pools and regardless of the increase in pool depth, the level of turbulence close to the axis is almost constant and around $0.15E_0$. This is rather intriguing. In fact, not only C_p values for the three TC1/2/3 pools are almost constant around 0.55 but also C'_p values are close and all around 0.16. The increase in pool depth does not provide additional cushioning.

For the DEP-STEP scenario, C'_p values with FC are still quite close to the flat initial stage of scour and decrease similarly in the radial direction. There is more turbulent fluctuations (and energy dissipation) at this stage this configuration that with TC1 in the DEP-VERT scenario. At y = 1.3D (i.e. $R_{fc}/2$), C'_p is still relatively important regarding centreline values.

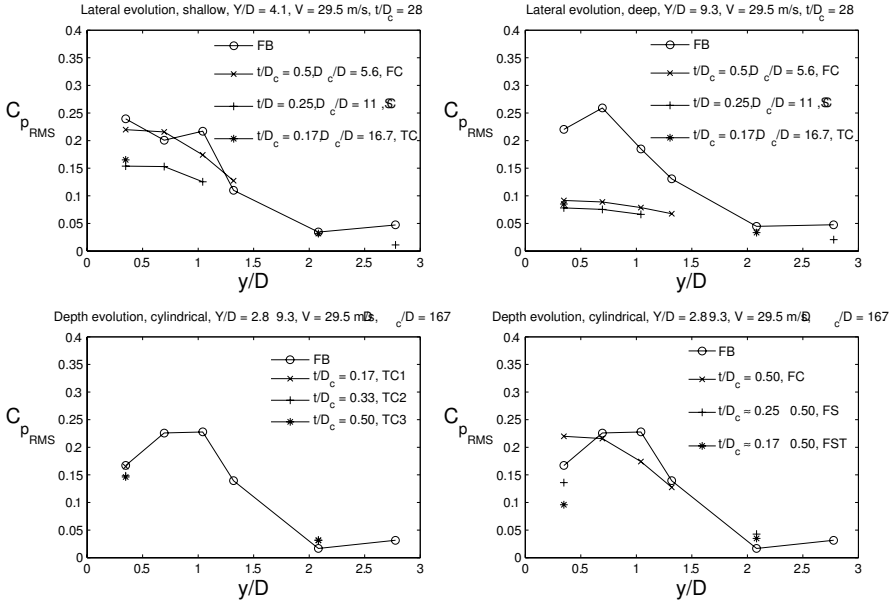

Figure 9.10.: Radial distribution of RMS pressure coefficients C'_p for the selected scour evolution scenarios. Similar to Figure 9.9

Table 9.3.: Ratio of RMS pressure coefficients at each evolution stage regarding the corresponding initial flat pool scenario, for the selected scour scenarios

		y/D					
	Compared series	0.35	0.69	1.04	1.32	2.08	2.78
Lateral, shallow	FC30/FB30	0.92	1.08	0.80	1.16	-	-
	SC30/FB30	0.64	0.76	0.58	-	-	0.23
	TC30/FB30	0.69	-	-	-	0.92	-
Lateral, deep	FC67/FB67	0.42	0.34	0.42	0.52	-	-
	SC67/FB67	0.35	0.29	0.36	-	-	0.44
	TC67/FB67	0.39	-	-	-	0.75	-
Depth, vertical	TC1-30/FB20	0.99	-	-	-	1.89	-
	TC2-50/FB20	0.89	-	-	-	1.90	-
	TC3-67/FB20	0.88	-	-	-	1.88	-
Depth, stepped	FC30/FB20	1.32	0.95	0.76	0.92	-	-
	FS50/FB20	0.82	-	-	-	2.57	-
	FST67/FB20	0.58	-	-	-	2.09	-

C'_p at the centreline decreases down to $0.10E_0$ with increasing pool depth (and depth of scour).

A direct comparison between C'_p values for the flat pool and the corresponding non-flat pools for the LAT-SHA and LAT-DEEP scenarios is presented in Table 9.3. The large majority of the ratios are less than 1 corresponding to a reduction in turbulent fluctuations. The few values higher than 1 correspond to the direct comparison between the widest (FB) and narrowest pools (FC).

In the same Table 9.3, a comparison between the turbulent fluctuations at a given **stage** of scour and the **initial** situation is presented for the DEP-VERT and DEP-STEP scenarios.

Close to the centreline, only the narrowest pool, "formed" at the beginning of scour (e.g. DEP-STEP) increases turbulent fluctuations, i.e. enhances jet development. The C'_p values close to the jet axis decrease as scour "grows" in depth. This is similar to what was observed by Ervine et al. (1997) and in the present data for pools with flat bottom and $Y/D > 6.9$. The C'_p values increase farther from the jet axis, e.g. at 2.8D, as a reflection of jet development the initial (shallow) stage with flat bottom.

9.3.3. Radial evolution of the pressure distribution

The procedure established in Chapter 6 to correlate the change in sign of the skewness parameter with the incoming or outgoing predominant pattern of pressure fluctuations is used to identify the characteristic length scales of flow phenomena in the impinging region.

An analysis of the kurtosis parameter, that concerns the intermittent character of the flow, is also applied to the four scour scenarios under investigation.

Figure 9.11 presents the radial evolution of the skewness C_s.

For the LAT-SHA case, C_s is positive in the FC pool up to 1.3D with a slight increase in positive fluctuations at halfway towards the wall (i.e. $R_{fc}/2$). In the SC pool, C_s values are also positive and also increase toward 2.8D (i.e. $R_{sc}/2$). The data for the wide (TC) pool seem to follow the same trend. However, for the widest pool (flat, FB), C_s is negative between 0.4D and 0.8D. This is due to the creation of a turbulent boundary layer by deflection of the core of the jet. Comparatively to the laterally confined pools, the absence of return currents in pools with flat bottom allows the core of the jet to impact the bottom. C_s becomes positive beyond 0.8D and reaches a local maximum at 1.3D. This maximum is thought to correspond to the interface between the turbulent shear layer (TSL) of the plunging jet and a depth-dependent roller, earlier described in Chapter 6. C_s decreases beyond 1.3D under the influence of such roller (less fluctuations, bottom wall jet). Assuming that C_s drops to zero at about y = 3D, this dissipative roller should have a length scale of about 3D (i.e. half the roller should be within y = 1.5D and y = 3D).

In the case of the LAT-DEEP scenario, C_s is positive for all the confinements tested, both close to the axis and laterally outwards, at least where assuming a linear evolution in between measured point is an adequate assumption. This is relatively similar to the reference flat case. The flat (FB) series presents slightly more positive turbulent fluctuations between 0.7 and 2D, which should correspond to the zone of impact of the developed jet and smooth transition into a wall jet. At 2.8D, C_s becomes negative. This is related to the upward

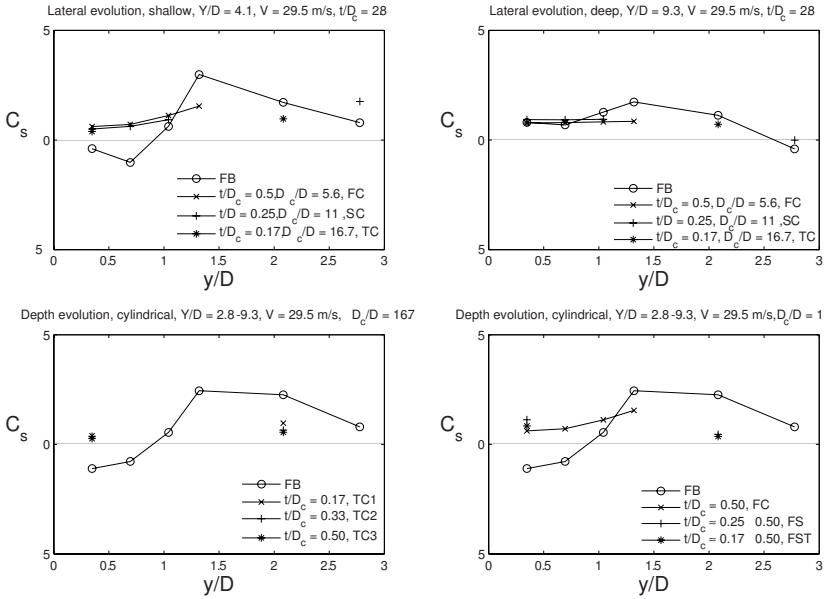

Figure 9.11.: Radial distribution of the skewness parameter C_s for the selected scour evolution scenarios. Similar to Figure 9.9

Table 9.4.: Evaluation of the change in local flow pattern in each pool geometry based on a comparison between the skewness C_s of the pressure distribution measurements, for the selected scour evolution scenarios

		y/D					
	Compared series	0.35	0.69	1.04	1.32	2.08	2.78
Lateral, shallow	FC30/FB30	Yes	Yes	No	No	-	-
	SC30/FB30	Yes	Yes	No	-	-	No
	TC30/FB30	Yes	-	-	-	No	-
Lateral, deep	FC67/FB67	No	No	No	No	-	-
	SC67/FB67	No	No	No	-	-	No
	TC67/FB67	No	-	-	-	No	-
Depth, cylindric	TC1-30/FB20	Yes	-	-	-	No	-
	TC2-50/FB20	Yes	-	-	-	No	-
	TC3-67/FB20	Yes	-	-	-	No	-
Depth, conical	FC30/FB20	Yes	Yes	No	No	-	-
	FS50/FB20	Yes	-	-	-	No	-
	FST67/FB20	Yes	-	-	-	No	-

detachment of the bottom wall jet, creating a turbulent boundary layer. This is an indication of the length scale of such roller in the y-direction: it should be in the order of 2D and not more than 4.2D in the x-direction (vertical).

For the DEP-VERT scenario, C_s data for the three confined pools are scarce and almost collapse. In this case, C_s does not seem to depend much on the pool depth. For these relatively wide confinements ($R_{tc} \approx 8.3D$), C_s close to the axis is positive but close to zero, i.e. the jet is in an almost "gaussian" transition between being compact and developed. The reference flat pool (FB20) presents similar features as the flat case in LAT-SHA (FB30) namely, from the centre to the periphery:

- negative C_s in the turbulent boundary layer created next to the impact of the jet core;
- positive C_s in the region where the shear layer of the plunging jets meets the depth-dependent roller (shear eddy or submerged hydraulic jump);
- decrease of C_s towards zero for an estimated distance of 3D, which may indicate the existence of a roller with a half-length scale of about 1.5D, above the wall jet, rotating between 1.5D and 4.5D.

In the case of the DEP-STEP scenario, the first stage of scour (FC) shows a change from negative from positive C_s. The measuring points closer to the jet axis no longer reflect the turbulent boundary layer created at core impact, but rather the impact of a developed jet. The radial increase in C_s up to 1.3D (i.e. $R_{fc}/2$) demonstrates the impact of the turbulent shear layer of such developed jet. Since the kurtosis follows exactly the same trend (see Figure 9.12) it is quite likely that for the narrow geometry (FC): (1) the transition from the plunging jet shear layer to the upward currents is done quite abruptly in space and (2) that it occurs at a location with high intermittency. The high intermittency in such confined space is related to the instability of the flow patterns, due to non-perfect symmetry of the jet and flow patterns along the jet perimeter. For the second (FS) and third (FST) stages of scour, C_s close to the axis is positive as expected for developed jet conditions and slightly higher than in the earlier stages of scour (i.e. slightly more weight of the positive extreme pressure fluctuations).

As documented in Table 9.4, C_s changes from negative to positive within $\approx$ 1.1D of the axis; this corresponds to a change from core impact conditions to those of developed jet impact conditions.

Changes in C_s with growing scour in depth or in width are also observed: in the LAT-SHA scenario, within less than 1D; in the DEE-VERT scenario at the vicinity of the axis. In these three examples, the change of sign of C_s close to the centreline reflects the enhancement of core development due to the flow patterns induced by the lateral confinement of jet diffusion.

In Figure 9.12, an equivalent analysis is repeated for the kurtosis. In the four cases, the radial evolution of K in flat pools shows an increase in intermittency or peakedness of the PDF functions between 1.3 and 2.1D. This is exactly the region of transition from the turbulent shear layer created by the plunging jet to the roller. It is close to zero in the turbulent boundary layer close to the jet axis.

For the LAT-SHA scenario, it tends to zero for y = 3D; at the vertical line that passes through the centre of the shear roller C_s and K are $\approx$ 0 and thus such roller should have a half-length scale of about 1.5D. For the SC pool, K is quite high at 2.8D (i.e. $R_{sc}/2$); this may indicate the interaction between the shear layer and the SC roller. For the FC pool, the

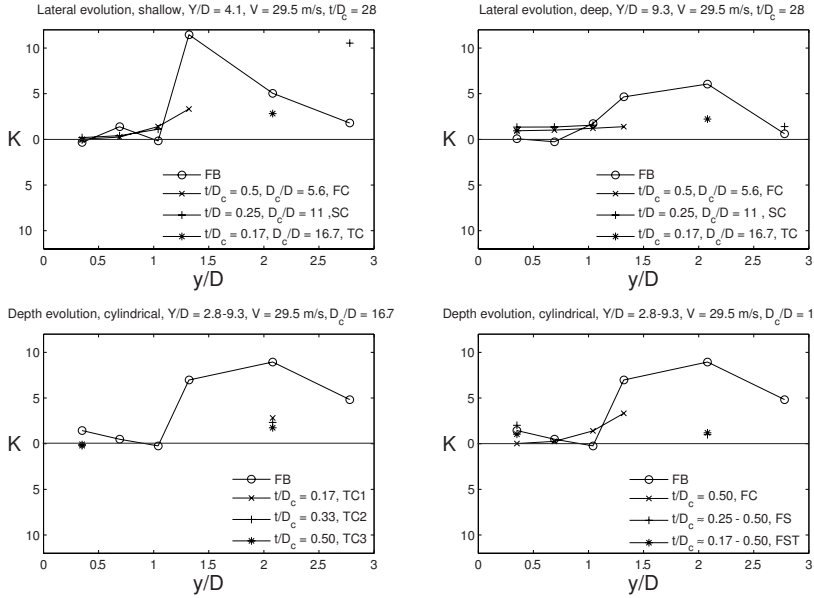

Figure 9.12.: Radial distribution of the kurtosis parameter K for the selected scour evolution scenarios. Similar to Figure 9.9

presence of a roller has not been confirmed, but there is a clear increase in K up to 1.3D (i.e. $R_{fc}/2$).

In the case of the LAT-DEEP scenario, the confined pools show more fluctuations close to the axis, than the flat (FB) pools. Therefore, K is slightly higher. Farther outwards, the fluctuating character of p' is less intense.

In the DEP-VERT scenario, K decreases with the evolution of scour in the two measuring points at 0.35 and 2.08D, respectively.

In the DEP-STEP scenario, the kurtosis decreases close to the centreline for the first scour stage (flat FB to a narrow FC geometry), but increases right afterwards (from narrow FC to intermediate SC and wide TC pools). At y = 2.08D kurtosis is considerably reduced regarding the initial flat stage.

In summary, the only situation for which K increased significantly within the documented region of y $<$ 3D corresponds to the SC shallow pools: at y = 2.8D the value of K is multiplied by five regarding a pool with flat bottom. At this point, the mean pressure value is relatively low, as well as the RMS pressure value. C_s is positive and higher than obtained in the flat reference case. Physically, this may correspond to the occurrence of positive fluctuations (C_s>0) of large amplitude (high K) regarding the RMS values. The high kurtosis value in this case is not high regarding the neighbouring points but high regarding the local RMS value (quite low). The fluctuations may be due to the incipient formation of a rotating cell with the axis at about y =2.8D.

9.3.4. Coherent motion in shallow laterally confined pools

Radial evolution of the impact pressure spectra

Power spectra are computed for the four pools of the LAT-SHA scenario - Figure 9.13.

The aim is to identify changes in spectral distribution that may be associated with the geometry, for a jet velocity of 29.5 m/s[1]. The majority of the spectra are obtained from cumulated data of 3 files; however, for V = 29.5 m/s experiments are performed in limit conditions of safety and in certain cases only one file is available. Spectral functions of impact wall pressures in pools with flat bottom were documented by Bollaert (2002b). Compared to the reference flat bottom geometry, the present results show:

- Spectra of measurements close to the axis decay slowly, with a -1 slope;
- Spectra at y/D = 2.08 and 2.78, have in general less energy (i.e. lower integral or lower σ^2), in particular at lower frequencies. In fact, for f > 40- 50 Hz all the spectra have a rather similar decay. The absence of a given amount of energy at lower frequencies is related with the formation of the bottom wall jet and reduction of the plunging jet's influence.

When confining laterally the propagation of such bottom wall jets, the power spectra are modified as a consequence of the induced flow patterns. For the wide (TC) pool, the spectrum at y/D = 0.35 is no longer characteristic of core impact (-1 slope). In fact, it has been modified to that of a developed jet, with a mild, almost flat slope up to frequencies in the order of 60-80 Hz, where it enters the dissipation range. The sub-inertial region (-5/3 slope) is very short and the spectrum's dissipation slope is between -7/3 and -9/3.

At y/D = 2.08, the spectrum may represent a coherent structure as a wall jet, with mild slopping spectra. By further narrowing the pool, spectra typical of developed jets are found at y/D = 0.35 to 1.04 (SC pool). At y/D = 2.78, the mild sloped spectra represents the bottom wall jet. At y/D = 5.6, a transducer that is flushed mounted horizontally in the wall of the confinement samples the impact pressures due to the bottom wall jet. However, this spectrum is again typical of developed jet impact, suggesting that the compact bottom wall jet that is identified at y/D = 2.78 diffuses and spreads between this point and the SC wall.

In an even narrower scour hole (FC pool), the bottom wall jet should even be more constrained. From y/D = 0.35 to 1.32, all spectra correspond to developed impact conditions. All the spectra, including the lateral one, enter the viscous dissipation region at frequencies between 70 and 100 Hz.

In summary, the three confinements tested ($D_c/D \leq 16.7$) enhance the development of the jet core for shallow pools with Y/D < 4.2, with the jets produced in the present experimental set-up.

Radial evolution of the space-time correlations

For the narrow (FC) pool, the space correlation becomes negative close to 1.3D (i.e. $R_{fc}/2$)- Figure 9.14. The integral scale in the y-direction (I_y) is < 4 cm, which is about $R_{fc}/5$ or $t/5$. In this case, the same turbulent shear layer impacts the bottom on the first half of the confinement, being abruptly deviated upwards, as shown in the increase of C_s and K in the radial direction. The bottom wall jet impacts the lateral wall in the same way as the

[1] The analysis can be pursued for other velocities.

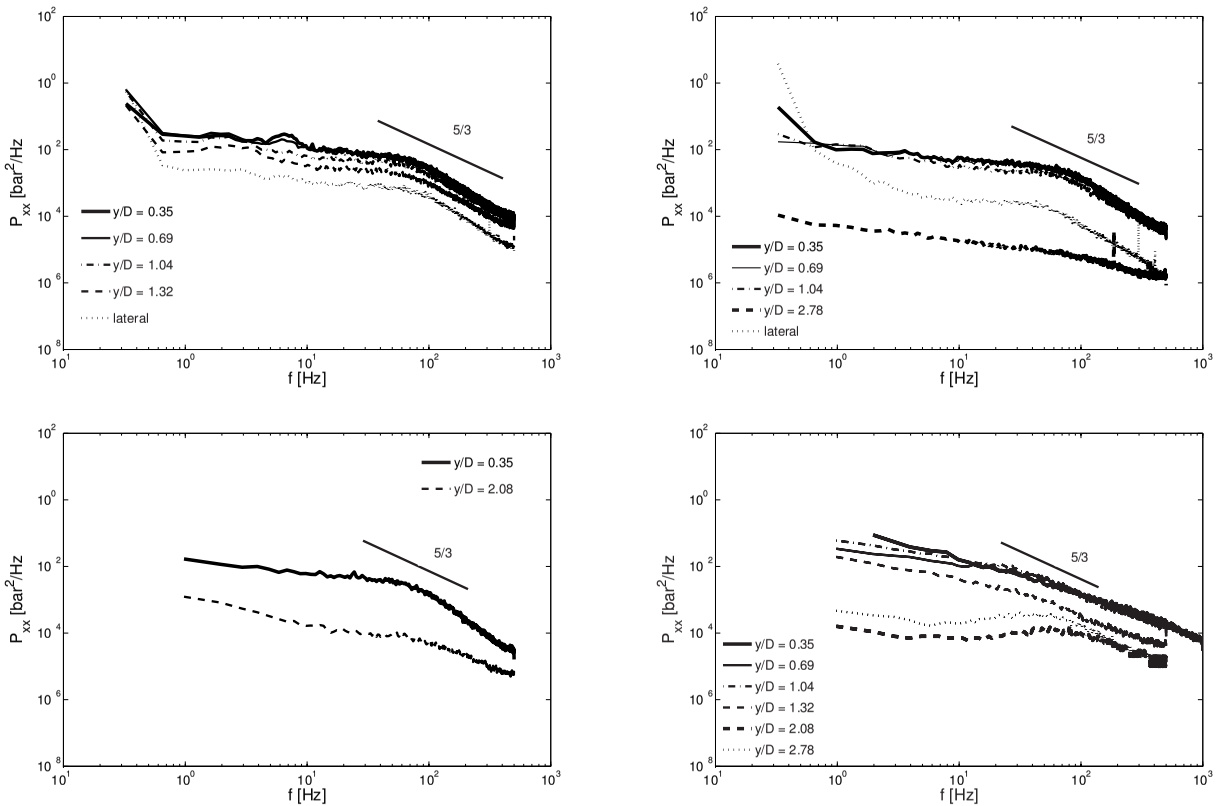

Figure 9.13.: Power spectra for "lateral evolution, shallow pools", from top to bottom (from narrow to wide) from series: FC30, SC30, TC30 and FB30. The position of the transducers is indicated in Figure 9.2. To be read clockwise.

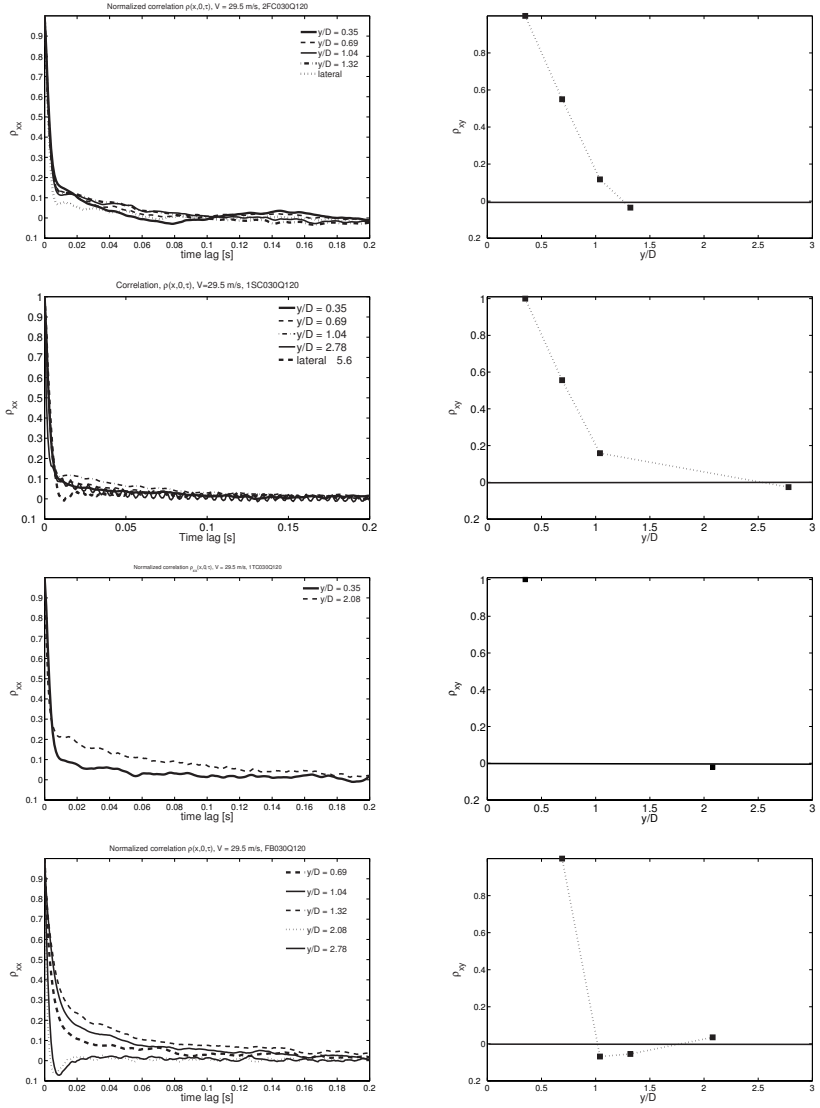

Figure 9.14.: Lateral evolution, shallow (from narrow to wide): FC30, SC30, TC30 and FB30. Left: ρ_{xx}; Right: ρ_{xy}, assumed linear.

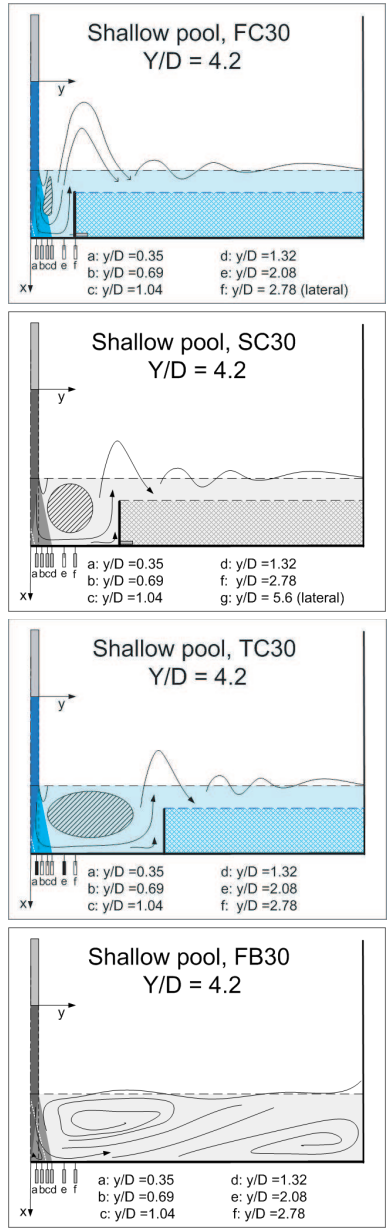

Figure 9.15.: Tentative flow patterns for "lateral evolution, shallow pools": FC30, SC30, TC30 and FB30. The solid elements have dimensions at scale, the flow patterns' scale are approximative.

plunging jet impacts the pool bottom, in agreement with the spectra presented for y/D = 0.35 and y/D = lateral (5.6).

In the case of the intermediate (SC) pool, ρ_{12} (with pivot point at y/D =0.35) becomes negative somewhere between 1.04D and 2.78D. In agreement with the previous interpretations, the impact of the turbulent shear layer should concern the points up 1.04D (all with positive C_s), whereas measurements at 2.8D concern the wall jet. The interpretation of the autocorrelation is similar to previous examples, save for the y/D = 2.8 case. A high frequency oscillation is superposed (observed also in the spectra at $\approx$ 110 Hz).

For the wide (TC) pool, ρ_{12} shows that the two measuring points are clearly influence by different structures. At y/D =0.35, ρ_{11} present two structures, one of very short duration (sharp decrease but always positive) and another long lasting (mild decrease). This corresponds to local small structures at stagnation, to which the impact of the TSL of the jet is superposed. At y/D = 2.08, the second structure is the bottom wall jet.

For the pool with flat bottom (FB), the space correlation (pivot at y/D = 0.69) drops sharply to negative, which is in agreement with the change in sign of the C_s. For the remaining three points, the correlation is almost zero, confirming that the region beyond 1D is no longer influenced by the turbulent boundary layer. The time (auto) correlations of the transducers at y/D = 2.08 and 2.78 are particularly interesting since they drop abruptly to negative values: there is no long-lasting impinging structure and therefore negative correlation (or "de-correlation") is attained rapidly.

In summary, the above interpretations based on C_p, C'_p, C_s, K and spectra, are corroborated by space-time correlations. However, it should be kept in mind that these correlations are representative of a small region of the entire pool.

Tentative flow patterns for shallow pools

Based on the previous interpretations, the most relevant flow features of the pools composing the LAT-SHA scenario are tentatively sketched in Figure 9.15. The "hatched" zones have not been assessed in detail. The main features are identified in the previous analytical analysis of the measurements and by visual observations during the tests.

9.3.5. Coherent motion in deep laterally confined pools

Radial evolution of the impact pressure spectra

For the narrowest confinement (FC pool), the spectrum at y/D = 0.35 corresponds to developed jet impact conditions. The other spectra are similar in shape. The transition to the dissipation range becomes less abrupt in the radial direction - Figure 9.16.

Enlarging scour (SC pool) pushed the "ring vortex" in the direction of the jet. At y/D = 2.8 (i.e. $R_c/2$), the spectrum is quite irregular: it seems to have low frequency disturbances around 2 - 3 Hz, superposed to the spectra of the transition to the wall jet region. The spectrum of the lateral transducer slopes fast into dissipation; there is little energy in p' at the corner.

When further enlargement of scour is produced (to wide TC pools), the spectrum at y/D = 0.35 becomes almost flat. At y/D = 2.08, there are traces of the large-scale pool oscillations identified in Section 9.2 for the same pool with lower velocities. At higher frequencies, the spectra decays mildly, as expected for a(n) (incipient) bottom wall jet.

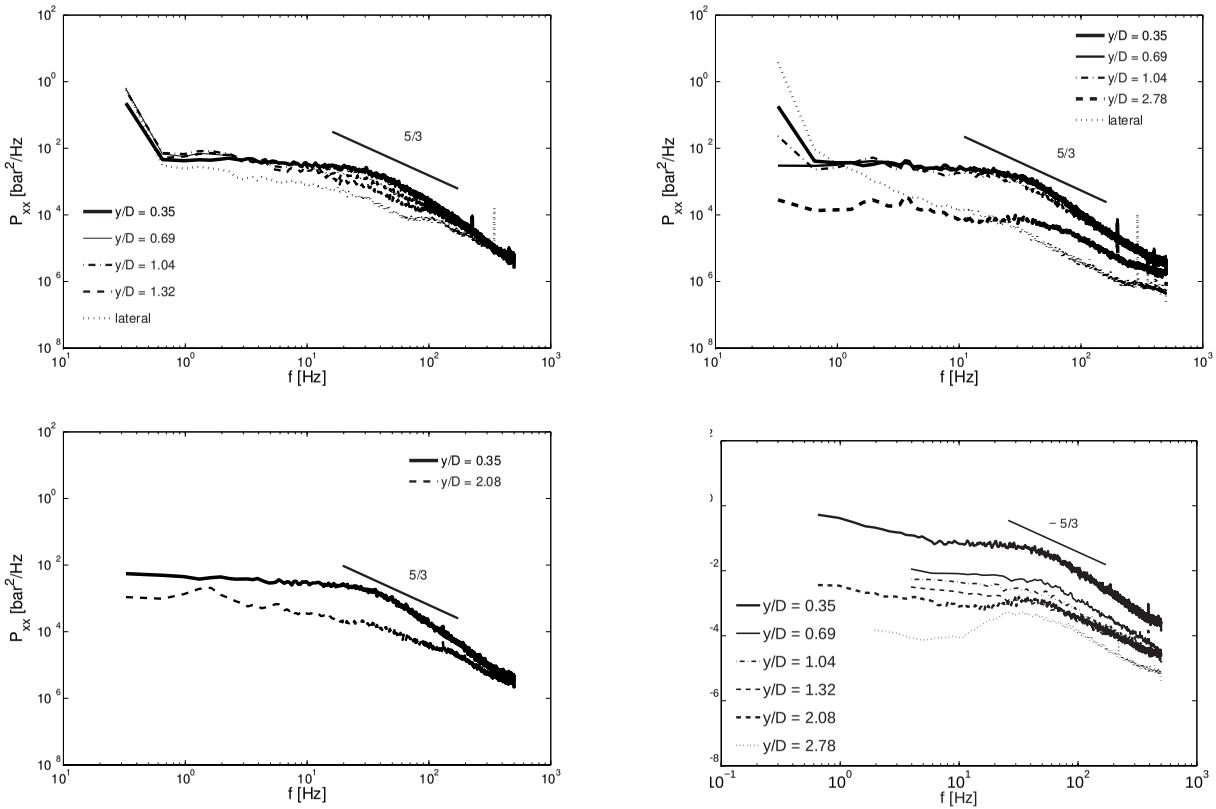

Figure 9.16.: Lateral evolution, deep pools: FC67, SC67, TC67 and FB67. Read clockwise.

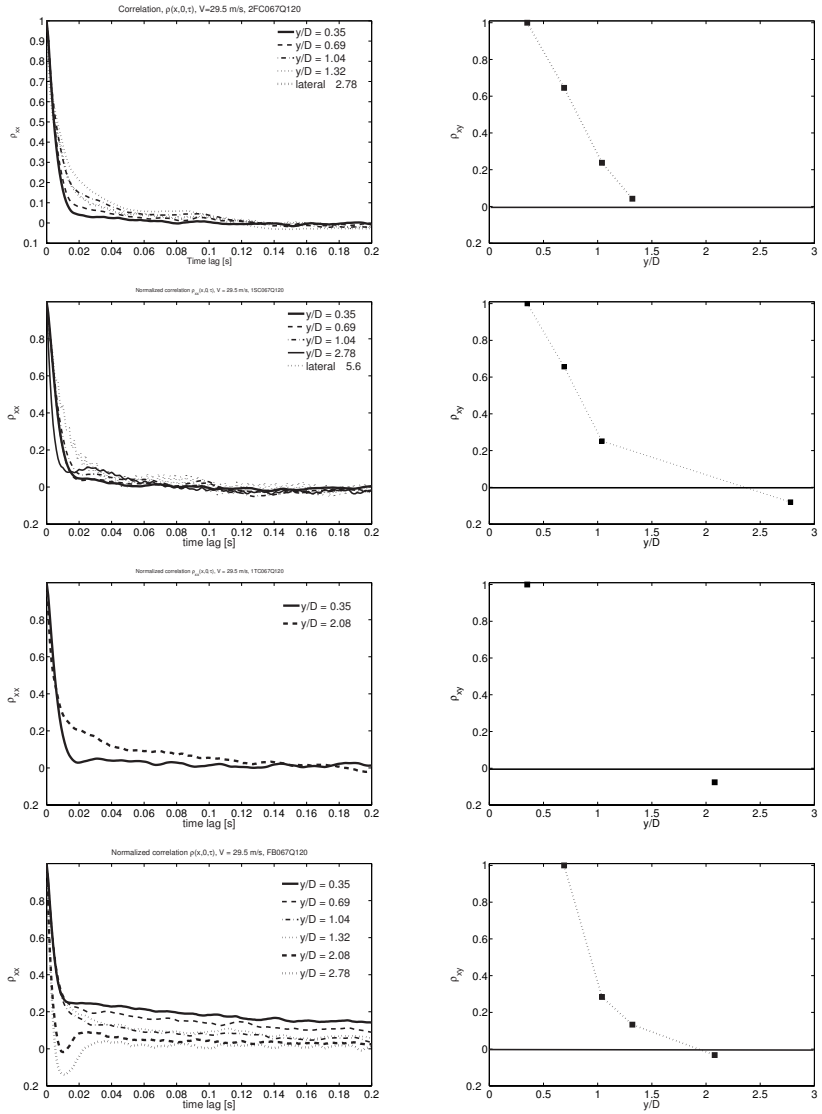

Figure 9.17.: Lateral evolution, deep pools: FC67, SC67, TC67 and FB67. Left: ρ_{xx}; Right: ρ_{yy}, assumed linear (pivot at y/D = 0.35, except for FB at y/D = 0.69).

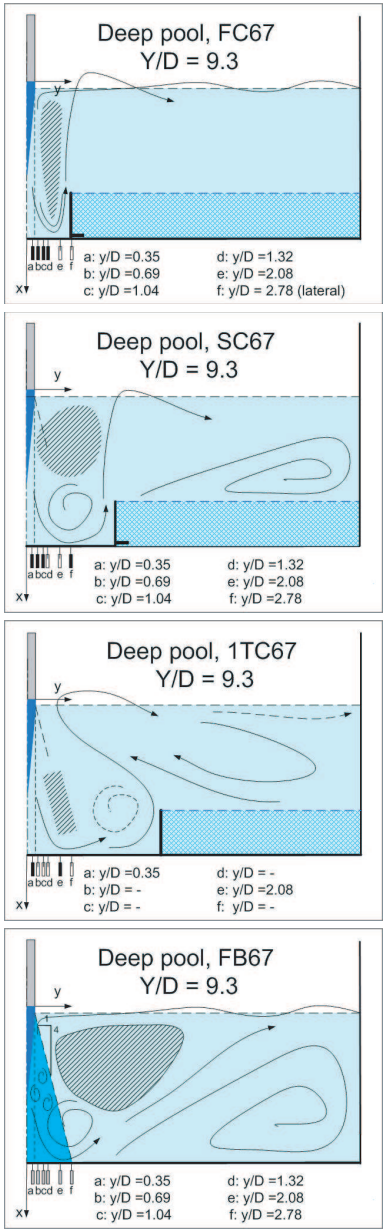

Figure 9.18.: Tentative flow patterns for "lateral evolution, deep pools": FC67, SC67, TC67 and FB67. The solid elements have dimensions at scale, the flow patterns' scale is approximative.

The flat reference case (FB) is characterized by the impact of developed jets. The spectra enter the viscous dissipation range at about 50 Hz . For y/D = 2.08 and 2.78 the energy content below 50 Hz is lower than that closer to the jet axis, since these two points are already under the influence of the bottom wall jet.

Radial evolution of the space-time correlations

The narrow (FC) pool presents integral scale I_y of $\approx$ 6 cm (i.e. $\approx R_{fc}/3$). The turbulent shear layer impacts up to 1.3D (i.e. $R_{fc}/2$). The autocorrelation functions are representative of the impact of the turbulent shear layer. For the point closer to the axis, the autocorrelation represents a stagnation turbulent scale, and a second long-lasting structure (the shear layer) with low correlation and mild slope - Figure 9.17.

In the intermediate (SC) pool, the autocorrelation functions closer to the axis are similar to those of the stagnation region. However, since the spatial correlation is positive, these points are under the influence of the shear layer. At y/D = 2.78, p' are non-correlated with the former and correspond to a bottom wall jet. The oscillations of the autocorrelation function ρ_{11} should correspond to pool surface oscillations.

In the wide (TC) pool, the two single points are clearly uncorrelated in space. One is under the influence of stagnation conditions (y/D = 0.35), and the other of the jet's TSL with slow decaying autocorrelation (y/D = 2.08).

The spatial correlation for the reference pool with flat bottom (FB) confirms the existence of a first region of correlated fluctuations up to about 2D. This should correspond to the impact of the shear layer (C_s and K>0). It is followed by the formation of a bottom wall jet, as shown in the autocorrelations for points y/D = 2.08 and 2.78.

Tentative flow patterns for deep pools

Based on the previous analysis, the main flow features in the LAT-DEEP scenario are schematically represented in Figure 9.18. the creation of a narrow hole and its enlargement induces:

- the vertical deflection of the bottom wall jet;
- the formation of shear eddy, its increase in size, and likely decrease in frequency, for the SC and TC pools.
- the "apparent" displacement of the shear eddy further outwards, when comparing the TC and FB pools;
- the inflection of upward currents inwards by the recirculation patterns (TC pool);

9.3.6. Coherent motion in cylindrical pools with vertical walls

Radial evolution of the impact pressure spectra

In the case of the DEE-VERT scenario, spectra for the initial flat case (FB) are characteristic of the impact of the jet core, at least up to y/D = 1.32 - Figure 9.19.

The remaining spectra at y/D = 2.08 and 2.78 are under the influence of the bottom wall jet (the energy at frequencies $<$ 50 Hz has been reduced). These point are under the influence of the turbulent shear layer, since the decay at high frequencies is somewhat similar to the previous spectra. In the dissipation range, the 2.08D spectra decays according with the

previous (at about f^{-1}). The 2.8D spectrum is slightly steeper than others, which can be associated with a higher degree of turbulence development.

The evolution of scour results in enhanced jet development at y/D = 0.35, already for Y/D = 4.2 (TC30). The transition from the energy redistribution range (low and intermediate frequencies) into the dissipation range occurs between 80-100 Hz. At y/D=2.08, the spectra are quite similar and should correspond to wall jets.

For the pools with Y/D = 6.9 (TC50) and 9.3 (TC67), the spectra present a small hump at about 40 Hz, which may indicate a superposition of the impact of the turbulent shear layer and the formation of the bottom wall jet, as mentioned for the initial flat stage.

Radial evolution of the space-time correlations

In the case of the pool with flat bottom, the cross-correlation ρ_{12} shows de-correlation between p' at y/D = 0.69 (pivot) and y/D = 1.04, Figure 9.20. This is good agreement with the change of sign of the C_s. For the three laterally confined pools, the cross-correlation functions confirm the absence of spatial-correlation between the turbulent flows at y/D = 0.35 and 2.08: the first is under the direct impact of the TSL, whereas the second is under the influence of an "incipient" bottom wall jet.

The autocorrelations ρ_{11} in the pool with flat bottom show:

- a double-structure function at y/D = 0.35, where the local stagnation fluctuations seem to be more relevant that the second long-lasting low-correlation structure;
- the same double-structure function for y/D = 0.69, 1.04 and 1.32 with increasing importance of the second structure (more fluctuations indicating the impact of the turbulent shear layer), regarding the first structure (turbulent boundary layer created by core impact);
- a autocorrelation that drops abruptly to negative values at y/D =2.08, indicating the transition to a bottom wall jet, with positive C_s and high K (local peak);
- a similar autocorrelation function at y/D = 2.78 as the previous but always positive, derived from small and almost de-correlated fluctuations (low persistence) which are superposed to a bottom wall jet. The slow decay of the function agrees with the evolution of C_s in suggesting the approach to the turning point of the shear eddy.

For the laterally confined pools, the autocorrelation functions are quite similar: at y/D = 0.35 there is decreasing importance of the 2^{nd} turbulent structure (TSL); whereas at y/D = 2.08, the slope of ρ_{11} becomes milder due to the influence of a more persistent (2^{nd}) turbulent structure like a bottom wall jet.

Tentative flow patterns for cylindrical pools with vertical walls

Based on the previous interpretation of the experimental results, relevant flow features are identified and are schematically represented Figure 9.21. For the three confinements, the main flow features that could be identified are rather similar. C_p and C'_p are almost constant with increasing depth. This suggests that relevant flow features that interfere in the development of the jet may exist in the non-assessed regions.

In any of the cases, direct friction between the plunging and ascending currents does not seem as important as in narrower pools. Comparing the 3TC67 pool with the TC67 pool of the LAT-DEEP scenario, the absence of important recirculation currents leads to a longer persistence of the jet core (i.e. C_p at y/D = 0.35 is higher in the 3TC67 case).

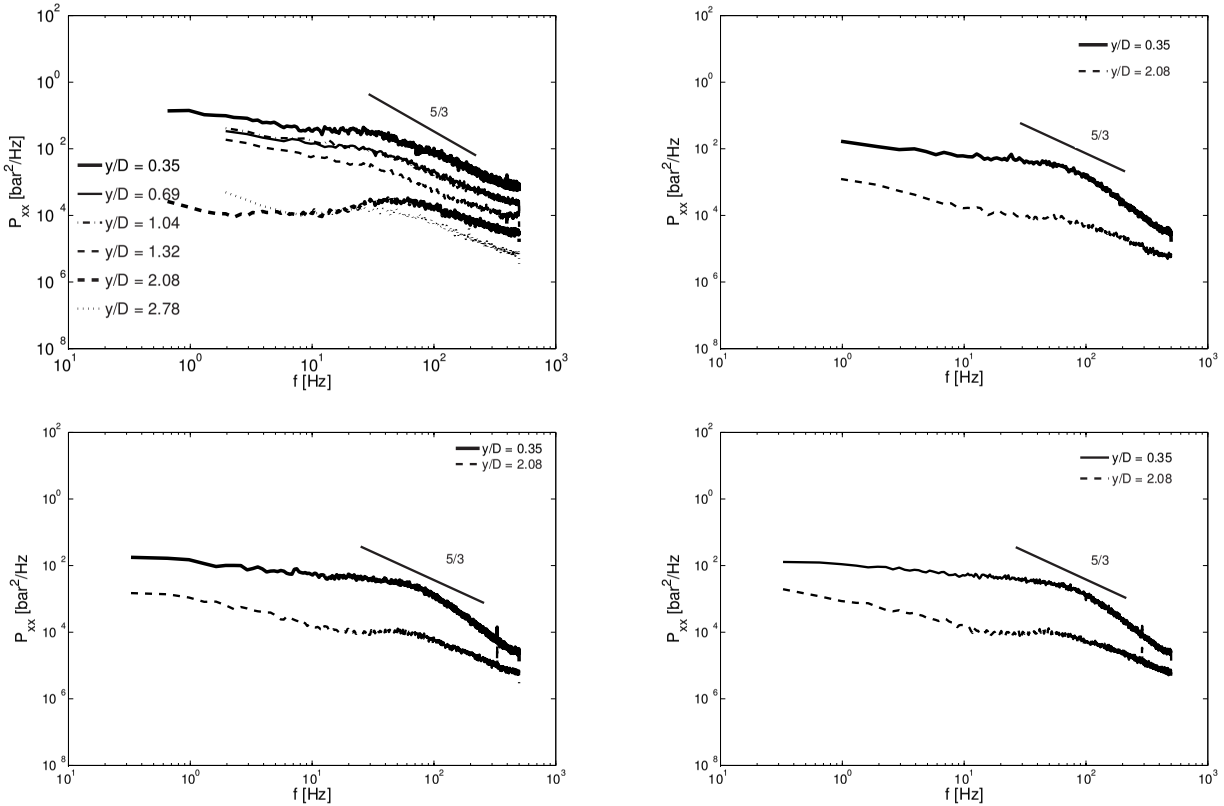

Figure 9.19.: Depth evolution, vertical, from shallow to deep: FB20, TC30, 2TC50 and 3TC67. Read clockwise.

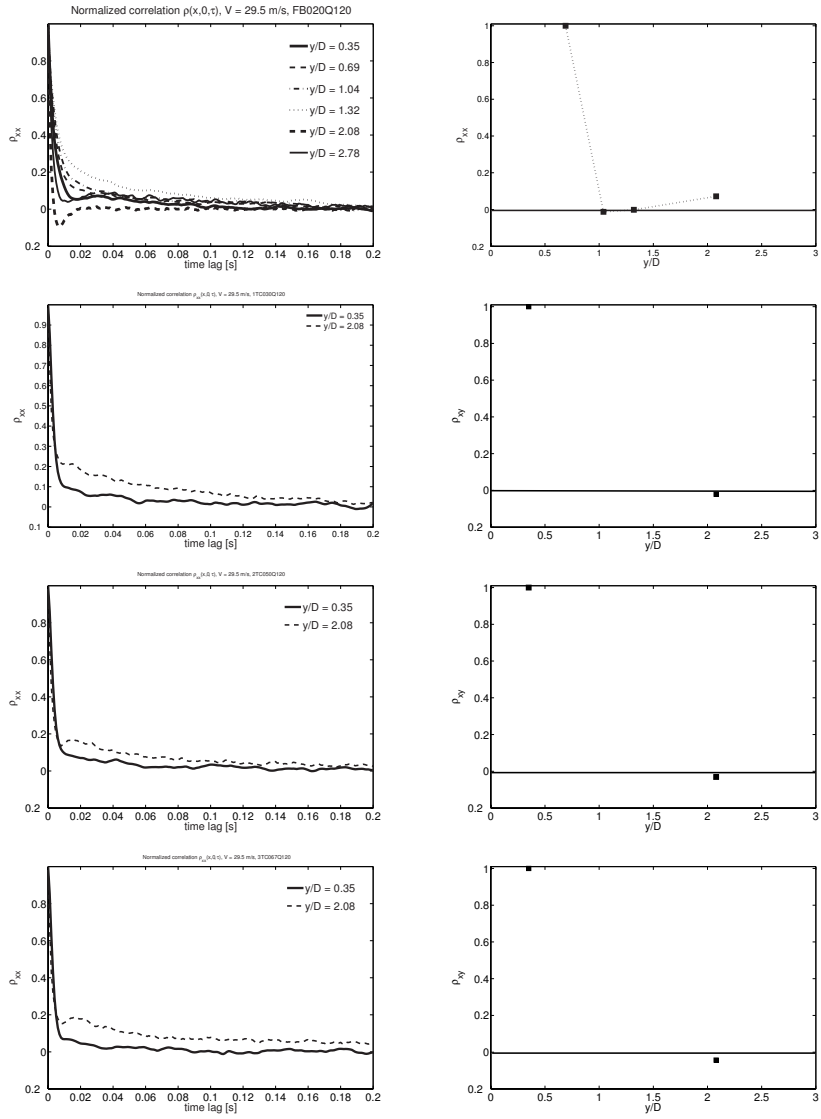

Figure 9.20.: Depth evolution, vertical pool (from shallow to deep): FB20, 1TC30, 2TC50 and 2TC67. Left: ρ_{xx}; Right: ρ_{yy}, assumed linear.

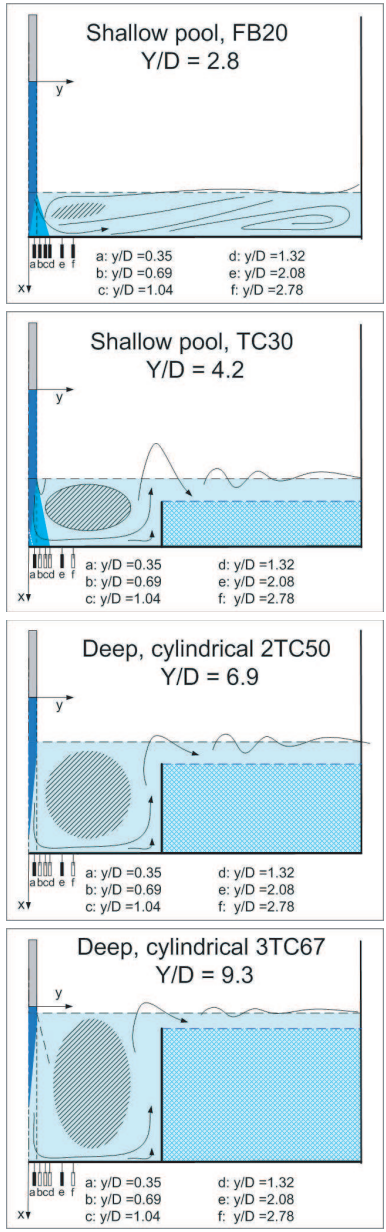

Figure 9.21.: Tentative flow patterns for "depth evolution, vertical", from top to bottom (from shallow to deep): FB20, TC30, 2TC50 and 3TC67. The solid elements have dimensions at scale, the flow patterns' scale is approximative.

9.3.7. Coherent motion in conical stepped pools

Radial evolution of the impact pressure spectra

The DEE-STEP scenario may be compared directly with the previous DEE-VERT. The initial pool with flat bottom is identical.

The first scour stage (FC) corresponds to a narrow confinement (Figure 9.22). It generates developed jet impact conditions for y = 0.35 to 1.32, which is in good agreement with the increase in C_s (positive) and K. Oscillations between 5 and 10 Hz may be due to surface disturbances (e.g. return flow directly upon the plunging jet). At y/D = 1.32, these oscillations are visible at 2 Hz. The lateral transducer shows the impact of a developed wall jet. The transition to the dissipation range occurs at about 60-80Hz.

In the second scour stage (FS), the spectrum at y/D =0.35 is slightly modified. It shows a mild decrease up to 40-60 Hz and evidence of low frequency oscillations at about 4 Hz. At y/D = 2.08 the spectrum is quite irregular and should correspond to the superposition of several flow features.

In the third stage of scour (FST), similar impact conditions are measured. The spectrum at y/D = 2.08 is closer to that at y/D = 0.35, in particular at f < 10 Hz, when compared to the preliminary stage of scour. There is no significant change in the corresponding C_s or K parameters. The spectrum at y/D =0.35 has less energy than in the previous stage of scour.

Radial evolution of the space-time correlations

For the first stage of scour (FC), the autocorrelation at y/D = 0.35 reflects the impact of the shear layer (Figure 9.23). A low frequency oscillation is superposed (undulating autocorrelation function). The autocorrelations for y/D = 0.69 and 1.04 are similar, reflecting the growing importance of the TSL.

At y/D = 1.32 the spatial correlation becomes negative. This should reflect the loss of influence of the fluctuations induced by the TSL. The increase in K at y/D = 1.32 suggests that some turbulent phenomena generating important fluctuations and with low persistence (autocorrelation becomes negative after 0.1 s) occurs above this measuring point. This is thought to correspond to the abrupt inflexion of the flow imposed by the FC wall at 2.8D. Unstable, intermittent flow conditions are generated at the interface between the plunging and the ascending currents. This, however, seems to have little relevance in the spectrum for 1.32D.

In the second stage of scour (FS), the two single points are clearly non-correlated (also for the third TC case). The autocorrelation of pressure fluctuations at y/D = 0.35 is similar to that of the first (FC) stage. At y/D = 2.08, the autocorrelation is almost identical, except for a slight increase in the correlation values for time lags <0.1 s. This corresponds to an increase in persistence of small turbulent structures.

For the third stage of scour (FST), the cross-correlation function and the autocorrelations are similar behaviour to the previous stage. However, the reduced time-correlation at y/D =0.35 should be mentioned, in particular when compared to that of the second (FS) stage of scour. There is a reduction of the importance of the TSL. In fact, it seems to disappear as sign of increased flow development and predominance of small turbulent structures. At y/D = 2.08 the autocorrelation seems less affected by the further development of the turbulent flow patterns in the pool.

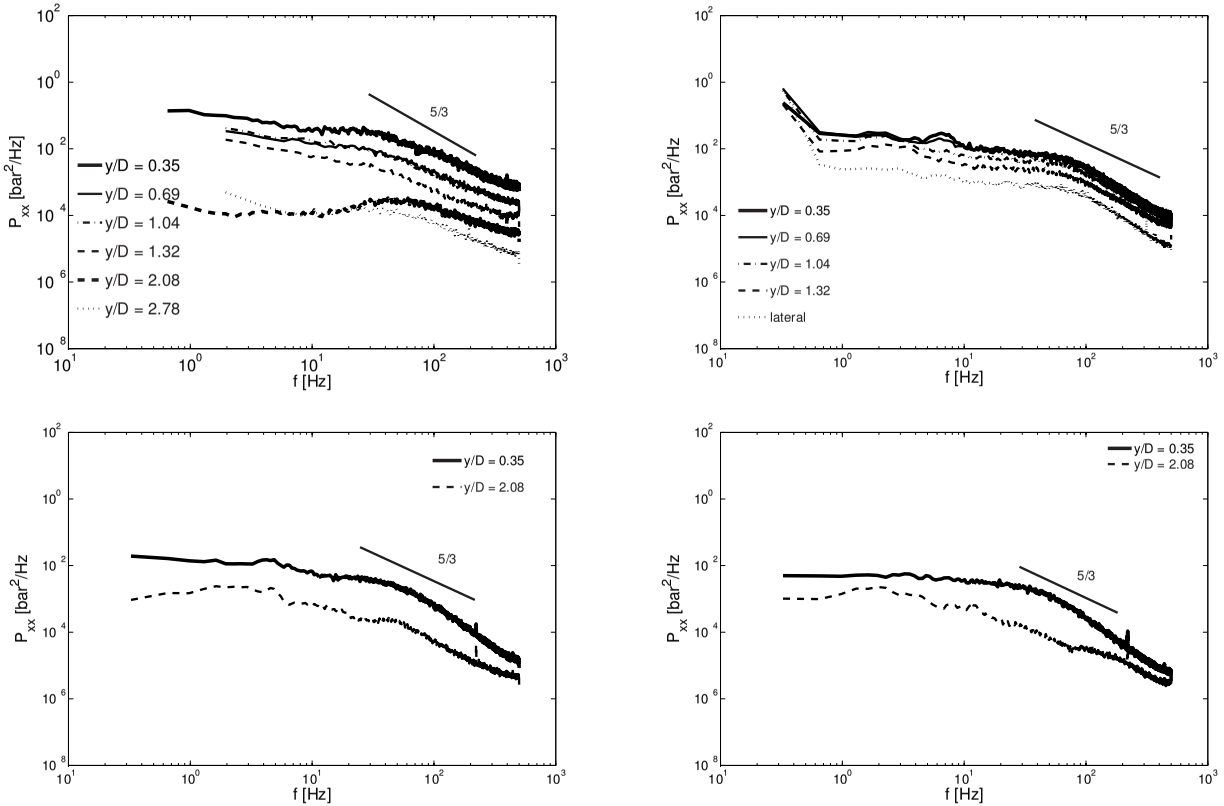

Figure 9.22.: Depth evolution, conical (from shallow to deep): FB20, FC30, FS50, FST67. Read clockwise.

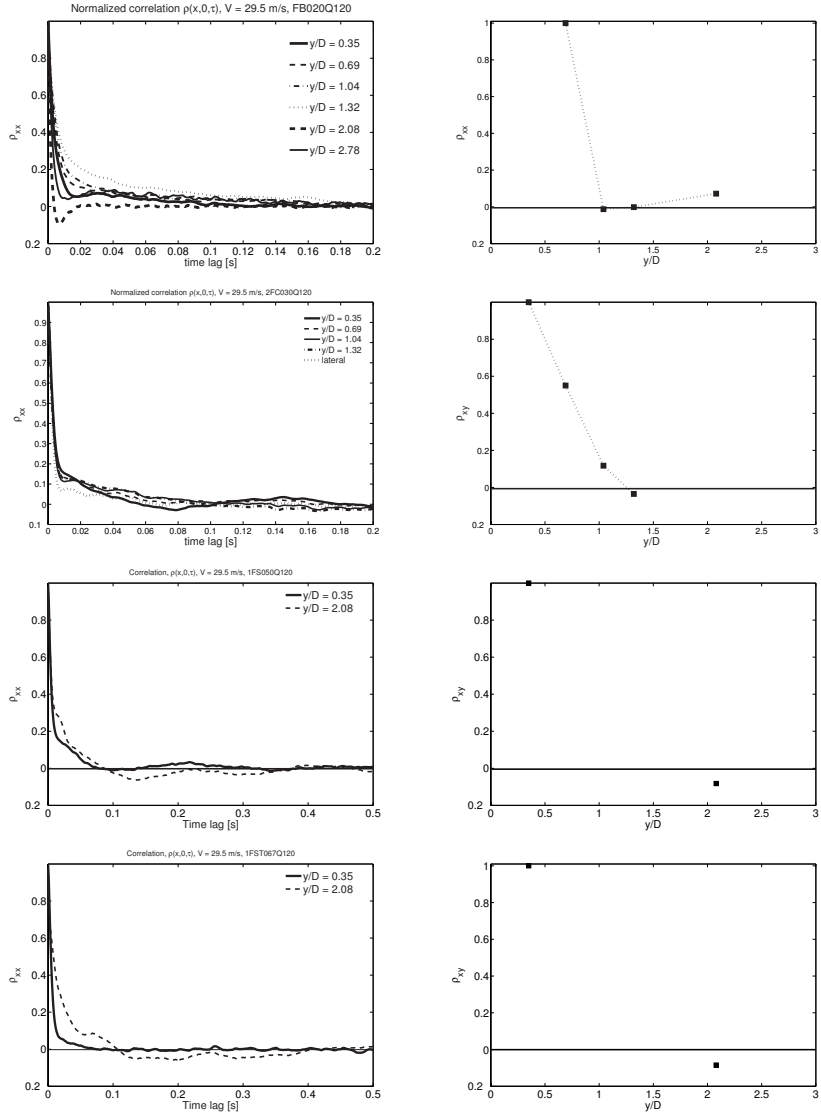

Figure 9.23.: Depth evolution, conical pool (from shallow to deep): FB20, FC30, FS50 and FST67. Left: ρ_{xx}; Right: ρ_{yy}, assumed linear. Note: the time scales of the last two plots on the left are larger than those of previous plots.

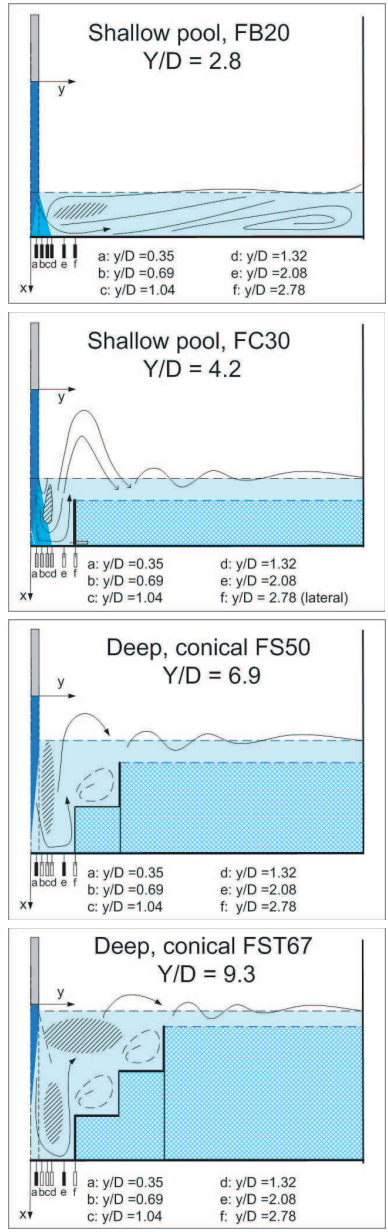

Figure 9.24.: Tentative flow patterns for "depth evolution, stepped", from top to bottom: FB20, FC30, FS50 and FST67. The solid elements have dimensions at scale, the flow patterns' scale is approximative.

Tentative flow patterns for conical stepped pools

The DEE-STEP scenario combines lateral and depth-wise evolution of scour. During the tests, the main flow is limited to the centre part of the pool, conditioned by the deepest and narrowest part of the FST geometry at the bottom. The analysis of the spectral density functions and of the cross and autocorrelation function suggest the flow patterns as a predominance of smaller structures, when compared to the three other scour scenarios LAT-SHA, LAT-DEEP and DEE-VERT. For the FS and FST stages of scour, complex spectral functions are obtained, suggesting the superposition of various relevant flow features. The mean pressure values are less than $0.20E_0$ and turbulent fluctuations do not exceed $0.05E_0$ at the bottom of the pool. The measured C_s and K are rather low. An estimated configuration of relevant flow features is presented in Figure 9.24. As schematically represented for the FST case, the upward currents are restricted to the centre of the pool.

Direct comparison between the FST67 and FB67 pools

A direct comparison of the final stage of scour (FST) with the equivalent pool with flat bottom (FB, Y/D = 9.3) reveals that C_p and C'_p values are, in general, lower in the FST pool. The spectral energy at y/D = 0.35 is reduced for all frequencies. At y/D = 2.08, the direct comparison shows lower energy contents at every frequency. Therefore, one can say that the FB pool provides conservative estimates of the dynamic pressures both in terms of mean values, RMS values and spectral distribution. The flow features in both cases are different, as shown by the autocorrelation functions of wall pressure fluctuation at several measuring stations.

9.4. Discussion on geometry-induced pool flow patterns

9.4.1. Induced-flow features

The most relevant induced flow patterns identified in the cases of shallow and deep laterally confined pools, as well as in cylindrical pools with vertical walls and conical stepped pools are:

- the shear eddy, between the turbulent shear layer(TSL) and the confinement;
- the upward currents generated by the reflection of the bottom wall jets on the pool boundaries;
- the pool recirculation currents, that set in motion the volume of water *outside* the scour hole.

The shear eddy (or dissipation cell) was also described by Puertas-Agudo (1994) based on visualisation of the flow structure during experiments. It can be considered similar to a submerged hydraulic jump roller that is pushed in the direction of the plunging jet by the deflected (upward) currents. Similar eddies have been described by Spurr (1985) as critical for the dissipation of the plunging jet's energy.

The shear cell is the most important of the three phenomena regarding impact pressures save for very narrow confinements. In the latter case, the shear cell may not develop and the deflected upward currents can oppose directly jet momentum. Depending on the direction of these upward currents and on their proximity to the diffusion region, they can also hinder air bubble penetration in the pool.

The pool circulation currents are generally less concerned in the definition of impact pressures. Depending on the tailwater level h, these currents may push the upward currents radially inwards and contribute to enhance dissipation and hinder air entrainment. However, for particular situations combining pool geometry, jet velocity and pool depth is can not be excluded that the generated circulation flow may reduce the tailwater level locally at the plunging section. This is observed in the present facility for pools with flat bottom and Y/D = 8.3. The local reduction of pool depth generated impact pressures quite similar to those obtained for Y/D = 6.9.

The participation of upward and recirculation currents in jet development is documented by video recording for vertical pool boundaries (D_c/D=16.7). In the case of the stepped pools, the available video recordings indicate that the direction of such currents is mainly induced by the narrowest (vertical) confinement placed at the bottom.

9.4.2. Developed flow impact conditions

The relative distance of the confinement to the axis of the jet has been pointed out as one relevant parameter for the definition of the induced flow pattern.

For the wide confined pools (TC), developed jet conditions are obtained starting from Y = 4.2D, which is $\approx R_{tc}/2$. In this case, developed impact conditions are obtained for:

$$Y \geq \frac{R_{tc}}{2} \tag{9.3}$$

However, for the intermediate (SC) pools ($R_{sc} = 5.6D$), C_p values similar to those in pools with flat bottom are found for Y = 2.8D (i.e. $R_{sc}/2$). To accommodate both situations, two expressions are proposed:

$$Y > R_c \quad \text{for } R_c/2 > 4\text{D} \tag{9.4}$$

and

$$Y > 1.5R_c \quad \text{for } R_c/2 < 4\text{D} \tag{9.5}$$

They can be resumed respectively in:

$$Y > R_c > 8D \tag{9.6}$$

or, more generally,

$$Y > 1.5R_c \quad \text{and} \quad R_c < 8D \tag{9.7}$$

The TC pool falls in the first group (i.e. $R_{tc}/2 = 4.2\text{D} > 4\text{D}$) whereas the SC and FC pools in the second (i.e. $R_{sc}/2 = 2.8\text{D} < 4\text{D}$ and $R_{fc}/2 = 1.4\text{D} < 4\text{D}$).

It should be stressed that Y/D = 4 is less than the core development length in pools with flat bottom in the present experimental set-up. This length is estimated in Y/D = 5.6 for an average velocity of 20 m/s (slightly longer if V > 20 m/s).

For $Y < R_c$ core impact conditions are observed, but few tests are performed in these conditions. For Y = 4 - 5.6 D, core impact conditions could occur for very large pools, i.e. $R_c > 8\text{D}$. For Y > 5.6 the core of the jet vanishes independently of the value of R_c.

In most practical situation, core jet impact is limited to the very early stages of scour or spillway operation. The most challenging conditions for research are the developed jet

impact conditions, which are shows to occur starting from very shallow pools in laterally confined pools. The main focus of the analysis of rock scour should thus be on the turbulent characteristics of the developed jet impact pressures.

9.4.3. Definition of the length scale of the shear cell

The observations of large-scale flow features (TC pool) allowed identifying the presence of a dissipation shear cell between the plunging jet and the upward currents. This cell varies in dimensions with R_c. It may vary with velocity, due to the influence of jet velocity on the definition of the interaction between the upward currents and the recirculation currents. The dimensions and frequency of such cell can be used to define a characteristic Strouhal number per pool geometry.

Despite the absence of direct velocity or pressure field measurements, some basic characteristics of such cells can be defined.

The width of the turbulent shear layer at impact with a flat bottom is assumed $\xi \approx$ Y/3, according to several authors (Cola, 1966; Beltaos and Rajaratnam, 1974) - see Table 5.3.

In the present set-up, the turbulent shear layer (TSL) impacts the bottom between 1.4D (for Y=2.8D) and 2.8D (for a maximum pool depth of 9.3D), assuming a diffusion spreading angle of 14°. The ξ is maximum 3D. Hence, the FC pool interferes directly with the TSL. The space between the axis and the confinement is shared between the "confined" shear layer and the upward currents.

The observation of the shear cell in the TC pool (in submerged jet conditions and for t/D =2.8 only) allows estimating the cell's dimension $\lambda_c < R_{tc}/2$. In these conditions Y = 11D and R_{tc}=8.3D. Therefore, $\lambda_c < 4.2D$ and is assumed circular. From visual interpretation of the flow field, $\lambda_c < Y/2$. The bundle of air bubbles that allowed visualisation did not exceeded 20 cm (i.e 2.8D).

This shear cell is bounded to move inwards, approaching the TSL for the SC and FC pools. This however could not be visually confirmed.

For the SC pool ($R_c = 5.6D$) and for t/D = 2.8, the jet core impacts the bottom only for the minimum Y/D, i.e. ξ = 0.33(2.8D) = 1.4D. For all the other pool depths Y/D, developed jet impact conditions are registered. One can consider that:

- with a TSL width of 1.8D for Y = 4.2D and a shear cell of 2.8D, the upwards currents can still occupy 1.4D and have little influence over the plunging jet. This is good agreement with the results.
- with a TSL width of 2.8D for Y = 9.3D, λ_c is lower than 2.8D. In this case two possibilities can be considered: either λ_c is 2.8D or the TSL has to be smaller.

The previous analysis of the three FC, SC and TC confinements with t/D = 2.8 suggests that the y-length scale of the shear eddy, when existing, is of about 2.8D. This corresponds to $R_{sc}/2$ or $R_{tc}/4$. The x-length scale (vertical) is likely related with t, i.e. the depth of scour below initial riverbed. In fact, for Y > t (i.e. h $\neq$ 0) the recirculation currents in the region outside of the confined zone may influence λ_c. This can be visually observed in the TC pool (t/D = 2.8) and Y/D = 9.3/11.4.

In summary, the **length scale of the shear cell** λ_c is assumed:

$$\text{if} \quad R_c = t \quad \text{and} \quad R_c > 2.8D \quad \text{and} \quad h \geq t \quad \Rightarrow \quad \lambda_c \approx t \tag{9.8}$$

For confinements that are *deeper than wider*, i.e. $R_c <$ t:

$$\text{if} \quad R_c > 2.8D \quad \text{and} \quad Y > 1.5t \quad \text{or} \quad Y \geq D_c \quad \Rightarrow \quad \lambda_c \approx R_c/2 \tag{9.9}$$

assuming Cola's hypothesis for the impinging zone (i.e. 0.33Y)

For confinements that are *wider than deeper*, i.e. $R_c >$ t:

$$\text{if} \quad 4D < Y \leq 1.5R_c \quad \text{and} \quad R_c > 4.2D \quad \Rightarrow \quad \lambda_c \approx t \tag{9.10}$$

For pools with flat bottom, an estimate of λ_c is obtained based on Cola's indication of the centre of gravity of the cells at 0.25Y. In these conditions,

$$\text{if} \quad Y > 5.6D \quad \Rightarrow \quad \lambda_c \approx 0.50Y \tag{9.11}$$

However, in the present set-up, the outflow is controlled by weirs. They define the pool level Y and influence the large recirculation currents in pools with flat bottom. Puertas-Agudo (1994) observed $\lambda_c < 0.50Y$ due to the same "weir" effect.

9.4.4. Evolution of the Strouhal number with scour depth

The rotation frequency of the shear cell can be computed by:

$$\widehat{f} = \frac{U_r}{\pi.\lambda_c} \tag{9.12}$$

where U_r is the rotation velocity, i.e. the velocity necessary to do one revolution of $\pi.\lambda_c$ (perimeter) in a given period T. The Strouhal number corresponding to this turbulent flow pattern can be defined as:

$$St = \frac{U_r}{\pi V} \tag{9.13}$$

which is similar to the expression proposed by Ervine et al. (1997).

The rotation velocity is assumed as the velocity of the plunging jet at the entry of the impinging region (i.e. 0.25Y). This depth corresponds to the x-coordinate of the centre of the cell (Cola, 1966; Puertas-Agudo, 1994).

Based on these assumptions, the characteristic frequencies of shear cells are presented in Table 9.5.

For the TC deep pool, the estimated frequencies range from 10 to 30 Hz, and are in agreement with the visual observations.

These estimates are very sensitive to the U_r assumptions. Since there is no centreline velocity decay law available for each pool geometry, coarse estimates are made based on the C_p values measured at y/D = 0.35.

For the FS and FST pools, λ_c is defined not by the total t or R_c but rather by the narrowest confinement at the bottom.

Rotating frequencies are estimated between 10-30 Hz in deep pools and 10-65 Hz in shallow pools. The spectra analysis suggests frequencies within this reach.

Table 9.5.: Definition of characteristic cell frequencies, based on assumptions and visual estimates of λ_c in the TC67 case.

Pool	Y/D	Y [m]	h [m]	R_c [m]	t [m]	V [m/s]	λ_c [m]	U_r [m/s]	f [Hz]	Str [-]
FB	4.2	0.30	0.30	-	-	29.5	0.15	29.5	63	0.32
				-	-	10	0.15	10	21	0.32
	9.3	0.67	0.67	-	-	29.5	0.34	20	19	0.22
				-	-	10	0.34	8	8	0.25
SC1	4.2	0.30	0.10	0.4	0.2	29.5	0.20	15	24	0.16
						10	0.20	6	10	0.19
	9.3	0.67	0.47	0.4	0.2	29.5	0.20	18	29	0.19
						10	0.20	5	8	0.16
TC1	4.2	0.30	0.10	0.6	0.2	29.5	0.20	20	32	0.22
						10	0.20	8	13	0.25
	9.3	0.67	0.47	0.6	0.2	29.5	0.20	11	18	0.12
						10	0.20	3	5	0.10
TC2	6.9	0.5	0.10	0.6	0.4	29.5	0.40	10	8	0.11
						10	0.40	4	3	0.13
TC3	9.3	0.67	0.07	0.6	0.6	29.5	0.30	11	12	0.12
						10	0.30	5	5	0.16
FS	6.9	0.50	0.30	0.2	0.2	29.5	0.20	10	16	0.11
						10	0.20	4	6	0.13
FST	9.3	0.67	0.47	0.2	0.2	29.5	0.20	10	16	0.11
						10	0.20	4	6	0.13

9.5. Synthesis and Conclusions

The diffusion of plunging jets in laterally confined plunge pools has been studied experimentally and compared with diffusion in pools with flat bottom. Dynamic pressures were sampled at the pool bottom and side slopes. Point statistics and a limited number of multi-point descriptions of the spatial turbulent pressure field are obtained. Analysis of pressure distributions, spectral energy content and visualisation of large-scale flow features allow concluding:

- that the geometry of the plunge pool is a key element in the definition of the mean and turbulent character of impact pressures on the pool boundaries;
- that the flow patterns induced by the interaction of the turbulent shear layer with the pool geometry may considerably alter jet diffusion and air bubble penetration in non-flat pools, compared to the most-documented case in literature of pools with flat bottom;
- that assuming the evolution of scour has a succession of scour stages with flat bottoms leads to overestimation of impact pressures for a given pool depth.

10. Transfer of impact pressures generated by high-velocity plunging jets to underlying rock fissures in laterally confined plunge pools

This chapter presents experimental evidence of the amplification of impact pressure fluctuations inside a closed-end fissure in pools with flat bottom and in laterally confined pools, i.e. in laterally unbounded and bounded jet diffusion conditions.

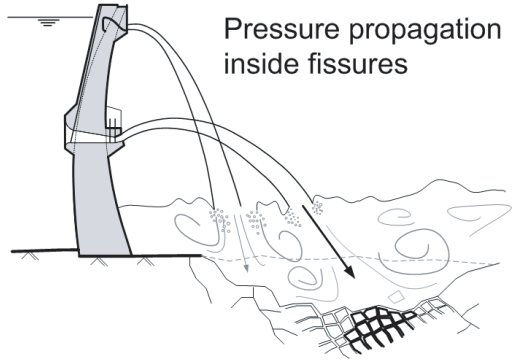

Figure 10.1.: Schematic representation of prototype rock scour (laterally confined pools) by propagation of hydrodynamic pressures generated by plunging jets, inside rock fissures (closed-end).

10.1. Transient flows inside rock fissures

Impact pressures at the water-rock interface propagate inside rock fissures. A pioneering study by Hartung and Häusler (1973) showed that fissured concrete plates can break under the impact of plunging jets. In rock, brittle failure may occur due to the local build-up of hydrodynamic pressures. Fatigue failure may also occur by repeated action of a given cyclic loading. Once blocks are formed, pressure build-up may eventually displace them. This is primarily the action of uplift forces that may unbalance stabilizing forces. These uplift forces may be generated by mean pressures, but also by fluctuating pressures. This idealisation of the scouring process was first presented by Yuditskii in 1961 in Moscow, before the Engineering Academy. Other research groups in the Soviet Union had different views, notably the group of Akhmedov, based on the predominance of the abrasion process. With time, both concepts were integrated in the present idealisation of the scouring process, with "ball-milling" following the ejection of blocks by a given pressure gradient.

A similar phenomena has been observed in stilling basins under hydraulic jumps and reproduced experimentally by Sanchez-Bribiesca and Fuentes-Mariles (1979). Fiorotto and Rinaldo (1988) developed a criteria for slab failure that was validated in experiments presented in Fiorotto and Rinaldo (1992a,b). They also proposed a mathematical method to simulate pressure propagation in the gap between the slabs and the foundation. Liu et al. (1998) used a similar waterhammer model to test the displacement of rock blocks in the reduced-scale hydraulic model for the Three Gorges dam in China. They observed that uplift forces can be generated by the propagation of pressure fluctuations in rock joints that are high enough to displace a loose block.

Transient flows correspond to intermediate flow conditions between two steady flow regimes that are created by some instability in an hydraulic system (e.g. opening or closure of a valve). The present case is quite atypical in terms of research in transient flows (i.e. the classic reservoir-pipe-valve system). The fissure system is excited by a highly fluctuating source of energy. The instability at the boundary of the system is created as soon as the jet starts impacting the entry of the fissure, and persists in time. Furthermore, the "upstream boundary" is not only fluctuating but may have energy in large ranges of frequencies. According to transient flow theory, e.g. Streeter and Wylie (1983), peak pressures higher than the incoming pressure head may be generated by superposition of pressure waves at frequencies that are characteristic of the system. Bollaert (2002b) measured pressure fluctuations inside simple-shaped rock fissures directly under the impact of a plunging jet with near-prototype dynamic characteristics. Jet impact pressures were amplified in several fissure configurations tested, under pools with flat bottom (closed-end, 2D closed-end, U-shaped open end, L-shaped closed-end). He observed and discussed pressure amplification and damping inside rock fissures for a wide range of jet velocities and relative pool depths.

Up to present no direct numerical simulation has succeeded in replicating the propagation of pressure fluctuations inside fissures excited by prototype plunging jets. Liu et al. (1998) attempt should be validated with prototype data. The model of Bollaert (2002b) was tested with near-prototype jet data and highlights potential sources of instability (e.g. variation of local air content) relying on an optimization algorithm.

10.2. Experimental work with plunging jets impacting at the entry of a closed-end fissure

Dynamic pressures were sampled at the pool bottom and inside a closed-end underlying fissure at 1 kHz. Detailed information on the experimental set-up and instrumentation are presented in Section 3.3.

The fissure was carefully filled with tap water at atmospheric pressure, systematically before each test. The fissure was cleaned periodically with a water-vacuum cleaner in order to prevent any obstruction by debris.

A selected number of cases that are representative of the diversity of situations encountered is presented and discussed hereafter. Data time series, pressure statistics, dynamic pressure coefficients and power spectra of pressure fluctuations are used to document the analysis.

10.3. Analysis of time series of impact and transient pressure signals

Time series of pressure measurements in pools with flat bottom, as well as several laterally confined pools are presented. The direct analysis of the time series illustrates flow phenomena inside the fissure.

Bollaert (2002b) documented and discussed the flat bottom case with several types of fissures. From the previously tested fissures, the closed-end configuration is selected herein to investigate the influence of jet impact conditions generated in pools with various geometries.

10.3.1. Pools with flat bottom

Pressure fluctuations at the bottom of the pool can generate higher fluctuations inside the fissure, in developed jet impact conditions (Bollaert, 2002b). This was also observed in the present experimental campaign. However, in the presents set-up, developed jet impact conditions correspond to pools with flat bottom and $Y/D > 5.6$ for $V < 15$ m/s, as well as for $Y/D \geq 6.9$. In the following some examples are presented and discussed.

Figure 10.2 (top) shows repeated pressure oscillations at the middle and end sections of the fissure. The positive cyclic peaks are spaced of ≈ 4 ms (i.e. 250 Hz in average). The maximum pressure of ≈ 8.1 bar is the highest value within 6.5 seconds. It is generated by a superposition of pressure waves that are subsequently damped by friction. Pressure peaks are quasi-simultaneous at the middle and end sections of the fissure. The time lag between peaks at the middle and end section is of the order of 0.5 ms over a distance of 0.4 m. In this case, the celerity of pressure waves a must be very high, i.e. in water ≈ 1000 m/s. This is in good agreement with the high rigidity of the experimental facility.

In the same data series, several higher peaks are obtained (in the same Figure, bottom plot). These high peaks follow time intervals with low pressures, close to the atmospheric pressure. In these circumstances, pressure remains almost constant during intervals of the order of magnitude of $O(10^{-2})$s. This is thought to correspond to the formation of gas cavities. This may occur by air bubble increase in volume and clustering, and eventually by gasification of dissolved gases in the water. In this case, the fissure is divided in liquid and gas regions, defining internal boundary conditions. The pressure in the gas region remains constant during the existence of the cavity. This has been observed in several prototype pumping systems (Jaeger, 1977). As an example, Mitosek (2000) observed the formation of vapour cavities in pipe under transient flow conditions and mentioned "vapourisation durations" (i.e. average lifetime of vapour cavities) between 2 and 8 ms. Furthermore, in classical transient flow analysis the collapse of vapour or gas cavities is expected to generate high pressure peaks due to the contact of the previously separated liquid columns, often estimated based on Joukovsky's formulae (Jaeger, 1977):

$$\Delta H = a\frac{U}{g} \tag{10.1}$$

where H is the piezometric head, U is the velocity of the flow inside the fissure and a is the average celerity of pressure wave propagation inside the fissure. The celerity of pressure

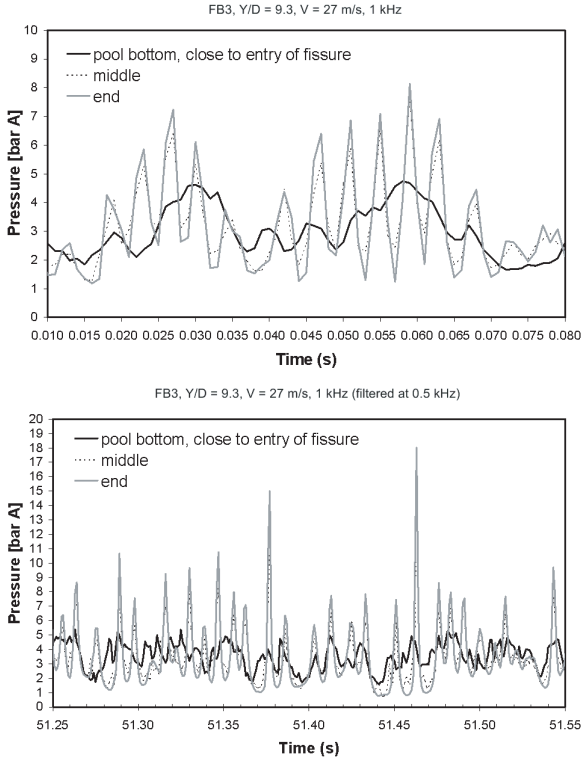

Figure 10.2.: Dynamic pressures at the pool bottom and inside the fissure for a pool with flat bottom, Y/D = 9.3, V = 27 m/s, f_s = 1 kHz (data series 3FB067Q110).

waves can be defined in pipe networks as (Wylie and Streeter, 1978):

$$a = \sqrt{\frac{K/\rho}{1 + \frac{K}{E}\frac{D}{e}}} \tag{10.2}$$

where K is the bulk modulus of the fluid of density ρ (two-phase pseudo-fluid), E is the elasticity modulus of the pipe with diameter D and thickness e.

For the present example, if a is kept constant (i.e. ≈ 1000 m/s) during the 0.5 ms mentioned, the velocity of the flow generated by cavity collapse can be estimated as $O(10^1)$ m/s for a $\Delta H \approx 17$ bar. Due to small dimensions of the fissure and the complex environment, flow velocities inside the fissure have not yet been measured. Nevertheless, $O(10^1)$ seems disproportionate as a first estimate. In pipe flow, velocities are rather $O(10^0)$ m/s. In this second timeframe, several peaks higher than 10 bar are observed within 0.3 s; they do not repeat at regular intervals.

10.3.2. Laterally confined pools with constant scour depth (t/D = 2.8)

Narrow pools (FC)

Tests with the FC pool (t/D = 2.8 and $D_c/D = 5.6$) have shown that pressure amplification can also occur in shallow pools with Y/D = 4.2 (Figure 10.3). Regular oscillations are found every 0.05 s, approximately 20 Hz. This may be assumed as the first harmonic frequency of resonance in the system. For a closed-end 1D fissure, resonance is achieved for frequencies (Bollaert, 2002b):

$$f_{res} = (1 + 2n)\frac{a}{4L} \tag{10.3}$$

in which n is the order of the multiple harmonic oscillations, in a fissure of length L. Taking n = 0 (fundamental harmonic), L = 0.8 m and f = 20 Hz, wave celerity would be estimated as 64 m/s. This value is dramatically low and would correspond to a quite deformable structure (or leaking fissure) or to a high content of air in the fissure. The former can be ruled out with the present experimental apparatus, but the latter not.

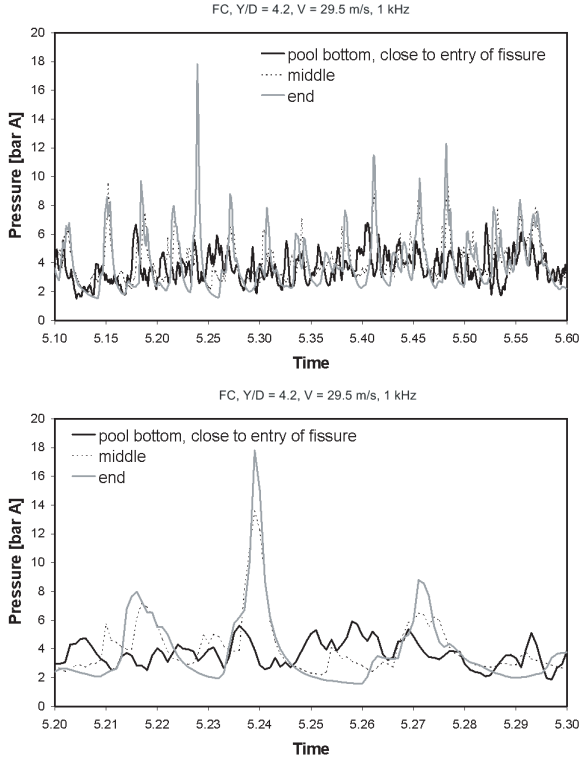

Figure 10.3.: Dynamic pressures at the pool bottom and inside the fissure for a laterally confined narrow pool (FC, t/D = 2.8, D_c/D = 5.6), Y/D = 4.2, V = 29.5 m/s, f_s = 1 kHz (data series 1FC030Q120)

Void fraction measurements presented in Chapter 7 revealed a maximum air content of 5 % (in volume) for V = 22 m/s at 2 cm from the pool bottom (Y/D = 4.2). It can not be excluded that some of these air bubbles are pushed into the fissure. Wylie and Streeter (1978) show that a can drop from 1250 m/s to 250 m/s if the volume of free gas in the fluid is 1%. The decay is sharp for air contents up to 1% and tends asymptotically to 150-200 m/s for higher C_{air}.

A detailed plot at the vicinity of one of the largest peaks (Figure 10.3, bottom) shows the occurrence of low-pressure intervals previous to the mentioned peak. However, three major differences in behaviour are observed regarding the previous case of a pool with flat bottom:

1. there is a time lag between the rise of the signal at the middle section and at the end section of the fissure;
2. pressure does not drop below 2 bar; and,
3. the low-pressure time window from [5.25 s; 5.26 s] is not followed by a peak as large as the previous.

The first point suggests that the pressure wave passing through the middle section needs some *time* to reach the end section and trigger the collapse of the cavity. In this case, the 0.40 m between the two sections would be covered in ≈ 5 ms at an average velocity of 80 m/s. Such straightforward analysis neglects the interaction between an eventual gas cavity and the liquid transient flow. Furthermore, for positive relative pressures, both series at the middle and end sections tend to follow a similar behaviour; even if not fully matching, the time lag between the signals is generally ≈1-2 ms. Therefore, the wave celerity should be closer to 1000 m/s than 80 m/s, in the "pseudo-fluid water hammer" region.

The second point suggests that high pressure peaks are generated without column separation, since pressures were never sub-atmospheric. These high peaks are generated by superposition of pressure waves, eventually resonance.

The first and third points shows that there is a different behaviour for low and high pressures. This indicates that the process is not merely hydrodynamic (i.e superposition of pressure waves) but also thermodynamic. There must be some type of variation of the air content along the fissure, depending on the exchanges of mass with the pool at the entry of the fissure and, eventually, solution and dissolution of air bubbles into and from the liquid phase. For the time being, this is just a scientific hypothesis without experimental validation. The observation of such peaks for such shallow pools is new.

Intermediate and wide pools (SC and TC)

Time series from tests series with wider pools (series SC and TC with t/D =2.8) are presented in Figure 10.4. Two examples are selected for pools with D_c/D =11 for which core impact conditions may still occur, i.e. Y/D = 2.8 and 4.2. The first example shows the impact of a compact jet with high mean value (≈ 5 bar) which seems to be interrupted occasionally. Pressure at impact drops sharply 2 - 3 bar. These pressure drops occur at frequencies of about 25 Hz and are thought to correspond to disturbances by deflected wall jets. In the fissure, measurements at the middle and end sections are paired. Wave celerity must be high, i.e. around 1000 m/s. A considerable difference between the pool surface and fissure signals can be signaled at 4.50 s.

The selected time series for the wide pools (test series TC067Q120 sampled at 15 kHz) shows a collapse of pressures at the middle and end sections of the fissure. This indicates a

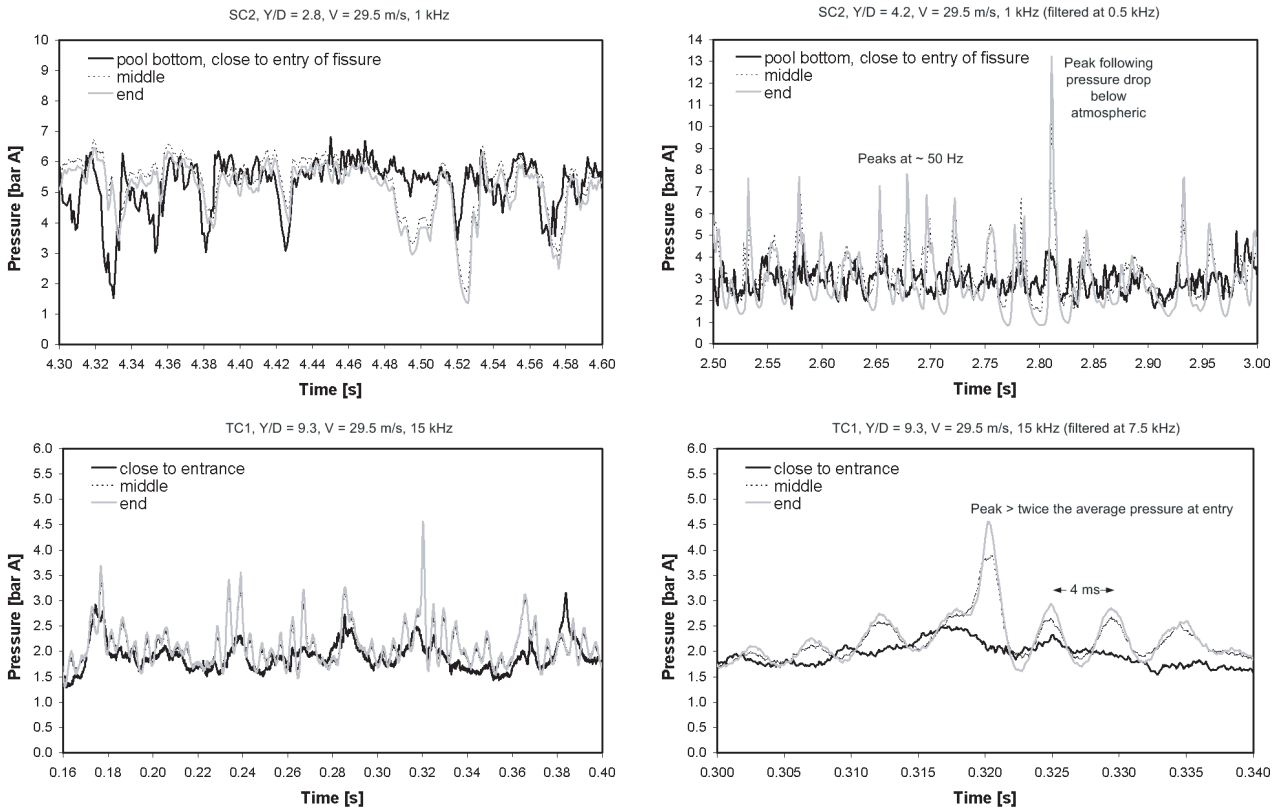

Figure 10.4.: Dynamic pressures at the pool bottom and inside the fissure for laterally confined pools.

high value of a in between these two sections. Peaks repeat at an average time intervals of 4 to 6 ms (i.e. 150-250 Hz). Assuming this is the first harmonic mode, celerity is $a = 4Lf$ and lies between 480 and 800 m/s. In such conditions, the mean air content should be less than 0.2% (Wylie and Streeter, 1978). A detail of this time series shows a succession of positive cyclic peaks spaced of 4 to 5 ms with decreasing amplitude. The maximum pressure of ≈5.6 bar is the highest value within 6.5 seconds. The time lag between peaks at the middle and end section is of the order of 0.5 ms and therefore $a \geq 1000$ m/s.

10.3.3. Stepped conical pools (FST)

A time series obtained with a deep stepped pool (Y/D = 8.3) with a very shallow tailwater level (h/D ≈ 0 - 1) is presented in Figure 10.5. The top image is a time window of 0.15 s sampled at 1 kHz showing low-pressure zones (eventual gas cavity), occasionally followed by high pressure peaks. There are also underlying oscillations with lower amplitude. The second image is a 0.05 s time window of data sampled at 15 kHz. Peaks of more than 12 bar are not regularly distributed: there can be a couple within 0.01 s or even none. The middle section signal follows quite closely the end section one, save in the (negative) relative pressure zones.

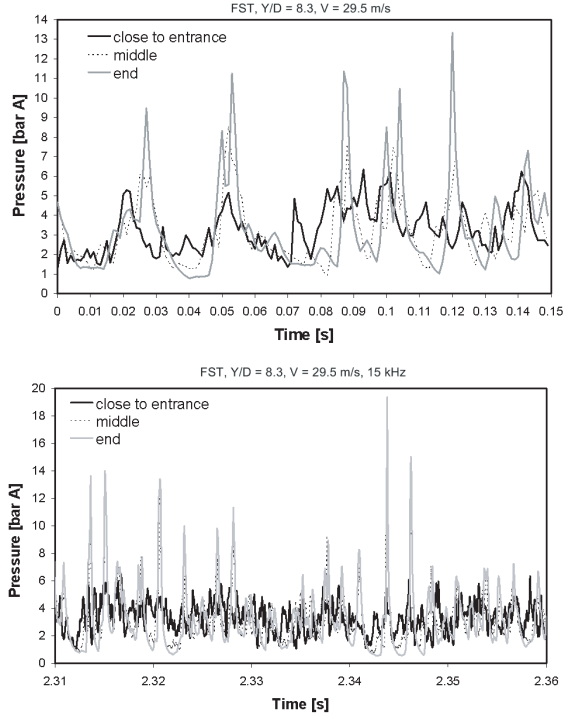

Figure 10.5.: Dynamic pressures at the pool bottom and inside the fissure for stepped confined pools (FST, t/D < 8.3, D_c/D ≤ 16.7), V = 29.5 m/s, Y/D = 8.3, f_s = 15 kHz

10.3.4. Summary

Transient flows inside a close-end fissure can generate pressure oscillations higher than the pressure fluctuations at the pool bottom. Three different transient regimes have been identified:

1. Quasi-simultaneous regular oscillations at middle and end sections of the fissure, generating peaks that may be 2 to 3 times the mean local pressure, and spikes that do not drop below atmospheric pressure (examples in Figure 10.4 c) and d);
2. Quasi-simultaneous regular oscillations at middle and end sections of the fissure for positive relative pressures, to which larger peaks superpose following pressure drops below atmospheric pressure. Peaks up to 5 times the corresponding average incoming kinetic energy of the jet are measured, i.e. 21 bar (examples in Figure 10.3);
3. Similar situations to previous but with time lags in the order of 1 - 4 ms between the time series at middle and end sections of the fissure (examples in Figure 10.5).

In the cases where the formation of a gas cavity is the most plausible explanation for the existence of constant low pressure intervals, the time series at the middle section do not seem to be concerned by the presence of such cavity. However, if collapse of the cavity occurs in between the middle and end sections, the time series at the middle section also shows a sudden rise of $p(t)$.

10.4. Amplification of pressure fluctuations inside a closed-end fissure

10.4.1. Comparison of dynamic pressure coefficients between pools with flat bottom (FB) and narrow pools (FC)

To illustrate the influence of pool geometry in pressure fluctuations inside a closed-end fissure, dynamic coefficients for a pool with flat bottom and the narrowest confined pool tested are presented in Figure 10.6 and in Figure 10.7. Others types of fissures have been studied by Bollaert (2002b) in pools with flat bottom.

$C_{p'}$ inside the fissure are higher in pools with flat bottom for Y/D values about the core development length and for deep pools, as a results of high intermittency at the water-rock interface and of fully developed impact conditions respectively. $C_{p'}$ estimates obtained with the FC pool are generally much lower than those obtained with a flat bottom for Y/D $>$ 5. For Y/D = 4.2 there is an increase in $C_{p'}$ in the laterally confined diffusion case. This corresponds to the enhancement of jet development induced by the geometry of the pool. For both types of pools, $C_{p'} > 0.12$. In submerged jet conditions, $C_{p'}$ is ≈ 0.15 for jet velocities between 10 and 30 m/s. $C_{p'}$ higher than 0.25 are observed for every velocity with the FB pool, whereas for the FC pool such cases occur only for V = 9.8 m/s and V $\geq$ 24 m/s. Overall, the FC pools reduce $C_{p'}$ values inside the fissure, save for shallow pools.

The corresponding positive extreme pressures (Figure 10.7) follow a similar trend. $C^+_{p'}$ estimates for deep FC pools are lower than the values obtained for Y/D = 5.6 and 9.3 with FB pools. For Y/D = 9.3, $C^+_{p'}$ drops from 4.8 to $\approx$ 1.5; for Y/D = 5.6, $C^+_{p'}$ drops from 4.5 to 2.5. Only for Y/D = 4.2 does $C^+_{p'}$ increase from 1.50 to 4.50 regarding the corresponding values in pools with flat bottom.

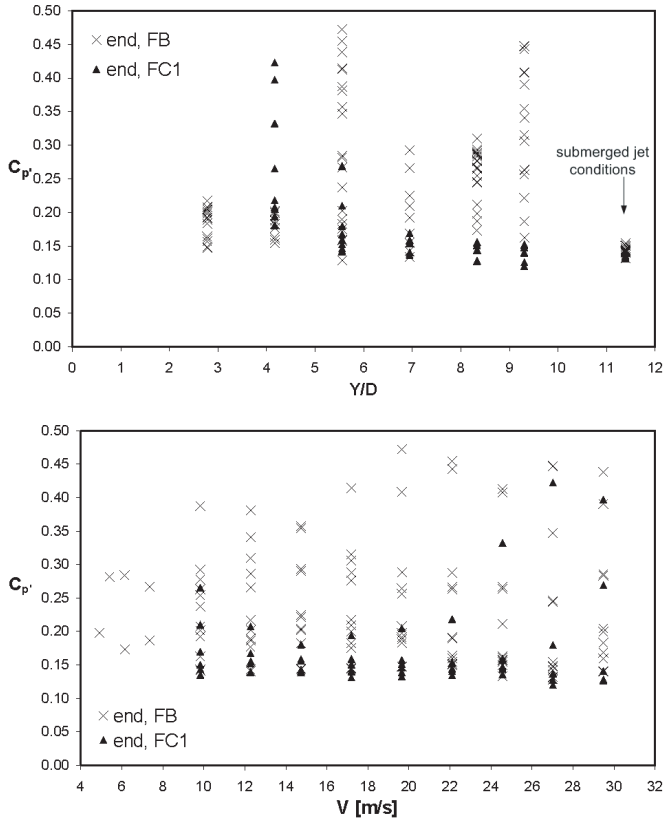

Figure 10.6.: Dynamic pressure coefficients $C_{p'}$ for V = 10 - 30 m/s. Test series FB3 and FC1.

In terms of velocities, $C_{p'}^{+} > 2$ are only found in FC pools for V > 24 m/s. In summary, positive extreme pressures in deep and transition FC pools tend to decrease regarding values in corresponding pools with flat bottom (FB). However, higher $C_{p'}^{+}$ may be generated in FC pools for shallow conditions; this is observed in the experimental tests for V > 24 m/s.

Negative extremes pressure fluctuations (i.e. C_p^{-}) are generally lower in FC pools than in pools with flat bottom (FB). C_p^{-} estimates in FC pools are not higher than 0.80, whereas for pools with flat bottom C_p^{-} can reach 1.50. Overall, these conclusions are valid for the range of velocities tested.

For narrow FC pools, generally $C_p^{-} < C_p^{+}$ and thus pressure PDFs inside the fissure are positively skewed.

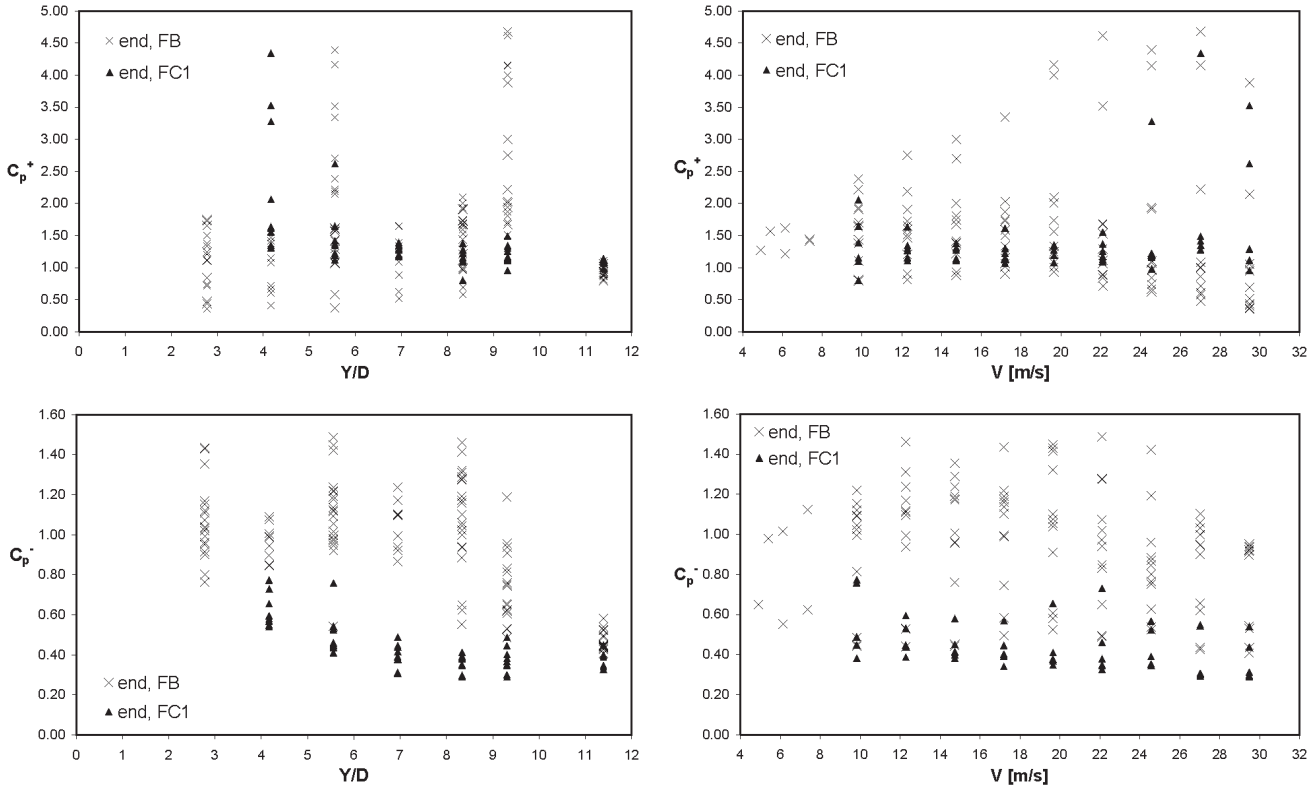

Figure 10.7.: Extreme pressure coefficients $C_{p'}^{+}$, $C_{p'}^{-}$ for V = 10 - 30 m/s. Test series FB3 and FC1.

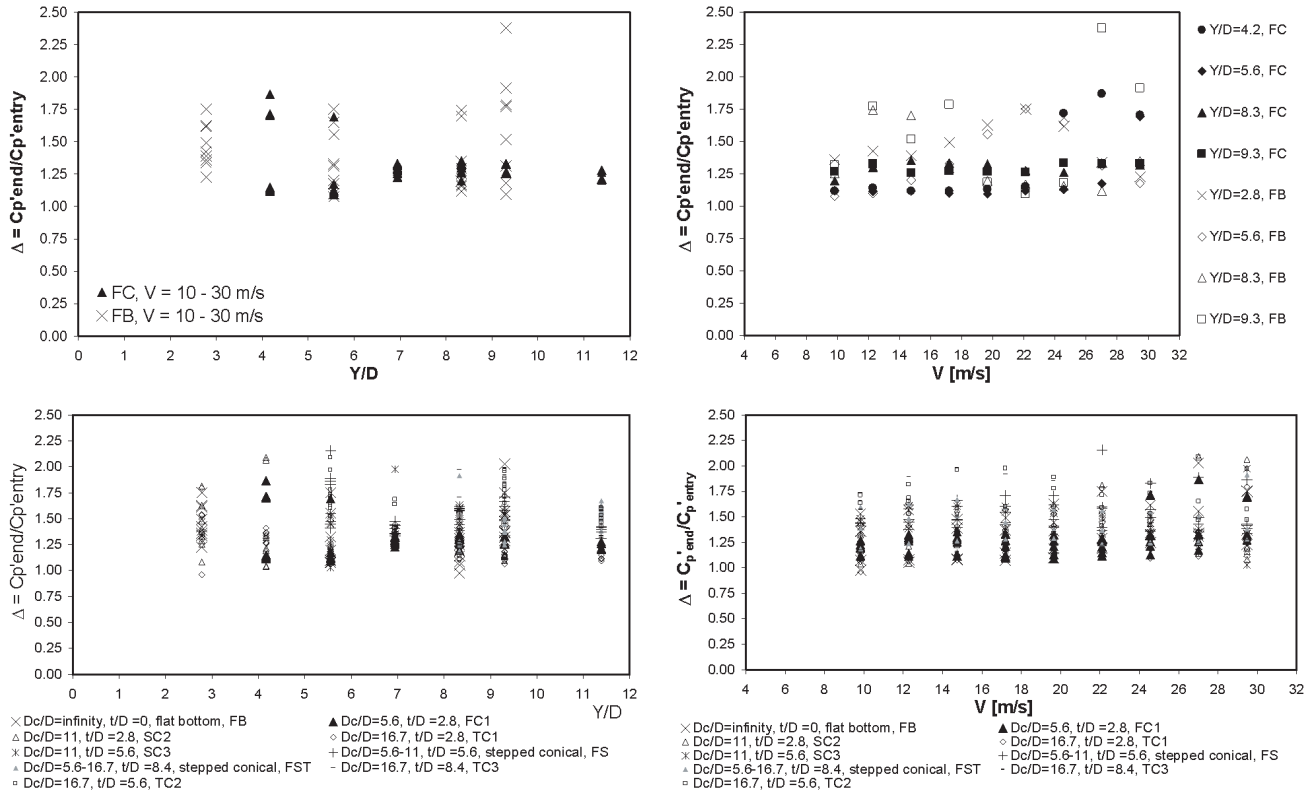

Figure 10.8.: Transient ratio Δ for V = 10 - 30 m/s: top row, direct comparison between pools with flat bottom (FB) and narrow pools (FC); bottom row, analysis of bundled data for all pool geometries (Note: these plots are meant to show envelope values and not for detailed interpretation of individual series). Test series FB3, FC1, SC2, TC1, SC3, TC2, TC3, FS, FST.

10.4.2. Amplification in terms of pressure fluctuations: the transient ratio

The ratio of the RMS values of transient pressure fluctuations at the end of the fissure to the impact pressure fluctuations close to the entry of the fissure is defined as:

$$\Delta = \frac{C_{p',end}}{C_{p',y/D=0.35}} = \frac{\sigma_{end}}{\sigma_{y/D=0.35}} \tag{10.4}$$

and is named transient ratio Δ. It is an ensemble parameter based on 3-min ergodic estimates of σ. The accuracy of σ estimates was discussed in Chapter 6. A direct comparison of pools with flat bottom and narrow pools is presented in Figure 10.8. An analysis of bundled data from all tests with the close-end fissure is presented in the same figure (bottom row).

A direct comparison of measurement in FB and FC pools shows that $\Delta > 1$ for all relative pool depths Y/D and jet velocities investigated. The most significant difference is that Δ values for narrow pools with Y/D = 8 - 10 are significantly lower that those measured in pools with flat bottom. In narrow pools (FC), Δ is only > 1.25 for a few cases with V > 24 m/s in shallow conditions (i.e. Y/D ≤ 5.6).

When considering the bundle of data from all tests for which measurements inside the fissure were performed, Δ is always larger than 1. There are many situations with $\Delta > 1.25$. Therefore, and without documenting each specific case, amplification of pressure fluctuations inside a closed-end fissure is shown to vary with jet velocity and degree of jet development in the pool. The latter has already been shown to depend on the relative pool depth Y/D and pool geometry.

As shown in classical theory of hydraulic transients, the oscillations depend not only on the boundary conditions at the both ends of the system, but also on the "pipe" mechanical characteristics and length. It should be kept in mind that a single type of fissures is being investigated in order to identify hydrodynamic phenomena in controlled conditions; it is by no means certain that similar fluctuations will occur in nature. Moreover, the increase in σ may not *per se* be relevant for scour, but rather the increase in energy at given frequencies.

10.4.3. Amplification in terms of extreme positive fluctuations: the instantaneous amplification ratio

A direct comparison between extreme positive pressures p'^{+} at the end of the fissure and the characteristic RMS-value at the entry of the fissure allows highlighting the importance of the transient regimes in generating high pressure values.

Sampling extreme fluctuations experimentally demands for very high acquisition frequencies and long duration runs. Sampling regular oscillatory patterns is less cumbersome. In this framework, the analysis of positive extreme pressures inside fissures should be seen as a means to complement, within reasonable laboratory hours, the analysis of transient pressures. As shown in Chapter 6, reasonable estimates of σ can be obtained from 3-min runs but third and fourth-order moments' estimates fall within larger margins.

The ratio of the p'^{+} at the end of the fissure to σ close to the entry of the fissure is herein named the **instantaneous amplification factor** and follows the definition given

by Bollaert and Schleiss (2002):

$$\Gamma = \frac{C_{p+,end}}{C_{p',y/D=0.35}} = \frac{p'^{+}_{end}}{\sigma_{y/D=0.35}} \tag{10.5}$$

This is an instantaneous ratio (1 ms) based on 3-min estimates of p'^{+} and therefore merely indicative of the phenomena. It provides an indication of magnitude of a single p' event and not of a succession of events.

Bollaert (2002b) presented values of Γ for pools with flat bottom and the same fissure, based on σ values obtained in 1-min runs. The FB3 test series that are herein used to define the reference scenario of a pool with flat bottom correspond to different jet issuance conditions that those used by Bollaert (2002b). In the present work, σ and p'^{+} estimates correspond to 3-min runs.

With the present experimental set-up, Γ in pools with flat bottom does not exceed 14, save for Y/D = 9.3 and very high velocities V = 27 - 29.5 m/s. A detailed comparison between narrow pools and pools with flat bottoms is presented hereafter.

Comparison between FB and FC pools

Amplification of impact pressures in underlying fissures is also observed in narrow pools. It occur in pool depths (Y/D < 4.2) typical of shallow pools, normally associated to core jet impact in pools with flat bottom. Γ values as high as 18 for Y/D = 5.6 (V =24.6 m/s) and 15 - 20 for Y/D = 4.2 are measured. They show that the enhancement of core development in FC pools compared to FB pools, can also impact pressures capable of exciting underlying fissures (Figure 10.9). For Y/D = 9.3, measured amplifications are lower for FC than FB. For submerged jet conditions, amplification does not exceed 11 in FC pools. Overall, most of the Γ values are between 6 and 13 for velocities from 10 to 22 m/s.

Ensemble analysis with all pools

The ensemble analysis of all pool geometries presented in Figure 10.9(bottom row) shows that:

- for Y/D = 2.8, Γ values in FB pools are not the highest;
- Γ values for FB and FC pools provide an upper bound of Γ for Y/D = 9.3;
- Γ can reach values as high as 16 in submerged conditions (these values correspond to FST stepped pools);
- in submerged conditions, Γ is ≈ 10 in narrow pools and decreases when the confinement is wider (TC1, the widest confined geometry), in the present experimental installation;
- pools with D_c/D $\leq$ 11 are able to generate Γ values as high as 30 in shallow or transition pools; and,
- a Γ value of 20 is an envelope value that accounts for the large majority of the tested cases, save for a few exceptions in shallow pools.

10.4.4. Summary

Jet diffusion in laterally confined pools may lead to unprecedentedly observed p'^{+} values in shallow pools ($Y/D < 5.6$). Similar values had only been measured previously in deeper

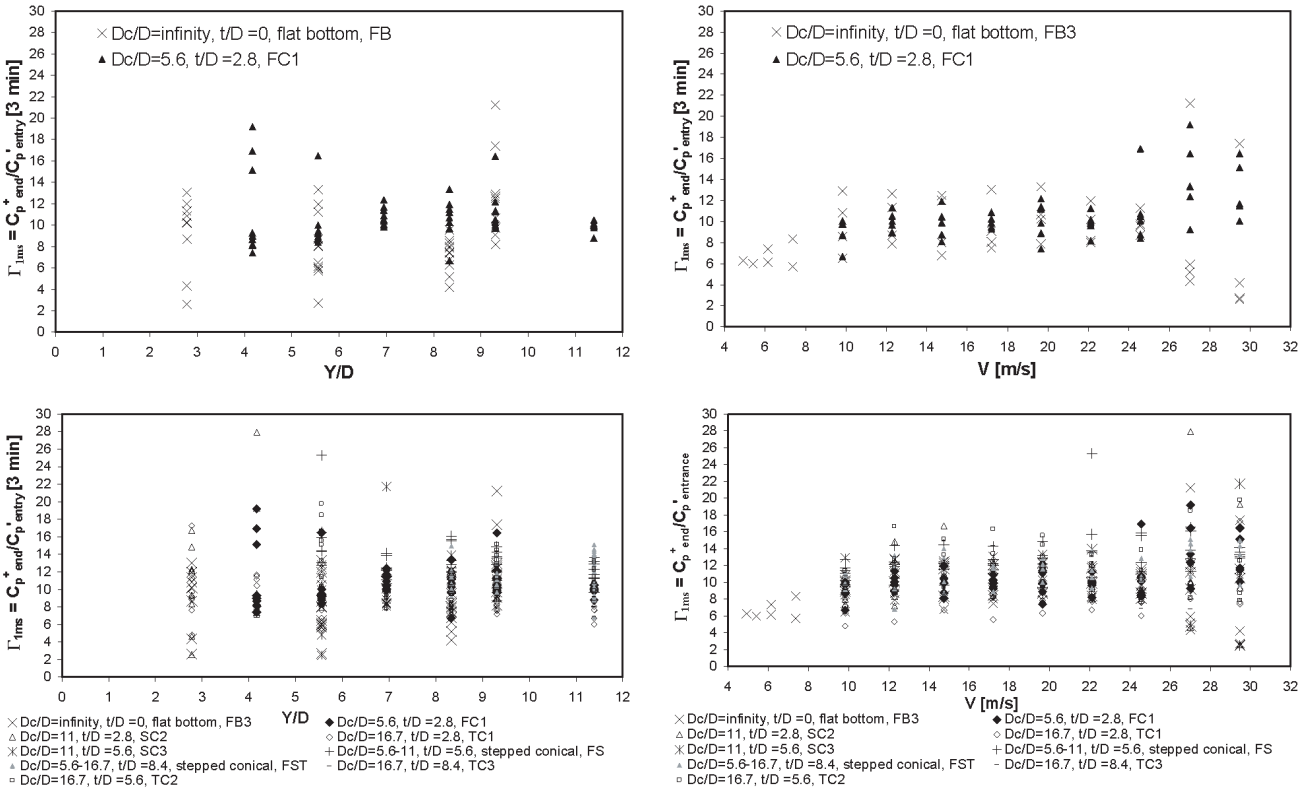

Figure 10.9.: Instantaneous amplification factor Γ for V = 10 - 30 m/s: top row, direct comparison between pools with flat bottom (FB) and narrow pools (FC); bottom row, analysis of bundled data for all pool geometries (Note: these plots are meant to show envelope values and not for detailed interpretation of individual series). Test series FB3, FC1, SC2, TC1, SC3, TC2, TC3, FS, FST.

pools with flat bottom. In deep pools, p'^{+}, p'^{-} and σ values are lower in laterally confined pools, compared to values measured in pools with flat bottom.

For all cases tested, the cumulated energy of pressure fluctuations at the end of the fissure is higher in presence of a lateral confinement (Δ >1). Amplification of pressure fluctuations inside a closed-end fissure is a function of V, Y/D, pool geometry and the characteristics of the fissure.

The experiments are performed in a simplified "rock fissure", i.e. rigid "rock mass", with smooth surfaced, no fissure filling, L = 800 mm, in order to identify hydrodynamic processes in controlled conditions. It is by no means certain that amplification of pressure fluctuations with similar amplitudes will occur in natural rock riverbeds. However, there is a high chance that tubular closed-end fissures with similar length are present at the water-rock interface.

10.5. Pressure distribution of impact and transient pressure signals

Data from several tests are selected to document the variation of pressure distribution from the pool bottom to the end of the fissure (Table 10.1). The evolution of PDF statistical parameters with increasing pool depth is documented in detail for the narrow pool geometry (FC).

Pressure distributions at the end section of the fissure are mainly positively skewed. For very shallow pools for which the core impacts the entrance of the fissure (e.g. Y/D = 2.8, SC2 series), $C_s < 0$ at impact and inside the fissure.

Kurtosis values are mostly positive, except for a few cases for which they are close to zero (i.e. Gaussian). The FC example shows that K inside the fissure decreases with increasing pool depth (i.e. jet development). In the majority of cases, the "propagation" of a PDF of impact pressures from the bottom of the pool to the end of the fissure leads to the increase of Z'_{max} and decrease of Z'_{min} (i.e. tends to zero). In none of these cases pressures inside the closed-end fissure are Gaussian.

10.6. Spectral energy distribution of impact and transient pressure signals

From the entire data base, spectra are computed for envelope cases of shallow pools (Y/D =2.8 or 4.2) and deep pools (Y/D = 8.3 or 9.3) and velocities between 24 and 30 m/s. The spectra computed from measurements inside fissures can be classified in five categories (Figures 10.10 and 10.11):

1. Type 1 - spectra that are originated by core impact conditions at the surface and show amplification peaks at $\approx$ 300 Hz. These spectra follow closely a f^{-1} decay law. Little to no air entrainment is expected in the fissure (direct impact of jet potential core at the entry). Considering the peak as the 1^{st} harmonic of a resonance mode, the mean celerity computed using equation 10.3 is a = 960 m/s. Observed with data from series 3FB020Q100, 2SC020Q100 and 1TC020Q100.

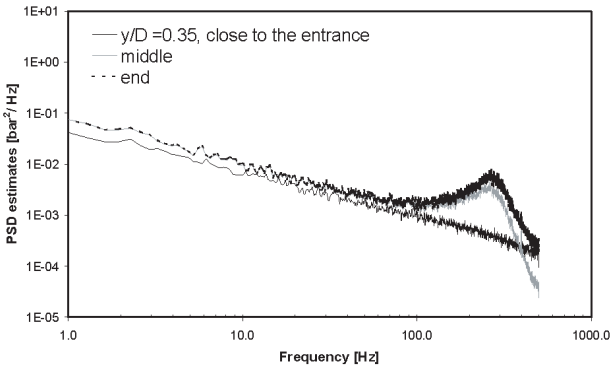

a) Type 1, FB3, Y/D = 2.8;

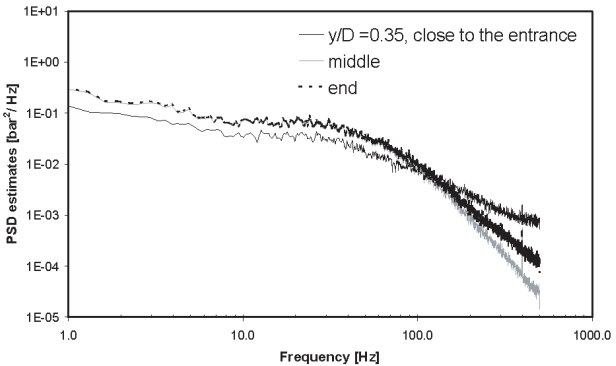

b) Type 2, FB3, Y/D = 2.8;

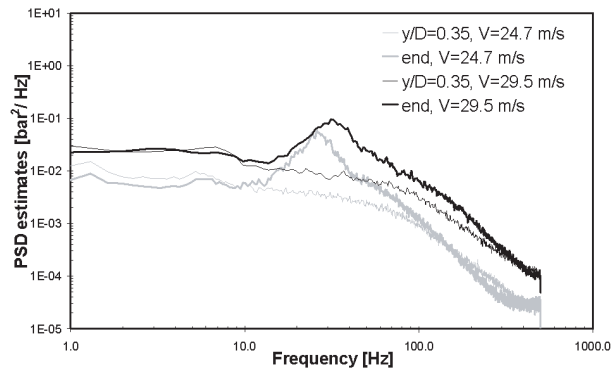

c) Type 3, 1FC, Y/D = 4.2;

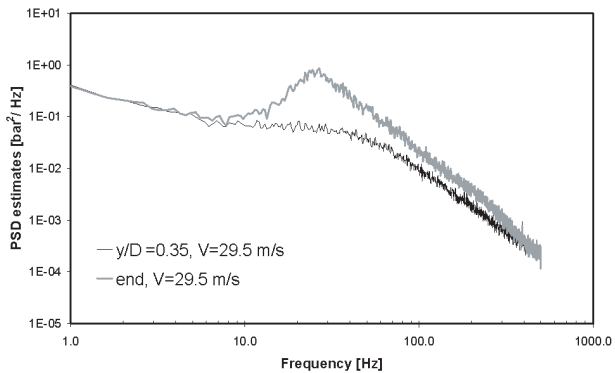

d) Type 3, FB3, Y/D = 9.3, 29.5 m/s;

Figure 10.10.: Types of spectra inside a closed-end fissure, as a function of pool geometry and jet impact conditions at the pool bottom, for velocities between 24.6 and 29.5 m/s.

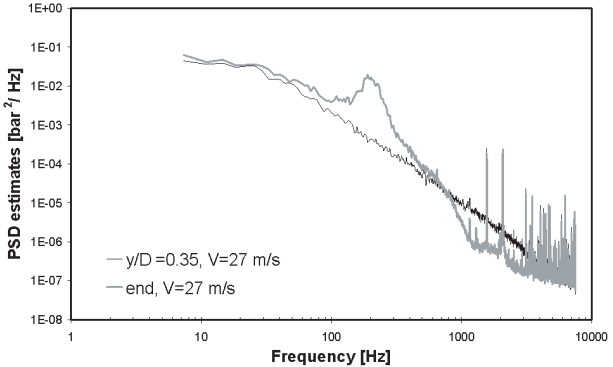

e) Type 4, 1TC, Y/D = 9.3;

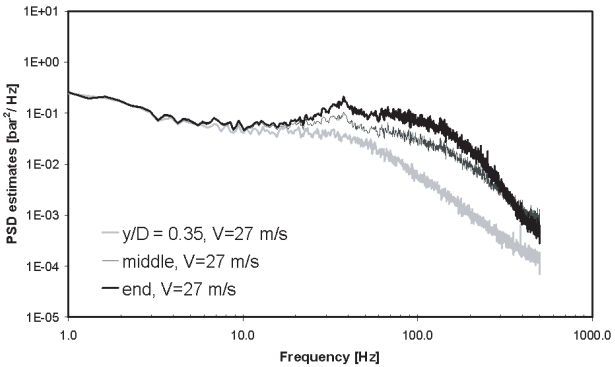

f) Type 5, FB3, Y/D = 9.3, 27 m/s;

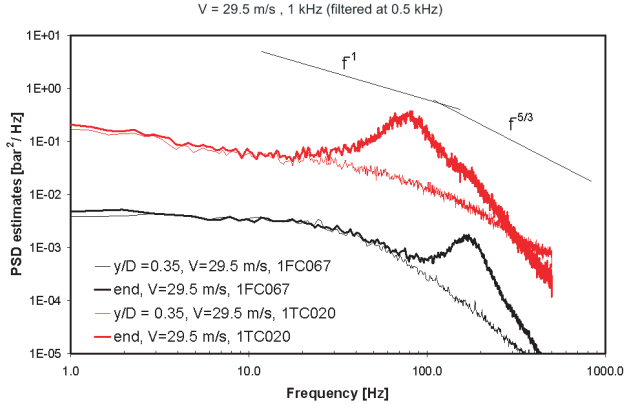

g) Type 6, 1FC Y/D = 9.3, 1TC Y/D = 2.8;

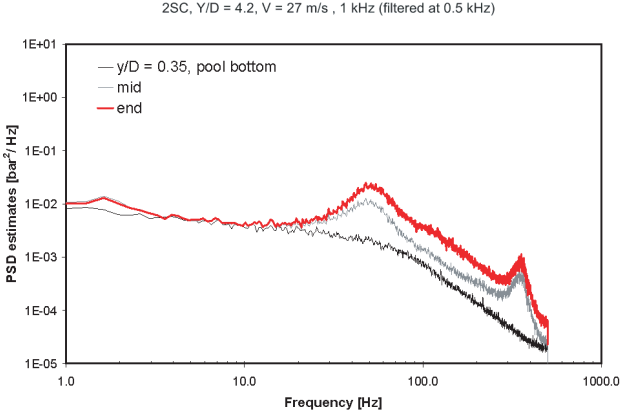

h) Type 7, 2SC, Y/D = 4.2.

Figure 10.11.: Idem to previous.

Table 10.1.: Selected statistical parameters of pressure measurements at the **end of the fissure** in several pools and V = 29.5 m/s. Statistics obtained from data sets with 3 x 65'536 points sampled at 1 kHz, save for FC and 2SC pools with 65'536 points. Time series 2SC for Y/D = 5.6 sampled at 15 kHz.

Pool	Y/D	y/D	$\overline{p}$	σ	p'^{+}	p'^{-}	C_s	K	Z'_{min}	Z'_{max}
			[bar]	[bar]	[bar]	[bar]				
FC1	4.2	0.35	3.000	1.032	7.228	0.572	0.56	-0.08	-2.4	4.1
		end	3.283	1.758	18.905	0.889	1.83	5.16	-1.4	8.9
	5.6	0.35	2.311	0.704	6.530	0.672	1.01	1.40	-2.3	6.0
		end	3.047	1.192	14.650	1.110	1.86	5.85	-1.6	9.7
	6.9	0.35	1.952	0.489	5.307	0.635	0.89	1.28	-2.7	6.9
		end	2.521	0.624	8.241	1.137	1.33	3.32	-2.2	9.2
	8.3	0.35	1.855	0.431	4.358	0.477	0.81	1.00	-3.2	5.8
		end	2.441	0.568	7.388	1.120	1.18	2.55	-2.3	8.7
	9.3	0.35	1.811	0.420	5.014	0.366	0.86	1.19	-3.4	7.6
		end	2.674	0.559	6.898	1.390	1.04	1.97	-2.3	7.6
3FB	9.3	0.35	2.980	0.988	7.635	0.551	0.86	0.27	-2.5	4.7
		end	3.020	1.728	20.200	0.670	2.11	7.63	-1.4	9.9
2SC	2.8	0.35	5.482	0.676	7.961	1.209	-1.67	4.19	-6.3	3.7
		end	5.340	0.730	6.963	0.888	-1.73	3.92	-6.1	2.2
	5.6	0.35	2.077	0.388	3.970	1.101	0.73	0.74	-2.5	4.9
		end	2.160	0.488	4.750	1.031	1.08	1.79	-2.3	5.3
1TC	9.3	0.35	2.009	0.377	4.448	0.796	0.78	0.93	-3.2	6.5
		end	1.077	0.444	4.513	-0.380	0.98	1.86	-3.3	7.7
2TC	6.9	0.35	3.293	0.657	6.144	1.327	0.36	-0.10	-3.0	4.3
		end	2.254	0.842	7.381	-0.409	0.68	0.56	-3.2	6.1
3TC	9.3	0.35	3.460	0.647	6.480	1.395	0.26	-0.22	-3.2	4.7
		end	2.367	0.858	7.555	-0.362	0.57	0.27	-3.2	6.0
FS	6.9	0.35	2.169	0.602	6.761	0.579	1.12	2.01	-2.6	7.6
		end	1.163	0.813	9.766	-0.643	1.45	3.64	-2.2	10.6
FST	9.3	0.35	1.938	0.425	4.733	0.648	0.84	1.04	-3.0	6.6
		end	0.990	0.539	5.070	-0.520	1.07	2.01	-2.8	7.6

2. Type 2 - spectra that have slopes milder than f^{-1} for f $<$ 40 Hz and show a transition into the dissipation range at $\approx$ 40 Hz. They are generated by transition impact conditions. Observed with data from series 3FB020Q120 and 2SC020Q120.

3. Type 3 - spectra that originate from developed jet impact conditions and show an amplification peak within 30-40 Hz. No other amplification peaks at frequencies multiple of these values are shown. Observed with data from series 3FB067Q120, 1FC030Q100-Q120 and FST060Q120.

4. Type 4 - spectra that originate from developed jet impact conditions and show a first amplification peak at about 200 Hz. Other amplification peaks can be identified at f $>$ 1 kHz. Between the first peak and the second one at $\approx$ 1.6 kHz, there is significant energy decay. In these conditions, n = 3 - 4 according to equation 10.2. Observed with data from series 1TC067Q110 (15 kHz).

5. Type 5 - spectra that originate from developed jet impact conditions and show an amplification hump covering a very large range of frequencies. Observed with data from series 3FB067Q110.

6. Type 6 - spectra that originate from developed jet impact conditions and show an amplification peak between 90-110 Hz and a large hump. Observed with data from

series 1FC067Q120, 1TC020Q120.

7. Type 7 - spectra that originate from developed jet impact conditions and show a first amplification peak at 50 Hz and a second one between 200-300 Hz. The time series shows that there might be column separation, similarly to the time series of spectra Type 3. Observed with data from series 2SC032Q110.

Pressure amplification inside fissures is not exclusive of deep pools. It is also observed in shallow laterally confined pools for which the jet is developed at impact. Amplification can hardly be associated with resonant conditions since multiple harmonic peaks are missing in most of the spectra. Higher harmonics may be out of the measured range of frequencies of 1 kHz, as shown in spectrum type 4.

10.7. Influence of the dimensions of the fissure's entry on the transfer of impact pressures to the rock

10.7.1. Transition from free surface to pressurized flow

The transition from free surface pool flows to pressurized "pipe" flow inside the fissure is a key feature of the rock scouring process. Kobus et al. (1979) showed that stagnation conditions are modified if the impact surface of the foundation is porous, e.g. loose blocks or gravel with voids in between. In the present case, the opening of the fissure is right at the jet axis. Mass exchange may occur between the pool and the fissure. Thus, velocity at stagnation may not be exactly nil.

The pressure gradient at the entry of the fissure is quite important ($\overline{p}$ between 0.2 and 1.00 $V_0^2/2g$), as well as the pressure fluctuations (σ between 0.1 and 0.30 $V_0^2/2g$) for the range of jet velocities and relative pool depths tested. The fissure being initially filled with water at atmospheric pressure, it can be assumed as non compressible. As soon as pressure fluctuations start stimulating the volume of water in the fissure, some exchange of mass may occur, including water and eventually air.

Transducer placed close to the fissure entry, inside the fissure already, were damaged by local pressure fluctuations, as reported by Bollaert (2002b). That location correspond to a reflection node for the transient regimes inside the fissure. Local pressure values may be very high.

As mentioned in Chapter 7, there is a high likelihood that air bubbles at stagnation are less than 1 mm in diameter; in fact, more than 50 % of the intercepted air bubbles are in this range at a distance of 1.4D from the pool bottom (point MP3). Furthermore, void fraction values between 2 to 10 % were measured close to the fissure's entry. Therefore, it is quite likely that some air bubbles are pushed through the 1 mm by 10 mmm fissure's entry section.

At the entry of the fissure, there is a transition from pool flow to pressurised flow. Only turbulent structures that are larger than the dimensions of the fissure's entry may influence the fissure evenly.

The energy of pressure fluctuations at impact is spread in a large range of frequencies. For developed jet impact conditions, energy is carried by large structures at low frequencies, redistributed down the energy cascade up to frequencies in the order of 20 to 200 Hz, when

spectra enter the dissipation range. If the dimension of the fissure is small, one may expected that it will interfere with the propagation of pressures generated by small structures (i.e. high frequencies). The influence of small structures will be averaged in space. The larger the fissure is, the lower are the frequencies concerned by this process. These hypothesis are the basis of the following mathematical analysis.

10.7.2. Frequency-domain analysis of scale-averaging of turbulent structures

Instantaneous pressures (i.e. $1/f_s$) may not influence the entire entry section of the fissure. Pressure measurements at several locations along the entry would be required to compute the actual pressure fluctuations acting on the fissure. Such data are not available. However, one can estimate the impact pressures over a given length based on measurements at the closest point to the fissure and on the Taylor Hypothesis of "frozen" turbulence.

The Taylor hypothesis of local turbulence homogeneity postulates that turbulent structures may be assumed to travel at given average velocity U during a given time span t (or over a given distance Δx). All scales of turbulence travel at the same velocity u within the reach Δx. This hypothesis can be found in reference books of turbulence theory , e.g. Chassaing (2000).

Based on this hypothesis the average pressure fluctuations over Δx can be obtained from the following procedure. Pressure fluctuations at a given point are defined in the frequency domain as (note: no $'$ is used for fluctuations in this development):

$$p(t) = \sum_k \widehat{p_k} e^{ikt} \tag{10.6}$$

where k is the wave number (i.e. $2\pi \mathrm{n}/\mathrm{T}$, where n is the number of spectral components) and $\hat{p_k}$ is the spectral component of index k. The pressure fluctuations after a given time interval $\Delta x/\mathrm{U}$ are:

$$p(t + \frac{\Delta x}{U}) = \sum_k \widehat{p_k} e^{ik(t + \frac{\Delta x}{U})} \tag{10.7}$$

The average pressure fluctuations over a distance L can thus be defined as:

$$p(t) = \int_0^L \sum_k \widehat{p_k} e^{ikt} e^{ik(\frac{\Delta x}{U})} dx \tag{10.8}$$

Replacing the space integral by a time integral, the average pressure fluctuations become:

$$p(t) = \sum_k \frac{1}{\Delta t} \int_t^{t+\Delta t} \widehat{p_k} e^{ikt} dt \tag{10.9}$$

which after some mathematical development becomes:

$$p(t) = \sum_k \frac{1}{\Delta t} \frac{\widehat{p_k}}{ik} (e^{ik(t+\Delta t)} - e^{ikt}) = \sum_k \frac{1}{\Delta t} \frac{\widehat{p_k}}{ik} e^{ikt} (e^{ik\Delta t} - 1) \tag{10.10}$$

The best way to compare the original signal at one point to that of the averaged pressure fluctuations over a given distance (or time interval) is to compute both spectra. The variance of the average pressure fluctuation series is:

$$\sigma^2 = \frac{1}{T}\int_0^\infty < p(t)p'(t) > dt \tag{10.11}$$

where $'$ is used to distinguish the conjugate function in the complex correlation. The spectrum of the averaged pressure fluctuations (i.e. space-averaged fluctuations) is:

$$< p(t)p'(t) >= \frac{1}{T}\sum_k\sum_{k'}\int_0^T \frac{1}{\Delta t}\frac{\widehat{p_k}}{ik}e^{ikt}(e^{ik\Delta t}-1)\frac{\widehat{p_{-k'}}}{ik'}e^{-ik't}(e^{-ik'\Delta t}-1)dt \tag{10.12}$$

For $k = k'$ (same frequencies) one obtains:

$$< p(t)p'(t) >= \frac{1}{T}\sum_k\int_0^T \frac{1}{\Delta t^2}\frac{1}{-k^2}\widehat{p_k}e^{ikt}(e^{ik\Delta t}-1)\widehat{p_{-k}}e^{-ikt}(e^{-ik\Delta t}-1)dt \tag{10.13}$$

which can be reduced to

$$< p(t)p'(t) >= \frac{1}{\Delta t^2}\sum_k \frac{\widehat{p_k}\widehat{p_{-k}}}{-k^2}(e^{ik\Delta t}-1)(e^{-ik\Delta t}-1) \tag{10.14}$$

By developing the terms within brackets using:

$$e^{ikt} = cos(kt) + isin(kt) \tag{10.15}$$

one obtains the final expression for the spectrum of the space-averaged pressure fluctuations:

$$< p(t)p'(t) >= \frac{1}{\Delta t^2}\sum_k \frac{\widehat{p_k}\widehat{p_{-k}}}{k^2}(2-2cos(k\Delta t)) \tag{10.16}$$

Therefore, one can compute the spectrum of the average pressures over Δt, i.e. over a given distance on the pool bottom, from the spectrum of the original pressure measurements at point y/D = 0.35. The real spectral components of the original spectrum $\widehat{p_k}\widehat{p_{-k}}$ are computed in author-made routines in MatLab.

The time intervals Δt should be larger than $1/f_s$ and of the same order of magnitude of the Taylor microscale, λ_t. The microscale provides an indication of the persistence of small turbulent scales. The microscale was estimated for pools with flat bottom as:

- 2 - 5 ms at y/D = 0.35 and Y/D = 2.8 to 9.3.
- 2 - 8 ms at y/D = 0.69 and Y/D = 2.8 to 9.3.
- 2 - 3 ms at y/D =2.78 and Y/D = 2.8 to 9.3.

from the autocorrelation function of the time series directly and from the FFT components (test series FB1, FB2 and FB3).

Figure 10.12 presents the results of the computations with Equation 10.16 for the pool with flat bottom, Y/D = 9.3 and jet velocity of 24.6 m/s (time series 1FB067Q100). The reduction of energy at high frequencies is proportional to k^2 (i.e. f^2) and is the more significant the

larger is Δt (i.e. the wider is the fissure's entry). Typically, small structures persisting $<$ 4-6 ms would be averaged out, the spectral energy being reduced for frequencies larger than 40 Hz. The fissure's width has does an important role in filtering out some of the turbulent scales impacting the pool bottom.

In the same figure, two images of measured spectra are also presented. They show spectra at the pool bottom (i.e. y/D = 0.35) compared to spectra at the end of the fissure for shallow pools. The variances at the pool surface and fissure sections are quite similar: they are just slightly higher at middle and end sections. In these two examples, pressure propagation inside the fissure *does not* lead to any particular amplification or transient regimes. The spectra reflect a reduction of energy at high frequencies, similar to the averaging effect computed in this section.

10.8. Modelling of pressure amplification inside fissures under high-fluctuating loading in low-air content conditions

10.8.1. Preliminary considerations

After analysis of the illustrative times series, pressure coefficients, PDF and spectra, several patterns of the response of a closed-end fissure to pool impact pressures have been identified. Several models exist to simulate mathematically transient regimes inside pipe systems. A few have been adapted to lining joints and fissures.

This section presents a model for simulation of transient regimes inside fissures based on the impedance method proposed by Wylie and Streeter (1978).

One of the key questions to answer is if resonance does occur inside fissures. Resonance is a mathematical concept and does not occur in reality like in theory. Peaks have finite amplitude due to the non-linearities of the system (e.g. friction losses) and do not correspond to a single frequency. The energy of a given harmonic is spread over a range of frequencies neighbouring the theoretical resonance frequency. Measured spectra show humps around characteristics frequencies that may correspond to the first harmonic of a resonating system. But the following multiple harmonics are missing. A full match of the acting hydrodynamic loading frequency f_H and the first resonant mode frequency of the fissure system f_F may not be necessary to generate considerable amplification. According Droz (2000), for hydromechanical equipment in power stations a ratio $f_H/f_F < 1$ is normally adopted as a design criteria (i.e. low tunning). However, values higher than 0.6 are known to create near-resonance responses with high amplification (e.g. of vibrations).

Another question is related with the air content in the fissure. If air is homogeneously distributed in the fissure, the liquid can be assumed as a pseudo-fluid with constant density. The wave celerity should be reduced accordingly. If the amount of free air changes, celerity should change. Bollaert (2002b) mentions solubility and gasification of air bubbles as one possible effect of pressure variation inside the fissure. This processes, however, require a given thermodynamic equilibrium (i.e. time) to occur. There have been no attempt yet to verify if this is possible or not. On the other hand, free air bubbles vary in volume with pressure and tend to migrate to lower pressure zones. Therefore, it is not clear what is the behaviour of free air bubbles trapped inside the fissure, if indeed there are some. Measurements at the pool bottom show that there is a high likelihood that some bubbles may enter.

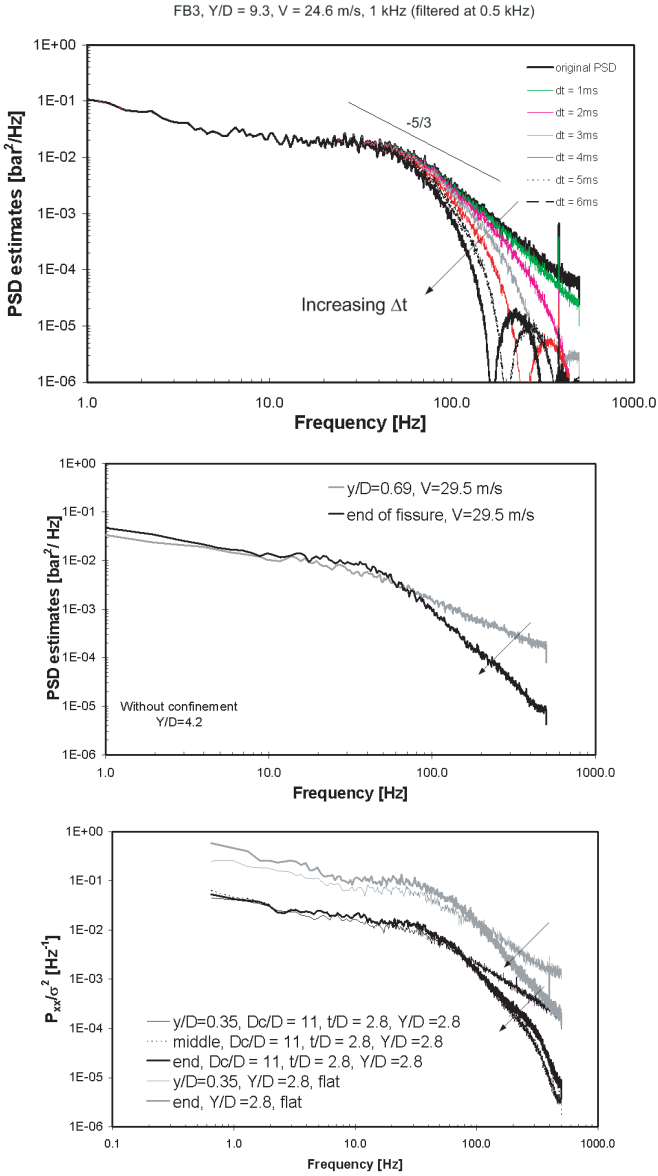

Figure 10.12.: Examples of PSD modification as function of f^2 for different averaging time intervals (or distances). Top: comparison between the **original spectrum** at y/D = 0.35 (test series FB3, V = 24.6 m/s, Y/D = 9.3) and **computed "averaged" spectra**. Middle: example of measured frequency modulation inside the fissure, test series FB1, V = 29.5 m/s, Y/D = 4.2; Bottom, example for SC2, V = 29 m/s, Y/D = 9.3).

Once inside the fissure, free air bubbles may cluster. If pressure drops locally below atmospheric pressure, gas may dissolve from the liquid phase. If it drops below vapour pressure, vapour cavities form. In any of these conditions, rupture of the liquid phase may occur (i.e. column separation) and the system is divided into liquid and gas regions.

10.8.2. Mathematical model for pressure propagation inside closed-end fissures

An analytical linear model solving the continuity and momentum equation is herein developed and compared with the experimental data, in the region not affected by the entrance conditions.

The model is developed in the frequency domain and is dependent on second moment estimations (i.e. variance and/or spectra).

Modelling of the transient regimes occurring inside a close-end fissure under impact of a high-velocity jet is done using the following set of equations, following Fiorotto and Rinaldo (1988); Liu et al. (1997); Bollaert (2002b):

$$\frac{g}{a^2}\frac{\partial h}{\partial t} + \frac{\partial V}{\partial x} + \frac{g}{a^2}V\frac{\partial h}{\partial x} = 0 \quad \text{mass conservation (continuity)} \tag{10.17}$$

$$\frac{\partial(\eta V)}{\partial t} + V\frac{\partial V}{\partial x} + g\frac{\partial h}{\partial x} + RV = 0 \quad \text{momentum conservation} \tag{10.18}$$

in which h is the pressure head (m), V the mean velocity (m/s), a the pressure wave celerity (m/s) and η a coefficient describing the shape of the velocity profile inside the fissure. R is a steady-state friction coefficient defined according to Poiseuille's formula for laminar flow between two parallel planes (Quintela, 1981; Schleiss, 1985):

$$J = RV = \frac{12\nu}{ge^2}V \tag{10.19}$$

where J is the friction slope, ν is the kinematic viscosity (1.16 x 10^{-6} m^2/s for 15°C) and e is the joint thickness (1 mm). For a joint between two parallel planes the hydraulic diameter D is considered $2e$. For conventional laboratory conditions R is 1.2 s/m.

The transient flow equation defined in terms of the piezometric head are used to simulate pressure wave propagation inside a closed-end fissure filled with a two-phase mixture fluid. Free air is assumed to be homogeneously distributed along the fissure. This system of equation does not consider slip or heat transfer between the two phases. The flow mixture is assumed as a pseudo-fluid with density equal to that of the water.

Flow regime is assumed laminar. In fact the narrow geometry of the fissure and the high stiffness of the experimental facility combine to limit flow velocity to $\approx O(10^{-2})$ as well as the Reynolds number to $\approx O(10^{2})$. The rigidity of the experimental metallic facility inhibits compression-expansion waves. For a change to turbulent flow regime to occur, velocity would need to reach 1 m/s, which highly unlikely inside the fissure.

Unsteady friction may be superposed to the steady-state friction in a second stage of model development. In fact, the effect of unsteady friction is considered of secondary importance

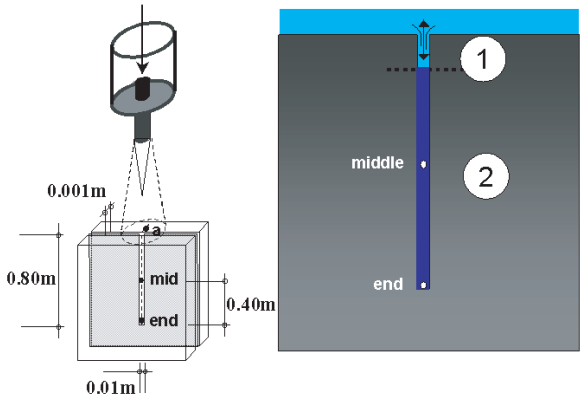

Figure 10.13.: Schematic representation of the fissure system and transducers positions (left hand side), and of the considered flow regions: (1) influenced by the exchange of mass (water and air) with the pool, (2) transient laminar flow region with non-supersaturated water (mobile upstream boundary).

for the calibration procedure, the current priority is identifying and simulating the most important flow features depending on linear friction.

As a first approach, the velocity profile is assumed uniform (η=1). The narrow geometry of the fissure is assumed to prevent any inflexion of the velocity profile over the width (10 mm) of the fissure.

The set of equations is hereafter solved by a spectral method based on the "Impedance method" presented by Wylie and Streeter (1978).

Two boundary conditions are set: a spectrum of the time series measured at the middle of the fissure, and a zero flow velocity at the closed-end. The set of equation is solved along a half length of the fissure (region 2) and extrapolated up to the surface (region 1) - see Figure 10.13.

Calibration is done in the frequency domain by comparing the spectra computed and measured at the downstream point (end of fissure). The integral of the spectra (variance) are also compared. The input data series correspond to a minimum of 25 s and often to 3 min of acquisition. This assures the ergodic character of the input series in terms of the 2^{nd} statistical moments.

Inverting the FFT function can translate results to the time domain, but an instantaneous comparison with an input time series is unrealistic, since the inversion process, as any derivative operation, will be shifted of a constant value. Histograms and spectra can be compared, as performed by Bollaert (2002b).

A mathematical model is developed from the initial set of equations assuming:

- the convection term for velocity in Equation 10.18 is relatively small comparing with the remaining terms;

- the variation of the $\frac{\partial h}{\partial x}$ is much smaller than $\frac{\partial h}{\partial t}$ and thus is normally neglected in Equation 10.17 in waterhammer applications (Streeter and Wylie, 1983);
- the stationary operation of the jet, neglecting variations in pool aeration and joint aeration;
- that pressure measurements with transducers smaller than the width of the fissure are representative of the mean characteristic of the flow and valid for 1D modelling.

The initial set of equation becomes:

$$\frac{g}{a^2}\frac{\partial h}{\partial t} + \frac{\partial V}{\partial x} = 0 \quad \text{mass conservation (continuity)} \tag{10.20}$$

$$\frac{\partial(\eta V)}{\partial t} + g\frac{\partial h}{\partial x} + RV = 0 \quad \text{momentum conservation} \tag{10.21}$$

By performing the time derivative to Equation 10.20 and spatial derivative to Equation 10.21:

$$\frac{\partial^2 V}{\partial t \partial x} = -\frac{g}{a^2}\frac{\partial^2 h}{\partial t^2} \tag{10.22}$$

and

$$\frac{\partial^2 V}{\partial t \partial x} + g\frac{\partial^2 h}{\partial x^2} + R\frac{\partial V}{\partial x} = 0 \tag{10.23}$$

Combining the results:

$$-\frac{g}{a^2}\frac{\partial^2 h}{\partial t^2} + g\frac{\partial^2 h}{\partial x^2} + R\frac{\partial V}{\partial x} = 0 \tag{10.24}$$

Replacing $\frac{\partial V}{\partial x}$ by Equation 10.20, the following expression depending solely on h is obtained:

$$-\frac{g}{a^2}\frac{\partial^2 h}{\partial t^2} + g\frac{\partial^2 h}{\partial x^2} - R\frac{g}{a^2}\frac{\partial h}{\partial t} = 0 \tag{10.25}$$

which can be reorder to finally obtain:

$$\frac{\partial^2 h}{\partial x^2} - \frac{1}{a^2}\frac{\partial^2 h}{\partial t^2} - \frac{R}{a^2}\frac{\partial h}{\partial t} = 0 \tag{10.26}$$

The pressure fluctuations are described as:

$$h(x,t) = \widehat{h_k(x)}e^{ikt} \tag{10.27}$$

and their derivative in time is:

$$\frac{\partial h}{\partial t} = ik\widehat{h_k}(x)e^{ikt} \tag{10.28}$$

where $\widehat{h_k(x)}$ are the spectral components of the fluctuations $h(x,t)$. Placing Equation 10.28 in Equation 10.26 leads to:

$$\frac{\partial^2 h}{\partial x^2} + \left(\frac{k^2}{a^2} - ik\frac{R}{a^2}\right)h = 0 \tag{10.29}$$

A known solution to this quadratic differential equation is (Fiorotto and Rinaldo, 1988):

$$z_k = \sqrt{-\frac{k^2}{a^2} + ik\frac{R}{a^2}} \tag{10.30}$$

where z_k is the hydraulic impedance (complex). According to the impedance method, the spectral components of the pressure fluctuations at a given point in the fissure can be defined as:

$$\hat{h_k}(x) = c_1 e^{z_k x} + c_2 e^{-z_k x} \tag{10.31}$$

where c_1 and c_2 are constants to be defined in terms of the boundary conditions. The input boundary conditions corresponds to the spectral components of measured p' at the middle section of the fissure, here defined as $\hat{P}_k$ (complex). Therefore, at the middle section (x=L/2):

$$\hat{h_k}(\frac{L}{2}) = \hat{P}_k = c_1 e^{z_k \frac{L}{2}} + c_2 e^{-z_k \frac{L}{2}} \tag{10.32}$$

And the end section (x=L), pressures are reflected, and thus:

$$\frac{\hat{h_k}(L)}{\partial x} = c_1 z_k e^{z_k L} - c_2 z_k e^{-z_k L} = 0 \tag{10.33}$$

Solving the 2 x 2 system with Equation 10.32 and Equation 10.33, one obtains:

$$c_1 = \frac{\hat{P}_k e^{-z_k \frac{L}{2}}}{e^{z_k \frac{L}{2}} + e^{-z_k \frac{L}{2}}} \tag{10.34}$$

and

$$c_2 = \hat{P}_k \left(\frac{1}{e^{-z_k \frac{L}{2}}} - \frac{e^{z_k \frac{L}{2}}}{e^{z_k \frac{L}{2}} + e^{-z_k \frac{L}{2}}} \right) \tag{10.35}$$

Thus, the spectral components of the pressure fluctuations are:

$$\hat{h_k}(x) = \hat{P}_k \left[\left(\frac{e^{-z_k \frac{L}{2}}}{e^{z_k \frac{L}{2}} + e^{-z_k \frac{L}{2}}} \right) e^{z_k x} + \left(\frac{1}{e^{-z_k \frac{L}{2}}} - \frac{e^{z_k \frac{L}{2}}}{e^{z_k \frac{L}{2}} + e^{-z_k \frac{L}{2}}} \right) e^{-z_k x} \right] \tag{10.36}$$

The terms inside the large square brackets vary for each wave number k and at every location x. For computational purposes they are named $g_1(x,k)$ and $g_2(x,k)$, the sum composing $g_k(x)$. To obtain the real part of $\hat{h_k}(x)$ the expected value is computed:

$$< \hat{h_k}(x) \hat{h_{-k}}(x) > = < \hat{P_k} \hat{P_{-k}} > < g_k(x) g_{-k}(x) > \tag{10.37}$$

where:

- $< \hat{h_k}(x) \hat{h_{-k}}(x) >$ is the spectra (real) of the pressure fluctuations at a given point x;
- $< \hat{P_k} \hat{P_{-k}} >$ is the input spectra (real) at the middle point of the closed-end fissure; and,
- $< g_k(x) g_{-k}(x) >$ is the real part of the **transfer function** $g_k(x)$.

This model is computed over the entire length of the fissure.

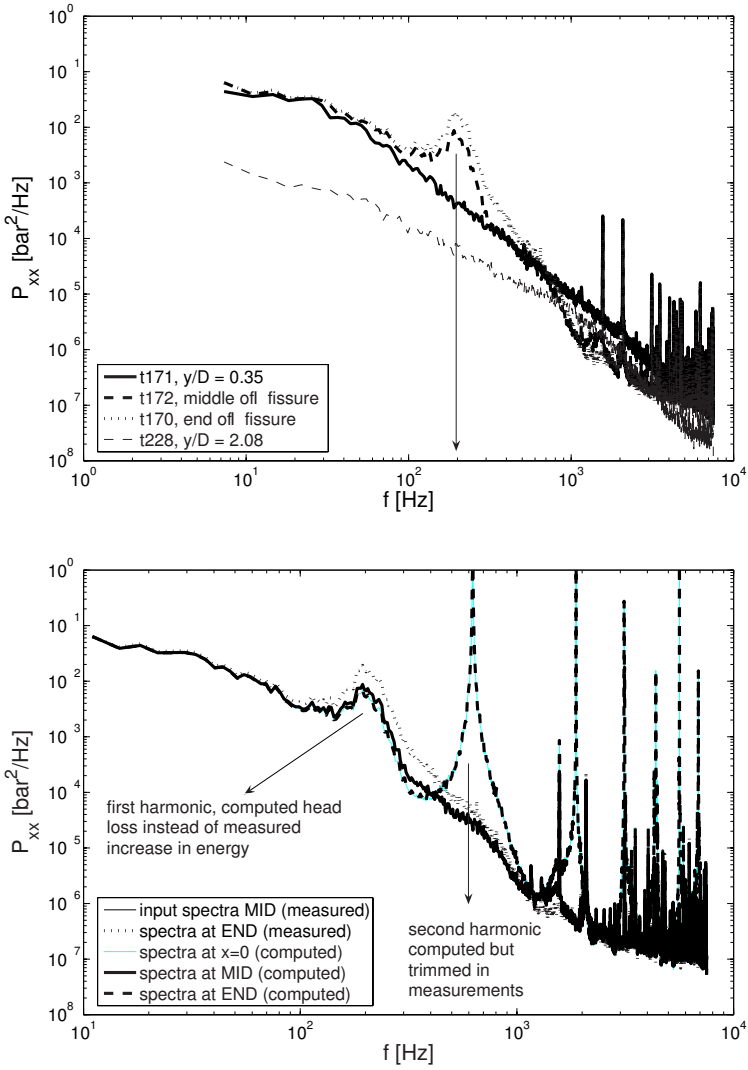

Figure 10.14.: Measured and computed spectra in a pool with flat bottom and inside a closed-end fissure, $D_c/D = 16.7$, t/D = 2.8, Y/D = 9.3 and V = 27 m/s, $f_s = 15$ kHz (test series 1TC067Q110): Top, original PSD function; bottom, $c = 1000$ m/s, computed spectra at "end" and at "x=0", as well as both spectra at "mid" section are superposed.

10.8.3. Analysis of computed spectra at the end of the fissure compared to measured spectra

The first case studied corresponds to the laterally confined pool D_c/D =16.7, t/D =2.8, Y/D =9.3 (1TC067Q110) with a jet at V = 27 m/s - Figure 10.14. Several runs at 15 kHz were performed, with the hardware filter set at 7.5 KHz. The previously measured spectra had a hump at $\approx$ 110 Hz. To check if such hump corresponded to a smeared resonance peak of the first harmonic it was necessary to sample higher frequencies to account for eventual multiple harmonics.

The computed spectra at the end section shows a peak at the same frequency as the measured spectra. A wave celerity of 1000 m/s allows reproducing multiple harmonics that are absent from measurements filtered at 0.5 kHz. Measurements filtered at 7.5 kHz have clearly more energy in between 500-1000 Hz where a second harmonic is expected. This second harmonic is produced numerically. The absence of the multiple harmonics in the measurements is thought to correspond to non-linear effects that are not reproduced in the mathematical model. In fact, the model is linear and does not include the non-linear convolution term, i.e. the convective term for velocity in Equation 10.18. This terms is responsible for the diffusion of energy over a wide range of frequencies. It's numerical implementation in the frequency domain requires extensive developments and was considered of secondary importance at the present stage of research.

The computed spectra at the entry section of the fissure (x = 0 in the local fissure axes) is similar in shape to that at the middle section and is different from the measured spectra at y/D = 0.35 for f $>$ 100 Hz.

The second example - Figure 10.15 - concerns a shallow pool with flat bottom with core impact conditions. Measurements show that there is amplification inside the fissure for peak frequencies of $\approx$ 250 Hz. Computed spectra show that high celerity values between 800 and 1000 m/s can generate transient regimes with a first harmonic oscillations precisely at that frequency. For c = 800 m/s, the second harmonic is perceptible at $\approx$ 500 Hz. One possible reason for wave celerity to be within this range of values could be the presence of a free air content of $<$ 1 %. This possibility can not be ruled out since void fraction measurements close to the entry of the fissure were in the order of 2 % for V = 22 m/s (shallow pools).

A deeper pool also with flat bottom is presented in Figure 10.16 from data sampled at 15 kHz. In this case, the air content measured close to the bottom is $\approx$ 8 % (point MP1 in Chapter 7). However, due to the advanced degree of development of the jet (Y/D =8.3), most of these air bubbles may be deviated to lower pressure zones and not enter the fissure. The entry of air bubbles in the fissure can not be excluded.A considerable difference of energy between the measured signals at the middle and end sections is observed in the range 200-1000 Hz. Numerically, wave celerity values of 600 and 800 m/s are tested. They produce harmonic oscillations that are not found in the measurements. Furthermore, the computed signal is more similar to the input (middle section) signal than to that at the end section. This confirms the occurrence of non-linear phenomena that are not included in the linear model.

A narrow pool that generates oscillations for unprecedented shallow conditions is presented in Figure 10.17. Once more a high wave celerity (i.e. $\geq$ 800 m/s) replicates the input spectra. The difference in energy between the spectra at the middle and end sections is not reproduced.

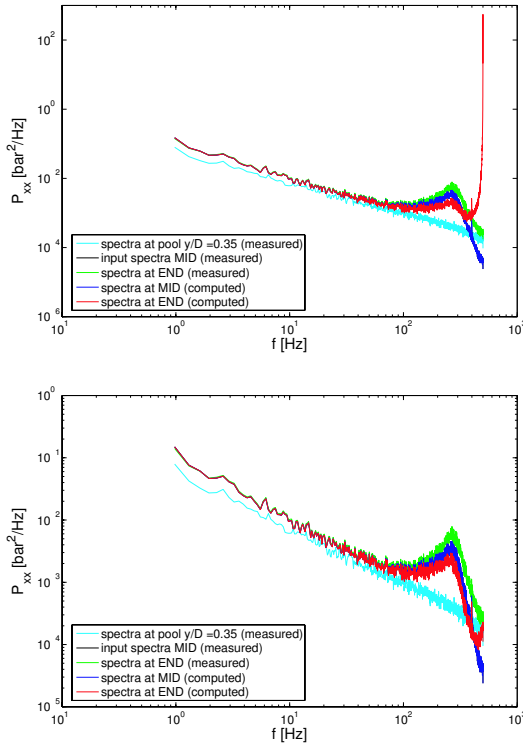

Figure 10.15.: Idem, pool with flat bottom, Y/D = 8.3 and V = 29.5 m/s, f_s = 15 kHz (Test series 3FB020Q120), top: c = 800 m/s; bottom: c = 1000 m/s.

10.8.4. Discussion of the spectral transient flow model

Overall, the measured and computed spectra are in accordance. For deep pools (Y/D=9.3) and high velocities from 27-29.5 m/s, numerical and experimental results fairly agree, within the range of frequencies up to 500 Hz, when assuming a celerity of 1000 m/s. Experimental results allow suspecting of resonance by energy amplification shown in spectra for frequencies as low as 100 Hz. Such peaks are well reproduced in the computational model. However, only the first harmonic frequency is reproduced experimentally, its multiples missing. The numerical model allows identifying the wave celerity of pressure waves, if the frequency of multiple harmonics is known.

In the majority of the computational tests, the spectra measured at the middle and end sections is similar in shape. This is well replicated in the model. However, there is more energy at the end of the fissure than in the middle. This is rather surprising. On the one hand, it may be related to the calibration of the transducers. On the other hand, it may be due to some particular transient phenomena occurring in between these two sections. Numerically, this increase in energy is not reproduced. In fact, the model dissipates energy

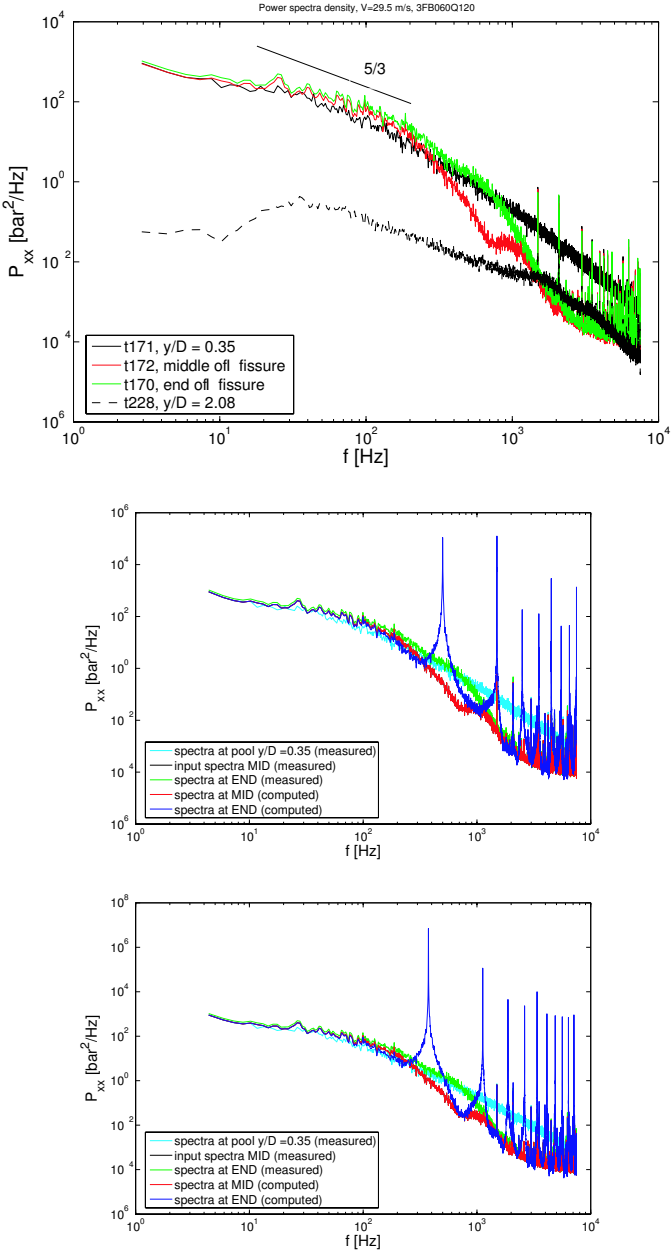

Figure 10.16.: Measured and computed spectra in a pool with flat bottom and inside a closed-end fissure, Y/D =8.3, V = 29.5 m/s, $f_s = 15$ kHz (test series 3FB060Q120): Top, original PSD function; middle, $c = 800$ m/s; bottom, $c = 600$ m/s.

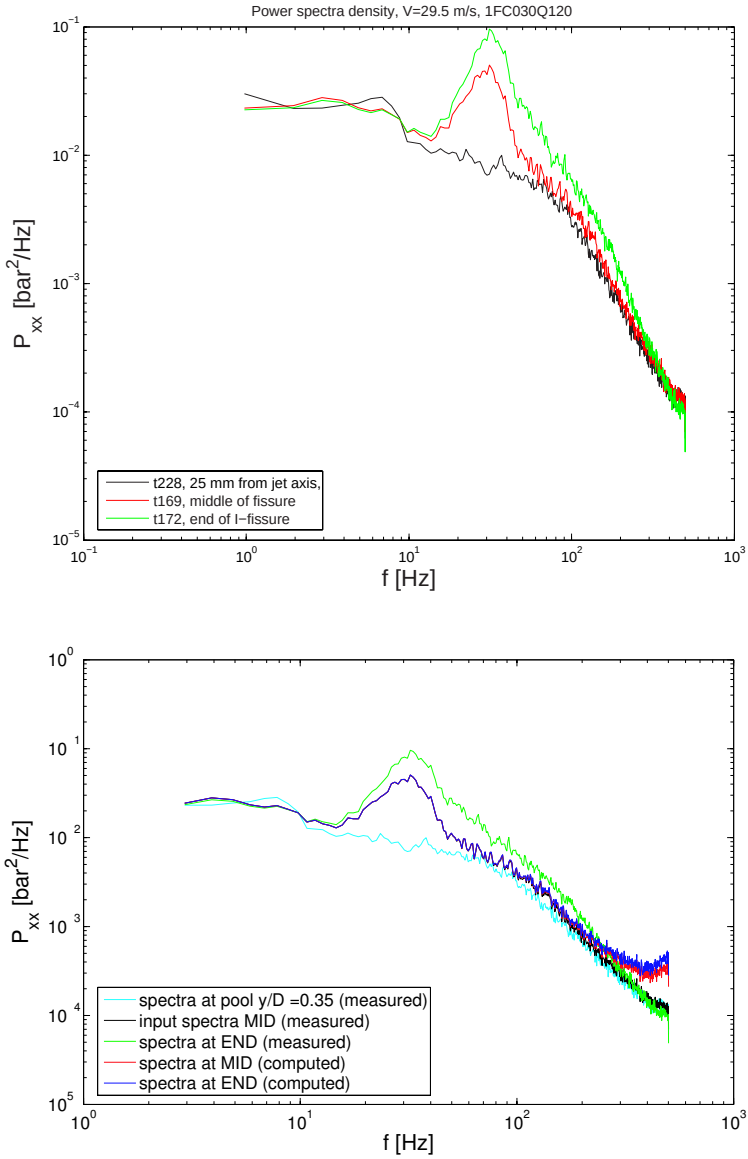

Figure 10.17.: Measured and computed spectra in a laterally confined pool (FC), Y/D = 4.2, V =29.5 m/s, f_s=1 kHz: top, original PSD; bottom, c = 800 m/s.

from the middle section to the end section. For high celerity values and such short distances, the input spectra is almost directly replicated at the end section.

Control runs performed at 15 kHz and filtered at 7.5 kHz show the occurrence of higher harmonics and confirm the resonance hypothesis. An improved correlation between the computed and measured signals is thought to depend on non-linear effects like pressure spreading over frequencies at the vicinity of resonance and unsteady friction effects.

10.9. Conclusions

1. Transient flows inside a close-end fissure can generate pressure oscillations higher than pressure fluctuations at the pool bottom.

2. The enhancement of jet development in the pool increases the energy of impacting pressures in the range of frequencies that are able to excite closed-end fissures. Amplification of pressure fluctuations up to 5 times the incoming kinetic energy is observed in pools with flat bottom for large pool depths (i.e. Y/D $>$ 9) and, for the first time, for shallow depths such as Y/D = 4.2 in laterally confined pools.

3. The analysis of time series of pressure measurements inside fissures allows identifying three different transient regimes, featuring regular oscillations, moderate amplification, very high amplification following pressure drops below atmospheric pressure, as well as combinations of the previous.

3. Jet diffusion in laterally confined pools may lead to unprecedentedly observed p'^{+} values in shallow and transition pools. Similar values had only been measured previously in deeper pools with flat bottom. In deep pools, p'^{+}, p'^{-} and σ values are lower in laterally confined pools, compared to values measured in pools with flat bottom. For all cases tested, the cumulated energy of pressure fluctuations at the end of the fissure is higher in presence of a lateral confinement. Amplification of pressure fluctuations inside a closed-end fissure is a function of V, Y/D, pool geometry and the characteristics of the fissure.

4. Different transient flows were documented. Based on the analyzed data, seven types of characteristic spectra inside close-end fissures have been identified.

5. Modeling of transient flows was performed with a mathematical model based on the numerical impedance method to solve the waterhammer equations in the frequency domain. The model was tested for several types of input spectra at the middle section of the fissure, away from the disturbances at the entry. Core impact and developed impact conditions were considered. Computed spectra at the end section of the fissure are in most cases similar to the input spectra (middle section). The model highlights the importance of non-linear phenomena in the transient regimes inside the fissures identified, for instance, by an increase in energy from the middle to the end sections over large ranges of frequencies. It provides fairly good estimates of power spectra if the air content in the fissure does not excess 0.2 %. Phenomena like air entrainment into the fissure and column separation inside the fissure merit further investigation.

6. The increase in energy at given frequencies may allow establishing a correlation between pressure fluctuations and scouring processes. The question if the frequency of occurrence of the peaks is of interest for rock scour is still matter of discussion.

7. The experiments are performed in a simplified "rock fissure", i.e. rigid "rock mass", with smooth surfaced, no fissure filling, L = 800 mm, in order to identify hydrodynamic processes in controlled conditions. It is by no means certain that amplification of pressure fluctuations with similar amplitudes will occur in natural rock riverbeds. However, there is a high chance that tubular closed-end fissures with similar length are present at the water-rock interface.

11. Analysis of the persistence of pressure pulses at impact and inside rock fissures in view of the definition of a probability-based model for rock block uplift

This chapter present new elements for the definition of the rock block displacement process (Fig. 11.1), based on an analysis of the energy content of pressure pulses of given probability and persistence.

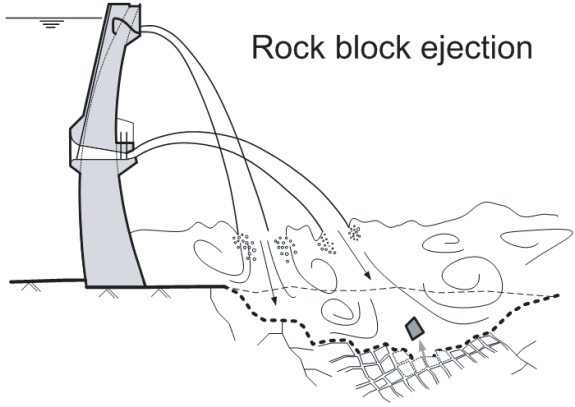

Figure 11.1.: Schematic representation of scour evolution due to the impact of plunging jets: process of block displacement by net uplift pressure gradient.

11.1. Duration of pressures pulses

Previous chapters have shown that pressure fluctuations may reach significant amplitudes both at impact and inside fissures. They may contribute to the process of rock scouring. Bollaert (2002b) compared hydrodynamic stresses at the tip of rock fissures with the local admissible stresses in the rock. The acting stress intensity was obtained from measurements of pressure fluctuations in laboratory using quasi-prototype jets. The resisting stress intensity is defined in terms of the rock characteristics. According to this criteria, the measured pressure fluctuations may cause brittle failure or/and fatigue failure of the rock mass. Several other authors active in the field of hydrodynamic loadings have also shown that

pressure fluctuations are relevant for the process of slab displacement under an hydraulic jump in lined stilling basins (Sanchez-Bribiesca and Fuentes-Mariles, 1979; Fiorotto and Rinaldo, 1992a,b; Bellin and Fiorotto, 1995). However, it is yet not clear which p' events are relevant for each scour process, namely crack propagation and block displacement. Regarding block displacement, Melo et al. (2006) presented experimental work and a stability model for concrete slabs in lined pools. They state that pressure fluctuations are of secondary importance in comparison with mean pressures, due to low spatial correlation of pressure fluctuations, both in the upper and lower faces of slabs, for open joint systems. Despite reproducing reliably aerated jets, their experiments were performed with low velocities. However, Melo et al. (2006) work show that the discussion about the role of pressure fluctuations in rock block uplift is far from finished.

Yuditskii (1963) performed extensive experimental work focusing on block displacement in a dam model at reduced-scale. He outlined the process of scouring, investigated the onset of displacement, registered the corresponding pressure gradient and described the influence of the joint thickness. Resulting pressure fluctuations were considered relevant for scouring, participating in the failure of the last bridges of rock connecting a block with the matrix. Displacement is defined as depending from a pressure field of amplitude larger than the mean uplift pressures and acting on the block for sufficient long time for water to fill in the gap. The notion of spatial correlation is implicit, excluding the high local pressure peaks from the main role on the displacement process. Accordingly, a given persistence in time seems required.

Montgomery (1984) studied the displacement of loose rock blocks under hydraulic jumps, focusing on the action of mean pressures. Annandale et al. (1998) performed large-scale experiments with concrete elements under plunging jets to validate the semi-empirical "Erodibility Index". Amelung (1996) investigated the movement of concrete cubes under the impact of submerged vertical jets. In any of these cases, the influence of dynamic pressures was not directly assessed. Several types of mechanisms and stages of rock displacement were identified. Blocks tend to vibrate, lift, emerging partially or fully from the rock mass, have their edges smeared by "ball-milling", and eventually end up being swept away by action of pool currents (e.g. by action of shear stresses at the pool boundaries). These tests have shown that displacement is hardly instantaneous. It is time dependent. Most of the previous research has been undertaken with loose material and, thus, the process of crack propagation under high hydrodynamic pressures is not considered. Crack propagation is also time-dependent since acting pressures vary in time: brittle fracturing of the rock mass depends on the frequency of high enough pressure peaks, whereas fatigue fracturing on the number of pressure cycles of given amplitude. Therefore, for crack propagation and block displacement a given compromise between pressure amplitude, duration and periodicity is necessary.

Duration curves of pressure fluctuations at impact with the pool bottom and at the end section of a closed-bed fissure are presented in Figure 11.2. If pulses of duration Δt larger than the duration of individual samples ($1/f_s$) and averaged during Δt are considered, the duration curves tend to flatten. The intervals of 4 and 8 ms are of the same order of magnitude as the microscale, i.e. of small turbulent structures, and the largest (128 ms) of that of the integral timescale. Very high pressure pulses inside the fissures persist for less than 4 ms (Figure 11.2d) and their lifetime is less than 2 % of the total time of a representative discharge (i.e. acquisition). Overall, pressure fluctuations at the pool bottom are 80 % of the time within 1 bar of $\overline{p}$, whereas inside the fissure it drops to 60 %.

Inside the fissure, the distribution of pressure fluctuations is positively skewed, as shown in

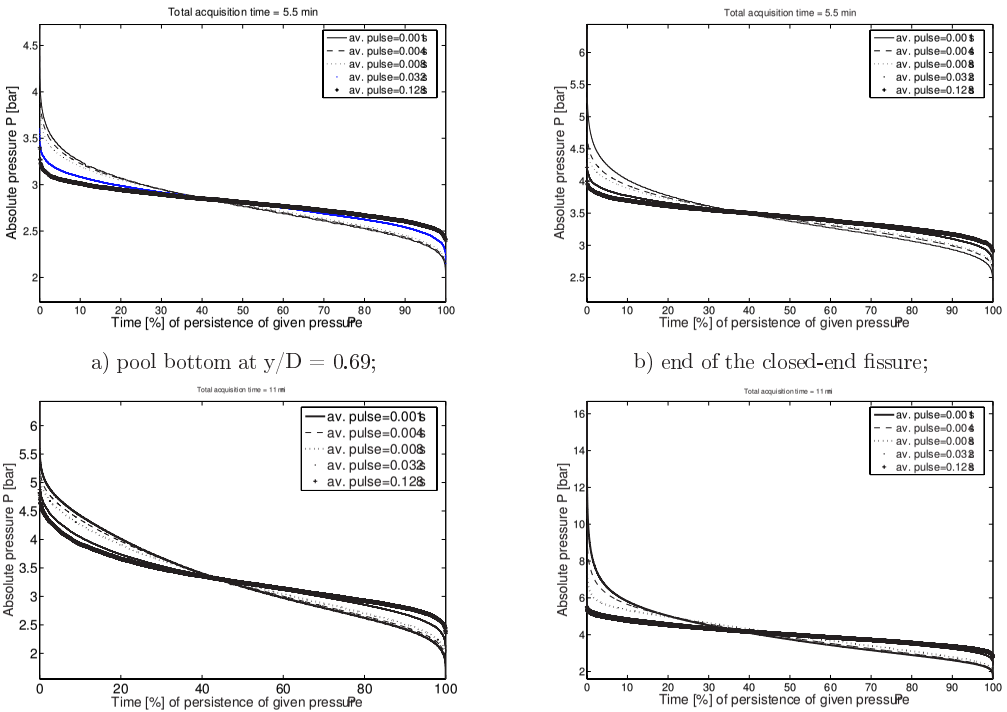

a) pool bottom at y/D = 0.69;

b) end of the closed-end fissure;

c) pool bottom at y/D = 0.69;

d) end of the closed-end fissure.

Figure 11.2.: Relative duration curves of pressures pulses of 1, 4, 8, 32 and 128 ms, in a pool with flat bottom and V=24.6 m/s (FB1 series): top row, Y/D = 11.4 (submerged jet outlet), total of 10 x 32'738 data point sampled at 1 kHz, ≈ 5.5 min); bottom row: Y/D = 9.3, total of 10 x 65'536 data point sampled at 1 kHz, ≈ 11 min (pressures vary from 0 to 6 bar on left figure) .

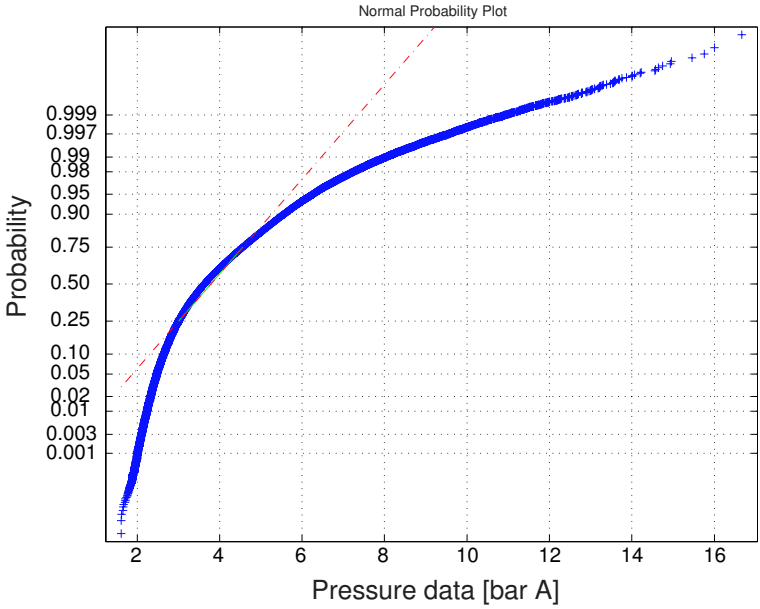

Figure 11.3.: Comparison between the data and a gaussian fit to the data at the end of the fissure, in a pool with flat bottom, V=24.6, Y/D = 9.3, 3 x 65'536 data point sampled at 1 kHz (FB1 series).

Chapter 10. In the example presented in Figure 11.3, a Gaussian pDf provides a reasonable fit to the data for probabilities within 0.20 and 0.90. Beyond those probabilities, differences between a gaussian fit and the measured data can be significant.

Pressure fluctuations at impact and inside the fissure have considerable spectral energy up to 150-200 Hz, but identifying what is the spectral content of pressure pulses with given persistence and probability is not straigthforward. If either the spectral content, the persistence, or the (cumulated) probability of a given pressure pulse is below a critical value, it may eventually be considered irrelevant for a given scouring process. The definition of such critical value is still a topic of research.

On the one hand, the amplification of pressure fluctuation inside fissures may generate high instantaneous pressure pulses. These pluses may lead to crack propagation. The duration of such pulses is small.

Amplification may also generate oscillating waves with regular frequency. They may contribute to crack propagation by fatigue and, once blocks are formed, to their vibration and milling. The duration of these oscillations may be of the order of magnitude of the integral scales I_t of the pressure field at surface, i.e. $O(10^{-1}\text{-}10^{-2})$s in the present facility.

On the other hand, pressure fluctuations in rock fissures may also contribute to the displacement of rock blocks. This process is analysed in detail in the following sections.

11.2. Three-dimensional dynamic uplift of rock blocks

11.2.1. Definition of rock block uplift

Uplift is the process of vertical block displacement out of the rock mass and into the pool flow. It occurs by overbalance of the stabilising loads (submerged weight, impact pressures, eventual contact forces with neighbouring rock) acting on the block, by the uplift pressures installed in the fissure around the block.

Rock block uplift is a three-dimensional process. It may, however, be assumed as a 2D or even a 1D process, depending on the relative dimensions of turbulent structures characteristic of the flow pattern (e.g. depth-dependent or geometry-dependent roller) and the rock blocks.

A schematic representation of theoretical approaches is presented in Figure 11.4 and discussed in the following paragraphs.

At the bottom of 3D scour hole, a rock block is submitted to a 3D hydrodynamic flow field. Depending on the degree of jet development, it may or may not be under the direct impact of the jet core. This would correspond to a highly correlated and persistent pressure field acting on the block.

For developed jets, the block is under a turbulent pressure field that can be characterised by two-dimensional integral scales in space and persistence (i.e. in time). Assessment of critical conditions for displacement requires a dense mesh of measuring points in the space.

Pressure fluctuations along the perimetrical fissure entry are responsible for the pressure field under the block. The uplift pressures created have to overbalance the stabilising action of the weight of the block and of the surface pressure field acting on the top of the block. The surface pressure field varies instantaneously. A balance between instantaneous surface pressures over a surface and correlated pressures over a perimetrical joint entry is the key for the definition of stabilising or destabilising conditions.

If blocks are larger than the integral scales, then the pressure loading along the perimetrical fissure entry is uneven. This unevenness is more important in reducing the surface pressure field than the fissure pressure field, since the travel time of pressure waves is at least 10 times higher inside the fissure.

If high pressure fluctuations are generated at a given location of the fissure they may propagate fast over the whole 3D joint, in particular if there is no opposing event generated elsewhere. However, the larger is the surface of the fissure's entry, the lower is the probability that very high pressure pulses are generated inside this joint. This is a direct consequence of the averaging of impact pressures transmitted to the fissure and of the 2D dispersion of local events over a given distance.

If the turbulent flow pattern is rather constant in one direction, a 2D approach can be used to investigate the stability of rock blocks. The analysis is done *per meter*. In this case, two loading scenarios can generate uplift:

- the block is under a turbulent structure of larger dimensions, transmitting higher pressures to the fissures than acting on top of the block[1]. The surface pressure field

[1] Turbulent rollers have lower pressures about the centreline.

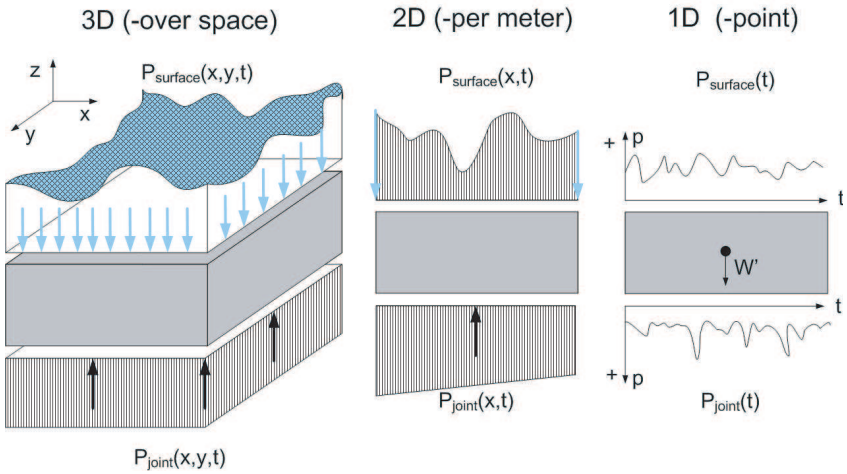

Figure 11.4.: Schematic representation of the 1D, 2D and 3D theoretical approaches to model block displacement: l_x, l_y are the characteristics dimensions of the rock block.

should persist at the surface long enough for pressures to build-up underneath the block;

- the block is under a highly turbulent flow of smaller structures than its own dimensions; correlated structures acting simultaneously at the entries of the fissure may lead to pressure build-up inside the joint. In this case, the persistence of the pressure field is less relevant; the key point is the correlation between the two (small) structures. A "low" pressure field over the block and pressure build-up in the joint.

As first approach, pressure propagation inside fissure is often assumed quasi-instantaneous. Wave celerity is O(10^2-10^3) m/s and blocks are O(10^0-10^1) m. Therefore, the time of travel is O(10^0-10^2) ms.

A simplified 1D approach may be considered for single pressure signals over and under the block. This approach neglects any notion of spatial correlation, considering that measurements at one point are characteristic of the pressure field over a given area. In these conditions, the difference between both pressure signals can be directly compared with the other acting loads. The resulting force acts on the gravity centre of the block.

If blocks are very small compared with typical turbulent scales in the pool, then a pressure field with low persistence may cause their ejection from the rock mass (i.e. "the saddle"). Hence, for small blocks, small turbulent structures may be relevant. In this case, if the wave celerity of pressure waves travelling in the joint between the block and the "saddle" is high (i.e. compared to block dimensions) or if the joint length is small, then uplift may occur within a very short time span.

As presented in section 2.3.5, block displacement was extensively investigated by Yuditskii (1963). In his experiments, displacement was not quasi-instantaneous and some time was required for pressures to build-up in the joint. Bollaert and Schleiss (2005) believe that once the block is in motion, with a given acceleration, it will be ejected even if the pressure

underneath disappears. They defined a quasi-instantaneous dynamic uplift. In the absence of physical evidence, this second concept may be applied to very small blocks.

Bollaert and Schleiss (2005) convert the impulse resulting from a net uplift force into a vertical displacement of a given height h_{up}. For a given value of $0 < h_{up} < 1$, the block comes out of the rock mass and may be swept away.

For blocks as large as the characteristic turbulent structures of the flow pattern, the acting pressures at the surface are lower than those at the entry of the fissure, when the structure is upon the block. In these conditions, the surface pressure field is less important below the center of the roller. Uplift may occur. Correlated turbulent flow structures may be depth-dependent roller, of large dimensions, but also geometry-dependent rollers that may vary from large to very small. A 1D approach is unable to replicate such variety of situations.

Moreover, if pressures build-up underneath the block generate a certain vertical displacement, then as soon as displacement occurs the pressures in the joint decrease. In this case, the block falls back again. A given persistence in time of the pressure field *inside* the joint is necessary or, in other words, the pulse that generates uplift is not likely to be "instantaneous". Hence, the time-line (i.e. history) of pressure fluctuations is important for block displacement. This notion is more perceptible in the 2D approach than in the 3D approach.

In general, a given minimum degree of correlation between the pressure fluctuations acting on top of the block and along the surface joint is necessary to generate a pressure field that may displace rock blocks. This correlated pressure field should persist long enough for the block to come out of the rock mass; the displacement should also be sufficient for the block to be swept away.

As shown in the previous section, very high pressure pulses have very low durations. In Figure 11.2d) and Figure 11.3, pressure pulses higher than 10 bar (the maximum is about 16.5 bar) persist less than 4 ms, occur less than 1 % of the time corresponding to V = 24.6 m/s and have probabilities higher than 0.997 (i.e. probability of not being exceeded).

After the previous theoretical considerations, it is legitimate to query whether pressure pulses with similar characteristics to this example are of any relevance for block displacement. Very high pressure pulses may contribute to crack opening but their contribution to block displacement is arguable. Block displacement requires a given level of space and time correlation of pressure fluctuations, relatively to block dimensions.

It would be highly advantageous for engineering practice to be able to estimate pressure fluctuations from a given probability law and identify their persistence. These values could then be combined with other data sets in order to study block displacement. The energy content of the generated pressure field could be integrated in space to assess the stability of the block. The frequency of repetition of relevant pressure fields for displacement could be identified.

On the other hand, if high pressure pulses of short duration are considered non relevant, then their energy content can be removed from the corresponding range of frequencies. Establishing a link between (1) the frequency and (2) the probability of a given pressure field, and (3) the characteristic block dimensions (eventually related with fissure spacing), could be helpful to estimating the frequency and probability of rock block ejection during a given flood. A contribution to this vast field of research is attempted in the following sections.

11.2.2. Upstream conditions

The probabilities of occurrence of upstream events define the exact framework for plunge pool analysis. The frequency of floods, the capacity of flood routing in the reservoir, and the number and operational guidelines of the spillways are necessary to define:

- the range of unit discharges at impact downstream (if the spillways are gated, the range can be narrowed);
- the duration of operation of each spillway.

These topics are normally dealt with in practice in deterministic terms, with a limited number of events being selected to study scour downstream (Quintela et al., 1987; Schleiss, 1993).

11.2.3. Stability model

Stability models for rock blocks have previously been defined by Yuditskii (1963) and Bollaert (2002b), as well as by Melo (2001) and Melo et al. (2006) for concrete slabs in lined plunge pools.

If a reliable estimate of characteristic rock block dimensions can be made from a geological survey of the natural site, preliminary computations of block stability may show what the critical conditions for block displacement are.

Assuming that there are no contact forces with the neighbouring rock mass, the critical uplift pressure field $p_{crit}(x, y, t)$ can be defined by the block's weight W and the hydrostatic lift. The latter accounts for the pool depth.

For a given scour stage, there is no block displacement if:

$$p_r(x, y, t) < p_{crit}(x, y, t) \tag{11.1}$$

where $p_r(x, y, t)$ is a pressure field acting on the gravity centre of a rock block, as a result of a fluctuating surface pressure field and a underlying-fissure pressure field. This is the **first criterion for block displacement**. This criterion can be, as a first approach, deterministic, unless probabilistic descriptions of rock block dimensions, pressure gradients and tailwater levels are available.

The rock block may eventually be ejected if these pressure fields are a result of the local correlation of instantaneous local pressures persisting long enough for the block to be lifted and swept away. A series of criteria are thus necessary.

11.2.4. Theoretical definition of a correlated and persistent pressure field capable of displacing typical rock blocks

The pressure field P_{up} is defined by the difference of the pressure fields at the surface P_s and underneath the block P_i.

The average pressure field underneath the block (i.e. acting at one point) can be defined as:

$$P_i = \overline{p} + \sum_k p'_{relevant} e^{ikt} + \sum_k p'_{irrelevant} e^{ikt} \tag{11.2}$$

where $p'_{relevant}(t)$ are the pressure fluctuations with probability between 0.5 and a given cut-off value P_{cut}. The third term of the equation corresponds to the fluctuations with P > P_{cut}. This is an alternative approach to the Reynolds decomposition, separating p' between **relevant** and irrelevant events.

The fluctuations $p'_{relevant}(t)$ can also be seen as:

$$p'_{relevant} = z'_{relevant}\sigma \tag{11.3}$$

where z' is the Gaussian reduced variable.

If the correlation function of $p'_{relevant}(t)$ in the x-direction and y-direction becomes negative at about half the length scales of the rock block, e.g.

$$\rho(x_1, x_2, 0) < 0 \quad \text{for} \quad 0.4l_x < \xi < 0.6l_x \tag{11.4}$$

and

$$\rho(y_1, y_2, 0) < 0 \quad \text{for} \quad 0.4l_y < \eta < 0.6l_y \tag{11.5}$$

then a typical turbulent scale is above the block. Considering a square-surfaced block and a turbulent structure with $I_y > I_x$ (e.g. hydraulic jump roller, shear eddy from Chapter 9):

- if $I_x > l_x$, then the entire block is under the influence of the roller, i.e. large persistent structure, and displacement occurs if pressures build-up inside the joint;
- if $I_x < l_x$, then the turbulent scale is above the block but it does not influence simultaneously both entries of the joint at x_{min} or x_{max}.

In laterally confined rock pools of irregular configuration (e.g. stepped conical), the integral scales of turbulence (I_x, I_y) tend to be related with the confinement dimensions or the pool depth, i.e.

$$(I_x, I_y) \propto k.R_c \quad \text{where} \quad k \leq 0.5 \tag{11.6}$$

11.2.5. Theoretical definition of a probabilistic displacement criteria for typical rock blocks

Displacement can be defined as a combined probability function of the events concerned in scouring. Mathematical description would be possible if probabilistic descriptions of the involved processes were available. Therefore, application of this concept in the short term is farfetched considering the present level of knowledge on some of the concerned processes.

The block will be dislodged after moving upward of a given distance z. Since the joints around the block are progressively enlarged by the vibrating action of the block, it is likely that a critical distance h_{up} inferior to the height of the block itself may suffice for it to be swept away. This corresponds to the deterministic criteria:

$$z \geq h_{up} \tag{11.7}$$

where z is obtained from the conversion of the kinetic energy $0.5mV^2$ corresponding to a given dynamic impulse, into potential energy mgz (m is the mass of the block). Bollaert

(2002b) described h_{up} as a site dependent parameter and found values around 0.2 for h_{up} in his case study of the Cabora-Bassa dam.

The notion of a probabilistic-based cut-off can be included defining:

$$V = \frac{1}{m} \int_{t_{up}}^{t_{down}} (p(t) - p_{cut}) dt \tag{11.8}$$

where t_{up} and t_{down} define the time interval during which p > p_{cut}, i.e the duration of a pressure field or pulse with probability equal to the cut-off value selected. Therefore:

$$z = \frac{1}{m^2 2g} \left[\int_{t_{up}}^{t_{down}} (p(t) - p_{cut}) dt \right]^2 \tag{11.9}$$

The definition of h_{up} is closely related with the characteristics of the pressure field and of the joints. If will certainly be larger the tighter the block is. Furthermore, the resulting pressure gradient acting on the block is modified with the opening of the joint. For instance, Yuditskii (1963) mentioned that the highest values of the uplift pressure gradient were achieved in his experiments for an opening of the joint equal to 40% of the total height of the tested elements.

11.3. Conditioned-probability analysis of pressure pulses in the time domain

A method is proposed to evaluate the energy content and the persistence of pressure pulses with probability of occurrence higher than selected cut-off values, i.e. conditioned to a given cut-off level.

The procedure presented in this chapter aims at associating the amplitude and time persistence of a given pressure fluctuation p' with its probability, energy content, and characteristic range of frequencies. It is a contribution to the definition of a more comprehensive model for block displacement. It aims to:

- define adequate levels of cut-off of extreme pressures;
- identify the persistence of pressure pulses of given probability;
- assess the energy content of pressure pulses and corresponding range of frequencies.

It addresses the question of knowing whether pressure extremes are relevant or not for scouring processes. Estimating extreme values requires long-acquisition runs in laboratory. Their amplitude being large, they may be contribute to crack opening. Their persistence in time and spatial influence is small and therefore it is arguable if they contribute to block displacement. If relevant pressures for block displacement fall within a range of probability from 0.10 to 0.90 a Gaussian distribution function may provide fairly good pressure estimates, as mentioned in Chapter 6.

Since only a few local pressure measurements are available, the method correspond to a 1D approach to block displacement. It assumes that point pressure measurements are representative of the loadings above and under (small) rock blocks.

11.3.1. Methodology to compute conditional pulse persistence

The methodology is presented hereafter. It is illustrated and documented in parallel with the example of a time series obtained in a pool with flat bottom, at the pool bottom (y/D=0.35) and at the end of the closed-end fissure (I-fissure). The first steps are:

- the selection of time series for analysis (e.g. FB3, Y/D = 9.3, V = 29.5 m/s) - Figure 11.5;
- the selection of pressure cut-off values higher than 0.5 for probability-conditional analysis; only positive pressures extremes are dealt with.

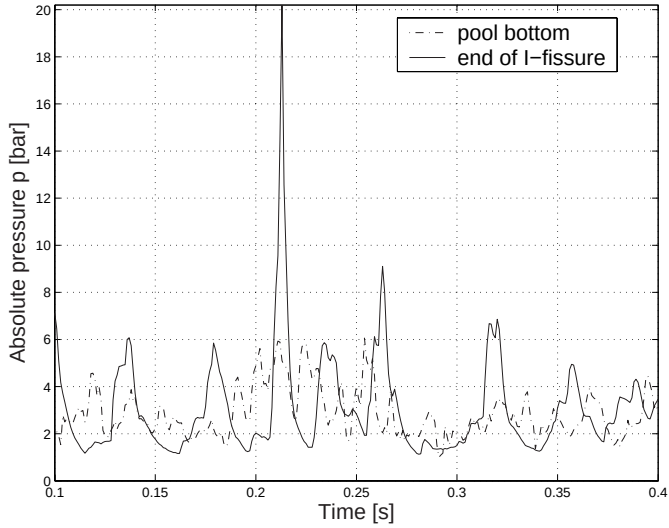

Figure 11.5.: Time series of $p^{'}$ in pool with flat bottom (FB), Y/D = 9.3, V =29.5 m/s, f_s=1 kHz.

Then, for each cut-off probability, the following tasks are performed:

- Identify the pressure value corresponding to cut-off probability from empirical cumulative distributions (epDf) of measured pressure fluctuations. The epDf's are obtained from data histograms with minimum 30 bins (100 bins were used) - Figure 11.6.
- Identify the duration of pressure fluctuations larger than the cut-off value from sorted time series, the duration being given in percentage of the total time of the event (event = operation scenario characterised by discharge, jet velocity, tailwater level, scour geometry) - Figure 11.7.
- Identify the energy content of pressure fluctuations $p^{'}$ larger than the cut-off value, as a percentage of the variance σ^2 of the entire time series.
- Identify the zero-crossing values at the intersection of the cut-off pressure value p_{cut} and the time series, separating upward and downward crossings according to the local first derivative $\frac{\partial p^{'}(t)}{\partial t}$ - Figure 11.8. The interval between an upward and downward crossing is defined as one pulse of $p^{'} \geq p_{cut}$.

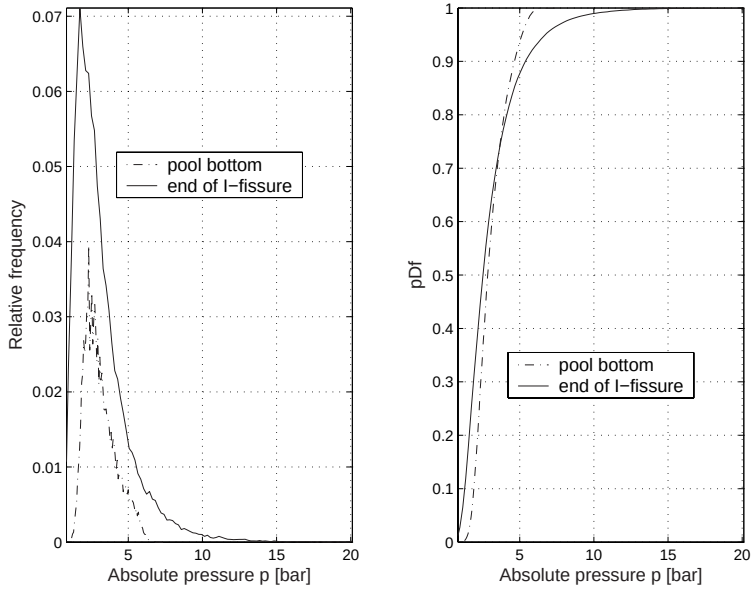

Figure 11.6.: Histograms and empirical probability Distribution function (epDf) in pool with flat bottom (FB), Y/D = 9.3, V =29.5 m/s, f_s=1 kHz.

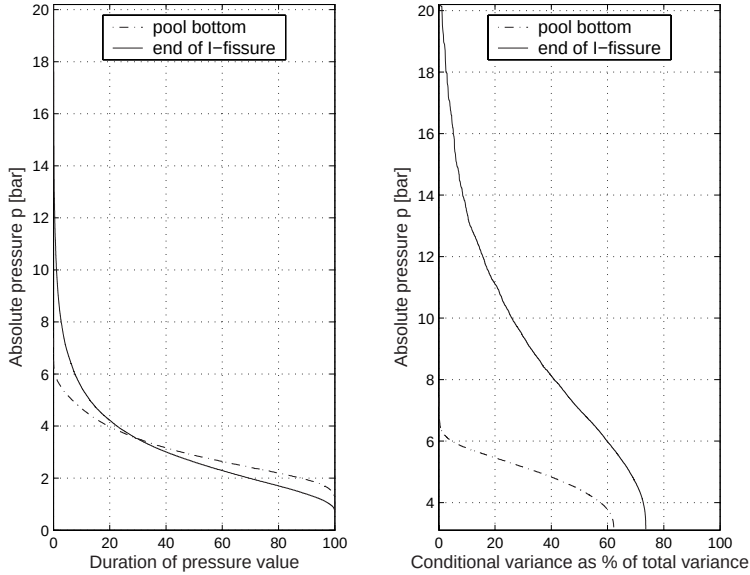

Figure 11.7.: Duration and conditional variance of positive $p^{'}$ in pool with flat bottom (FB), Y/D = 9.3, V =29.5 m/s, f_s=1 kHz

- Computation of the persistence time of each individual pulse τ_i and of the cumulated persistence of $p^{'} \geq p_{cut}$. The average of the time intervals is defined as the persistence τ_{cut} of a given pressure cut-off value. It should not be taken by the persistence of a given pressure field obtained from the integral scale I_t. The persistence of a pulse i is defined as:

$$\tau_i = t_{down} - t_{up} \tag{11.10}$$

and the persistence of pressure pulses larger than p_{cut} is

$$\tau_{cut} = \frac{1}{N} \sum_{i=1}^{N} \tau_i \quad \text{where N is the number of pulses with } p^{'} \geq p_{cut} \tag{11.11}$$

- Computation of the dynamic impulse of each pulse as well as the cumulated impulse $p^{'} \geq p_{cut}$. The impulse is defined as:

$$I_i = \int_{\Omega} \int_{t_{down}}^{t_{up}} [p(t) - p_{cut}(t)] dt d\Omega \tag{11.12}$$

where Ω is the surface where the pressure field is acting (i.e. in 1D approach is the surface of the block).

- Definition of the peak time of each individual pulse i in terms of the position in the time series. This task depends on the typology of pressure pulses above the cut-off pressure (e.g. single peaked, with multiple peaks, symmetric, skewed). Three solutions are compared, based on the sum of t_{up} with either (1) $\frac{\tau}{2}$, half of the average pulse persistence, or (2) $\frac{\tau_i}{2}$, half of the pulse persistence, or finally (3) τ_{50}, the instant corresponding to 50% of the impulse (i.e. surface) for each pulse.
- Definition of the series of time distances between pulse peaks, T_i with $p^{'} \geq p_{cut}$.
- Definition of characteristic frequencies of pressure pulses, f_{cut} based on the range of values of T_i.

This procedure allows establishing a connection between a cut-off probability and the corresponding energy, persistence and range of frequencies of pressure pulses.

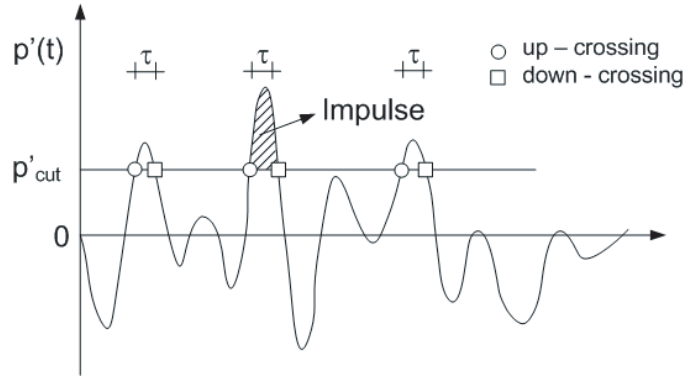

Figure 11.8.: Definition of the impulse of pressure events between up and down crossings for a given cut-off probability, adapted from Fiorotto and Salandin (2000).

The definition of the periods between peaks and the range of frequencies is, for the time being, approximative. As observed in the time series, peaks of high probability may not be evenly spaced. Therefore, T_i may vary considerably. In such case, the obtained range of frequencies is too large to be useful.

11.3.2. Selected data series for analysis

The previous methodology is implemented in ©Matlab scripts made by the author. For the definition of pulses, tangential points to the cut-off pressure level are not considered. Truncation errors due to the discretization (i.e. number of bins) necessary for computation of the histograms and epDf's are weighted, by performing interpolation between points, in order to reduce inaccuracies.

The analysis procedure was tested with six time series selected from the data base - Table 11.1.

Table 11.1.: Data series of pressure fluctuations at the pool bottom (y/D =0.35) and inside the fissure, V =29.5 m/s, 65'536 points.

Pool	Y [m]	Y/D	f_s [kHz]	Name
flat bottom	0.20	2.8	1	FB20
	0.40	5.6	1	FB40
	0.67	9.3	1	FB67
narrow	0.30	4.2	1	FC30
	0.67	9.3	1	FC67

11.3.3. Average persistence of probability-conditioned pressure pulses

The persistence τ of pressure pulses corresponding to cut-off probabilities of 0.5 (mean value), 0.75, 0.80, 0.85, 0.90, 0.95, 0.99 and 0.999 are presented in Figure 11.9, in terms of probability and of the corresponding cut-off pressure value P_{cut}.

For all the cases investigated, τ decreases with the probability. At the bottom of the pool, $\tau \leq 6$ ms for P > 0.75. In fact, for Y/D ≤ 5.6 (i.e. Y = 0.4 m) τ values are even less than 4 ms. For developed jet impact conditions (i.e series FB67, FC30 and FC67), the persistence for equivalent probability values is higher than for core impact conditions (i.e. series FB20 and FB40).

Inside the fissure, τ may be larger than 6 ms for probabilities less than 0.75 in the cases for which very significant amplification inside the fissure is observed, i.e. FB67 and FC30, or core impact was observed, i.e. FB20 and FB40. Whenever there is significant amplification, the pressure cut-off value drops sharply with the decrease of probability. In these series, pressure peaks of about 20 bar have been recorded, which have P$\geq$0.999 and $\tau \leq 1.5$ ms. For instance, for P = 0.99, τ is ≈ 2 ms but pressure values are in both cases about 10 - 11 bar, i.e. about **half** the maximum pressure values measured.

For a deep narrow pool (i.e. FC67), $\tau \leq 4$ ms inside the fissure and pressure values are about twice those found at the pool bottom.

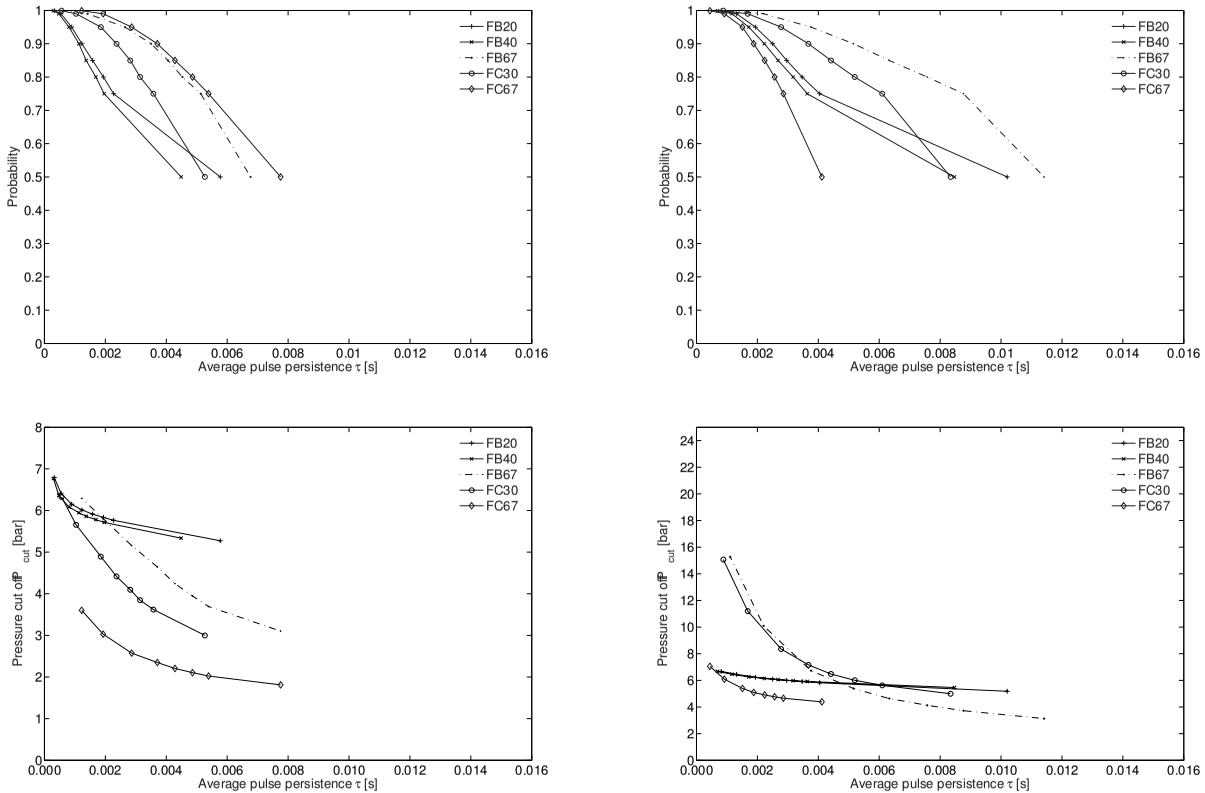

Figure 11.9.: Average pulse persistence τ of pressure pulses conditioned by given cut-off probability and pressure (in absolute pressures): left, pool bottom (y/D =0.35); right, end of closed-end fissure. Assumed linear between points for interpretation.

11.3.4. Statistical distribution of pulse persistence

Figures 11.10 and 11.11 present duration curves of τ_i for a selected number of test series, as well as histograms of τ_i for a probability of 0.75, as well as the corresponding Rayleigh function fits. These examples correspond to test cases for which significant p' amplification was measured inside the fissure. For increasing cut-off probability, persistence drops to values close to the acquisition duration $1/f_s$. At the pool bottom, there are more pulses with intermediate persistence between 5 - 15 ms than inside the fissure (i.e. duration curves are flatter in the first case).

Gaussian pressure fluctuations are expected to generate pulse persistence intervals τ_i following a Rayleigh distribution (Fiorotto and Salandin, 2000). For the selected examples, the Rayleigh distribution does not fit the series of τ_i data at the pool bottom. Inside the fissure it fails in representing the existence of several peaks of higher probability. It provides a reasonable trend curve. The deviation from a Rayleigh distribution may be related to the sampling frequency and the amount of data used for the histograms. This comparison may be pursued in the future with other cut-off probabilities and using more data.

11.3.5. Dynamic impulse of probability-conditioned pressure pulses inside a closed-end fissure

Histograms of the dynamic impulse series obtained for each cut-off probability value are presented in - Figure 11.12. The selected example corresponds to a time series for which significant amplification is measured inside the fissure. Pulses with high probability are quite sharp. The large majority of impulses is of less than 0.05 bar.s; only few are higher, for low cut-off probabilities. For a given impulse values, the variation of the number of pulse with the cut-off probability is significant, i.e. curves are quite mild sloped.

11.3.6. Average peak frequency of probability-conditioned pressure pulses

The average peak frequency is computed from the average period between pulse peaks. Results are presented in Figure 11.13. Frequency estimates hardly vary with cut-off probability. This is partly due to the fact that the periods between pulses have been averaged, but also to the nature of the pulses themselves. Indeed, if pulses are very sharp and short in time, different cut-off pressure values intersect the same "event" at different pressure values: the interval between consecutive pulses almost does not change for various cut-off probabilities.

A second coarse attempt to estimate the periodicity of pulses of a given cut-off probability can be made by dividing the number of pulses by the total duration of the time series used for the analysis. Figure 11.14 presents such analysis for the selected test series. Extreme pressures being of random nature, they are not represented in such analysis simply because they may not occur within the considered time frame.

11.3.7. Discussion

The probability analysis in the time domain allows defining the events to investigate in terms of extreme pressures, which is not possible in a traditional Fourier analysis.

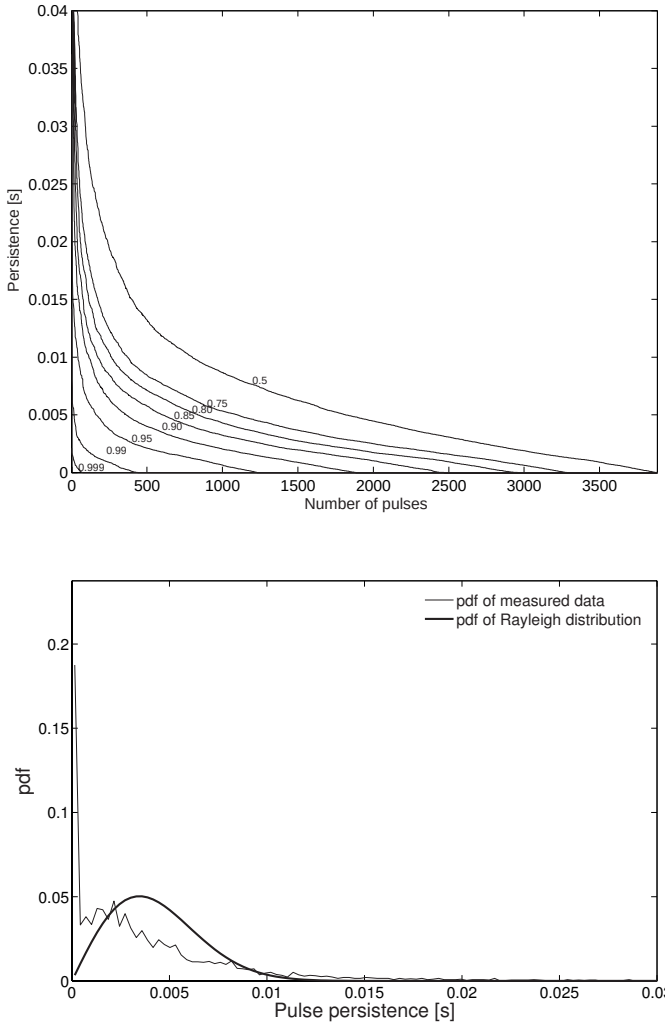

Figure 11.10.: Conditioned pulse persistence **at the pool bottom** (V=29.5 m/s, y/D = 0.69, FB67, 1000 bins): top, histograms; bottom, statistical distribution for P = 0.75 compared to Rayleigh fit of the data.

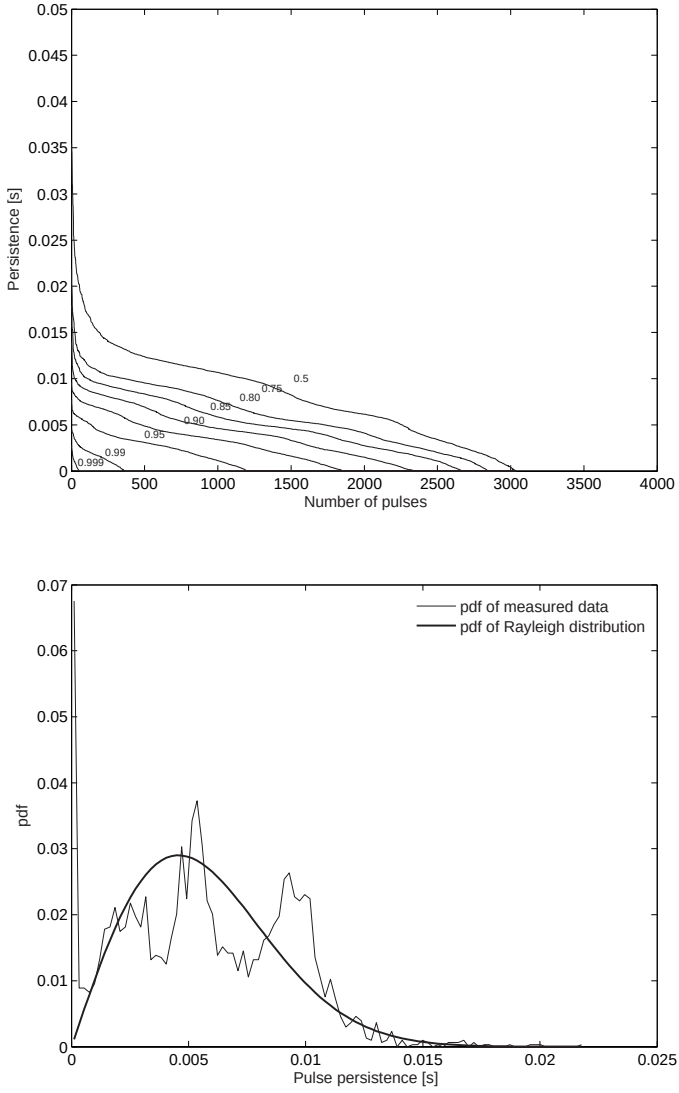

Figure 11.11.: Conditioned pulse persistence at the **end of the fissure** (V=29.5 m/s, FC30, 100 bins): top, histograms; bottom, statistical distribution for P = 0.75 compared to Rayleigh fit of the data.

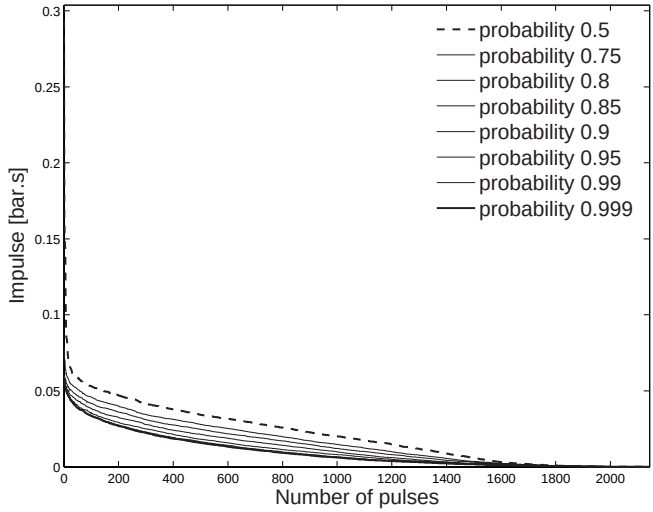

Figure 11.12.: Histogram of conditioned dynamic impulse I at the end of the closed-end fissure (V = 29.5 m/s, FB67, data set of 65 s).

Persistence of pulses is identified, as well as their energy content in terms of the corresponding % of σ^2 and dynamic impulse.

For signals that have randomly distributed extreme events, the definition of the frequency of such events is rather qualitative. The range of possible frequencies obtained from T_{max} and T_{min} is too wide; the estimate of average frequency may not have a sound physical meaning. Depending on the type of signal (e.g. pool bottom or inside fissure, unconfined/confined, with/without amplification in fissures, with/without column separation), the time intervals between pulses of given conditioned-probability may be correlated with the flow conditions.

The method presented before considers pressure measurement at one point as representative for (small) rock blocks. This is a simplification that allows exploring a 1D approach of the block displacement process. It allows advancing into the definition of of the methodology for analysis. The 1D approach should be validated in the future with additional experimental work. Once 2D or even 3D pressure field measurements are available, part of the theoretical background will have already been settled. A 1D approach based on force measurements would already be more representative than the present approach with pressures since:

...pressure fluctuations over a given surface have PDF closer to Gaussian than pressure fluctuations at any point within that surface...

according to the Theorem of Central Limit (Pinheiro, 1995). If the "relevant" pressure fields over the block could be described with Gaussian pDf's, then it would be much simpler to combine analytically the probability of block displacement with the probability of occurrence

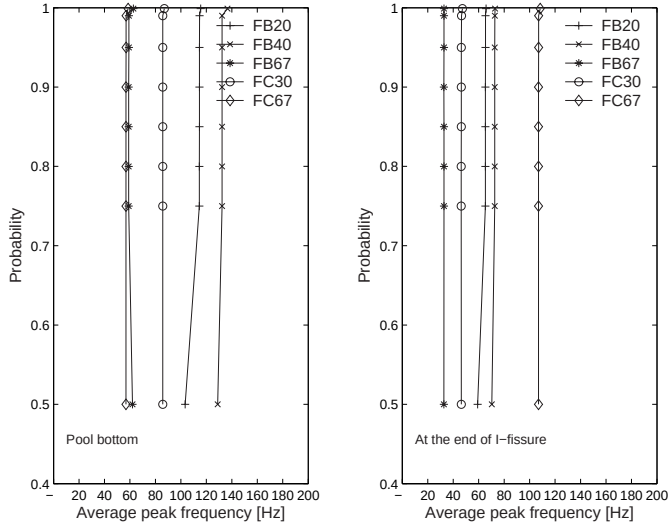

Figure 11.13.: Average peak frequency of pressure pulses conditioned by given cut-off probability: left, pool bottom; right, at the end of the fissure. Assumed linear between points for interpretation purposes.

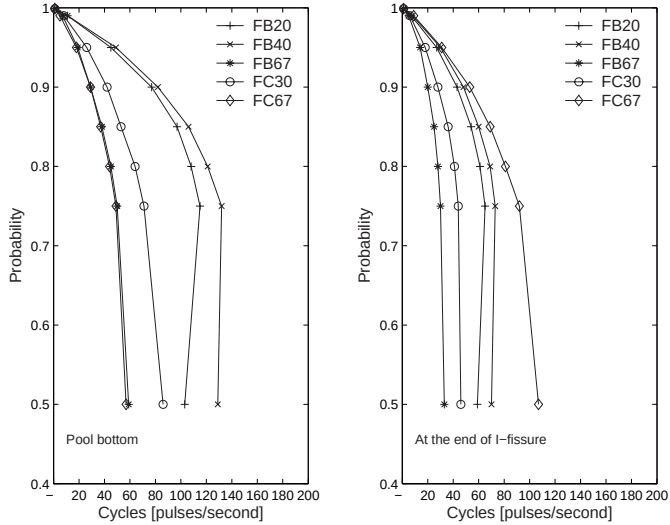

Figure 11.14.: Relative frequency of pressure pulses conditioned by given cut-off probability: left, pool bottom; right, at the end of the fissure. Assumed linear between points for interpretation purposes.

of other processes situated upstream in the rock scour process (flood event, flood routing, spillway operation, impact pressures, crack propagation, rock block dimensions, a.s.o)

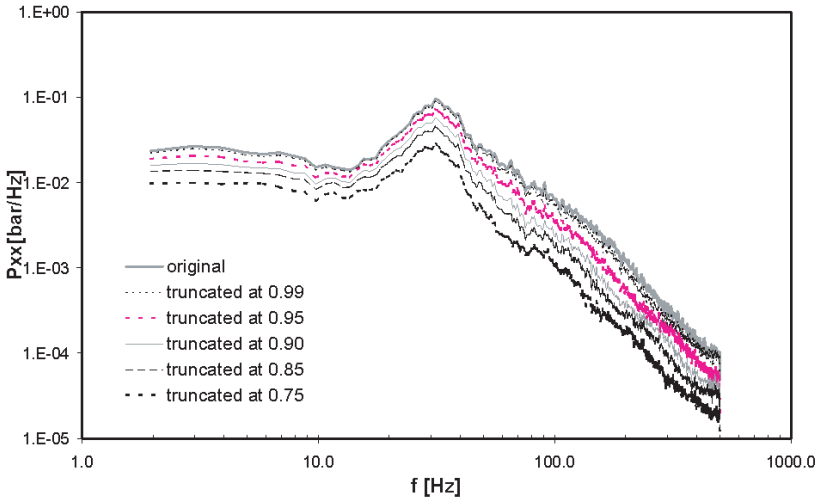

Figure 11.15.: Power spectra of p' inside the fissure in a narrow pool with Y/D = 4.2 and V = 29.5 m/s (test series FC030). Example of power spectra obtained from probability-conditioned truncated signals and the spectrum of the original signal.

Extreme pressure pulses with very high probability have low persistence. They do not occur at constant spaced intervals. Such isolated events are poorly represented in the Fourier analysis presented in the previous chapters.

A conditioned-probability analysis may also be used to truncate the time series, removing the energy content of pulse *above* a given cut-off. By comparing the power spectra of the truncated series with that of the original signal, an estimate of the reduction in spectral energy may be obtained. In this approach the pulses are replaced by a constant pressure value (i.e. the cut-off), which biases the Fourier analysis. The shorter these truncated intervals are, the less inaccurate the Fourier Analysis is.

An example is provided in Figure 11.15 and table 11.2, for p' values inside the fissure. Pressure fluctuations with $P \geq 0.95$ last less than 5 % of the entire event but account for about 30 % of the variance, i.e. the energy of pressure fluctuations. However, since $\tau \leq 3$ ms these events are small structures of the order of magnitude of the Taylor micro-scale. They may contribute to crack propagation by brittle failure or fatigue failure but it is rather unlikely that they will participate in the process of block displacement.

Isolated extreme events are not regular oscillations at given frequency and, therefore, their energy is distributed throughout a large range of frequencies. The analysis of such isolated events may be done with the help of available wavelet functions. However, the wavelet method does not allow a direct link with the probability of a given pressure value. The Fourier and wavelet approaches may be considered complementary to the probabilistic time-domain analysis presented in this work.

Table 11.2.: Example of cut-off analysis results inside the fissure in a narrow pool with Y/D=4.2 and V = 29.5 m/s (test series FC030)

P_{cut}	σ^2	$\frac{\sigma_p^2}{\sigma_{100\%}^2}$	$\tau_{P>P_{cut}}$
	$[bar^2]$	[%]	[s]
0.750	0.80	26	0.006
0.850	1.28	42	0.004
0.900	1.65	53	0.004
0.950	2.16	70	0.003
0.990	2.81	91	0.002
original	3.09	100	-

11.4. Conclusions

This chapter discusses the importance of pressure fluctuations in the process of rock scour based on the evaluation of their persistence in time. Persistence can be of importance whenever processes may not be considered instantaneous, i.e. whenever a given permanence in time is necessary for a given event to occur.

Previous analyses of time series and spectral energy content of pressure fluctuations inside fissures have shown that a sequence of pressure events may build-up high pressures inside fissures. These extremely high pulses can reach values several times larger than the incoming kinetic energy. They are expected to contribute to crack propagation and eventually to block displacement. In order to assess whether these extreme values are relevant for rock scour, their persistence in time needs to be evaluated.

Duration curves of pressure values defined in terms of the % of total duration of a given event (i.e. discharge, diffusion, pool geometry, a.s.o) are presented. At the pool bottom, pressure fluctuations for developed jet conditions remain within $\pm 1\sigma$ of the mean value for about 80% of the total time of the event considered. Inside the fissure, this range decreases to 60 % of the total duration. Extreme pressure events last a relatively low % of the total duration of the event.

The processes of block displacement is analysed in detail. A theoretical definition of the 3D dimensional process of displacement is presented, as well as the assumption made when considering a 2D or 1D approach of the problem. The three approaches are discussed. The basis for the identification of a correlated pressure field that should be capable of displacing rock blocks is presented. This allows defining theoretically a probabilistic criteria for rock block displacement.

According to this, the available pressure measurements allow a 1D approach. This can be considered appropriate for rock blocks smaller than the characteristic integral scales of turbulence in the scour hole.

In view of contributing to the mentioned theoretical endeavours, an analytical models for a conditioned-probability analysis of pressure pulses is presented. It allows the selection of pressure pulses with probability higher than given cut-off values. Individual pressure pulses are identified and analyzed in terms of their persistence and dynamic impulse.

The results for two typical pressure time series in a pool with flat bottom (FB) and a narrow pool (FC) show that:

- pressure fluctuations with P $>$ 0.75 persist less than 6 ms at the pool bottom. For core jet conditions, this value drops to 4 ms. For developed jet impact conditions, the persistence for equivalent probability values is higher than for core impact conditions;
- pressure fluctuations with P $<$ 0.75 may be larger than 6 ms inside closed-end fissures, e.g. for cases with significant amplification inside the fissure or for core impact conditions;
- whenever there is significant amplification (e.g. transient regimes with column separation), the pressure cut-off value drops sharply with the decrease of probability. As an example, pressure peaks with P $\geq$ 0.999 last $\leq$ 1.5 ms, whereas for P = 0.99 they may persist for $\approx$ 2 ms an be about **half** the maximum pressures.

In summary, extreme pressure values have very low persistence. It is likely that their participation in the process of block displacement is secondary, unless the area of application is of the order of magnitude of the rock block's dimensions (i.e. very small blocks in comparison with main flow patterns); otherwise, a given spatial correlation seems to be required, as shown by Melo et al. (2006) for concrete slabs. Research should now focus on the establishment of a correlation between the dimensions of rock blocks, the characteristic turbulent scales of the flow in the pool, and given cut-off probabilities. The displacement of rock block could then be defined in terms of the pressure field fluctuations with (cumulative) probabilities *lower* than that of the cut-off.

The methodology outlined is implemented numerically and is ready for application. It allows a straightforward identification of pressure pulses with given probability, as well as the corresponding average persistence. The analysis presented herein is based on the positive part of the signal only. This reasoning, however, can also be applied to the pressure signal resulting from the difference between pressures at the surface and inside the fissure, e.g. at y/D = 0.35 and at the end of the fissure. Such analysis could be considered a 1D approach to rock block displacement.

The large variety of pressure fluctuation series justifies pursuing this analysis to the most typical pressure signal at impact with the pool bottom and inside fissures.

12. Conclusions, practical recommendations and future research

12.1. Concluding remarks

Rock scour by plunging jets is a three-dimensional water-air-rock interaction problem. Impact pressures are the driving agent of the scouring process.

This investigation presents experimental evidence of the influence of plunge pool geometry in the definition of dynamic pressures at the water-rock interface. Different pool geometries typical of prototype conditions were tested and compared with pools with a flat bottom used as a reference case. Pressure measurements at the jet outlet, at the pool bottom and inside a closed-end fissure are presented. The development of plunging jets in the water is clearly modified by the boundaries of the plunge pool, depending considerably of the degree of lateral confinement relatively to the dimensions of the jet.

The hydraulic characteristics of jets at issuance were investigated. It is shown that for non-aerated compact jets, the turbulence intensity decreases with increasing velocity. The velocity profile tends to become uniform as function of the contraction at issuance. The turbulent jets produced in the experimental set-up are similar to those issued from overfall spillways and orifices. Based on experimental data and literature review, the issuance characteristic in typical water-releasing structures of dams are defined.

The dissipation of energy of high-velocity plunging jets is estimated based on measurements of mean impact pressures at the pool bottom. An analytical model is compiled in this study based on previous literature. The experimental results are compared with the analytical estimates for the diffusion of turbulent aerated jets in pools with a flat bottom. The analytical model provides good estimates of energy dissipation efficiency in the pool, in the early stages of scour and in deep flat pools. For pool depths about the core development length (i.e. transitional pools), analytical estimates are quite sensitive to the initial assumptions on the centreline velocity decay, dimension of impinging zone and pool aeration.

Turbulent impact pressures in pools with a flat bottom were investigated in terms of their probabilistic distribution at stagnation, for increasing pool depths. This allowed dividing jet development conditions at impact in core and developed impact conditions, based on an evaluation of high-order moments and autocorrelations of pressure fluctuations. Core impact conditions are typical of shallow pools and generate negative skewness at stagnation. The end of core development is associated with intermittent flow conditions indicated by high kurtosis. For developed impact conditions, pressure fluctuations at stagnation are positively skewed. A Gaussian distribution was shown to fit satisfactorily the data, save for extreme high and low probabilities.

Air-water measurements were carried out at selected points in pools with a flat bottom. They allow describing the behaviour of air bubbles before, at, and after stagnation. Void fraction

estimates close to the entry of rock fissures show that air bubbles reduce in size under the influence of the high-pressure gradient at stagnation. Characteristic bubble dimensions are similar to typical rock fissures' dimensions, which suggests that air bubbles may enter in rock fissures.

The present results show that mean impact pressures at the pool bottom are lower in laterally confined pools than in pools with a flat bottom. The length of core development can be reduced, depending on the degree of confinement and pool depth. The corresponding power spectra density and probabilistic distribution functions of pressure fluctuations transmitted to the rocky riverbed are modified when compared with pools with a flat bottom. The flow currents created by deflection of the jet on the lateral boundaries of the pool may interfere with the development of the jet, generate additional dissipation and hinder the penetration of air bubbles in the pool.

For shallow and transitional pool depths in laterally confined pools, pressure fluctuations may have more energy than in corresponding pools with a flat bottom. Power spectra of pressure fluctuations have higher energy content in the lower frequencies range and extreme positive pressures increase, in comparison to pools with a flat bottom. For deep laterally confined pools, the energy of pressure fluctuations is lower than in pools with a flat bottom. The extreme positive pressures are not reduced in absolute terms when compared to values for pools with a flat bottom, and increase relatively to the total energy of pressure fluctuations. Negative extreme pressures are lower in laterally confined pools of any depth compared to pools with a flat bottom.

Based on direct observations of flow patterns and on the turbulent characteristics of the dynamic loading at the pool bottom, large-scale pool flow features like surface oscillations, shear eddies and air-water ejections are identified and described. The induced flow patterns in four typical scour scenarios are presented and discussed. They allow explaining the evolution of flow features and dynamic loadings with scour development, for variable confinements and pool depths. The role of deflected upward currents, shear eddies and recirculation currents in the development of plunging jets and in air entrainment in the pool is discussed. These flow features are shown to have an important role in the energy dissipation process.

Measurements of transient pressures inside fissures show that the dynamic response of rock fissures varies with the turbulent character of impact pressures at the rock interface. The influence of the dimensions of the entry in averaging turbulent pressure fluctuations in the transition to fissure is identified and this filtering effect is described analytically. The energy of pressure fluctuations inside the fissure is always higher than at the entry, for all pool configurations tested. The energy of pressure fluctuations inside rock fissures is lower in narrow confined pools for transitional and deep pools, but higher in shallow pools, compared with pools with a flat bottom. This is also valid for positive extreme pressures. Negative extreme pressures are generally lower. Amplification of pressure peaks is observed inside a closed-end fissure for both shallow and deep pools; it is described as a function of jet development, i.e. of relative pool depth, pool geometry and jet turbulent characteristics. The occurrence of column separation inside the fissure is documented. The occurrence of resonance inside fissures is investigated numerically. Multiple resonant harmonics are replicated solving the waterhammer equations inside the fissure with the hydraulic impedance method.

A probabilistic-based event analysis is developed to correlate the probability, persistence, duration and energy content of extreme pressure pulses. The persistence reduces abruptly for

pressure pulses with high extreme (cumulated) probabilities; these extreme pressures have an important energy content. The role of extreme pressure events in the scouring processes of crack propagation and block displacement is discussed.

In conclusion, this analysis of jet diffusion in pools with a flat bottom and laterally confined pools shows the importance of detailed knowledge of pool flow patterns for the definition of impact pressures and transient pressures inside rock fissures. It provides detailed information on hydrodynamic processes involved in rock scour. It contributes to the development, the use and the interpretation of mathematical models for the simulation of pool flows and transient flows inside fissures.

This dissertation is a contribution to the knowledge of scouring agents and processes. Rock scour in being studied for decades and a comprehensive tool to assess scour evolution is yet to be produced. In-depth insight on the physics of the driving processes is the core information required for that endeavour and this dissertation is envisaged as a milestone on this quest.

12.2. Influence of plunge pool geometry for scour assessment

As stated, this dissertation focuses on physical processes. There is no intention of presenting engineering tools or procedures to estimate scour. However, the enhanced knowledge on pool flow patterns and impact pressures in laterally confined plunge pools allow presenting recommendations for practical application (next section). The work herein presented allows presenting a number of statements that summarize the influence of plunge pool geometry in the process of rock scour.

- The geometry of the pool contributes to the definition of the flow patterns inside the pool and also in the zone around the impact region. Recirculation currents can lead to bank erosion and eventual danger to structures.
- The geometry of the plunge pool is a key element in the definition of the mean and turbulent character of impact pressures on the pool boundaries, as well as transient pressures inside rock fissures. Pressure amplification inside fissures is directly related with the turbulent pattern of dynamic pressures at the water-rock interface.
- The mean dynamic pressures transmitted to the foundation are lower in laterally confined pools in comparison with pools with a flat bottom. For a given lateral confinement, the reduction of mean pressures increases with velocity. For a given velocity and pool depth, the reduction is more significant the narrower the pool is.
- Jet development may be enhanced in the presence of lateral confinements; the geometry of the pool may induce currents that interfere with the diffusion of the plunging jet. This effect is more important for shallow and transitional pools. The roller (shear eddy) created by deflection of the jet at the pool boundaries is a key element in the dissipation of energy through the water column and in jet development. The narrower the pool the closer such roller will be of the plunging jet, enhancing friction.
- Pool currents may reduce the penetration of air in the pool; this may have opposing consequences: on the one hand, a lower air content in the pool leads to an increase in mean pressures at impact; on the other hand, it reduces the turbulent character of

pressure fluctuations in the pool boundaries. The former is unfavourable for shallow pools, whereas the latter is unfavourable for deep pools.

- Pressure fluctuations in laterally confined pools are lower than in pools with a flat bottom, if the pool depth is sufficient for jet development (in equivalent free diffusion conditions). They may be higher in shallow pools, as indicated by the parameter ϕ in Chapter 8.
- Extreme positive and negative impact pressures in laterally confined pools do not increase in absolute terms, in comparison with pools with a flat bottom. The extreme positive pressures p'^{+} may reach 8 times the RMS values of local pressure fluctuations. Extreme negative pressures p'^{-} do not exceed 2-3 times the corresponding RMS values.
- For shallow confined pools, the energy of pressure fluctuations at impact may increase in the range of frequencies capable of exciting rock fissures, in comparison with very wide plunge pools. For deep confined pools, spectral energy of p' at impact is generally reduced for all frequencies.
- Assuming the evolution of scour as a succession of scour stages with flat bottoms leads to overestimation of impact pressures.
- The previous indications are helpful for the definition of the geometry of pre-excavated pools, taking into account the type of flow patterns and dynamic loadings described in this dissertation.

12.3. Recommendations regarding existing scour estimation models

The developments and finding presented herein may be helpful to improve the prediction capabilities of existing scour models based on the pressure-gradient concept (see section 2.3.5). The suggestions presented hereafter concern mainly the model presented by Bollaert and Schleiss (2005), since it allows improving explicitly the definition of relevant physical processes.

The model of Bollaert and Schleiss (2005) is based on pressure measurements with near-prototype velocities and aeration, follows the idealisation of the scour process first identified by Yuditskii (1963) himself, and is so far unique in considering explicitly the process of crack propagation. It is divided in three modules: the falling jet module, the plunge pool module and the rock mass module.

Concerning the falling jet module, description of several types of jet issuance conditions can be accounted for taking into consideration the investigations presented in Chapter 4 of the present dissertation, in particular the indications resumed in Table 4.1, and in equations 4.6 and 4.7 for the jet turbulence intensity Tu and kinetic energy correction factor α.

Regarding the plunge pool module, the accuracy of impact pressures estimates being used for scour simulations can now be evaluated based on the ergodicity and error-estimation analysis presented in Chapter 6. Similarly, the assumptions necessary for estimation of jet diffusion (i.e. core development length, impinging jet zone, reduction of mean pressures due to pool aeration, etc.) can be discussed based on the limited-depth diffusion model presented in Chapter 5. The values of the mean pressure coefficient Cp can be obtained from Figure 8.2 for a stable jet, or use those presented in the original paper for a more

unstable jet. Similarly, for the RMS coefficient Cp', the values presented in Figure 8.9 or those indicated by Ervine et al. (1997) are suggested for stable jets. Figure 8.10 allows simplifying the previous approach assuming $Cp' = 0.25$ for deep pools and $Cp' = 0.15$ for shallow pools if jet velocities are higher than 15 m/s. The values presented in the original paper by Bollaert and Schleiss (2005) can be assumed for unstable jets. It should be kept in mind that the use of Cp and Cp' values obtained in pools with a flat bottom leads to an overestimation of mean pressures for any pool depth, as well as an overestimation of RMS-values for deep pools, in comparison with prototype plunge pools.

The present study has shown that mean and RMS-values of pressure fluctuations are highly dependent on pool geometry and on the induced flow-patterns. Aeration conditions also. The relationships used to describe Cp in Bollaert and Schleiss (2005) can be replaced by equations 8.4 8.5 8.6, or by those resumed in table 8.1. Apart from the relationships presented in Chapter 8, several other geometries can be simulated using the extensive pressure value database acquired during the experimental work presented in this dissertation. The Cp' relationships obtained for pools with flat bottom have to be replaced for prototype plunge pools (i.e. laterally confined pools). This can be achieved by (1) using values presented in Figure 8.9, (2) multiplying the Cp' obtained in pools with flat bottom by envelope ϕ values, i.e. $\phi = 0.8$ for deep pools and $\phi = 1.4$ - 2.0 for shallow pools according Figure 8.11 or (3) searching in the pressure database the most adequate values for each specific case and scour stage. The modifications to pool aeration due to pool geometry are already accounted for in the pressure values, which were obtained in near-prototype aeration conditions. A detailed evaluation of the main flow features in each scour stage and pool geometry will be instrumental in the selection of the most suitable database to consider; a comparison with the flow patterns and observation presented in Chapter 10 is suggested.

Concerning the rock mass module, a distinction between the crack propagation sub-module and the block uplift module is necessary. In terms of crack propagation, the existing expression for the definition of a maximum hydrodynamic pressure at the tip of a crack can be revised by either:

- replacing the definition of the instantaneous amplification factor Γ by an envelope value of 20, as defined in Figure 10.9 for the ensemble of all tested pool geometries; or,
- explicitly considering Cp^+ values from the pressure database.

In terms of the block uplift module, there is little physical evidence sustaining a 1D approach, as discussed in Chapter 11. The procedure presented in Bollaert and Schleiss (2005) is adequate for small blocks compared with coherent flow patterns, the dimensions of which range several orders of magnitude in prototype plunge pools. Therefore, and until further evidence is provided, this sub-module can either be replaced by (1) the model of Yuditskii (1963) accepting the scale effects associated with tests at reduced-scale, or (2) the model of Melo et al. (2006) if the flow conditions are somewhat similar to those in a lined plunge pool, or (3) limit the application of the dynamic uplift model to pressure pulses with persistence in the range from 0.005 to 0.05 s (i.e corresponding to integral scales between 0.05 and 0.5 s, one order of magnitude higher than the computed microscales). In the latter case, the pressure values that should be considered for the computation of net uplift impulse correspond to the pressure cut-off values for which such average persistence is obtained. According to Figure 11.9, such assumption corresponds to pressure fluctuations with cumulated probabilities between 60 and 80 %, which correspond to values between 2 - 4 times σ inside the fissure. Until significant physical evidence is presented, the discussion

of which pressure events are relevant or irrelevant for block displacement is conditioned by the observations of Yuditskii (1963) cited in section 2.3.5.

In summary, scour models based on the pressure-gradient method may benefit directly from the results of the present experimental work and analysis. The aforementioned suggestions can be directly integrated in the model presented by Bollaert and Schleiss (2005) which is already used in practice. This integration is part of the long-term research goal of the LCH-EPFL to achieve a comprehensive model for scour prediction based on sound physical background.

12.4. Future research

The following topics could be addressed in future research:

1. Describe the **mean and turbulent flow fields** in limited depth pools and laterally confined pools. This could be done both experimentally and numerically. In both cases, the highly turbulent and aerated character of the flow renders any development quite challenging. In practical terms, these investigations could allow improving the description of jet diffusion (centreline velocity, diffusion angles, core contraction, etc.).

2. Pursue the investigation on **pool and fissure aeration** in limited-depth pools. This can be done by using phase-detection probes (e.g. fiber-optic) and high-velocity video recordings. Selection of the measuring zone and installation of such equipment in the current facility presents many practical difficulties; significant changes to the set-up would be required. Two main topis would be of interest: (1) the **interaction of air bubbles with the turbulent flow field** in the pool (e.g. bubble induced turbulence, slip conditions); and (2) **the transition from the pool to the fissure**. The former is particularly important to understand the influence of air bubbles in pool turbulence and in impact pressures. The latter could allow a detailed investigation of the exchanges of mass with the fissure and of the behaviour of air bubbles at the fissure's entry. The low air content at the water-rock interface may allow measuring the velocity flow field (e.g. PIV or ADV), and simultaneously the dynamic pressures and air-water characteristics in the close vicinity of the entry of the fissure. Local phenomena like the transition from free surface flow to pressurized flow, cavitation, air bubble compression and migration could thus be investigated.

3. Describe the process of **block displacement**, collecting experimental evidence of the governing mechanisms and critical stability conditions, based on the work of Yuditskii (1963) at reduced-scale, of Melo et al. (2006) in lined plunge pools, and of Bollaert and Schleiss (2005) and the present dissertation with near-prototype jet velocities and aeration. A systematic evaluation of the correlation between the dimensions of the block dimensions and the the dynamic characteristics of the pressure field could allow defining in which circumstances a 1D, 2D or 3D approach, as proposed in Chapter 11, is suitable to evaluate block displacement. This investigation could also pursue the conditioned-probability analysis of extreme events aforementioned, to select the relevant pressure events for each physical process concerned in scouring (e.g. implement a probabilistic displacement criteria; implement the study of gradient time series instead of time series of impact pressures, a.s.o). Such investigations could allow also deciding the pertinence of studying extreme pressure events at impact for variable pool depths in **long duration acquisition runs**. Sufficiently long data could allow

for the study of the most adequate probability density function to estimate extreme pressure events. The main objective could be the development of a **probabilistic-based model for block displacemen**t by relevant pressure gradients.

4. Initiate experimental research with rock samples under the impact of high-velocity jets to evaluate: (1) the process of **crack opening** from local flaws in the rock surface; (2) the process of **crack propagation** by hydrodynamic pressures; (3) the differences between vertical/sub-horizontal crack propagation. This would require considerably modifications to the experimental apparatus. The first topic would require an statistical description of existing fissure types based on prototype observations. The second topic could considerably benefit from recent findings in fracture mechanics obtained in other domains of the Civil and Materials Engineering sciences. To investigate the third point, an initial step could be to introduce in the rock mass module of the present facility a zone of lower rigidity.

5. A number of relatively straightforward experimental studies with high value for the current research could still be performed with minor changes to the existing facility, such as: (1) jet diffusion and impact pressures in **asymmetric plunge pools**; (2) pressure propagation in **fissures with different characteristics** of roughness, angles, branching; (3) evaluation of **scale effects** related with the diameter of the jet.

6. The existing **library of dynamic pressure measurements** can be used to pursue analysis of, for example: (1) extreme pressure values for other geometries and velocities, eventually other scouring scenarios than those presented in Chapter 9; (2) idem, for the corresponding PDF's; and (3) to develop a probabilistic-based version of the analytical model presented in Chapter 5.

Notation

Roman Lower Case

a	sound celerity; celerity of pressure waves
b	diffusion layer half-width; energy decay rate
d	length scale
d_m	mean grain/bubble diameter
d_S, d_{Sauter}	Sauter diameter of air bubbles
d_{p50}	diameter corresponding to a probability of 0.50
d_{90}	characteristic diameter of a grain sample
e	joint thickness
f	frequency
f_{cut}	cut-off frequency
f_{res}	resonance frequency
f_s	sampling frequency
g	gravitational acceleration
h	tailwater level
$\hat{h_k}$	k-spectral component of pressure fluctuations
h_{up}	critical displacement
i	index
k	wave number
l	length of the outlet nozzle
l_y, l_x	x- and y-dimensions of a rock block
m	mass
n	number of acquisition runs; exponent for velocity profile; index for multiple harmonics
n_{bins}	number of classes for histograms
p	total pressure
$\overline{p}$	mean local pressure
p'	pressure fluctuations
p_k, p_{-k}	complex spectral component; idem, conjugate
p_r	relevant /irrelevant pressure
q	unit discharge
r^2	correlation coefficient
t	depth of scour hole; height of pool clylinders
t_{hyd}	ultimate scour depth, from purely hydrodynamic considerations
u'	velocity fluctuations
x	vertical coordinate in the pool; longitudinal coordinate in the fissure
x_A	free diffusion length
x_c	core development length
y	radial coordinate of jet section; radial (horizontal) coordinate at pool bottom
z	normalized variable of Gaussian pdf ($= \frac{p-\mu}{\sigma}$); vertical co-ordinate
z_k	hydraulic impedance (complex)

Roman Capital

A	nozzle section surface; amplitude of p'
B, B_0	plane jet thickness; idem, at issuance; stagnation
C	turbulent constant; void fraction
C_p, C_{paxis}	mean pressure coefficient; idem, at jet axis
$C_{p'}$	turbulent pressure coefficient
$C^+_{p'}$, $C^-_{p'}$	extreme positive/negative pressure coefficient
C_{air}	void fraction; air concentration;
C_d, C_v	diffusion coefficient; idem, for centreline velocity decay
C_s	skewness coefficient
D, D_0	nozzle diameter; jet diameter; idem, at issuance
D_c	diameter of the lateral confinement in the pool
D_m	mean diameter of scour hole in mobile-bed rivers
D_p	depth of air bubble penetration
E	elasticity modulus of the pipe
E_c	kinetic energy
E_u	Euler number
F_0	jet Froude number
F_{aw}	densimetric air-water Froude number
Fr_c	confinement Froude number
F_r	Froude number
H, H_0	energy head, piezometric head; idem, at issuance
I_i	dynamic impulse
I_t	time integral scale
I_x, I_y	integral scales of turbulent flow
J	friction slope
K	excess kurtosis coefficient; bulk modulus of the fluid
L	jet travel distance in the air; length of I-fissure
L_b	jet break-up length in the air
M_a	Sarrau-Mach Number
N	number of samples; Normal/Gaussian distribution
N_b	number of intercepted interfaces air-water
P_{cut}	cut-off probability
P_s, $P_{surface}$	pressure field at the surface of a rock block
P_{up}	pressure field inside the fissure; uplift pressure
P_{xx}	one-sided power spectra estimates
Q, Q_w, Q_0	flow discharge; flow discharge at issuance
Q_a, Q_T	amount of entrained air; total amount of entrained air
R	steady-state friction coefficient
R_c	confinement radius
Re	Reynolds number ($= UD/\nu$)
St	Strouhal number
T	duration of acquisition; discharge duration; time
T_u, Tu_0	jet turbulence intensity; idem, at issuance
U, U_0	mean flow velocity, idem, at issuance
U_i	velocity at entry in pool surface
V, V_0, V_w	velocity; idem, at issuance; idem, of water
V_{air}	volume of air
V_{aw}	interfacial velocity
V_r	bubble rise velocity
W	breadth of scour hole; riverbed width; block weight
We	Weber number
Y, Y_0	pool depth; idem, initial conditions

Greek symbols

α	angle of the flip bucket lip; void fraction; kinetic energy correction factor
α_1	core contraction angle; free diffusion core contraction angle
α_2	spreading angle; free diffusion spreading angle
β	air-water ratio; impinging angle
β_A	free diffusion length in limited-depth pools
β_i	air-water ratio at entry in the pool
γ_w	water specific weigh
Γ	instantaneous amplification factor
Δ	amplification ratio
Δ_t	time interval
ϵ	surface roughness; jet surface disturbances
η	energy dissipation efficiency
θ	exponent for mean pressure reduction in aerated flows
λ_c	length scale of the shear cell
λ_t	Taylor microscale
μ	mean value of dynamic viscosity
ν	kinematic viscosity
ξ	radial dimension of the impinging zone
Π	dimensionless number
ρ, ρ_w	water density
ρ_{xx}	autocorrelation
ρ_{xy}	spatial cross correlation
σ	standard deviation; surface tension
τ	time lag, persistence
τ_{ch}	bubble chord time
τ_{cut}	cut-off persistence
τ_i	persistence of pressure pulse above cut-off
ϕ	confinement ratio for turbulent impact pressures (Chapter 8)
Ω	surface

Acronyms

CJ	core jet
DAC	data acquisition system
DEP-STEP	depth evolution of scour in conical-stepped pools
DEP-VERT	depth evolution of scour in vertical pools
DJ	developed jet
DLC	degree of Lateral Confinement
epdf,Epdf	empirical probability density function
epDf	empirical cumulative distribution
FB	pool with flat bottom
FC	pool with first cylinder
FDZ	flow development zone
FFT	Fast Fourier Transform
FS	stepped pool with first and second cylinders
FSO	full scale output
FST	stepped pool with first, second and third cylinders
Gu	Gumbel
Gpdf	Gumbel probability density function
LAT-DEEP	lateral evolution of scour in deep pools
LAT-SHA	lateral evolution of scour in shallow pools
LCH	Laboratoire de Constructions Hydrauliques
LCP	laterally confined pools
LDDM	limited-depth diffusion model
LMH	Laboratoire de Machines Hydrauliques
LNEC	Laboratório Nacional de Engenharia Civil
LUP	laterally unbounded pools
MLT	mass, length, time
MP1	measuring point 1, Chapter 7
MP2	measuring point 2, Chapter 7
MP3	measuring point 3, Chapter 7
Npdf	Gaussian probability density function
pdf	probability density function
PSD	power spectra density
RMS	root-mean-square
SC	pool with second Cylinder
SHR	scour hole ratio
TC	pool with Third Cylinder
TSL	Turbulent shear layer
ZEF	zone of established flow

Bibliography

Abramovich, G. N. (1963). *The theory of turbulent jets*, M.I.T. Press.

Akhmedov, T. K. (1988). Calculation of the depth of scour in rock downstream of a spillway, *Water Power and Dam Construction* (12): 25–27.

Albertson, M., Dai, Y., Jensen, R. and Rouse, H. (1948). Diffusion of submerged jets, *Transactions of the ASCE* **Paper No. 2409**: 639–664.

Amanian, N. (1993). *Scour below a flip bucket spillway*, Ph. D., Utah State University.

Amanian, N. and Urroz, G. E. (1993). Design of pre-excavated scour hole below flip bucket spillways, *in* H. W. Shen, S. Su and F. Wen (eds), *Hydraulic Engineering '93*, Vol. 1, American Society of Civil Engineers, San Francisco, pp. 856–860.

Amelung, M. (1996). *Auskolkung klüftiger Felssohlen durch Entlastungsstrahlen*, Ph.D. Thesis, TU Braunschweig.

Amri, A. E. and Verrette, J. (2005). Étude quantitative de l'érosion en aval des dissipateurs d'énergie type auge, *Canadian Journal of Civil Engineering* **32**(2): 400–412.

André, S. (2004). *High velocity aerated flows on stepped chutes with macro-roughness elements*, PhD Thesis No. 2993, EPFL.

Annandale, G. W. (1995). Erodibility, *Journal of Hydraulic Research* **33**(4): 471–494.

Annandale, G., Wittler, R., Ruff, J. and Lewis, T. (1998). Prototype validation of erodibility index for scour in fractured rock media, *in* ASCE (ed.), *Proc. Int. Water Resources Eng. Conference*, ASCE, Memphis, pp. 1096–1001.

Armenio, V., T. P. and Fiorotto, V. (1999). On the effects of a negative step in pressure fluctuations at the bottom of a hydraulic jump, *Journal of Hydraulic Research* **38**(5): 359–368.

Arndt, R. E. A. and Ippen, A. T. (1970). Turbulence measurements in liquids using an improved total pressure probe, *Journal of Hydraulic Research* **8**(2): 131–158.

Attari, J., Arefi, F. and Golzari, F. (2002). A review on physical models of scour holes below large dams in Iran, *in* Schleiss and Bollaert (eds), *Rock scour due to falling high-velocity jets*, Swets and Zeitlinger, Lisse, pp. 73–80.

Barata, J. M. M., Durão, D. F. G., Heitor, M. V. and McGuirk, J. (1993). On the analysis of an impinging jet on ground effects, *Experiments in Fluids* **15**: 117–129.

Bellin, A. and Fiorotto, V. (1995). Direct dynamic force measurement on slabs in spillway stilling basins, *Journal of Hydraulic Engineering* **121**(10): 686–693.

Beltaos, S. and Rajaratnam, N. (1973). Plane turbulent impinging jets, *Journal of Hydraulic Research* **11**(1): 29–59.

Beltaos, S. and Rajaratnam, N. (1974). Impinging circular turbulent jets, *Journal of the Hydraulics Division* **100**(10): 1313–1328.

Beltaos, S. and Rajaratnam, N. (1977). Impingement of axisymmetric developing jets, *Journal of Hydraulic Research* **14**(4): 311–326.

Bendat, J. S. and Piersol, A. G. (1971). *Random data: analysis and measuremenst procedures*, Wiley, New York.

Bergant, A. and Simpson, A. R. (1999). Pipeline column separation flow regimes, *Journal of Hydraulic Engineering* **125**(8): 835–848.

Bín, A. K. (1984). Air entrainment by plunging jets, *Proc. Symp. on Scale Effects*, pp. 5.5:1–6.

Bín, A. K. (1993). Gas entrainment by plunging liquid jets, *Chemical Engineering Science* **48**(21): 3585–3630.

Boes, R. (2000). *Zweiphasenströmung und energieumsetzung an grosskaskaden*, PhD Thesis, Mitteilungen No. 166 VAW, ETH Zürich, Switzerland.

Boes, R. M. and Hager, W. H. (1998). Fiber-optical experimentation in two-phase cascade flow, *in* K. Hansen (ed.), *Proc. Int. RCC Dams seminar*, Denver, USA.

Bohrer, J. G., Abt, S. R. and Wittler, R. J. (1998). Predicting plunge pool velocity decay of free falling, rectangular jet, *Journal of Hydraulic Engineering* **124**(10): 1043–1048.

Bollaert, E. (2002a). The influence of plunge pool air entrainment on the presence of free air in rock joints, *in* Schleiss and Bollaert (eds), *Rock scour due to falling high-velocity jets*, Lisse, Swets and Zeitlinger, pp. 137–151.

Bollaert, E. (2004). A comprehensive model to evaluate scour formation in plunge pools, *Hydropower and Dams* (1): 94–101.

Bollaert, E. F. (2002b). *Transient water pressures in joints and formation of rock scour due to high-velocity jet impact*, Communication of the Laboratory of Hydraulic Constructions (LCH) No. 13, EPFL, Lausanne, ISSN 1661-1179.

Bollaert, E. F. R. and Schleiss, A. J. (2003a). Scour of rock due to the impact of plunging high velocity jets. Part I: a state-of-the art review, *Journal of Hydraulic Research* **41**(5): 451–464.

Bollaert, E., Falvey, H. T. and Schleiss, A. (2002). Assessment of turbulent jet impingement on rocky riverbeds: the particular properties of a near-prototype physical model study, *Proc. of Riverflow 2002*, Louvain-la-Neuve, pp. 395–403.

Bollaert, E., Manso, P. and Schleiss, A. (2004). Dynamic pressure fluctuations at real-life plunge pool bottoms, *in* Y. a. Attari (ed.), *Hydraulics of Dams and River Structures*, Balkema, pp. 117–124.

Bollaert, E. and Schleiss, A. (2002). Discussion of "Simulation of scour process in plunging pool of loose bed-material" by Yafei Jia, Tadanori Kitamura, and Sam S. Y. Wang, *Journal of Hydraulic Engineering* **128**(7): 721–723.

Bollaert, E. and Schleiss, A. (2003b). Scour of rock due to the impact of plunging high velocity jets Part II: Experimental results of dynamic pressures at pool bottoms and in one-and two-dimensional closed end rock joints, *Journal of Hydraulic Research* **41**(5): 465–480.

Bollaert, E. and Schleiss, A. (2005). Physically based model for evaluation of rock scour due to high-velocity jet impact, *Journal of Hydraulic Engineering* **131**(3): 153–165.

Bonetto, F. and Lahey Jr, R. T. (1993). An experimental study of air carryunder due to a plunging liquid jet, *International Journal of Multiphase Flow* **19**(2): 281–294.

Brattberg, T. and Chanson, H. (1998). Air entrapment and air bubble dispersion at two-dimensional plunging water jets, *Chemical Engineering Science* **53**(24): 4113–4127.

Burattini, P., Antonia, R. A., Rajagopalan, S. and Stephens, M. (2004). Effect of initial conditions on the near-field development of a round jet, *Experiments in Fluids* **37**: 56–64.

Cain, P. and Wood, I. R. (1981). Instrumentation for aerated flow on spillways, *Journal of Hydraulic Engineering* **107**(11): 1407–1424.

Canepa, S. and Hager, W. H. (2003). Effect of air content on plunge pool scour, *Journal of Hydraulic Engineering* **129**(5): 358–365.

Carbone, V., Regnoli, G., Martines, E. and Antoni, V. (2000). Intermittency and self-similarity in plasma edge fluctuations, *Physics of Plasmas* **7**(2): 445–447.

Carreras, B. A., Milligen, B. P. v., Pedrosa, M., Balbín, R., Hidalgo, C., Newman, D., Sanchéz, E., Frances, M., García-Cortés, I., Bleuel, J., Endler, M., Riccardi, C., Davies, S., Matthews, G. F., Martines, E., Antoni, V., Latten, A. and Klinger, T. (1998). Self-similarity of the plasma edge fluctuations, *Physics of Plasmas* **5**(10): 3632–3643.

Cartellier, A. (1992). Simultaneous vodi fraction measurement, bubble velocity and size estimate using a single optical porbe in gas-liquid two-phase flows, *Review of Scientific Instruments* **63**(11): 5442–5453.

Cartellier, A. and Achard, J. L. (1991). Local phase detection probes in fluid/fluid two-phase flows, *Review of Scientific Instruments* **62**(2): 279–303.

Chanson, H. (1997). *Air bubble entrainment in free-surface turbulent shear flows*, Academic Press.

Chanson, H. (2004a). Air-water flows in water engineering and hydraulic structures. Basic processes and metrology., *in* Yazandoost and Attari (eds), *Hydraulics of dams and river structures*, Taylor and Francis Group, Tehran, pp. 3–16.

Chanson, H. (2004b). The compressibility of extra-high-velocity aerated flow, *Journal of Hydraulic Research* **42**(2): 213–215.

Chanson, H., Aoki, S. and Hoque, A. (2004). Physical modelling and similitude of air bubble entrainment at vertical circular plunging jets, *Chemical Engineering Science* **59**: 747–758.

Chassaing, P. (2000). *Turbulence en Mécanique des fluides - Analyse du phénomène en vue de sa modélisation à l'usage de l'ingénieur (in French)*, POLYTECH, Cépaduès-Editions, Toulouse.

Clanet, C. and Lasheras, J. C. (1997). Depth of penetration of bubbles entrained by a plunging water jet, *Physics of Fluids* **9**(7): 1864–1866.

Cola, R. (1965). Energy dissipation of a high-velocity vertical jet entering a basin, *Proc. Xxi iahr congress*, Vol. I, paper 1.52, IAHR, Leninegrad, pp. 1–13.

Cola, R. (1966). Diffusione di un getto piano verticale in un bacino d'acqua d'altezza limitata, *L'Energia Elettrica* **43**(11): 649–664.

Comte-Bellot, G. and Corrsin, S. (1966). The use of a contraction to improve the isotropy of grid-generated turbulence, *Journal of Fluid Mechanics* **25**(4): 657–682.

Covas, D., Ramos, H. and Almeida, A. B. (2005). Impulse response method for solving hydraulic transients in viscoelastic pipes, *XXXI IAHR Congress*, Vol. 1 - CD-Rom, IAHR, Seoul, pp. 676–686.

Cummings, P. D. and Chanson, H. (1997). Air entrainment in the developing flow region of plunging jets - Part 2: experimental, *Journal of Fluids Engineering* **119**(9): 603–608.

Droz, P. (2000). *Problèmes dynamiques des fondations de machines hydrauliques*, Lecture notes of the Advanced Master in Hydraulic Schemes, Laboratoire de Constructions Hydrauliques, Lausanne.

Ervine, A. and Falvey, H. T. (1987). Behaviour of turbulent water jets in the atmosphere and in plunge pools, *Paper 9136, Water Eng. Group, Proc. of the Institution of Civil Engineers, Part 2,*, Vol. 83:, pp. 295–314.

Ervine, D. A., Falvey, H. R. and Withers, W. (1997). Pressure fluctuations on plunge pool floors, *Journal of Hydraulic Research* **35**(2): 257–279.

Fahlbusch, F. E. (1994). Scour in rock riverbeds downstream of large dams, *International Journal on Hydropower and Dams* **46**(7): 30–32.

Falvey, H. T. (1980). *Air-water flow in hydraulic structures*, Vol. Engineering Monograph No. 41, Denver.

Falvey, H. T. (1990). *Cavitation in chutes and spillways*, Vol. Engineering Monograph No. 42, Denver.

Falvey, H. T. and Ervine, D. A. (1988). Aeration in jets and high-velocity flows, *in* P. Burgi (ed.), *Proc. Symp. Model-prototype correlation*, Colorado, pp. 25–55.

Ferrando, A. M. and Rico, J. R. (2002). On the incipient aerated flow in chutes and spillways, *Journal of Hydraulic Research* **40**(1): 95–97.

Fiorotto, V. and Rinaldo, A. (1988). Sul dimensionamento delle protezioni di fondo in bacini di dissipazione a risalto: nuovi risultati teorici e sperimentali, *Giornale del Genio Civile* **7-8-9**: 179–201.

Fiorotto, V. and Rinaldo, A. (1992a). Fluctuating uplift and lining design in spillway stilling basins, *Journal of Hydraulic Engineering* **118**(4): 578–596.

Fiorotto, V. and Rinaldo, A. (1992b). Turbulent pressure fluctuations below hydraulic jumps, *Journal of Hydraulic Research* **30**(4): 499–520.

Fiorotto, V. and Salandin, P. (2000). Design of anchored slabs in spillway stilling basins, *Journal of Hydraulic Engineering* **126**(7).

Furstenburg, L., Huraut, J. P., Blake, K. R. K. and Zwanborn, J. A. (1991). The influence of foundation conditions on spillway and plunge pool design at Katse dam, *Proc. XVII ICOLD Congress*, ICOLD, Vienne, pp. Q.66 R93, 1727 – 1743.

Gilard, V. and Brizzi, L.-E. (2005). Slot jet impinging on a concave curved wall, *Journal of Fluids Engineering* **127**(5): 595–603.

Gunko, F. G., Burkov, A. F., Isachenko, N. B., Rubinstein, G. L., Soloviova, A. G. and Yuditskii, G. A. (1965). Research on the hydraulic regime and local scour of river bed

below spillways of high-head dams, *Proc. XI IARH Congress*, Vol. paper 1.50, IAHR, Leninegrad.

Gutmark, G., Wolfshtein, M. and Wygnanski, I. (1978). The plane turbulent impinging jet, *Journal of Fluid Mechanics* **88**(4): 737–756.

Hartung, F. and Häusler, E. (1973). Scours, stilling basins and downstream protection under free overfall jets at dams, *Proc. of the 11th Congress on Large Dams*, Vol. Q41 R3, ICOLD, Madrid, pp. 39–56.

Henderson, J. B., McCarthy, M. and Molloy, N. (1970). Entrainment by plunging jets, *Proc. of CHEMECA '70*, Vol. Section 2, Melbourne, pp. 86–100.

Ho, C.-M. and Nosseir, N. S. (1981). Dynamics of an impinging jet: the feedback phenomena, *Journal of Fluid Mechanics* **105**: 119–142.

Ho, C.-M., Plocher, D. A. and Leve, H. L. (1977). Surface pressure fluctuation generated by a jet impinging on a curved plate, *AIAA Journal* **15**(9): 1348–1350.

Holdhusen, J. S. (1948). Discussion of "Diffusion of submerged jets" by Albertson et al. (1948), *Transactions of the ASCE* **Paper No. 2409**: 665–671.

Jaeger, C. (1977). *Fluid transients: in hydro-electric engineering practice*, Blackie, Glasgow and London.

Jia, Y., Kitamura, T. and Wang, S. S. Y. (2001). Simulation of scour process in plunging pool of loose-bed material, *Journal of Hydraulic Engineering* **127**(3): 219–229.

Juon, R. and Hager, W. H. (2000). Flip bucket without and with deflectors, *Journal of Hydraulic Engineering* **126**(11): 837–845.

Kamoi, A. and Tanaka, H. (1972). Measurements of wall shear stress, wall pressure and fluctuations in the stagnation region produced by oblique jet impingement, *in* D. J. Cockrell (ed.), *Fluid Dynamic Measurements Conference Papers*, Vol. 1, pp. 217–227.

Knowles, K. and Myszko, M. (1998). Turbulence measurements in radial wall-jets, *Experimental Thermal and Fluid Sciences* **17**: 71–78.

Kobus, H. (1984). Local air entrainment and detrainment, *in* IAHR (ed.), *Proc. Symp. "Scale effects in modelling hydraulic structures"*, Vol. paper 4.10, IAHR, Esslingen.

Kobus, H., Leister, P. and Westrich, B. (1979). Flow field and scouring effects on steady and pulsating jets impinging on a movable bed, *Journal of Hydraulic Research* **17**(3): 175–192.

Kraatz, W. (1965). Flow characteristics of a free circular water jet, *Proc. of the XXI IAHR Congress, paper 1.44*, Vol. I, IAHR, Leninegrad.

Lemos, F. (1982). Behaviour of hydraulic structures of some dams built in narrow valleys (in Portuguese), *Trans. of the Int. Symp on the Layout of Dams in Narrow Gorges*, ICOLD, Brazil, pp. 241–252.

Lesleighter, E. J. (1988). Cavitation in Hydraulic structures, *in* P. Burgi (ed.), *Proc. of the Int. Symp. on Model-Prototype Correlation of Hydraulic Structures*, pp. 74–94.

Levi, E. (1995). *The science of water: the foundation of modern hydraulics*, ASCE Press, New York.

Löfdahl, L. and Gad-el Hak, M. (1999). MEMS-based pressure and shear stress sensors for turbulent flows, *Measurement Science and Technology* **10**(8): 665–686.

Liu, P. (2005). A new method for calculating depth of scour pit caused by overflow water jets, *Journal of Hydraulic Research* **43**(6): 695–701.

Liu, P., Gao, J., Li, Z. and Li, Y. (1997). Mechanism of energy dissipation and hydraulic design for plunge pools downstream of large dams, *Proc. XXVII Congress*, IAHR, San Francisco, pp. 417–422.

Liu, P., Li, F. and Yin, W. (2003). Experimental study on controlling parameters of flow patterns downstream of high dams, Vol. Theme D, IAHR, pp. 839–844.

Liu, P. Q., Dong, J. and Yu, C. (1998). Experimental investigations of fluctuation uplift on rock blocks at the bottom of the scour pool downstream of Three Gorges spillway, *Journal of Hydraulic Research* **36**(1): 55.

Locher, F. A. and Hsu, S. T. (1984). Energy dissipation at high-dams, *in* P. Novak (ed.), *Developments in Hydraulic Engineering*, Vol. 2 of *Hydraulic Engineering - Periodicals*, Elsevier, pp. 183–238.

Lopardo, R. A. and Henning, R. E. (1985). Experimental advances on pressure fluctuations beneath hydraulic jumps, *Proc. 21st IAHR Congress*, Vol. 3, IAHR, Melbourne, pp. 633–638.

Lyons, R. G. (1997). *Understanding digital signal processing*, Addison Wesley Longman, Inc.

Malmström, T. G., Kirkpatrick, A. T., Christensen, B. and Knappmiller, K. D. (1997). Centreline velocity decay measurements in low-velocity axysymmetric jets, *Journal of Fluid Mechanics* **346**: 363–377.

Mandelbrot, B. B. (2002). *Gaussian self-affinity and fractals*, Springer.

Manso, P., Bollaert, E. F. and Schleiss, A. J. (2005a). Impact pressures generated by high-velocity jets in a flat pool, *submitted to the Journal "Experiments in Fluids"* .

Manso, P., Bollaert, E. and Schleiss, A. (2004a). Influence of rock scour geometry on dynamic pressures due to jet impact, *Proc. of the 2nd Int. Conference on Scour and Erosion, 14-17 Nov., CD-Rom*, Singapore.

Manso, P., Bollaert, E. and Schleiss, A. (2005b). Evaluation of high-velocity plunging jet issuance characteristics as a basis for plunge pool analysis, *submitted to the Journal of Hydraulic Research* .

Manso, P., Bollaert, E. and Schleiss, A. J. (2004b). Experimental investigation on high-velocity jet characteristics and its influence on plunge pool scour, *in* Yazdandoost and Attari (eds), *Hydraulics of dams and river structures*, Balkema, Tehran, Iran, pp. 173–180.

Manso, P., Bollaert, E. and Schleiss, A. J. (2005c). Dynamic pressures generated by plunging jets in confined pools under extreme flood discharges, *Proc. XXXI IAHR Congress*, Vol. CD, IAHR, Seoul.

Manso, P., Fiorotto, V., Bollaert, E. F. and Schleiss, A. J. (2004). Discussion to "Effect of jet air content on plunge pool scour" by Stefano Canepa and Willi H. Hager, *Journal of Hydraulic Engineering* **130**(11): 1128–1130.

Martins, R. (1973a). Contribution to the knowledge on the scour action of free jets on rocky riverbeds, *Proc. of the 11th Congress on Large Dams*, Vol. Q41 R44, ICOLD, Madrid, pp. 799–814.

Martins, R. (1973b). *Scouring action of free jets downstream of hydraulic structures (in Portuguese)*, Vol. Memória LNEC No. 424, LNEC.

Martins, R. (1975). Scouring of rocky riverbeds and free-jet spillways, *Int. Water Power and Dam Construction* **27**(4): 152–153.

Martins, R. (ed.) (1977). *Kinematics of the free jet in the field of hydraulic structures (in Portuguese)*, Vol. Memória LNEC No. 486, LNEC, Lisbon.

Mason, P. J. (1993). Practical guidelines for the design of flip buckets and plunge pools, *Water Power and Dam Construction* **45**(September/October): 40–45.

Mason, P. J. and Arumugam, K. (1985). Free jet scour below dams and flip buckets, *Journal of Hydraulic Engineering* **111**(2): 220–235.

Matos, J., Frizell, K., André, S. and Frizell, W. (2002). On the performance of velocity measurement techniques in air-water flows, *in* Wahl (ed.), *Proc. Conf. on Hydraulic Measurements and Experimental Methods*, ASCE, Estes Park, USA, p. CD.

May, R. W. P. and Willoughby, I. R. (1991). Impact pressures in plunge basins due to vertical falling jets, *Report SR242*, HR-Wallingford.

McKeogh, E. J. and Elsawy, E. M. (1980). Air retained in pool by plunging water jet, *Journal of the Hydraulic Division* **106**(10): 1577–1593.

McKeogh, E. J. and Ervine, D. A. (1981). Air entrainment rate and diffusion pattern of plunging liquid jets, *Chemical Engineering Science* **36**: 1161–1172.

Melo, J. (2002a). Presentation at the International Workshop on Rock Scour.

Melo, J. F. (2001). *Hydrodynamic loads acting on floor slabs of energy dissipation basins by plunging jets (in Portuguese)*, Ph. D. Thesis, Instituto Superior Técnico, Lisbon, Portugal.

Melo, J. F. (2002b). Reduction of plunge pool floor dynamic pressure due to jet air entrainment, *in* Schleiss and Bollaert (eds), *Rock scour due to falling High-velocity Jets*, Swets and Zeitlinger, Lisse, pp. 125–136.

Melo, J. F., Pinheiro, A. N. and Ramos, C. M. (2006). Forces on plunge pool slabs: influence of joints location and width, *Journal of Hydraulic Engineering* **132**(1): 49–60.

Mih, W. C. and Kabir, J. (1983). Impingement of water jets on nonuniform streambed, *Journal of Hydraulic Engineering* **109**(4): 536–548.

Mitosek, M. (2000). Study of transient vapor cavitation in series pipe systems, *Journal of Hydraulic Engineering* **126**(12): 904–911.

Montgomery, R. (1984). *Investigations into rock erosion by high-velocity water flows*, Ph. D., The Royal Institute of Technology.

Nezu, I. and Nakagawa, H. (1993). *Turbulence in open-channel flows*, Monograph series, A.A. Balkema, Rotterdam.

Pinheiro, A. (1995). *Acções hidrodinâmicas em soleiras de bacias de dissipação de energia por ressalto*, Ph. D. Thesis, Instituto Superior Técnico, Lisbon, Portugal.

Puertas-Agudo, J. (1994). *Hydraulic criteria for the design of energy dissipation basins in arch dams with free crest overfall*, Ph. D. Thesis, Universitat Politècnica de Catalunya.

Puertas, J. and Dolz, J. (2002). Pressure fields due to the impingement of free falling jets on a riverbed, *in* Schleiss and Bollaert (eds), *Rock scour due to falling high-velocity jets*, Swets and Zeitlinger, Lisse, pp. 105 – 114.

Quintela, A. C. (1981). *Hidráulica*, 4th edn, Fundação Calouste Gulbenkian.

Quintela, A. C. and Cruz, A. A. d. (1982). Cahora-Bassa dam spillway. Conception, hydraulic model studies and prototype behaviour, *Trans. of the Int. Symp on the Layout of Dams in Narrow Gorges*, ICOLD, Brazil, pp. 301–309.

Quintela, A. C., Cruz, A. A. and Fernandes, J. S. (1987). Cahora-Bassa dam spilway. Design and prototype behaviour (in Portuguese), *Iberian-American Conference on Hydraulic Schemes*, Lisbon, pp. C197–C206.

Rajaratnam, N. (1976). *Turbulent jets*, Vol. 5 of *Developments in Water Science*, Elsevier.

Rajaratnam, N. (1981). Erosion by plane turbulent plane jets, *Journal of Hydraulic Engineering* **19**(4): 339–358.

Rajaratnam, N. and Mazurek, K. A. (2002). Erosion of a polysterene bed by obliquely impinging circular turbulent air jets, *Journal of Hydraulic Research* **40**(6): 709–716.

Rajaratnam, N. and Mazurek, K. A. (2003). Erosion of sand by circular impinging water jets with small tailwater, *Journal of Hydraulic Engineering* **129**(3): 225–229.

Ramos, C. M. (1982). Energy dissipation on free jet spillways. Bases for its study in hydraulic models, *Trans. of the Int. Symp on the Layout of Dams in Narrow Gorges*, Vol. 1, ICOLD, Brazil, pp. 263–268.

RBI (1999). Logiciel VIN 2.0 - Etude des écoulements diphasiques: Manuel d'utilisation.

Renna, F., Fratino, U. and Matos, J. (2005). Air-water flow features in skimming flow over steeply sloping stepped spillways, *IAHR Congress*, Vol. CD Rom, IAHR, Seoul, pp. 2664–2674.

Rinaldi, P. and Valentin, F. (2005). Non-dimensional scaling of turbulent jets in confined spaces, *in* Lee and Lam (eds), *Environmental Hydraulics and Sustainable Water Management*, Taylor and Francis Group, London, pp. 319–324.

Rouse, H., Howe, J. and Metzler, D. (1951). Experimental investigations of fire monitors and nozzles, *Proc. of the ASCE Hydraulics Division* **77**(Separate 92): 1–29.

Salehi-Neyshabouri, A., Silva, A. M. F. d. and Barron, R. (2003). Numerical simulation of scour by a free falling jet, *Journal of Hydraulic Research* **41**(5): 533–539.

Sanchez-Bribiesca, J. L. and Fuentes-Mariles, O. A. (1979). Experimental analysis of macroturbulence effects on the lining of stilling basins, *XXXIII Congress on Large Dams*, Vol. Q50-R6, ICOLD, New Delhi, pp. 85–103.

Sarkaria, G. S., Piasentin, C., Fiorini, A. S. and Carvalho, E. (2003). Operational efficiency of large spillways: eight Brasilian case studies, *International Journal on Hydropower and Dams* **55**(4): 47–57.

Schleiss, A. (1985). *Bemessung von Druckstollen*, Vol. Teil 1, Mitteilungen de Versuchsanstalt für Wasserbau, Hydrologie und Glaziologie No. 78, ETH Zürich, VAW.

Schleiss, A. (1993). Estimation of scour depth at plunge pool for Karun I dam in Iran.

Schleiss, A. J. (2002). Scour evaluation in pace and time - the challenge of dam designers, *in* Schleiss and Bollaert (eds), *Rock scour due to falling high-velocity jets*, Swets and Zweitinger, pp. 3–22.

Sene, K. J. (1988). Air entrainment by plunging jets, *Chemical Engineering Science* **43**(10): 2615–2623.

Spurr, K. J. W. (1985). Energy approach to estimating scour downstream of a large dam, *International Water Power and Dam Construction* **37**(11): 81–89.

Stearns, S. D. (2003). *Digital signal processing with examples in MATLAB*, CRC Press, Boca Raton.

Streeter, V. L. and Wylie, E. B. (1983). *Fluid Mechanics*, Civil and Mechanical Engineering Series, Mc-Graw Hill.

Taraimovich, I. I. (1979). Deformations of channels below high-head spillways on rock foundations, *Hydrotech. Constr. translated from Gidro. Stroit. 1978, 9: 38-42 by Plenum Publishing Corporation* pp. 917–923.

Taraimovich, I. I. (1981). Calculation of local scour of rock foundations by high-velocity flows, *Hydrotech. Constr. translated from Gidro. Stroit. 1980, 8: 19-22 by Plenum Publishing Corporation* pp. 791–796.

Toso, J. W. and Bowers, C. E. (1988). Extreme pressures in hydraulic-jump stilling basins, *Journal of Hydraulic Engineering* **114**(8): 829–843.

Ursino, N., S. P. and Da Leppo, L. (2003). Fluctuating pressures at the bottom of a plunge pool, *Proc. of the XXX IAHR Congress*, Vol. Theme C, IAHR, Thessaloniki, pp. 191–198.

Vischer, D. L. and Hager, W. H. (1998). *Dam Hydraulics*, John Wiley and Sons, West Sussex (UK).

Weilin, X., Huasheng, L., Yongquan, Y. and Chigong, W. (2002). Turbulent flow and energy dissipation in plunge pool of high arch dam, *Journal of Hydraulic Research* **40**(4): 471–476.

Weilin, X., Jun, D., Jingxue, Q., Shanjun, L. and Wei, W. (2004). Experimental investigation on influence of aeration on plane jet scour, *Journal of Hydraulic Engineering* **130**(2): 160–164.

Whittaker, J. G. and Schleiss, A. J. (1984). *Scour related to energy dissipators for high head structures*, Vol. VAW Mitteilungen N.73, VAW - ETHZ, Zürich.

Wood, I. R. (1991). *Air entrainment in free-surface flows*, Vol. 4 of *Hydraulic structures design manual*, Balkema, Rotterdam.

Wood, I. R., Ackers, P. and Loveless, J. (1983). General method for critical point on spillways, *Journal of Hydraulic Engineering* **109**(2): 308–312.

Wylie, E. and Streeter, V. L. (1978). *Fluid Transients*, Mc-Graw Hill.

Yuditskii, G. (1963). *Hydrodynamic loading of a falling nappe over blocks of a rocky riverbed and its failure conditions (Acção hidrodinâmica de uma lâmina descarregada sobre blocos de um leito rochoso e condições de rotura deste), (in Portuguese)*, LNEC, Lisbon, Translation No 442 of the publication "Silovoe vozdeistvie padayushchei strui

na otdel'nosti skal'nogo osnovaniya i usloviya ego razrusheniya" from "Izvestiya VNII GidroTekhniki, Moskva", Leninegrad, No. 62, 1963, pp: 35-60.

Zaman, K. B. M. Q. (1999). Spreading characteristics of compressible jets from nozzles of various geometries, *Journal of Fluid Mechanics* **383**: 197–228.

Zhao, J. F. and Li, W. (2000). Investigation of the compressibility of extra-high-velocity aerated flows, *Journal of Hydraulic Research* **38**(5): 351–358.

Acknowledgements

This research project was performed at the Laboratory of Hydraulic Constructions of the *Ecole Polytechnique Fédérale de Lausanne* under the supervision of Prof. Anton Schleiss. I would like to thank him for welcoming me in his team. I thank him for the autonomy and the opportunities granted, his restless support, his open-mind and for the wise technical, scientific and personal advice. It has been a great pleasure working with him.

The present research project was funded by the Federal Office for Water and Geology (FOWG, Switzerland) and by the grant $SFRH/BD/6894/2001$ of the Foundation for Science and Technology (FCT, Portugal). I thank in particular Mr. Henri Poutgasch, former Director of the Department of Dams of the FOWG, for his vivid interested for my research and his continuous support.

I thank the members of the jury, Profs. François Avellan, Virgilio Fiorotto, Pierino Lestuzzi, Jorge Matos, Anton Schleiss and Ian Smith for their comments and proof reading.

The experimental part of this work was accomplished with the dedicated assistance of Mr. Louis Schneiter, Mr. Marc-Eric Pantillon, Mr. Rene Fontannelaz, Mr. Michel Teuscher and the hydraulic intuition of Dr. Jean-Louis Boillat. The efficient start in the use of the fiber optical probe for air-water flows was made possible due to the kind assistance of Dr. Stéphanie André.

Monthly progress meetings were regularly held with Prof. Anton Schleiss, and often with Dr. Erik Bollaert. I acknowledge Erik's participation in these meetings as well as his comments on the spin-off publications of my research.

I thank the Laboratory of Hydraulic Machinery of EPFL of Prof. François Avellan for their support in the calibration of the pressure transducers, namely Dr. Mohammed Farhat, Ms. Silvia Natal, Mr. Louis Bézençon and Mr. Daniel Rouiller.

In Spring 2002, while preparing the enrollment as Ph. D. candidate at EPFL, I followed a course in "Instability and Turbulence" given by Dr. Emannuel Leriche from the LIN - Laboratory of Numeric Engineering, as well as a course in "Application-oriented introduction to Digital Signal Processing" given by Dr. Jean-Marc Vesin from the LDST - Laboratory of Digital Signal Treatment, which were both quite useful for my research work. Their enthusiasm for these topics was a good motivation for the initial steps of my research.

In 2003 I participated in the $21st$ Congress of the International Committee on Large Dams (ICOLD) in Montreal, Canada, after being selected by the Swiss Committee on Dams (SCOD) to participate in the "Next Generation" poster competition. I thank the SCOD as well as the Canadian Organizing Committee for this opportunity, that was rewarded with a Prize.

I thank also all of those who gave me positive input in discussions or send me valuable literature and data, namely Emil Hopfinger (LEGI-INP Grenoble/France), António

Pinheiro (IST-UT Lisbon/Portugal) Henry Falvey (USA), Mustafa Altinakar (CCHE-MU, Mississipi/USA), Victor Saouma (CSU- Colorado/USA), Hubert Chanson (QU, Queensland/Australia), António Quintela (IST-UT Lisbon/Portugal), Ascensio Lara (Coyne et Bélier/France), Wim Uitjewall (TU Delft/Netherlands), António Amador (ESTB-IP Setúbal/Portugal), Soheila Talebi (Mahab Ghodss/Iran), Jeronimo Puertas Agudo (CITEE Coruna/Spain), Soleyman Emami (Mahab Ghodss/Iran), Marcelo Giulian Marques (IPH-UF Rio Grande do Sul/Brazil) and Farid Boushaba (Univ. Oujda/Morocco).

Throughout these last years I had the opportunity to supervise the laboratory works and projects of several undergraduate students, some of which concerned directly the topic of my research. The former students (now good colleagues) Rémi Martinerie, Sophie Crisinel, Jonathan Nieto and Matteo Federspiel gave me very positive input with their excellent reports and enthusiasm.

I had the opportunity to work directly with several external experts. In 2003, Prof. Virgilio Fiorotto from the University of Trieste (Italy) visited the LCH. In 2004, I spend some time at the CEHIDRO - Center for the study of Hydrosystems in Lisbon in June to work with Prof. Jorge Matos (UTL/IST, Portugal). I also have good memories of nice discussions with Floriana Renna and Rui Ferreira on air-water flows, pressure fluctuations and the outside world in general. In September 2004, it was my turn to visit Trieste, where I was warmly welcomed. For that I thank Elpidio Caroni, Cristian Marson, Daniel Tirelli, Luca Falconer, Mauro Castelarin, and Davide Russo and his friends. In 2005, both Jorge Matos and Virgilio Fiorotto visited EPFL in July for some intense days of discussion. These discussions were some of the best moments I had while preparing this thesis. In December 2005, right after the Ph.D. exam, I visited the National Laboratory of Civil Engineering (LNEC, Portugal) to work with Dr. José Falcão de Melo at the Hydraulic Department. His support, comments and recommendations were capital at the beginning and throughout the preparation of this thesis. In 2004 and 2005 I had the pleasure of working with Prof. Michel Pirotton (University of Liege/Belgium) on transient flows inside fissures and also on pool flows. I would like to thank him for his interest and open-mind.

In all these visits and partnerships I was able to find experts whose intellectual generosity and scientific curiosity have greatly inspired me.

A word of appreciation is also due to Fabrice Ribblet and Bruno Livramento from the Chemistry Department of EPFL for their help in defining the thermodynamic equilibrium conditions for gas solubility in water.

Apart from the professional life, my living experience in Lausanne was spiced up with the friendship of many: the members of Entrelaçar; the several batches of the MAS in Hydraulic Schemes; the rowing family of the LS-Aviron; the IAPHS universe; former LRH now LHE members; my Chinese-French tandem partners; the CDM crew; the sound environment created by the LCH's past & present staff; and, in particular, the lusophone communities of EPFL. Among these, I thank personally Marcelo Ribeiro for his eternal good spirit and readiness, Luisa Lopes for her deep-rooted friendship and incredible laugh, and Mário Franca for our enthusiastic discussions and day-dreaming exercises.

My family and my friends in Portugal and around the world were always over supportive; such trust kept me going at all times and I thank them for that. This work is dedicated to the memory of my grandparents, whose life example I keep well casted in my backbone, to my loving parents, sister and brother-in-law. I thank my wife Janina with all my heart for her incredible support throughout these years.

A. Review of prototype plunge pools

Table A.1.: Geology and feedback from pool operation for cases in Table 2.1

Dam	Riverbed characteristics	Plunge pool characteristics	Feedback from operation and interventions
CB	Sound granitoid gneiss with very little cracking, block size: $d_{85} = 2.625$ m, $d_{50} = 2.1$ m and $d_{15} = 0.975$ m	In operation since late 1974, *symmetrical* pool both axial-wise, depth of ≈ 30 m below initial river bed, 200 m long, axial slopes ≈ 14° and lateral slopes between 33° (left bank) and 50° (right bank). Riverbed width ≈ 80-100 m. D/s section rating curve imposes 50 m deep tailwater level for design flood.	Observations after eight and twelve years of operation and several major floods afterwards (1975, 1977/78) show scour is less deep than expected and more extended longitudinally. The bar downstream is not so high as in the 1:75 model. Surveys in 1975, 1980 and 1982. Second model tests performed with a cohesive mixture of gravel, sand, aluminous cement and water, in good agreement with the observed prototype conditions. Visual inspection by divers in 1985 showed large loose blocks in the pool (potential for "ball milling"). Operation with 8 orifices revealed very high and sporadic upward flow ejections from pool. Up to 1987 two orifices had worked 5.7 over 12 years.
K	Gneiss, fracture spacing (≈ d_m) was 0.5 m. Also mentioned 88 kN prototype blocks.	Deep pool, u/s slope milder than steep d/s slope. In operation since 1960, by 1966 the scour hole was ≈ 50 m deep (≈ . 88 m in 1979) and 130 m long. Upstream slope approximately 1V: 1.5H (33°)	First model test (before commissioning) with non-cohesive material overestimated scour, second model (after first years of operation) with a cohesive mixture of gravel, clay and water, agreed fairly well with the observed scour at that time (1973). Risk of instability of pool slopes identified soon afterwards. Stabilizing works were done in the 1990's.
P	Granite, block size ≈ 1.0 m	In operation since 1958, by 1965 a 20 m deep and 120 m long symmetrical scour hole had developed. Longitudinal slopes of 1V:3H (18.4°) and very steep side slopes. The river is 80 m wide at pool section.	After major floods in 1962, the scour hole was 20 m deep and a 15 m high bar had formed. In 1979 scour was 22 m deep, 163 m long. Scour was punctually deeper than predicted in feasibility model tests, despite not being so extensive. Tests were repeated after major flooding. Stabilizing works in the 1960's for the plunge pool and margins.
Kr	Granite, 5 m of weathered rock at the surface	In operation since the late 1950's, upstream pool slope of 21°	14 m of scour in 1964, 16 m in 1966, 17 m in 1979 from floods during construction with higher unit discharge than expected for operation. 17 % less than predicted in model.
I	Fractured limestone	In operation since 1980, upstream slope of 32°	80 m of scour observed as of 1994.
Kar	-	In operation since 1976, u/s slope of 35°, d/s slope of 1V: 5H (11°). Side slopes 30° - 40°	Scour of ≈ 18 m (1993). Scour was less deep than predicted in model.

Table A.2.: cont.

Dam	Riverbed characteristics	Plunge pool characteristics	Feedback from operation and interventions
E	300 m-thick strata of fine grained quartzite	-	The spillway has operated for about 10 % of total operational life. Lack of pre-excavated pool contributed to an irregular erosive process. Current concentration at left bank lead to asymmetric lateral erosion. Modifications and repairs were necessary to the spillway chute and buckets structures, that resulted in a decrease in intensity of the counter currents.
FdA	Dense basalts	Pre-excavated pool with exiting channel. Scour depth of 25 m (1983)	Very large floods in 1983 (86 % of design flood), 1985 and 1992. Erosion close to the lateral walls.
F	Laminated quartzite, dipping 10° d/s	-	Important flood in 1992. Minor repairs. Operated for 11 % of operational life.
It	Basalt, breccia	Several meters deeper than pre-excavation. Survey in 1988 showed a 30-m deep hole at the right bucket.	Concrete slabs, light shotcrete protection and pre-excavated pool. Large floods in 1982 and 1983. Continuous operation from 1982 till 1991. Scouring greater than expected, partial collapse of right bank rock slope, largely because of the highly jointed natural rock surfaces and continuous operation. Repair consisted in the construction of massive reinforced concrete walls anchored to the rock. 1991 survey results were similar to model tests.
SS	Fractured and weathered basalt, dense basalt underneath	5 m deep, 300 m long scour pit	Scouring lead to bar formation and intensification of return currents. Repair and protection work was necessary. After 23 years and spillway operation for 43 % of total operational life, scour has stabilized.
Tu	-	Pre-excavated pool.	Continuous operation of spillways for 93 months from 1984 to 1992. During 18 years, 6 floods $> 31000\ m^3/s$ were recorded. 1984 survey showed accumulation of sediments in low velocity region of plunge pool, which were removed after the larger floods. Only minor erosion was observed in the pool regarding the pre-excavated geometry.
X	-	Pre-excavated pool 70-100 m long and 100 m wide.	Tailwater levels are low. Main purpose is to confine low discharges. Scour observed at discontinuities of the rock mass.
SL	Quartzite	-	In operation since 1942, in 2001 first operation of spillways lead to 7 m of scour
Kat	Basalt with interposed breccia horizontal layers, micro-fracture spacing of 0.30 m	Tailpond dam	Model studies at 1:30. Plunge pool created by a 17 m high tailpond dam, natural tailwater would be only of a few metres

B. List of pool geometries tested, hydraulic and geometric parameters, and measuring positions

Table B.1.: Schematic representation of pool geometries used in the experimental tests. For each series, the number of pool depths, jet velocities and transducers is indicated, as well as the geometric characteristics of the confinements

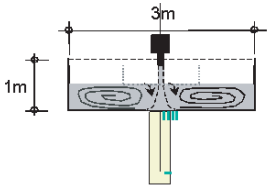

Y/ D = variable (0.075, 0.20//0.10/0.60, sub, #8)

V variable (#10)

Transducers: 25/50/75/95/150 + end -fissure (#6)

FB1

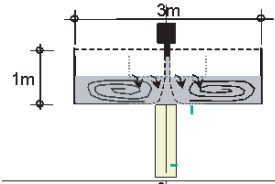

Y/ D = variable (0.075, 0.20//0.10/0.60, sub #8)

V variable (#10)

Transducers: 200 (5//10°) + end-fissure (#6)

FB2

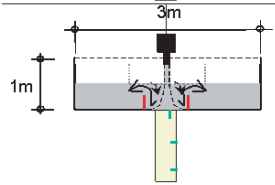

Y/ D = variable (0.30//0.10/0.60, 0.67, sub #6)

V variable (#10)

Transducers: 25, end-fissure, mid-fissure (#3)

FC1

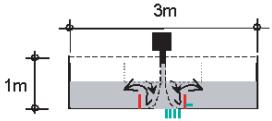

Y/ D = variable (0.30//0.10 > 0.82, #6)

t/D=2.8 ; D/ D= 5.6

V variable (#10)

Transducers: 25/50/75/95 + lateral (#5)

FC2

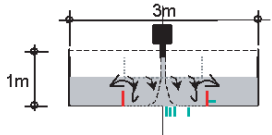

Y/ D = variable (0.30//0.10 > 0.82, #6)

t/D=2.8; Dc/ D= 11

V variable (#10)

Transducers: 25/50/75/(95 or 200)/Lat (#5)

SC1

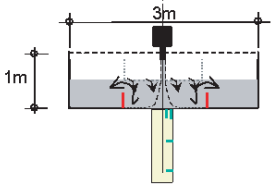

Y/ D = variable (0.20, 0.30,0.40,0.67, #4)

t/D=2.8; Dc/ D= 11

V variable (#10)

Transducers: 25 (50) end-fissure, mid-fissure (#3-4)

SC2

Table B.2.: cont.

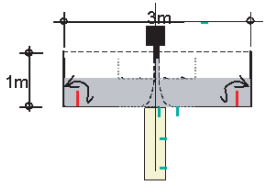	Y/ D = variable (0.20//0.10/0.60, O.67,0.82) **t/D=2.8;** Dc/ D= 16.7 V variable (#9) Transducers: 25, 150 ,end-f, mid-f (#4)	TC1
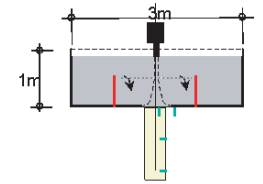	Y/ D = variable (0.40/0.50/0.60/0.67….sub, #5) **t/D=5.6;** Dc/ D= 11 V variable (#9) Transducers: 25, 150, end-f, mid-f (#4)	SC3
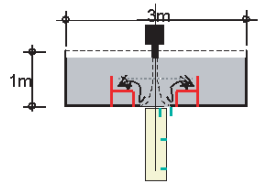	Y/ D = variable (0.40,0.50, 0.60, 0.67, sub, #5) **t/D=5.6;** Dc/ D= 5.6 – 11 V variable (#10) Transducers: 25, 150, end-f, mid-f (#3/4)	FS1
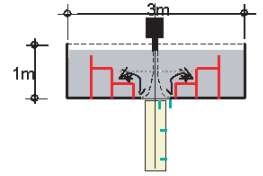	Y/ D = variable (0.60, 0.67, 0.82, #3) **t/D=max 8.3;** Dc/ D= 5.6 – 16.7 V variable (#10) Transducers: 25, 150, end-f, mid-f (#3/4)	FST1
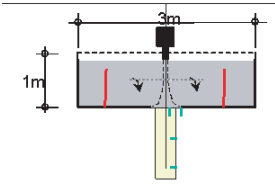	Y/ D = variable (0.60.0.67, sub, #3) **t/D =8.3;** Dc/ D= 16.7 V variable (#10) Transducers: 25, 150, end-f, mid-f (#4)	TC3
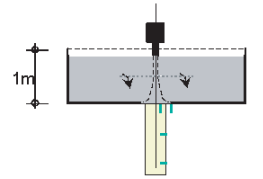	Y/ D = variable (0.20, 0.67, 0.40, 0.60 #4) V variable (#10) Transducers: 25, 150, end-f, mid-f (#4)	FB3

C. Complementary remarks on the development of the boundary layer in free surface chutes

The distance to the inception point (Figure C.1) can be computed **directly** (Ferrando and Rico, 2002) considering the boundary layer thickness development as given by Wood et al. (1983).

$$\Delta x = (\frac{q}{0.05642k^{0.056}(sin\theta)^{0.34}})^F \tag{C.1}$$

$$F = (1.46443k^{0.0054}(sin\theta)^{0.0027})^{-1} \tag{C.2}$$

where q is the unit discharge, k is the equivalent sand grain roughness, and θ is the chute slope. The boundary layer thickness δ at the inception pointis obtained from Wood et al. (1983):

$$\frac{\delta}{\Delta x} = 0.0212(\frac{\Delta x}{H_s})^{-0.11}(\frac{\Delta x}{k})^{-0.10} \tag{C.3}$$

where H_s is the local energy head at the surface. It provides a good estimate of the flow depth $h_{\Delta x}$ at that location. For short chutes, computing the boundary layer thickness at the issuing lip δ_L (replacing Δx by the chute length in the same expression), allows estimating the potential flow depth h_p at a given location by simply $h_p = h_{\Delta x} - \delta_L$. For a typical case where $q = 10\ m^2/s$, $k = 2$ mm and $\theta = 45°$ a distance of about 54 m would be required to reach inception. In most practical cases of overfall weirs, the chute length does not exceeds 20 m and h_p is larger than 50 % of $h_{\Delta x}$. The issuing jet can thus be treated as having a non-aerated core with a uniform velocity profile and turbulence intensity of less than 3 %. These data can be used as input for the jet trajectory and spreading computations.

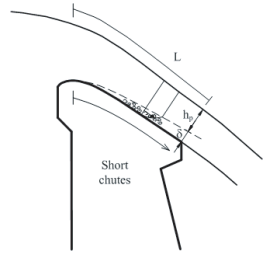

Figure C.1.: Typical non-gated spillway chute

D. Mean pressure statistics complementary to Chapter 8

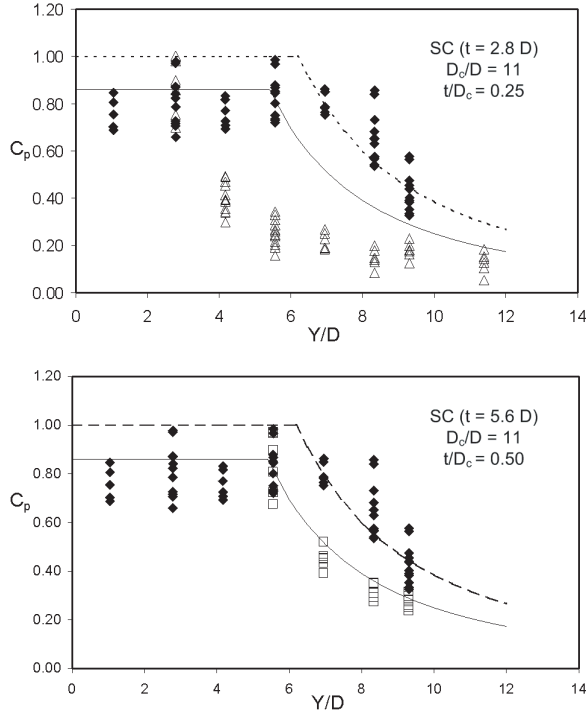

Figure D.1.: "Evolution in depth, cylindrical", dimensionless mean pressure coefficient C_p close to the jet axis ($y/D = 0.35$) as a function of the relative pool depth ratio for pools with D_c/D=11 (SC) and growing scour depth. Comparison with Ervine et al. (1997)'s best fit of data (continuous line) and submerged jet data (dotted line). All data from tests with $V > 17$ m/s. From top to bottom: SC1/2 and SC3 test series.

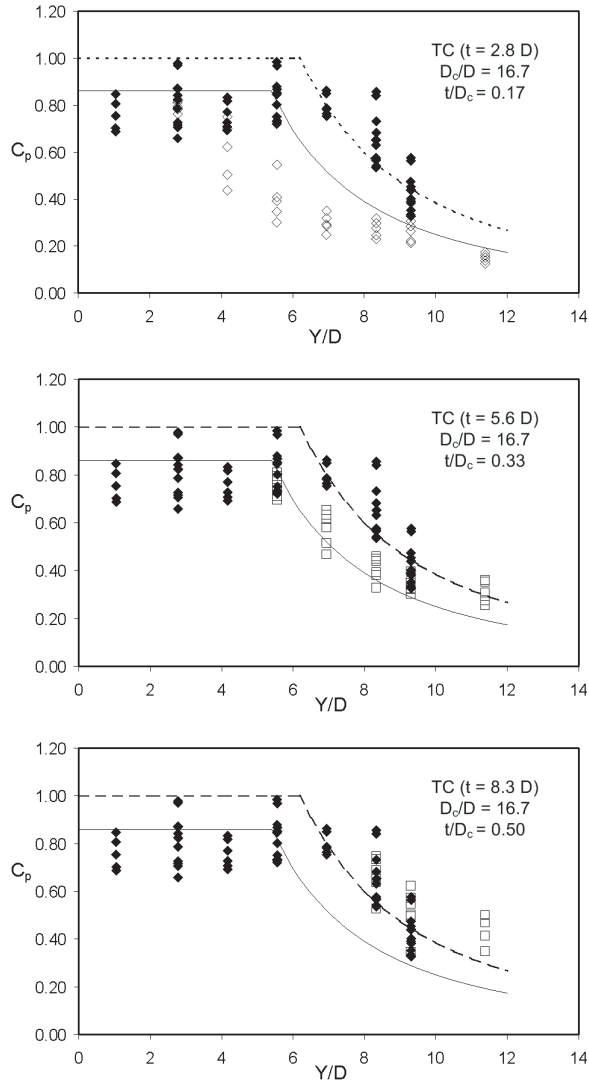

Figure D.2.: "Evolution in depth, cylindrical", dimensionless mean pressure coefficient C_p close to the jet axis ($y/D = 0.35$) as a function of the relative pool depth ratio for pools with D_c/D=16.7 (TC) and growing scour depth. Comparison with Ervine et al. (1997)'s best fit of data (continuous line) and submerged jet data (dotted line). All data from tests with $V > 17$ m/s. From top to bottom: TC1, TC2 and TC3 test series.

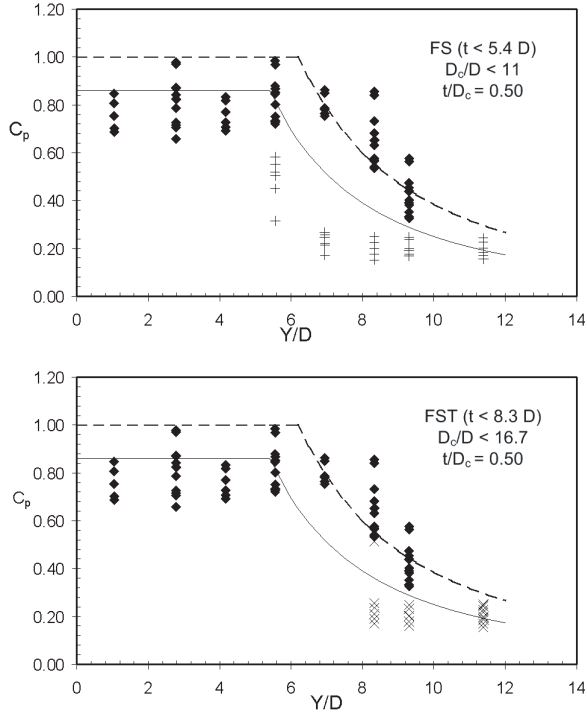

Figure D.3.: "Evolution in depth, conical", dimensionless mean pressure coefficient C_p close to the jet axis ($y/D = 0.35$) as a function of the relative pool depth ratio for pools with $D_c/D <$16.7 and growing scour depth. Comparison with Ervine et al. (1997)'s best fit of data (continuous line) and submerged jet data (dotted line). All data from tests with $V > 17$ m/s. From top to bottom: FC1/2, FS and FST test series.

E. Notes on the use of spectral and correlation functions

From the FFT independent terms (complex) $Y(k)$ one can compute the power spectrum components (real) by:

$$P_{xx} = Y.conj(Y)/N \tag{E.1}$$

where N is the number of independent terms. If one is dealing with relative pressures the first term of the spectrum should be excluded since it corresponds to the mean value. If one is dealing solely with the fluctuations (without the mean), this is not necessary. To verify the correctness of the obtained FFT estimates, the integral of the power spectrum density (PSD) can be compared with the variance of the input data.

Since the FFT function is symmetrical regarding the origin, P_{xx} is only the one-sided positive part of the spectrum and the total power can be estimated with:

$$\sigma^2 = 2\sum P_{xx}/N \tag{E.2}$$

Care should be taken when using the ready-made algorithms of the different software for digital signal treatment (e.g. ©MatLab, ©Labview, etc.) since the definition of the outcome is not always the same, in terms of units, number of terms, one-sided or two-sided spectra, with/without the mean, frequency resolution, and so forth. One small example of this is the fact that Welch's PSD estimates are presented in $[unit^2/\mathrm{Hz}]$ instead of $[unit^2]$ and the number of one-sided PSD Fourier terms is $k_{Welch} = N/N_b/2 + 1$ instead of $N - 1$ (where N_b is the number of data sub-sets selected).

The PSD estimates presented in this dissertation have been obtained using:

- Files that were either 65'024 or 65356 points long (note: this is the limit of rows one can have in Excel, for instance);
- Acquisition frequencies: 2 kHz (Chapter 4), 1 kHz (the large majority) and 10 or 15 kHz (for control runs in Chapter 10);
- Three data files, 64 blocks, 50 % overlapping and Hamming windowing whenever the Welch's method was used;
- A single file whenever the direct FFT method was used.

The correlation function C(x,0,τ) can be computed from the spectral components. For a given time lag τ, the correlation is obtained from:

$$C(i) = 1/N \sum_{n=1}^{k} P_{xx}(n) 2cos(2\pi/N.n)\tau \tag{E.3}$$

The normalized correlation $\rho(x, 0, \tau)$ can be obtained from $C(x, 0, \tau)$ by:

$$\rho(x, 0, \tau) = \frac{C(x, 0, \tau)}{C(x, 0, 0)} \tag{E.4}$$

The time scale I_t is the integral of the positive part of $\rho(x, 0, \tau)$ before the first zero-crossing. When the correlation decays exponentially, i.e.:

$$\rho \approx e^{-\alpha.\tau} \tag{E.5}$$

the integral scale may be obtained analytically from α, i.e.:

$$\hat{I}_t \approx \frac{1}{\alpha} \tag{E.6}$$

The micro (or Taylor) scale λ_t is the x-ordinate of the zero-crossing of a parabola tangent to the $\rho(x, 0, \tau)$ function at the origin. This is equivalent to assuming that the derivatives of $\rho(x, 0, \tau)$ and of the parabola are equal at the vicinity of τ=0.

In practical terms, the quality of the estimate of λ_t depends on the computation of such local derivative, e.g. on the selection of the number of τ time steps to consider regarding the shape of the $\rho(x, 0, \tau)$ function.

In physical terms, the micro scale provides an indication on the persistence of small turbulent structures. The integral scale I_t provides an indication of the type and relevance of the turbulent structures at a given point.

The correlation functions presented in this dissertation have been obtained using:

- The FFT terms, but only for single-point correlation ;
- The direct computation of step-by-step correlations from the time series using the original data files, with frequencies as mentioned for the PSD functions, for single-point but also for cross-correlation of instantaneous pressure data;

Autocorrelations were also computed from the time series and compared with the equivalent estimates obtained from the FFT terms. The results showed a very good agreement. However, it should be stressed that the correlation estimates obtained from the FFT terms are based on three data files (ergodic sampling) whereas those obtained from the time series are based on only one data file. The use of non-consecutive data (due to the acquisition/storage interruption) in the time domain provides erroneous results.

The cross-correlation $C(x_1, x_2, 0)$ is the correlation between simultaneous time series in two-different points and allows inferring the degree of correlation of the turbulent flow field over these points.

If several points are considered, characteristic properties of the turbulent pressure field can be obtained. The integral of the positive surface of the normalized cross-correlation function $\rho(y_1, y_2, 0)$ up to the first zero-crossing in the radial direction y is named the integral scale I_y. It corresponds to a length scale of the turbulent structure that is governing the turbulent pressure field above the mentioned measuring points. In the present context, it can provide an indication of the length scale of a hydraulic jump roller or other characteristic eddy size.

To profit properly from the analysis of cross-correlation the number of measuring points should be spatially displaced in a way to intercept the most important flow features.

Communications du Laboratoire de constructions hydrauliques ISSN 1661-1179
Ecole Polytechnique Fédérale de Lausanne
Editeur: Prof. R. Sinniger

N° 1 1986 W. H. Hager
Discharge measurement structures

N° 2 1988 N. V. Bretz
Ressaut hydraulique forcé par seuil

N° 3 1990 R. Bremen
Expanding stilling basin

N° 4 1996 Dr R. Bremen
Ressaut hydraulique et bassins amortisseurs, aspects hydrauliques particuliers

N° 5 1997 Compte-rendu du séminaire à l'EPFL
Recherche dans le domaine des barrages, crues extrêmes

Communications du Laboratoire de constructions hydrauliques
Ecole Polytechnique Fédérale de Lausanne
Editeur: Prof. Dr A. Schleiss

N° 6 1998 N. Beyer Portner
Erosion des bassins versants alpins suisse par ruissellement de surface

N° 7 1998 G. De Cesare
Alluvionnement des retenues par courants de turbidité

N° 8 1998 J. Dubois
Comportement hydraulique et modélisation des écoulements de surface

N° 9 2000 J. Dubois, J.-L. Boillat
Routing System - Modélisation du routage de crues dans des systèmes hydrauliques à surface libre

N° 10 2002 J. Dubois, M. Pirotton
Génération et transfert des crues extrêmes - Le logiciel Faitou

N° 11 2002 A. Lavelli, G. De Cesare, J.-L. Boillat
Modélisation des courants de turbidité dans le bassin Nord du Lac de Lugano

N° 12 2002 P. de Almeida Manso
Stability of linings by concrete elements for surface protection of overflow earthfill dams

N° 13 2002 E. Bollaert
Transient water pressures in joints and formation of rock scour due to high-velocity jet impact

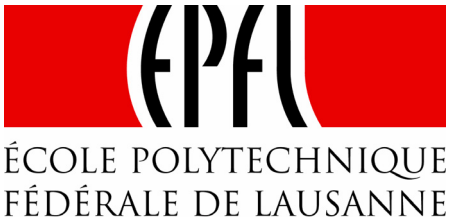

ISSN 1661-1179

Prof. Dr A. Schleiss
Laboratoire de constructions hydrauliques - LCH
EPFL, Bât. GC, Station 18, CH-1015 Lausanne
http://lchwww.epfl.ch
e-mail: secretariat.lch@epfl.ch